Measurement and relevance of rhythmic and aperiodic human brain dynamics

DISSERTATION

zur Erlangung des akademischen Grades
Doctor rerum naturalium (Dr. rer. nat.)

eingereicht an der
Lebenswissenschaftlichen Fakultät der Humboldt-Universität zu Berlin

von
Julian Q. Kosciessa (M.Sc.)

Präsidentin
der Humboldt-Universität zu Berlin
Prof. Dr.-Ing. Dr. Sabine Kunst

Dekan der Lebenswissenschaftlichen Fakultät
der Humboldt-Universität zu Berlin
Prof. Dr. Bernhard Grimm

Gutachter

1. Prof. Dr. Ulman Lindenberger
2. Prof. Dr. Bradley Voytek
3. Prof. Dr. Jonas Obleser

Tag der mündlichen Prüfung: 02.10.2020

Summary

Non-invasive signals recorded from the human scalp provide a window on the neural dynamics that shape perception, cognition and action. Historically motivating the assessment of large-scale network dynamics, rhythms are a ubiquitous sign of neural coordination, and a major signal of interest in the cognitive, systems, and computational neurosciences. However, typical descriptions of rhythmicity lack detail, e.g., failing to indicate when and for how long rhythms occur. Moreover, neural times series exhibit a wealth of dynamic patterns, only some of which appear rhythmic. While aperiodic contributions are traditionally relegated to the status of irrelevant 'noise', they may be informative of latent processing regimes in their own right. Crucially, the measurement of rhythmic and aperiodic components is mutually confounded in space, time and magnitude, thus challenging their separate characterization.

This cumulative dissertation summarizes and discusses work that (a) aims to methodologically dissociate rhythmic and aperiodic contributions to human electroencephalogram (EEG) signals, and (b) probes their relevance for flexible cognition. Specifically, ***Project 1*** highlights the necessity, feasibility and limitations of dissociating rhythmic from aperiodic activity at the single-trial level. ***Project 2*** inverts this perspective, and examines the utility of multi-scale entropy as an index for the irregularity of brain dynamics, with a focus on the relation to rhythmic and aperiodic descriptions. By highlighting prior biases and proposing solutions, this work indicates future directions for measurements of temporal irregularity. Finally, ***Project 3*** examines the neurocognitive relevance of rhythmic and aperiodic regimes with regard to the neurophysiological context in which they may be engaged. Using a parallel multi-modal EEG-fMRI design with concurrent pupillometry, this project provides initial evidence that elevated demands shift cortical dynamics from a rhythmic to an irregular regime; and implicates concurrent phasic neuromodulation and subcortical thalamic engagement in these regime shifts.

By combining advances in the characterization of rhythmic and aperiodic activity with their application to a novel behavioral probe, this cumulative dissertation advances insights into how contextual demands shape cortical rhythms as well as irregularity, highlights improvements in the ability to selectively characterize these regimes, and discusses their potential interpretation at the latent level of human brain function.

Zusammenfassung

Menschliche Hirnsignale von der Kopfhaut bieten einen Einblick in die neuronalen Prozesse, denen Wahrnehmung, Denken und Verhalten zugrunde liegen. Rhythmen, die historisch den Grundstein für die Erforschung großflächiger Hirnsignale legten, sind ein häufiges Zeichen neuronaler Koordination, und damit von weitem Interesse für die kognitiven, systemischen und komputationalen Neurowissenschaften. Typischen Messungen von Rhythmizität fehlt es jedoch an Details, z. B. wann und wie lange Rhythmen auftreten. Darüber hinaus weisen neuronale Zeitreihen zahlreiche dynamische Muster auf, von denen nur einige rhythmisch erscheinen. Obwohl aperiodischen Beiträgen traditionell der Status irrelevanten „Rauschens“ zugeschrieben wird, attestieren neuere Erkenntnisse ihnen ebenfalls eine Signalrolle in Bezug auf latente Hirndynamik. Eine separate Charakterisierung rhythmischer und aperiodischer Komponenten ist jedoch nur eingeschränkt möglich, da beide Anteile räumlich, zeitlich und in ihrer Amplitude vermischt sind.

Diese kumulative Dissertation fasst Projekte zusammen, die darauf abzielen, rhythmische und aperiodische Beiträge zum menschlichen Elektroenzephalogramm (EEG) methodisch zu dissoziieren, und ihre Relevanz für die flexible Wahrnehmung zu untersuchen. Projekt 1 ermittelt insbesondere die Notwendigkeit und Durchführbarkeit der Trennung rhythmischer von aperiodischer Aktivität in kontinuierlichen Signalen. Projekt 2 kehrt diese Perspektive um und prüft Multiscale Entropy als Index für die Unregelmäßigkeit von Zeitreihen. Diese Arbeit weist auf methodische Probleme in der klassischen Messung zeitlicher Unregelmäßigkeit hin, und schlägt Lösungen für zukünftige Anwendungen vor. Abschließend untersucht Projekt 3 die neurokognitive Relevanz rhythmischer und aperiodischer Zustände. Anhand eines parallelen multimodalen EEG-fMRT-Designs mit gleichzeitiger Pupillenmessung liefert dieses Projekt erste Hinweise dafür, dass erhöhte kognitive Anforderungen Hirnsignale von einem rhythmischen zu einem unregelmäßigen Regime verschieben und impliziert gleichzeitige Neuromodulation und thalamische Aktivierung in diesem Regimewechsel.

Auf der Basis von Fortschritten in der Charakterisierung rhythmischer und aperiodischer Zustände sowie ihrer Erforschung in einem funktionalen Design diskutiert diese kumulative Dissertation wie kontextuale Anforderungen Rhythmen sowie Unregelmäßigkeiten in Zeitreihen beeinflussen, wie diese Komponenten methodisch separiert werden können, sowie welche möglichen Interpretationen diesen Komponenten auf der latenten Ebene der menschlichen Gehirnfunktion zugrunde liegen.

Acknowledgements

This dissertation represents the culmination of multiple years of work on individual projects, none of which would have been possible without the support from people and institutions around me. These include, but are not limited to:

- my advisors, formal (Dr. Douglas D. Garrett, Prof. Dr. Ulman Lindenberger) and informal (Dr. Markus Werkle-Bergner) for their unwavering conceptual and practical support
- the entire LNDG lab, including all of its time-varying members, as well as the student assistants LNDG and otherwise, who have contributed to this work
- the LIP-IT, the IT-helpdesk and especially Michael Krause for swift and encompassing technical support
- numerous colleagues who provided helpful technical feedback at conferences
- the COMP2PSYCH research school for their numerous resources and for providing me the freedom to pursue my research topics of interest
- the Max Planck Institute for Human Development for their outstanding facilities, including all of the support staff
- the whole LIP team for great talks, chats and a very sociable atmosphere
- the DAAD and COMP2PSYCH for their travel grants
- my wife, Chen Yunyue, least of all for improving my Illustrator skills and assisting with the cover design
- my family for providing me with endless support of all kinds
- the reviewers, open and anonymous, who have substantially contributed to many manuscript revisions, the benefits of which are directly visible in different BioRxiv versions
- the numerous researchers and lecturers at the Freie Universität Berlin, National University of Singapore, the Berlin School of Mind and Brain, University College London and Humboldt Universität, who have accompanied my academic development

And last but not least, the countless researchers, whose work inspired this dissertation, informs my (limited) understanding of human cognition, and whose work continually makes me question my own assumptions and practices in the best possible way.

Abbreviations

ACh: acetylcholine
AMPA: α-amino-3-hydroxy-5-methyl-4-isoxazolepropionic acid
BOLD: blood-oxygen-level-dependent
BOSC: Better OSCillation detection
CPP: Centroparietal Positive Potential
CTC: communication through coherence
eBOSC: extended Better OSCillation detection
E-I: excitation-inhibition
EEG: electroencephalogram/electroencephalography
fMRI: functional magnetic resonance topography
FOOOF: Fitting Oscillations & One-Over F
GABA: gamma-aminobutyric acid
IRASA: Irregularly Resampled AutoSpectral Analysis
L-FPN: Lateral Frontoparietal Network
LFP: local field potential
LGN: lateral geniculate nucleus
LRTC: long-range temporal correlation
M-CIN: Midcingulo-Insular Network
MAAT**:** Multi-Attribute Attention Task
MEG: magnetoencephalogram/magnetoencephalography
MSE: multi-scale entropy
mMSE: modified multi-scale entropy
NA: noradrenaline
RT: reaction time
SampEn: sample entropy
SNR: signal-to-noise ratio
TC: thalamocortical
TRN: thalamic reticular nucleus

Table of Contents

1. Introduction

Human cognition requires a flexible coordination of neural activity to shape information processing in contextually adaptive ways (Malsburg, Phillips, & Singer, 2010). Potentials measured at the human scalp (e.g., via electroencephalography) provide a non-invasive and information-rich window on such coordinative processes, and offer the opportunity to bridge observations across multiple spatial scales in cognitive and systems neuroscience (Panzeri, Macke, Gross, & Kayser, 2015). However, the characterization of the constituent components of scalp potentials remains challenging. Neural rhythms/oscillations (e.g., Buzsáki, 2006; Steriade, 2006) are a dominant graphoelement that has been observed since the early days of electrophysiological recordings (Berger, 1929). By virtue of their periodic synchrony, rhythms may orchestrate local and distributed neural activity, and provide a principled framework for the coordination of neural processing. However, rhythmic activity is but one index of brain function, whereas most of the variance in neural recordings can be characterized as aperiodic, arrhythmic, and/or scale-free[1]. Although this aperiodic signal component may prove sensitive to neural computations *sui generis*, our understanding of it remains limited. This partly arises from a traditional focus on narrowband rhythms, which relegates aperiodic activity to the status of 'background' activity or irrelevant 'noise'. The work summarized in this dissertation aims to improve the measurement of rhythmic (*Chapter 2*) and aperiodic regimes (*Chapter 3*) in humans, as well as to advance our knowledge about their functional relevance for flexible attention (*Chapter 4*). *Chapter 1* briefly reviews these two signal components, their measurement, as well as the suggested underlying mechanisms of their generation, and is followed by the specific aims of the work in this dissertation. *Chapters 2-4* provide brief summaries of the individual Projects encompassing this cumulative dissertation, which are reprinted in the Appendix. Finally, I summarize and discuss implications and future directions of the present work in *Chapter 5*. In general, I attempt to embed the work described in the individual Projects into the broader cognitive/systems neuroscience literature, while expanding on various aspects that may not have received sufficient discussion in each of the individual papers.

---

[1] Rhythmic (or oscillatory) fluctuations exhibit a specific time scale that is defined by the period of repetitions (or the frequency, as the inverse). In contrast, aperiodic (or arrhythmic/irregular) fluctuations encompass multiple time scales, in extreme cases rendering them 'scale-free'.

1.1. Electrophysiological rhythms as markers of periodic activity fluctuations

The observation of rhythmic (or oscillatory) graphoelements at the scalp initially motivated the use of electroencephalography (EEG) as a means to study large-scale brain dynamics in humans (Adrian & Matthews, 1934; Berger, 1929; Jasper, 1948; Jasper & Andrews, 1938)[2]. Since those initial descriptions, a great amount of work assigned neural rhythms a computational role in structured information processing and communication in the brain (for reviews see Buzsáki & Draguhn, 2004; Fiebelkorn & Kastner, 2019; Heeger & Mackey, 2019; Helfrich & Knight, 2016; E. K. Miller & Buschman, 2013; E. K. Miller, Lundqvist, & Bastos, 2018; Salinas & Sejnowski, 2001; Siegel, 2013; Ward, 2003). In particular, information (e.g., about the external environment) is represented in the timing and rate of neural 'unit' firing in circumscribed neural networks (Montemurro, Rasch, Murayama, Logothetis, & Panzeri, 2008; Quiroga & Panzeri, 2013; Rolls & Treves, 2011). This all-or-none 'unit' activity in turn depends on the subthreshold states of membrane potentials, i.e., the current 'context' of ongoing fluctuations (Lashley, 1951; Okun et al., 2015). Neurons constantly receive a barrage of excitatory and inhibitory synaptic inputs, which robustly alter membrane potentials and thereby regulate the firing rate probability of postsynaptic neurons (Destexhe, Rudolph, & Pare, 2003). Neural populations undergo collective fluctuations in their membrane potentials, and thus their excitability and firing patterns, giving rise to measurable signals of synchrony (Engel et al., 2001; Singer, 1999) in local field or scalp potentials (Haider, Schulz, Hausser, & Carandini, 2016)[3]. Periodic rhythms reflect rapid temporal imbalances between excitation and inhibition on the order of tens of milliseconds (see Figure 8 in Poo and Isaacson (2009); Figure 5 in Atallah and Scanziani (2009)), which give rise to transient temporal 'windows of opportunity' (Buzsáki, 2006) for local information processing and for distributed neural communication if those windows are synchronized across space (Canolty

[2] An excellent historical analysis on the scientific origins of human electrophysiology is provided by Borck (2005); Borck and Hentschel (2018).

[3] The scalp EEG signal primarily reflects the magnitude and synchrony (Musall, von Pfostl, Rauch, Logothetis, & Whittingstall, 2014) of postsynaptic potentials in the dendrites of cortical pyramidal cells (Buzsáki, Anastassiou, & Koch, 2012; Nunez & Srinivasan, 2006), although spike contributions have also been reported (Suzuki & Larkum, 2017). This signal shares sensitivity to mass synaptic flux with its magnetic counterpart (MEG) (Lopes da Silva, 2013), as well as local field potentials (LFPs) as 'building blocks' of summed synaptic potentials closer to the recording site (Einevoll, Kayser, Logothetis, & Panzeri, 2013; Kajikawa & Schroeder, 2011). This establishes a link between latent dynamics at the level of synaptic inputs, membrane potential fluctuations, and their modulation of mass neural firing to observations at a coarser scale of measurement (Hari & Puce, 2017).

et al., 2010; Fries, 2005, 2015; F. Varela, Lachaux, Rodriguez, & Martinerie, 2001; Womelsdorf et al., 2007). Due to the shared nature of excitability fluctuations, gross population firing (but not necessarily activation of single neurons) fluctuates periodically as a function of the rhythmic phase, alongside behavioral outputs (e.g., Gross et al., 2002). Specifically, depending on whether momentary excitation or inhibition dominates, population firing rates increase and decrease during the rhythmic trough and peak, respectively. By indicating the average modulation of neural discharge, measures of population synchrony thus offer a complementary perspective on neural 'unit' activity that may bridge spatial scales of analysis (Bullock, 1997; Panzeri et al., 2015; Singer, 2013).

Synchronized population firing occurs within and between local and distant neural populations. Such short- and long-range synchrony can emerge from distinct structural circuit motifs that shape different intrinsic time scales (Womelsdorf, Valiante, Sahin, Miller, & Tiesinga, 2014). In particular, local synchrony and feedforward processing are closely associated with high-frequency (gamma) rhythms arising from the proximal interactions between excitatory pyramidal cells and inhibitory interneurons (Buzsáki & Wang, 2012; X. J. Wang, 2010). In contrast, slower rhythms are thought to be generated by the interaction of proximal and distal drive, the latter via long-range cortico-cortical or thalamo-cortical circuits (von Stein & Sarnthein, 2000). This architecture may particularly support top-down feedback communication (Engel, Fries, & Singer, 2001; Markov et al., 2014) and is supported by laminar-specific[4] engagement of fast and slow rhythms (for a review see Scheeringa & Fries, 2019). Whereas slower (alpha) rhythms are observed in cortico-cortical feedback, (i.e., superficial and deep) layers (Bollimunta, Chen, Schroeder, & Ding, 2008; Bollimunta, Mo, Schroeder, & Ding, 2011; Haegens et al., 2015; M. Halgren et al., 2019; van Kerkoerle et al., 2014), propagation of high frequencies may follow a feedforward direction from granular to superficial and deep layers (van Kerkoerle et al., 2014). Moreover, an anticorrelated modulation between alpha and gamma has been observed across cortical layers (Spaak, Bonnefond, Maier, Leopold, & Jensen, 2012) as well as cortical hierarchies in visual cortex (Michalareas et al., 2016). Such a relationship between frequency architecture and

[4] The cerebral cortex exhibits a systematic layer structure with distinct cell and connectivity profiles, that constitute canonical microcircuits (for a review see Bastos et al., 2012 and references therein).

feedforward vs. feedback connectivity has since been supported by computational models (Mejias, Murray, Kennedy, & Wang, 2016). Hence, the time scale of macroscopic fluctuations is thought to be a crucial index of structural circuit properties (Avena-Koenigsberger, Misic, & Sporns, 2018).

Neural rhythms may coordinate neural firing and information processing in space, time and across time scales. This is best exemplified by travelling waves[5] that sequentially engage local and increasingly distal neural populations into a common temporal reference frame, as observed in both humans and non-human animal models (Bahramisharif et al., 2013; M. Halgren et al., 2019; J. R. Hughes, 1995; Lozano-Soldevilla & VanRullen, 2019; Roberts et al., 2019; Zhang, Watrous, Patel, & Jacobs, 2018). In addition to spatial coordination, multiplexing of information at different temporal channels (i.e., frequencies) can structure and integrate cortical processing (T. Akam & Kullmann, 2014; Bonnefond, Kastner, & Jensen, 2017; Buzsáki & Wang, 2012; Fries, 2015; Helfrich & Knight, 2016; Jensen & Colgin, 2007; Knight & Eichenbaum, 2013; Palva & Palva, 2007; Whittingstall & Logothetis, 2009). For example, visual sampling involves an interplay between high-frequency gamma power and the phase of low-frequency theta and alpha rhythms (Jensen, Bonnefond, & VanRullen, 2012; Michalareas et al., 2016). Similarly, memory encoding and retention have been conceptualized as a coupling of item-specific gamma cycles that are sequentially ordered by the phase of a slower theta rhythm (Bahramisharif, Jensen, Jacobs, & Lisman, 2018; Heusser, Poeppel, Ezzyat, & Davachi, 2016; Kajikawa & Schroeder, 2011; J. E. Lisman & Idiart, 1995; J. E. Lisman & Jensen, 2013; Siegel, Warden, & Miller, 2009). As such, neural rhythms observed in scalp recordings may signify rapid information coordination at different time scales.

1.2. A brief overview of rhythmic frequency bands

Neural rhythms can be reliably grouped into different frequency bands (Penttonen & Buzsáki, 2003; Shackman, McMenamin, Maxwell, Greischar, & Davidson, 2010), with high consistency across species (Buzsáki, Logothetis, & Singer, 2013), and idiosyncratic 'spectral fingerprints' in different cortical regions (Keitel & Gross, 2016; Rosanova et al., 2009). The canonical bands consist of delta (~ 1-4 Hz), theta (~4-8 Hz), alpha (~8-15 Hz), beta (~15-30 Hz)

[5] Note that there are observations of both planar rhythms as discussed here and concentric waves in mammalian cortex (for reviews see Muller, Chavane, Reynolds, & Sejnowski, 2018; Sato, Nauhaus, & Carandini, 2012), although the relation between them is unclear. Conceptually, they have been differentially likened to planar waves that wind produce in a body of water vs. the effects of a raindrop that concentrically propagates waves (Sato et al., 2012).

and gamma (~30-120 Hz) frequencies, although exact ranges vary and diverse circuits may generate rhythms even within the same frequency band (Buzsáki et al., 2013; Womelsdorf et al., 2014). These narrow-band rhythms have been implicated in a plethora of cognitive functions, and will only be briefly covered here (for a broader perspective see textbooks, e.g., Buzsáki, 2006; Mike X. Cohen, 2014; Hari & Puce, 2017; Nunez & Srinivasan, 2006; Schomer & Silva, 2017). **Delta (~1-4 Hz) rhythms** (and infra-slow fluctuations < 1 Hz) modulate broadband excitability on longer timescales in primates (Lakatos, Karmos, Mehta, Ulbert, & Schroeder, 2008; Lakatos et al., 2005; Schroeder & Lakatos, 2009; Whittingstall & Logothetis, 2009) and humans (Besle et al., 2011; Helfrich, Huang, Wilson, & Knight, 2017; Monto, Palva, Voipio, & Palva, 2008). Functionally, this modulation may serve stimulus selection via the coupling of distant populations e.g., in fronto-parietal networks (Nacher, Ledberg, Deco, & Romo, 2013). **Theta rhythms (~4-8 Hz)** are dominantly associated with spatial navigation, and memory formation in hippocampus (for a review see Korotkova et al., 2018; Vanderwolf, 1969). Such hippocampal theta signals make limited contribution to scalp signals however (Backus, Schoffelen, Szebenyi, Hanslmayr, & Doeller, 2016). In contrast, frontal theta rhythms at the scalp have been linked to cognitive control and decision making with links to the more proximal anterior cingulate cortex (Beulen, 2011; Cavanagh & Frank, 2014; M. X. Cohen & Donner, 2013). Theta rhythms also coordinate perceptual sampling when attention is allocated to multiple objects (Fiebelkorn, Saalmann, & Kastner, 2013; Helfrich, Breska, & Knight, 2019; Landau & Fries, 2012; Re, Inbar, Richter, & Landau, 2019). **Alpha rhythms (~8-15 Hz)** have initially been associated with passive cortical idling (Adrian & Matthews, 1934) due to strong amplitude increases upon eye closure (Berger, 1929). Recent studies have revised this account, suggesting an active inhibitory gating of information processing (Basar, 2012; Buschman, Denovellis, Diogo, Bullock, & Miller, 2012; Foxe & Snyder, 2011; Jensen & Mazaheri, 2010; Klimesch, Sauseng, & Hanslmayr, 2007; Peterson & Voytek, 2017; Pfurtscheller, 2001). According to the inhibition-timing hypothesis (Klimesch et al., 2007), both the magnitude and phase of alpha rhythms modulate local excitability. Via 'pulsed inhibition', spike probability increases at the rhythmic trough and decreases during the peak. Such relationship between sinusoidal phase and multi-unit firing has found empirical support in rats (Poo & Isaacson, 2009), cats (Lorincz, Kekesi, Juhasz, Crunelli, & Hughes, 2009), monkeys (Haegens, Nacher, Luna, Romo, & Jensen, 2011) and humans (Coon et al., 2016; Schalk, Marple, Knight, & Coon, 2017). Via phasic modulation of cortical excitability, alpha rhythms can temporally gate perception (Busch & VanRullen, 2010; Jensen et al., 2012; Mathewson, Gratton, Fabiani, Beck, & Ro, 2009; Romei, Gross, & Thut, 2012), while decreases in alpha amplitude (and thus the presumed magnitude of pulsed inhibition) track increases in excitability (Haegens et al., 2011; Lange, Oostenveld, & Fries, 2013; Pfurtscheller & da Silva, 1999; Romei et al., 2012), active information representation (Griffiths et

al., 2019; Hanslmayr, Staudigl, & Fellner, 2012) and attention in space and time (e.g., see reviews: Foster, Sutterer, Serences, Vogel, & Awh, 2017; Foxe & Snyder, 2011; Jensen & Mazaheri, 2010; Palva & Palva, 2007; Sadaghiani & Kleinschmidt, 2016). Due to their large amplitude in non-invasive EEG recordings, and their relevance for cortical processing, much work in this dissertation focusses on the identification and functional role of alpha rhythms. Events in the **Beta (~15-25 Hz)** frequency band have been associated with motor inhibition, the protection of current cortical states from external interruption (Engel & Fries, 2010) and transient content reactivation for current task demands (Spitzer & Haegens, 2017). Recent evidence questions the prevalence of sustained beta rhythms however, and rather suggests a transient 'burst' appearance (Feingold, Gibson, DePasquale, & Graybiel, 2015; Little, Bonaiuto, Barnes, & Bestmann, 2019; Lundqvist et al., 2016; M. A. Sherman et al., 2016; Tinkhauser, Pogosyan, Little, et al., 2017; Tinkhauser, Pogosyan, Tan, et al., 2017; Tinkhauser et al., 2018) as well as prominent non-sinusoidal features of motoric beta rhythms (Cole et al., 2017; Schaworonkow & Nikulin, 2019). Finally, **Gamma (approx. > 25 Hz)** 'rhythms' have been associated with active cortical processing, and the binding of information within and across cortical areas via temporal synchrony (Bruno & Sakmann, 2006; Engel et al., 2001; Fries, 2005, 2009; Jagadeesh, Gray, & Ferster, 1992; Ni et al., 2016; X. J. Wang, 2010; Womelsdorf, Fries, Mitra, & Desimone, 2006; Womelsdorf et al., 2007). Gamma represents a relative outlier among the frequency ranges reported here, as both narrow- and broadband components exist (e.g., Bartoli et al., 2019; Belitski et al., 2008; Henrie & Shapley, 2005; Saleem et al., 2017), with some evidence for non-stationary narrowband gamma bursts (Burns, Xing, & Shapley, 2011; Palmigiano, Geisel, Wolf, & Battaglia, 2017; Xing et al., 2012). Notably, the gamma range is difficult to characterize in non-invasive EEG recordings due to the low sensitivity to high-frequency content, and a spectral overlap with non-neural noise contributions (Hipp & Siegel, 2013; Yuval-Greenberg, Tomer, Keren, Nelken, & Deouell, 2008).

1.3. Fundamental characteristics of neural rhythms

Multiple indices of scalp-level rhythmicity provide insights into latent[6] properties of neural dynamics. The **amplitude** of rhythmic events is traditionally assumed to reflect the strength and synchrony of neural population activity (Buzsáki et al., 2012; Buzsáki & Draguhn, 2004; Mike X. Cohen, 2014; Musall et al., 2014)[7]. Narrowband (putatively rhythmic) amplitudes wax and wane over time (e.g., Linkenkaer-Hansen, Nikouline, Palva, & Ilmoniemi, 2001) alongside systematic changes in neural firing and behavioral outputs (e.g., Nelli, Itthipuripat, Srinivasan, & Serences, 2017; Sauseng, Klimesch, Gerloff, & Hummel, 2009; Schalk et al., 2017). However, conventional estimation methods conflate rhythmic and aperiodic components in magnitude, space and time, thereby rendering amplitude estimates ambiguous to the presence of rhythmicity (see *Section 1.4*).

The **rhythmic frequency** band is considered to relate at least in part to the conduction delay and thus the size of the engaged network (Buzsáki & Draguhn, 2004; Buzsáki et al., 2013; von Stein & Sarnthein, 2000), although long-range synchrony has also been observed at high frequencies (Gregoriou, Gotts, Zhou, & Desimone, 2009). Within these bands, smaller, yet robust and systematic frequency variations are observed across development (Knyazeva, Barzegaran, Vildayski, & Demonet, 2018; Lindsley, 1939; Marshall, Bar-Haim, & Fox, 2002; H. S. Wang & Busse, 1969), between subjects (Bazanova & Vernon, 2014; Furman et al., 2018; Grandy, Werkle-Bergner, Chicherio, Lovden, et al., 2013; Grandy, Werkle-Bergner, Chicherio, Schmiedek, et al., 2013; Gray & Emmanouil, 2020; Gulbinaite, van Viegen, Wieling, Cohen, & VanRullen, 2017; Haegens, Cousijn, Wallis, Harrison, & Nobre, 2014), and as a function of behavioral or task state (Atallah & Scanziani, 2009; Babu Henry Samuel, Wang, Hu, & Ding, 2018; Benwell et al., 2019; Haegens et al., 2014; Mierau, Klimesch, & Lefebvre, 2017; Wutz, Melcher, & Samaha, 2018). Long-term developmental changes in rhythmic frequency are thought to depend on the morphology of thalamocortical feedback loops due to the maturation of synaptic connectivity and myelination (Knyazeva et al., 2018), with inter-individual differences reflecting the relative efficiency and

---

[6] The term 'latent' is used here, as the neural dynamics of interest are generally not directly observed in EEG recordings (cf. Heitmann & Breakspear, 2018), which at best provide imperfect proxy estimates among diverse sources of measurement noise (Hari & Puce, 2017).

[7] For inter-individual assessments, conductivity differences arising from differences in tissue conductivity (e.g., grey matter density, skull and skin thickness) can impact amplitude measures at the scalp level especially in EEG recordings (Hagemann, Hewig, Walter, & Naumann, 2008; Leissner, Lindholm, & Petersen, 1970).

speed of neural information transfer (Grandy, Werkle-Bergner, Chicherio, Schmiedek, et al., 2013; Samaha & Postle, 2015; Wutz et al., 2018). In addition, transient alpha/beta frequency shifts across different task states assumedly index different arousal levels (Mierau et al., 2017), while increases in narrowband gamma frequency as a function of stimulation intensity (Jia, Xing, & Kohn, 2013; Mejias et al., 2016; Ray & Maunsell, 2010; Saleem et al., 2017) may reflect rapid variations in the temporal lag between excitation and inhibition (Atallah & Scanziani, 2009; Xing et al., 2012).

Finally, the **phase** of a sinusoidal process is considered important for coordinated information flow through coherence (Fell & Axmacher, 2011; Fries, 2005, 2015; F. Varela et al., 2001) as well as for chunking continuous input streams into segregated packets of information. Accordingly, measures of population activity (Coon et al., 2016; Haegens et al., 2011; Snyder, Morais, Willis, & Smith, 2015; Whittingstall & Logothetis, 2009) and stimulus information (Kayser, Montemurro, Logothetis, & Panzeri, 2009; Montemurro et al., 2008; Ng, Logothetis, & Kayser, 2013) vary as a function of low-frequency phase. At the behavioral level, such chunking via phasic excitability variations motivated the concept of *perceptual cycles* (VanRullen, 2016), which proposes a rhythmic sampling (or scanning) of the environment at discrete excitability phases (Busch & VanRullen, 2010; Helfrich, 2018). Such idea predicts 'visual sampling rates', estimated for example via periodic fluctuations in perceptual performance (Romei et al., 2012), that covary with the frequency of cortical rhythms (VanRullen & Koch, 2003; F. J. Varela, Toro, John, & Schwartz, 1981). Such relation has indeed been observed for posterior alpha rhythms (Minami & Amano, 2017; Samaha & Postle, 2015). Moreover, a division of the sampling frequency (i.e., to theta frequencies) occurs when attention is coordinated between multiple spatial locations (Crouzet & VanRullen, 2017; Fiebelkorn, Pinsk, & Kastner, 2018; Fiebelkorn et al., 2013; Helfrich et al., 2018; Landau & Fries, 2012; Mo et al., 2019; Re et al., 2019). As such, the rhythmic phase of mass potentials may signify the temporal coordination of active information processing (for a review see Panzeri et al., 2015).

Relative to these fundamental characteristics of rhythms, the **timing**, **duration,** and **rate** of rhythmic events are traditionally neglected features in the field due to a common reliance on average summary statistics[8]. Such oversight is unfortunate, as the duration or rate of events may

[8] Sleep scoring provides an exception, as the presence or absence of specific graphoelements as indicated by manual labeling is used as a sleep stage index (Silber et al., 2007). However, this manual scoring is not without problems, as threshold criteria are somewhat arbitrarily fixed (Muehlroth & Werkle-Bergner, 2020).

be of functional importance (Palmigiano et al., 2017; Peterson & Voytek, 2017, 2019; Xing et al., 2012). Rare work that estimates the presence and duration of non-stationary alpha events suggests that their incidence, but not their duration or amplitude, changes with neurofeedback training (Ossadtchi, Shamaeva, Okorokova, Moiseeva, & Lebedev, 2017). Moreover, increasing work in the beta frequency range suggests that beta power reflects "specifically timed synaptic events […], which occur intermittently in time" (M. A. Sherman et al., 2016, p. E4893), while the duration statistics of such transient events change alongside cortical development (Gireesh & Plenz, 2008). As such, rhythm timing, duration, and rate may provide important indices of neural processes that remain underappreciated at least in part due to methodological difficulties that I discuss next.

1.4. Pitfalls of current practices in the characterization of neural rhythms

The assessment of neural rhythms has a long-standing history, with visual assessments of manually derived time series dominating early work on rhythm identification (Borck, 2005) before spectral decomposition approaches automated the characterization of periodic signal components, initially of paper recordings (Dietsch, 1932) and later in electrical circuits (Walter, 1943a). While such techniques allow for efficient analyses and remain in prevalent use (Mike X. Cohen, 2014), they do not unambiguously indicate whether – and if so when – a rhythm occurred. As such, not all features derived by careful manual labelling (e.g., timing and event duration) can yet be retrieved by automated, high-throughput procedures. Moreover, the interpretation of traditional rhythm characteristics (see *Section 1.3*) requires that a rhythm is present during their measurement. This assumption is rarely checked however, and is complicated by multiple methodological limitations.

Rhythms are typically assessed by means of a Fourier transform (Gross, 2014) that deconstructs a time-domain signal into a sum of sinusoids that vary in amplitude and phase (for textbooks see e.g., Mike X. Cohen, 2014; Van Drongelen, 2018). Notably, this conversion is lossless, meaning that any signal can be exhaustively decomposed into sinusoids, even if it consists exclusively of structured or unstructured noise. Notably, such noise components are characterized by stereotypic amplitude (and power) spectra, specifically a 1/f fall-off in the case of pink noise, as observed in many empirical brain signals (see *Section 1.6*). As such, rhythmicity can be defined as a local amplitude peak above this 'noise' background in the frequency domain. However, this also means that narrowband power estimates reflect an amalgamation of both the rhythmic 'signal' and the aperiodic 'noise' profile (Donoghue, Dominguez, & Voytek, 2020; Haller et al., 2018; Voytek & Knight, 2015). Hence, the reverse inference that spectral power reflects the presence of a rhythm, is not warranted. As such, it has been claimed that "[m]ost of the time in

most animals there is little evidence of really rhythmic oscillators in the ongoing cerebral activity, let alone that rhythms account for much of the total energy" (Bullock, 1997, p. 5), although a quantification of the rhythmic content in neural recordings remains challenging[9]. Crucially, higher-order characterizations of rhythms, such as phase-based functional connectivity estimates, assume that estimates are directly linked to the presence of periodicity, therefore leading to interpretational difficulties when it is unclear whether this condition is met (Aru et al., 2015; Muthukumaraswamy & Singh, 2011).

Moreover, many applications (as well as the Fourier transform itself) operate with at least, "a 'soft assumption' of signal stationarity, which means that the spectral and other features of the signal remain constant over time" (M. X. Cohen, 2019, p. 81). Brain dynamics may rarely be stationary however. For example, increasing evidence highlights that beta events occur as transients in time (Bartolo & Merchant, 2015; Feingold et al., 2015; Karvat et al., 2020; Little et al., 2019; Lundqvist et al., 2016; M. A. Sherman et al., 2016; Tinkhauser, Pogosyan, Little, et al., 2017; Tinkhauser, Pogosyan, Tan, et al., 2017; Tinkhauser et al., 2018), with suggestions of a behaviorally-relevant burst or latency code for motor outputs (Little et al., 2019; Shin, Law, Tsutsui, Moore, & Jones, 2017) and working memory storage (Lundqvist et al., 2016; Lundqvist, Herman, Warden, Brincat, & Miller, 2018). Similar observations have been made in the gamma range (Burns et al., 2011; Palmigiano et al., 2017; Xing et al., 2012), arguing in favor of transient pulses of synchronization rather than continuous generators akin to a clock or a heartbeat. From a measurement perspective, misfits between transient events and implicit stationarity introduces ambiguities in empirical estimates. Fundamentally, if temporal averages of power estimates

[9] This claim was more systematically examined by Bullock, McClune, and Enright (2003) who compared Fourier-derived power spectra with an alternative rhythm definition based on averaging multiple phase-aligned segments at a period-defined time lag. Notably, this method assumes periodicity to be stationary for "a reasonable number of cycles […], we propose, on the order of 10 cycles" (Bullock et al., 2003, p. 234). While the work nicely illustrates problems with the reverse inference of rhythms from power spectra, such criteria appear overly strict for anything but stationary rhythms with high signal-to-noise ratios. A similar phase-progression logic was later implemented by Fransen, van Ede, and Maris (2015). Their 'lagged coherence' index operationalizes rhythmicity as periods during which upcoming phase estimates can be temporally predicted a given number of cycles in advance; ***Project 1*** compares this index to power-based rhythm detection criteria using eBOSC.

include periods of absent rhythmicity, resulting amplitude estimates are reduced at the frequency of interest. As such, spectral power averages conflate the presence (i.e., duration) and the magnitude of a rhythm in time (Figure 1). This problem is as old as spectral EEG decomposition itself (Figure 1AB; Walter, 1943b), but is still in need of a principled solution[10].

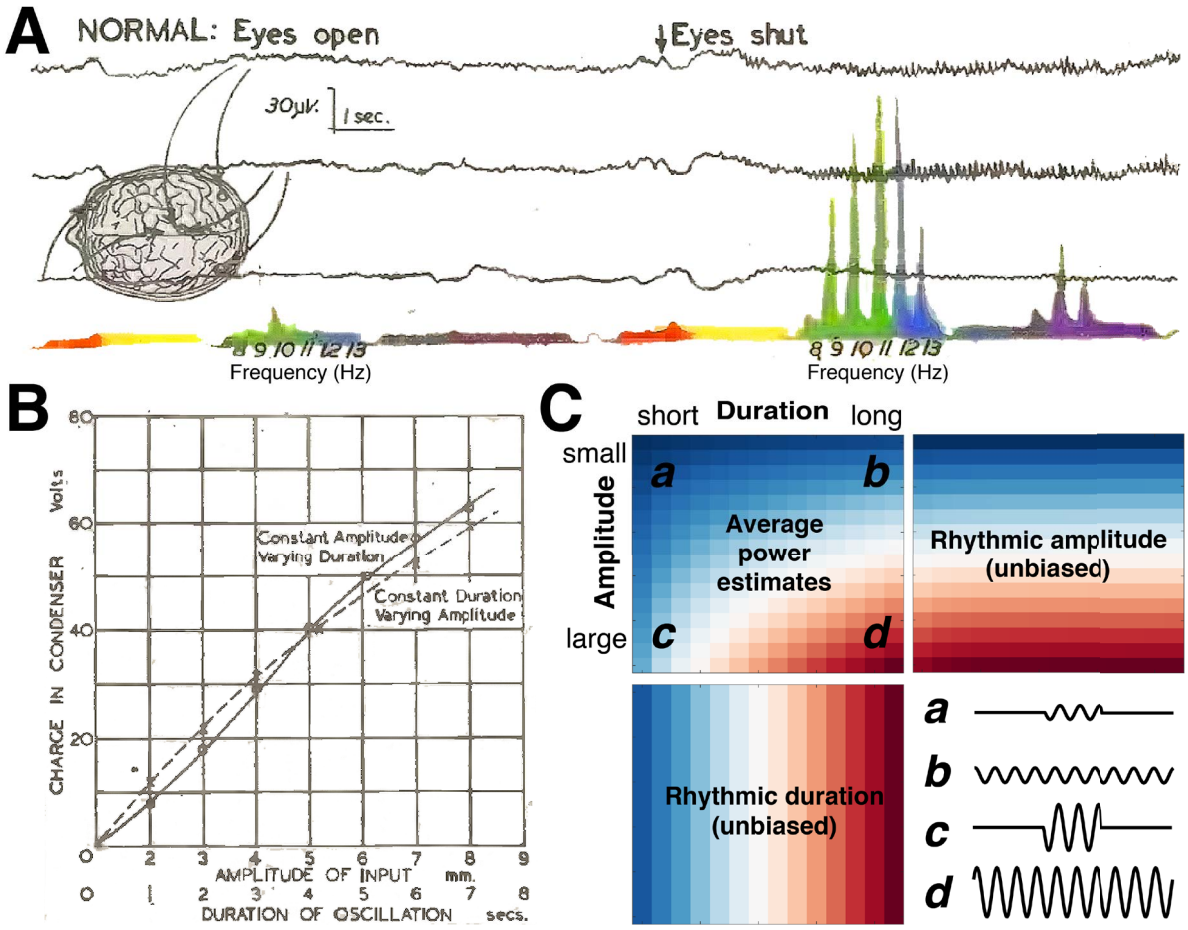

Figure 1. Traditional spectral power estimates ambiguate rhythmic amplitude and duration. (A) Early example of spectral decomposition by Walter (1943b), visualizing the classic Berger (1929) effect of eye closure. (B) In his early frequency decompositions, Walter (1943b) noted the ambiguity of rhythmic amplitude and duration in resulting currents, a crucial problem that remains relevant today. (C) Rhythm

[10] Time-resolved spectral estimation approaches (e.g., using transient Fourier-, Hilbert- or wavelet-based kernels; Bruns, 2004) alleviate the stationarity assumptions of the static Fourier transform by assuming that signals are quasi-stationary for shorter time windows (Bodenstein & Praetorius, 1977). However, many applications average resulting estimates, e.g., to increase the rhythmic signal-to-noise ratio (in part because the absence of a dedicated error term during spectral decomposition forces system noise to be represented in the resulting estimates; Pardey, Roberts, & Tarassenko, 1996). Such 'post-hoc averaging' similarly assumes stationary spectral properties (see also next paragraph).

detection provides a method for disambiguating rhythmic amplitude and duration. Heat maps present amplitude estimates from Fourier-transformed signals of sinusoids with varying amplitudes and durations. Panels A and B are reproduced from Walter (1943b) according to fair use. Copyrights may be held by the respective publisher and/or author and are not subject to the license of this dissertation. Panel C adapted with permission from Kosciessa, Grandy, Garrett, and Werkle-Bergner (2020). For a similar schematic, see Figure 1 in Fransen et al. (2015).

Ambiguity regarding the presence of rhythms in temporal data averages extends to the stationary or transient appearance of narrowband events when spectral estimates are averaged across trials (van Ede, Quinn, Wookich, & Nobre, 2018). Traditional power spectra are computed as the squared amplitude spectrum, thus producing exclusively positive estimates. As positive estimates do not cancel in trial averages, such summary statistics – commonly calculated to increase the rhythmic signal-to-noise ratio – can produce an illusory impression of sustained rhythms (Figure 2A) if transient events occur with a temporal jitter (S. R. Jones, 2016; M. A. Sherman et al., 2016; Xing et al., 2012). Hence, a dedicated detection of rhythmic events at the single-trial level is necessary to validly estimate the duration of rhythmic events, and to avoid potential biases that may arise from signal averaging.

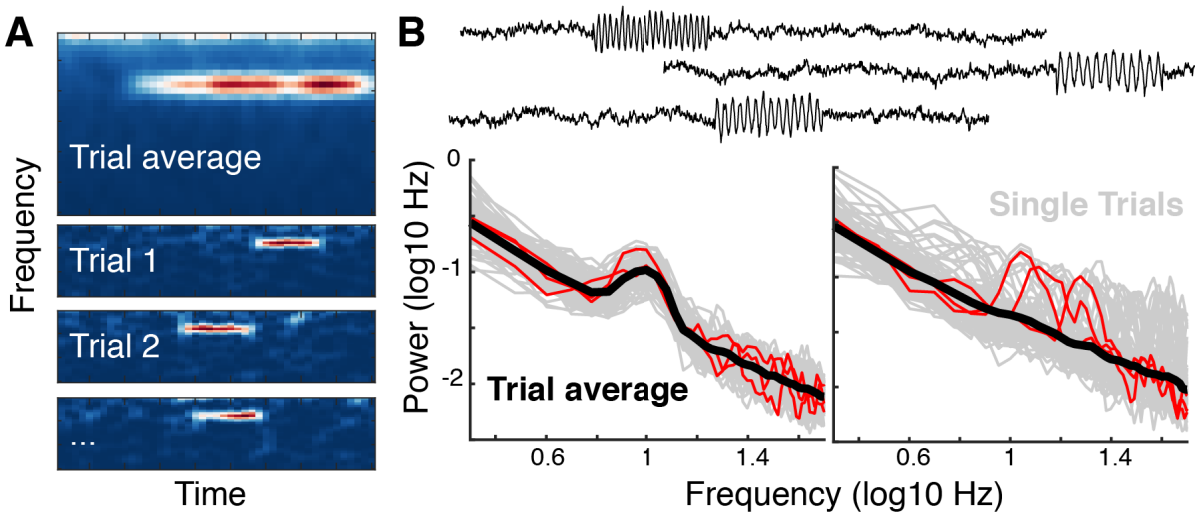

Figure 2. Trial averages of spectral power may not adequately capture single-trial rhythm appearance. (**A**) Trial averaging can give a stationary appearance to transient narrowband events. For a similar schematic see S. R. Jones (2016). (**B**) The appearance of time-varying rhythmic episodes in average spectra depends on single-trial characteristics. Top traces depict three example trials with trial-varying frequency. Bottom left: Rhythmic single-trial events with systematic frequency (here 10 Hz) induce a peak both in single trials (grey, 3 synthetic example trials shown in red) and in the average spectrum (albeit at reduced amplitude). Bottom right: Non-stationary rhythms with variable frequency (e.g., quasi-periodic rhythms) across trials exhibit clear peaks in single trials but not in the average spectrum. All data are based on simulated sine waves superimposed on a 1/f^1 background signal. For a similar schematic, see Palva and Palva (2018).

1.5. Towards a separation of narrow- and broadband neural signal components

Due to the issues noted above (*Section 1.4*), neural rhythms and broadband components (see also *Section 1.7*) are often ambiguously related based on narrowband power analysis of the raw power spectrum (Voytek & Knight, 2015), an analysis that provides the starting point for a large body of the EEG literature. To overcome this limitation, a range of methods have been proposed to separate the power spectrum into overlapping oscillatory and non-oscillatory components. These include 'whitening' the data (Roehri, Lina, Mosher, Bartolomei, & Benar, 2016), removing the across-condition average spectrum (Demanuele, James, & Sonuga-Barke, 2007), elevating a spectral peak from 'flanking' frequency bands (Nikulin, Nolte, & Curio, 2011), subtracting the signal's autocorrelation (see also Makinen, May, & Tlitinen, 2005; Yamamoto & Hughson, 1993), performing a linear regression fit in log(frequency)-log(power) coordinates (Caplan, Madsen, Raghavachari, & Kahana, 2001), or in a more sophisticated form by modelling and removing gaussian peaks on a linear log-log fit (Haller et al., 2018). Notably, while these approaches remove aperiodic influences from the overall spectrum – and thus improve the average specificity to rhythmic content – they do not allow one to determine the presence of rhythms in time. As such, rhythmic contributions, especially when temporally sparse, may go unnoticed (Figure 2B). Alternative approaches such as IRASA (**I**rregularly **R**esampled **A**uto**S**pectral **A**nalysis; H. Wen & Z. Liu, 2016) have been proposed to resample time series and separate rhythmic and aperiodic periods in time. However, IRASA only provides a summary description of rhythmic and aperiodic segments, and does not produce an index of when and for how long rhythmic episodes are present.

Existing approaches to indicate the presence and duration of rhythmic events generally apply an amplitude threshold to narrowband-filtered signals (e.g., Karvat et al., 2020; M. A. Sherman et al., 2016; Shin et al., 2017; Tinkhauser, Pogosyan, Little, et al., 2017). For example, Shin et al. (2017) identified transient beta events as time points during which narrowband beta power surpassed a fixed threshold based on average pre-stimulus power. Similarly, Feingold et al. (2015) defined beta events as exceeding 1.5 or 3 times the median beta power of that channel, while Tinkhauser, Pogosyan, Little, et al. (2017) applied a 75th percentile threshold to beta amplitudes. Likewise, M. Halgren et al. (2019) detected alpha 'bursts' as exceeding 3* the average of adjacent theta and beta power, while Ossadtchi et al. (2017) detect alpha spindles as exceeding 2* the median of alpha power. These approaches therefore use a spectrally local power criterion, with varying criteria and baselines. While existing approaches capture the largest fluctuations in a given frequency band, they lack a principled definition of an aperiodic baseline (conflating

aperiodic and periodic components) and may thus be unreliable; and at worst, systematically biased towards differences in narrowband power[11].

In theory, the joint benefits of rhythmic specificity and temporal sensitivity are combined by estimating the aperiodic background and detecting temporal narrowband deviations from it in continuous signals (i.e., at the level of single trials). This may produce dual improvements on the signal-to-noise of rhythmic estimates by reducing aperiodic background contributions (Doyle, Toussaint, & Evans, 2019), while simultaneously 'amplifying' the rhythmic component in time (Figure 2B). This has been suggested for the BOSC method (Better OSCillation Detection; Caplan, Bottomley, Kang, & Dixon, 2015; Caplan et al., 2001; Whitten, Hughes, Dickson, & Caplan, 2011), which identifies rhythmic segments in single trials by using the average linear broadband slope as a basis for a power threshold that momentary narrowband power has to cross for a specified duration of cycles. However, the method does not account for spectral peaks that may bias the linear fitting procedure, and also does not produce an index for the timing of individual rhythmic episodes. ***Project 1*** therefore sought to extend the BOSC method to identify rhythmic episodes at the single-trial level, and to benchmark its performance in simulated and empirical data.

1.6. Characterizing the scale-free (aperiodic) background signal

While neurophysiological signals contain rhythms at characteristic time scales, they are dominated by aperiodic broadband activity (Bullock et al., 1995) that can be phenomenologically characterized by a power-law form[12] (i.e., systematic amplitude reductions with increasing frequency $\frac{1}{f^x}$) (Buzsáki, 2006; for a review see B. Y. J. He, 2014; K. J. Miller, Sorensen, Ojemann, & den Nijs, 2009; K. J. Miller, Zanos, Fetz, den Nijs, & Ojemann, 2009; Robinson et al., 2001). Albeit

---

[11] Intuitively, the threshold for the rhythmic 'signal' is circularly defined as a proportion of said signal, rather than as a proportion of an independently operationalized noise component. This can introduce systematic variations in the liberality of detection criteria, for example across channels or subjects. Specifically, the threshold for rhythmic events will be more stringent when overall narrowband power is high, than if narrowband power is low, independent of the magnitude of the scale-free 'noise' component.

[12] The term 1/f is often used as a short-hand for the appearance of aperiodic dynamics in the frequency domain, although different mathematical distributions (e.g., Lorentzian, Weibull, log-logistic and Gamma functions) can provide aesthetically similar fits as beautifully illustrated by Benguigui and Marinov (2015). A differentiation between these different shapes is beyond the scope of the work presented here and I use the terms 1/f, power-law and scale-free as simplified approximations for the (loglog-linear) aperiodic power distribution.

traditionally treated as 'noise' relative to the rhythmic component of interest, this scale-free activity may constitute a signal *sui generis*. Broadband contributions to the signal variation (or power) of electrophysiological recordings better approximate aggregate spiking activity in humans (Manning, Jacobs, Fried, & Kahana, 2009; see also broadband relations in Snyder et al., 2015), as well as modeled (Hermes, Nguyen, & Winawer, 2017) and empirical (H. G. Wen & Z. M. Liu, 2016) BOLD responses, than narrowband rhythms. As such, narrowband rhythms and broadband power may provide differential insights regarding the synchrony and level of neural population activity (Manning et al., 2009; K. J. Miller et al., 2012; K. J. Miller et al., 2014; K. J. Miller, Sorensen, et al., 2009; K. J. Miller, Zanos, et al., 2009), respectively. This coheres with earlier notions that "[t]he degree of stochasticity (which is not necessarily noise), as distinct from synchrony, may be a prime variable among brain states, regions, stages, and taxa." (Bullock, 1997, p. 6). However, insights regarding temporal variations of this aperiodic component, and its neuro-cognitive modulation are only starting to emerge.

Scale-free contributions to neural signals are ubiquitous at multiple spatial scales, such as in the spiking activity of neural populations (Beggs & Plenz, 2003), their membrane potentials (Destexhe et al., 2003; El Boustani et al., 2009; Hasenstaub et al., 2005), and in coarser field potentials measured by invasive electrocorticography (ECoG; Dehghani et al., 2012; Freeman & Zhai, 2009; B. J. He, Zempel, Snyder, & Raichle, 2010; Henrie & Shapley, 2005; Manning et al., 2009; K. J. Miller, Sorensen, et al., 2009; Sheehan, Sreekumar, Inati, & Zaghloul, 2018; Voytek et al., 2015), as well as non-invasive EEG (e.g., Colombo et al., 2019; Dehghani, Bedard, Cash, Halgren, & Destexhe, 2010; Haller et al., 2018; W. He et al., 2019; Lendner et al., 2019; Miskovic, MacDonald, Rhodes, & Cote, 2019; Pereda, Gamundi, Rial, & Gonzalez, 1998; Peterson, Rosen, Campbell, Belger, & Voytek, 2018; Pritchard, 1992; Voytek et al., 2015), and MEG (Dehghani et al., 2010). Linear slope coefficients vary between analysis techniques (likely in part due to differences in conductance, spatial sensitivity and intrinsic system noise: Benar, Grova, Jirsa, & Lina, 2019; Dehghani et al., 2010), but typically lie in pink noise ranges between .5 and 1.5 (Dehghani et al., 2010; B. J. He et al., 2010; K. J. Miller, Sorensen, et al., 2009; Pritchard, 1992). Importantly, slope coefficients do not only provide a static snapshot of generic network properties, but dynamically vary across different task states (Billig et al., 2019; El Boustani et al., 2009; B. J. He et al., 2010; Kardan et al., 2020; Podvalny et al., 2015; Sheehan et al., 2018), alongside pharmacological interventions (Colombo et al., 2019; Huang et al., 2019; Muthukumaraswamy & Liley, 2018), and across the lifespan (W. He et al., 2019; McIntosh, Kovacevic, & Itier, 2008; McIntosh et al., 2014;

Voytek et al., 2015; H. Wang, McIntosh, Kovacevic, Karachalios, & Protzner, 2016)[13]. In particular, compared with periods of wakeful rest, invasive recordings indicate a shallowing of spectral slopes in motor (B. J. He et al., 2010), auditory (Billig et al., 2019) and visual (El Boustani et al., 2009; Podvalny et al., 2015) cortex with respect to movement and audio-visual stimulation, respectively, suggesting that cortical activation is accompanied by slope shallowing.

A wide range of mechanisms can generate power-laws in local field potentials and related modalities. Low-level explanations include a frequency-dependent filtering of current via resistance in the extracellular medium (i.e., scalp, skull and brain tissues; Bedard & Destexhe, 2009; Bedard, Gomes, Bal, & Destexhe, 2017; Bedard, Kroger, & Destexhe, 2006; Weissman, 1988), intrinsic low-pass filtering of current flow at the dendrite (Linden, Pettersen, & Einevoll, 2010; K. J. Miller, 2010; K. J. Miller, Sorensen, et al., 2009; Pettersen & Einevoll, 2008), refractory periods in distance-dependent feedback connectivity (Chaudhuri, He, & Wang, 2018; Freeman & Zhai, 2009), or a mixture of damped oscillators with a distribution of relaxation rates (see Section 5.3 for a discussion; Muthukumaraswamy & Liley, 2018). From a functional perspective, computational models (Destexhe & Rudolph, 2004; Gao, Peterson, & Voytek, 2017; see also Lombardi, Herrmann, & de Arcangelis, 2017) relate the slope of LFP power-laws to the ratio of excitatory (E) and inhibitory (I) synaptic contributions to membrane potentials. The level of membrane conductance is largely shaped by mass synaptic inputs (Ferguson & Cardin, 2020; S. L. Zhou & Yu, 2018). During normal function, excitation and inhibition are globally balanced (Adesnik & Scanziani, 2010; Dehghani et al., 2016; Deneve & Machens, 2016; Isaacson & Scanziani, 2011; Okun & Lampl, 2008; Xue, Atallah, & Scanziani, 2014), which computationally affords robust sensitivity to external inputs (Renart et al., 2010; Rubin, Abbott, & Sompolinsky, 2017; vanVreeswijk & Sompolinsky, 1996). During these globally balanced states, variations in the excitatory (largely AMPA-mediated) and inhibitory (largely GABA-mediated) inputs shape membrane currents, and thereby modulate neural firing (Monier, Fournier, & Fregnac, 2008). Notably, the temporal shape of synaptic input currents can be characterized as $\frac{1}{f^x}$ in the frequency domain, with differences in spectral exponent x as a function of the rise and decay times of excitatory and inhibitory currents (Destexhe & Rudolph, 2004; Gao et al., 2017). In particular,

[13] Scale-free dynamics have also been observed for functional magnetic resonance imaging (fMRI; Bullmore et al., 2001; Ciuciu, Varoquaux, Abry, Sadaghiani, & Kleinschmidt, 2012; B. J. He, 2011) signals, with dynamic modulations thereof (Churchill et al., 2016; B. J. He, 2011; Tagliazucchi et al., 2013). However, evidence for reliable associations between scale-free exponents in these two modalities remains an open question for future research.

spectral slopes of excitatory currents are flatter than those of inhibitory currents (Destexhe & Rudolph, 2004). Accordingly, simulations show that spectral slopes flatten when excitation rises quickly in a neural network (Freeman & Zhai, 2009) and when such excitatory contributions dominate mixture currents (Gao et al., 2017). Given such model assumptions, broadband shifts can be used to infer relative differences in cortical excitability in comparative experimental designs (Gao et al., 2017), even if influences from assumedly time-invariant conductance properties contribute to the generic power-law appearance (see Figure 1 in K. J. Miller, 2010 for a schematic).

Complementing a spectral perspective that optimally identifies sinusoidal fluctuations at distinct time scales, measures based on information theory (Dayan & Abbott, 2001; Shannon, 1948) such as sample entropy (Richman & Moorman, 2000) have become popular tools to characterize the overall irregularity or 'complexity' of neural time series, also in a time-resolved fashion (e.g., Grandy, Garrett, Schmiedek, & Werkle-Bergner, 2016; Waschke, Wostmann, & Obleser, 2017)[14]. Notably, one major source of temporal predictability stems from scale-free signal autocorrelations (Pardey et al., 1996; Vakorin & McIntosh, 2012) as discussed above. Phenomenologically, a flattening of spectral slopes mirrors a relative reduction in long-range dependencies and temporal signal predictability. Hence, such shallowing corresponds to an increase in irregularity and is generally associated with a 'noisy' appearance of time series based on visual inspection. However, these two views require some degree of reconciliation, as signal entropy is theoretically sensitive to non-linear signal properties that cannot be captured purely by spectral power estimates (Glass & Kaplan, 1993; McIntosh, 2019; Penny, 2000). In particular, a linear system's dynamics are governed by a set of linear generative processes (e.g., sinusoids), and can thus be sufficiently described by probability measures that include means, variances, and variance spectra. Similarly, a time-varying (non-stationary) system can be linear if a fixed set of linear terms (e.g., spectra) are transiently engaged in time. In contrast, nonlinear terms (e.g., f =

[14] Entropy extends time domain approaches that make limited assumptions regarding a specific time function X(t) (e.g., a sinusoid). A wide variety of time domain approaches are available, many of which share substantial information about linear characteristics with power spectral characteristics (e.g., Wiener–Khinchin theorem; see also Hjorth, 1970). These methods will not be discussed here, but comprehensive reviews are available for the interested reader (Kay & Marple, 1981; Pardey et al., 1996; Penny, 2000).

x^2y) render future states of the system highly sensitive to small changes in present values, which gives rise to low temporal predictability, and signs of 'complex chaos' (Heitmann & Breakspear, 2018)[15]. In line with these theoretical dissociations of linear and non-linear dynamics, the study of moment-to-moment variability has emphasized variance and entropy as potentially complementary indices of healthy, efficient, and flexible neural function (for a review see Garrett et al., 2013a). However, given that the empirical dissociation of rhythmic and aperiodic linear, as well as non-linear components remains practically challenging, a clarification of the con- and divergence between estimates in the time, frequency, and 'complexity domain' (Mariani et al., 2016) is necessary (e.g., Kaffashi, Foglyano, Wilson, & Loparo, 2008; Pincus & Goldberger, 1994; Vakorin & McIntosh, 2012). This is particularly urgent for extensions of entropy that aim to describe the irregularity of fluctuations at multiple time scales (Costa, Goldberger, & Peng, 2002, 2005). Notably, such scale-specific approach contrasts with the notion of a scale-independent measure, but adheres to the putative relevance of *neural* time scales. While previous studies aimed at validating such extensions (Costa et al., 2002; Courtiol et al., 2016), they may have suffered from algorithmic biases (Nikulin & Brismar, 2004; Valencia et al., 2009) that deserve consideration. ***Project 2*** attended these issues to probe the practical utility of (multi-scale) entropy for characterizing rhythmic and aperiodic fluctuations.

1.7. Rhythmic and aperiodic signal components as indicators of cortical excitability states in experimental cognitive neuroscience

The exact relation between the proposed mesoscopic mechanisms of rhythmic and aperiodic signal generation requires empirical validation/falsification attempts using an invasive approach that concurrently measures membrane currents, neural spiking and coarse scalp potentials. However, from a cognitive neuroscience perspective, the functional relevance and modulation of rhythmic and aperiodic contributions may nonetheless be assessed. ***Project 3*** pursued such an avenue, with a specific focus on the flexible modulation and coordination of visual attention.

---

[15] See also the appendix of Stam, Breakspear, van Walsum, and van Dijk (2003) for more fine-grained definitions and mathematical formulations of linear and non-linear properties. Importantly, the apparent time series complexity as operationalized via its temporal predictability should not be equated with the physiological complexity of the generating system (Burggren & Monticino, 2005).

To adaptively process overwhelming amounts of dynamically changing information in the world, the human brain must flexibly extract and prioritize relevant information. Such a fundamental capacity – broadly construed as 'attention' – requires a stable, yet flexible encoding of information depending on contextual goals. Neural gain modulation (Ferguson & Cardin, 2020) – a multiplicative (or divisive) modulation of neural firing output as a function of synaptic inputs (Carandini & Heeger, 2012) – increases signal discrimination in the presence of external noise and acts as a model of attention and working memory (Ferguson & Cardin, 2020; Fries, Reynolds, Rorie, & Desimone, 2001; Reynolds & Heeger, 2009; Saalmann & Kastner, 2009). In particular, feature-based attention increases the response gain (Herrmann, Heeger, & Carrasco, 2012) to selective features in visual cortex (Martinez-Trujillo & Treue, 2004), thus conceptually establishing discrete feature 'attractors' (Niyogi & Wong-Lin, 2013; Thiele & Bellgrove, 2018)[16]. However, theoretical and empirical work also suggests that intermediate levels of 'noise' may benefit the traversal of different attractors in uncertain or rapidly changing environments (Deco, Jirsa, & McIntosh, 2013; Garrett et al., 2013b; Ghosh, Rho, McIntosh, Kotter, & Jirsa, 2008). As such, the brain may implement dual control to process different features in complex tasks: selective gain increases to support the creation of feature-specific attractors, and neural noise to benefit traversal between them.

Rhythmic and aperiodic signal components may index such complementary aspects of neural coordination (Figure 3). Neural rhythms have been linked to phasic gain control in sensory cortex (see Figure 1D in Obleser & Kayser, 2019; Womelsdorf et al., 2014) as putatively shaped by short time delays between excitation and inhibition (Atallah & Scanziani, 2009; Lorincz et al., 2009; Poo & Isaacson, 2009). In particular, alpha rhythms are thought to selectively inhibit task-irrelevant stimulus dimensions (e.g., Wöstmann, Alavash, & Obleser, 2019) via rhythmic modulations of feedforward excitability (Dugue, Marque, & VanRullen, 2011; Haegens et al., 2011; Lorincz et al., 2009), thereby providing temporal 'windows of opportunity' for high-frequency gamma synchronization in sensory cortex (Popov, Kastner, & Jensen, 2017; Spaak et al., 2012; van Kerkoerle et al., 2014) and increased cortical gain (Ni et al., 2016; Peterson & Voytek, 2017).

[16] Attractor models suggest that neuro-cognitive computations (e.g. perception, attention, decision-making, working memory) involve the creation and stochastic traversal of low-dimensional, stable states (i.e., 'attractors') within a high-dimensional energy landscape (Deco, Rolls, & Romo, 2009).

However, increasing the fidelity of single stimulus dimensions is theoretically insufficient when uncertain environments require a high sensitivity to multiple stimulus features. During high uncertainty, ***tonic*** increases to the excitation-inhibition (E-I) ratio (Gao et al., 2017) in sensory cortex provide a principled mechanism for elevated sensitivity to – and a more faithful processing of – high-dimensional stimuli (Castro-Alamancos, 2009; Destexhe et al., 2003; K. D. Harris & Thiele, 2011; Marguet & Harris, 2011). More tonic variations in excitability shape the sensitivity to incoming sensory information (for a review see Castro-Alamancos, 2009; Schwalm & Jubal, 2017) by altering evoked magnitudes, trial-by-trial firing variability, and/or 'noise correlations'[17] (for a review see McGinley, Vinck, et al., 2015). As eloquently stated by Lashley (1951), "behavior is the result of ***interaction*** of this background of excitation with input from any designated stimulus" (Lashley, 1951, p. 112; emphasis added). 'Desynchronized' states of elevated excitability afford a largely veridical relay of external sensory inputs during behavioral activation (Curto, Sakata, Marguet, Itskov, & Harris, 2009; Marguet & Harris, 2011; Milton, Shahidi, & Dragoi, 2020; Pachitariu, Lyamzin, Sahani, & Lesica, 2015), whereas input communication is more sparse and temporally modulated in the presence of large, slow membrane fluctuations (e.g., see Figure 1 in Marguet & Harris, 2011). Notably, strategic shifts between such synchronized and

[17] 'Noise' correlations refer to intrinsic activity fluctuations of experimentally unknown origin (Masquelier, 2013) that are shared across populations with differential specificity across repeated stimulus presentations. Recent work indicates that such fluctuations contain multidimensional codes of current behavioral state (Musall, Kaufman, Juavinett, Gluf, & Churchland, 2019; Stringer et al., 2019), including but not limited to arousal (McGinley, David, & McCormick, 2015; Vinck, Batista-Brito, Knoblich, & Cardin, 2015). Functionally, reduced noise correlations are key features of attention-related improvements in stimulus coding in monkeys (M. R. Cohen & Maunsell, 2009; J. F. Mitchell, Sundberg, & Reynolds, 2009). However, "[w]hether 'residual' correlations of this nature will have a strong impact on coding will depend on the extent to which downstream networks are able to disambiguate modulations in activity due to different sources" (Renart et al., 2010). As such, noise correlations may not impair stimulus coding, as their representation is orthogonal (and dominant in feedback layers: Hansen, Chelaru, & Dragoi, 2012) to the local, distributed stimulus code, for which correlations are low (Ecker et al., 2010; Rumyantsev et al., 2020; Stringer et al., 2019). Rather, shared variability may reflect internally generated signals (Goris, Movshon, & Simoncelli, 2014) that diffusely disseminate contextual information, potentially to integrate incoming sensory information into the ongoing model of the animal's internal state (e.g., Buzsáki, 2019). As eloquently phrased by Pinneo (1966), "stimuli are always superimposed upon the tonic activity of the entire brain, and […] the perception and 'meaning' of a [phasic] stimulus must depend upon the relative amounts of tonic activity in the various parts of the nervous system" (Pinneo, 1966, p. 245). Noise correlations closely relate to mass synaptic flux as assessed via LFPs, likely via slow (< 4 Hz) excitability fluctuations (Cui, Liu, McFarland, Pack, & Butts, 2016).

desynchronized cortical states may support top-down attention (for a review see K. D. Harris & Thiele, 2011). ***Project 3*** introduced a novel paradigm to test this hypothesis. In particular, subjects had to monitor an increasing amount of target features in a joint display depending on the known uncertainty regarding the probed feature. The project tested the hypothesis that increasing the number of relevant features would engage a state of enhanced excitability, whereas a single relevant attribute would afford a selective attention mode, engaging phasic excitability modulations via alpha rhythms.

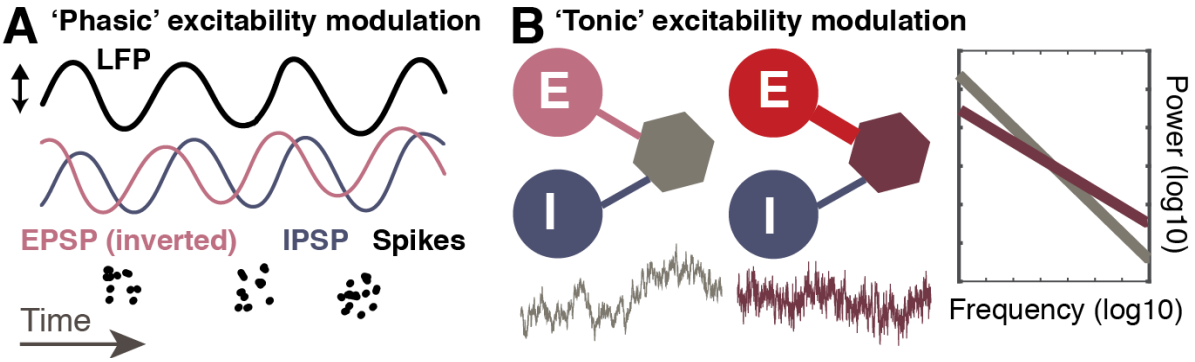

Figure 3. Schematic of presumed functional relevance of rhythmic and aperiodic signal components for phasic and tonic excitability modulation. (**A**) Rhythmic fluctuations in local field potential (LFP) signals as a temporal imbalance between excitatory and inhibitory inputs into a neural population as theorized (Klimesch et al., 2007) and empirically observed (Atallah & Scanziani, 2009; Poo & Isaacson, 2009). Rhythmic amplitude assumedly reflects the extent of phasic firing modulation (Haegens et al., 2011; Klimesch et al., 2007). (**B**) Potential tonic excitability modulation via changes in excitation-inhibition (E-I) ratio (see *Section 1.6*). Relative increases in excitatory contributions to mixture currents (Gao et al., 2017) during globally balanced states (Destexhe et al., 2003) can increase the irregular appearance of global dynamics, reflected in a flattening of spectral slopes in the frequency domain (right). Color saturation indicates the magnitude of schematic synaptic inputs (circles) into a neural population (hexagon).

The excitability state of cortical networks, and gain on feedforward inputs, can be shaped by a variety of mechanisms (for reviews see Ferguson & Cardin, 2020; McGinley, Vinck, et al.,

2015; Zagha & McCormick, 2014), including stimulus drive[18], cortical feedback[19], subcortical activity, and diffuse neuromodulation (reviewed in Castro-Alamancos, 2004; Lee & Dan, 2012; McCormick & Bal, 1997; Saper, Fuller, Pedersen, Lu, & Scammell, 2010). In particular, the thalamus – a subcortical nexus for rhythmogenesis and neuromodulation – may play a major role in the contextual modulation of cortical state (see also *Section 5.7*). The thalamus provides the main interface between cortex and the external world, and thalamo-cortical interactions are critical for sensation, cognition and action (E. G. Jones, 1998, 2001, 2009; S. M. Sherman, 2016). "To destroy the thalamus is to kill" (Ward, 2013, p. 609) as the thalamus is indispensable for conscious activation (for a review see Penfield, 1975; N. D. Schiff, 2008), while electrical or chemical stimulation activates intact cortex (Alkire, McReynolds, Hahn, & Trivedi, 2007; Redinbaugh et al., 2020; Shirvalkar, Seth, Schiff, & Herrera, 2006) and can recover cognitive function even years following brain injury (N. D. Schiff et al., 2007). While its role has traditionally been restricted to an initial 'relay' for sensory information at the beginning of a serial processing hierarchy (Ward, 2013), "the thalamus is not to be regarded merely as a set of nuclei that relay afferent impulses *en route* to the cerebral cortex" (Steriade & Llinas, 1988, p. 250). Rather, emerging models suggest the thalamus' dynamic involvement along the entirety of the cortical

---

[18] Shared synaptic inputs from external sources provide a straightforward mechanism for population-wide membrane fluctuations (J. N. Yu & Ferster, 2010), cortical state (Hirata & Castro-Alamancos, 2010; Lewis et al., 2015; Poulet, Fernandez, Crochet, & Petersen, 2012), and spiking variability (for a review see Doiron, Litwin-Kumar, Rosenbaum, Ocker, & Josic, 2016; Ponce-Alvarez, Thiele, Albright, Stoner, & Deco, 2013). However, while sensory drive potently shifts sensory cortex from synchronous to asynchronous states (Tan, Chen, Scholl, Seidemann, & Priebe, 2014), with dose-dependent effects on the probability of spontaneous cortical activation (Anderson, Lampl, Reichova, Carandini, & Ferster, 2000), state variations also occur in the absence of changes in feedforward sensory drive (e.g., during attention: Kanashiro, Ocker, Cohen, & Doiron, 2017).

[19] One of the primary characteristics of cerebral cortex is its' dense recurrent connectivity (Braitenberg, Schüz, & Braitenberg, 1998). Cortico-cortical feedback thus provides a primary source of cortical excitability fluctuations (Sanchez-Vives & McCormick, 2000; Stringer et al., 2016) that increase in magnitude from feedforward thalamic relays (Kara, Reinagel, & Reid, 2000; Malina, Mohar, Rappaport, & Lampl, 2016; Scholvinck, Saleem, Benucci, Harris, & Carandini, 2015; Shapcott et al., 2016). Moreover, cortical feedback circuits can intrinsically generate (Timofeev, Grenier, Bazhenov, Sejnowski, & Steriade, 2000) and modulate low frequency fluctuations (Zagha, Casale, Sachdev, McGinley, & McCormick, 2013) with high efficacy, as single neuron activity can change population activity spanning multiple millimeters (C. Y. Li, Poo, & Dan, 2009).

hierarchy (for reviews see Dehghani & Wimmer, 2019; Halassa & Sherman, 2019; Hayworth & Marblestone, 2018; Honjoh et al., 2018; Nakajima & Halassa, 2017; Rikhye, Wimmer, & Halassa, 2018; Wolff & Vann, 2019), succinctly summarized by the notion that "[t]he thalamus forms a functional backbone that sustains, coordinates and switches distributed cortical computations" (Schmitt et al., 2017). This notion mirrors early speculation of "[…] some centrally placed integrating center which is capable of a general control, inhibitory and facilitatory, upon the multitude of potentially conscious processes whose patterns of elaboration lie in the cortex." (Jasper, 1948, p. 346). However, especially non-invasive human evidence for such a role remains sparse, at least in part due to the technical challenge of assessing thalamic links to rapid cortical signals measured via EEG (due to its' low sensitivity to subcortical signal sources; Hari & Puce, 2017). In ***Project 3***, we therefore used a multi-modal design, in which participants performed the same visual attention task in both an EEG and a fMRI session, the latter of which permits estimation of thalamic activity. Data were acquired in separate sessions to reduce artifacts encountered during simultaneous EEG-fMRI assessments (e.g., Fellner et al., 2016).

Moreover, since initial reports of a 'reticular activating system' (Moruzzi & Magoun, 1949), multiple neuromodulators, in particular acetylcholine (ACh) and noradrenaline (NA), have been implicated in the control of neuro-behavioral state either by directly innervating cortex or acting via thalamus (reviewed in Castro-Alamancos, 2004; Froemke, 2015; Lee & Dan, 2012; McCormick, 1989; McCormick & Bal, 1997; McCormick, Pape, & Williamson, 1991; Saper et al., 2010). Cholinergic projections from the brainstem or basal forebrain to thalamus and cortex (for a review see Thiele, 2013) provide an activation signal following the occurrence of behaviorally-relevant stimuli (for a review see Ballinger, Ananth, Talmage, & Role, 2016). As such, they increase the firing rate of task-relevant neurons, while 'desynchronizing' spontaneous fluctuations as reported in early reports that electrical stimulation of the reticular forebrain is "marked in the EEG by the replacement of high-voltage slow waves with low-voltage fast activity" (Moruzzi & Magoun, 1949, p. 251). In parallel, forebrain stimulation or ACh application in sensory cortices improves stimulus discrimination and facilitates the processing of specific stimuli (Pinto et al., 2013; Runfeldt, Sadovsky, & MacLean, 2014; Thiele, Herrero, Distler, & Hoffmann, 2012), while diffuse increases in neural firing (i.e., elevated sensitivity) have also been observed (Hirata, Aguilar, & Castro-Alamancos, 2006). Noradrenaline (or norepinephrine) projections from the locus coeruleus throughout the central nervous system similarly activate cortex and cognition (for a review see Sara, 2009). Phasic firing of locus coeruleus neurons can potently desynchronize global cortical state (Carter et al., 2010; Constantinople & Bruno, 2011; McCormick et al., 1991) and increase receptivity to external stimuli (also called arousal; McGinley, Vinck, et al., 2015; Vazey, Moorman, & Aston-Jones, 2018). Notably, the importance of neuromodulation for cortical function, e.g.,

during attention (Aston-Jones & Cohen, 2005), stresses the necessity for a non-invasive assessment of neuromodulatory drive. Pupil dilation provides a sensitive (yet unspecific) proxy of particularly noradrenergic neuromodulation in mice (Breton-Provencher & Sur, 2019; Reimer et al., 2014; Zerbi et al., 2019), monkeys (Aston-Jones & Cohen, 2005; Joshi, Li, Kalwani, & Gold, 2016) and humans (de Gee et al., 2017; Murphy, O'Connell, O'Sullivan, Robertson, & Balsters, 2014). Larger pupil dilation relates to increased single unit spiking excitability in ferret auditory cortex (Schwartz, Buran, & David, 2020), while phasic increases in pupil diameter indicate shifts to an elevated attentional state of cortical desynchronization in ferrets (Stitt, Zhou, Radtke-Schuller, & Frohlich, 2018) and humans (Dahl, Mather, Sander, & Werkle-Bergner, 2020; Murphy, Wilming, Hernandez-Bocanegra, Prat Ortega, & Donner, 2020). We therefore simultaneously assessed pupil dilation as a proxy of neuromodulatory drive in ***Project 3***.

1.8. Aims of the dissertation

Rhythmic and aperiodic components of human brain signals reflect methodologically separable indices of brain function, although their relevance for observed effects is often ambiguous in traditional assessments. Improvements for their separation in time, space and magnitude are thus necessary to derive specific insights into their joint or separate neurocomputational modulation. As such, we first aimed to methodologically separate them before probing their functional relevance in a novel task.

Project 1: The aim of this study was to extend and test a rhythm detection method in EEG data. In particular, we probed the extent to which dedicated detection of rhythmic events may alleviate ambiguities regarding the amplitude and duration of rhythmic events arising from a mixing with aperiodic signal contributions.

Project 2: The aim of this study was to assess multi-scale entropy (MSE) as an index of neural time series (ir)regularity. In particular, MSE characterizes signals from a time domain perspective, which reduces assumptions on the fixed sinusoidal form of temporal patterns. Motivated by previously reported biases (Nikulin & Brismar, 2004), we used simulations and empirical data to probe how entropy at different time scales reflects rhythmic signals with a known time scale, as well as scale-free dynamics.

Project 3: Finally, we investigated the contextual modulation of rhythmic and aperiodic signatures using a novel behavioral probe of visual attention. Specifically, we examined the joint impact of environmental uncertainty on cortical excitability, neuromodulation, and thalamic activity during stimulus encoding, as well as their consequences for subsequent perceptual decisions. The aim of this study was to investigate whether EEG signals over parieto-visual cortex would shift from a

rhythmic mode during selective attention to an aperiodic regime during attentional uncertainty, and whether neuromodulation and subcortical thalamic activity would parallel such shifts. We performed a multi-modal EEG-fMRI experiment in parallel sessions to capture both subcortical and rapid cortical activity with high spatio-temporal precision, while recording pupil dilation as a proxy for neuromodulatory drive.

2. Single-trial characterization of neural rhythms: Potential and challenges

Kosciessa, J. Q., Grandy, T. H., Garrett, D. D., & Werkle-Bergner, M. (2020). Single-trial characterization of neural rhythms: Potential and challenges. *NeuroImage, 206,* 116331. doi:10.1016/j.neuroimage.2019.116331

A copy of this Project and its Supplementary Materials is attached in Appendix 1.

Rhythms are a conspicuous sign of brain function, and hence, the precise characterization of rhythmic neural activity is of high importance for neuroscience on methodological and conceptual grounds. Methodologically, many advanced synchronization measures depend on the presence of rhythmic activity, an assumption rarely checked, although it's violation might invalidate any derived indices of neural synchronization (e.g., Aru et al., 2015; S. R. Jones, 2016). At the same time, the temporal occurrence and duration of rhythmic neural events sheds light on mechanistic models of neural coordination (e.g., by distinguishing between sustained or transient processes). However, methods that permit a temporally precise characterization of rhythmic neural activity are not widely available. In ***Project 1***, we (a) extended a previously proposed single-trial rhythm detection method (BOSC) for electrophysiological data (Caplan et al., 2001; Whitten et al., 2011), (b) systematically benchmarked its sensitivity and specificity in simulations, and (c) applied it in the context of a micro-longitudinal dataset to investigate inter-individual differences and intra-individual stability in rhythmicity during both rest and task states.

In particular, our method (extended Better OSCillation detection, or eBOSC) defines rhythmic episodes (Figure 4A) as events with power exceeding a linear scale-free background power spectrum for a predefined number of cycles (Figure 4B). eBOSC can identify rhythmic episodes with high specificity, but with slightly impaired sensitivity compared to its predecessor BOSC (Figure 4C). More generally, we demonstrate that the signal-to-noise ratio (SNR) constrains the efficacy of rhythm detection, resulting (at least in part) in striking associations between amplitude and duration estimates (Figure 4D). While this poses problems for the unambiguous separation of the duration and amplitude of rhythmic events, eBOSC affords the specific extraction of rhythmic signals by removing the aperiodic background in space and time (Figure 4E, F), thus 'amplifying' rhythmic contributions. By detecting continuous rhythmic episodes, eBOSC further enables a post-hoc separation of rhythmic and aperiodic periods allowing to clearly distinguish transient from sustained events (Figure 4G). In a working memory application, we highlight the applied benefit of single-trial rhythm identification, as the effect size of load-related increases in the alpha and theta band increased when aperiodic activity was excluded, and a frontal theta frequency decrease was only observed after removing aperiodic contributions in time.

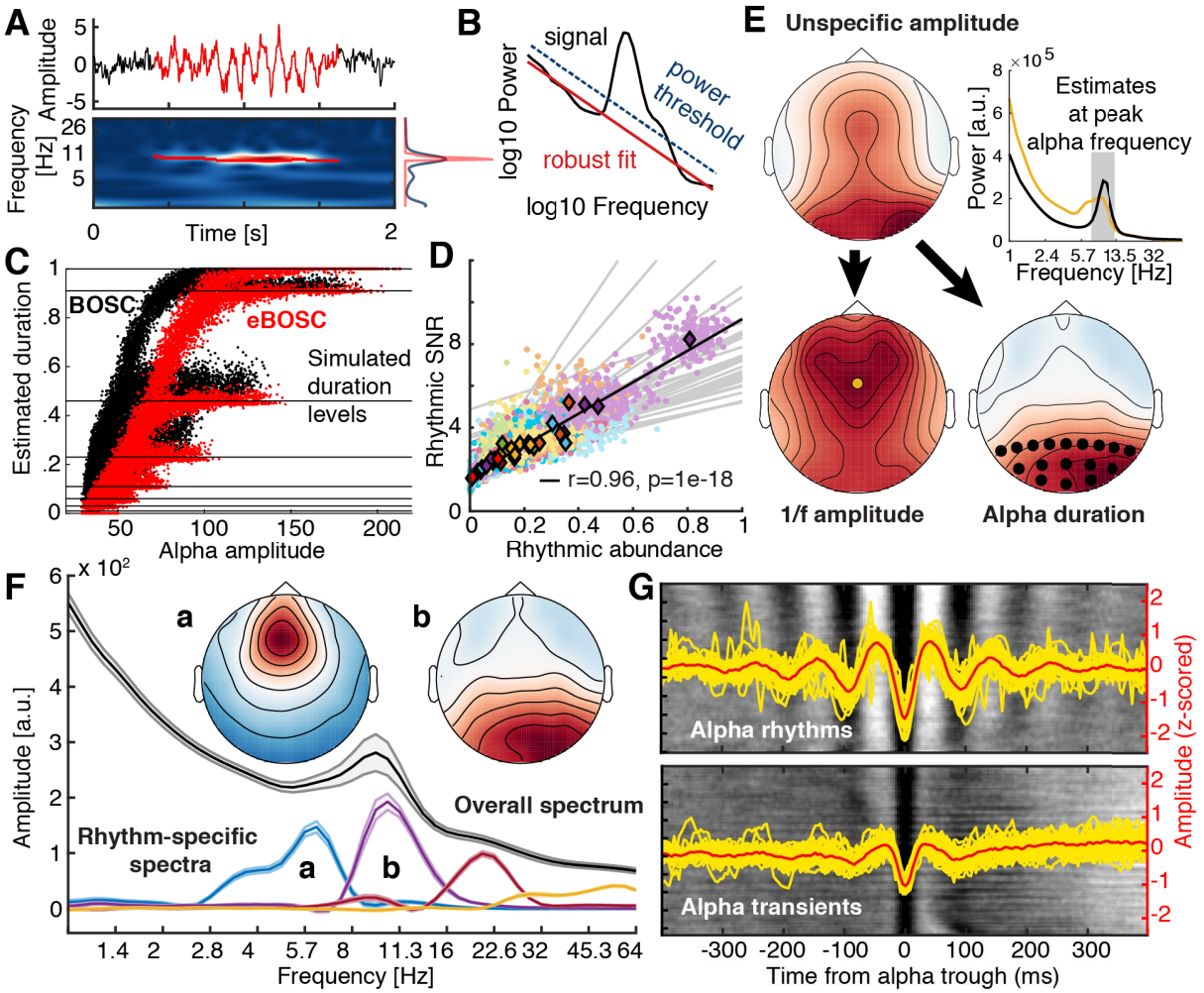

Figure 4: Summary overview of Project 1. (A, B) Principle of extended Better Oscillation Detection (eBOSC). eBOSC increases specificity to temporal rhythmic episodes, thereby enhancing their amplitudes over background noise (red vs. grey avgerage power spectrum on the right). (B) eBOSC defines rhythmic events as spectral peaks exceeding a linear scale-free background power spectrum. Specifically, rhythmic events are temporal periods whose power exceeds a positive statistical threshold from this background distribution for a chosen number of cycles. (**C**) The extension achieves more accurate duration estimates over the BOSC method in simulations, at the slight loss of sensitivity (rightward shift of red dots). (**D**) Empirically, rhythmic amplitude and duration are strongly coupled within- and across-subject, either due to intrinsic coupling between the two parameters, or due to methodological sensitivity issues at low signal-to-noise ratios (SNRs). (**E**) eBOSC successfully dissociates rhythmic signal from aperiodic noise background in space and magnitude, as shown here for alpha rhythms. (**F**) This is achieved across frequencies, highlighting a regionally-specific peak frequency structure (see topography insets for (a) theta and (b) alpha rhythms). (**G**) Due to the creation of continuous rhythmic episodes, eBOSC affords the selective investigation of spectral events with a given duration of interest (e.g., rhythms > 3 cycles or transient spectral events < 3 cycles here). All panels are adapted with permission from Kosciessa, Grandy, et al. (2020).

In sum, ***Project 1*** provides important theoretical and empirical insights into the potential and challenges of rhythm detection at the single-trial level, which is of increasing importance to the field (van Ede et al., 2018). Results from this work highlight that a detection of time-varying rhythmic events may overcome fundamental limitations arising from traditional averaging procedures, rendering estimates more specific to rhythmic contributions, and more sensitive to classic task effects.

3. Standard multiscale entropy reflects neural dynamics at mismatched temporal scales: What's signal irregularity got to do with it?

Kosciessa, J. Q., Kloosterman, N. A., & Garrett, D. D. (2020). Standard multiscale entropy reflects neural dynamics at mismatched temporal scales: What's signal irregularity got to do with it? *PLOS Computational Biology, 16(5),* e1007885. doi:10.1371/journal.pcbi.1007885

A copy of this Project and its Supplementary Materials is attached in Appendix 2.

Due to the dynamic interaction of neural networks across multiple spatio-temporal scales, brain dynamics may be inherently non-stationary and non-linear (Heitmann & Breakspear, 2018; Mckenna, Mcmullen, & Shlesinger, 1994). However, non-linear signal dynamics such as "active transients that persist after the cessation of stimuli, limit cycle oscillations, or spatially inhomogeneous stable steady states" (Wilson & Cowan, 1973) cannot be differentiated by static snapshots such as spectral power estimates alone (i.e., the discussed narrowband rhythms and the background slopes), thus motivating a search for alternative descriptors of time series fluctuations (Stam, 2005). Approaches from information theory may be appropriate and in theory provide sensitivity beyond spectral decomposition approaches. In particular, entropy characterizes the information capacity of a system of interest (Dayan & Abbott, 2001; Shannon, 1948). Sample entropy (Richman & Moorman, 2000) is a computational analogue that characterizes the temporal predictability of time series. In theory, sample entropy indicates the relative amount of irregularity and stochasticity ('noise') in the system; whereas patterns that can be predicted in time such as stationary or periodic patterns yield low entropy, stochastic signals are highly entropic due to their lack of temporal predictability. A trade-off between structure and randomness would introduce intermediate levels of predictability that may suggest a complex, potentially non-linear, interaction between multiple processes (see Figure 1 in Silva, Cabella, Neves, & Murta, 2015 for a schematic).

Multi-scale entropy (MSE; Costa et al., 2002, 2005) extends sample entropy to characterize dynamics at multiple time scales (Figure 5A, B). This extension is motivated by the assumption that time scales provide useful insights into neural dynamics relating, for example, to the spatial scale of their engagement (see *Section 1.1*). Within this framework, multiple studies have observed entropy differences across groups and in relation to cognitive performance at both fine (thought to indicate faster dynamics) and coarse (thought to index slower dynamics) time scales, sometimes in inverted directions of effect (for reviews see Garrett et al., 2013a; McIntosh, 2019). Moreover, a common suggestion in many applications is that such results indicate the presence – and behavioral significance – of *non-linear* brain dynamics (e.g., Park, Kim, Kim, Cichocki, & Kim,

2007), given that power spectral analyses of the same data are insufficient to recover MSE effects. However, known issues regarding MSEs computation (e.g., Nikulin & Brismar, 2004) may fundamentally invalidate intuitive interpretations of scale-specific results.

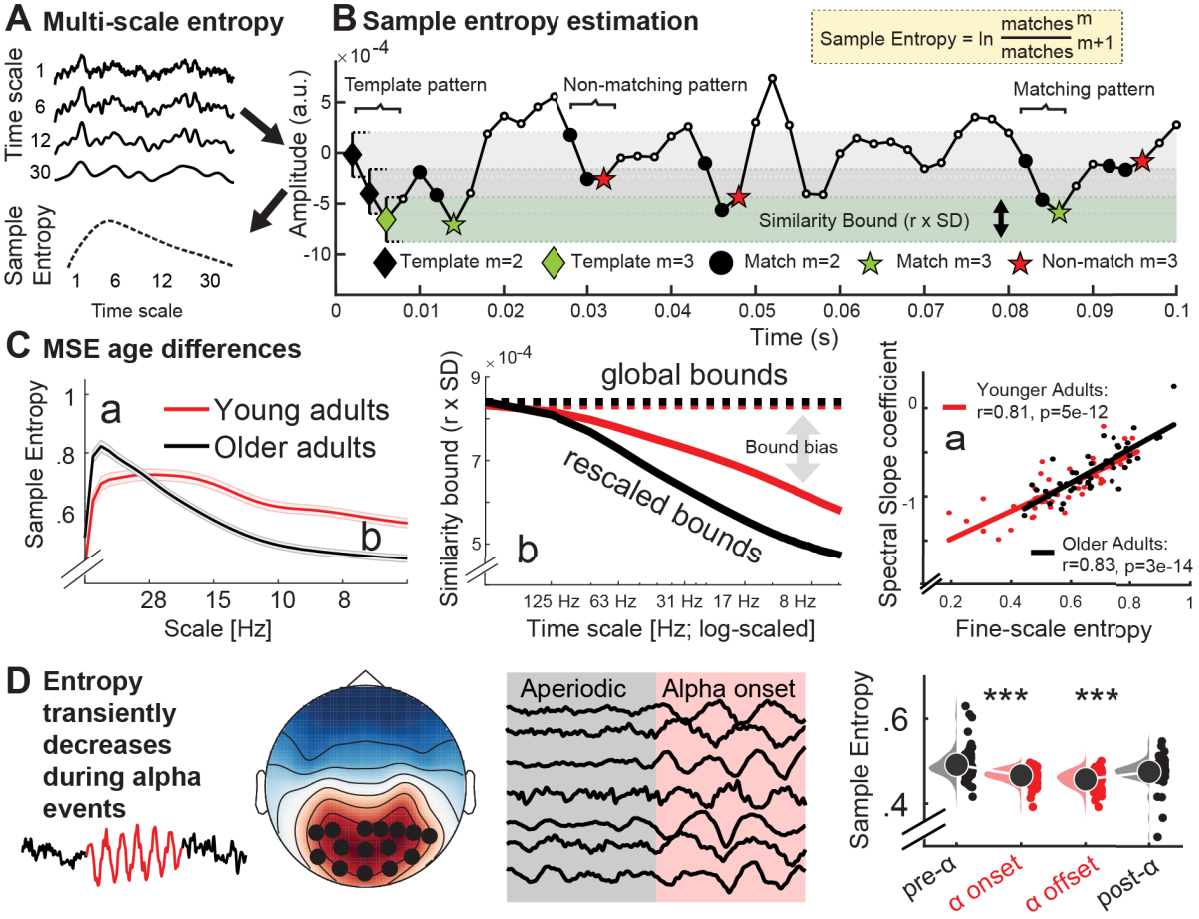

Figure 5. Summary overview of Project 2. (**A, B**) MSE estimation procedure. (**A**) Multi-scale entropy is intended to describe the temporal irregularity of time series data. To estimate entropy for different time scales, the original signal is traditionally 'coarse-grained' using low-pass filters, followed by the calculation of the sample entropy. (**B**) Sample entropy estimation procedure. Sample entropy measures the conditional probability that two amplitude patterns of sequence length m (here, 2) remain similar (or matching) when the next sample ***m*** + 1 is included in the sequence. Hence, sample entropy increases with temporal irregularity, i.e., with the number of m-length patterns that do not remain similar at length m+1 (non-matches). To discretize temporal patterns from continuous amplitudes, similarity bounds (defined as a proportion ***r*** of the signal's standard deviation [SD]) define amplitude ranges around each sample in a given template sequence, within which matching samples are identified in the rest of the time series. These are indicated by horizontal grey and green bars around the first three template samples. This procedure is applied to each template sequence in time, and the pattern counts are summed to estimate the signal's entropy. (**C**) Using simulations (see paper) and empirical data of cross-sectional age differences during eyes open rest, we highlight that (a) coarse-scale effects (thought to reflect slow dynamics) can be attributed to

an estimation bias (present in ~ 90% of previous MSE work) that counterintuitively renders coarse scales sensitive to differences in high-frequency power, and (b) fine-scale differences relate to scale-free dynamics. (**D**) Along with recommending approaches to overcome these challenges (see paper in Appendix 3), we indicate that spectral control for narrowband characteristics can render fine-scale entropy a useful index of temporal fluctuations in broadband irregularity, as illustrated by a transient reduction in broadband signal irregularity during non-stationary alpha events (as uniquely indicated by eBOSC rhythm detection). All panels are adapted with permission from Kosciessa, Kloosterman, and Garrett (2020).

To assess the impact of such issues for time-scale inference, ***Project 2*** assessed the relation of multi-scale entropy to rhythmic patterns with a known time scale and regularity. Specifically, we used simulations and empirical resting-state EEG data to (a) indicate strong and previously underappreciated associations between multiscale entropy and spectral power; (b) highlight how such relations may invalidate common inferences regarding the time scale of neural irregularity (Figure 5C); (c) demonstrate how such issues may be alleviated by controlling the spectral signal content; and (d) recommend best practices for more specific inferences regarding neural signal irregularity. ***Project 2*** thus provides significant methodological insights that pave the way for more principled and valid interpretations of MSE estimates. Beyond highlighting challenges, this work also suggests concrete steps to advance a better understanding of the role of neural signal irregularity for brain function, especially highlighting the utility of phase-shuffled surrogate analyses to verify potential non-linear contributions. Additionally, this work indicates a relation of scale-specific irregularity to the rate of non-stationary rhythmic events as detected by eBOSC, and highlights how sample entropy can be combined with targeted filtering to achieve insights into rapid changes in broadband dynamics (Figure 5D).

4. Thalamocortical excitability adjustments guide human perception under uncertainty

Kosciessa, J. Q., Lindenberger, U., & Garrett, D. D. (2020). Thalamocortical excitability adjustments guide human perception under uncertainty. Manuscript submitted for publication.

A preprint of this Project and its Supplementary Materials is attached in Appendix 3.

Cognitive functions are implemented in distributed cortical networks whose activity is embedded in the context in which these functions are performed (Bastos et al., 2012; Heeger, 2017; Mesulam, 1990; Murray, Jaramillo, & Wang, 2017; Siegel, Buschman, & Miller, 2015). However, how brain activity within and between cortical sites is dynamically adjusted to serve varying contextual demands remains a major question in neuroscience (von der Malsburg, Phillips, & Singer, 2010). We designed a multi-faceted visual attention task (Figure 6A,B; e.g., Schmitt et al., 2017; Wimmer et al., 2015) to probe whether rhythmic and aperiodic signal components index neural adaptations to the environmental context to support upcoming perceptual decisions.

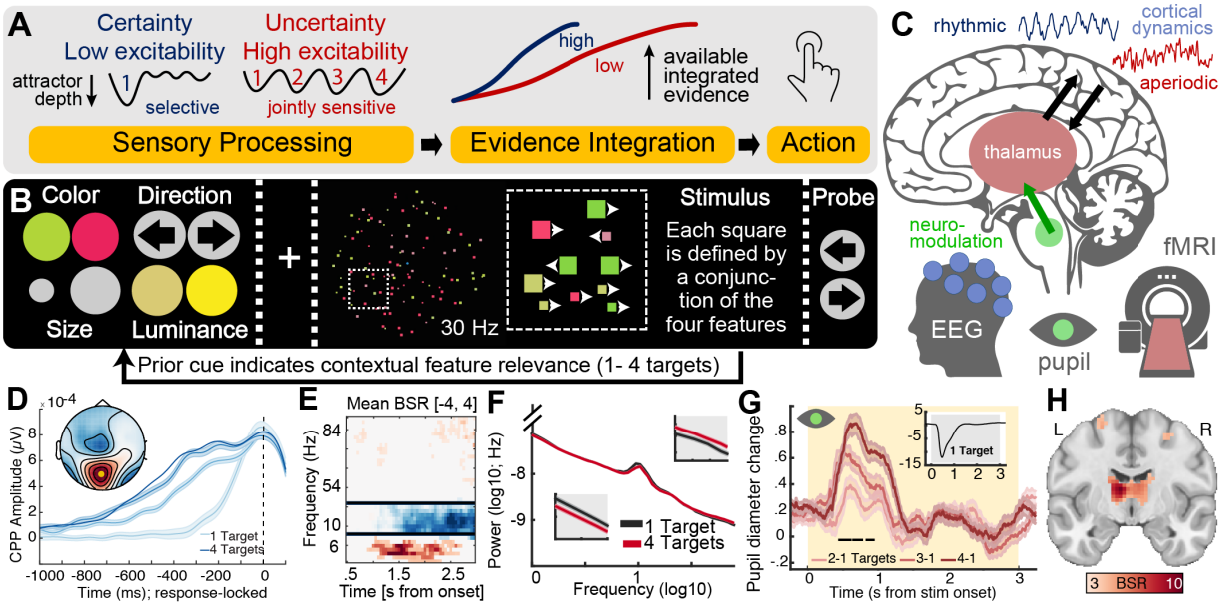

Figure 6. Summary overview of Project 3. (**A**) We probed whether subjects modulate cortical excitability during stimulus processing to guide subsequent evidence accumulation. We hypothesized that when valid attentional cues about a single target feature are available in advance, a low excitability regime may optimize subsequent choices via the targeted selection of relevant – and inhibition of irrelevant – information. This can be conceptualized as the creation of a single feature attractor. In contrast, under high probe uncertainty, higher excitability may afford the concurrent sampling of multiple relevant features, but at the cost of a relative reduction of subsequently available evidence for any individual feature. (**B**) Subjects performed a **M**ulti-**A**ttribute **A**ttention **T**ask ('MAAT') during which they had to sample up to four visual

features in a joint display for immediate subsequent recall. Prior to stimulus presentation, subjects were validly cued to a set of potential target probes. The number and identity of cues were varied to modulate the level of expected probe uncertainty. (**C**) We hypothesized that increasing probe uncertainty would induce a joint increase in neuromodulation and thalamic activity, associated with shifts from a phasic gain control mode (implemented via neural alpha rhythms) toward tonic increases in cortical excitability (as indicated by aperiodic activity). Subjects performed the same task in both an EEG and an fMRI session, allowing us to assess joint inter-individual differences in rapid cortical signals (EEG) and subcortical sources (fMRI). (**D**) Probe uncertainty during sensation decreased the rate of subsequent evidence integration as indicated by the Centroparietal Positive Potential (CPP) and drift-diffusion modelling. (**E, F**) Cortical excitability increases under uncertainty guide subsequent evidence integration, as indicated by a disengagement of alpha rhythms (E) and simultaneous increases in aperiodic activity (F). (**G**) Increases in phasic pupil diameter relate to transient excitability adjustments. (**H**) Thalamic BOLD modulation tracked changes in EEG-based excitability and pupil-based arousal during sensation, as well as drift rate decreases during subsequent decisions. All panels are adapted with permission from Kosciessa et al. (in prep.).

Project 3 investigated the impact of uncertainty on cortical excitability, neuromodulation, and thalamic activity during stimulus encoding, as well as their consequences for subsequent perceptual decisions in humans (Figure 6C). We performed a multi-modal EEG-fMRI experiment in parallel sessions to capture subcortical activity (fMRI) and rapid cortical (EEG) activity with high spatio-temporal precision, while recording pupil dilation as a proxy for neuromodulatory drive. Subjects performed a visual attention task which (a) parametrically modulated the number of relevant stimulus dimensions in a dynamic square display, yet (b) held bottom-up stimulus characteristics constant. By applying drift diffusion modeling to participants' choice behavior while assessing electrophysiological signatures of decision processes, we show that uncertainty during sensation reduces the rate of subsequent evidence integration (Figure 6D). To establish a neural mechanism for such sensory adjustments, we demonstrate that this reduction in available sensory evidence is associated with increased cortical excitability (as indexed by joint low-frequency (~alpha) desynchronization and high-frequency (~gamma) synchronization; Figure 6E) and an increase in E-I ratio (as indicated by increased sample entropy and flatter scale-free 1/f slopes; Figure 6F) during sensation. These excitability adjustments occurred in parallel with increases in pupil-based arousal (Figure 6G). Finally, individual modulation of visual excitability, drift rates and arousal was associated with increases in thalamic BOLD signal magnitudes (Figure 6H), providing evidence for an important subcortical role in the contextual modulation of cortical state. Together, these findings suggest that (i) thalamus and neuromodulation jointly shape cortical excitability states in humans, and that (ii) shifts from alpha-rhythmic towards aperiodic neural dynamics contextually adjust the processing fidelity of external stimuli in service of upcoming decisions.

5. Discussion: Implications, limitations and future directions

5.1. Methodological insights for valid inference regarding neural dynamics

Projects 1 and 2 challenge traditional assumptions in the measurement of rhythmic and irregular dynamics and provide suggestions of how such challenges may be overcome. In particular, ***Project 1*** highlights that traditional averages derived from the Fourier transform do not unambiguously indicate the presence or strength of a rhythm, although this is tentatively assumed in many applications[20]. ***Project 2*** highlights that analyses regarding non-linear brain dynamics have to control for shared sensitivity to linear features, including narrowband rhythms and scale-free autocorrelations. On a more granular level, this project highlights how variance biases in the standard MSE algorithm ambiguate effects observed at coarse 'time scales.' This bias is crucial to highlight for the MSE community given that the very reason for using MSE in the first place (instead of only single scale sample entropy) is that 'slower' entropy processes are presumed to be estimable *and* viable. From a broader perspective, ***Projects 1 and 2*** provide evidence that a simultaneous appreciation of both spectral and temporal signal descriptions is mutually beneficial.

Underappreciation of these various methodological issues in a large number of neuroscientific applications threatens the validity of previous results (as simulations are highly reliable, and biases such as those highlighted in ***Project 2*** can be conceptually replicated with minimal empirical data). Notably, the sensitivity of specific features to behavior or cognitive status – key targets of data-driven prediction approaches (e.g., Brunton & Beyeler, 2019; Choudhury, Fishman, McGowan, & Juengst, 2014; Krakauer, Ghazanfar, Gomez-Marin, MacIver, & Poeppel, 2017) – is not a panacea to these problems. For example, prior work indicated the relevance of coarse-scale entropy estimates for disease state prediction (e.g., Takahashi et al., 2010; A. C. Yang

[20] This issue is also prevalent in fMRI research, where spectral power estimates are used to infer the presence of 'oscillations' (Baria, Baliki, Parrish, & Apkarian, 2011; Zuo et al., 2010), also in the absence of spectral peaks (Baria et al., 2011; B. J. He et al., 2010; but see McAvoy et al., 2008). Notably, the estimation of the spectrum is more difficult in fMRI due to the sparse temporal sampling, and the sluggishness of the hemodynamic response. However, terms such as 'low frequency fluctuations' (Zou et al., 2008) should be preferred if there is no sufficient evidence for a spectral peak.

et al., 2013); ***Project 2*** shows that such results are ambiguous, and may reflect processes at completely different temporal scales than those reported. Similarly, variations in the 'sustained' power of beta rhythms has long been a predictor of motor performance (Engel & Fries, 2010), but single-trial analyses argue that this association arises from variations in the timing and rate of transient beta events (Shin et al., 2017)[21]. By highlighting such specific methodological issues and indicating potential solutions, insights from ***Projects 1 and 2*** may increase sensitivity to effects of interests while jointly avoiding biases, thus providing more veridical/valid estimates of neural dynamic regimes of interest.

5.2. Dissociating rhythmic and aperiodic signals in space and time

"If we believe that oscillations underlie the function of the brain (Buzsaki, 2006), then the fine details of the behaviors of these oscillations–when they arise, where they arise, for how long and in what relation to other oscillations–must contain interesting information about how the brain works and what happens to it in disease." (Hsu, Hsu, Grabenstatter, Worrell, & Sutula, 2010, p. 189). ***Project 1*** highlights how rhythm detection elucidates such details in practice by separating non-stationary rhythms from the scale-free background in space, time, and magnitude. First, by indicating *when* rhythms occur in time, eBOSC removes aperiodic amplitude biases (see Figure 4A), thereby increasing amplitude estimates (especially for sparse rhythms) even when no overt peak is observed at the average level (see Figure 4F)[22]. Second, by removing spatial correlations of the aperiodic background signal, rhythm detection increases spatial specificity in determining *where* rhythms are observed (Figure 4E; while intrinsic uncertainty remains regarding the exact spatial sources). Third, by indicating for *how long* rhythms occur, eBOSC

[21] Notably, timing variability can be crucial for assessing neurocomputational arguments, such as communication through coherence (CTC; Fries, 2005; Fries, 2015). Previous arguments have questioned CTC by arguing that the power of gamma rhythms is on average too low and their engagement temporally too sporadic (Burns et al., 2011; Xing et al., 2012) to achieve reliable communication (T. E. Akam & Kullmann, 2012). However, recent modeling work that explicitly reproduces transient gamma 'sync pulses' highlights that *when* gamma events occur, they possess sufficient power to impact information transfer between regions (Palmigiano et al., 2017).

[22] By systematically recovering spectral content on the single-trial level, our results agree with previous conclusions that "[t]he wide-band cortical EEG […] is not likely to be primarily based on a mixture of real rhythms of many frequencies" (Bullock et al., 1995, p. 11572). If narrow-band signals were strongly modulated by transient rhythms at quasi-random frequencies (e.g., Figure 2B), one would expect to see a general baseline of detected rhythmicity in rhythm-conditional spectra, which we do not observe in empirical data with segregated peak structures (see Figure 4F).

separates transient and sustained events in a principled manner (Figure 4G). Fourth, rhythm-conditional spectra afford insights into the temporal simultaneity of rhythms (Figure 4F), while *relations between rhythms* can be specifically probed using cross-frequency analyses at times when the carrier rhythm is present (see ***Project 3***). Fifth, as rhythm indices such as the 'rhythmic signal-to-noise ratio' are defined on an absolute scale relative to individual backgrounds, they emphasize an individual-centric approach in cognitive neuroscience. In sum, the addition of eBOSC to the field's electrophysiological toolkit can thus advance our understanding of (potentially time-limited) rhythmic contributions to brain function.

While eBOSC relaxes the assumption of rhythm stationarity, it introduces assumptions in its own right. As ***Project 1*** highlights, the practical accuracy of rhythm detection depends on the presence and correct specification of a linear background spectrum. Given that eBOSC fits linear slopes after manually removing overt frequency peaks at the group level, potential biases may remain due to inter-individual or spatial variations in narrowband content, as well as 'knee' frequencies at which the spectrum deviates from linearity (Gao, 2016). While we did not observe such deviations at the group level, the shape of the aperiodic spectrum may deviate substantially from a linear power-law shape at the individual level – especially for short signals. Prior tests of linear power-law scaling using model comparison (Ton & Daffertshofer, 2016) and alternative estimation approaches of spectral slopes may reduce such limitations. In particular, **I**rregularly **R**esampled **A**uto**S**pectral **A**nalysis (IRASA; H. Wen & Z. Liu, 2016) repeatedly subsamples a time-series to quantify and characterize the temporal contribution of rhythmic and scale-free components to average estimates. Another tool, FOOOF ('**F**itting **O**scillations & **O**ne-**O**ver **F**') fits narrowband rhythms as Gaussian peaks on top of an aperiodic background and in principle allows for the unbiased estimation of spectral slopes in temporal averages (Haller et al., 2018). Such automatic approaches likely prove useful in future implementations of time-varying rhythm detection to reduce potential misfits of aperiodic slopes (see ***Project 1***). A more conceptual issue concerns the general validity of a stationary aperiodic 'background', especially given evidence that spectral slopes rapidly change in systematic ways (see ***Projects 2 and 3***). The current projects largely circumvent this problem by fitting linear slopes to short periods with similar cognitive demands. However, this proves difficult in the absence of a task structure (e.g., for spontaneous activity at rest). Temporal resampling, as implemented in IRASA, may provide a solution to incorporate dynamic changes of aperiodic signal components into continuous rhythm detection. Alternatively, ***Project 2*** highlights that modified MSE (mMSE) allows a time-resolved estimation of signal irregularity with high temporal resolution by estimating irregularity across trials (Grandy et al., 2016). While more work is necessary on determining optimal dynamic thresholds,

their implementation may further refine the dissociation of rhythmic and aperiodic signal components in time.

Project 1 also indicated technical limitations arising from the rhythmic signal-to-noise ratio (SNR) of EEG recordings, providing yet another challenge to distinguishing rhythms from aperiodic signals. In short, when rhythmic contributions are faint, it will be unclear whether a rhythm was present and not detected ('miss') or truly absent ('correct rejection'). Further work is necessary to establish the utility of other modalities with higher rhythmic SNR and/or methods that increase the precision of the spectral decomposition (and thus the sensitivity to target features) prior to rhythm detection (e.g., de Cheveigne & Arzounian, 2015; de Cheveigne & Parra, 2014; Hsu et al., 2010; Nikulin et al., 2011). In particular, such approaches can maximize narrowband SNRs when prior knowledge exists regarding a specific frequency range of interest. Moreover, as they reduce the spatial dimensionality of signals prior to rhythm detection, they can improve analysis efficiency. Independent component analysis, as a related method has been validated with the original BOSC algorithm (Whitten et al., 2011), which highlights the general feasibility for combining signal separation approaches and rhythm detection into a common workflow. Given that both eBOSC and mMSE permit high-throughput estimation efficiency, their application presents a promising avenue to investigate the role of rhythmic and aperiodic activity for neuro-cognitive function in large datasets.

5.3. Periodic events as a subset of time-varying brain dynamics

Projects 1-3 argue that the characterization of non-stationary signal components permits not only the identification of *what* activity patterns occur, but also *when* and *how frequently* they appear in time. This supports a general shift away from static descriptions of signal averages towards a focus on the temporal aspects of macroscopic dynamics in neuroscience (Lurie et al., 2020). An intriguing alternative to the identification of rhythmic events (***Project 1***) is the use of data-driven latent state approaches that are increasingly used to investigate transient functional networks in fMRI and EEG/MEG (e.g., Karahanoglu & Van De Ville, 2015; Lurie et al., 2020; Taghia et al., 2018; Vidaurre, Abeysuriya, et al., 2018). For example, Hidden Markov Models allow estimation of a limited number of temporally recurrent latent states with e.g., specific spectral profiles (Vidaurre, Hunt, et al., 2018), which can subsequently be analyzed with regard to their transition probabilities, dwell times/durations and switching rates. These methods also successfully detect transient beta events (Heidema, Quinn, Woolrich, van Ede, & Nobre, 2020; Quinn et al., 2019; Seedat et al., 2020), indicating their sensitivity to spectral features. Crucially, many of these models assume that only a single state is active at each time point, whereas rhythmic views of brain function often emphasize a simultaneous multiplexing of information at

different temporal scales. While both approaches theoretically afford novel insights into time-varying neural dynamics, which approach proves more useful and/or accurate remains an interesting and open question. Alternative methods are also available to decompose neural time series into specific graphoelements, of which periodic patterns represent only a subset. Most prominently, matching pursuit (Chandran, Mishra, Shirhatti, & Ray, 2016; Mallat & Zhang, 1993) and dynamic mode decomposition (Brunton, Johnson, Ojemann, & Kutz, 2016) deconstruct signals into underlying 'atoms' or modes, either from a predefined dictionary or based on statistical covariation. An alternative nonparametric approach to pattern identification that is popular in genomics involves the testing of temporally binned time series against a specific morphology (e.g., including 'sawtooth' features) or a fixed library of waveforms (M. E. Hughes, Hogenesch, & Kornacker, 2010; Michael et al., 2008; Thaben & Westermark, 2014). Similar to eBOSC (***Project 1***), such approaches may identify the contribution of specific graphoelements to neural time series.

Interestingly, despite the prevalent assumption of sinusoidal features in neuroscience, temporal dynamics may not be perfectly rhythmic, but instead systematically vary in form (Cole & Voytek, 2017, 2019; Lozano-Soldevilla, 2018a; Schaworonkow & Nikulin, 2019). However, due to the mathematics of the Fourier algorithm, even non-sinusoidal shapes are separated into a combination of sinusoids, at a loss of morphological information. This overemphasis of sinusoidal features in spectral analysis (even when the signal does not warrant it) was noted early on (see also Rohracher, 1937): "Even though it may be possible to analyze the complex forms of brain waves into a number of different sine-wave frequencies, this may lead only to what might be termed a 'Fourier fallacy,' if one assumes ad hoc that all of the necessary frequencies actually occur as periodic phenomena in cell groups within the brain." (Jasper, 1948, p. 345; see also Rohracher, 1937)[23]. Dedicated rhythm detection (***Project 1***) can assist in detecting periods that *per se* qualify as sinusoidal, but given the wavelet transform involved in their detection, does not provide strict

[23] Unfortunately, no English translation of Rohracher's concise discussion is yet available: "[W]enn jedoch die Tätigkeit eines Organs in einer charakteristischen Kurvenform des Spannungsverlaufes zum Ausdruck kommt, dann verliert die harmonische Analyse ihren Sinn; denn sie löst die Kurve in Sinusschwingungen auf, also in Komponenten, von denen man nicht ohne weiteres annehmen darf, dass sie in Wirklichkeit bei der Entstehung der untersuchten Potentialschwankung beteiligt sind." (Rohracher, 1937, p. 544). In coarse translation: "However, if the function of an organ is expressed in a characteristic shape of the voltage curve, then harmonic analysis loses its sense; it reduces the curve to sine waves, that is to components of which one may not without further ado assume that they are in reality involved in the generation of the examined potential fluctuation."

evidence for it. As discussed in ***Project 1***, a dedicated follow-up analysis that characterizes the time series morphology of rhythmic episodes (e.g., Cole & Voytek, 2019) may prove fruitful to further pursue such questions (e.g., Neymotin, Barczak, et al., 2020; Spyropoulos et al., 2020). More generally, determining the sinusoidality of generative processes remains challenging given that a sinusoidal appearance at the scalp can arise from non-sinusoidal dynamics with different degrees of spatio-temporal mixing (Schaworonkow & Nikulin, 2019). This morphological uncertainty represents an ill-posed inverse problem, as sinusoidal events do not unequivocally suggest the presence of a sinusoidal generator, while a superposition of periodic generators can produce complex patterns (Lorincz et al., 2009). On a methodological note, entropy (***Project 2***) is invariant to the shape of repeating patterns, but captures the degree to which any pattern repeats. Entropy applications may therefore prove advantageous when a strong assumption of sinusoidality is not warranted.

While analyses that are agnostic to time series shape remain productive, efforts toward better characterizing (quasi-)periodic or sinusoidal patters and deviations thereof (e.g., Cole & Voytek, 2019) are poised to improve our understanding of the latent regimes that shape observed brain signals (e.g., Figure 1 in Breakspear, 2017). For example, a stable fixed-point attractor is expected to give rise to periodic signals, even in the presence of added noise that adds temporal amplitude and frequency fluctuations. In contrast, more complex patterns arise in the presence of a chaotic attractor (Breakspear, 2017)[24]. While various circuit properties (e.g., spatio-temporal excitation-inhibition profiles) can instantiate periodic and chaotic regimes, large-scale models of neural circuits (e.g., Mejias et al., 2016; Neymotin, Daniels, et al., 2020; Robinson et al., 2001; Schirner, McIntosh, Jirsa, Deco, & Ritter, 2018) can further constrain the space of biophysically-realistic implementations. Prior work (e.g., M. A. Sherman et al., 2016) has elegantly used such

[24] Challenges regarding nonlinear contributions to measures such as entropy (highlighted in ***Project 2***) are particularly relevant for inference of chaotic systems as suggested by neural mass models, given that "the presence of such nonlinear waveforms in macroscopic signals such as EEG would provide compelling support for these models and, more deeply, for the implicit assumption on which they rest: namely, that through synchrony, collective neuronal dynamics retain the nonlinearities present at the microscopic scale." (Breakspear, 2017, p. 346). Similar to previous work (for reviews see Lancaster, Iatsenko, Pidde, Ticcinelli, & Stefanovska, 2018; Stam, 2005), ***Project 2*** argues that such inference regarding non-linear contributions requires stringent null models, as provided by surrogate data.

large-scale approaches to explain the emergence of transient beta events from an interaction of proximal and distal cortical input, while confirming model predictions using electrophysiological recordings. The methods highlighted here provide useful tools to further advance such efforts.

Together, ***Projects 1-3*** encourage a wholistic perspective on features in both the time and frequency domains, in line with early conclusions that "[f]requency analysis, when related at all times to the original recording, is proving to be a useful adjunct to the electroencephalographer's armamentarium, if and when the various spectra thus obtained can receive adequate and valid interpretation." (Jasper, 1948, p. 345). In the end, questions such as "When is fluctuating activity a rhythm? and How do we tell a real rhythm from an artifact of our analysis?"[25] (Bullock, 1997, p. 5) remain challenging and relevant.

5.4. Links between aperiodic signal components, neural 'variability', and 'noise'

Brain activity is naturally variable at multiple spatio-temporal scales (Faisal, Selen, & Wolpert, 2008). This variability includes both periodic and irregular fluctuations at the level of population signals, and may index latent dynamic regimes that are considered important for healthy, efficient and flexible neural function (Breakspear, 2017). However, the mapping between neural variability moment-to-moment, trial-by-trial, and the multiple proxy measures thereof often remains unclear in application (Dinstein, Heeger, & Behrmann, 2015; Doiron et al., 2016; Garrett et al., 2013a; but see B. J. He, 2011; Kumral et al., 2020). As a result, the notion of neuro-behavioral variability (and associated functional interpretations) may encompass a wide variety of metrics that potentially index different aspects of neural dynamics (cf. Garrett et al., 2015; Shafiei et al., 2019)[26]. ***Project 2*** provides a unifying perspective on time series irregularity (or

---

[25] Any generative caveats regarding the latent neural nature (cf. inhalation, muscle sources) or intrinsic origin (cf. entrainment; Obleser & Kayser, 2019) of rhythms at the level of observed time series naturally also apply to rhythm detection.

[26] Given that metrics vary in their descriptive order (mean, total variation, variance structure, variance and phase interactions), lower-order indices should be controlled for when specific claims are to be made about the unique relevance of a higher-order index, e.g., using surrogate analyses (as highlighted in ***Project 2***). These two studies illustrate how interpretations may diverge depending on whether overall signal variation or entropy are considered, even if effects largely converge given the strong anticorrelation between these indices.

'complexity') and aperiodic slopes (and rhythms) in the frequency domain. It thereby indicates previously underappreciated links between measurements of signal complexity and variance structure (Garrett et al., 2013a) that may bridge disparate findings. In particular, a strong link of temporal irregularity to aperiodic slopes is appealing, given that such slopes may provide a *bona fide* index of neural excitability (see *Section 1.6*) and have conceptually been associated with the stochasticity (i.e., 'noise'[27] level) of neural firing via links to mass synaptic and membrane potential flux (Voytek & Knight, 2015).

Functionally, two alternative expectations exist regarding the role of noise for information processing. While overwhelming intrinsic noise constrains the reliability of computations (for a review see Faisal et al., 2008), intermediate levels of random input can benefit neural processing via stochastic facilitation (Garrett, McIntosh, & Grady, 2011; Garrett et al., 2013b; McDonnell & Ward, 2011; Stein, Gossen, & Jones, 2005). As such, elevated stochasticity may contribute to a state of 'stable flexibility' that characterizes a balance between reliable stimulus responses and large dynamic range (Dinstein et al., 2015; Garrett et al., 2013a). Such a suggestion is conceptually similar to the notion of 'critical' dynamics (Beggs, 2008; Palva & Palva, 2018)[28] that operate at the boundary of order and disorder (Stanley, 1971) (e.g., at the transition between periodic and chaotic regimes; Breakspear, 2017). Importantly, networks that are critically balanced between excitation and inhibition theoretically (Kinouchi & Copelli, 2006; Peterson & Voytek, 2015; Shew

---

[27] The notion of noise can only be defined with reference to a target signal of interest; e.g., "Random or unpredictable fluctuations and disturbances that are not part of a signal." (Faisal et al., 2008, p. 292) Given that there is no canonical model of a brain 'signal' (e.g., Buzsáki, 2019), the definition of 'noise' for brain function is non-trivial outside of computational models that implement a clear operational definition of both components (e.g., with regards to the neural 'representation' of experimentally measurable external variables). I use the term 'noise' here to refer to the level of (largely scale-free) stochasticity of synaptic inputs and neural firing, albeit those components may constitute signals (a) in the brain itself, and as such (b) for experimenters recording those signals.

[28] Power-law dynamics have been observed across a range of systems, although phenomenological similarity does not imply mechanistic equality (Stumpf & Porter, 2012). Scale-free dynamics have been proposed as a signature of self-organized criticality (e.g., Bak, Tang, & Wiesenfeld, 1987; Beggs, 2008; de Arcangelis, Perrone-Capano, & Herrmann, 2006; De Los Rios & Zhang, 1999; Lin & Chen, 2005; Mandelbrot, 1999; Markovic & Gros, 2014), as an emergent property of dynamically interacting systems. However, the inference of such principles from power-law dynamics has received criticism (for a review see Beggs & Timme, 2012) and the applicability of such broad models to electrophysiological features (Touboul & Destexhe, 2017) remains unclear.

& Plenz, 2013) and empirically support efficient, large, and dynamic information transfer (Deneve & Machens, 2016; H. D. Yang, Shew, Roy, & Plenz, 2012; Y. G. Yu, Migliore, Hines, & Shepherd, 2014; S. L. Zhou & Yu, 2018). At a global network level, such critical states may facilitate the exploration of different network attractors (Cocchi, Gollo, Zalesky, & Breakspear, 2017; Palva & Palva, 2018) during rested wakefulness (Deco & Jirsa, 2012; Lynn, Cornblath, Papadopoulos, Bertolero, & Bassett, 2020), whereas specific networks may stabilize activity when 'expected uncertainty' (Friston, Breakspear, & Deco, 2012) regarding upcoming events decreases during specific tasks (Fagerholm et al., 2015; Hellyer et al., 2014; Lynn et al., 2020). By controlling the number of concurrently relevant feature attractors during attention, ***Project 3*** similarly proposes that E-I regulation fine-tunes dynamic range during attentional states, although the determination of whether optimal excitability regimes for sensory processing exist (e.g., McGinley, David, et al., 2015) and how or when they are instantiated requires further work.

In parallel with the power-law (1/f) appearance of broadband time series, narrowband-filtered (i.e., putatively rhythmic) EEG or MEG signals also exhibit long-range temporal correlations (Linkenkaer-Hansen et al., 2001; Monto et al., 2008; Poil, van Ooyen, & Linkenkaer-Hansen, 2008) in their amplitude fluctuations. Narrowband amplitudes depend on their past values with a probability falling off according to a power-law[29]. This amplitude autocorrelation further argues against stationary rhythms with constant amplitude, and – like broadband 1/f slopes – has been proposed to covary with cortical excitability (Bruining et al., 2020; Stephani et al., 2020). A unified perspective on these narrow- and broadband characteristics emerges from the observation that E-I balance gives rise to spatial power-law distributions of spreading activity ('neuronal avalanches'; Beggs & Plenz, 2003; Shew, Yang, Yu, Roy, & Plenz, 2011) at short time scales (Lombardi et al., 2017; Poil, Hardstone, Mansvelder, & Linkenkaer-Hansen, 2012), that are nested within emerging alpha rhythms at longer times scales (Poil et al., 2012). Similarly, injection of empirical alpha-band signals (including their autocorrelative amplitude structure) into large-scale mean field models can emulate BOLD-like signals (Schirner et al., 2018), indicating close (but likely non-exclusive) links between the 1/f appearance of BOLD signals and the scale-free

[29] Others have noted bimodality in alpha power distributions at rest to argue that cortical dynamics stochastically switch between an aperiodic and a rhythmic fix-point regime (Freyer, Aquino, Robinson, Ritter, & Breakspear, 2009; Freyer et al., 2011), although the continuous vs. discrete nature of rhythmic amplitude fluctuations remains unresolved. Given that these results are more generally based exclusively on narrowband-filtered fluctuations, the characteristics of the 'low-amplitude' episodes deserve further attention, as the absence of a rhythm conceptually differs from the continued presence of rhythmicity, albeit of decreased amplitude.

distribution of alpha-band amplitudes. This provides an interesting perspective on potential generative links between alpha rhythms and aperiodic slopes, and may partially account for the robustly observed empirical covariation between them (see next section).

5.5. Plausible biological relations between rhythmic and scale-free dynamics

Projects 1-3 treat the non-invasive human EEG signal as high-dimensional and information-rich, and argue for benefits of a systematic dissociation between narrow- and broadband spectral content. While their potential divergence is a stimulating prospect (e.g., Fellner et al., 2019; Ouyang, Hildebrandt, Schmitz, & Herrmann, 2020)[30], ***Projects 2 and 3*** also suggest relations between the two components when care is taken to methodically separate them. Hence, a complementary view may be warranted, in which the substantive question of interest concerns the neurobiological relation between rhythmic and aperiodic features, as well as the contexts for which their relative predominance proves adaptive. Indeed, correlations between spectral slopes and narrowband rhythms are frequently observed. For example, rhythmic alpha power covaried with spectral exponents in high frequency ranges, both across time and subjects (Muthukumaraswamy & Liley, 2018). Likewise, Podvalny et al. (2015) observed a positive association between alpha power and aperiodic slopes across channels, while changes in 1/f slope were correlated with broadband gamma power over visual cortex (Hermes, Miller, Wandell, & Winawer, 2015; Podvalny et al., 2015) and in the subthalamic nucleus (Huang et al., 2019). Similarly, intracranial theta power related to 1/f slopes during an associative memory task and jointly predicted memory performance (Sheehan et al., 2018). Finally, a previous EEG/MEG study suggests that alpha rhythms precede a reduction in long-range temporal correlations, estimated from both EEG and MEG resting state data (Becker, Van de Ville, & Kleinschmidt, 2018). This was interpreted as alpha rhythms reducing temporal integration windows in cortex, akin to a 'window wiping' mechanism (Sadaghiani & Kleinschmidt, 2016). Notably, results in ***Project 2*** provide evidence against this observation, and rather suggest that strong alpha events co-occur with

[30] Ouyang et al. (2020) suggest that visual 1/f slopes predict inter-individual differences in processing speed over and above rhythm-specific alpha power. However, they did not assess the predictive power of differences in alpha frequency, which relates to perceptual speed (Samaha & Postle, 2015) and empirically predicts differences in generalized intelligence (Grandy, Werkle-Bergner, Chicherio, Lovden, et al., 2013).

steeper spectral slopes (as also reported in the evoked scenario in auditory cortex: Billig et al., 2019), perhaps as a signature of reduced broadband excitability (Voytek & Knight, 2015).

The frequently observed covariation between rhythm parameters and spectral slopes has been used to argue that both features jointly reflect a latent oscillatory damping mechanism. Damping is a resistive force (opposite resonance) that reduces the amplitude of an oscillation over time. Muthukumaraswamy and Liley (2018) argued that variations in scale-free 1/f slopes arise from a stochastic distribution of non-stationary damped oscillators: "[r]eductions in the damping of this system will lead to higher amplitude oscillations in the time domain and a narrowing of the spectral resonance in the frequency domain" and "[t]he narrowing of this spectral resonance will be associated with a steeper falloff in power for higher frequencies." (Muthukumaraswamy & Liley, 2018, p. 590). This argument is based on their observation that shallower slopes are reliably related to larger alpha power, and the associated width narrowing of the power distribution. However, the authors carefully separated rhythmic and aperiodic components via IRASA (see *Section 5.2*) and found that the distributional width of alpha power only minimally overlapped with the aperiodic spectra, thus questioning a perfect fit between theory and data. While their model offers an interesting perspective on generative links between rhythmic features and spectral slopes as observed in ***Projects 2 and 3***, it deserves further validation, and may functionally be reconciled with other models depending on the origin of rhythmic amplitude fluctuations.

Notably, interactions between the excitatory tone of neural networks and synchrony are expected at the generative level. Shared stochastic inputs into two processing sites can induce synchrony between them (Ermentrout, Galan, & Urban, 2008), allowing for transient communication via coherence (Deco & Kringelbach, 2016; Fries, 2005, 2015; Palmigiano et al., 2017) even in the absence of structural connections (Galan, Fourcaud-Trocme, Ermentrout, & Urban, 2006; T. S. Zhou, Chen, & Aihara, 2005)[31]. As neurons differ in their responses to identical input (Nowak, Sanchez-Vives, & McCormick, 1997; Tsubo, Takada, Reyes, & Fukai, 2007), even white noise can in theory elicit synchronization between neural populations with similar functional response profiles (Brette, 2012; Stiefel & Ermentrout, 2016). At a more macroscopic level, thalamo-cortical models highlight that the level of background stochasticity in the network predicts the empirical efficacy of non-invasive periodic stimulation on cortical alpha rhythms

[31] This extends physical principles of induced synchrony between chaotic oscillators (Abarbanel, Rulkov, & Sushchik, 1996; Rosenblum, Pikovsky, & Kurths, 1996; Teramae & Tanaka, 2004).

(Lefebvre, Hutt, & Frohlich, 2017), highlighting that optimal levels of synaptic background activity benefit rhythmogenesis (Tiesinga & Sejnowski, 2004). In computational models, local E-I balance reproduces spontaneous network fluctuations as observed with fMRI (Deco et al., 2014) and MEG (Abeysuriya et al., 2018) and facilitates the emergence of alpha rhythms (Poil et al., 2012). In parallel, empirical work indicates an emergence of LFP rhythms from short delays in coupled excitation and inhibition (Atallah & Scanziani, 2009; Lorincz et al., 2009; Poo & Isaacson, 2009), while pharmacological blocking of either excitation or inhibition reduces rhythmic alpha power (Lozano-Soldevilla, 2018b). As Palva and Palva (2018) succinctly put it: "The dynamic [N.B.: excitability] state could contribute significantly to the ability of neuronal oscillations to express flexible synchronization, phase resetting, and entrainment." (p. 741). Hence, joint relations between narrow- and broadband signal characteristics may arise from a generative coupling.

5.6. Relevance of alpha-rhythmic and aperiodic dynamics for cognitive control

A source of major theoretical appeal of rhythmic and aperiodic signal components lies in the potential to link observations across spatial scales of investigation (Panzeri et al., 2015). While validation attempts of the underlying models require an invasive systems neuroscience approach, cognitive neuroscience offers alternative insights into the cognitive relevance of rhythmic and aperiodic components. ***Project 3*** exploited such an approach and probed the conceptual model of rhythmic and tonic (aperiodic) excitability modes (Figure 3) in a novel task (the '**M**ulti-**A**ttribute **A**ttention **T**ask', or MAAT) that required the flexible coordination of attention in time (Figure 6). On the MAAT, subjects were asked to attend to a parametrically varying number of features in a dynamic visual display. This task imposed multifaceted task demands at the cost of decreased specificity to individual facets of flexible cognition, such as arousal, alertness, selective attention, working memory and adaptive control (Cocchi, Zalesky, Fornito, & Mattingley, 2013; Dajani & Uddin, 2015; Sadaghiani & Kleinschmidt, 2016). The multifaceted nature of the task adheres to the view that "the very notion of attention, decision-making and working memory being individual neural processes may be replaced by a common set of thalamo-cortical circuit operations whose deployments vary according to behavioral demands and give rise to varying degrees of behavioral overlap among such cognitive constructs" (Halassa & Kastner, 2017, p. 1677). When the number of relevant features increased, posterior alpha engagement decreased, while aperiodic activity increased. Moreover, these effects were tracked at an individual level by BOLD signal magnitudes dominantly in thalamus, as well as elevations in phasic pupil diameter.

Alpha rhythms in particular are thought to support selective processing via a phase-dependent modulation of excitability that scales with their amplitude (for reviews see Foxe & Snyder, 2011; Jensen & Mazaheri, 2010; Klimesch, 2012; Klimesch et al., 2007; Lozano-Soldevilla,

2018b; Mathewson et al., 2011; Palva & Palva, 2007; Pfurtscheller, 2001). Based on this framework, a model by Sadaghiani and Kleinschmidt (2016) proposes that three components of alpha engagement are associated with different facets of control: an increase in unspecific alpha amplitudes in task-irrelevant regions as a sign of tonic alertness[32], a local desynchronization serving active information processing, and a modulation of distant alpha phase-locking as an expression of flexible attentional selection ('phasic adaptive control')[33]. In line with this model, alpha power increases in task-irrelevant regions (e.g., ipisilateral during attention; Capilla, Schoffelen, Paterson, Thut, & Gross, 2014; Wöstmann et al., 2019), while desynchronization in task-relevant regions benefits active information representation (de Pesters et al., 2016; Griffiths et al., 2019; Hanslmayr et al., 2012; Klimesch, 2012; Klimesch et al., 2007). While further assessment of the global vs. local engagement of alpha rhythms is required and may be facilitated by designs that include laterality contrasts to probe alpha engagement as a function of hemispheric recruitment, ***Project 3***'s results are in line with an active role of alpha rhythms in selective processing, while alpha engagement decreases when contexts require a more faithful processing of complex visual stimuli.

Given limited work on a task-related modulation of aperiodic slopes, evidence for their role in cognition remains scarce. A recent study suggests that the Hurst exponent (which directly scales with spectral slope coefficients; B. J. He, 2011) monotonically decreases with working memory set size, whereas alpha power reductions closely tracked memory capacity (Kardan et al., 2020). These results converge with the results of slope shallowing alongside target load in

---

[32] They ascribe globally unspecific alpha increases to tonic alertness, a state of nonselective readiness for perception and action (Posner, 2008). Tonic alertness and stimulus salience are associated with activity in a Midcingulo-Insular Network [M-CIN] (Sturm & Willmes, 2001), whose fluctuations at rest positively covary with global alpha amplitudes (Sadaghiani et al., 2010). Converging with a putative cholinergic role in upregulating alpha power (see discussion of ***Project 3***) (Suffczynski, Kalitzin, Pfurtscheller, & da Silva, 2001), the M-CIN network includes the highest density of the nicotinic acetylcholine receptors (Picard et al., 2013), while cholinergic reuptake inhibitors increase contralateral alpha power during selective attention (Bauer et al., 2012).

[33] Adaptive control entails the establishment, shifting and maintenance of attentional sets. Such control has been associated with the Lateral Frontoparietal Network (L-FPN) and may manifest via reconfiguration of long-range alpha phase relations (Sadaghiani & Kleinschmidt, 2016), in line with evidence that lateral prefrontal cortex lesions impair alpha phase synchrony and flexible cognition (Sadaghiani et al., 2019). As the MAAT not only requires switches between simultaneously presented visual features in the current attentional set (as analyzed in ***Project 3***), but also enforces a regular updating of attentional sets, future work will probe the task's utility for elucidating the multi-modal correlates of set switching.

Project 3. However, the authors speculate that this may reflect a relative reduction of a 'free-roaming', critical system at rest towards a more targeted processing mode under enhanced cognitive effort (see also Fagerholm et al., 2015). Given that high levels of alertness are required *throughout* the MAAT, ***Project 3*** suggests an alternative interpretation; specifically, the shallowing of aperiodic slopes may reflect transient increases in cortical excitability to allow for a flexible sampling of multiple contextually relevant features. While these perspectives are not mutually exclusive, this scenario illustrates the emerging challenge of unifying expectations regarding the directionality and functional interpretation of changes in scale-free dynamics.

Notably, neural rhythms also have a coordinative role in cortical processing, and previous work indicates that perceptual sampling (also of multiple concurrent locations or features) is implemented via rhythmic selection of neural representations at theta frequencies (Fiebelkorn et al., 2013; Helfrich et al., 2019; Landau & Fries, 2012; Re et al., 2019). While such modulation is not straightforward to test in the MAAT (as it is unclear whether and when individual features have been sampled), the concept of rhythmic sampling is not at odds with the present view that multi-feature attention is supported by excitability boosts. Indeed, a concurrent activation of populations that code simultaneously relevant features has been proposed as a basis for parallel representations, that such rhythmic sampling can select from (Mo et al., 2019). As such, a theta-rhythmic sampling in fronto-parietal networks, potentially coordinated by thalamus (Fiebelkorn, Pinsk, & Kastner, 2019), may resolve competition during increased excitability.

5.7. Contextual modulation of cortical processing via thalamocortical circuits

Project 3 indicates a central role of the thalamus in modulating behaviorally-relevant cortical excitability. Given that the thalamus' role in cognitive function remains underappreciated relative to cortex, this section provides a brief overview of converging evidence for a substantial thalamic role in the contextual coordination of cortical dynamics at the service of cognitive flexibility, with a particular focus on the relation to rhythmic and aperiodic activity as briefly discussed in ***Project 3***.

Already at birth (Toulmin et al., 2015), the thalamus is integrated with cortex (J. A. Harris et al., 2019) and constrains how it receives and processes information (Dehghani & Wimmer, 2019; Halassa & Sherman, 2019; J. A. Harris et al., 2019; A. S. Mitchell, 2015; Rikhye, Wimmer, et al., 2018). Although typically considered a simple relay of information into cortex, the thalamus can also modulate activity along the hierarchy of cortical processing (for reviews see Dehghani & Wimmer, 2019; Halassa & Sherman, 2019; Hayworth & Marblestone, 2018; Honjoh et al., 2018; Nakajima & Halassa, 2017; Rikhye, Wimmer, et al., 2018; Wolff & Vann, 2019). The difference

between information relay and modulation is apparent at the level of different nuclei (S. M. Sherman & Guillery, 2013); whereas relay nuclei respond maximally to transients, such as the on- and offsets of sensory stimuli (Alonso & Swadlow, 2005; Bruno & Sakmann, 2006; Rose & Metherate, 2005; Theyel, Llano, & Sherman, 2010), modulatory (i.e., higher-order) nuclei increase activity particularly during high cognitive demands (Bolkan et al., 2018; Cruikshank et al., 2012; Delevich, Tucciarone, Huang, & Li, 2015; Parnaudeau et al., 2013; Schmitt et al., 2017). This differentiation is also apparent between cell types; whereas 'core' cells feed sensory-motor information forward to granular cortical layers, 'matrix' cells can selectively target superficial cortical layers (Barbas, Garcia-Cabezas, & Zikopoulos, 2013; Cruikshank et al., 2012; E. G. Jones, 2001) to align cortical membrane excitability to momentary behavioral goals (Rikhye, Gilra, & Halassa, 2018; Rikhye, Wimmer, et al., 2018) without necessarily eliciting activity (Reichova & Sherman, 2004; S. M. Sherman, 2017). In humans, the gradient of core-to-matrix projections aligns with sensory-to-associative cortical areas, myelination profiles, and short-to-long cortical timescales (Müller et al., 2020), arguing for a key thalamic role in shaping cortical timescales and functional hierarchies (Gao, van den Brink, Pfeffer, & Voytek, 2020). Accordingly, human fMRI studies feature the thalamus as an integrative hub for macroscopic networks (Garrett, Epp, Perry, & Lindenberger, 2018; Hwang, Bertolero, Liu, & D'Esposito, 2017), with activity particularly in higher-order midline nuclei relating to temporal network fluctuations important for executive function (Shine et al., 2019). Hence, the thalamus may contextually coordinate information flow within and across cortical areas, potentially to track and optimize the efficiency and metabolic cost of cortical computations (Dehghani & Wimmer, 2019).

Such relevance of thalamus for cortical processing also extends to cognitive function in non-human animal models. Recent studies in mice assign higher-order thalamic nuclei a causal role in mediating connectivity within fronto-parietal control networks required for dynamic sensory selection (Rikhye, Gilra, et al., 2018) and sustained attention (Schmitt et al., 2017; Wimmer et al., 2015). Notably, prefrontal cortex is defined based on structural connections (i.e., *hodologically*) to mediodorsal thalamus (A. S. Mitchell, 2015). Accordingly, thalamo-prefrontal interactions are involved in establishing (Rikhye, Gilra, et al., 2018), sustaining (Bolkan et al., 2018), and switching (Marton, Seifikar, Luongo, Lee, & Sohal, 2018; Parnaudeau et al., 2013; Wright, Vann, Aggleton, & Nelson, 2015) prefrontal representations given contextual demands. Thus, the thalamus is poised to play a fundamental role in cognitive control and executive function (Browning, Chakraborty, & Mitchell, 2015; Halassa & Kastner, 2017; Krol, Wimmer, Halassa, & Feng, 2018; Ouhaz, Fleming, & Mitchell, 2018; Schmitt et al., 2017), at least in part by controlling sensory excitability (Lewis et al., 2015). The MAAT ('**M**ulti-**A**ttribute **A**ttention **T**ask') in ***Project 3*** responds to calls for "tasks with multifaceted cognitive demands" (Pergola et al., 2018, p. 1017)

to study the role of higher-order thalamic nuclei in cognitive neuroscience. Accordingly, it modulates BOLD signals particularly in antero-medial nuclei with prefrontal projection patterns (see ***Project 3***), implying their importance for flexible cognition also in humans.

Thalamic activity itself is under potent control of neuromodulation (Kinomura, Larsson, Gulyas, & Roland, 1996; Paus, 2000; N. Schiff & Purpura, 2002; N. D. Schiff, 2008; N. D. Schiff et al., 2007; Steriade & Glenn, 1982; Wyder, Massoglia, & Stanford, 2004). Anterior intralaminar and centro-medial association nuclei in particular receive dense inputs from cholinergic (Kolmac & Mitrofanis, 1999), noradrenergic (Oke, Carver, Gouvion, & Adams, 1997) and serotonergic afferents (Lavoie & Parent, 1991; Oke et al., 1997), and are thus key stations of neuromodulatory pathways (Dringenberg & Olmstead, 2003; J. Liu et al., 2015; Song et al., 2017; Steriade & Glenn, 1982) and control circuits (Van der Werf, Witter, & Groenewegen, 2002). Such known relation to neuromodulation (largely from non-human animals) converges with the strong link we noted for the first time in humans (***Project* 3)** between task-related thalamic BOLD increases and phasic increases in pupil diameter, potentially reflecting upregulation in noradrenergic drive[34].

Finally, the thalamus contributes to cortical rhythms (for reviews see Crunelli et al., 2018; Huguenard & McCormick, 2007; E. G. Jones, 2009; Ketz, Jensen, & O'Reilly, 2015; McCormick, McGinley, & Salkoff, 2015; Saalmann & Kastner, 2009), particularly in the alpha frequency range (Andersen & Andersson, 1968; Isaichev, Derevyankin, Koptelov Yu, & Sokolov, 2001; G. S. Li, Henriquez, & Frohlich, 2017; Lorincz et al., 2009; Schreckenberger et al., 2004; Vijayan & Kopell,

[34] While (non-luminance-mediated) pupil responses have been linked to activity dominantly within the noradrenergic system in mice (Breton-Provencher & Sur, 2019; Reimer et al., 2014; Zerbi et al., 2019), monkeys (Aston-Jones & Cohen, 2005; Joshi et al., 2016) and humans (de Gee et al., 2017; Murphy et al., 2014), evidence for an overlap with cholinergic activation has also been reported (Reimer et al., 2014), albeit with reduced cholinergic associations with the first derivative of pupil dilation as calculated in ***Project 3***. As discussed in ***Project 3***, the potential separability of these systems, and their importance for selective and sensitive processing, remain open and interesting questions.

2012)[35]. These links are based on phase-locking and amplitude covariation between concurrent alpha rhythms in thalamus and posterior cortex (Chatila, Milleret, Rougeul, & Buser, 1993; M. Halgren et al., 2019; Lopes da Silva, van Lierop, Schrijer, & van Leeuwen, 1973; Lopes da Silva, Vos, Mooibroek, & Van Rotterdam, 1980; Lorincz et al., 2009), which inspired models of thalamo-cortical circuits that spontaneously generate alpha rhythms (Bazhenov, Timofeev, Steriade, & Sejnowski, 1999; Becker, Knock, Ritter, & Jirsa, 2015; Breakspear et al., 2006; Contreras, Destexhe, Sejnowski, & Steriade, 1996; Destexhe, Mccormick, & Sejnowski, 1993; Golomb, Wang, & Rinzel, 1994; Lopes da Silva, Hoeks, Smits, & Zetterberg, 1974; McCormick & Huguenard, 1992; Robinson et al., 2001; Suffczynski et al., 2001). Moreover, multimodal studies consistently indicate positive relationships between hemodynamic signals in thalamus and spontaneous alpha power at rest (Becker, Reinacher, Freyer, Villringer, & Ritter, 2011; de Munck et al., 2007; DiFrancesco, Holland, & Szaflarski, 2008; Feige et al., 2005; Goldman, Stern, Engel, & Cohen, 2002; Z. M. Liu et al., 2012; Moosmann et al., 2003; Olbrich et al., 2009; Sadaghiani et al., 2010)[36]. Thalamic rhythms have been observed in multiple centers of the visual thalamus (for a review see Saalmann & Kastner, 2011), ranging from relay nuclei, such as the lateral geniculate nucleus (LGN) (S. W. Hughes, Cope, Blethyn, & Crunelli, 2002; S. W. Hughes & Crunelli, 2007; S. W. Hughes et al., 2008; S. W. Hughes et al., 2004; Lorincz, Crunelli, & Hughes, 2008; Lorincz et al., 2009), to higher-order nuclei such as the pulvinar and the thalamic reticular nucleus (TRN). In particular, the TRN (McAlonan, Cavanaugh, & Wurtz, 2008) is considered the 'guardian of the thalamic gateway' (Crick, 2003) as it inhibits otherwise excitatory thalamic nuclei. The TRN's capacity to control both widespread

[35] However, the cortical or thalamic origin of rhythmogenesis remains debated (e.g., Bollimunta et al., 2011; M. Halgren et al., 2019; Stitt et al., 2018) and may systematically vary between different thalamocortical circuits and neuro-behavioral states (e.g., Fiebelkorn et al., 2019; Stitt et al., 2018).

[36] Notably, we observed the opposite relation during task performance in ***Project 3***, i.e., increases in thalamic BOLD signal magnitude accompanied stronger task-related reduction of alpha power. Notably these two results are not irreconcilable. Speculating, thalamocortical alpha rhythms may coordinate more global ongoing activity during wakeful rest, whereas elevated thalamo-cortical activity may serve a targeted local desynchronization for specific task processing (Sadaghiani & Kleinschmidt, 2016). Moreover, alpha rhythms during task and rest may relate to partially differentiable thalamo-cortical circuits (see *Section 5.8*). More work is necessary to elucidate these different possibilities, with a stronger focus on alpha rhythms during task performance in concurrent EEG-fMRI measurements.

and focal brain rhythms (Drover, Schiff, & Victor, 2010; MacDonald, Fifkova, Jones, & Barth, 1998) has been noted early on (Morison & Dempsey, 1943), leading to speculation that "[…] in this thalamic reticular system are the specific central controlling mechanisms for processes of attention, and that the spontaneous rhythms of the cortex may in some manner reflect the influence this thalamic system exerts upon the function of specific cortical areas involved in the momentary limelight directed here and there in the central stream of consciousness" (Jasper, 1948, p. 346). Finally, the pulvinar nucleus has been closely linked to attentional gain control[37] over bottom-up processing via the modulation of posterior alpha (Cortes & van Vreeswijk, 2015; Fiebelkorn et al., 2019; Lopes da Silva et al., 1973; Lopes da Silva et al., 1980; computational model: Quax, Jensen, & Tiesinga, 2017; Saalmann, Pinsk, Wang, Li, & Kastner, 2012) and gamma rhythms (Roux, Wibral, Singer, Aru, & Uhlhaas, 2013).

While this suggests a key role of the sensory thalamus in a phasic modulation of excitability during selective attention (e.g., Suffczynski et al., 2001), the thalamus also facilitates the occurrence and duration of cortical activation (J. Liu et al., 2015; MacLean, Watson, Aaron, & Yuste, 2005; Redinbaugh et al., 2020; Rigas & Castro-Alamancos, 2007) by changing the membrane potential and the firing level of thalamocortical cells (Hirata & Castro-Alamancos, 2010; Steriade & Llinas, 1988). When thalamic cells are relatively hyperpolarized (i.e., farther from firing threshold), transient inputs induce a synchronous 'burst' mode (S. M. Sherman, 2001). In contrast, during relative depolarization close to firing threshold (i.e., increased excitability), neurons exhibit desynchronized, 'tonic' responses (Steriade & Llinas, 1988) during which

[37] The pulvinar has been closely linked to control over attentional salience (for a review see Grieve, Acuna, & Cudeiro, 2000). Lesions to the pulvinar produce deficits in attentional selection (Arend et al., 2008; Danziger, Ward, Owen, & Rafal, 2004; Rafal & Posner, 1987; Snow, Allen, Rafal, & Humphreys, 2009; Zihl & von Cramon, 1979), while selective attention increases pulvinar blood flow and glucose uptake (Kastner & Pinsk, 2004; Laberge & Buchsbaum, 1990; Smith, Cotton, Bruno, & Moutsiana, 2009). Recent modelling (Jaramillo, Mejias, & Wang, 2019) and empirical work (Saalmann, Ly, Pinsk, & Kastner, 2018) indicate that the pulvinar sustains top-down information in parietal cortex (Saalmann & Kastner, 2009), and establishes connectivity with visual pathways to regulate feedforward processing (Purushothaman, Marion, Li, & Casagrande, 2012). In line with an encoding of top-down priors (Kanai, Komura, Shipp, & Friston, 2015; O'Reilly, Wyatte, & Rohrlich, 2017; Rikhye, Wimmer, et al., 2018), pulvinar neurons are sensitive to the expected precision or confidence in perceptual information (Jaramillo et al., 2019; Komura, Nikkuni, Hirashima, Uetake, & Miyamoto, 2013).

peripheral signals are faithfully transmitted to cortex (Hartings, Temereanca, & Simons, 2003). As discussed in ***Project 3***, BOLD increases (and shallowing of spectral slopes) as a function of attentional demands may relate to a switch between thalamic 'burst' and 'tonic' firing modes (S. M. Sherman, 2001). Interestingly, recent multi-modal work in rats indicates that 10 Hz stimulation of central thalamus evokes negative cortical BOLD responses, whereas high-frequency stimulation increases positive cortical BOLD responses, widens the extent of thalamic BOLD activation, and induces behavioral arousal (J. Liu et al., 2015; see also Logothetis et al., 2010). Hence, the thalamus may be critical for cortical regime switches, as also suggested by computational models of thalamo-cortical switches between high-amplitude alpha rhythms and low-amplitude, putatively aperiodic states, at rest (Freyer et al., 2011; Freyer, Roberts, Ritter, & Breakspear, 2012)[38].

Notably, the specific contribution of individual nuclei to task performance is difficult to ascertain in ***Project 3*** due to the spatial spread of BOLD signals. Previously, Hwang et al. (2017) argued for little BOLD specificity for individual nuclei in resting state recordings at a magnetic field strength of 3 Tesla. While some separability was observed with task engagement in ***Project 3***, the specific nucleus attribution should thus be interpreted with some reservation. An interesting prospect is the use of higher field strengths to improve spatial sensitivity (Shine et al., 2019), and/or the parcellation of nuclei in individual subjects based on anatomical images (Su et al., 2019) or tractography (Battistella et al., 2017; Behrens et al., 2003; Horn & Blankenburg, 2016; O'Muircheartaigh, Keller, Barker, & Richardson, 2015) to reduce the required amount of spatial smoothing, potentially increasing signal-to-noise ratios. Furthermore, as our results are constrained to inter-individual covariations, future work may benefit from the assessment of trial-by-trial associations in simultaneous EEG-fMRI setups, if the data quality affords such analyses.

[38] In particular, these models reproduce bimodal amplitude distributions of alpha power – presumably reflecting switches between alpha rhythms and aperiodic states – by driving a thalamo-cortical mean field model with stochastic inputs into specific thalamic nuclei, while including state-dependent cortical feedback that controls the noise gain from thalamus to cortex. This incorporates assumed cortical feedback from cortex, as observed empirically (Contreras et al., 1996; Crandall, Cruikshank, & Connors, 2015; Rigas & Castro-Alamancos, 2007, 2009), and in line with prevalent cortical inputs to thalamus (Castro-Alamancos, 2004, 2009; Halassa & Sherman, 2019; S. M. Sherman, 2017; S. M. Sherman & Guillery, 1996).

5.8. A note regarding the potential diversity of rhythmic sources

Projects 1-3 used a simplified view of rhythmic engagement by focusing on scalp signals and assuming a unitary, shared spatial source. However, rhythmic (e.g., alpha) generators vary spatially (e.g., Barzegaran, Vildavski, & Knyazeva, 2017; de Pesters et al., 2016; Popov, Gips, Kastner, & Jensen, 2019), inter-individually, and between tasks (Barry, De Blasio, Fogarty, & Clarke, 2020; Michels, Moazami-Goudarzi, Jeanmonod, & Sarnthein, 2008). The use of signal source reconstruction techniques may enhance spatial insights in future work, potentially even into thalamic sources with sufficient priors (Attal, Yelnik, Bardinet, Chupin, & Baillet, 2010; Krishnaswamy et al., 2017; Roux et al., 2013). Crucially however, generative mechanisms likely vary within a given frequency band and circuit architecture (Vijayan & Kopell, 2012; Womelsdorf et al., 2014). An enticing (albeit speculative) possibility is that large-amplitude alpha rhythms during rest (e.g., ***Projects 1 & 2***) and low-amplitude alpha rhythms during task (e.g., ***Projects 1 & 3***) reflect different generative circuits (Fiebelkorn et al., 2019). There is some invasive evidence for differentiable propagation directions, evoked effects and behavioral relations of alpha rhythms in varying regions and cortical layers[39]. In V2 and V4, alpha power was found to exhibit regional variations in laminar profile (propagating from infragranular to supragranular layers in visual cortex; from supragranular to infragranular layers in inferior temporal cortex) and importantly, inverse behavioral consequences (Bollimunta et al., 2008). Whereas higher alpha power in visual cortex was associated with lower reaction times, higher alpha power in inferior temporal cortex predicted slower responses. Similarly, Buffalo, Fries, Landman, Buschman, and Desimone (2011) reported opposite effects of visual stimulation on alpha generators in the supra-

[39] Widespread associative connections, both cortico- and thalamo-cortical, target supra- and infragranular layers but not the granular layer that is associated with feedforward input (for a review see Bastos et al., 2012). Slow delta and theta fluctuations in humans are strongest in superficial layers (Csercsa et al., 2010; E. Halgren et al., 2015; M. Halgren et al., 2018) that contain dense interneuron networks that can spread inhibition throughout the cortical column to potently modulate feedforward processing. For alpha rhythms, there is mixed evidence for a dominance in superficial layers (Haegens et al., 2015; M. Halgren et al., 2019), deep layers (Bastos, Loonis, Kornblith, Lundqvist, & Miller, 2018) and/or the presence across layers (Bollimunta et al., 2008; Haegens et al., 2015; Scheeringa, Koopmans, van Mourik, Jensen, & Norris, 2016; van Kerkoerle et al., 2014), while recording issues such as volume conduction from deep sources (Haegens et al., 2015) complicate principled inference.

and infragranular layers of early visual cortex: while visual stimulation reduced supragranular alpha, it enhanced infragranular alpha (Buffalo et al., 2011). As noted by Schmid, Singer, and Fries (2012) the latter may be more closely related to thalamic activity, as the main driving input to pulvinar arises from infragranular cortical layers (Sherman, 2007).

This potential diversity of sources provides a challenge for non-invasive investigations, as scalp signals are thought to be particularly sensitive to superficial layers with vertical currents, while deeper layers may dominantly form closed loops to which EEG/MEG are insensitive (Schmid et al., 2012). Such divergence may also contribute to increasing evidence against alpha rhythms in primary sensory regions, as compared to significant rhythmicity in higher order associative regions (Billig et al., 2019; Zhigalov & Jensen, 2020). Concurrent recordings of EEG and layer-specific fMRI at high field strengths (Scheeringa & Fries, 2019) provide a fascinating avenue for non-invasive insights into rhythmogenesis[40]. Moreover, given that the laminar constellation (i.e., the directional arrangement of current sources and sinks) defines whether the surface potential will be positive or negative (see Figure 7 in Mitzdorf, 1985), and excitability is assumedly maximized during either the positive or the negative part of the oscillatory cycle, a differential coupling of higher-frequencies to different sub-cycles during e.g., rest and task could non-invasively indicate different laminar origins. However, whether this is empirically the case is unclear. Systematic variability in observed waveform shape, amplitude, and duration characteristics (Peterson & Voytek, 2017) potentially provide another source of insights into generative differences. In particular, a model by Peterson and Voytek (2017) suggests that 'sustained' alpha events (> 5 cycles, as typically observed during rest) extensively inhibit inputs (see ***Projects 1 and 2***), whereas more transient 'bursts' (~ 1-3 cycles) during task states (see ***Projects 1 and 3***) enhance neural activity and variability therein[41]. Duration-specific rhythm

[40] This is equally true for scale-free dynamics, whose layer-dependence is virtually unknown (as pointed out also by B. J. He et al., 2010).

[41] A potential concern with this model and the associated data is the strong empirical covariation between the estimated duration and amplitude of events as highlighted in ***Project 1***. As such, differences in event amplitude may drive differential high-frequency power (e.g., Klimesch et al., 2007), rather than the duration of events.

detection as afforded by eBOSC (see ***Project 1***) provides a principled solution to investigate such models empirically in future work.

5.9. Cortical excitability across the lifespan, in health and disease

Insights into rhythmic and aperiodic signal components suggest fruitful perspectives for further work that focuses on baseline excitability and its functional modulation across the lifespan[42]. With increasing adult age, 1/f spectra shallow (***Project 2***; Dave, Brothers, & Swaab, 2018; Tran, Rolle, Gazzaley, & Voytek, 2020; Voytek et al., 2015) with parallel changes in multiscale entropy (McIntosh, 2019). Given that slope shallowing mirrors behavioral declines with advanced adult age (Tran et al., 2020; Voytek et al., 2015) and is reliable across task states (Dave et al., 2018), shallowing may reflect adverse increases in excitatory tone with senescence, potentially due to deficits in homeostatic inhibition (Legon et al., 2016; Rozycka & Liguz-Lecznar, 2017). This aligns with an increasing decline of the GABA system with age (Leventhal, Wang, Pu, Zhou, & Ma, 2003; Porges et al., 2017; Rozycka & Liguz-Lecznar, 2017) that may lead to functional dedifferentiation (Lalwani et al., 2019; S. C. Li, Lindenberger, & Sikstrom, 2001). Furthermore, the task-related recruitment of inhibitory alpha rhythms decreases with age (Borghini et al., 2018), at least in part alongside behavioral deficits in inhibition (Hasher & Zacks, 1988; Kennedy & Mather, 2019; Salthouse & Meinz, 1995; Sander, Lindenberger, & Werkle-Bergner, 2012; Zanto & Gazzaley, 2017). Moreover, adult age differences in thalamic structure and function (for a review see Fama & Sullivan, 2015) have been reported, potentially leading to reduced control over cortical circuits[43]. In the face of alterations in structural anatomy and neuromodulation, tasks such

---

[42] Given the link between fine-scale sample entropy and 1/f slopes (see ***Project 2)***, previous cross-sectional evidence of increases in fine-scale entropy across childhood may tentatively also be attributed to a shallowing of spectral slopes as observed in recent data (W. He et al., 2019). However, little evidence exists on the longitudinal development of aperiodic signatures, which thus deserves attention.

[43] Age-related changes in the thalamus may also involve the dopamine system. In addition to the prevalent striatal targets, the primate (but not rodent; Garcia-Cabezas, Martinez-Sanchez, Sanchez-Gonzalez, Garzon, & Cavada, 2009) thalamus is a key target for brain dopamine (Sanchez-Gonzalez, Garcia-Cabezas, Rico, & Cavada, 2005), with particularly high receptor density in higher-order nuclei (Rieck, Ansari, Whetsell, Deutch, & Kessler, 2004). Given that reductions in dopamine efficacy reflect a prominent model of age-related changes in neural processing and cognition (for reviews see Backman, Lindenberger, Li, & Nyberg, 2010; Backman, Nyberg, Lindenberger, Li, & Farde, 2006; S. C. Li et al., 2001), the potential separability of the dopamine systems (e.g., de Manzano, Cervenka, Karabanov, Farde, & Ullen, 2010) and the implications of potential challenges in the thalamic dopamine system present exciting questions for future work.

as the MAAT (***Project 3***) may help to elucidate whether/how putative changes in cortical excitability shape and constrain adaptive perception, cognition and action in complex environments across the lifespan.

A further fertile area for future work concerns potential impairments in adaptive excitability modulations (***Project 3***) and E-I plasticity in disorders (J. Lisman, 2012; Nelson & Valakh, 2015; Yizhar et al., 2011). Challenges to E-I homeostasis provide a simplified description of neuro-sensory hyperexcitability, as observed in autism (Crane, Goddard, & Pring, 2009; Neil, Olsson, & Pellicano, 2016; Nelson & Valakh, 2015; Pettine, Louie, Murray, & Wang, 2020; Rubenstein & Merzenich, 2003; Sinha et al., 2014; Takarae & Sweeney, 2017) and schizophrenia (Anticevic & Lisman, 2017; Gao & Penzes, 2015; Uhlhaas & Singer, 2010; G. J. Yang et al., 2016). Similarly, states of heightened metabolic stress such as sleep deprivation are characterized by heightened somatosensory sensitivity (Krause, Prather, Wager, Lindquist, & Walker, 2019) and thalamic aberrations (C. L. Liu, Kong, Liu, Zhou, & Wu, 2014; Ma, Dinges, Basner, & Rao, 2015; Shokri-Kojori et al., 2018). Finally, thalamocortical dysrhythmia (i.e., hypersynchrony) due to pathological intra-thalamic inhibition may be involved in functional disorders including epilepsy, chronic pain and depression (Huguenard & McCormick, 2007; E. G. Jones, 2010; Llinas, Ribary, Jeanmonod, Kronberg, & Mitra, 1999; Proske, Jeanmonod, & Verschure, 2011). Further research into thalamocortical excitability, and its top-down control, may thus shed light on the mechanisms contributing to neuro-behavioral flexibility in health and disease.

5.10. Conclusions

In this cumulative dissertation, I summarized and discussed evidence that rhythmic and aperiodic scalp activity provide methodologically separable, and potentially complementary, indicators of neuro-behavioral states. However, the measurement of rhythmic and aperiodic signatures is traditionally confounded, thus requiring principled techniques that separate these components in time, space and magnitude. In multiple applications (dominantly in ***Project 1***), I demonstrated the potential to determine and investigate rhythmic events in a time-resolved manner using the eBOSC algorithm. Complementary to rhythm characterization, ***Project 2*** focused on the measurement of temporal irregularity (entropy), and highlighted a series of biases and potential solutions to aid veridical characterization of irregular neural dynamics. Finally, ***Project 3*** investigated the modulation of aperiodic (i.e., irregular) and rhythmic activity in a novel paradigm that manipulated levels of contextual uncertainty, thereby providing correlational evidence that thalamo-cortical loops shape momentary cortical network states alongside neuromodulation in service of contextual demands.

Many of the chapters in this dissertation focused on methodological advances in the non-invasive characterization of rhythmic and aperiodic states. While such developments are necessary on methodological and conceptual grounds, they will likely be most fruitful when future research questions are driven by theoretical frameworks seeking to elucidate the principles of flexible thalamocortical coordination, as briefly reviewed here. Moreover, the rapid development of large-scale, biophysically-inspired models of neural circuits (e.g., Mejias et al., 2016; Neymotin, Daniels, et al., 2020; Robinson et al., 2001; Schirner et al., 2018) promises an exciting avenue for exploring time series features, and to gain insights into their generative mechanisms (e.g., M. A. Sherman et al., 2016). However, the thalamus (with its diverse circuit motifs, deep location and small subdivisions) provides substantial challenges for non-invasive *in vivo* investigations. Given increasing evidence of the thalamus' fundamental importance for the coordination of neural dynamics and cognitive function, these challenges provide urgent targets for research on neural computations in health and disease.

6. References

Abarbanel, H. D. I., Rulkov, N. F., & Sushchik, M. M. (1996). Generalized synchronization of chaos: The auxiliary system approach. *Physical Review E, 53*(5), 4528-4535. doi:10.1103/PhysRevE.53.4528

Abeysuriya, R. G., Hadida, J., Sotiropoulos, S. N., Jbabdi, S., Becker, R., Hunt, B. A. E., . . . Woolrich, M. W. (2018). A biophysical model of dynamic balancing of excitation and inhibition in fast oscillatory large-scale networks. *Plos Computational Biology, 14*(2). doi:10.1371/journal.pcbi.1006007

Adesnik, H., & Scanziani, M. (2010). Lateral competition for cortical space by layer-specific horizontal circuits. *Nature, 464*(7292), 1155-U1171. doi:10.1038/nature08935

Adrian, E. D., & Matthews, B. H. C. (1934). The berger rhythm potential changes from the occipital lobes in man. *Brain, 57*, 355-385. doi:10.1093/brain/57.4.355

Akam, T., & Kullmann, D. M. (2014). Oscillatory multiplexing of population codes for selective communication in the mammalian brain. *Nature Reviews Neuroscience, 15*(2), 111-122. doi:10.1038/nrn3668

Akam, T. E., & Kullmann, D. M. (2012). Efficient "communication through coherence" requires oscillations structured to minimize interference between signals. *Plos Computational Biology, 8*(11). doi:10.1371/journal.pcbi.1002760

Alkire, M. T., McReynolds, J. R., Hahn, E. L., & Trivedi, A. N. (2007). Thalamic microinjection of nicotine reverses sevoflurane-induced loss of righting reflex in the rat. *Anesthesiology, 107*(2), 264-272. doi:10.1097/01.anes.0000270741.33766.24

Alonso, J. M., & Swadlow, H. A. (2005). Thalamocortical specificity and the synthesis of sensory cortical receptive fields. *Journal of Neurophysiology, 94*(1), 26-32. doi:10.1152/jn.01281.2004

Andersen, P., & Andersson, S. A. (1968). *Physiological basis of the alpha rhythm*. New York: Appleton-Century-Crofts.

Anderson, J., Lampl, I., Reichova, I., Carandini, M., & Ferster, D. (2000). Stimulus dependence of two-state fluctuations of membrane potential in cat visual cortex. *Nature Neuroscience, 3*(6), 617-621. doi:10.1038/75797

Anticevic, A., & Lisman, J. (2017). How can global alteration of Excitation/Inhibition balance lead to the local dysfunctions that underlie schizophrenia? *Biological Psychiatry, 81*(10), 818-820. doi:10.1016/j.biopsych.2016.12.006

Arend, I., Machado, L., Ward, R., McGrath, M., Ro, T., & Rafal, R. D. (2008). The role of the human pulvinar in visual attention and action: Evidence from temporal-order judgment, saccade decision, and antisaccade tasks. *Using Eye Movements as an Experimental Probe of Brain Function - a Symposium in Honor of Jean Buttner-Ennever, 171*, 475-483. doi:10.1016/S0079-6123(08)00669-9

Aru, J., Aru, J., Priesemann, V., Wibral, M., Lana, L., Pipa, G., . . . Vicente, R. (2015). Untangling cross-frequency coupling in neuroscience. *Current Opinion in Neurobiology, 31*, 51-61. doi:10.1016/j.conb.2014.08.002

Aston-Jones, G., & Cohen, J. D. (2005). An integrative theory of locus coeruleus-norepinephrine function: Adaptive gain and optimal performance. *Annual Review of Neuroscience, 28*, 403-450. doi:10.1146/annurev.neuro.28.061604.135709

Atallah, B. V., & Scanziani, M. (2009). Instantaneous modulation of gamma oscillation frequency by balancing excitation with inhibition. *Neuron, 62*(4), 566-577. doi:10.1016/j.neuron.2009.04.027

Attal, Y., Yelnik, J., Bardinet, E., Chupin, M., & Baillet, S. (2010). MEG detects alpha-power modulations in pulvinar. *17th International Conference on Biomagnetism Advances in Biomagnetism - Biomag2010, 28*, 211-214.

Avena-Koenigsberger, A., Misic, B., & Sporns, O. (2018). Communication dynamics in complex brain networks. *Nature Reviews Neuroscience, 19*(1), 17-33. doi:10.1038/nrn.2017.149

Babu Henry Samuel, I., Wang, C., Hu, Z., & Ding, M. (2018). The frequency of alpha oscillations: Task-dependent modulation and its functional significance. *NeuroImage, 183*, 897-906. doi:10.1016/j.neuroimage.2018.08.063

Backman, L., Lindenberger, U., Li, S. C., & Nyberg, L. (2010). Linking cognitive aging to alterations in dopamine neurotransmitter functioning: Recent data and future avenues. *Neurosci Biobehav Rev, 34*(5), 670-677. doi:10.1016/j.neubiorev.2009.12.008

Backman, L., Nyberg, L., Lindenberger, U., Li, S. C., & Farde, L. (2006). The correlative triad among aging, dopamine, and cognition: Current status and future prospects. *Neuroscience and Biobehavioral Reviews, 30*(6), 791-807. doi:10.1016/j.neubiorev.2006.06.005

Backus, A. R., Schoffelen, J. M., Szebenyi, S., Hanslmayr, S., & Doeller, C. F. (2016). Hippocampal-prefrontal theta oscillations support memory integration. *Current Biology, 26*(4), 450-457. doi:10.1016/j.cub.2015.12.048

Bahramisharif, A., Jensen, O., Jacobs, J., & Lisman, J. (2018). Serial representation of items during working memory maintenance at letter-selective cortical sites. *PLoS Biology, 16*(8). doi:10.1371/journal.pbio.2003805

Bahramisharif, A., van Gerven, M. A. J., Aarnoutse, E. J., Mercier, M. R., Schwartz, T. H., Foxe, J. J., . . . Jensen, O. (2013). Propagating neocortical gamma bursts are coordinated by traveling alpha waves. *Journal of Neuroscience, 33*(48), 18849-18854. doi:10.1523/Jneurosci.2455-13.2013

Bak, P., Tang, C., & Wiesenfeld, K. (1987). Self-organized criticality: An explanation of the 1/f noise. *Physical Review Letters, 59*(4), 381-384. doi:10.1103/PhysRevLett.59.381

Ballinger, E. C., Ananth, M., Talmage, D. A., & Role, L. W. (2016). Basal forebrain cholinergic circuits and signaling in cognition and cognitive decline. *Neuron, 91*(6), 1199-1218. doi:10.1016/j.neuron.2016.09.006

Barbas, H., Garcia-Cabezas, M. A., & Zikopoulos, B. (2013). Frontal-thalamic circuits associated with language. *Brain and Language, 126*(1), 49-61. doi:10.1016/j.bandl.2012.10.001

Baria, A. T., Baliki, M. N., Parrish, T., & Apkarian, A. V. (2011). Anatomical and functional assemblies of brain BOLD oscillations. *Journal of Neuroscience, 31*(21), 7910-7919. doi:10.1523/JNEUROSCI.1296-11.2011

Barry, R. J., De Blasio, F. M., Fogarty, J. S., & Clarke, A. R. (2020). Natural alpha frequency components in resting EEG and their relation to arousal. *Clinical Neurophysiology, 131*(1), 205-212. doi:10.1016/j.clinph.2019.10.018

Bartoli, E., Bosking, W., Chen, Y., Li, Y., Sheth, S. A., Beauchamp, M. S., . . . Foster, B. L. (2019). Functionally distinct gamma range activity revealed by stimulus tuning in human visual cortex. *Current Biology, 29*(20), 3345-3358. doi:10.1016/j.cub.2019.08.004

Bartolo, R., & Merchant, H. (2015). Beta oscillations are linked to the initiation of sensory-cued movement sequences and the internal guidance of regular tapping in the monkey. *Journal of Neuroscience, 35*(11), 4635-4640. doi:10.1523/Jneurosci.4570-14.2015

Barzegaran, E., Vildavski, V. Y., & Knyazeva, M. G. (2017). Fine structure of posterior alpha rhythm in human EEG: Frequency components, their cortical sources, and temporal behavior. *Scientific Reports, 7*. doi:10.1038/s41598-017-08421-z

Basar, E. (2012). A review of alpha activity in integrative brain function: Fundamental physiology, sensory coding, cognition and pathology. *International Journal of Psychophysiology, 86*(1), 1-24. doi:10.1016/j.ijpsycho.2012.07.002

Bastos, A. M., Loonis, R., Kornblith, S., Lundqvist, M., & Miller, E. K. (2018). Laminar recordings in frontal cortex suggest distinct layers for maintenance and control of working memory. *Proceedings of the National Academy of Sciences of the United States of America, 115*(5), 1117-1122. doi:10.1073/pnas.1710323115

Bastos, A. M., Usrey, W. M., Adams, R. A., Mangun, G. R., Fries, P., & Friston, K. J. (2012). Canonical microcircuits for predictive coding. *Neuron, 76*(4), 695-711. doi:10.1016/j.neuron.2012.10.038

Battistella, G., Najdenovska, E., Maeder, P., Ghazaleh, N., Daducci, A., Thiran, J. P., . . . Fornari, E. (2017). Robust thalamic nuclei segmentation method based on local diffusion magnetic resonance properties. *Brain Structure & Function, 222*(5), 2203-2216. doi:10.1007/s00429-016-1336-4

Bauer, M., Kluge, C., Bach, D., Bradbury, D., Heinze, H. J., Dolan, R. J., & Driver, J. (2012). Cholinergic enhancement of visual attention and neural oscillations in the human brain. *Current Biology, 22*(5), 397-402. doi:10.1016/j.cub.2012.01.022

Bazanova, O. M., & Vernon, D. (2014). Interpreting EEG alpha activity. *Neurosci Biobehav Rev, 44*, 94-110. doi:10.1016/j.neubiorev.2013.05.007

Bazhenov, M., Timofeev, I., Steriade, M., & Sejnowski, T. J. (1999). Self-sustained rhythmic activity in the thalamic reticular nucleus mediated by depolarizing GABA(A) receptor potentials. *Nature Neuroscience, 2*(2), 168-174. doi:10.1038/5729

Becker, R., Knock, S., Ritter, P., & Jirsa, V. (2015). Relating alpha power and phase to population firing and hemodynamic activity using a thalamo-cortical neural mass model. *Plos Computational Biology, 11*(9). doi:10.1371/journal.pcbi.1004352

Becker, R., Reinacher, M., Freyer, F., Villringer, A., & Ritter, P. (2011). How ongoing neuronal oscillations account for evoked fMRI variability. *Journal of Neuroscience, 31*(30), 11016-11027. doi:10.1523/Jneurosci.0210-11.2011

Becker, R., Van de Ville, D., & Kleinschmidt, A. (2018). Alpha oscillations reduce temporal long-range dependence in spontaneous human brain activity. *Journal of Neuroscience, 38*(3), 755-764. doi:10.1523/JNEUROSCI.0831-17.2017

Bedard, C., & Destexhe, A. (2009). Macroscopic models of local field potentials and the apparent 1/f noise in brain activity. *Biophysical Journal, 96*(7), 2589-2603. doi:10.1016/j.bpj.2008.12.3951

Bedard, C., Gomes, J. M., Bal, T., & Destexhe, A. (2017). A framework to reconcile frequency scaling measurements, from intracellular recordings, local-field potentials, up to EEG and MEG signals. *Journal of Integrative Neuroscience, 16*(1), 3-18. doi:10.3233/Jin-160001

Bedard, C., Kroger, H., & Destexhe, A. (2006). Does the 1/f frequency scaling of brain signals reflect self-organized critical states? *Physical Review Letters, 97*(11). doi:10.1103/PhysRevLett.97.118102

Beggs, J. M. (2008). The criticality hypothesis: How local cortical networks might optimize information processing. *Philosophical Transactions of the Royal Society a-Mathematical Physical and Engineering Sciences, 366*(1864), 329-343. doi:10.1098/rsta.2007.2092

Beggs, J. M., & Plenz, D. (2003). Neuronal avalanches in neocortical circuits. *Journal of Neuroscience, 23*(35), 11167-11177.

Beggs, J. M., & Timme, N. (2012). Being critical of criticality in the brain. *Frontiers in Physiology, 3*. doi:10.3389/fphys.2012.00163

Behrens, T. E. J., Johansen-Berg, H., Woolrich, M. W., Smith, S. M., Wheeler-Kingshott, C. A. M., Boulby, P. A., . . . Matthews, P. M. (2003). Non-invasive mapping of connections between human thalamus and cortex using diffusion imaging. *Nature Neuroscience, 6*(7), 750-757. doi:10.1038/nn1075

Belitski, A., Gretton, A., Magri, C., Murayama, Y., Montemurro, M. A., Logothetis, N. K., & Panzeri, S. (2008). Low-frequency local field potentials and spikes in primary visual cortex convey independent visual information. *Journal of Neuroscience, 28*(22), 5696-5709. doi:10.1523/Jneurosci.0009-08.2008

Benar, C. G., Grova, C., Jirsa, V. K., & Lina, J. M. (2019). Differences in MEG and EEG power-law scaling explained by a coupling between spatial coherence and frequency: A simulation study. *Journal of Computational Neuroscience, 47*(1), 31-41. doi:10.1007/s10827-019-00721-9

Benguigui, L., & Marinov, M. (2015). *A classification of natural and social distributions. Part one: The descriptions*. (1507.03408). arXiv.

Benwell, C. S. Y., London, R. E., Tagliabue, C. F., Veniero, D., Gross, J., Keitel, C., & Thut, G. (2019). Frequency and power of human alpha oscillations drift systematically with time-on-task. *NeuroImage, 192*, 101-114. doi:10.1016/j.neuroimage.2019.02.067

Berger, H. (1929). Über das elektrenkephalogramm des menschen. *Archiv für Psychiatrie und Nervenkrankheiten, 87*(1), 527-570. doi:10.1007/BF01797193

Besle, J., Schevon, C. A., Mehta, A. D., Lakatos, P., Goodman, R. R., McKhann, G. M., . . . Schroeder, C. E. (2011). Tuning of the human neocortex to the temporal dynamics of attended events. *Journal of Neuroscience, 31*(9), 3176-3185. doi:10.1523/JNEUROSCI.4518-10.2011

Beulen, M. A. (2011). *The role of theta oscillations in memory and decision making.* (Master thesis), University of Utrecht, Utrecht, The Netherlands.

Billig, A. J., Herrmann, B., Rhone, A. E., Gander, P. E., Nourski, K. V., Snoad, B. F., . . . Johnsrude, I. S. (2019). A sound-sensitive source of alpha oscillations in human non-primary auditory cortex. *Journal of Neuroscience, 39*(44), 8679-8689. doi:10.1523/Jneurosci.0696-19.2019

Bodenstein, G., & Praetorius, H. M. (1977). Feature extraction from electroencephalogram by adaptive segmentation. *Proceedings of the Ieee, 65*(5), 642-652. doi:Doi 10.1109/Proc.1977.10543

Bolkan, S. S., Stujenske, J. M., Parnaudeau, S., Spellman, T. J., Rauffenbart, C., Abbas, A. I., . . . Kellendonk, C. (2018). Thalamic projections sustain prefrontal activity during working memory maintenance (vol 20, pg 987, 2017). *Nature Neuroscience, 21*(8), 1138-1138. doi:10.1038/s41593-018-0132-2

Bollimunta, A., Chen, Y., Schroeder, C. E., & Ding, M. (2008). Neuronal mechanisms of cortical alpha oscillations in awake-behaving macaques. *Journal of Neuroscience, 28*(40), 9976-9988. doi:10.1523/JNEUROSCI.2699-08.2008

Bollimunta, A., Mo, J., Schroeder, C. E., & Ding, M. (2011). Neuronal mechanisms and attentional modulation of corticothalamic alpha oscillations. *Journal of Neuroscience, 31*(13), 4935-4943. doi:10.1523/JNEUROSCI.5580-10.2011

Bonnefond, M., Kastner, S., & Jensen, O. (2017). Communication between brain areas based on nested oscillations. *Eneuro, 4*(2). doi:10.1523/ENEURO.0153-16.2017

Borck, C. (2005). *Hirnströme : Eine kulturgeschichte der elektroenzephalographie*. Göttingen: Wallstein.

Borck, C., & Hentschel, A. (2018). *Brainwaves : A cultural history of electroencephalography*. London ; New York: Routledge/Taylor & Francis Group.

Borghini, G., Candini, M., Filannino, C., Hussain, M., Walsh, V., Romei, V., . . . Cappelletti, M. (2018). Alpha oscillations are causally linked to inhibitory abilities in ageing. *Journal of Neuroscience, 38*(18), 4418-4429. doi:10.1523/Jneurosci.1285-17.2018

Braitenberg, V., Schüz, A., & Braitenberg, V. (1998). *Cortex : Statistics and geometry of neuronal connectivity* (2nd thoroughly rev. ed.). Berlin ; New York: Springer.

Breakspear, M. (2017). Dynamic models of large-scale brain activity. *Nature Neuroscience, 20*(3), 340-352. doi:10.1038/nn.4497

Breakspear, M., Roberts, J. A., Terry, J. R., Rodrigues, S., Mahant, N., & Robinson, P. A. (2006). A unifying explanation of primary generalized seizures through nonlinear brain modeling and bifurcation analysis. *Cerebral Cortex, 16*(9), 1296-1313. doi:10.1093/cercor/bhj072

Breton-Provencher, V., & Sur, M. (2019). Active control of arousal by a locus coeruleus GABAergic circuit. *Nature Neuroscience, 22*(2), 218-228. doi:10.1038/s41593-018-0305-z

Brette, R. (2012). Computing with neural synchrony. *Plos Computational Biology, 8*(6). doi:10.1371/journal.pcbi.1002561

Browning, P. G. F., Chakraborty, S., & Mitchell, A. S. (2015). Evidence for mediodorsal thalamus and prefrontal cortex interactions during cognition in macaques. *Cerebral Cortex, 25*(11), 4519-4534. doi:10.1093/cercor/bhv093

Bruining, H., Hardstone, R., Juarez-Martinez, E. L., Sprengers, J., Avramiea, A. E., Simpraga, S., . . . Linkenkaer-Hansen, K. (2020). Measurement of excitation-inhibition ratio in autism spectrum disorder using critical brain dynamics. *Scientific Reports, 10*(1), 9195. doi:10.1038/s41598-020-65500-4

Bruno, R. M., & Sakmann, B. (2006). Cortex is driven by weak but synchronously active thalamocortical synapses. *Science, 312*(5780), 1622-1627. doi:10.1126/science.1124593

Bruns, A. (2004). Fourier-, hilbert- and wavelet-based signal analysis: Are they really different approaches? *Journal of Neuroscience Methods, 137*(2), 321-332. doi:10.1016/j.jneumeth.2004.03.002

Brunton, B. W., & Beyeler, M. (2019). Data-driven models in human neuroscience and neuroengineering. *Current Opinion in Neurobiology, 58*, 21-29. doi:10.1016/j.conb.2019.06.008

Brunton, B. W., Johnson, L. A., Ojemann, J. G., & Kutz, J. N. (2016). Extracting spatial-temporal coherent patterns in large-scale neural recordings using dynamic mode decomposition. *Journal of Neuroscience Methods, 258*, 1-15. doi:10.1016/j.jneumeth.2015.10.010

Buffalo, E. A., Fries, P., Landman, R., Buschman, T. J., & Desimone, R. (2011). Laminar differences in gamma and alpha coherence in the ventral stream. *Proceedings of the National Academy of Sciences of the United States of America, 108*(27), 11262-11267. doi:10.1073/pnas.1011284108

Bullmore, E. T., Long, C., Suckling, J., Fadili, J., Calvert, G., Zelaya, F., . . . Brammer, M. (2001). Colored noise and computational inference in neurophysiological (fMRI) time series analysis: Resampling methods in time and wavelet domains. *Human Brain Mapping, 12*(2), 61-78. doi:10.1002/1097-0193(200102)

Bullock, T. H. (1997). Signals and signs in the nervous system: The dynamic anatomy of electrical activity is probably information-rich. *Proceedings of the National Academy of Sciences of the United States of America, 94*(1), 1-6. doi:10.1073/pnas.94.1.1

Bullock, T. H., Mcclune, M. C., Achimowicz, J. Z., Iraguimadoz, V. J., Duckrow, R. B., & Spencer, S. S. (1995). Temporal fluctuations in coherence of brain waves. *Proceedings of the National Academy of Sciences of the United States of America, 92*(25), 11568-11572. doi:DOI 10.1073/pnas.92.25.11568

Bullock, T. H., McClune, M. C., & Enright, J. T. (2003). Are the electroencephalograms mainly rhythmic? Assessment of periodicity in wide-band time series. *Neuroscience, 121*(1), 233-252. doi:10.1016/S0306-4522(03)00208-2

Burggren, W. W., & Monticino, A. G. (2005). Assessing physiological complexity. *Journal of Experimental Biology, 208*(17), 3221-3232. doi:10.1242/jeb.01762

Burns, S. P., Xing, D. J., & Shapley, R. M. (2011). Is gamma-band activity in the Local Field Potential of V1 cortex a "clock" or filtered noise? *Journal of Neuroscience, 31*(26), 9658-9664. doi:10.1523/Jneurosci.0660-11.2011

Busch, N. A., & VanRullen, R. (2010). Spontaneous EEG oscillations reveal periodic sampling of visual attention. *Proceedings of the National Academy of Sciences of the United States of America, 107*(37), 16048-16053. doi:10.1073/pnas.1004801107

Buschman, T. J., Denovellis, E. L., Diogo, C., Bullock, D., & Miller, E. K. (2012). Synchronous oscillatory neural ensembles for rules in the prefrontal cortex. *Neuron, 76*(4), 838-846. doi:10.1016/j.neuron.2012.09.029

Buzsáki, G. (2006). *Rhythms of the brain*. Oxford ; New York: Oxford University Press.

Buzsáki, G. (2019). *The brain from inside out*. New York, NY: Oxford University Press.

Buzsáki, G., Anastassiou, C. A., & Koch, C. (2012). The origin of extracellular fields and currents--EEG, ECoG, LFP and spikes. *Nature Reviews: Neuroscience, 13*(6), 407-420. doi:10.1038/nrn3241

Buzsáki, G., & Draguhn, A. (2004). Neuronal oscillations in cortical networks. *Science, 304*(5679), 1926-1929. doi:10.1126/science.1099745

Buzsáki, G., Logothetis, N., & Singer, W. (2013). Scaling brain size, keeping timing: Evolutionary preservation of brain rhythms. *Neuron, 80*(3), 751-764. doi:10.1016/j.neuron.2013.10.002

Buzsáki, G., & Wang, X. J. (2012). Mechanisms of gamma oscillations. *Annual Review of Neuroscience, Vol 35, 35*, 203-225. doi:10.1146/annurev-neuro-062111-150444

Canolty, R. T., Ganguly, K., Kennerley, S. W., Cadieu, C. F., Koepsell, K., Wallis, J. D., & Carmena, J. M. (2010). Oscillatory phase coupling coordinates anatomically dispersed functional cell assemblies. *Proceedings of the National Academy of Sciences of the United States of America, 107*(40), 17356-17361. doi:10.1073/pnas.1008306107

Capilla, A., Schoffelen, J. M., Paterson, G., Thut, G., & Gross, J. (2014). Dissociated alpha-band modulations in the dorsal and ventral visual pathways in visuospatial attention and perception. *Cerebral Cortex, 24*(2), 550-561. doi:10.1093/cercor/bhs343

Caplan, J. B., Bottomley, M., Kang, P., & Dixon, R. A. (2015). Distinguishing rhythmic from non-rhythmic brain activity during rest in healthy neurocognitive aging. *NeuroImage, 112*, 341-352. doi:10.1016/j.neuroimage.2015.03.001

Caplan, J. B., Madsen, J. R., Raghavachari, S., & Kahana, M. J. (2001). Distinct patterns of brain oscillations underlie two basic parameters of human maze learning. *Journal of Neurophysiology, 86*(1), 368-380. doi:10.1152/jn.2001.86.1.368

Carandini, M., & Heeger, D. J. (2012). Normalization as a canonical neural computation. *Nature Reviews Neuroscience, 13*(1), 51-62. doi:10.1038/nrn3136

Carter, M. E., Yizhar, O., Chikahisa, S., Nguyen, H., Adamantidis, A., Nishino, S., . . . de Lecea, L. (2010). Tuning arousal with optogenetic modulation of locus coeruleus neurons. *Nature Neuroscience, 13*(12), 1526-1533. doi:10.1038/nn.2682

Castro-Alamancos, M. A. (2004). Dynamics of sensory thalamocortical synaptic networks during information processing states. *Progress in Neurobiology, 74*(4), 213-247. doi:10.1016/j.pneurobio.2004.09.002

Castro-Alamancos, M. A. (2009). Cortical up and activated states: Implications for sensory information processing. *Neuroscientist, 15*(6), 625-634. doi:10.1177/1073858409333074

Cavanagh, J. F., & Frank, M. J. (2014). Frontal theta as a mechanism for cognitive control. *Trends in Cognitive Sciences, 18*(8), 414-421. doi:10.1016/j.tics.2014.04.012

Chandran, K. S. S., Mishra, A., Shirhatti, V., & Ray, S. (2016). Comparison of matching pursuit algorithm with other signal processing techniques for computation of the time-frequency power spectrum of brain signals. *Journal of Neuroscience, 36*(12), 3399-3408. doi:10.1523/Jneurosci.3633-15.2016

Chatila, M., Milleret, C., Rougeul, A., & Buser, P. (1993). Alpha-rhythm in the cat thalamus. *Comptes Rendus De L Academie Des Sciences Serie Iii-Sciences De La Vie-Life Sciences, 316*(1), 51-58.

Chaudhuri, R., He, B. J., & Wang, X. J. (2018). Random recurrent networks near criticality capture the broadband power distribution of human ECoG dynamics. *Cerebral Cortex, 28*(10), 3610-3622. doi:10.1093/cercor/bhx233

Choudhury, S., Fishman, J. R., McGowan, M. L., & Juengst, E. T. (2014). Big data, open science and the brain: Lessons learned from genomics. *Frontiers in Human Neuroscience, 8*. doi:10.3389/fnhum.2014.00239

Churchill, N. W., Spring, R., Grady, C., Cimprich, B., Askren, M. K., Reuter-Lorenz, P. A., . . . Berman, M. G. (2016). The suppression of scale-free fMRI brain dynamics across three different sources of effort: Aging, task novelty and task difficulty. *Scientific Reports, 6*, 30895. doi:10.1038/srep30895

Ciuciu, P., Varoquaux, G., Abry, P., Sadaghiani, S., & Kleinschmidt, A. (2012). Scale-free and multifractal time dynamics of fMRI signals during rest and task. *Frontiers in Physiology, 3*. doi:10.3389/fphys.2012.00186

Cocchi, L., Gollo, L. L., Zalesky, A., & Breakspear, M. (2017). Criticality in the brain: A synthesis of neurobiology, models and cognition. *Progress in Neurobiology, 158*, 132-152. doi:10.1016/j.pneurobio.2017.07.002

Cocchi, L., Zalesky, A., Fornito, A., & Mattingley, J. B. (2013). Dynamic cooperation and competition between brain systems during cognitive control. *Trends in Cognitive Sciences, 17*(10), 493-501. doi:10.1016/j.tics.2013.08.006

Cohen, M. R., & Maunsell, J. H. (2009). Attention improves performance primarily by reducing interneuronal correlations. *Nature Neuroscience, 12*(12), 1594-1600. doi:10.1038/nn.2439

Cohen, M. X. (2014). *Analyzing neural time series data : Theory and practice*. Cambridge, Massachusetts: The MIT Press.

Cohen, M. X. (2019). A better way to define and describe Morlet wavelets for time-frequency analysis. *NeuroImage, 199*, 81-86. doi:10.1016/j.neuroimage.2019.05.048

Cohen, M. X., & Donner, T. H. (2013). Midfrontal conflict-related theta-band power reflects neural oscillations that predict behavior. *Journal of Neurophysiology, 110*(12), 2752-2763. doi:10.1152/jn.00479.2013

Cole, S. R., van der Meij, R., Peterson, E. J., de Hemptinne, C., Starr, P. A., & Voytek, B. (2017). Nonsinusoidal beta oscillations reflect cortical pathophysiology in Parkinson's Disease. *Journal of Neuroscience, 37*(18), 4830-4840. doi:10.1523/Jneurosci.2208-16.2017

Cole, S. R., & Voytek, B. (2017). Brain oscillations and the importance of waveform shape. *Trends in Cognitive Sciences, 21*(2), 137-149. doi:10.1016/j.tics.2016.12.008

Cole, S. R., & Voytek, B. (2019). Cycle-by-cycle analysis of neural oscillations. *Journal of Neurophysiology, 122*(2), 849-861. doi:10.1152/jn.00273.2019
Colombo, M. A., Napolitani, M., Boly, M., Gosseries, O., Casarotto, S., Rosanova, M., . . . Sarasso, S. (2019). The spectral exponent of the resting EEG indexes the presence of consciousness during unresponsiveness induced by propofol, xenon, and ketamine. *NeuroImage, 189*, 631-644. doi:10.1016/j.neuroimage.2019.01.024
Constantinople, C. M., & Bruno, R. M. (2011). Effects and mechanisms of wakefulness on local cortical networks. *Neuron, 69*(6), 1061-1068. doi:10.1016/j.neuron.2011.02.040
Contreras, D., Destexhe, A., Sejnowski, T. J., & Steriade, M. (1996). Control of spatiotemporal coherence of a thalamic oscillation by corticothalamic feedback. *Science, 274*(5288), 771-774. doi:10.1126/science.274.5288.771
Coon, W. G., Gunduz, A., Brunner, P., Ritaccio, A. L., Pesaran, B., & Schalk, G. (2016). Oscillatory phase modulates the timing of neuronal activations and resulting behavior. *NeuroImage, 133*, 294-301. doi:10.1016/j.neuroimage.2016.02.080
Cortes, N., & van Vreeswijk, C. (2015). Pulvinar thalamic nucleus allows for asynchronous spike propagation through the cortex. *Frontiers in Computational Neuroscience, 9*. doi:10.3389/fncom.2015.00060
Costa, M., Goldberger, A. L., & Peng, C. K. (2002). Multiscale entropy analysis of complex physiologic time series. *Physical Review Letters, 89*(6). doi:10.1103/PhysRevLett.89.068102
Costa, M., Goldberger, A. L., & Peng, C. K. (2005). Multiscale entropy analysis of biological signals. *Physical Review E, 71*(2). doi:10.1103/PhysRevE.71.021906
Courtiol, J., Perdikis, D., Petkoski, S., Muller, V., Huys, R., Sleimen-Malkoun, R., & Jirsa, V. K. (2016). The multiscale entropy: Guidelines for use and interpretation in brain signal analysis. *Journal of Neuroscience Methods, 273*, 175-190. doi:10.1016/j.jneumeth.2016.09.004
Crandall, S. R., Cruikshank, S. J., & Connors, B. W. (2015). A corticothalamic switch: Controlling the thalamus with dynamic synapses. *Neuron, 86*(3), 768-782. doi:10.1016/j.neuron.2015.03.040
Crane, L., Goddard, L., & Pring, L. (2009). Sensory processing in adults with autism spectrum disorders. *Autism, 13*(3), 215-228. doi:10.1177/1362361309103794
Crick, F. (2003). Function of the thalamic reticular complex: The searchlight hypothesis. *Essential Sources in the Scientific Study of Consciousness*, 263-272.
Crouzet, S. M., & VanRullen, R. (2017). The rhythm of attentional stimulus selection during visual competition. *bioRxiv*.
Cruikshank, S. J., Ahmed, O. J., Stevens, T. R., Patrick, S. L., Gonzalez, A. N., Elmaleh, M., & Connors, B. W. (2012). Thalamic control of layer 1 circuits in prefrontal cortex. *Journal of Neuroscience, 32*(49), 17813-17823. doi:10.1523/Jneurosci.3231-12.2012
Crunelli, V., Lorincz, M. L., Connelly, W. M., David, F., Hughes, S. W., Lambert, R. C., . . . Errington, A. C. (2018). Dual function of thalamic low-vigilance state oscillations: Rhythm-regulation and plasticity. *Nature Reviews Neuroscience, 19*(2), 106-118. doi:10.1038/nrn.2017.151
Csercsa, R., Dombovari, B., Fabo, D., Wittner, L., Eross, L., Entz, L., . . . Ulbert, I. (2010). Laminar analysis of slow wave activity in humans. *Brain, 133*, 2814-2829. doi:10.1093/brain/awq169
Cui, Y., Liu, L. D., McFarland, J. M., Pack, C. C., & Butts, D. A. (2016). Inferring cortical variability from local field potentials. *Journal of Neuroscience, 36*(14), 4121-4135. doi:10.1523/JNEUROSCI.2502-15.2016
Curto, C., Sakata, S., Marguet, S., Itskov, V., & Harris, K. D. (2009). A simple model of cortical dynamics explains variability and state dependence of sensory responses in urethane-anesthetized auditory cortex. *Journal of Neuroscience, 29*(34), 10600-10612. doi:10.1523/JNEUROSCI.2053-09.2009
Dahl, M. J., Mather, M., Sander, M. C., & Werkle-Bergner, M. (2020). Noradrenergic responsiveness supports selective attention across the adult lifespan. *Journal of Neuroscience, 40*(22), 4372-4390. doi:10.1523/JNEUROSCI.0398-19.2020
Dajani, D. R., & Uddin, L. Q. (2015). Demystifying cognitive flexibility: Implications for clinical and developmental neuroscience. *Trends in Neurosciences, 38*(9), 571-578. doi:10.1016/j.tins.2015.07.003
Danziger, S., Ward, R., Owen, V., & Rafal, R. (2004). Contributions of the human pulvinar to linking vision and action. *Cognitive Affective & Behavioral Neuroscience, 4*(1), 89-99. doi:10.3758/Cabn.4.1.89
Dave, S., Brothers, T. A., & Swaab, T. Y. (2018). 1/f neural noise and electrophysiological indices of contextual prediction in aging. *Brain Research, 1691*, 34-43. doi:10.1016/j.brainres.2018.04.007
Dayan, P., & Abbott, L. F. (2001). *Theoretical neuroscience : Computational and mathematical modeling of neural systems*. Cambridge, Mass.: Massachusetts Institute of Technology Press.
de Arcangelis, L., Perrone-Capano, C., & Herrmann, H. J. (2006). Self-organized criticality model for brain plasticity. *Physical Review Letters, 96*(2). doi:10.1103/PhysRevLett.96.028107
de Cheveigne, A., & Arzounian, D. (2015). Scanning for oscillations. *J Neural Eng, 12*(6), 066020. doi:10.1088/1741-2560/12/6/066020

de Cheveigne, A., & Parra, L. C. (2014). Joint decorrelation, a versatile tool for multichannel data analysis. *NeuroImage, 98*, 487-505. doi:10.1016/j.neuroimage.2014.05.068
de Gee, J. W., Colizoli, O., Kloosterman, N. A., Knapen, T., Nieuwenhuis, S., & Donner, T. H. (2017). Dynamic modulation of decision biases by brainstem arousal systems. *Elife, 6*. doi:10.7554/eLife.23232
De Los Rios, P., & Zhang, Y. C. (1999). Universal 1/f noise from dissipative self-organized criticality models. *Physical Review Letters, 82*(3), 472-475. doi:10.1103/PhysRevLett.82.472
de Manzano, O., Cervenka, S., Karabanov, A., Farde, L., & Ullen, F. (2010). Thinking outside a less intact box: Thalamic dopamine D2 receptor densities are negatively related to psychometric creativity in healthy individuals. *PloS One, 5*(5), e10670. doi:10.1371/journal.pone.0010670
de Munck, J. C., Goncalves, S. I., Huijboom, L., Kuijer, J. P., Pouwels, P. J., Heethaar, R. M., & Lopes da Silva, F. H. (2007). The hemodynamic response of the alpha rhythm: An EEG/fMRI study. *NeuroImage, 35*(3), 1142-1151. doi:10.1016/j.neuroimage.2007.01.022
de Pesters, A., Coon, W. G., Brunner, P., Gunduz, A., Ritaccio, A. L., Brunet, N. M., . . . Schalk, G. (2016). Alpha power indexes task-related networks on large and small scales: A multimodal ECoG study in humans and a non-human primate. *NeuroImage, 134*, 122-131. doi:10.1016/j.neuroimage.2016.03.074
Deco, G., & Jirsa, V. K. (2012). Ongoing cortical activity at rest: Criticality, multistability, and ghost attractors. *Journal of Neuroscience, 32*(10), 3366-3375. doi:10.1523/Jneurosci.2523-11.2012
Deco, G., Jirsa, V. K., & McIntosh, A. R. (2013). Resting brains never rest: Computational insights into potential cognitive architectures. *Trends in Neurosciences, 36*(5), 268-274. doi:10.1016/j.tins.2013.03.001
Deco, G., & Kringelbach, M. (2016). Metastability and coherence: Extending the communication through coherence hypothesis using a whole-brain computational perspective (vol 39, pg 125, 2016). *Trends in Neurosciences, 39*(6), 432-432. doi:10.1016/j.tins.2016.04.006
Deco, G., Ponce-Alvarez, A., Hagmann, P., Romani, G. L., Mantini, D., & Corbetta, M. (2014). How local excitation-inhibition ratio impacts the whole brain dynamics. *Journal of Neuroscience, 34*(23), 7886-7898. doi:10.1523/Jneurosci.5068-13.2014
Deco, G., Rolls, E. T., & Romo, R. (2009). Stochastic dynamics as a principle of brain function. *Progress in Neurobiology, 88*(1), 1-16. doi:10.1016/j.pneurobio.2009.01.006
Dehghani, N., Bedard, C., Cash, S. S., Halgren, E., & Destexhe, A. (2010). Comparative power spectral analysis of simultaneous elecroencephalographic and magnetoencephalographic recordings in humans suggests non-resistive extracellular media. *Journal of Computational Neuroscience, 29*(3), 405-421. doi:10.1007/s10827-010-0263-2
Dehghani, N., Hatsopoulos, N. G., Haga, Z. D., Parker, R. A., Greger, B., Halgren, E., . . . Destexhe, A. (2012). Avalanche analysis from multielectrode ensemble recordings in cat, monkey, and human cerebral cortex during wakefulness and sleep. *Frontiers in Physiology, 3*. doi:10.3389/fphys.2012.00302
Dehghani, N., Peyrache, A., Telenczuk, B., Le Van Quyen, M., Halgren, E., Cash, S. S., . . . Destexhe, A. (2016). Dynamic balance of excitation and inhibition in human and monkey neocortex. *Scientific Reports, 6*, 23176. doi:10.1038/srep23176
Dehghani, N., & Wimmer, R. D. (2019). A computational perspective of the role of the thalamus in cognition. *Neural Computation, 31*(7), 1380-1418. doi:10.1162/neco_a_01197
Delevich, K., Tucciarone, J., Huang, Z. J., & Li, B. (2015). The mediodorsal thalamus drives feedforward inhibition in the anterior cingulate cortex via parvalbumin interneurons. *Journal of Neuroscience, 35*(14), 5743-5753. doi:10.1523/Jneurosci.4565-14.2015
Demanuele, C., James, C. J., & Sonuga-Barke, E. J. S. (2007). Distinguishing low frequency oscillations within the 1/f spectral behaviour of electromagnetic brain signals. *Behavioral and Brain Functions, 3*. doi:10.1186/1744-9081-3-62
Deneve, S., & Machens, C. K. (2016). Efficient codes and balanced networks. *Nature Neuroscience, 19*(3), 375-382. doi:10.1038/nn.4243
Destexhe, A., Mccormick, D. A., & Sejnowski, T. J. (1993). A model for 8-10 hz spindling in interconnected thalamic relay and reticularis neurons. *Biophysical Journal, 65*(6), 2473-2477. doi:10.1016/S0006-3495(93)81297-9
Destexhe, A., & Rudolph, M. (2004). Extracting information from the power spectrum of synaptic noise. *Journal of Computational Neuroscience, 17*(3), 327-345. doi:Doi 10.1023/B:Jcns.0000044875.90630.88
Destexhe, A., Rudolph, M., & Pare, D. (2003). The high-conductance state of neocortical neurons in vivo. *Nature Reviews: Neuroscience, 4*(9), 739-751. doi:10.1038/nrn1198
Dietsch, G. (1932). Fourier-analyse von elektrencephalogrammen des menschen. *Pflüger's Archiv für die gesamte Physiologie des Menschen und der Tiere, 230*(1), 106-112. doi:10.1007/BF01751972
DiFrancesco, M. W., Holland, S. K., & Szaflarski, J. P. (2008). Simultaneous EEG/functional magnetic resonance imaging at 4 tesla: Correlates of brain activity to spontaneous alpha rhythm during relaxation. *Journal of Clinical Neurophysiology, 25*(5), 255-264. doi:10.1097/WNP.0b013e3181879d56

Dinstein, I., Heeger, D. J., & Behrmann, M. (2015). Neural variability: Friend or foe? *Trends in Cognitive Sciences, 19*(6), 322-328. doi:10.1016/j.tics.2015.04.005
Doiron, B., Litwin-Kumar, A., Rosenbaum, R., Ocker, G. K., & Josic, K. (2016). The mechanics of state-dependent neural correlations. *Nature Neuroscience, 19*(3), 383-393. doi:10.1038/nn.4242
Donoghue, T., Dominguez, J., & Voytek, B. (2020). Electrophysiological frequency band ratio measures conflate periodic and aperiodic neural activity. *bioRxiv*.
Doyle, J. A., Toussaint, P.-J., & Evans, A. C. (2019). Amplifying the neural power spectrum. *bioRxiv*.
Dringenberg, H. C., & Olmstead, M. C. (2003). Integrated contributions of basal forebrain and thalamus to neocortical activation elicited by pedunculopontine tegmental stimulation in urethane-anesthetized rats. *Neuroscience, 119*(3), 839-853. doi:10.1016/S0306-4522(03)00197-0
Drover, J. D., Schiff, N. D., & Victor, J. D. (2010). Dynamics of coupled thalamocortical modules. *Journal of Computational Neuroscience, 28*(3), 605-616. doi:10.1007/s10827-010-0244-5
Dugue, L., Marque, P., & VanRullen, R. (2011). The phase of ongoing oscillations mediates the causal relation between brain excitation and visual perception. *Journal of Neuroscience, 31*(33), 11889-11893. doi:10.1523/JNEUROSCI.1161-11.2011
Ecker, A. S., Berens, P., Keliris, G. A., Bethge, M., Logothetis, N. K., & Tolias, A. S. (2010). Decorrelated neuronal firing in cortical microcircuits. *Science, 327*(5965), 584-587. doi:10.1126/science.1179867
Einevoll, G. T., Kayser, C., Logothetis, N. K., & Panzeri, S. (2013). Modelling and analysis of local field potentials for studying the function of cortical circuits. *Nature Reviews Neuroscience, 14*(11), 770-785. doi:10.1038/nrn3599
El Boustani, S., Marre, O., Behuret, S., Baudot, P., Yger, P., Bal, T., . . . Fregnac, Y. (2009). Network-state modulation of power-law frequency-scaling in visual cortical neurons. *Plos Computational Biology, 5*(9). doi:10.1371/journal.pcbi.1000519
Engel, A. K., & Fries, P. (2010). Beta-band oscillations - signalling the status quo? *Current Opinion in Neurobiology, 20*(2), 156-165. doi:10.1016/j.conb.2010.02.015
Engel, A. K., Fries, P., & Singer, W. (2001). Dynamic predictions: Oscillations and synchrony in top-down processing. *Nature Reviews Neuroscience, 2*(10), 704-716. doi:10.1038/35094565
Ermentrout, G. B., Galan, R. F., & Urban, N. N. (2008). Reliability, synchrony and noise. *Trends in Neurosciences, 31*(8), 428-434. doi:10.1016/j.tins.2008.06.002
Fagerholm, E. D., Lorenz, R., Scott, G., Dinov, M., Hellyer, P. J., Mirzaei, N., . . . Leech, R. (2015). Cascades and cognitive state: Focused attention incurs subcritical dynamics. *Journal of Neuroscience, 35*(11), 4626-4634. doi:10.1523/JNEUROSCI.3694-14.2015
Faisal, A. A., Selen, L. P., & Wolpert, D. M. (2008). Noise in the nervous system. *Nature Reviews: Neuroscience, 9*(4), 292-303. doi:10.1038/nrn2258
Fama, R., & Sullivan, E. V. (2015). Thalamic structures and associated cognitive functions: Relations with age and aging. *Neuroscience and Biobehavioral Reviews, 54*, 29-37. doi:10.1016/j.neubiorev.2015.03.008
Feige, B., Scheffler, K., Esposito, F., Di Salle, F., Hennig, J., & Seifritz, E. (2005). Cortical and subcortical correlates of electroencephalographic alpha rhythm modulation. *Journal of Neurophysiology, 93*(5), 2864-2872. doi:10.1152/jn.00721.2004
Feingold, J., Gibson, D. J., DePasquale, B., & Graybiel, A. M. (2015). Bursts of beta oscillation differentiate postperformance activity in the striatum and motor cortex of monkeys performing movement tasks. *Proceedings of the National Academy of Sciences of the United States of America, 112*(44), 13687-13692. doi:10.1073/pnas.1517629112
Fell, J., & Axmacher, N. (2011). The role of phase synchronization in memory processes. *Nature Reviews: Neuroscience, 12*(2), 105-118. doi:10.1038/nrn2979
Fellner, M. C., Gollwitzer, S., Rampp, S., Kreiselmeyr, G., Bush, D., Diehl, B., . . . Hanslmayr, S. (2019). Spectral fingerprints or spectral tilt? Evidence for distinct oscillatory signatures of memory formation. *PLoS Biology, 17*(7), e3000403. doi:10.1371/journal.pbio.3000403
Fellner, M. C., Volberg, G., Mullinger, K. J., Goldhacker, M., Wimber, M., Greenlee, M. W., & Hanslmayr, S. (2016). Spurious correlations in simultaneous EEG-fMRI driven by in-scanner movement. *NeuroImage, 133*, 354-366. doi:10.1016/j.neuroimage.2016.03.031
Ferguson, K. A., & Cardin, J. A. (2020). Mechanisms underlying gain modulation in the cortex. *Nature Reviews: Neuroscience, 21*(2), 80-92. doi:10.1038/s41583-019-0253-y
Fiebelkorn, I. C., & Kastner, S. (2019). A rhythmic theory of attention. *Trends in Cognitive Sciences, 23*(2), 87-101. doi:10.1016/j.tics.2018.11.009
Fiebelkorn, I. C., Pinsk, M. A., & Kastner, S. (2018). A dynamic interplay within the frontoparietal network underlies rhythmic spatial attention. *Neuron, 99*(4), 842-853. doi:10.1016/j.neuron.2018.07.038

Fiebelkorn, I. C., Pinsk, M. A., & Kastner, S. (2019). The mediodorsal pulvinar coordinates the macaque fronto-parietal network during rhythmic spatial attention. *Nat Commun, 10*(1), 215. doi:10.1038/s41467-018-08151-4

Fiebelkorn, I. C., Saalmann, Y. B., & Kastner, S. (2013). Rhythmic sampling within and between objects despite sustained attention at a cued location. *Current Biology, 23*(24), 2553-2558. doi:10.1016/j.cub.2013.10.063

Foster, J. J., Sutterer, D. W., Serences, J. T., Vogel, E. K., & Awh, E. (2017). Alpha-band oscillations enable spatially and temporally resolved tracking of covert spatial attention. *Psychological Science, 28*(7), 929-941. doi:10.1177/0956797617699167

Foxe, J. J., & Snyder, A. C. (2011). The role of alpha-band brain oscillations as a sensory suppression mechanism during selective attention. *Frontiers in Psychology, 2*, 154. doi:10.3389/fpsyg.2011.00154

Fransen, A. M. M., van Ede, F., & Maris, E. (2015). Identifying neuronal oscillations using rhythmicity. *NeuroImage, 118*, 256-267. doi:10.1016/j.neuroimage.2015.06.003

Freeman, W. J., & Zhai, J. (2009). Simulated power spectral density (PSD) of background electrocorticogram (ECoG). *Cognitive Neurodynamics, 3*(1), 97-103. doi:10.1007/s11571-008-9064-y

Freyer, F., Aquino, K., Robinson, P. A., Ritter, P., & Breakspear, M. (2009). Bistability and non-gaussian fluctuations in spontaneous cortical activity. *Journal of Neuroscience, 29*(26), 8512-8524. doi:10.1523/Jneurosci.0754-09.2009

Freyer, F., Roberts, J. A., Becker, R., Robinson, P. A., Ritter, P., & Breakspear, M. (2011). Biophysical mechanisms of multistability in resting-state cortical rhythms. *Journal of Neuroscience, 31*(17), 6353-6361. doi:10.1523/Jneurosci.6693-10.2011

Freyer, F., Roberts, J. A., Ritter, P., & Breakspear, M. (2012). A canonical model of multistability and scale-invariance in biological systems. *Plos Computational Biology, 8*(8). doi:10.1371/journal.pcbi.1002634

Fries, P. (2005). A mechanism for cognitive dynamics: Neuronal communication through neuronal coherence. *Trends in Cognitive Sciences, 9*(10), 474-480. doi:10.1016/j.tics.2005.08.011

Fries, P. (2009). Neuronal gamma-band synchronization as a fundamental process in cortical computation. *Annual Review of Neuroscience, 32*, 209-224. doi:10.1146/annurev.neuro.051508.135603

Fries, P. (2015). Rhythms for cognition: Communication through coherence. *Neuron, 88*(1), 220-235. doi:10.1016/j.neuron.2015.09.034

Fries, P., Reynolds, J. H., Rorie, A. E., & Desimone, R. (2001). Modulation of oscillatory neuronal synchronization by selective visual attention. *Science, 291*(5508), 1560-1563. doi:10.1126/science.1055465

Friston, K. J., Breakspear, M., & Deco, G. (2012). Perception and self-organized instability. *Frontiers in Computational Neuroscience, 6*. doi:10.3389/fncom.2012.00044

Froemke, R. C. (2015). Plasticity of cortical excitatory-inhibitory balance. *Annual Review of Neuroscience, 38*, 195-219. doi:10.1146/annurev-neuro-071714-034002

Furman, A. J., Meeker, T. J., Rietschel, J. C., Yoo, S., Muthulingam, J., Prokhorenko, M., . . . Seminowicz, D. A. (2018). Cerebral peak alpha frequency predicts individual differences in pain sensitivity. *NeuroImage, 167*, 203-210. doi:10.1016/j.neuroimage.2017.11.042

Galan, R. F., Fourcaud-Trocme, N., Ermentrout, G. B., & Urban, N. N. (2006). Correlation-induced synchronization of oscillations in olfactory bulb neurons. *Journal of Neuroscience, 26*(14), 3646-3655. doi:10.1523/Jneurosci.4605-05.2006

Gao, R. (2016). Interpreting the electrophysiological power spectrum. *Journal of Neurophysiology, 115*(2), 628-630. doi:10.1152/jn.00722.2015

Gao, R., & Penzes, P. (2015). Common mechanisms of excitatory and inhibitory imbalance in schizophrenia and autism spectrum disorders. *Current Molecular Medicine, 15*(2), 146-167. doi:10.2174/1566524015666150303003028

Gao, R., Peterson, E. J., & Voytek, B. (2017). Inferring synaptic excitation/inhibition balance from field potentials. *NeuroImage, 158*, 70-78. doi:10.1016/j.neuroimage.2017.06.078

Gao, R., van den Brink, R. L., Pfeffer, T., & Voytek, B. (2020). Neuronal timescales are functionally dynamic and shaped by cortical microarchitecture. *bioRxiv*.

Garcia-Cabezas, M. A., Martinez-Sanchez, P., Sanchez-Gonzalez, M. A., Garzon, M., & Cavada, C. (2009). Dopamine innervation in the thalamus: Monkey versus rat. *Cerebral Cortex, 19*(2), 424-434. doi:10.1093/cercor/bhn093

Garrett, D. D., Epp, S. M., Perry, A., & Lindenberger, U. (2018). Local temporal variability reflects functional integration in the human brain. *NeuroImage, 183*, 776-787. doi:10.1016/j.neuroimage.2018.08.019

Garrett, D. D., McIntosh, A. R., & Grady, C. L. (2011). Moment-to-moment signal variability in the human brain can inform models of stochastic facilitation now. *Nature Reviews: Neuroscience, 12*(10), 612; author reply 612. doi:10.1038/nrn3061-c1

Garrett, D. D., Nagel, I. E., Preuschhof, C., Burzynska, A. Z., Marchner, J., Wiegert, S., . . . Lindenberger, U. (2015). Amphetamine modulates brain signal variability and working memory in younger and older adults. *Proceedings of the National Academy of Sciences of the United States of America, 112*(24), 7593-7598. doi:10.1073/pnas.1504090112

Garrett, D. D., Samanez-Larkin, G. R., MacDonald, S. W., Lindenberger, U., McIntosh, A. R., & Grady, C. L. (2013a). Moment-to-moment brain signal variability: A next frontier in human brain mapping? *Neurosci Biobehav Rev, 37*(4), 610-624. doi:10.1016/j.neubiorev.2013.02.015

Garrett, D. D., Samanez-Larkin, G. R., MacDonald, S. W. S., Lindenberger, U., McIntosh, A. R., & Grady, C. L. (2013b). Moment-to-moment brain signal variability: A next frontier in human brain mapping? *Neuroscience and Biobehavioral Reviews, 37*(4), 610-624. doi:10.1016/j.neubiorev.2013.02.015

Ghosh, A., Rho, Y., McIntosh, A. R., Kotter, R., & Jirsa, V. K. (2008). Noise during rest enables the exploration of the brain's dynamic repertoire. *PLoS Computational Biology, 4*(10), e1000196. doi:10.1371/journal.pcbi.1000196

Gireesh, E. D., & Plenz, D. (2008). Neuronal avalanches organize as nested theta- and beta/gamma-oscillations during development of cortical layer 2/3. *Proceedings of the National Academy of Sciences of the United States of America, 105*(21), 7576-7581. doi:10.1073/pnas.0800537105

Glass, L., & Kaplan, D. (1993). Time-series analysis of complex dynamics in physiology and medicine. *Medical Progress Through Technology, 19*(3), 115-128.

Goldman, R. I., Stern, J. M., Engel, J., & Cohen, M. S. (2002). Simultaneous EEG and fMRI of the alpha rhythm. *Neuroreport, 13*(18), 2487-2492. doi:10.1097/00001756-200212200-00022

Golomb, D., Wang, X. J., & Rinzel, J. (1994). Synchronization properties of spindle oscillations in a thalamic reticular nucleus model (vol 72, pg 1109, 1994). *Journal of Neurophysiology, 72*(6), U26-U26.

Goris, R. L., Movshon, J. A., & Simoncelli, E. P. (2014). Partitioning neuronal variability. *Nature Neuroscience, 17*(6), 858-865. doi:10.1038/nn.3711

Grandy, T. H., Garrett, D. D., Schmiedek, F., & Werkle-Bergner, M. (2016). On the estimation of brain signal entropy from sparse neuroimaging data. *Scientific Reports, 6*, 23073. doi:10.1038/srep23073

Grandy, T. H., Werkle-Bergner, M., Chicherio, C., Lovden, M., Schmiedek, F., & Lindenberger, U. (2013). Individual alpha peak frequency is related to latent factors of general cognitive abilities. *NeuroImage, 79*, 10-18. doi:10.1016/j.neuroimage.2013.04.059

Grandy, T. H., Werkle-Bergner, M., Chicherio, C., Schmiedek, F., Lovden, M., & Lindenberger, U. (2013). Peak individual alpha frequency qualifies as a stable neurophysiological trait marker in healthy younger and older adults. *Psychophysiology, 50*(6), 570-582. doi:10.1111/psyp.12043

Gray, M. J., & Emmanouil, T. A. (2020). Individual alpha frequency increases during a task but is unchanged by alpha-band flicker. *Psychophysiology, 57*(2). doi:10.1111/psyp.13480

Gregoriou, G. G., Gotts, S. J., Zhou, H. H., & Desimone, R. (2009). High-frequency, long-range coupling between prefrontal and visual cortex during attention. *Science, 324*(5931), 1207-1210. doi:10.1126/science.1171402

Grieve, K. L., Acuna, C., & Cudeiro, J. (2000). The primate pulvinar nuclei: Vision and action. *Trends in Neurosciences, 23*(1), 35-39. doi:10.1016/S0166-2236(99)01482-4

Griffiths, B. J., Mayhew, S. D., Mullinger, K. J., Jorge, J., Charest, I., Wimber, M., & Hanslmayr, S. (2019). Alpha/beta power decreases track the fidelity of stimulus-specific information. *Elife, 8*. doi:10.7554/eLife.49562

Gross, J. (2014). Analytical methods and experimental approaches for electrophysiological studies of brain oscillations. *Journal of Neuroscience Methods, 228*, 57-66. doi:10.1016/j.jneumeth.2014.03.007

Gross, J., Timmermann, J., Kujala, J., Dirks, M., Schmitz, F., Salmelin, R., & Schnitzler, A. (2002). The neural basis of intermittent motor control in humans. *Proceedings of the National Academy of Sciences of the United States of America, 99*(4), 2299-2302. doi:10.1073/pnas.032682099

Gulbinaite, R., van Viegen, T., Wieling, M., Cohen, M. X., & VanRullen, R. (2017). Individual alpha peak frequency predicts 10 hz flicker effects on selective attention. *Journal of Neuroscience, 37*(42), 10173-10184. doi:10.1523/Jneurosci.1163-17.2017

Haegens, S., Barczak, A., Musacchia, G., Lipton, M. L., Mehta, A. D., Lakatos, P., & Schroeder, C. E. (2015). Laminar profile and physiology of the alpha rhythm in primary visual, auditory, and somatosensory regions of neocortex. *Journal of Neuroscience, 35*(42), 14341-14352. doi:10.1523/JNEUROSCI.0600-15.2015

Haegens, S., Cousijn, H., Wallis, G., Harrison, P. J., & Nobre, A. C. (2014). Inter- and intra-individual variability in alpha peak frequency. *NeuroImage, 92*, 46-55. doi:10.1016/j.neuroimage.2014.01.049

Haegens, S., Nacher, V., Luna, R., Romo, R., & Jensen, O. (2011). alpha-Oscillations in the monkey sensorimotor network influence discrimination performance by rhythmical inhibition of neuronal

spiking. *Proceedings of the National Academy of Sciences of the United States of America, 108*(48), 19377-19382. doi:10.1073/pnas.1117190108
Hagemann, D., Hewig, J., Walter, C., & Naumann, E. (2008). Skull thickness and magnitude of EEG alpha activity. *Clinical Neurophysiology, 119*(6), 1271-1280. doi:10.1016/j.clinph.2008.02.010
Haider, B., Schulz, D. P., Hausser, M., & Carandini, M. (2016). Millisecond coupling of local field potentials to synaptic currents in the awake visual cortex. *Neuron, 90*(1), 35-42. doi:10.1016/j.neuron.2016.02.034
Halassa, M. M., & Kastner, S. (2017). Thalamic functions in distributed cognitive control. *Nature Neuroscience, 20*(12), 1669-1679. doi:10.1038/s41593-017-0020-1
Halassa, M. M., & Sherman, S. M. (2019). Thalamocortical circuit motifs: A general framework. *Neuron, 103*(5), 762-770. doi:10.1016/j.neuron.2019.06.005
Halgren, E., Kaestner, E., Marinkovic, K., Cash, S. S., Wang, C., Schomer, D. L., . . . Ulbert, I. (2015). Laminar profile of spontaneous and evoked theta: Rhythmic modulation of cortical processing during word integration. *Neuropsychologia, 76*, 108-124. doi:10.1016/j.neuropsychologia.2015.03.021
Halgren, M., Fabo, D., Ulbert, I., Madsen, J. R., Eross, L., Doyle, W. K., . . . Halgren, E. (2018). Superficial slow rhythms integrate cortical processing in humans. *Scientific Reports, 8*(1), 2055. doi:10.1038/s41598-018-20662-0
Halgren, M., Ulbert, I., Bastuji, H., Fabo, D., Eross, L., Rey, M., . . . Cash, S. S. (2019). The generation and propagation of the human alpha rhythm. *Proceedings of the National Academy of Sciences of the United States of America, 116*(47), 23772-23782. doi:10.1073/pnas.1913092116
Haller, M., Donoghue, T., Peterson, E., Varma, P., Sebastian, P., Gao, R., . . . Voytek, B. (2018). Parameterizing neural power spectra. *bioRxiv*.
Hansen, B. J., Chelaru, M. I., & Dragoi, V. (2012). Correlated variability in laminar cortical circuits. *Neuron, 76*(3), 590-602. doi:10.1016/j.neuron.2012.08.029
Hanslmayr, S., Staudigl, T., & Fellner, M. C. (2012). Oscillatory power decreases and long-term memory: The information via desynchronization hypothesis. *Frontiers in Human Neuroscience, 6*, 74. doi:10.3389/fnhum.2012.00074
Hari, R., & Puce, A. (2017). *MEG-EEG primer*: Oxford University Press.
Harris, J. A., Mihalas, S., Hirokawa, K. E., Whitesell, J. D., Choi, H., Bernard, A., . . . Zeng, H. K. (2019). Hierarchical organization of cortical and thalamic connectivity. *Nature, 575*(7781), 195-202. doi:10.1038/s41586-019-1716-z
Harris, K. D., & Thiele, A. (2011). Cortical state and attention. *Nature Reviews Neuroscience, 12*(9), 509-523. doi:10.1038/nrn3084
Hartings, J. A., Temereanca, S., & Simons, D. J. (2003). State-dependent processing of sensory stimuli by thalamic reticular neurons. *Journal of Neuroscience, 23*(12), 5264-5271.
Hasenstaub, A., Shu, Y. S., Haider, B., Kraushaar, U., Duque, A., & McCormick, D. A. (2005). Inhibitory postsynaptic potentials carry synchronized frequency information in active cortical networks. *Neuron, 47*(3), 423-435. doi:10.1016/j.neuron.2005.06.016
Hasher, L., & Zacks, R. T. (1988). Working memory, comprehension, and aging: A review and a new view. In G. H. Bower (Ed.), *The psychology of learning and motivation* (Vol. 22, pp. pp. 193-225). San Diego, CA: Academic Press.
Hayworth, K. J., & Marblestone, A. H. (2018). How thalamic relays might orchestrate supervised deep training and symbolic computation in the brain. *bioRxiv*.
He, B. J. (2011). Scale-free properties of the functional magnetic resonance imaging signal during rest and task. *Journal of Neuroscience, 31*(39), 13786-13795. doi:10.1523/JNEUROSCI.2111-11.2011
He, B. J., Zempel, J. M., Snyder, A. Z., & Raichle, M. E. (2010). The temporal structures and functional significance of scale-free brain activity. *Neuron, 66*(3), 353-369. doi:10.1016/j.neuron.2010.04.020
He, B. Y. J. (2014). Scale-free brain activity: Past, present, and future. *Trends in Cognitive Sciences, 18*(9), 480-487. doi:10.1016/j.tics.2014.04.003
He, W., Donoghue, T., Sowman, P. F., Seymour, R. A., Brock, J., Crain, S., . . . Hillebrand, A. (2019). Co-increasing neuronal noise and beta power in the developing brain. *bioRxiv*, 839258. doi:10.1101/839258
Heeger, D. J. (2017). Theory of cortical function. *Proceedings of the National Academy of Sciences of the United States of America, 114*(8), 1773-1782. doi:10.1073/pnas.1619788114
Heeger, D. J., & Mackey, W. E. (2019). Oscillatory recurrent gated neural integrator circuits (ORGaNICs), a unifying theoretical framework for neural dynamics. *Proceedings of the National Academy of Sciences of the United States of America, 116*(45), 22783-22794. doi:10.1073/pnas.1911633116
Heidema, S. G., Quinn, A. J., Woolrich, M. W., van Ede, F., & Nobre, A. C. (2020). Dissecting beta-state changes during timed movement preparation in parkinson's disease. *Progress in Neurobiology, 184*. doi:10.1016/j.pneurobio.2019.101731

Heitmann, S., & Breakspear, M. (2018). Putting the "dynamic" back into dynamic functional connectivity. *Network Neuroscience, 2*(2), 150-174. doi:10.1162/netn_a_00041
Helfrich, R. F. (2018). The rhythmic nature of visual perception. *Journal of Neurophysiology, 119*(4), 1251-1253. doi:10.1152/jn.00810.2017
Helfrich, R. F., Breska, A., & Knight, R. T. (2019). Neural entrainment and network resonance in support of top-down guided attention. *Current Opinion in Psychology, 29*, 82-89. doi:10.1016/j.copsyc.2018.12.016
Helfrich, R. F., Fiebelkorn, I. C., Szczepanski, S. M., Lin, J. J., Parvizi, J., Knight, R. T., & Kastner, S. (2018). Neural mechanisms of sustained attention are rhythmic. *Neuron, 99*(4), 854-865. doi:10.1016/j.neuron.2018.07.032
Helfrich, R. F., Huang, M., Wilson, G., & Knight, R. T. (2017). Prefrontal cortex modulates posterior alpha oscillations during top-down guided visual perception. *Proceedings of the National Academy of Sciences of the United States of America, 114*(35), 9457-9462. doi:10.1073/pnas.1705965114
Helfrich, R. F., & Knight, R. T. (2016). Oscillatory dynamics of prefrontal cognitive control. *Trends in Cognitive Sciences, 20*(12), 916-930. doi:10.1016/j.tics.2016.09.007
Hellyer, P. J., Shanahan, M., Scott, G., Wise, R. J., Sharp, D. J., & Leech, R. (2014). The control of global brain dynamics: Opposing actions of frontoparietal control and default mode networks on attention. *Journal of Neuroscience, 34*(2), 451-461. doi:10.1523/JNEUROSCI.1853-13.2014
Henrie, J. A., & Shapley, R. (2005). LFP power spectra in V1 cortex: The graded effect of stimulus contrast. *Journal of Neurophysiology, 94*(1), 479-490. doi:10.1152/jn.00919.2004
Hermes, D., Miller, K. J., Wandell, B. A., & Winawer, J. (2015). Stimulus dependence of gamma oscillations in human visual cortex. *Cerebral Cortex, 25*(9), 2951-2959. doi:10.1093/cercor/bhu091
Hermes, D., Nguyen, M., & Winawer, J. (2017). Neuronal synchrony and the relation between the blood-oxygen-level dependent response and the local field potential. *PLoS Biology, 15*(7). doi:10.1371/journal.pbio.2001461
Herrmann, K., Heeger, D. J., & Carrasco, M. (2012). Feature-based attention enhances performance by increasing response gain. *Vision Research, 74*, 10-20. doi:10.1016/j.visres.2012.04.016
Heusser, A. C., Poeppel, D., Ezzyat, Y., & Davachi, L. (2016). Episodic sequence memory is supported by a theta-gamma phase code. *Nature Neuroscience, 19*(10), 1374-1380. doi:10.1038/nn.4374
Hipp, J. F., & Siegel, M. (2013). Dissociating neuronal gamma-band activity from cranial and ocular muscle activity in EEG. *Frontiers in Human Neuroscience, 7*. doi:10.3389/fnhum.2013.00338
Hirata, A., Aguilar, J., & Castro-Alamancos, M. A. (2006). Noradrenergic activation amplifies bottom-up and top-down signal-to-noise ratios in sensory thalamus. *Journal of Neuroscience, 26*(16), 4426-4436. doi:10.1523/JNEUROSCI.5298-05.2006
Hirata, A., & Castro-Alamancos, M. A. (2010). Neocortex network activation and deactivation states controlled by the thalamus. *Journal of Neurophysiology, 103*(3), 1147-1157. doi:10.1152/jn.00955.2009
Hjorth, B. (1970). EEG analysis based on time domain properties. *Electroencephalography and Clinical Neurophysiology, 29*(3), 306-310. doi:Doi 10.1016/0013-4694(70)90143-4
Honjoh, S., Sasai, S., Schiereck, S. S., Nagai, H., Tononi, G., & Cirelli, C. (2018). Regulation of cortical activity and arousal by the matrix cells of the ventromedial thalamic nucleus. *Nat Commun, 9*(1), 2100. doi:10.1038/s41467-018-04497-x
Horn, A., & Blankenburg, F. (2016). Toward a standardized structural-functional group connectome in mni space. *NeuroImage, 124*(Pt A), 310-322. doi:10.1016/j.neuroimage.2015.08.048
Hsu, D., Hsu, M., Grabenstatter, H. L., Worrell, G. A., & Sutula, T. P. (2010). Time-frequency analysis using damped-oscillator pseudo-wavelets: Application to electrophysiological recordings. *Journal of Neuroscience Methods, 194*(1), 179-192. doi:10.1016/j.jneumeth.2010.09.019
Huang, Y., Hu, K., Green, A. L., Ma, X., Gillies, M. J., Wang, S., . . . Sun, B. (2019). Dynamic changes in rhythmic and arrhythmic neural signatures in the subthalamic nucleus induced by anaesthesia and intubation. *bioRxiv*.
Hughes, J. R. (1995). The phenomenon of travelling waves: A review. *Clinical Electroencephalography, 26*(1), 1-6. doi:10.1177/155005949502600103
Hughes, M. E., Hogenesch, J. B., & Kornacker, K. (2010). JTK_CYCLE: An efficient nonparametric algorithm for detecting rhythmic components in genome-scale data sets. *Journal of Biological Rhythms, 25*(5), 372-380. doi:10.1177/0748730410379711
Hughes, S. W., Cope, D. W., Blethyn, K. L., & Crunelli, V. (2002). Cellular mechanisms of the slow (<1 hz) oscillation in thalamocortical neurons in vitro. *Neuron, 33*(6), 947-958. doi:10.1016/s0896-6273(02)00623-2
Hughes, S. W., & Crunelli, V. (2007). Just a phase they're going through: The complex interaction of intrinsic high-threshold bursting and gap junctions in the generation of thalamic alpha and theta rhythms. *International Journal of Psychophysiology, 64*(1), 3-17. doi:10.1016/j.ijpsycho.2006.08.004

Hughes, S. W., Errington, A., Lorincz, M. L., Kekesi, K. A., Juhasz, G., Orban, G., . . . Crunelli, V. (2008). Novel modes of rhythmic burst firing at cognitively-relevant frequencies in thalamocortical neurons. *Brain Research, 1235*, 12-20. doi:10.1016/j.brainres.2008.06.029
Hughes, S. W., Lorincz, M., Cope, D. W., Blethyn, K. L., Kekesi, K. A., Parri, H. R., . . . Crunelli, V. (2004). Synchronized oscillations at alpha and theta frequencies in the lateral geniculate nucleus. *Neuron, 42*(2), 253-268. doi:10.1016/S0896-6273(04)00191-6
Huguenard, J. R., & McCormick, D. A. (2007). Thalamic synchrony and dynamic regulation of global forebrain oscillations. *Trends in Neurosciences, 30*(7), 350-356. doi:10.1016/j.tins.2007.05.007
Hwang, K., Bertolero, M. A., Liu, W. B., & D'Esposito, M. (2017). The human thalamus is an integrative hub for functional brain networks. *Journal of Neuroscience, 37*(23), 5594-5607. doi:10.1523/JNEUROSCI.0067-17.2017
Isaacson, J. S., & Scanziani, M. (2011). How inhibition shapes cortical activity. *Neuron, 72*(2), 231-243. doi:10.1016/j.neuron.2011.09.027
Isaichev, S. A., Derevyankin, V. T., Koptelov Yu, M., & Sokolov, E. N. (2001). Rhythmic alpha-activity generators in the human EEG. *Neurosci Behav Physiol, 31*(1), 49-53. doi:10.1023/a:1026622229972
Jagadeesh, B., Gray, C. M., & Ferster, D. (1992). Visually evoked oscillations of membrane-potential in cells of cat visual-cortex. *Science, 257*(5069), 552-554. doi:10.1126/science.1636094
Jaramillo, J., Mejias, J. F., & Wang, X. J. (2019). Engagement of pulvino-cortical feedforward and feedback pathways in cognitive computations. *Neuron, 101*(2), 321-336 e329. doi:10.1016/j.neuron.2018.11.023
Jasper, H. H. (1948). Charting the sea of brain waves. *Science, 108*(2805), 343-347. doi:10.1126/science.108.2805.343
Jasper, H. H., & Andrews, H. L. (1938). Brain potentials and voluntary muscle activity in man. *Journal of Neurophysiology, 1*(2), 87-100.
Jensen, O., Bonnefond, M., & VanRullen, R. (2012). An oscillatory mechanism for prioritizing salient unattended stimuli. *Trends in Cognitive Sciences, 16*(4), 200-206. doi:10.1016/j.tics.2012.03.002
Jensen, O., & Colgin, L. L. (2007). Cross-frequency coupling between neuronal oscillations. *Trends in Cognitive Sciences, 11*(7), 267-269. doi:10.1016/j.tics.2007.05.003
Jensen, O., & Mazaheri, A. (2010). Shaping functional architecture by oscillatory alpha activity: Gating by inhibition. *Frontiers in Human Neuroscience, 4*. doi:10.3389/fnhum.2010.00186
Jia, X. X., Xing, D. J., & Kohn, A. (2013). No consistent relationship between gamma power and peak frequency in macaque primary visual cortex. *Journal of Neuroscience, 33*(1), 17-U421. doi:10.1523/Jneurosci.1687-12.2013
Jones, E. G. (1998). Viewpoint: The core and matrix of thalamic organization. *Neuroscience, 85*(2), 331-345. doi:10.1016/s0306-4522(97)00581-2
Jones, E. G. (2001). The thalamic matrix and thalamocortical synchrony. *Trends in Neurosciences, 24*(10), 595-601. doi:10.1016/S0166-2236(00)01922-6
Jones, E. G. (2009). Synchrony in the interconnected circuitry of the thalamus and cerebral cortex. *Annals of the New York Academy of Sciences, 1157*, 10-23. doi:10.1111/j.1749-6632.2009.04534.x
Jones, E. G. (2010). Thalamocortical dysrhythmia and chronic pain. *Pain, 150*(1), 4-5. doi:10.1016/j.pain.2010.03.022
Jones, S. R. (2016). When brain rhythms aren't 'rhythmic': Implication for their mechanisms and meaning. *Current Opinion in Neurobiology, 40*, 72-80. doi:10.1016/j.conb.2016.06.010
Joshi, S., Li, Y., Kalwani, R. M., & Gold, J. I. (2016). Relationships between pupil diameter and neuronal activity in the locus coeruleus, colliculi, and cingulate cortex. *Neuron, 89*(1), 221-234. doi:10.1016/j.neuron.2015.11.028
Kaffashi, F., Foglyano, R., Wilson, C. G., & Loparo, K. A. (2008). The effect of time delay on Approximate & Sample Entropy calculations. *Physica D-Nonlinear Phenomena, 237*(23), 3069-3074. doi:10.1016/j.physd.2008.06.005
Kajikawa, Y., & Schroeder, C. E. (2011). How local is the Local Field Potential? *Neuron, 72*(5), 847-858. doi:10.1016/j.neuron.2011.09.029
Kanai, R., Komura, Y., Shipp, S., & Friston, K. (2015). Cerebral hierarchies: Predictive processing, precision and the pulvinar. *Philosophical Transactions of the Royal Society B-Biological Sciences, 370*(1668), 69-81. doi:10.1098/rstb.2014.0169
Kanashiro, T., Ocker, G. K., Cohen, M. R., & Doiron, B. (2017). Attentional modulation of neuronal variability in circuit models of cortex. *Elife, 6*. doi:10.7554/eLife.23978
Kara, P., Reinagel, P., & Reid, R. C. (2000). Low response variability in simultaneously recorded retinal, thalamic, and cortical neurons. *Neuron, 27*(3), 635-646. doi:10.1016/s0896-6273(00)00072-6

Karahanoglu, F. I., & Van De Ville, D. (2015). Transient brain activity disentangles fMRI resting-state dynamics in terms of spatially and temporally overlapping networks. *Nature Communications, 6*. doi:10.1038/ncomms8751

Kardan, O., Adam, K. C. S., Mance, I., Churchill, N. W., Vogel, E. K., & Berman, M. G. (2020). Distinguishing cognitive effort and working memory load using scale-invariance and alpha suppression in EEG. *NeuroImage, 211*. doi:10.1016/j.neuroimage.2020.116622

Karvat, G., Schneider, A., Alyahyay, M., Steenbergen, F., Tangermann, M., & Diester, I. (2020). Real-time detection of neural oscillation bursts allows behaviourally relevant neurofeedback. *Communications Biology, 3*(1). doi:10.1038/s42003-020-0801-z

Kastner, S., & Pinsk, M. A. (2004). Visual attention as a multilevel selection process. *Cognitive, Affective, & Behavioral Neuroscience, 4*(4), 483-500. doi:10.3758/CABN.4.4.483

Kay, S. M., & Marple, S. L. (1981). Spectrum analysis - a modern perspective. *Proceedings of the Ieee, 69*(11), 1380-1419. doi:Doi 10.1109/Proc.1981.12184

Kayser, C., Montemurro, M. A., Logothetis, N. K., & Panzeri, S. (2009). Spike-phase coding boosts and stabilizes information carried by spatial and temporal spike patterns. *Neuron, 61*(4), 597-608. doi:10.1016/j.neuron.2009.01.008

Keitel, A., & Gross, J. (2016). Individual human brain areas can be identified from their characteristic spectral activation fingerprints. *PLoS Biology, 14*(6). doi:10.1371/journal.pbio.1002498

Kennedy, B. L., & Mather, M. (2019). Neural mechanisms underlying age-related changes in attentional selectivity. In G. R. Samanez-Larkin (Ed.), *The aging brain: Functional adaptation across adulthood* (pp. 45–72). Washington, DC: American Psychological Association.

Ketz, N. A., Jensen, O., & O'Reilly, R. C. (2015). Thalamic pathways underlying prefrontal cortex-medial temporal lobe oscillatory interactions. *Trends in Neurosciences, 38*(1), 3-12. doi:10.1016/j.tins.2014.09.007

Kinomura, S., Larsson, J., Gulyas, B., & Roland, P. E. (1996). Activation by attention of the human reticular formation and thalamic intralaminar nuclei. *Science, 271*(5248), 512-515. doi:10.1126/science.271.5248.512

Kinouchi, O., & Copelli, M. (2006). Optimal dynamical range of excitable networks at criticality. *Nature Physics, 2*(5), 348-352. doi:10.1038/nphys289

Klimesch, W. (2012). Alpha-band oscillations, attention, and controlled access to stored information. *Trends in Cognitive Sciences, 16*(12), 606-617. doi:10.1016/j.tics.2012.10.007

Klimesch, W., Sauseng, P., & Hanslmayr, S. (2007). EEG alpha oscillations: The inhibition-timing hypothesis. *Brain Research Reviews, 53*(1), 63-88. doi:10.1016/j.brainresrev.2006.06.003

Knight, R. T., & Eichenbaum, H. (2013). Multiplexed memories: A view from human cortex. *Nature Neuroscience, 16*(3), 257-258. doi:10.1038/nn.3341

Knyazeva, M. G., Barzegaran, E., Vildayski, V. Y., & Demonet, J. F. (2018). Aging of human alpha rhythm. *Neurobiology of Aging, 69*, 261-273. doi:10.1016/j.neurobiolaging.2018.05.018

Kolmac, C., & Mitrofanis, J. (1999). Organization of the basal forebrain projection to the thalamus in rats. *Neuroscience Letters, 272*(3), 151-154. doi:10.1016/S0304-3940(99)00614-X

Komura, Y., Nikkuni, A., Hirashima, N., Uetake, T., & Miyamoto, A. (2013). Responses of pulvinar neurons reflect a subject's confidence in visual categorization. *Nature Neuroscience, 16*(6), 749-755. doi:10.1038/nn.3393

Korotkova, T., Ponomarenko, A., Monaghan, C. K., Poulter, S. L., Cacucci, F., Wills, T., . . . Lever, C. (2018). Reconciling the different faces of hippocampal theta: The role of theta oscillations in cognitive, emotional and innate behaviors. *Neuroscience and Biobehavioral Reviews, 85*, 65-80. doi:10.1016/j.neubiorev.2017.09.004

Kosciessa, J. Q., Grandy, T. H., Garrett, D. D., & Werkle-Bergner, M. (2020). Single-trial characterization of neural rhythms: Potential and challenges. *NeuroImage, 206*, 116331. doi:10.1016/j.neuroimage.2019.116331

Kosciessa, J. Q., Kloosterman, N. A., & Garrett, D. D. (2020). Standard multiscale entropy reflects neural dynamics at mismatched temporal scales: What's signal irregularity got to do with it? *PLoS Computational Biology, 16*(5), e1007885. doi:10.1371/journal.pcbi.1007885

Krakauer, J. W., Ghazanfar, A. A., Gomez-Marin, A., MacIver, M. A., & Poeppel, D. (2017). Neuroscience needs behavior: Correcting a reductionist bias. *Neuron, 93*(3), 480-490. doi:10.1016/j.neuron.2016.12.041

Krause, A. J., Prather, A. A., Wager, E. D., Lindquist, M. A., & Walker, M. P. (2019). The pain of sleep loss: A brain characterization in humans. *Journal of Neuroscience, 39*(12), 2291-2300. doi:10.1523/Jneurosci.2408-18.2018

Krishnaswamy, P., Obregon-Henao, G., Ahveninen, J., Khan, S., Babadi, B., Iglesias, J. E., . . . Purdon, P. L. (2017). Sparsity enables estimation of both subcortical and cortical activity from MEG and EEG. *Proceedings of the National Academy of Sciences of the United States of America, 114*(48), E10465-E10474. doi:10.1073/pnas.1705414114

Krol, A., Wimmer, R. D., Halassa, M. M., & Feng, G. (2018). Thalamic reticular dysfunction as a circuit endophenotype in neurodevelopmental disorders. *Neuron, 98*(2), 282-295. doi:10.1016/j.neuron.2018.03.021

Kumral, D., Sansal, F., Cesnaite, E., Mahjoory, K., Al, E., Gabeler, M., . . . Villringer, A. (2020). BOLD and EEG signal variability at rest differently relate to aging in the human brain. *NeuroImage, 207*. doi:10.1016/j.neuroimage.2019.116373

Laberge, D., & Buchsbaum, M. S. (1990). Positron emission tomographic measurements of pulvinar activity during an attention task. *Journal of Neuroscience, 10*(2), 613-619.

Lakatos, P., Karmos, G., Mehta, A. D., Ulbert, I., & Schroeder, C. E. (2008). Entrainment of neuronal oscillations as a mechanism of attentional selection. *Science, 320*(5872), 110-113. doi:10.1126/science.1154735

Lakatos, P., Shah, A. S., Knuth, K. H., Ulbert, I., Karmos, G., & Schroeder, C. E. (2005). An oscillatory hierarchy controlling neuronal excitability and stimulus processing in the auditory cortex. *Journal of Neurophysiology, 94*(3), 1904-1911. doi:10.1152/jn.00263.2005

Lalwani, P., Gagnon, H., Cassady, K., Simmonite, M., Peltier, S., Seidler, R. D., . . . Polk, T. A. (2019). Neural distinctiveness declines with age in auditory cortex and is associated with auditory GABA levels. *NeuroImage, 201*. doi:10.1016/j.neuroimage.2019.116033

Lancaster, G., Iatsenko, D., Pidde, A., Ticcinelli, V., & Stefanovska, A. (2018). Surrogate data for hypothesis testing of physical systems. *Physics Reports-Review Section of Physics Letters, 748*, 1-60. doi:10.1016/j.physrep.2018.06.001

Landau, A. N., & Fries, P. (2012). Attention samples stimuli rhythmically. *Current Biology, 22*(11), 1000-1004. doi:10.1016/j.cub.2012.03.054

Lange, J., Oostenveld, R., & Fries, P. (2013). Reduced occipital alpha power indexes enhanced excitability rather than improved visual perception. *Journal of Neuroscience, 33*(7), 3212-3220. doi:10.1523/JNEUROSCI.3755-12.2013

Lashley, K. S. (1951). The problem of serial order in behavior. In L. A. Jeffress (Ed.), *Cerebral mechanisms in behavior* (pp. 112-147). New York: Wiley.

Lavoie, B., & Parent, A. (1991). Serotoninergic innervation of the thalamus in the primate - an immunohistochemical study. *Journal of Comparative Neurology, 312*(1), 1-18. doi:10.1002/cne.903120102

Lee, S. H., & Dan, Y. (2012). Neuromodulation of brain states. *Neuron, 76*(1), 209-222. doi:10.1016/j.neuron.2012.09.012

Lefebvre, J., Hutt, A., & Frohlich, F. (2017). Stochastic resonance mediates the state dependent effect of periodic stimulation on cortical alpha oscillations. *Elife, 6*. doi:10.7554/eLife.32054

Legon, W., Punzell, S., Dowlati, E., Adams, S. E., Stiles, A. B., & Moran, R. J. (2016). Altered prefrontal Excitation/Inhibition balance and prefrontal output: Markers of aging in human memory networks. *Cerebral Cortex, 26*(11), 4315-4326. doi:10.1093/cercor/bhv200

Leissner, P., Lindholm, L. E., & Petersen, I. (1970). Alpha amplitude dependence on skull thickness as measured by ultrasound technique. *Electroencephalography and Clinical Neurophysiology, 29*(4), 392-399. doi:10.1016/0013-4694(70)90047-7

Lendner, J. D., Helfrich, R. F., Mander, B. A., Romundstad, L., Lin, J. J., Walker, M. P., . . . Knight, R. T. (2019). An electrophysiological marker of arousal level in humans. *bioRxiv*.

Leventhal, A. G., Wang, Y. C., Pu, M. L., Zhou, Y. F., & Ma, Y. Y. (2003). GABA and its agonists improved visual cortical function in senescent monkeys. *Science, 300*(5620), 812-815. doi:10.1126/science.1082874

Lewis, L. D., Voigts, J., Flores, F. J., Schmitt, L. I., Wilson, M. A., Halassa, M. M., & Brown, E. N. (2015). Thalamic reticular nucleus induces fast and local modulation of arousal state. *Elife, 4*, e08760. doi:10.7554/eLife.08760

Li, C. Y., Poo, M. M., & Dan, Y. (2009). Burst spiking of a single cortical neuron modifies global brain state. *Science, 324*(5927), 643-646. doi:10.1126/science.1169957

Li, G. S., Henriquez, C. S., & Frohlich, F. (2017). Unified thalamic model generates multiple distinct oscillations with state-dependent entrainment by stimulation. *Plos Computational Biology, 13*(10). doi:10.1371/journal.pcbi.1005797

Li, S. C., Lindenberger, U., & Sikstrom, S. (2001). Aging cognition: From neuromodulation to representation. *Trends in Cognitive Sciences, 5*(11), 479-486. doi:10.1016/S1364-6613(00)01769-1

Lin, M., & Chen, T. L. (2005). Self-organized criticality in a simple model of neurons based on small-world networks. *Physical Review E, 71*(1). doi:10.1103/PhysRevE.71.016133
Linden, H., Pettersen, K. H., & Einevoll, G. T. (2010). Intrinsic dendritic filtering gives low-pass power spectra of local field potentials. *Journal of Computational Neuroscience, 29*(3), 423-444. doi:10.1007/s10827-010-0245-4
Lindsley, D. B. (1939). A longitudinal study of the occipital alpha rhythm in normal children frequency and amplitude standards. *Pedagogical Seminary and Journal of Genetic Psychology, 55*(1), 197-213.
Linkenkaer-Hansen, K., Nikouline, V. V., Palva, J. M., & Ilmoniemi, R. J. (2001). Long-range temporal correlations and scaling behavior in human brain oscillations. *Journal of Neuroscience, 21*(4), 1370-1377.
Lisman, J. (2012). Excitation, inhibition, local oscillations, or large-scale loops: What causes the symptoms of schizophrenia? *Current Opinion in Neurobiology, 22*(3), 537-544. doi:10.1016/j.conb.2011.10.018
Lisman, J. E., & Idiart, M. A. P. (1995). Storage of 7+/-2 short-term memories in oscillatory subcycles. *Science, 267*(5203), 1512-1515. doi:10.1126/science.7878473
Lisman, J. E., & Jensen, O. (2013). The theta-gamma neural code. *Neuron, 77*(6), 1002-1016. doi:10.1016/j.neuron.2013.03.007
Little, S., Bonaiuto, J., Barnes, G., & Bestmann, S. (2019). Human motor cortical beta bursts relate to movement planning and response errors. *PLoS Biology, 17*(10). doi:10.1371/journal.pbio.3000479
Liu, C. L., Kong, X. Z., Liu, X. Y., Zhou, R. L., & Wu, B. (2014). Long-term total sleep deprivation reduces thalamic gray matter volume in healthy men. *Neuroreport, 25*(5), 320-323. doi:10.1097/Wnr.0000000000000091
Liu, J., Lee, H. J., Weitz, A. J., Fang, Z., Lin, P., Choy, M., . . . Lee, J. H. (2015). Frequency-selective control of cortical and subcortical networks by central thalamus. *Elife, 4*, e09215. doi:10.7554/eLife.09215
Liu, Z. M., de Zwart, J. A., Yao, B., van Gelderen, P., Kuo, L. W., & Duyn, J. H. (2012). Finding thalamic BOLD correlates to posterior alpha EEG. *NeuroImage, 63*(3), 1060-1069. doi:10.1016/j.neuroimage.2012.08.025
Llinas, R. R., Ribary, U., Jeanmonod, D., Kronberg, E., & Mitra, P. P. (1999). Thalamocortical dysrhythmia: A neurological and neuropsychiatric syndrome characterized by magnetoencephalography. *Proceedings of the National Academy of Sciences of the United States of America, 96*(26), 15222-15227. doi:10.1073/pnas.96.26.15222
Logothetis, N. K., Augath, M., Murayama, Y., Rauch, A., Sultan, F., Goense, J., . . . Merkle, H. (2010). The effects of electrical microstimulation on cortical signal propagation. *Nature Neuroscience, 13*(10), 1283-1291. doi:10.1038/nn.2631
Lombardi, F., Herrmann, H. J., & de Arcangelis, L. (2017). Balance of excitation and inhibition determines 1/f power spectrum in neuronal networks. *Chaos, 27*(4). doi:10.1063/1.4979043
Lopes da Silva, F. H. (2013). EEG and MEG: Relevance to neuroscience. *Neuron, 80*(5), 1112-1128. doi:10.1016/j.neuron.2013.10.017
Lopes da Silva, F. H., Hoeks, A., Smits, H., & Zetterberg, L. H. (1974). Model of brain rhythmic activity - alpha-rhythm of thalamus. *Kybernetik, 15*(1), 27-37. doi:Doi 10.1007/Bf00270757
Lopes da Silva, F. H., van Lierop, T. H., Schrijer, C. F., & van Leeuwen, W. S. (1973). Organization of thalamic and cortical alpha rhythms - spectra and coherences. *Electroencephalography and Clinical Neurophysiology, 35*(6), 627-639. doi:10.1016/0013-4694(73)90216-2
Lopes da Silva, F. H., Vos, J. E., Mooibroek, J., & Van Rotterdam, A. (1980). Relative contributions of intracortical and thalamo-cortical processes in the generation of alpha rhythms, revealed by partial coherence analysis. *Electroencephalography and Clinical Neurophysiology, 50*(5-6), 449-456. doi:10.1016/0013-4694(80)90011-5
Lorincz, M. L., Crunelli, V., & Hughes, S. W. (2008). Cellular dynamics of cholinergically induced alpha (8-13 hz) rhythms in sensory thalamic nuclei in vitro. *Journal of Neuroscience, 28*(3), 660-671. doi:10.1523/JNEUROSCI.4468-07.2008
Lorincz, M. L., Kekesi, K. A., Juhasz, G., Crunelli, V., & Hughes, S. W. (2009). Temporal framing of thalamic relay-mode firing by phasic inhibition during the alpha rhythm. *Neuron, 63*(5), 683-696. doi:10.1016/j.neuron.2009.08.012
Lozano-Soldevilla, D. (2018a). Nonsinusoidal neuronal oscillations: Bug or feature? *Journal of Neurophysiology, 119*(5), 1595-1598. doi:10.1152/jn.00744.2017
Lozano-Soldevilla, D. (2018b). On the physiological modulation and potential mechanisms underlying parieto-occipital alpha oscillations. *Frontiers in Computational Neuroscience, 12*, 23. doi:10.3389/fncom.2018.00023

Lozano-Soldevilla, D., & VanRullen, R. (2019). The hidden spatial dimension of alpha: 10-hz perceptual echoes propagate as periodic traveling waves in the human brain. *Cell Reports, 26*(2), 374-380. doi:10.1016/j.celrep.2018.12.058
Lundqvist, M., Rose, J., Herman, P., Brincat, S. L., Buschman, T. J., & Miller, E. K. (2016). Gamma and beta bursts underlie working memory. *Neuron, 90*(1), 152-164. doi:10.1016/j.neuron.2016.02.028
Lurie, D. J., Kessler, D., Bassett, D. S., Betzel, R. F., Breakspear, M., Kheilholz, S., . . . Calhoun, V. D. (2020). Questions and controversies in the study of time-varying functional connectivity in resting fMRI. *Netw Neurosci, 4*(1), 30-69. doi:10.1162/netn_a_00116
Lynn, C. W., Cornblath, E. J., Papadopoulos, L., Bertolero, M. A., & Bassett, D. S. (2020). *Non-equilibrium dynamics and entropy production in the human brain*. (2005.02526). arXiv.
Ma, N., Dinges, D. F., Basner, M., & Rao, H. Y. (2015). How acute total sleep loss affects the attending brain: A meta-analysis of neuroimaging studies. *Sleep, 38*(2), 233-240. doi:10.5665/sleep.4404
MacDonald, K. D., Fifkova, E., Jones, M. S., & Barth, D. S. (1998). Focal stimulation of the thalamic reticular nucleus induces focal gamma waves in cortex. *Journal of Neurophysiology, 79*(1), 474-477.
MacLean, J. N., Watson, B. O., Aaron, G. B., & Yuste, R. (2005). Internal dynamics determine the cortical response to thalamic stimulation. *Neuron, 48*(5), 811-823. doi:10.1016/j.neuron.2005.09.035
Makinen, V. T., May, P. J. C., & Tlitinen, H. (2005). The use of stationarity and nonstationarity in the detection and analysis of neural oscillations. *NeuroImage, 28*(2), 389-400. doi:10.1016/j.neuroimage.2005.06.004
Malina, K. C. K., Mohar, B., Rappaport, A. N., & Lampl, I. (2016). Local and thalamic origins of correlated ongoing and sensory-evoked cortical activities. *Nature Communications, 7*. doi:10.1038/ncomms12740
Mallat, S. G., & Zhang, Z. F. (1993). Matching pursuits with time-frequency dictionaries. *Ieee Transactions on Signal Processing, 41*(12), 3397-3415. doi:Doi 10.1109/78.258082
Mandelbrot, B. B. (1999). *Multifractals and 1/f noise : Wild self-affinity in physics (1963-1976) : Selecta volume n*. New York: Springer.
Manning, J. R., Jacobs, J., Fried, I., & Kahana, M. J. (2009). Broadband shifts in Local Field Potential power spectra are correlated with single-neuron spiking in humans. *Journal of Neuroscience, 29*(43), 13613-13620. doi:10.1523/Jneurosci.2041-09.2009
Marguet, S. L., & Harris, K. D. (2011). State-dependent representation of amplitude-modulated noise stimuli in rat auditory cortex. *Journal of Neuroscience, 31*(17), 6414-6420. doi:10.1523/Jneurosci.5773-10.2011
Mariani, S., Borges, A. F. T., Henriques, T., Thomas, R. J., Leistedt, S. J., Linkowski, P., . . . Costa, M. D. (2016). Analysis of the sleep EEG in the complexity domain. In J. Patton, R. Barbieri, J. Ji, E. Jabbari, S. Dokos, R. Mukkamala, D. Guiraud, E. Jovanov, Y. Dhaher, D. Panescu, M. Vangils, B. Wheeler, & A. P. Dhawan (Eds.), *2016 38th annual international conference of the ieee engineering in medicine and biology society* (pp. 6429-6432).
Markov, N. T., Vezoli, J., Chameau, P., Falchier, A., Quilodran, R., Huissoud, C., . . . Kennedy, H. (2014). Anatomy of hierarchy: Feedforward and feedback pathways in macaque visual cortex. *Journal of Comparative Neurology, 522*(1), 225-259. doi:10.1002/cne.23458
Markovic, D., & Gros, C. (2014). Power laws and self-organized criticality in theory and nature. *Physics Reports-Review Section of Physics Letters, 536*(2), 41-74. doi:10.1016/j.physrep.2013.11.002
Marshall, P. J., Bar-Haim, Y., & Fox, N. A. (2002). Development of the EEG from 5 months to 4 years of age. *Clinical Neurophysiology, 113*(8), 1199-1208. doi:10.1016/S1388-2457(02)00163-3
Martinez-Trujillo, J. C., & Treue, S. (2004). Feature-based attention increases the selectivity of population responses in primate visual cortex. *Current Biology, 14*(9), 744-751. doi:10.1016/j.cub.2004.04.028
Marton, T. F., Seifikar, H., Luongo, F. J., Lee, A. T., & Sohal, V. S. (2018). Roles of prefrontal cortex and mediodorsal thalamus in task engagement and behavioral flexibility. *Journal of Neuroscience, 38*(10), 2569-2578. doi:10.1523/JNEUROSCI.1728-17.2018
Masquelier, T. (2013). Neural variability, or lack thereof. *Frontiers in Computational Neuroscience, 7*, 7. doi:10.3389/fncom.2013.00007
Mathewson, K. E., Gratton, G., Fabiani, M., Beck, D. M., & Ro, T. (2009). To see or not to see: Prestimulus alpha phase predicts visual awareness. *Journal of Neuroscience, 29*(9), 2725-2732. doi:10.1523/Jneurosci.3963-08.2009
Mathewson, K. E., Lleras, A., Beck, D. M., Fabiani, M., Ro, T., & Gratton, G. (2011). Pulsed out of awareness: EEG alpha oscillations represent a pulsed-inhibition of ongoing cortical processing. *Frontiers in Psychology, 2*. doi:10.3389/fpsyg.2011.00099
McAlonan, K., Cavanaugh, J., & Wurtz, R. H. (2008). Guarding the gateway to cortex with attention in visual thalamus. *Nature, 456*(7220), 391-394. doi:10.1038/nature07382
McAvoy, M., Larson-Prior, L., Nolan, T. S., Vaishnavi, S. N., Raichle, M. E., & d'Avossa, G. (2008). Resting states affect spontaneous BOLD oscillations in sensory and paralimbic cortex. *Journal of Neurophysiology, 100*(2), 922-931. doi:10.1152/jn.90426.2008

McCormick, D. A. (1989). Cholinergic and noradrenergic modulation of thalamocortical processing. *Trends in Neurosciences, 12*(6), 215-221. doi:10.1016/0166-2236(89)90125-2
McCormick, D. A., & Bal, T. (1997). Sleep and arousal: Thalamocortical mechanisms. *Annual Review of Neuroscience, 20*, 185-215. doi:10.1146/annurev.neuro.20.1.185
McCormick, D. A., & Huguenard, J. R. (1992). A model of the electrophysiological properties of thalamocortical relay neurons. *Journal of Neurophysiology, 68*(4), 1384-1400.
McCormick, D. A., McGinley, M. J., & Salkoff, D. B. (2015). Brain state dependent activity in the cortex and thalamus. *Current Opinion in Neurobiology, 31*, 133-140. doi:10.1016/j.conb.2014.10.003
McCormick, D. A., Pape, H. C., & Williamson, A. (1991). Actions of norepinephrine in the cerebral cortex and thalamus: Implications for function of the central noradrenergic system. *Progress in Brain Research, 88*, 293-305. doi:10.1016/s0079-6123(08)63817-0
McDonnell, M. D., & Ward, L. M. (2011). The benefits of noise in neural systems: Bridging theory and experiment. *Nature Reviews: Neuroscience, 12*(7), 415-426. doi:10.1038/nrn3061
McGinley, M. J., David, S. V., & McCormick, D. A. (2015). Cortical membrane potential signature of optimal states for sensory signal detection. *Neuron, 87*(1), 179-192. doi:10.1016/j.neuron.2015.05.038
McGinley, M. J., Vinck, M., Reimer, J., Batista-Brito, R., Zagha, E., Cadwell, C. R., . . . McCormick, D. A. (2015). Waking state: Rapid variations modulate neural and behavioral responses. *Neuron, 87*(6), 1143-1161. doi:10.1016/j.neuron.2015.09.012
McIntosh, A. R. (2019). Neurocognitive aging and brain signal complexity: Oxford University Press.
McIntosh, A. R., Kovacevic, N., & Itier, R. J. (2008). Increased brain signal variability accompanies lower behavioral variability in development. *Plos Computational Biology, 4*(7). doi:10.1371/journal.pcbi.1000106
McIntosh, A. R., Vakorin, V., Kovacevic, N., Wang, H., Diaconescu, A., & Protzner, A. B. (2014). Spatiotemporal dependency of age-related changes in brain signal variability. *Cerebral Cortex, 24*(7), 1806-1817. doi:10.1093/cercor/bht030
Mckenna, T. M., Mcmullen, T. A., & Shlesinger, M. F. (1994). The brain as a dynamic physical system. *Neuroscience, 60*(3), 587-605. doi:10.1016/0306-4522(94)90489-8
Mejias, J. F., Murray, J. D., Kennedy, H., & Wang, X. J. (2016). Feedforward and feedback frequency-dependent interactions in a large-scale laminar network of the primate cortex. *Science Advances, 2*(11). doi:10.1126/sciadv.1601335
Mesulam, M. M. (1990). Large-scale neurocognitive networks and distributed processing for attention, language, and memory. *Annals of Neurology, 28*(5), 597-613. doi:10.1002/ana.410280502
Michael, T. P., Mockler, T. C., Breton, G., McEntee, C., Byer, A., Trout, J. D., . . . Chory, J. (2008). Network discovery pipeline elucidates conserved time-of-day-specific cis-regulatory modules. *PLoS Genetics, 4*(2). doi:10.1371/journal.pgen.0040014
Michalareas, G., Vezoli, J., van Pelt, S., Schoffelen, J. M., Kennedy, H., & Fries, P. (2016). Alpha-beta and gamma rhythms subserve feedback and feedforward influences among human visual cortical areas. *Neuron, 89*(2), 384-397. doi:10.1016/j.neuron.2015.12.018
Michels, L., Moazami-Goudarzi, M., Jeanmonod, D., & Sarnthein, J. (2008). EEG alpha distinguishes between cuneal and precuneal activation in working memory. *NeuroImage, 40*(3), 1296-1310. doi:10.1016/j.neuroimage.2007.12.048
Mierau, A., Klimesch, W., & Lefebvre, J. (2017). State-dependent alpha peak frequency shifts: Experimental evidence, potential mechanisms and functional implications. *Neuroscience, 360*, 146-154. doi:10.1016/j.neuroscience.2017.07.037
Miller, E. K., & Buschman, T. J. (2013). Cortical circuits for the control of attention. *Current Opinion in Neurobiology, 23*(2), 216-222. doi:10.1016/j.conb.2012.11.011
Miller, E. K., Lundqvist, M., & Bastos, A. M. (2018). Working memory 2.0. *Neuron, 100*(2), 463-475. doi:10.1016/j.neuron.2018.09.023
Miller, K. J. (2010). Broadband spectral change: Evidence for a macroscale correlate of population firing rate? *Journal of Neuroscience, 30*(19), 6477-6479. doi:10.1523/Jneurosci.6401-09.2010
Miller, K. J., Hermes, D., Honey, C. J., Hebb, A. O., Ramsey, N. F., Knight, R. T., . . . Fetz, E. E. (2012). Human motor cortical activity is selectively phase-entrained on underlying rhythms. *Plos Computational Biology, 8*(9). doi:10.1371/journal.pcbi.1002655
Miller, K. J., Honey, C. J., Hermes, D., Rao, R. P. N., denNijs, M., & Ojemann, J. G. (2014). Broadband changes in the cortical surface potential track activation of functionally diverse neuronal populations. *NeuroImage, 85*, 711-720. doi:10.1016/j.neuroimage.2013.08.070
Miller, K. J., Sorensen, L. B., Ojemann, J. G., & den Nijs, M. (2009). Power-law scaling in the brain surface electric potential. *Plos Computational Biology, 5*(12). doi:10.1371/journal.pcbi.1000609

Miller, K. J., Zanos, S., Fetz, E. E., den Nijs, M., & Ojemann, J. G. (2009). Decoupling the cortical power spectrum reveals real-time representation of individual finger movements in humans. *Journal of Neuroscience, 29*(10), 3132-3137. doi:10.1523/Jneurosci.5506-08.2009
Milton, R., Shahidi, N., & Dragoi, V. (2020). Dynamic states of population activity in prefrontal cortical networks of freely-moving macaque. *Nat Commun, 11*(1), 1948. doi:10.1038/s41467-020-15803-x
Minami, S., & Amano, K. (2017). Illusory jitter perceived at the frequency of alpha oscillations. *Current Biology, 27*(15), 2344-2351. doi:10.1016/j.cub.2017.06.033
Miskovic, V., MacDonald, K. J., Rhodes, L. J., & Cote, K. A. (2019). Changes in EEG multiscale entropy and power-law frequency scaling during the human sleep cycle. *Human Brain Mapping, 40*(2), 538-551. doi:10.1002/hbm.24393
Mitchell, A. S. (2015). The mediodorsal thalamus as a higher order thalamic relay nucleus important for learning and decision-making. *Neuroscience and Biobehavioral Reviews, 54*, 76-88. doi:10.1016/j.neubiorev.2015.03.001
Mitchell, J. F., Sundberg, K. A., & Reynolds, J. H. (2009). Spatial attention decorrelates intrinsic activity fluctuations in macaque area v4. *Neuron, 63*(6), 879-888. doi:10.1016/j.neuron.2009.09.013
Mitzdorf, U. (1985). Current source-density method and application in cat cerebral-cortex - investigation of evoked-potentials and eeg phenomena. *Physiological Reviews, 65*(1), 37-100.
Mo, C., Lu, J., Wu, B., Jia, J., Luo, H., & Fang, F. (2019). Competing rhythmic neural representations of orientations during concurrent attention to multiple orientation features. *Nat Commun, 10*(1), 5264. doi:10.1038/s41467-019-13282-3
Monier, C., Fournier, J., & Fregnac, Y. (2008). In vitro and in vivo measures of evoked excitatory and inhibitory conductance dynamics in sensory cortices. *Journal of Neuroscience Methods, 169*(2), 323-365. doi:10.1016/j.jneumeth.2007.11.008
Montemurro, M. A., Rasch, M. J., Murayama, Y., Logothetis, N. K., & Panzeri, S. (2008). Phase-of-firing visual stimuli in coding of natural primary visual cortex. *Current Biology, 18*(5), 375-380. doi:10.1016/j.cub.2008.02.023
Monto, S., Palva, S., Voipio, J., & Palva, J. M. (2008). Very slow EEG fluctuations predict the dynamics of stimulus detection and oscillation amplitudes in humans. *Journal of Neuroscience, 28*(33), 8268-8272. doi:10.1523/Jneurosci.1910-08.2008
Moosmann, M., Ritter, P., Krastel, I., Brink, A., Thees, S., Blankenburg, F., . . . Villringer, A. (2003). Correlates of alpha rhythm in functional magnetic resonance imaging and near infrared spectroscopy. *NeuroImage, 20*(1), 145-158. doi:10.1016/s1053-8119(03)00344-6
Morison, R. S., & Dempsey, E. W. (1943). Mechanism of thalamocortical augmentation and repetition. *American Journal of Physiology, 138*(2), 0297-0308.
Moruzzi, G., & Magoun, H. W. (1949). Brain stem reticular formation and activation of the EEG. *Electroencephalography and Clinical Neurophysiology, 1*(4), 455-473.
Muehlroth, B. E., & Werkle-Bergner, M. (2020). Understanding the interplay of sleep and aging: Methodological challenges. *Psychophysiology, 57*(3). doi:10.1111/psyp.13523
Müller, E., Munn, B., Hearne, L. J., Smith, J. B., Fulcher, B., Cocchi, L., & Shine, J. M. (2020). Core and matrix thalamic sub-populations relate to spatio-temporal cortical connectivity gradients. *bioRxiv*.
Muller, L., Chavane, F., Reynolds, J., & Sejnowski, T. J. (2018). Cortical travelling waves: Mechanisms and computational principles. *Nature Reviews Neuroscience, 19*(5), 255-268. doi:10.1038/nrn.2018.20
Murphy, P. R., O'Connell, R. G., O'Sullivan, M., Robertson, I. H., & Balsters, J. H. (2014). Pupil diameter covaries with BOLD activity in human locus coeruleus. *Human Brain Mapping, 35*(8), 4140-4154. doi:10.1002/hbm.22466
Murphy, P. R., Wilming, N., Hernandez-Bocanegra, D. C., Prat Ortega, G., & Donner, T. H. (2020). Normative circuit dynamics across human cortex during evidence accumulation in changing environments. *bioRxiv*.
Murray, J. D., Jaramillo, J., & Wang, X. J. (2017). Working memory and decision-making in a frontoparietal circuit model. *Journal of Neuroscience, 37*(50), 12167-12186. doi:10.1523/JNEUROSCI.0343-17.2017
Musall, S., Kaufman, M. T., Juavinett, A. L., Gluf, S., & Churchland, A. K. (2019). Single-trial neural dynamics are dominated by richly varied movements. *Nature Neuroscience, 22*(10), 1677-1686. doi:10.1038/s41593-019-0502-4
Musall, S., von Pfostl, V., Rauch, A., Logothetis, N. K., & Whittingstall, K. (2014). Effects of neural synchrony on surface EEG. *Cerebral Cortex, 24*(4), 1045-1053. doi:10.1093/cercor/bhs389
Muthukumaraswamy, S. D., & Liley, D. T. J. (2018). 1/f electrophysiological spectra in resting and drug-induced states can be explained by the dynamics of multiple oscillatory relaxation processes. *NeuroImage, 179*, 582-595. doi:10.1016/j.neuroimage.2018.06.068

Nacher, V., Ledberg, A., Deco, G., & Romo, R. (2013). Coherent delta-band oscillations between cortical areas correlate with decision making. *Proceedings of the National Academy of Sciences of the United States of America, 110*(37), 15085-15090. doi:10.1073/pnas.1314681110
Nakajima, M., & Halassa, M. M. (2017). Thalamic control of functional cortical connectivity. *Current Opinion in Neurobiology, 44*, 127-131. doi:10.1016/j.conb.2017.04.001
Neil, L., Olsson, N. C., & Pellicano, E. (2016). The relationship between intolerance of uncertainty, sensory sensitivities, and anxiety in autistic and typically developing children. *Journal of Autism and Developmental Disorders, 46*(6), 1962-1973. doi:10.1007/s10803-016-2721-9
Nelli, S., Itthipuripat, S., Srinivasan, R., & Serences, J. T. (2017). Fluctuations in instantaneous frequency predict alpha amplitude during visual perception. *Nature Communications, 8*. doi:10.1038/s41467-017-02176-x
Nelson, S. B., & Valakh, V. (2015). Excitatory/inhibitory balance and circuit homeostasis in autism spectrum disorders. *Neuron, 87*(4), 684-698. doi:10.1016/j.neuron.2015.07.033
Neymotin, S. A., Barczak, A., O'Connell, M. N., McGinnis, T., Markowitz, N., Espinal, E., . . . Lakatos, P. (2020). Taxonomy of neural oscillation events in primate auditory cortex. *bioRxiv*.
Neymotin, S. A., Daniels, D. S., Caldwell, B., McDougal, R. A., Carnevale, N. T., Jas, M., . . . Jones, S. R. (2020). Human Neocortical Neurosolver (HNN), a new software tool for interpreting the cellular and network origin of human MEG/EEG data. *Elife, 9*. doi:10.7554/eLife.51214
Ng, B. S. W., Logothetis, N. K., & Kayser, C. (2013). EEG phase patterns reflect the selectivity of neural firing. *Cerebral Cortex, 23*(2), 389-398. doi:10.1093/cercor/bhs031
Ni, J. G., Wunderle, T., Lewis, C. M., Desimone, R., Diester, I., & Fries, P. (2016). Gamma-rhythmic gain modulation. *Neuron, 92*(1), 240-251. doi:10.1016/j.neuron.2016.09.003
Nikulin, V. V., & Brismar, T. (2004). Comment on "multiscale entropy analysis of complex physiologic time series". *Physical Review Letters, 92*(8). doi:10.1103/PhysRevLett.92.089803
Nikulin, V. V., Nolte, G., & Curio, G. (2011). A novel method for reliable and fast extraction of neuronal EEG/MEG oscillations on the basis of spatio-spectral decomposition. *NeuroImage, 55*(4), 1528-1535. doi:10.1016/j.neuroimage.2011.01.057
Niyogi, R. K., & Wong-Lin, K. (2013). Dynamic excitatory and inhibitory gain modulation can produce flexible, robust and optimal decision-making. *Plos Computational Biology, 9*(6). doi:10.1371/journal.pcbi.1003099
Nowak, L. G., Sanchez-Vives, M. V., & McCormick, D. A. (1997). Influence of low and high frequency inputs on spike timing in visual cortical neurons. *Cerebral Cortex, 7*(6), 487-501. doi:10.1093/cercor/7.6.487
Nunez, P. L., & Srinivasan, R. (2006). *Electric fields of the brain : The neurophysics of EEG* (2nd ed.). Oxford ; New York: Oxford University Press.
O'Muircheartaigh, J., Keller, S. S., Barker, G. J., & Richardson, M. P. (2015). White matter connectivity of the thalamus delineates the functional architecture of competing thalamocortical systems. *Cerebral Cortex, 25*(11), 4477-4489. doi:10.1093/cercor/bhv063
O'Reilly, R. C., Wyatte, D. R., & Rohrlich, J. (2017). Deep predictive learning: A comprehensive model of three visual streams. Retrieved from doi:arXiv:1709.04654
Obleser, J., & Kayser, C. (2019). Neural entrainment and attentional selection in the listening brain. *Trends in Cognitive Sciences, 23*(11), 913-926. doi:10.1016/j.tics.2019.08.004
Oke, A. F., Carver, L. A., Gouvion, C. M., & Adams, R. N. (1997). Three-dimensional mapping of norepinephrine and serotonin in human thalamus. *Brain Research, 763*(1), 69-78. doi:10.1016/S0006-8993(97)00404-6
Okun, M., & Lampl, I. (2008). Instantaneous correlation of excitation and inhibition during ongoing and sensory-evoked activities. *Nature Neuroscience, 11*(5), 535-537. doi:10.1038/nn.2105
Okun, M., Steinmetz, N. A., Cossell, L., Iacaruso, M. F., Ko, H., Bartho, P., . . . Harris, K. D. (2015). Diverse coupling of neurons to populations in sensory cortex. *Nature, 521*(7553), 511-U189. doi:10.1038/nature14273
Olbrich, S., Mulert, C., Karch, S., Trenner, M., Leicht, G., Pogarell, O., & Hegerl, U. (2009). EEG-vigilance and BOLD effect during simultaneous EEG/fMRI measurement. *NeuroImage, 45*(2), 319-332. doi:10.1016/j.neuroimage.2008.11.014
Ossadtchi, A., Shamaeva, T., Okorokova, E., Moiseeva, V., & Lebedev, M. A. (2017). Neurofeedback learning modifies the incidence rate of alpha spindles, but not their duration and amplitude. *Scientific Reports, 7*. doi:10.1038/s41598-017-04012-0
Ouhaz, Z., Fleming, H., & Mitchell, A. S. (2018). Cognitive functions and neurodevelopmental disorders involving the prefrontal cortex and mediodorsal thalamus. *Frontiers in Neuroscience, 12*. doi:10.3389/fnins.2018.00033

Ouyang, G., Hildebrandt, A., Schmitz, F., & Herrmann, C. S. (2020). Decomposing alpha and 1/f brain activities reveals their differential associations with cognitive processing speed. *NeuroImage, 205*, 116304. doi:10.1016/j.neuroimage.2019.116304

Pachitariu, M., Lyamzin, D. R., Sahani, M., & Lesica, N. A. (2015). State-dependent population coding in primary auditory cortex. *Journal of Neuroscience, 35*(5), 2058-2073. doi:10.1523/JNEUROSCI.3318-14.2015

Palmigiano, A., Geisel, T., Wolf, F., & Battaglia, D. (2017). Flexible information routing by transient synchrony. *Nature Neuroscience, 20*(7), 1014-1022. doi:10.1038/nn.4569

Palva, S., & Palva, J. M. (2007). New vistas for alpha-frequency band oscillations. *Trends in Neurosciences, 30*(4), 150-158. doi:10.1016/j.tins.2007.02.001

Palva, S., & Palva, J. M. (2018). Roles of brain criticality and multiscale oscillations in temporal predictions for sensorimotor processing. *Trends in Neurosciences, 41*(10), 729-743. doi:10.1016/j.tins.2018.08.008

Panzeri, S., Macke, J. H., Gross, J., & Kayser, C. (2015). Neural population coding: Combining insights from microscopic and mass signals. *Trends in Cognitive Sciences, 19*(3), 162-172. doi:10.1016/j.tics.2015.01.002

Pardey, J., Roberts, S., & Tarassenko, L. (1996). A review of parametric modelling techniques for EEG analysis. *Medical Engineering & Physics, 18*(1), 2-11. doi:Doi 10.1016/1350-4533(95)00024-0

Park, J. H., Kim, S., Kim, C. H., Cichocki, A., & Kim, K. (2007). Multiscale entropy analysis of EEG from patients under different pathological conditions. *Fractals-Complex Geometry Patterns and Scaling in Nature and Society, 15*(4), 399-404. doi:10.1142/S0218348x07003691

Parnaudeau, S., O'Neill, P. K., Bolkan, S. S., Ward, R. D., Abbas, A. I., Roth, B. L., . . . Kellendonk, C. (2013). Inhibition of mediodorsal thalamus disrupts thalamofrontal connectivity and cognition. *Neuron, 77*(6), 1151-1162. doi:10.1016/j.neuron.2013.01.038

Paus, T. (2000). Functional anatomy of arousal and attention systems in the human brain. *Cognition, Emotion and Autonomic Responses: The Integrative Role of the Prefrontal Cortex and Limbic Structures, 126*, 65-77.

Penfield, W. (1975). *The mystery of the mind : A critical study of consciousness and the human brain*. Princeton, N.J.: Princeton University Press.

Penny, W. D. (Producer). (2000). Signal processing course. Retrieved from https://www.fil.ion.ucl.ac.uk/~wpenny/course/course.html

Penttonen, M., & Buzsáki, G. (2003). Natural logarithmic relationship between brain oscillators. *Thalamus & Related Systems, 2*(2), 145-152. doi:10.1016/S1472-9288(03)00007-4

Pereda, E., Gamundi, A., Rial, R., & Gonzalez, J. (1998). Non-linear behaviour of human EEG: Fractal exponent versus correlation dimension in awake and sleep stages. *Neuroscience Letters, 250*(2), 91-94. doi:10.1016/s0304-3940(98)00435-2

Pergola, G., Danet, L., Pitel, A. L., Carlesimo, G. A., Segobin, S., Pariente, J., . . . Barbeau, E. J. (2018). The regulatory role of the human mediodorsal thalamus. *Trends in Cognitive Sciences, 22*(11), 1011-1025. doi:10.1016/j.tics.2018.08.006

Peterson, E. J., Rosen, B. Q., Campbell, A. M., Belger, A., & Voytek, B. (2018). 1/f neural noise is a better predictor of schizophrenia than neural oscillations. *bioRxiv*.

Peterson, E. J., & Voytek, B. (2015). Balanced oscillatory coupling improves information flow. *bioRxiv*.

Peterson, E. J., & Voytek, B. (2017). Alpha oscillations control cortical gain by modulating excitatory-inhibitory background activity. *bioRxiv*.

Peterson, E. J., & Voytek, B. (2019). Homeostatic mechanisms may shape the type and duration of oscillatory modulation. *bioRxiv*.

Pettersen, K. H., & Einevoll, G. T. (2008). Amplitude variability and extracellular low-pass filtering of neuronal spikes. *Biophysical Journal, 94*(3), 784-802. doi:10.1529/biophysj.107.111179

Pettine, W. W., Louie, K., Murray, J. D., & Wang, X.-J. (2020). Hierarchical network model excitatory-inhibitory tone shapes alternative strategies for different degrees of uncertainty in multi-attribute decisions. *bioRxiv*.

Pfurtscheller, G. (2001). Functional brain imaging based on ERD/ERS. *Vision Research, 41*(10-11), 1257-1260. doi:10.1016/S0042-6989(00)00235-2

Pfurtscheller, G., & da Silva, F. H. L. (1999). Event-related EEG/MEG synchronization and desynchronization: Basic principles. *Clinical Neurophysiology, 110*(11), 1842-1857. doi:10.1016/S1388-2457(99)00141-8

Picard, F., Sadaghiani, S., Leroy, C., Courvoisier, D. S., Maroy, R., & Bottlaender, M. (2013). High density of nicotinic receptors in the cingulo-insular network. *NeuroImage, 79*, 42-51. doi:10.1016/j.neuroimage.2013.04.074

Pincus, S. M., & Goldberger, A. L. (1994). Physiological time-series analysis - what does regularity quantify. *American Journal of Physiology, 266*(4), H1643-H1656. doi:DOI 10.1152/ajpheart.1994.266.4.H1643

Pinneo, L. R. (1966). On noise in the nervous system. *Psychological Review, 73*(3), 242-247. doi:10.1037/h0023240
Pinto, L., Goard, M. J., Estandian, D., Xu, M., Kwan, A. C., Lee, S. H., . . . Dan, Y. (2013). Fast modulation of visual perception by basal forebrain cholinergic neurons. *Nature Neuroscience, 16*(12), 1857-1863. doi:10.1038/nn.3552
Podvalny, E., Noy, N., Harel, M., Bickel, S., Chechik, G., Schroeder, C. E., . . . Malach, R. (2015). A unifying principle underlying the extracellular field potential spectral responses in the human cortex. *Journal of Neurophysiology, 114*(1), 505-519. doi:10.1152/jn.00943.2014
Poil, S. S., Hardstone, R., Mansvelder, H. D., & Linkenkaer-Hansen, K. (2012). Critical-state dynamics of avalanches and oscillations jointly emerge from balanced Excitation/Inhibition in neuronal networks. *Journal of Neuroscience, 32*(29), 9817-9823. doi:10.1523/Jneurosci.5990-11.2012
Poil, S. S., van Ooyen, A., & Linkenkaer-Hansen, K. (2008). Avalanche dynamics of human brain oscillations: Relation to critical branching processes and temporal correlations. *Human Brain Mapping, 29*(7), 770-777. doi:10.1002/hbm.20590
Ponce-Alvarez, A., Thiele, A., Albright, T. D., Stoner, G. R., & Deco, G. (2013). Stimulus-dependent variability and noise correlations in cortical mt neurons. *Proceedings of the National Academy of Sciences of the United States of America, 110*(32), 13162-13167. doi:10.1073/pnas.1300098110
Poo, C., & Isaacson, J. S. (2009). Odor representations in olfactory cortex: "Sparse" coding, global inhibition, and oscillations. *Neuron, 62*(6), 850-861. doi:10.1016/j.neuron.2009.05.022
Popov, T., Gips, B., Kastner, S., & Jensen, O. (2019). Spatial specificity of alpha oscillations in the human visual system. *Human Brain Mapping, 40*(15), 4432-4440. doi:10.1002/hbm.24712
Popov, T., Kastner, S., & Jensen, X. (2017). FEF-controlled alpha delay activity precedes stimulus-induced gamma-band activity in visual cortex. *Journal of Neuroscience, 37*(15), 4117-4127. doi:10.1523/Jneurosci.3015-16.2017
Porges, E. C., Woods, A. J., Edden, R. A. E., Puts, N. A. J., Harris, A. D., Chen, H. H., . . . Cohen, R. A. (2017). Frontal gamma-aminobutyric acid concentrations are associated with cognitive performance in older adults. *Biological Psychiatry-Cognitive Neuroscience and Neuroimaging, 2*(1), 38-44. doi:10.1016/j.bpsc.2016.06.004
Poulet, J. F., Fernandez, L. M., Crochet, S., & Petersen, C. C. (2012). Thalamic control of cortical states. *Nature Neuroscience, 15*(3), 370-372. doi:10.1038/nn.3035
Pritchard, W. S. (1992). The brain in fractal time - 1/f-like power spectrum scaling of the human electroencephalogram. *International Journal of Neuroscience, 66*(1-2), 119-129. doi:10.3109/00207459208999796
Proske, J. H., Jeanmonod, D., & Verschure, P. F. M. J. (2011). A computational model of thalamocortical dysrhythmia. *European Journal of Neuroscience, 33*(7), 1281-1290. doi:10.1111/j.1460-9568.2010.07588.x
Purushothaman, G., Marion, R., Li, K., & Casagrande, V. A. (2012). Gating and control of primary visual cortex by pulvinar. *Nature Neuroscience, 15*(6), 905-U136. doi:10.1038/nn.3106
Quax, S., Jensen, O., & Tiesinga, P. (2017). Top-down control of cortical gamma-band communication via pulvinar induced phase shifts in the alpha rhythm. *Plos Computational Biology, 13*(5). doi:10.1371/journal.pcbi.1005519
Quinn, A. J., van Ede, F., Brookes, M. J., Heideman, S. G., Nowak, M., Seedat, Z. A., . . . Woolrich, M. W. (2019). Unpacking transient event dynamics in electrophysiological power spectra. *Brain Topography, 32*(6), 1020-1034. doi:10.1007/s10548-019-00745-5
Quiroga, R., & Panzeri, S. (2013). *Principles of neural coding*. Boca Raton: CRC Press.
Rafal, R. D., & Posner, M. I. (1987). Deficits in human visual spatial attention following thalamic lesions. *Proceedings of the National Academy of Sciences of the United States of America, 84*(20), 7349-7353. doi:10.1073/pnas.84.20.7349
Ray, S., & Maunsell, J. H. R. (2010). Differences in gamma frequencies across visual cortex restrict their possible use in computation. *Neuron, 67*(5), 885-896. doi:10.1016/j.neuron.2010.08.004
Re, D., Inbar, M., Richter, C. G., & Landau, A. N. (2019). Feature-based attention samples stimuli rhythmically. *Current Biology, 29*(4), 693-699. doi:10.1016/j.cub.2019.01.010
Redinbaugh, M. J., Phillips, J. M., Kambi, N. A., Mohanta, S., Andryk, S., Dooley, G. L., . . . Saalmann, Y. B. (2020). Thalamus modulates consciousness via layer-specific control of cortex. *Neuron, 106*(1), 66-75. doi:10.1016/j.neuron.2020.01.005
Reichova, I., & Sherman, S. M. (2004). Somatosensory corticothalamic projections: Distinguishing drivers from modulators. *Journal of Neurophysiology, 92*(4), 2185-2197. doi:10.1152/jn.00322.2004

Reimer, J., Froudarakis, E., Cadwell, C. R., Yatsenko, D., Denfield, G. H., & Tolias, A. S. (2014). Pupil fluctuations track fast switching of cortical states during quiet wakefulness. *Neuron, 84*(2), 355-362. doi:10.1016/j.neuron.2014.09.033

Renart, A., de la Rocha, J., Bartho, P., Hollender, L., Parga, N., Reyes, A., & Harris, K. D. (2010). The asynchronous state in cortical circuits. *Science, 327*(5965), 587-590. doi:10.1126/science.1179850

Reynolds, J. H., & Heeger, D. J. (2009). The normalization model of attention. *Neuron, 61*(2), 168-185. doi:10.1016/j.neuron.2009.01.002

Richman, J. S., & Moorman, J. R. (2000). Physiological time-series analysis using approximate entropy and sample entropy. *American Journal of Physiology: Heart and Circulatory Physiology, 278*(6), H2039-H2049.

Rieck, R. W., Ansari, M. S., Whetsell, W. O., Jr., Deutch, A. Y., & Kessler, R. M. (2004). Distribution of dopamine D2-like receptors in the human thalamus: Autoradiographic and PET studies. *Neuropsychopharmacology, 29*(2), 362-372. doi:10.1038/sj.npp.1300336

Rigas, P., & Castro-Alamancos, M. A. (2007). Thalamocortical up states: Differential effects of intrinsic and extrinsic cortical inputs on persistent activity. *Journal of Neuroscience, 27*(16), 4261-4272. doi:10.1523/Jneurosci.0003-07.2007

Rigas, P., & Castro-Alamancos, M. A. (2009). Impact of persistent cortical activity (up states) on intracortical and thalamocortical synaptic inputs. *Journal of Neurophysiology, 102*(1), 119-131. doi:10.1152/jn.00126.2009

Rikhye, R. V., Gilra, A., & Halassa, M. M. (2018). Thalamic regulation of switching between cortical representations enables cognitive flexibility. *Nature Neuroscience, 21*(12), 1753-1763. doi:10.1038/s41593-018-0269-z

Rikhye, R. V., Wimmer, R. D., & Halassa, M. M. (2018). Toward an integrative theory of thalamic function. *Annual Review of Neuroscience, Vol 41, 41*, 163-183. doi:10.1146/annurev-neuro-080317-062144

Roberts, J. A., Gollo, L. L., Abeysuriya, R. G., Roberts, G., Mitchell, P. B., Woolrich, M. W., & Breakspear, M. (2019). Metastable brain waves. *Nature Communications, 10*. doi:10.1038/s41467-019-08999-0

Robinson, P. A., Rennie, C. J., Wright, J. J., Bahramali, H., Gordon, E., & Rowe, D. L. (2001). Prediction of electroencephalographic spectra from neurophysiology. *Physical Review E, 63*(2). doi:10.1103/PhysRevE.63.021903

Roehri, N., Lina, J. M., Mosher, J. C., Bartolomei, F., & Benar, C. G. (2016). Time-frequency strategies for increasing high-frequency oscillation detectability in intracerebral EEG. *IEEE Transactions on Biomedical Engineering, 63*(12), 2595-2606. doi:10.1109/TBME.2016.2556425

Rohracher, H. (1937). Über die kurvenform cerebraler potentialschwankungen. *Pflüger's Archiv für die gesamte Physiologie des Menschen und der Tiere, 238*(1), 535-545. doi:10.1007/BF01767659

Rolls, E. T., & Treves, A. (2011). The neuronal encoding of information in the brain. *Progress in Neurobiology, 95*(3), 448-490. doi:10.1016/j.pneurobio.2011.08.002

Romei, V., Gross, J., & Thut, G. (2012). Sounds reset rhythms of visual cortex and corresponding human visual perception. *Current Biology, 22*(9), 807-813. doi:10.1016/j.cub.2012.03.025

Rosanova, M., Casali, A., Bellina, V., Resta, F., Mariotti, M., & Massimini, M. (2009). Natural frequencies of human corticothalamic circuits. *Journal of Neuroscience, 29*(24), 7679-7685. doi:10.1523/Jneurosci.0445-09.2009

Rose, H. J., & Metherate, R. (2005). Auditory thalamocortical transmission is reliable and temporally precise. *Journal of Neurophysiology, 94*(3), 2019-2030. doi:10.1152/jn.00860.2004

Rosenblum, M. G., Pikovsky, A. S., & Kurths, J. (1996). Phase synchronization of chaotic oscillators. *Physical Review Letters, 76*(11), 1804-1807. doi:10.1103/PhysRevLett.76.1804

Roux, F., Wibral, M., Singer, W., Aru, J., & Uhlhaas, P. J. (2013). The phase of thalamic alpha activity modulates cortical gamma-band activity: Evidence from resting-state MEG recordings. *Journal of Neuroscience, 33*(45), 17827-17835. doi:10.1523/JNEUROSCI.5778-12.2013

Rozycka, A., & Liguz-Lecznar, M. (2017). The space where aging acts: Focus on the GABAergic synapse. *Aging Cell, 16*(4), 634-643. doi:10.1111/acel.12605

Rubenstein, J. L. R., & Merzenich, M. M. (2003). Model of autism: Increased ratio of excitation/inhibition in key neural systems. *Genes Brain and Behavior, 2*(5), 255-267. doi:10.1034/j.1601-183X.2003.00037.x

Rubin, R., Abbott, L. F., & Sompolinsky, H. (2017). Balanced excitation and inhibition are required for high-capacity, noise-robust neuronal selectivity. *Proceedings of the National Academy of Sciences of the United States of America, 114*(44), E9366-E9375. doi:10.1073/pnas.1705841114

Rumyantsev, O. I., Lecoq, J. A., Hernandez, O., Zhang, Y. P., Savall, J., Chrapkiewicz, R., . . . Schnitzer, M. J. (2020). Fundamental bounds on the fidelity of sensory cortical coding. *Nature*. doi:10.1038/s41586-020-2130-2

Runfeldt, M. J., Sadovsky, A. J., & MacLean, J. N. (2014). Acetylcholine functionally reorganizes neocortical microcircuits. *Journal of Neurophysiology, 112*(5), 1205-1216. doi:10.1152/jn.00071.2014
Saalmann, Y. B., & Kastner, S. (2009). Gain control in the visual thalamus during perception and cognition. *Current Opinion in Neurobiology, 19*(4), 408-414. doi:10.1016/j.conb.2009.05.007
Saalmann, Y. B., & Kastner, S. (2011). Cognitive and perceptual functions of the visual thalamus. *Neuron, 71*(2), 209-223. doi:10.1016/j.neuron.2011.06.027
Saalmann, Y. B., Ly, R., Pinsk, M. A., & Kastner, S. (2018). Pulvinar influences parietal delay activity and information transmission between dorsal and ventral visual cortex in macaques. *bioRxiv*.
Saalmann, Y. B., Pinsk, M. A., Wang, L., Li, X., & Kastner, S. (2012). The pulvinar regulates information transmission between cortical areas based on attention demands. *Science, 337*(6095), 753-756. doi:10.1126/science.1223082
Sadaghiani, S., Dombert, P. L., Lovstad, M., Funderud, I., Meling, T. R., Endestad, T., . . . D'Esposito, M. (2019). Lesions to the fronto-parietal network impact alpha-band phase synchrony and cognitive control. *Cerebral Cortex, 29*(10), 4143-4153. doi:10.1093/cercor/bhy296
Sadaghiani, S., & Kleinschmidt, A. (2016). Brain networks and alpha-Oscillations: Structural and functional foundations of cognitive control. *Trends in Cognitive Sciences, 20*(11), 805-817. doi:10.1016/j.tics.2016.09.004
Sadaghiani, S., Scheeringa, R., Lehongre, K., Morillon, B., Giraud, A. L., & Kleinschmidt, A. (2010). Intrinsic connectivity networks, alpha oscillations, and tonic alertness: A simultaneous electroencephalography/functional magnetic resonance imaging study. *Journal of Neuroscience, 30*(30), 10243-10250. doi:10.1523/Jneurosci.1004-10.2010
Saleem, A. B., Lien, A. D., Krumin, M., Haider, B., Roson, M. R., Ayaz, A., . . . Harris, K. D. (2017). Subcortical source and modulation of the narrowband gamma oscillation in mouse visual cortex. *Neuron, 93*(2), 315-322. doi:10.1016/j.neuron.2016.12.028
Salinas, E., & Sejnowski, T. J. (2001). Correlated neuronal activity and the flow of neural information. *Nature Reviews Neuroscience, 2*(8), 539-550. doi:10.1038/35086012
Salthouse, T. A., & Meinz, E. J. (1995). Aging, inhibition, working-memory, and speed. *Journals of Gerontology Series B-Psychological Sciences and Social Sciences, 50*(6), P297-P306. doi:DOI 10.1093/geronb/50B.6.P297
Samaha, J., & Postle, B. R. (2015). The speed of alpha-band oscillations predicts the temporal resolution of visual perception. *Current Biology, 25*(22), 2985-2990. doi:10.1016/j.cub.2015.10.007
Sanchez-Gonzalez, M. A., Garcia-Cabezas, M. A., Rico, B., & Cavada, C. (2005). The primate thalamus is a key target for brain dopamine. *Journal of Neuroscience, 25*(26), 6076-6083. doi:10.1523/Jneurosci.0968-05.2005
Sanchez-Vives, M. V., & McCormick, D. A. (2000). Cellular and network mechanisms of rhythmic recurrent activity in neocortex. *Nature Neuroscience, 3*(10), 1027-1034.
Sander, M. C., Lindenberger, U., & Werkle-Bergner, M. (2012). Lifespan age differences in working memory: A two-component framework. *Neuroscience and Biobehavioral Reviews, 36*(9), 2007-2033. doi:10.1016/j.neubiorev.2012.06.004
Saper, C. B., Fuller, P. M., Pedersen, N. P., Lu, J., & Scammell, T. E. (2010). Sleep state switching. *Neuron, 68*(6), 1023-1042. doi:10.1016/j.neuron.2010.11.032
Sara, S. J. (2009). The locus coeruleus and noradrenergic modulation of cognition. *Nature Reviews: Neuroscience, 10*(3), 211-223. doi:10.1038/nrn2573
Sato, T. K., Nauhaus, I., & Carandini, M. (2012). Traveling waves in visual cortex. *Neuron, 75*(2), 218-229. doi:10.1016/j.neuron.2012.06.029
Sauseng, P., Klimesch, W., Gerloff, C., & Hummel, F. C. (2009). Spontaneous locally restricted EEG alpha activity determines cortical excitability in the motor cortex. *Neuropsychologia, 47*(1), 284-288. doi:10.1016/j.neuropsychologia.2008.07.021
Schalk, G., Marple, J., Knight, R. T., & Coon, W. G. (2017). Instantaneous voltage as an alternative to power- and phase-based interpretation of oscillatory brain activity. *NeuroImage, 157*, 545-554. doi:10.1016/j.neuroimage.2017.06.014
Schaworonkow, N., & Nikulin, V. V. (2019). Spatial neuronal synchronization and the waveform of oscillations: Implications for EEG and MEG. *PLoS Computational Biology, 15*(5), e1007055. doi:10.1371/journal.pcbi.1007055
Scheeringa, R., & Fries, P. (2019). Cortical layers, rhythms and BOLD signals. *NeuroImage, 197*, 689-698. doi:10.1016/j.neuroimage.2017.11.002
Scheeringa, R., Koopmans, P. J., van Mourik, T., Jensen, O., & Norris, D. G. (2016). The relationship between oscillatory EEG activity and the laminar-specific BOLD signal. *Proceedings of the National Academy of Sciences of the United States of America, 113*(24), 6761-6766. doi:10.1073/pnas.1522577113

Schiff, N., & Purpura, K. (2002). Towards a neurophysiological foundation for cognitive neuromodulation through deep brain stimulation. *Thalamus & Related Systems, 2*(1), 55-69. doi:10.1017/S1472928802000286
Schiff, N. D. (2008). Central thalamic contributions to arousal regulation and neurological disorders of consciousness. *Annals of the New York Academy of Sciences, 1129*, 105-118. doi:10.1196/annals.1417.029
Schiff, N. D., Giacino, J. T., Kalmar, K., Victor, J. D., Baker, K., Gerber, M., . . . Rezai, A. R. (2007). Behavioural improvements with thalamic stimulation after severe traumatic brain injury. *Nature, 448*(7153), 600-U610. doi:10.1038/nature06041
Schirner, M., McIntosh, A. R., Jirsa, V., Deco, G., & Ritter, P. (2018). Inferring multi-scale neural mechanisms with brain network modelling. *Elife, 7*. doi:10.7554/eLife.28927
Schmid, M. C., Singer, W., & Fries, P. (2012). Thalamic coordination of cortical communication. *Neuron, 75*(4), 551-552. doi:10.1016/j.neuron.2012.08.009
Schmitt, L. I., Wimmer, R. D., Nakajima, M., Happ, M., Mofakham, S., & Halassa, M. M. (2017). Thalamic amplification of cortical connectivity sustains attentional control. *Nature, 545*(7653), 219-223. doi:10.1038/nature22073
Scholvinck, M. L., Saleem, A. B., Benucci, A., Harris, K. D., & Carandini, M. (2015). Cortical state determines global variability and correlations in visual cortex. *Journal of Neuroscience, 35*(1), 170-178. doi:10.1523/JNEUROSCI.4994-13.2015
Schomer, D. L., & Silva, F. H. L. d. (2017). *Niedermeyer's electroencephalography: Basic principles, clinical applications, and related fields*: Oxford University Press.
Schreckenberger, M., Lange-Asschenfeld, C., Lochmann, M., Mann, K., Siessmeier, T., Buchholz, H. G., . . . Grunder, G. (2004). The thalamus as the generator and modulator of EEG alpha rhythm: A combined PET/EEG study with lorazepam challenge in humans. *NeuroImage, 22*(2), 637-644. doi:10.1016/j.neuroimage.2004.01.047
Schroeder, C. E., & Lakatos, P. (2009). Low-frequency neuronal oscillations as instruments of sensory selection. *Trends in Neurosciences, 32*(1), 9-18. doi:10.1016/j.tins.2008.09.012
Schwalm, M., & Jubal, E. R. (2017). Back to pupillometry: How cortical network state fluctuations tracked by pupil dynamics could explain neural signal variability in human cognitive neuroscience. *Eneuro, 4*(6). doi:10.1523/ENEURO.0293-16.2017
Schwartz, Z. P., Buran, B. N., & David, S. V. (2020). Pupil-associated states modulate excitability but not stimulus selectivity in primary auditory cortex. *Journal of Neurophysiology, 123*(1), 191-208. doi:10.1152/jn.00595.2019
Seedat, Z. A., Quinn, A. J., Vidaurre, D., Liuzzi, L., Gascoyne, L. E., Hunt, B. A. E., . . . Brookes, M. J. (2020). The role of transient spectral 'bursts' in functional connectivity: A magnetoencephalography study. *NeuroImage, 209*. doi:10.1016/j.neuroimage.2020.116537
Shackman, A. J., McMenamin, B. W., Maxwell, J. S., Greischar, L. L., & Davidson, R. J. (2010). Identifying robust and sensitive frequency bands for interrogating neural oscillations. *NeuroImage, 51*(4), 1319-1333. doi:10.1016/j.neuroimage.2010.03.037
Shafiei, G., Zeighami, Y., Clark, C. A., Coull, J. T., Nagano-Saito, A., Leyton, M., . . . Misic, B. (2019). Dopamine signaling modulates the stability and integration of intrinsic brain networks. *Cerebral Cortex, 29*(1), 397-409. doi:10.1093/cercor/bhy264
Shannon, C. E. (1948). A mathematical theory of communication. *Bell System Technical Journal, 27*(3), 379-423. doi:10.1002/j.1538-7305.1948.tb01338.x
Shapcott, K. A., Schmiedt, J. T., Saunders, R. C., Maier, A., Leopold, D. A., & Schmid, M. C. (2016). Correlated activity of cortical neurons survives extensive removal of feedforward sensory input. *Scientific Reports, 6*. doi:10.1038/srep34886
Sheehan, T. C., Sreekumar, V., Inati, S. K., & Zaghloul, K. A. (2018). Signal complexity of human intracranial EEG tracks successful associative-memory formation across individuals. *Journal of Neuroscience, 38*(7), 1744-1755. doi:10.1523/Jneurosci.2389-17.2017
Sherman, M. A., Lee, S., Law, R., Haegens, S., Thorn, C. A., Hamalainen, M. S., . . . Jones, S. R. (2016). Neural mechanisms of transient neocortical beta rhythms: Converging evidence from humans, computational modeling, monkeys, and mice. *Proceedings of the National Academy of Sciences of the United States of America, 113*(33), E4885-E4894. doi:10.1073/pnas.1604135113
Sherman, S. M. (2001). Tonic and burst firing: Dual modes of thalamocortical relay. *Trends in Neurosciences, 24*(2), 122-126. doi:10.1016/s0166-2236(00)01714-8
Sherman, S. M. (2016). Thalamus plays a central role in ongoing cortical functioning. *Nature Neuroscience, 19*(4), 533-541. doi:10.1038/nn.4269

Sherman, S. M. (2017). Functioning of circuits connecting thalamus and cortex. *Compr Physiol, 7*(2), 713-739. doi:10.1002/cphy.c160032
Sherman, S. M., & Guillery, R. W. (1996). Functional organization of thalamocortical relays. *Journal of Neurophysiology, 76*(3), 1367-1395. doi:10.1152/jn.1996.76.3.1367
Sherman, S. M., & Guillery, R. W. (2013). Functional connections of cortical areas: A new view from the thalamus. *Functional Connections of Cortical Areas: A New View from the Thalamus*, 1-279.
Shew, W. L., & Plenz, D. (2013). The functional benefits of criticality in the cortex. *Neuroscientist, 19*(1), 88-100. doi:10.1177/1073858412445487
Shew, W. L., Yang, H. D., Yu, S., Roy, R., & Plenz, D. (2011). Information capacity and transmission are maximized in balanced cortical networks with neuronal avalanches. *Journal of Neuroscience, 31*(1), 55-63. doi:10.1523/Jneurosci.4637-10.2011
Shin, H., Law, R., Tsutsui, S., Moore, C. I., & Jones, S. R. (2017). The rate of transient beta frequency events predicts behavior across tasks and species. *Elife, 6*. doi:10.7554/eLife.29086
Shine, J. M., Hearne, L. J., Breakspear, M., Hwang, K., Muller, E. J., Sporns, O., . . . Cocchi, L. (2019). The low-dimensional neural architecture of cognitive complexity is related to activity in medial thalamic nuclei. *Neuron, 104*(5), 849-855 e843. doi:10.1016/j.neuron.2019.09.002
Shirvalkar, P., Seth, M., Schiff, N. D., & Herrera, D. G. (2006). Cognitive enhancement with central thalamic electrical stimulation. *Proceedings of the National Academy of Sciences of the United States of America, 103*(45), 17007-17012. doi:10.1073/pnas.0604811103
Shokri-Kojori, E., Wang, G. J., Wiers, C. E., Demiral, S. B., Guo, M., Kim, S. W., . . . Volkow, N. D. (2018). Beta-amyloid accumulation in the human brain after one night of sleep deprivation. *Proceedings of the National Academy of Sciences of the United States of America, 115*(17), 4483-4488. doi:10.1073/pnas.1721694115
Siegel, M. (2013). Spectral fingerprints of large-scale neuronal interactions. *Journal of Psychophysiology, 27*, 40-40.
Siegel, M., Buschman, T. J., & Miller, E. K. (2015). Cortical information flow during flexible sensorimotor decisions. *Science, 348*(6241), 1352-1355. doi:10.1126/science.aab0551
Siegel, M., Warden, M. R., & Miller, E. K. (2009). Phase-dependent neuronal coding of objects in short-term memory. *Proceedings of the National Academy of Sciences of the United States of America, 106*(50), 21341-21346. doi:10.1073/pnas.0908193106
Silber, M. H., Ancoli-Israel, S., Bonnet, M. H., Chokroverty, S., Grigg-Damberger, M. M., Hirshkowitz, M., . . . Iber, C. (2007). The visual scoring of sleep in adults. *Journal of Clinical Sleep Medicine, 3*(2), 121-131.
Silva, L. E. V., Cabella, B. C. T., Neves, U. P. D., & Murta, L. O. (2015). Multiscale entropy-based methods for heart rate variability complexity analysis. *Physica a-Statistical Mechanics and Its Applications, 422*, 143-152. doi:10.1016/j.physa.2014.12.011
Singer, W. (2013). Cortical dynamics revisited. *Trends in Cognitive Sciences, 17*(12), 616-626. doi:10.1016/j.tics.2013.09.006
Sinha, P., Kjelgaard, M. M., Gandhi, T. K., Tsourides, K., Cardinaux, A. L., Pantazis, D., . . . Held, R. M. (2014). Autism as a disorder of prediction. *Proceedings of the National Academy of Sciences of the United States of America, 111*(42), 15220-15225. doi:10.1073/pnas.1416797111
Smith, A. T., Cotton, P. L., Bruno, A., & Moutsiana, C. (2009). Dissociating vision and visual attention in the human pulvinar. *Journal of Neurophysiology, 101*(2), 917-925. doi:10.1152/jn.90963.2008
Snow, J. C., Allen, H. A., Rafal, R. D., & Humphreys, G. W. (2009). Impaired attentional selection following lesions to human pulvinar: Evidence for homology between human and monkey. *Proceedings of the National Academy of Sciences of the United States of America, 106*(10), 4054-4059. doi:10.1073/pnas.0810086106
Snyder, A. C., Morais, M. J., Willis, C. M., & Smith, M. A. (2015). Global network influences on local functional connectivity. *Nature Neuroscience, 18*(5), 736-743. doi:10.1038/nn.3979
Song, A. H., Kucyi, A., Napadow, V., Brown, E. N., Loggia, M. L., & Akeju, O. (2017). Pharmacological modulation of noradrenergic arousal circuitry disrupts functional connectivity of the locus ceruleus in humans. *Journal of Neuroscience, 37*(29), 6938-6945. doi:10.1523/Jneurosci.0446-17.2017
Spaak, E., Bonnefond, M., Maier, A., Leopold, D. A., & Jensen, O. (2012). Layer-specific entrainment of gamma-band neural activity by the alpha rhythm in monkey visual cortex. *Current Biology, 22*(24), 2313-2318. doi:10.1016/j.cub.2012.10.020
Spitzer, B., & Haegens, S. (2017). Beyond the status quo: A role for beta oscillations in endogenous content (re)activation. *Eneuro, 4*(4). doi:10.1523/Eneuro.0170-17.2017
Spyropoulos, G., Dowdall, J. R., Schölvinck, M. L., Bosman, C. A., Lima, B., Peter, A., . . . Fries, P. (2020). Spontaneous variability in gamma dynamics described by a linear harmonic oscillator driven by noise. *bioRxiv*.

Stam, C. J. (2005). Nonlinear dynamical analysis of EEG and MEG: Review of an emerging field. *Clinical Neurophysiology, 116*(10), 2266-2301. doi:10.1016/j.clinph.2005.06.011
Stam, C. J., Breakspear, M., van Walsum, A. M. V., & van Dijk, B. W. (2003). Nonlinear synchronization in EEG and whole-head MEG recordings of healthy subjects. *Human Brain Mapping, 19*(2), 63-78. doi:10.1002/hbm.10106
Stanley, H. E. (1971). *Introduction to phase transitions and critical phenomena*. New York: Oxford University Press.
Stein, R. B., Gossen, E. R., & Jones, K. E. (2005). Neuronal variability: Noise or part of the signal? *Nature Reviews: Neuroscience, 6*(5), 389-397. doi:10.1038/nrn1668
Stephani, T., Waterstraat, G., Haufe, S., Curio, G., Villringer, A., & Nikulin, V. V. (2020). Temporal signatures of criticality in human cortical excitability as probed by early somatosensory responses. *bioRxiv*.
Steriade, M. (2006). Grouping of brain rhythms in corticothalamic systems. *Neuroscience, 137*(4), 1087-1106. doi:10.1016/j.neuroscience.2005.10.029
Steriade, M., & Glenn, L. L. (1982). Neocortical and caudate projections of intralaminar thalamic neurons and their synaptic excitation from midbrain reticular core. *Journal of Neurophysiology, 48*(2), 352-371.
Steriade, M., & Llinas, R. R. (1988). The functional-states of the thalamus and the associated neuronal interplay. *Physiological Reviews, 68*(3), 649-742.
Stiefel, K. M., & Ermentrout, G. B. (2016). Neurons as oscillators. *Journal of Neurophysiology, 116*(6), 2950-2960. doi:10.1152/jn.00525.2015
Stitt, I., Zhou, Z. C., Radtke-Schuller, S., & Frohlich, F. (2018). Arousal dependent modulation of thalamo-cortical functional interaction. *Nat Commun, 9*(1), 2455. doi:10.1038/s41467-018-04785-6
Stringer, C., Pachitariu, M., Steinmetz, N., Reddy, C. B., Carandini, M., & Harris, K. D. (2019). Spontaneous behaviors drive multidimensional, brainwide activity. *Science, 364*(6437), 255. doi:10.1126/science.aav7893
Stringer, C., Pachitariu, M., Steinmetz, N. A., Okun, M., Bartho, P., Harris, K. D., . . . Lesica, N. A. (2016). Inhibitory control of correlated intrinsic variability in cortical networks. *Elife, 5*. doi:10.7554/eLife.19695
Stumpf, M. P. H., & Porter, M. A. (2012). Critical truths about power laws. *Science, 335*(6069), 665-666. doi:10.1126/science.1216142
Sturm, W., & Willmes, K. (2001). On the functional neuroanatomy of intrinsic and phasic alertness. *NeuroImage, 14*(1 Pt 2), S76-84. doi:10.1006/nimg.2001.0839
Su, J. H., Thomas, F. T., Kasoff, W. S., Tourdias, T., Choi, E. Y., Rutt, B. K., & Saranathan, M. (2019). Thalamus optimized multi atlas segmentation (THOMAS): Fast, fully automated segmentation of thalamic nuclei from structural MRI. *NeuroImage, 194*, 272-282. doi:10.1016/j.neuroimage.2019.03.021
Suffczynski, P., Kalitzin, S., Pfurtscheller, G., & da Silva, F. H. L. (2001). Computational model of thalamo-cortical networks: Dynamical control of alpha rhythms in relation to focal attention. *International Journal of Psychophysiology, 43*(1), 25-40. doi:Doi 10.1016/S0167-8760(01)00177-5
Suzuki, M., & Larkum, M. E. (2017). Dendritic calcium spikes are clearly detectable at the cortical surface. *Nature Communications, 8*. doi:10.1038/s41467-017-00282-4
Taghia, J., Cai, W. D., Ryali, S., Kochalka, J., Nicholas, J., Chen, T. W., & Menon, V. (2018). Uncovering hidden brain state dynamics that regulate performance and decision-making during cognition. *Nature Communications, 9*. doi:10.1038/s41467-018-04723-6
Tagliazucchi, E., von Wegner, F., Morzelewski, A., Brodbeck, V., Jahnke, K., & Laufs, H. (2013). Breakdown of long-range temporal dependence in default mode and attention networks during deep sleep. *Proceedings of the National Academy of Sciences of the United States of America, 110*(38), 15419-15424. doi:10.1073/pnas.1312848110
Takahashi, T., Cho, R., Mizuno, T., Kikuchi, M., Murata, T., Takahashi, K., & Wada, Y. (2010). Antipsychotics reverse abnormal EEG complexity in drug-naive schizophrenia: A multiscale entropy analysis. *International Journal of Neuropsychopharmacology, 13*, 242-243.
Takarae, Y., & Sweeney, J. (2017). Neural hyperexcitability in autism spectrum disorders. *Brain Sci, 7*(10). doi:10.3390/brainsci7100129
Tan, A. Y., Chen, Y., Scholl, B., Seidemann, E., & Priebe, N. J. (2014). Sensory stimulation shifts visual cortex from synchronous to asynchronous states. *Nature, 509*(7499), 226-229. doi:10.1038/nature13159
Teramae, J., & Tanaka, D. (2004). Robustness of the noise-induced phase synchronization in a general class of limit cycle oscillators. *Physical Review Letters, 93*(20). doi:10.1103/PhysRevLett.93.204103
Thaben, P. F., & Westermark, P. O. (2014). Detecting rhythms in time series with RAIN. *Journal of Biological Rhythms, 29*(6), 391-400. doi:10.1177/0748730414553029

Theyel, B. B., Llano, D. A., & Sherman, M. (2010). The corticothalamocortical circuit drives higher-order cortex in the mouse. *Nature Neuroscience, 13*(1), 84-U246. doi:10.1038/nn.2449
Thiele, A. (2013). Muscarinic signaling in the brain. *Annual Review of Neuroscience, Vol 36, 36*, 271-294. doi:10.1146/annurev-neuro-062012-170433
Thiele, A., & Bellgrove, M. A. (2018). Neuromodulation of attention. *Neuron, 97*(4), 769-785. doi:10.1016/j.neuron.2018.01.008
Thiele, A., Herrero, J. L., Distler, C., & Hoffmann, K. P. (2012). Contribution of cholinergic and GABAergic mechanisms to direction tuning, discriminability, response reliability, and neuronal rate correlations in macaque middle temporal area. *Journal of Neuroscience, 32*(47), 16602-16615. doi:10.1523/Jneurosci.0554-12.2012
Tiesinga, P. H. E., & Sejnowski, T. J. (2004). Rapid temporal modulation of synchrony by competition in cortical interneuron networks. *Neural Computation, 16*(2), 251-275. doi:10.1162/089976604322742029
Timofeev, I., Grenier, F., Bazhenov, M., Sejnowski, T. J., & Steriade, M. (2000). Origin of slow cortical oscillations in deafferented cortical slabs. *Cerebral Cortex, 10*(12), 1185-1199. doi:10.1093/cercor/10.12.1185
Tinkhauser, G., Pogosyan, A., Little, S., Beudel, M., Herz, D. M., Tan, H., & Brown, P. (2017). The modulatory effect of adaptive deep brain stimulation on beta bursts in parkinson's disease. *Brain, 140*, 1053-1067. doi:10.1093/brain/awx010
Tinkhauser, G., Pogosyan, A., Tan, H. L., Herz, D. M., Kuhn, A. A., & Brown, P. (2017). Beta burst dynamics in parkinson's disease OFF and ON dopaminergic medication. *Brain, 140*, 2968-2981. doi:10.1093/brain/awx252
Tinkhauser, G., Torrecillos, F., Duclos, Y., Tan, H. L., Pogosyan, A., Fischer, P., . . . Brown, P. (2018). Beta burst coupling across the motor circuit in parkinson's disease. *Neurobiology of Disease, 117*, 217-225. doi:10.1016/j.nbd.2018.06.007
Ton, R., & Daffertshofer, A. (2016). Model selection for identifying power-law scaling. *NeuroImage, 136*, 215-226. doi:10.1016/j.neuroimage.2016.01.008
Touboul, J., & Destexhe, A. (2017). Power-law statistics and universal scaling in the absence of criticality. *Phys Rev E, 95*(1-1), 012413. doi:10.1103/PhysRevE.95.012413
Toulmin, H., Beckmann, C. F., O'Muircheartaigh, J., Ball, G., Nongena, P., Makropoulos, A., . . . Edwards, A. D. (2015). Specialization and integration of functional thalamocortical connectivity in the human infant. *Proceedings of the National Academy of Sciences of the United States of America, 112*(20), 6485-6490. doi:10.1073/pnas.1422638112
Tran, T. T., Rolle, C. E., Gazzaley, A., & Voytek, B. (2020). Linked sources of neural noise contribute to age-related cognitive decline. *Journal of Cognitive Neuroscience*, 1-110. doi:10.1162/jocn_a_01584
Tsubo, Y., Takada, M., Reyes, A. D., & Fukai, T. (2007). Layer and frequency dependencies of phase response properties of pyramidal neurons in rat motor cortex. *European Journal of Neuroscience, 25*(11), 3429-3441. doi:10.1111/j.1460-9568.2007.05579.x
Uhlhaas, P. J., & Singer, W. (2010). Abnormal neural oscillations and synchrony in schizophrenia. *Nature Reviews Neuroscience, 11*(2), 100-113. doi:10.1038/nrn2774
Vakorin, V. A., & McIntosh, A. R. (2012). Mapping the multiscale information content of complex brain signals. *Principles of Brain Dynamics: Global State Interactions*, 183-208.
Valencia, J. F., Porta, A., Vallverdu, M., Claria, F., Baranowski, R., Orlowska-Baranowska, E., & Caminal, P. (2009). Refined multiscale entropy: Application to 24-h holter recordings of heart period variability in healthy and aortic stenosis subjects. *IEEE Transactions on Biomedical Engineering, 56*(9), 2202-2213. doi:10.1109/Tbme.2009.2021986
Van der Werf, Y. D., Witter, M. P., & Groenewegen, H. J. (2002). The intralaminar and midline nuclei of the thalamus. Anatomical and functional evidence for participation in processes of arousal and awareness. *Brain Research Reviews, 39*(2-3), 107-140. doi:10.1016/S0165-0173(02)00181-9
Van Drongelen, W. (2018). *Signal processing for neuroscientists*: Academic Press.
van Ede, F., Quinn, A. J., Wookich, M. W., & Nobre, A. C. (2018). Neural oscillations: Sustained rhythms or transient burst-events? *Trends in Neurosciences, 41*(7), 415-417. doi:10.1016/j.tins.2018.04.004
van Kerkoerle, T., Self, M. W., Dagnino, B., Gariel-Mathis, M. A., Poort, J., van der Togt, C., & Roelfsema, P. R. (2014). Alpha and gamma oscillations characterize feedback and feedforward processing in monkey visual cortex. *Proceedings of the National Academy of Sciences of the United States of America, 111*(40), 14332-14341. doi:10.1073/pnas.1402773111
Vanderwolf, C. H. (1969). Hippocampal electrical activity and voluntary movement in the rat. *Electroencephalography and Clinical Neurophysiology, 26*(4), 407-418. doi:10.1016/0013-4694(69)90092-3

VanRullen, R. (2016). Perceptual cycles. *Trends in Cognitive Sciences, 20*(10), 723-735. doi:10.1016/j.tics.2016.07.006
VanRullen, R., & Koch, C. (2003). Is perception discrete or continuous? *Trends in Cognitive Sciences, 7*(5), 207-213. doi:10.1016/S1364-6613(03)00095-0
vanVreeswijk, C., & Sompolinsky, H. (1996). Chaos in neuronal networks with balanced excitatory and inhibitory activity. *Science, 274*(5293), 1724-1726.
Varela, F., Lachaux, J. P., Rodriguez, E., & Martinerie, J. (2001). The brainweb: Phase synchronization and large-scale integration. *Nature Reviews: Neuroscience, 2*(4), 229-239. doi:10.1038/35067550
Varela, F. J., Toro, A., John, E. R., & Schwartz, E. L. (1981). Perceptual framing and cortical alpha-rhythm. *Neuropsychologia, 19*(5), 675-686.
Vazey, E. M., Moorman, D. E., & Aston-Jones, G. (2018). Phasic locus coeruleus activity regulates cortical encoding of salience information. *Proceedings of the National Academy of Sciences of the United States of America, 115*(40), E9439-E9448. doi:10.1073/pnas.1803716115
Vidaurre, D., Abeysuriya, R., Becker, R., Quinn, A. J., Alfaro-Almagro, F., Smith, S. M., & Woolrich, M. W. (2018). Discovering dynamic brain networks from big data in rest and task. *NeuroImage, 180*, 646-656. doi:10.1016/j.neuroimage.2017.06.077
Vidaurre, D., Hunt, L. T., Quinn, A. J., Hunt, B. A. E., Brookes, M. J., Nobre, A. C., & Woolrich, M. W. (2018). Spontaneous cortical activity transiently organises into frequency specific phase-coupling networks. *Nature Communications, 9*. doi:10.1038/s41467-018-05316-z
Vijayan, S., & Kopell, N. J. (2012). Thalamic model of awake alpha oscillations and implications for stimulus processing. *Proceedings of the National Academy of Sciences of the United States of America, 109*(45), 18553-18558. doi:10.1073/pnas.1215385109
Vinck, M., Batista-Brito, R., Knoblich, U., & Cardin, J. A. (2015). Arousal and locomotion make distinct contributions to cortical activity patterns and visual encoding. *Neuron, 86*(3), 740-754. doi:10.1016/j.neuron.2015.03.028
von der Malsburg, C., Phillips, W. A., & Singer, W. (2010). *Dynamic coordination in the brain: From neurons to mind*. Cambridge, MA: MIT Press.
von Stein, A., & Sarnthein, J. (2000). Different frequencies for different scales of cortical integration: From local gamma to long range alpha/theta synchronization. *International Journal of Psychophysiology, 38*(3), 301-313. doi:10.1016/S0167-8760(00)00172-0
Voytek, B., & Knight, R. T. (2015). Dynamic network communication as a unifying neural basis for cognition, development, aging, and disease. *Biological Psychiatry, 77*(12), 1089-1097. doi:10.1016/j.biopsych.2015.04.016
Voytek, B., Kramer, M. A., Case, J., Lepage, K. Q., Tempesta, Z. R., Knight, R. T., & Gazzaley, A. (2015). Age-related changes in 1/f neural electrophysiological noise. *Journal of Neuroscience, 35*(38), 13257-13265. doi:10.1523/Jneurosci.2332-14.2015
Walter, W. G. (1943a). An automatic low frequency analyser. *Electronic Engineering, 16*(184), 9-13.
Walter, W. G. (1943b). An improved low frequency analyser. *Electronic Engineering, 16*, 236–238.
Wang, H., McIntosh, A. R., Kovacevic, N., Karachalios, M., & Protzner, A. B. (2016). Age-related multiscale changes in brain signal variability in pre-task versus post-task resting-state EEG. *Journal of Cognitive Neuroscience, 28*(7), 971-984. doi:10.1162/jocn_a_00947
Wang, H. S., & Busse, E. W. (1969). EEG of healthy old persons--a longitudinal study. I. Dominant background activity and occipital rhythm. *Journal of Gerontology, 24*(4), 419-426. doi:10.1093/geronj/24.4.419
Wang, X. J. (2010). Neurophysiological and computational principles of cortical rhythms in cognition. *Physiological Reviews, 90*(3), 1195-1268. doi:10.1152/physrev.00035.2008
Ward, L. M. (2003). Synchronous neural oscillations and cognitive processes. *Trends in Cognitive Sciences, 7*(12), 553-559. doi:10.1016/j.tics.2003.10.012
Ward, L. M. (2013). The thalamus: Gateway to the mind. *Wiley Interdisciplinary Reviews: Cognitive Science, 4*(6), 609-622. doi:10.1002/wcs.1256
Waschke, L., Wostmann, M., & Obleser, J. (2017). States and traits of neural irregularity in the age-varying human brain. *Scientific Reports, 7*. doi:10.1038/s41598-017-17766-4
Weissman, M. B. (1988). 1/f noise and other slow, nonexponential kinetics in condensed matter. *Reviews of Modern Physics, 60*(2), 537-571. doi:10.1103/RevModPhys.60.537
Wen, H., & Liu, Z. (2016). Separating fractal and oscillatory components in the power spectrum of neurophysiological signal. *Brain Topography, 29*(1), 13-26. doi:10.1007/s10548-015-0448-0
Wen, H. G., & Liu, Z. M. (2016). Broadband electrophysiological dynamics contribute to global resting-state fMRI signal. *Journal of Neuroscience, 36*(22), 6030-6040. doi:10.1523/Jneurosci.0187-16.2016

Whitten, T. A., Hughes, A. M., Dickson, C. T., & Caplan, J. B. (2011). A better oscillation detection method robustly extracts EEG rhythms across brain state changes: The human alpha rhythm as a test case. *NeuroImage, 54*(2), 860-874. doi:10.1016/j.neuroimage.2010.08.064

Whittingstall, K., & Logothetis, N. K. (2009). Frequency-band coupling in surface EEG reflects spiking activity in monkey visual cortex. *Neuron, 64*(2), 281-289. doi:10.1016/j.neuron.2009.08.016

Wilson, H. R., & Cowan, J. D. (1973). A mathematical theory of the functional dynamics of cortical and thalamic nervous tissue. *Kybernetik, 13*(2), 55-80. doi:10.1007/bf00288786

Wimmer, R. D., Schmitt, L. I., Davidson, T. J., Nakajima, M., Deisseroth, K., & Halassa, M. M. (2015). Thalamic control of sensory selection in divided attention. *Nature, 526*(7575), 705-709. doi:10.1038/nature15398

Wolff, M., & Vann, S. D. (2019). The cognitive thalamus as a gateway to mental representations. *Journal of Neuroscience, 39*(1), 3-14. doi:10.1523/JNEUROSCI.0479-18.2018

Womelsdorf, T., Fries, P., Mitra, P. P., & Desimone, R. (2006). Gamma-band synchronization in visual cortex predicts speed of change detection. *Nature, 439*(7077), 733-736. doi:10.1038/nature04258

Womelsdorf, T., Schoffelen, J. M., Oostenveld, R., Singer, W., Desimone, R., Engel, A. K., & Fries, P. (2007). Modulation of neuronal interactions through neuronal synchronization. *Science, 316*(5831), 1609-1612. doi:10.1126/science.1139597

Womelsdorf, T., Valiante, T. A., Sahin, N. T., Miller, K. J., & Tiesinga, P. (2014). Dynamic circuit motifs underlying rhythmic gain control, gating and integration. *Nature Neuroscience, 17*(8), 1031-1039. doi:10.1038/nn.3764

Wöstmann, M., Alavash, M., & Obleser, J. (2019). Alpha oscillations in the human brain implement distractor suppression independent of target selection. *Journal of Neuroscience, 39*(49), 9797-9805. doi:10.1523/JNEUROSCI.1954-19.2019

Wright, N. F., Vann, S. D., Aggleton, J. P., & Nelson, A. J. (2015). A critical role for the anterior thalamus in directing attention to task-relevant stimuli. *Journal of Neuroscience, 35*(14), 5480-5488. doi:10.1523/JNEUROSCI.4945-14.2015

Wutz, A., Melcher, D., & Samaha, J. (2018). Frequency modulation of neural oscillations according to visual task demands. *Proceedings of the National Academy of Sciences of the United States of America, 115*(6), 1346-1351. doi:10.1073/pnas.1713318115

Wyder, M. T., Massoglia, D. P., & Stanford, T. R. (2004). Contextual modulation of central thalamic delay-period activity: Representation of visual and saccadic goals. *Journal of Neurophysiology, 91*(6), 2628-2648. doi:10.1152/jn.01221.2003

Xing, D., Shen, Y., Burns, S., Yeh, C. I., Shapley, R., & Li, W. (2012). Stochastic generation of gamma-band activity in primary visual cortex of awake and anesthetized monkeys. *Journal of Neuroscience, 32*(40), 13873-13880a. doi:10.1523/JNEUROSCI.5644-11.2012

Xue, M. S., Atallah, B. V., & Scanziani, M. (2014). Equalizing excitation-inhibition ratios across visual cortical neurons. *Nature, 511*(7511), 596-600. doi:10.1038/nature13321

Yamamoto, Y., & Hughson, R. L. (1993). Extracting fractal components from time-series. *Physica D, 68*(2), 250-264. doi:10.1016/0167-2789(93)90083-D

Yang, A. C., Wang, S. J., Lai, K. L., Tsai, C. F., Yang, C. H., Hwang, J. P., . . . Fuh, J. L. (2013). Cognitive and neuropsychiatric correlates of EEG dynamic complexity in patients with alzheimer's disease. *Progress in Neuro-Psychopharmacology and Biological Psychiatry, 47*, 52-61. doi:10.1016/j.pnpbp.2013.07.022

Yang, G. J., Murray, J. D., Wang, X. J., Glahn, D. C., Pearlson, G. D., Repovs, G., . . . Anticevic, A. (2016). Functional hierarchy underlies preferential connectivity disturbances in schizophrenia. *Proceedings of the National Academy of Sciences of the United States of America, 113*(2), E219-E228. doi:10.1073/pnas.1508436113

Yang, H. D., Shew, W. L., Roy, R., & Plenz, D. (2012). Maximal variability of phase synchrony in cortical networks with neuronal avalanches. *Journal of Neuroscience, 32*(3), 1061-1072. doi:10.1523/Jneurosci.2771-11.2012

Yizhar, O., Fenno, L. E., Prigge, M., Schneider, F., Davidson, T. J., O'Shea, D. J., . . . Deisseroth, K. (2011). Neocortical excitation/inhibition balance in information processing and social dysfunction. *Nature, 477*(7363), 171-178. doi:10.1038/nature10360

Yu, J. N., & Ferster, D. (2010). Membrane potential synchrony in primary visual cortex during sensory stimulation. *Neuron, 68*(6), 1187-1201. doi:10.1016/j.neuron.2010.11.027

Yu, Y. G., Migliore, M., Hines, M. L., & Shepherd, G. M. (2014). Sparse coding and lateral inhibition arising from balanced and unbalanced dendrodendritic excitation and inhibition. *Journal of Neuroscience, 34*(41), 13701-13713. doi:10.1523/Jneurosci.1834-14.2014

Yuval-Greenberg, S., Tomer, O., Keren, A. S., Nelken, I., & Deouell, L. Y. (2008). Transient induced gamma-band response in EEG as a manifestation of miniature saccades. *Neuron, 58*(3), 429-441. doi:10.1016/j.neuron.2008.03.027

Zagha, E., Casale, A. E., Sachdev, R. N., McGinley, M. J., & McCormick, D. A. (2013). Motor cortex feedback influences sensory processing by modulating network state. *Neuron, 79*(3), 567-578. doi:10.1016/j.neuron.2013.06.008

Zagha, E., & McCormick, D. A. (2014). Neural control of brain state. *Current Opinion in Neurobiology, 29*, 178-186. doi:10.1016/j.conb.2014.09.010

Zanto, T. P., & Gazzaley, A. (2017). Selective attention and inhibitory control in the aging brain *Cognitive neuroscience of aging: Linking cognitive and cerebral aging, 2nd ed.* (pp. 207-234). New York, NY, US: Oxford University Press.

Zerbi, V., Floriou-Servou, A., Markicevic, M., Vermeiren, Y., Sturman, O., Privitera, M., . . . Bohacek, J. (2019). Rapid reconfiguration of the functional connectome after chemogenetic locus coeruleus activation. *Neuron, 103*(4), 702-718 e705. doi:10.1016/j.neuron.2019.05.034

Zhang, H., Watrous, A. J., Patel, A., & Jacobs, J. (2018). Theta and alpha oscillations are traveling waves in the human neocortex. *Neuron, 98*(6), 1269-1281 e1264. doi:10.1016/j.neuron.2018.05.019

Zhigalov, A., & Jensen, O. (2020). Alpha oscillations do not implement gain control in early visual cortex but rather gating in parieto-occipital regions. *bioRxiv*.

Zhou, S. L., & Yu, Y. G. (2018). Synaptic E-I balance underlies efficient neural coding. *Frontiers in Neuroscience, 12*. doi:10.3389/fnins.2018.00046

Zhou, T. S., Chen, L. N., & Aihara, K. (2005). Molecular communication through stochastic synchronization induced by extracellular fluctuations. *Physical Review Letters, 95*(17). doi:10.1103/PhysRevLett.95.178103

Zihl, J., & von Cramon, D. (1979). The contribution of the 'second' visual system to directed visual attention in man. *Brain, 102*(4), 835-856. doi:10.1093/brain/102.4.835

Zou, Q. H., Zhu, C. Z., Yang, Y. H., Zuo, X. N., Long, X. Y., Cao, Q. J., . . . Zang, Y. F. (2008). An improved approach to detection of amplitude of low-frequency fluctuation (ALFF) for resting-state fMRI: Fractional ALFF. *Journal of Neuroscience Methods, 172*(1), 137-141. doi:10.1016/j.jneumeth.2008.04.012

Zuo, X. N., Di Martino, A., Kelly, C., Shehzad, Z. E., Gee, D. G., Klein, D. F., . . . Milham, M. P. (2010). The oscillating brain: Complex and reliable. *NeuroImage, 49*(2), 1432-1445. doi:10.1016/j.neuroimage.2009.09.037

7. Appendices

The appendix section contains the following main manuscripts as well as their Supplementary Materials. Continuous page numbers are presented on the top throughout the appendices.

NeuroImage 206 (2020) 116331

Contents lists available at ScienceDirect

NeuroImage

journal homepage: www.elsevier.com/locate/neuroimage

Single-trial characterization of neural rhythms: Potential and challenges

Julian Q. Kosciessa [a,b,c,*], Thomas H. Grandy [b], Douglas D. Garrett [a,b], Markus Werkle-Bergner [b,**]

[a] Max Planck UCL Centre for Computational Psychiatry and Ageing Research, Lentzeallee 94, 14195, Berlin, Germany
[b] Center for Lifespan Psychology, Max Planck Institute for Human Development, Lentzeallee 94, 14195, Berlin, Germany
[c] Department of Psychology, Humboldt-Universität zu Berlin, Rudower Chaussee 18, 12489, Berlin, Germany

ARTICLE INFO

Keywords:
Rhythm detection
Rhythmic duration
Rhythmic amplitude
Inter-individual differences
Single-trial rhythm estimates

ABSTRACT

The average power of rhythmic neural responses as captured by MEG/EEG/LFP recordings is a prevalent index of human brain function. Increasing evidence questions the utility of trial-/group averaged power estimates however, as seemingly sustained activity patterns may be brought about by time-varying transient signals in each single trial. Hence, it is crucial to accurately describe the duration and power of rhythmic and arrhythmic neural responses on the single trial-level. However, it is less clear how well this can be achieved in empirical MEG/EEG/LFP recordings. Here, we extend an existing rhythm detection algorithm (**e**xtended **B**etter **OSC**illation detection: "eBOSC"; cf. Whitten et al., 2011) to systematically investigate boundary conditions for estimating neural rhythms at the single-trial level. Using simulations as well as resting and task-based EEG recordings from a micro-longitudinal assessment, we show that alpha rhythms can be successfully captured in single trials with high specificity, but that the quality of single-trial estimates varies greatly between subjects. Despite those signal-to-noise-based limitations, we highlight the utility and potential of rhythm detection with multiple proof-of-concept examples, and discuss implications for single-trial analyses of neural rhythms in electrophysiological recordings. Using an applied example of working memory retention, rhythm detection indicated load-related increases in the duration of frontal theta and posterior alpha rhythms, in addition to a frequency decrease of frontal theta rhythms that was observed exclusively through amplification of rhythmic amplitudes.

1. Introduction

1.1. Towards a single-trial characterization of neural rhythms

Episodes of rhythmic neural activity in electrophysiological recordings are of prime interest for research on neural representations and computations across multiple scales of measurement (e.g. Buzsáki, 2006; Wang, 2010). At the macroscopic level, the study of rhythmic neural signals has a long heritage, dating back to Hans Berger's classic investigations into the Alpha rhythm (Berger, 1938). Since then, advances in recording and processing techniques have facilitated large-scale spectral analysis schemes (e.g. Gross, 2014) that were not available to the pioneers of electrophysiological research, who often depended on the manual analysis of single time series to indicate the presence and magnitude of rhythmic events. Interestingly, improvements in analytic methods still do not capture all of the information that can be extracted by manual inspection. For example, current analysis techniques are largely naïve to the specific temporal presence of rhythms in the continuous recordings, as they often employ windowing of condition- or group-based averages to extract putative rhythm-related characteristics (Cohen, 2014). However, the underlying assumption of stationary, sustained rhythms within the temporal window of interest might not consistently be met (Jones, 2016; Stokes and Spaak, 2016), thus challenging the appropriateness of the averaging model (i.e., the ergodicity assumption (Molenaar and Campbell, 2009)). Furthermore, in certain situations, single-trial characterizations become necessary to derive unbiased individual estimates of neural rhythms (Cohen, 2017). For example, this issue becomes important when asking whether rhythms appear in transient or in sustained form (van Ede et al., 2018), or when only single-shot acquisitions are feasible (i.e., resting state or sleep recordings).

1.2. Duration as a powerful index of rhythmicity

The presence of rhythmicity is a necessary prerequisite for the accurate interpretation of measures of amplitude, power, and phase (Aru et al., 2015; Jones, 2016; Muthukumaraswamy and Singh, 2011). This is

* Corresponding author. Center for Lifespan Psychology, Max Planck Institute for Human Development, Lentzeallee 94, 14195, Berlin, Germany.
** Corresponding author.
E-mail addresses: kosciessa@mpib-berlin.mpg.de (J.Q. Kosciessa), werkle@mpib-berlin.mpg.de (M. Werkle-Bergner).

https://doi.org/10.1016/j.neuroimage.2019.116331
Received 2 September 2019; Accepted 1 November 2019
Available online 8 November 2019

exemplified by the bias that arrhythmic periods exert on rhythmic power estimates. Most current time-frequency decomposition methods of neurophysiological signals (such as the electroencephalogram (EEG)) are based on the Fourier transform (Gross, 2014). Following Parceval's theorem (e.g. Hansen, 2014), the Fast Fourier Transform (FFT) decomposes an arbitrary time series into a sum of sinusoids at different frequencies. Importantly, FFT-derived power estimates do not differentiate between high-amplitude transients and low-amplitude sustained signals. In the case of FFT power, this is a direct result of the violated assumption of stationarity in the presence of a transient signal. Short-time FFT and wavelet techniques alleviate (but do not eliminate) this problem by analyzing shorter epochs, during which stationarity is more likely to be obtained. However, whenever spectral power is averaged across these episodes, both high-amplitude rhythmic and low-amplitude arrhythmic signal components may once again become intermixed. In the presence of arrhythmic content (often referred to as the "signal background," or "noise"), this results in a reduced amplitude estimate of the underlying rhythm, the extent of which relates to the duration of the rhythmic episode relative to the length of the analysed segment (which we will refer to as 'abundance') (see Fig. 1A). Therefore, integration across epochs that contain a mixture of rhythmic and arrhythmic signals results in an inherent ambiguity between the strength of the rhythmic activity (as indexed by power/amplitude) and its duration (as indexed by the abundance of the rhythmic episode within the segment) (see Fig. 2B).

Crucially, the strength and duration of rhythmic activity theoretically differ in their neurophysiological interpretation. Rhythmic power most readily indexes the magnitude of synchronized changes in membrane potentials within a network (Buzsáki et al., 2012), and is thus related to the size of the participating neural population. The duration of a rhythmic episode, by contrast, tracks how long population synchrony is upheld. Notably, measures of rhythm duration have recently gained interest as they may provide additional information regarding the biophysical mechanisms that give rise to the recorded signals (Peterson and Voytek, 2017; Sherman et al., 2016), for example, by differentiating between transient and sustained rhythmic events (van Ede et al., 2018).

1.3. Single-trial rhythm detection as a methodological challenge

In general, the accurate estimation of process parameters depends on a sufficiently strong signal in the neurophysiological recordings under investigation. Especially for scalp-level M/EEG recordings it remains elusive whether neural rhythms are sufficiently strong to be clearly detected in single trials. Here, a large neural population has to be synchronously active to give rise to potentials that are visible at the scalp surface. This problem intensifies further by signal attenuation through the skull (in the case of EEG) and the superposition of signals from diverse sources of no interest both in- and outside the brain (Schomer & Lopes da Silva, 2017). In sum, these considerations lead to the proposal that the signal-to-noise ratio (SNR), here operationally defined as the ratio of rhythmic to arrhythmic variance, may fundamentally constrain the accurate characterization of single-trial rhythms.

Following those considerations, we set out to answer the following hypotheses and questions: (1) A precise differentiation between rhythmic and arrhythmic timepoints can disambiguate the strength and the duration of rhythmicity. (2) To what extent does the single-trial rhythm representation in empirical data allow for an accurate estimation of rhythmic strength and duration in the face of variations in the signal-to-noise ratio of rhythmicity? (3) What are the empirical benefits of separating rhythmic (and arrhythmic) duration and power?

Recently, the Better OSCillation Detection (BOSC; Caplan et al., 2001; Whitten et al., 2011) method has been proposed to identify rhythmicity at the single-trial level. BOSC defines rhythmicity based on the presence of a spectral peak that is superimposed on an arrhythmic 1/f background and that remains present for a minimum number of cycles. Here, we extend the BOSC method (i.e., extended BOSC; eBOSC) to derive rhythmic temporal episodes that can be used to further characterize rhythmicity. Using simulations, we derive rhythm detection benchmarks and probe the boundary conditions for unbiased rhythm indices. Furthermore, we apply the eBOSC algorithm to resting- and task-state data from a micro-longitudinal dataset to systematically investigate the feasibility to derive reliable and valid indices of neural rhythmicity from single-trial scalp EEG data and to probe their modulation by working memory load.

We focus on alpha rhythms (~8–15 Hz; defined here based on individual FFT-peaks) due to (a) their high amplitude in human EEG recordings, (b) the previous focus on the alpha band in the rhythm detection literature (Caplan et al., 2015; Fransen et al., 2015; Whitten et al., 2011), and (c) their importance for human cognition (Grandy et al., 2013a; Klimesch, 2012; Sadaghiani and Kleinschmidt, 2016). We present examples beyond the alpha range to highlight the ability to apply eBOSC in multiple, diverse frequency ranges.

2. Methods

2.1. Study design

Resting state and task data were collected in the context of a larger assessment, consisting of eight sessions in which an adapted Sternberg short-term memory task (Sternberg, 1966) and three additional cognitive tasks were repeatedly administered. Resting state data are from the first session, task data are from sessions one, seven and eight, during which EEG data were acquired. Sessions one through seven were completed on consecutive days (excluding Sundays) with session seven completed seven days after session one by all but one participant (eight days due to a two-day break). Session eight was conducted approximately one week after session seven (M = 7.3 days, SD = 1.4) to estimate the stability of the behavioral practice effects. The reported EEG sessions lasted approximately three and a half to 4 h, including approximately one and a half hours of EEG preparation. For further details on the study protocol and results of the behavioural tasks see (Grandy et al., 2017).

2.2. Participants

The sample contained 32 young adults (mean age = 23.3 years, SD = 2.0, range 19.6–26.8 years; 17 women; 28 university students) recruited from the participant database of the Max Planck Institute for Human Development, Berlin, Germany (MPIB). Participants were right-handed, as assessed with a modified version of the Edinburgh Handedness Inventory (Oldfield, 1971), and had normal or corrected-to-normal vision, as assessed with the Freiburg Visual Acuity test (Bach, 1996, 2007). Participants reported to be in good health with no known history of neurological or psychiatric incidences and were paid for their participation (8.08 € per hour, 25.00 € for completing the study within 16 days, and a performance-dependent bonus of 28.00 €; see below). All participants gave written informed consent according to the institutional guidelines of the ethics committee of the MPIB, which approved the study.

2.3. Procedure

Participants were seated at a distance of 80 cm in front of a 60 Hz LCD monitor in an acoustically and electrically shielded chamber. A resting state assessment was conducted prior to the initial performance of the adapted Sternberg task. Two resting state periods were used: the first encompassed a duration of 2 min of continuous eyes open (EO1) and eyes closed (EC1) periods, respectively; the second resting state was comprised of two 80 s runs, totalling 16 repetitions of 5 s interleaved eyes open (EO2) – eyes closed (EC2) periods. An auditory beep indicated to the subjects when to open and close their eyes.

Following the resting assessments, participants performed an adapted version of the Sternberg task. Digits were presented in white on a black

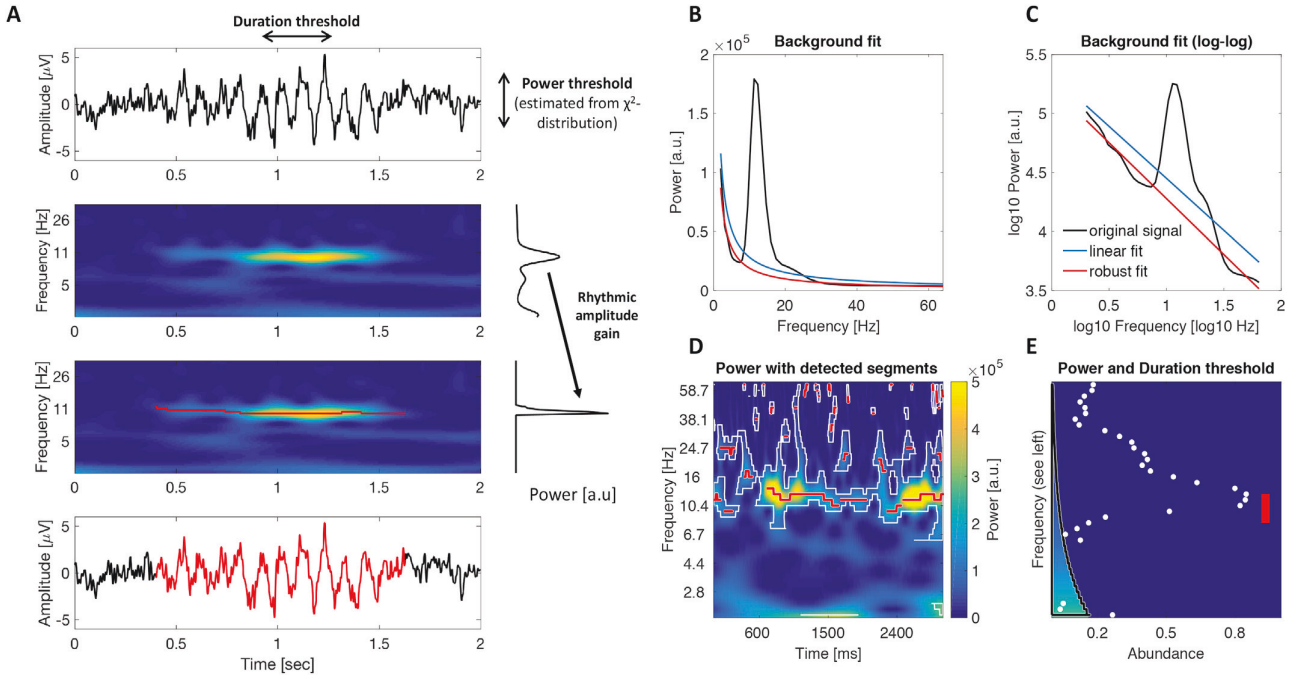

Fig. 1. Schematic illustration of rhythm detection. (A) Average amplitude estimates (right) increase with the focus on rhythmic episodes within the averaged time interval. The left plots show simulated time series and the corresponding time-frequency power. Superimposed red traces indicate rhythmic time points. The upper right plot shows the average power spectrum averaged across the entire epoch, the lower plot presents amplitudes averaged exclusively across rhythmic time points. An amplitude gain is observed due to the exclusion of arrhythmic low amplitude time points. (B–E) Comparison of standard and extended BOSC. (B + C) Rhythms were detected based on a power threshold estimated from the arrhythmic background spectrum. Standard BOSC applies a linear fit in log-log space to define the background power, which may overestimate the background at the frequencies of interest in the case of data with large rhythmic peaks. Robust regression following peak removal alleviates this problem. (D) Example of episode detection. White borders circumfuse time frequency points, at which standard BOSC indicated rhythmic content. Red traces represent the continuous rhythmic episodes that result from the extended post-processing. (E) Applied thresholds and detected rhythmic abundance. The black border denotes the duration threshold at each frequency (corresponding to D), i.e., for how long the power threshold needed to be exceeded to count as a rhythmic period. Note that this threshold can be set to zero for a post-hoc characterization of the duration of episodes (see Methods 2.12). The color scaling within the demarcated area indicates the power threshold at each frequency. Abundance corresponds to the relative length of the segment on the same time scale as presented in D. White dots correspond to the standard BOSC measure of rhythmic abundance at each frequency (termed Pepisode). Red lines indicate the abundance measure used here, which is defined as the proportion of sample points at which a rhythmic episode between 8 and 15 Hz was indicated (shown as red traces in D).

background and subtended ~2.5° of visual angle in the vertical and ~1.8° of visual angle in the horizontal direction. Stimulus presentation and recording of behavioral responses were controlled with E-Prime 2.0 (Psychology Software Tools, Inc., Pittsburgh, PA, USA). The task design followed the original report (Sternberg, 1966). Participants started each trial by pressing the left and right response key with their respective index fingers to ensure correct finger placement and to enable fast responding. An instruction to blink was given, followed by the sequential presentation of 2, 4 or 6 digits from zero to nine. On each trial, the memory set size (i.e., load) varied randomly between trials, and participants were not informed about the upcoming condition. Also, the single digits constituting a given memory set were randomly selected in each trial. Each stimulus was presented for 200 ms, followed by a fixed 1000 ms blank inter-stimulus interval (ISI). The offset of the last stimulus coincided with the onset of a 3000 ms blank retention interval, which concluded with the presentation of a probe item that was either contained in the presented stimulus set (*positive probe*) or not (*negative probe*). Probe presentation lasted 200 ms, followed by a blank screen for 2000 ms, during which the participant's response was recorded. A beep tone indicated the end of the trial. The task lasted about 50 min.

For each combination of load x probe type, 31 trials were conducted, cumulating in 186 trials per session. Combinations were randomly distributed across four blocks (block one: 48 trials; blocks two through four: 46 trials). Summary feedback of the overall mean RT and accuracy within the current session was shown at the end of each block. At the beginning of session one, 24 practice trials were conducted to familiarize participants with the varying set sizes and probe types. To sustain high motivation throughout the study, participants were paid a 28 € bonus if their current session's mean RT was faster or equal to the overall mean RT during the preceding session, while sustaining accuracy above 90%. Only correct trials were included in the analyses.

2.4. EEG recordings and pre-processing

EEG was continuously recorded from 64 Ag/AgCl electrodes using BrainAmp amplifiers (Brain Products GmbH, Gilching, Germany). Sixty scalp electrodes were arranged within an elastic cap (EASYCAP GmbH, Herrsching, Germany) according to the 10% system (cf. Oostenveld et al., 2011) with the ground placed at AFz. To monitor eye movements, two electrodes were placed on the outer canthi (horizontal EOG) and one electrode below the left eye (vertical EOG). During recording, all electrodes were referenced to the right mastoid electrode, while the left mastoid electrode was recorded as an additional channel. Prior to recording, electrode impedances were retained below 5 kΩ. Online, signals were recorded with an analog pass-band of 0.1–250 Hz and digitized at a sampling rate of 1 kHz.

Preprocessing and analysis of EEG data were conducted with the FieldTrip toolbox (Oostenveld et al., 2011) and using custom-written MATLAB (The MathWorks Inc., Natick, MA, USA) code. Offline, EEG data were filtered using a 4th order Butterworth filter with a pass-band of 0.5–100 Hz, and were linearly detrended. Resting data with interleaved eye closure were epoched relative to the auditory cue to open and close the eyes. An epoch of −2 s to +3 s relative to on- and offsets was chosen to include padding for the analysis. During the eBOSC procedure, 3 s of

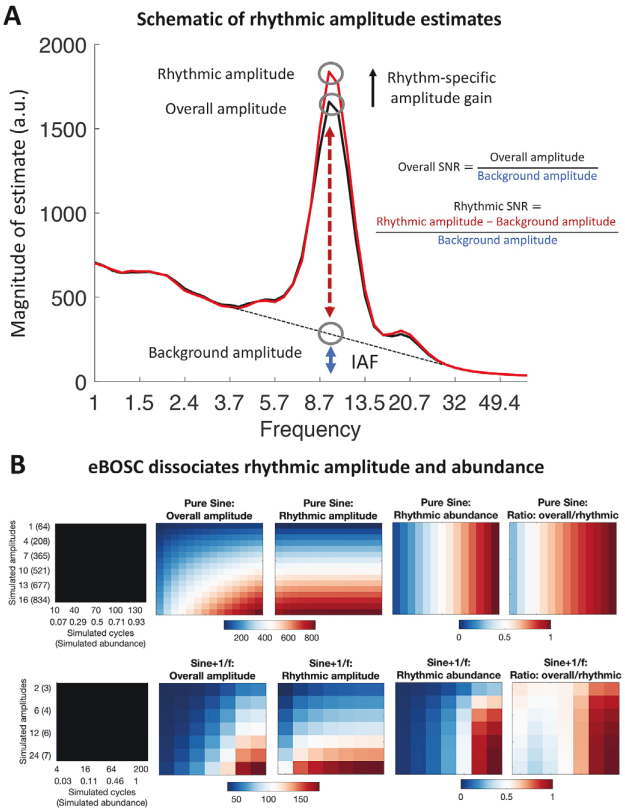

Fig. 2. eBOSC disambiguates the magnitude and duration of rhythmic episodes. (**A**) Schema of different amplitude metrics. (**B**) Rhythm-detection disambiguates rhythmic amplitude and duration. Overall amplitudes represent a mixture of rhythmic power and duration. In the absence of noise (upper row), eBOSC perfectly orthogonalizes rhythmic amplitude from abundance. Superimposed noise leads to an imperfect separation of the two metrics (lower row). The duration of rhythmicity is similarly indicated by abundance and the overlap between rhythmic and overall amplitudes. This can be seen by comparing the two rightmost plots in each row.

signal were removed from both edges (see below), resulting in an effective epoch of 4 s duration that excludes evoked components following the cue onset. Continuous eyes open/closed recordings were segmented to the cue on- and offset. For the interleaved data, the first and last trial for each condition were removed, resulting in an effective trial number of 14 trials per condition. For the task data, we analysed two intervals: an extended interval to assess the overall dynamics of detected rhythmicity and a shorter interval that focused on the retention period. Unless otherwise noted, we refer to the extended interval when presenting task data. For the extended segments, task data were segmented to 21 s epochs ranging from −9 s to +12 s with regard to the onset of the 3 s retention interval for analyses including peri-retention data. For analyses including only the retention phase, data were segmented to −2 s to +3 s around the retention interval. Note that for all analyses, 3 s of signal were removed on each side of the signal during eBOSC detection, effectively removing the evoked cue activity (2 s to account for edge artifacts following wavelet-transformation and 1 s to account for eBOSC's duration threshold, see section 2.6), except during the extended task interval. Hence, detected segments were restricted to occur from 1s after period onset until period offset, thereby excluding evoked signals. Blink, movement and heart-beat artifacts were identified using Independent Component Analysis (ICA; Bell and Sejnowski, 1995) and removed from the signal. Subsequently, data were downsampled to 250 Hz and all channels were re-referenced to mathematically averaged mastoids. Artifact-contaminated channels (determined across epochs) were automatically detected (a) using the FASTER algorithm (Nolan et al., 2010) and (b) by detecting outliers exceeding three standard deviations of the kurtosis of the distribution of power values in each epoch within low (0.2–2 Hz) or high (30–100 Hz) frequency bands, respectively. Rejected channels were interpolated using spherical splines (Perrin et al., 1989). Subsequently, noisy epochs were likewise excluded based on FASTER and recursive outlier detection, resulting in the rejection of approximately 13% of trials. To prevent trial rejection due to artifacts outside the signal of interest, artifact detection was restricted to epochs that included 2.4 s of additional signal around the on- and offset of the retention interval, corresponding to the longest effective segment that was used in the analyses. A further 2.65% of incorrectly answered trials from the task were subsequently excluded.

2.5. Rhythm-detection using extended BOSC

We applied an extended version of the Better OSCillation detection method (eBOSC; cf. Caplan et al., 2001; Whitten et al., 2011) to automatically separate rhythmic from arrhythmic episodes. The BOSC method reliably identifies rhythms using data-driven thresholds based on theoretical assumptions of the signal characteristics. Briefly, the method defines rhythms as time points during which wavelet-derived power at a particular frequency exceeds a *power threshold* based on an estimate of the arrhythmic signal background. The theoretical *duration threshold* defines a minimum duration of cycles this power threshold has to be exceeded to exclude high amplitude transients. Previous applications of the BOSC method focused on the analysis of resting-state data or long data epochs, where reliable detection has been established regardless of specific parameter setups (Caplan et al., 2001, 2015; Whitten et al., 2011). We introduce the following adaptations here (for details see section 2.6, Fig. 1 & Fig. S1): (1) we remove the spectral alpha peak and use robust regression to establish power thresholds; (2) we combine detected time points into continuous rhythmic episodes and (3) we reduce the impact of wavelet convolution on abundance estimates. We benchmarked the algorithm and compared it to standard BOSC using simulations (see section 2.8).

2.6. Specifics of rhythm-detection using extended BOSC

Rhythmic events were detected within subjects for each channel and condition. Time-frequency transformation of single trials was performed using 6-cycle Morlet wavelets (Grossmann and Morlet, 1985) with 49 logarithmically-spaced center frequencies ranging from 1 to 64 Hz. Following the wavelet transform, 2 s were removed at each segment's borders to exclude edge artifacts. To estimate the background spectrum, the time-frequency spectra from all trials were temporally concatenated within condition and channel and log-transformed, followed by temporal averaging. For eyes-closed and eyes-open resting states, both continuous and interleaved exemplars were included in the background estimation for the respective conditions. The resulting power spectrum was fit linearly in log(frequency)-log(power) coordinates using a robust regression, with the underlying assumption that the EEG background spectrum is characterized by coloured noise of the form A*f(−α) (Buzsáki and Mizuseki, 2014; He et al., 2010; Linkenkaer-Hansen et al., 2001). A robust regression with bisquare weighting (e.g. Holland and Welsch, 2007) was chosen to improve the linear fit of the background spectrum (cf. Haller et al., 2018), which was characterized by frequency peaks in the alpha range for almost all subjects (Fig. S4). In contrast to ordinary least squares regression, robust regression iteratively down-weights outliers (in this case spectral peaks) from the linear background fit. To improve the definition of rhythmic power estimates as outliers during the robust regression, power estimates within the wavelet pass-band around the

individual alpha peak frequency were removed prior to fitting.[1] The passband of the wavelet (e.g. Linkenkaer-Hansen et al., 2001) was calculated as

$$Passband\ [Hz] = IAF\ \pm\ 0.5*\frac{2}{WL}*IAF \quad (1)$$

in which IAF denotes the individual alpha peak frequency and WL refers to wavelet length (here, six cycles in the main analysis). IAF was determined based on the peak magnitude within the 8–15 Hz average spectrum for each channel and condition (Grandy et al., 2013b). This ensures that the maximum spectral deflection is removed across subjects, even in cases where no or multiple peaks are present.[2] This procedure effectively removes a bias of the prevalent alpha peak on the arrhythmic background estimate (see Fig. 1B and C & Fig. 3C). The power threshold for rhythmicity at each frequency was set at the 95th percentile of a χ^2(2)-distribution of power values, centered on the linearly fitted estimate of background power at the respective frequency (for details see Whitten et al., 2011). This essentially implements a significance test of single-trial power against arrhythmic background power. A three-cycle threshold was used as the duration threshold to exclude transients, unless indicated otherwise (see section 2.12). The conjunctive power and duration criteria produce a binary matrix of 'detected' rhythmicity for each time-frequency point (see Fig. S1C). To account for the duration criterion, 1000 ms were discarded from each edge of this 'detected' matrix.

The original BOSC algorithm was further extended to define rhythmic events as continuous temporal episodes that allow for an event-wise assessment of rhythm characteristics (e.g. duration). The following steps were applied to the binary matrix of 'detected' single-trial rhythmicity to derive such sparse and continuous episodes. First, to account for the spectral extension of the wavelet, we selected time-frequency points with maximal power within the wavelet's spectral smoothing range (i.e. the pass-band of the wavelet; $\frac{2}{WL}$*frequency; see Formula 1). That is, at each time point, we selected the frequency with the highest indicated rhythmicity within each frequency's pass-band. This served to exclude super-threshold timepoints that may be accounted for by spectral smoothing of a rhythm at an adjacent frequency. Note that this effectively creates a new frequency resolution for the resulting rhythmic episodes, thus requiring sufficient spectral resolution (defined by the wavelet's pass-band) to differentiate simultaneous rhythms occurring at close frequencies. Finally, continuous rhythmic episodes were formed by temporally connecting extracted time points, while allowing for moment-to-moment frequency transitions (i.e. within-episode frequency non-stationarities; Atallah and Scanziani, 2009) (for a single-trial illustration see Fig. 1D and Fig. S1D).

In addition to the spectral extension of the wavelet, the choice of wavelet parameter also affects the extent of temporal smoothing, which may bias rhythmic duration estimates. To decrease such temporal bias, we compared observed rhythmic amplitudes at each time point within each rhythmic episode with those expected by smoothing adjacent amplitudes using the wavelet (Fig. S1E). By retaining only those time points where amplitudes exceeded the smoothing-based expectations, we removed supra-threshold time points that can be explained by temporal smoothing of nearby rhythms (e.g., 'ramping' up and down signals). In more detail, we simulated the positive cycle of a sine wave at each frequency, zero-shouldered each edge and performed (6-cycle) wavelet convolution. The resulting amplitude estimates at the zero-padded time points reflect the temporal smoothing bias of the wavelet on adjacent arrhythmic time points. This bias is maximal (*BiasMax*) at the time point immediately adjacent to the rhythmic on-/offset and decreases with temporal distance to the rhythm. Within each rhythmic episode, the 'convolution bias' of a time-frequency (TF) point's amplitude on surrounding points was estimated by scaling the points' amplitude by the modelled temporal smoothing bias.

$$Amplitudes_{F,T+1-L:L-T} = \left[(Amplitude_{TF} - PT_F) * \frac{BiasVector_{F,T+1-L:L-T:}}{BiasMax_F}\right] + PT_F \quad (2)$$

Subscripts F and T denote frequency and time within each episode, respectively. *BiasVector* is a vector with the length of the current episode (L) that is centered around the current TF-point. It contains the wavelet's symmetric convolution bias around *BiasMax*. Note that both BiasVector and BiasMax respect the possible frequency variations within an episode (i.e., they reflect the differences in convolution bias between frequencies). The estimated wavelet bias was then scaled to the amplitude of the rhythmic signal at the current TF-point. PT refers to the condition- and frequency-specific power threshold applied during rhythm detection. We subtracted the power threshold to remove arrhythmic contributions. This effectively sensitizes the algorithm to near-threshold values, rendering them more likely to be excluded. Finally, time points with lower amplitudes than expected by the convolution model were removed and new rhythmic episodes were created (Fig. S1F). The resulting episodes were again checked for adhering to the duration threshold.

As an alternative to the temporal wavelet correction based on the wavelet's simulated maximum bias ('MaxBias'; as described above), we investigated the feasibility of using the wavelet's full-width half maximum ('FWHM') as a criterion. Within each continuous episode and for each "rhythmic" sample point, 6-cycle wavelets at the frequency of the neighbouring points were created and scaled to the point's amplitude. We then used the amplitude of these wavelets at the FWHM as a threshold for rhythmic amplitudes. That is, points within a rhythmic episodes that had amplitudes below those of the scaled wavelets were defined as arrhythmic. The resulting continuous episodes were again required to pass the duration threshold. As the FWHM approach indicated decreased specificity of rhythm detection in the simulations (Fig. S2) we used the 'MaxBias' method for our analyses.

Furthermore, we considered a variant where total amplitude values were used (vs. supra-threshold amplitudes) as the basis for the temporal wavelet correction. Our results suggest that using supra-threshold power values leads to a more specific detection at the cost of sensitivity (Fig. S2). Crucially, this eliminated false alarms and abundance overestimation, thus rendering the method highly specific to the occurrence of rhythmicity. As we regard this as a beneficial feature, we used supra-threshold amplitudes as the basis for the temporal wavelet correction throughout the manuscript.

[1] This procedure is similar to calculating the background spectrum from conditions with attenuated alpha power (e.g., the eyes open resting state; Caplan et al. (2015)). However, here we ensure that alpha power is sufficiently removed, whereas if conditions with reduced alpha peak magnitudes are selected, alpha power may still remain sufficiently elevated to influence slope or intercept estimates. Furthermore, the reliance on conditions with decreased rhythmicity appears less suitable given inter-individual differences in alpha engagement in e.g., the eyes open condition. This may induce an implicit contrast to eyes open rhythmicity. Note that when the frequency range is chosen so that the alpha peak represents the middle of the chosen interval, the alpha-induced bias would be captured by a linear increment in the intercept of the background fit, which may also be alleviated by choosing a higher percentile for the power threshold. Notably, removing the alpha peak as done here attenuates such bias, even in cases where the alpha peak biases the slope of the background fit, as would happen if the alpha peak is not centered within the range of sampled frequencies.

[2] When multiple alpha-band peaks are present or the peak has a broader appearance, the spectral peak may not be removed entirely, which could result in misfits of the background spectrum. For this purpose, we employed robust regression to down-weight potential residuals around the alpha peak. Our current implementation only accounts for a peak in the alpha range, but could be extended to other frequency ranges using the same logic (see discussion on limitations in section 4.6).

2.7. Definition of abundance, rhythmic probability and amplitude metrics

A central goal of rhythm detection is to disambiguate rhythmic power and duration (Fig. 2). For this purpose, eBOSC provides multiple indices. We describe the different indices for the example case of alpha rhythms. Please note that eBOSC can be applied in a similar fashion to any other frequency range. The ***abundance*** of alpha rhythms denotes the duration of rhythmic episodes with a mean frequency in the alpha range (8–15 Hz), relative to the duration of the analysed segment. This frequency range was motivated by clear peaks within this range in individual resting state spectra (Fig. S4). Note that abundance is closely related to standard BOSC's Pepisode metric (Whitten et al., 2011), with the difference that abundance refers to the duration of the continuous rhythmic episodes and not the 'raw' detected rhythmicity of BOSC (cf. Figs. S1C and D). We further define ***rhythmic probability*** as the *across trials* probability to observe a detected rhythmic episode within the alpha frequency range at a given point in time. It is therefore the within-time, across-trial equivalent of abundance.

As a result of rhythm detection, the magnitude of spectral events can be described using multiple metrics (see Fig. 2A for a schematic). Amplitudes were calculated as the square-root of wavelet-derived power estimates and are used interchangeably throughout the manuscript. The standard measure of window-averaged amplitudes, ***overall amplitudes*** were computed by averaging across the entire segment at its alpha peak frequency. In contrast, ***rhythmic amplitudes*** correspond to the amplitude estimates during detected rhythmic episodes. If no alpha episode was indicated, abundance was set to zero, and amplitude was set to missing. Unless indicated otherwise, both amplitude measures were normalized by subtracting the amplitude estimate of the fitted background spectrum. This step represents a parameterization of rhythmic power (cf. Haller et al., 2018) and is conceptually similar to baseline normalization, without requiring an explicit baseline segment. This highlights a further advantage of rhythm-detection procedures like (e)BOSC. In addition, we calculated an ***overall signal-to-noise ratio (SNR)*** as the ratio of the overall amplitude to the background amplitude: $\frac{Overall}{Background}$. In addition, we defined ***rhythmic SNR*** as the background-normalized rhythmic amplitude as a proxy for the rhythmic representation: $\frac{Rhythmic-Background}{Background}$.

Unless stated differently, subject-, and condition-specific amplitude and abundance values were averaged within and across trials, and across posterior-occipital channels (P7, P5, P3, P1, Pz, P2, P4, P6, P8, PO7, PO3, POz, PO4, PO8, O1, Oz, O2), in which alpha power was maximal (Fig. 4A, Fig. 8).

2.8. eBOSC validation via alpha rhythm simulations

To assess eBOSC's detection performance, we simulated 10 Hz sine waves with varying amplitudes (0, 2, 4, 6, 8, 12, 16, 24 [a.u.]) and durations (2, 4, 8, 16, 32, 64, 128, 200 [cycles]) that were symmetrically centered within random 1/f-filtered white noise signals (20 s; 250 Hz sampling rate). Amplitudes were scaled relative to the power of the 8–12 Hz 6th order Butterworth-filtered background signal in each trial to approximate SNRs. To ensure comparability with the empirical analyses, we computed overall SNR analogously to the empirical data, which tended to be lower than the target SNR. We chose the maximum across simulated durations as an upper bound (i.e., conservative estimate) on overall SNR. For each amplitude-duration combination we simulated 500 "trials". We assessed three different detection pipelines regarding their detection efficacy: the standard BOSC algorithm (i.e., linear background fit incorporating the entire frequency range with no post-editing of the detected matrix); the eBOSC method using wavelet correction by simulating the maximum bias introduced by the wavelet ("MaxBias); and the eBOSC method using the full-width-at-half-maximum amplitude for convolution correction ("FWHM"). The background was estimated separately for each amplitude-duration combination. 500 edge points were removed bilaterally following wavelet estimation, 250 additional samples were removed bilaterally following BOSC detection to account for the duration threshold, effectively retaining 14 s of simulated signal.

Detection efficacy was indexed by signal detection criteria regarding the identification of rhythmic time points between 8 and 12 Hz (i.e., hits = simulated and detected points; false alarms = detected, but not simulated points). These measures are presented as ratios to the full amount of possible points within each category (e.g., hit rate = hits/all simulated time points). For the eBOSC pipelines, abundance was calculated identically to the analyses of empirical data. As no consecutive episodes (cf. Pepisode and abundance) are available in standard BOSC, abundance was defined as the relative amount of time points with detected rhythmicity between 8 and 12 Hz.

A separate simulation aimed at establishing the ability to accurately recover amplitudes. For this purpose, we simulated a whole-trial alpha signal (i.e., duration = 1) and a quarter-trial alpha signal (duration = .25) with a larger range of amplitudes (1:16 [a.u.]) and performed otherwise identical procedures as described above. To assess eBOSC's ability to disambiguate power and duration (Fig. 2B), we additionally performed simulations in the absence of noise across a larger range of simulated amplitudes and durations.

A major change in eBOSC compared to standard BOSC is the exclusion of the rhythmic peak prior to estimating the background. To investigate to what extent the two methods induce a bias between rhythmicity and the estimated background magnitude (for a schematic see Fig. 1C and D), we calculated Pearson correlations between the overall amplitude and the estimated background amplitude across all levels of simulated amplitudes and durations (Fig. 3C).

As the empirical data suggested a trial-wise association between amplitude and abundance estimates also at high levels of signal-to-noise ratios (Fig. 7), we investigated whether such associations were also present in the simulations. For each pair of simulated amplitude and duration, we calculated Pearson correlations between the overall amplitude and abundance across single trials. Note that due to the stationarity of simulated duration, trial-by-trial fluctuations indicate the bias under fluctuations of the noise background (as amplitudes were scaled to the background in each trial). For each cell, we performed Fisher's r-to-z transform to account for unequal trial sizes due to missing amplitude/abundance estimates (e.g. when no episodes are detected).

2.9. Calculation of phase-based lagged coherence

To investigate the convergence between the power-based duration estimate (abundance) and a phase-based alternative (Fransen et al., 2015), we calculated lagged coherence at 40 linearly scaled frequencies in the range of 1–40 Hz for each resting-state condition. Lagged coherence assesses the consistency of phase clustering at a single sensor for a chosen cycle lag (see Fransen et al., 2015 for formulas). Instantaneous power and phase were estimated via 3-cycle wavelets. Data were segmented to be identical to eBOSC's effective interval (i.e., same removal of signal shoulders as described above). In reference to the duration threshold for power-based rhythmicity, we calculated the averaged lagged coherence using two adjacent epochs à three cycles. We computed an index of alpha rhythmicity by averaging values across epochs and posterior-occipital channels, finally extracting the value at the maximum lagged coherence peak in the 8–15 Hz range.

2.10. Dynamics of rhythmic probability and rhythmic power during task performance

To investigate the detection properties in the task data, we analysed the temporal dynamics of rhythmic probability and power in the alpha band. We created time-frequency representations as described in section 2.6 and extracted the alpha peak power time series, separately for each person, condition, channel and trial. At the single-trial level, values were allocated to rhythmic vs. arrhythmic time points according to whether a rhythmic episode with mean frequency in the respective range was

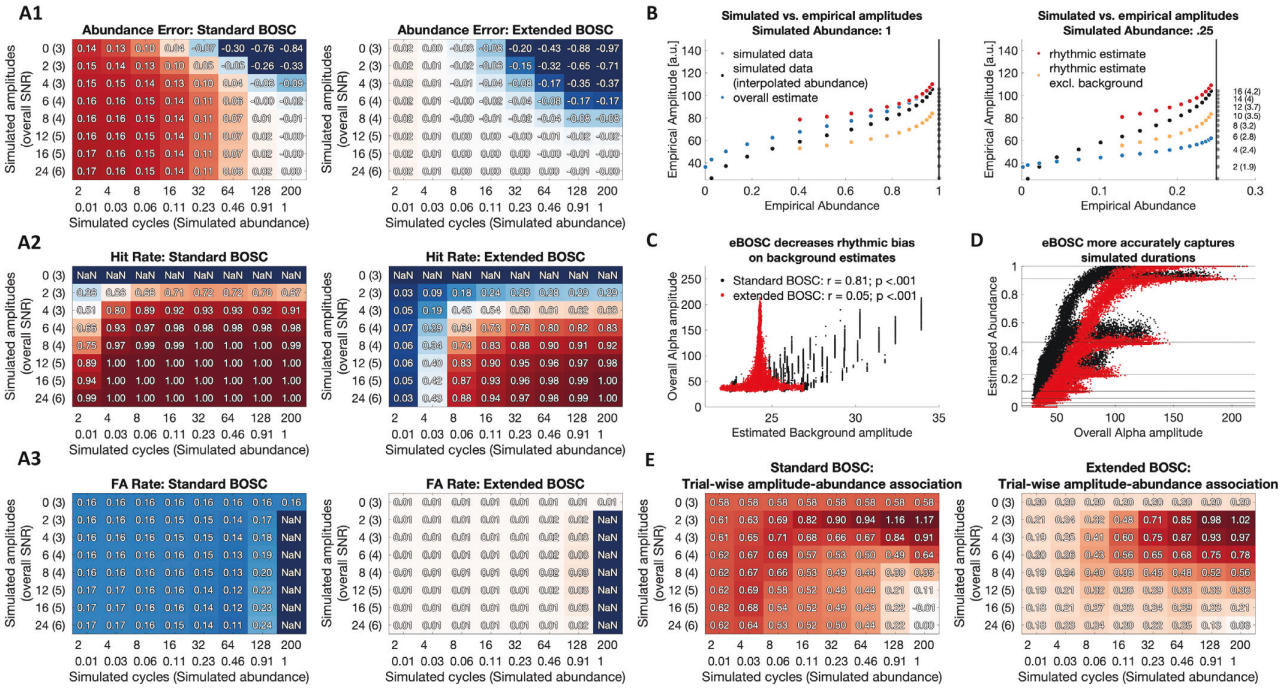

Fig. 3. Rhythm detection performance of standard and extended BOSC in simulations. (**A**) Signal detection properties of the two algorithms. For short simulated rhythmicity, abundance is overestimated by standard BOSC, but not eBOSC, whereas eBOSC underestimates the duration of prolonged rhythmicity at low SNRs (A1). Extended BOSC has decreased sensitivity (A2), but higher specificity (A3) compared with extended BOSC. Note that for simulated zero alpha amplitude, all sample points constitute potential false alarms, while by definition no sample point constitutes a potential hit. (**B**) Amplitude and abundance estimate for signals with sustained (left) and short rhythmicity (right). Black dots indicate reference estimates for a pure sine wave without noise, coloured dots indicate the respective estimates for data with the 1/f background. [Note that the reference estimates were interpolated at the empirical abundance of the 1/f data. Gray dots indicate the perfect abundance estimates in the absence of background noise.] When rhythms are sustained (left), impaired rhythm detection at low SNRs causes an overestimation of the rhythmic amplitude. At low rhythmic duration (right), this deficit is outweighed by the severe bias of arrhythmic duration on overall amplitude estimates (e.g., Fig. 9). Simulated amplitudes (and corresponding empirical SNRs in brackets) are shown on the right. Vertical lines indicate the simulated rhythmic duration. (**C**) eBOSC successfully reduces the bias of the rhythmic peak on the estimation of the background amplitude. In comparison, standard BOSC induces a strong coupling between the peak magnitude and the background estimate. (**D**) eBOSC indicates abundance more accurately than standard BOSC at high amplitudes (i.e., high SNR; see also A1). The leftward shift indicates a decrease in sensitivity. Horizontal lines indicate different levels of simulated duration. Dots are single-trial estimates across levels of simulated amplitude and duration. (**E**) Standard BOSC and eBOSC induce trial-wise correlations between amplitude and abundance. eBOSC exhibits reduced trial-by-trial coupling at higher SNR compared to standard BOSC. Values are r-to-z-transformed correlation coefficients.

indicated by eBOSC. These time series were averaged within subject to create individual averages of rhythm dynamics. Subsequently, we z-scored the power time series to accentuate signal dynamics and attenuate between-subject power differences. To highlight global dynamics, these time series were further averaged within- and between-subjects. Figure captions indicate which average was used.

2.11. Rhythm-conditional spectra and abundance for multiple canonical frequencies

To assess the general feasibility of rhythm detection outside the alpha range, we analysed the retention interval of the adapted Sternberg task, where the occurrence of theta, alpha and beta rhythms has been reported in previous studies (Brookes et al., 2011; Jensen et al., 2002; Jokisch and Jensen, 2007; Lundqvist et al., 2016; Raghavachari et al., 2001; Tuladhar et al., 2007). For this purpose, we re-segmented the data to cover the final 2 s of the retention interval +- 3 s of edge signal that was removed during the eBOSC procedure. We performed eBOSC rhythm detection with otherwise identical parameters to those described in section 2.6. We then calculated spectra across those time points where rhythmic episodes with a mean frequency in the range of interest were indicated, separately for four frequency ranges: 3–8 Hz (theta), 8–15 Hz (alpha), 15–25 Hz (beta) and 25–64 Hz (gamma). We subtracted spectra across the remaining arrhythmic time-points for each range from these 'rhythm-conditional' spectra to derive the spectra that are unique to those time points with rhythmic occurrence in the band of interest. For the corresponding topographic representations, we calculated the abundance metric as described in section 2.7 for the apparent peak frequency ranges.

2.12. Post-hoc characterization of sustained rhythms vs. transients

Instead of exclusively relying on a fixed *a priori* duration threshold as done in previous applications, eBOSC's continuous 'rhythmic episodes' also allow for a post-hoc separation of rhythms and transients based on the duration of identified rhythmic episodes. This is afforded by our extended post-processing that results in a more specific identification of rhythmic episodes (see Fig. 3) and an estimated length for each episode. For this analysis (Fig. 10), we set the *a priori* duration threshold to zero and separated the resulting episodes post-hoc based on their duration (shorter vs. longer than 3 cycles) at their mean frequency. That is, any episode crossing the amplitude threshold was retained and episodes were sorted by their 'transient' or sustained appearance afterwards. We conducted this analysis in the extended task data to illustrate the temporal dynamics of rhythmic and transient events. To investigate the modulation of rhythm- and transient-specific metrics between the retention phase and the probe phase, we averaged metrics within these two intervals and performed a paired *t*-test between the two respective intervals for four indices: episode number, duration, frequency and power. Cluster-based permutation tests (Maris and Oostenveld, 2007) as implemented in FieldTrip were performed to control for multiple

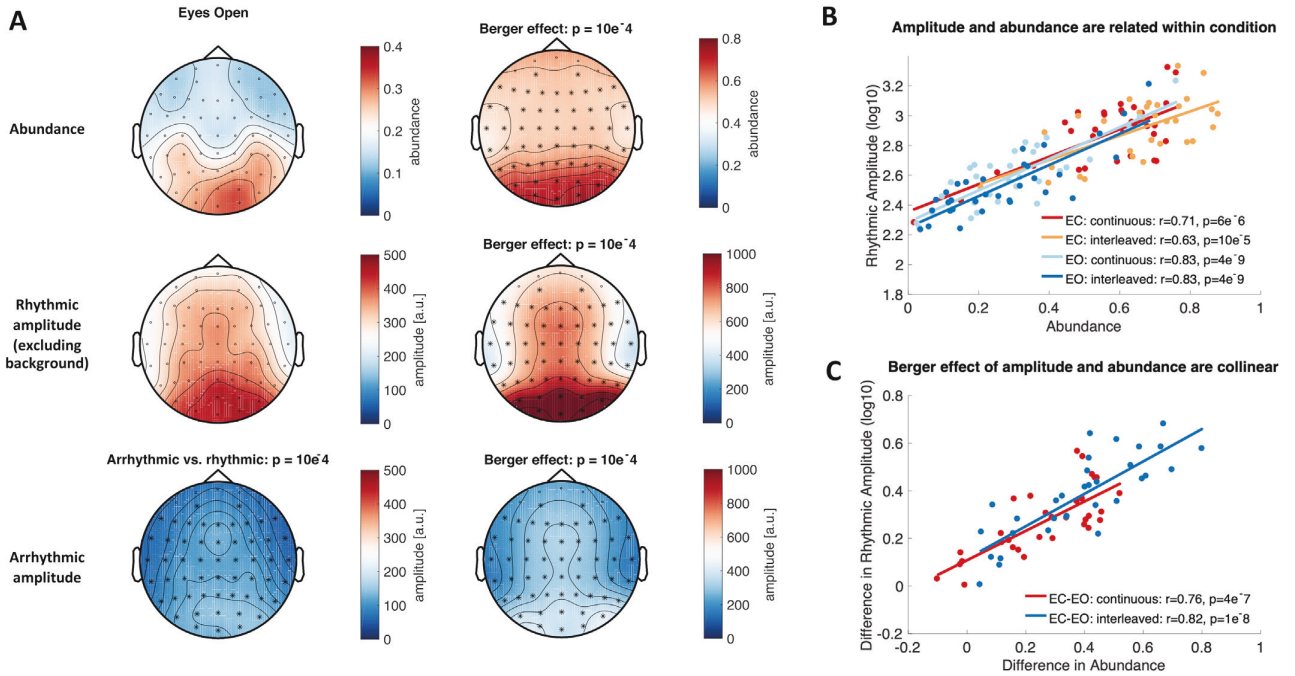

Fig. 4. Rhythmic alpha abundance and amplitude during rest. (**A**) eBOSC identifies high occipital alpha abundance and rhythmic amplitude especially during the Eyes Closed resting state. White asterisks indicate significant decreases for arrhythmic from rhythmic amplitudes (cluster is identical between conditions). Black asterisks indicate significant increases upon eye closure. (**B**) Rhythmic amplitude and abundance are inter-individually related during rest (**C**) The modulation of eye closure has similar effects on amplitude and abundance. Estimates were extracted from posterior-occipital channels.

comparisons. Initially, a clustering algorithm formed clusters based on significant t-tests of individual data points ($p < .05$; cluster entry threshold) with the spatial constraint of min. three adjacent channels. Then, the significance of the observed cluster-level statistic, based on the summed t-values within the cluster, was assessed by comparison to the distribution of all permutation-based cluster-level statistics. The final cluster p-value that we report in Figures was assessed as the proportion of 1000 Monte Carlo iterations in which the cluster-level statistic was exceeded. Cluster significance was indicated by p-values below .025 (two-sided cluster significance threshold).

2.13. Time series representations of detected rhythmic events

To visualize the stereotypic depiction of single-trial rhythmic events, we extracted the time series during individual rhythmic episodes that exceeded a post-hoc duration threshold of three cycles. Individual time series were time-locked to the trough of individual rhythmic episodes and averaged across episodes (Sherman et al., 2016). To avoid unequal sample counts at the edges of episodes, we included additional data padding around the trough prior to averaging. The trough was chosen to be the local minimum during the spectral episode that was closest to the maximum power of the wavelet-transformed signal. To better estimate the local minimum, the time domain signal was low-pass filtered at 25 Hz for alpha and beta, 10 Hz for theta and high-pass-filtered at 20 Hz for gamma using a 6th order Butterworth filter. Filters only served the identification of local minima, whereas unfiltered data were used for plotting. Averaged event dynamics during the first session were visualized for theta at Fz, alpha at O2, beta at FCz and gamma at Fz. To visualize single-trial time-domain signals, we computed moving averages of 150 trials across rhythmic episodes concatenated across all subjects.

We further assessed a potential load-modulation of the rate of rhythmic events during working memory retention by counting the number of individual rhythmic episodes with a mean frequency that fell in a moving window of 3 adjacent center frequencies. This produced a channel-by-frequency representation of spectral event rates, which were the basis for subsequent significance testing using dependent sample regression t-tests and implemented in permutation tests as described in section 2.12.

2.14. Modulation of rhythm estimates by working memory load and eye closure

To assess the sensitivity of rhythm-derived indices to experimental manipulations, we compared (1) the effect of eye closure ("Berger effect") and (2) the effect of working memory load between select rhythm indices. To compare rhythm-specific results with traditional approaches, traditional wavelet estimates were derived using identical parameters as used for eBOSC. We performed confirmatory tests of a parametric increase in posterior alpha power and frontal theta power with memory load based on previous reports in the literature (Jensen et al., 2002; Jensen and Tesche, 2002; Jokisch and Jensen, 2007; Meltzer et al., 2008; Michels et al., 2008; Onton et al., 2005; Scheeringa et al., 2009; Tuladhar et al., 2007). In addition, we explored a decrease in frontal theta frequency with load. To reduce the amount of statistical contrasts, we averaged all metrics across sessions before submitting them to statistical tests. Load effects for within-subject trial averages between load conditions were assessed by means of a dependent sample regression *t*-test, implemented within permutation tests (see section 2.12 for details). Similar cluster-based permutation tests were performed for the effect of eye closure on rhythmic and arrhythmic amplitudes and abundance using a paired samples *t*-test.

Beyond probing effects on each estimate individually, we probed whether rhythm-specific estimates of duration and magnitude uniquely captured task effects over and above traditional indices. For this purpose, we performed post-hoc linear mixed effects analyses, averaging within the abundance effects clusters. Prior to modelling, values were z-scored across subjects and conditions. In each model, a rhythm-specific index (e.g. abundance) served as the dependent variable, while traditional

amplitudes served as a fixed dependent variable. Load or eye closure were modelled as fixed effects with random subject intercepts, assuming compound symmetry. For the load effect, we assessed uniquely explained variance with a post-hoc ANOVA, using marginal sums-of-squares ('Type III'). Linear mixed effects modelling was performed in R 3.6.1 (R Core Team, 2019) with the nlme package (Pinheiro et al., 2019).

In addition, we explored effects on theta frequency with cluster-based permutations. To visualize frequency modulations, we performed a post-hoc Fast Fourier Transform (FFT) to specifically characterize rhythmic episodes, while normalizing for their duration. To retain an identical frequency resolution across episodes, we zero-padded episodes of variable duration to a fixed duration of 2 s. We then computed a discrete-time Fourier Transform of individual rhythmic episodes: $Y(k) = \sum_{j=1}^{n} X(j) W_n^{(j-1)(k-1)}$, where n is the length of the zero-padded time series X and $W_n = e^{(-2\pi i)/n}$, normalized the resulting absolute spectral values by the length of the rhythmic episode $N_{rhythmic}$ and calculated the single-sided amplitude spectrum. This resulted in rhythm-specific amplitude values with an identical frequency resolution across episodes. In contrast, to derive rhythm-unspecific FFT amplitude estimates, we included the entire two-second retention period in the estimation and used the respective length for normalization, thus resulting in traditional 'overall' FFT amplitude estimates that were unspecific to rhythmic occurrence. To assess, whether a theta frequency modulation would be observed with traditional FFT spectra, we detected condition-dependent theta frequency peaks. Peaks were defined as frequencies at which the first derivative of the spectrum changed from positive to negative (Grandy et al., 2013b). In case no peak was identified, the frequency with peak amplitude was selected. Finally, we performed paired-t-tests to estimate potential load effects.

In figures, we display within-subject standard errors (Cousineau, 2005) to highlight condition differences. For these, individual data were centered by subtracting the subject condition average and adding the grand condition average to individual within-condition values.

3. Results

3.1. Extended BOSC (eBOSC) increases specificity of rhythm detection

We extended the BOSC rhythm detection method to characterize rhythmicity at the single-trial level by creating continuous 'rhythmic episodes' (see Fig. 1 & Fig. S1). A central goal of this approach is the disambiguation of rhythmic power and duration, which can be achieved perfectly in data without background noise (upper row in Fig. 2B). However, the addition of 1/f noise reintroduces a partial coupling of the two parameters (lower row in Fig. 2B). To better understand the boundary conditions to derive specific amplitude and duration estimates, we compared the detection properties of the standard and the extended (eBOSC) pipeline by simulating varying levels of rhythm magnitude and duration. Considering the sensitivity and specificity of detection, both pipelines performed adequately at high levels of SNR with high hit and low false alarm rates (Fig. 3A). However, whereas standard BOSC showed perfect sensitivity above SNRs of ~4, specificity was lower than for eBOSC as indicated by higher false alarm rates (grand averages: 0.160 for standard BOSC; 0.015 for eBOSC). This specificity increase was observed across simulation parameters, suggesting a general abundance overestimation by standard BOSC (see also Fig. 3D). In addition, standard BOSC did not show a reduced detection of transient rhythms below the duration threshold of three cycles, whereas hit rates for those transients were clearly reduced with eBOSC (Fig. 3A2). This suggests that wavelet convolution extended the effective duration of transient rhythmic episodes, resulting in an exceedance of the temporal threshold. In contrast, by creating explicit rhythmic episodes and reducing convolution effects, eBOSC more strictly adhered to the specified target duration. However, there was also a notable reduction in sensitivity for rhythms just above the duration threshold, suggesting a sensitivity-specificity trade-off (Fig. 3A2). In addition to decreasing false alarms, eBOSC also more accurately estimated the duration of rhythmicity (Fig. 3A1), although an underestimation of abundance persisted (and was increased) at low SNRs. In sum, while eBOSC improved the specificity of identifying rhythmic content, there were also noticeable decrements in sensitivity (grand averages: 0.909 for standard BOSC; 0.614 for eBOSC), especially at low SNRs. Comparable results were obtained with a 3-cycle wavelet (Fig. S3). Notably, while sensitivity remains an issue, the high specificity of detection suggests that the estimated rhythmic abundance serves as a lower bound on the actual duration of rhythmicity.

In a second set of simulations, we considered eBOSC's potential to accurately estimate rhythmic amplitudes. As expected, in signals with stationary rhythms (duration = 1), the time-invariant 'overall' amplitude estimate most accurately represented simulated amplitudes (Fig. 3B left), as any methods-induced underestimation biased rhythm-specific amplitudes. Specifically, at low SNRs, underestimation of rhythmic content resulted in an overestimation of rhythmic amplitudes, as some low-amplitude time points were incorrectly excluded prior to averaging. At those low SNRs, subtraction of the background estimate (cf. baseline normalization) alleviated this overestimation. The general impairment at low SNRs was however outweighed by the advantage of rhythm-specific amplitude estimates in time series where rhythmic duration was low and thus arrhythmicity was prevalent (Fig. 3B right). Here, rhythm-specific estimates accurately tracked simulated amplitudes, whereas a strong underestimation was observed for unspecific power indices. In both scenarios, we observed an underestimation of rhythmic abundance with decreasing amplitudes (cf. Fig. 3A1).

An adaptation of the eBOSC method is the exclusion of the rhythmic alpha peak prior to fitting the arrhythmic background. This serves to reduce a potential bias of rhythmic content on the estimation of the arrhythmic content (see Fig. 1C for a schematic). Our simulations indeed indicated a bias of the spectral peak amplitude on the background estimate in the standard BOSC algorithm, which was substantially reduced in eBOSC's estimates (Fig. 3C).

To gain a visual representation of duration estimation performance, we plotted abundance against amplitude estimates across all simulated trials, regardless of simulation parameters (Fig. 3D). This revealed multiple modes of abundance at high amplitude levels, which in the eBOSC case more closely tracked the simulated duration. This further visualizes the decreased error in abundance estimates, especially at high SNRs (e.g., Fig. 3A), while an observed rightward shift towards higher amplitudes indicated the more pronounced underestimation of rhythmicity at low SNRs.

Finally, we investigated the trial-wise association between amplitude and duration estimate based on the observed coupling in empirical data (see Fig. 7). Our simulations suggest that both standard BOSC and eBOSC can induce spurious positive correlations between amplitude and abundance estimates, which are most pronounced at low levels of SNR (Fig. 3E). Notably, these associations are strongly reduced in eBOSC, especially when rhythmic power is high. This indicates that eBOSC provides a better separation between the two (here independent) parameters, although a spurious association remains.

In sum, our simulations suggest that eBOSC specifically separates rhythmic and arrhythmic time points in simulated data at the expense of decreased sensitivity, especially when SNR is low. However, the increase in specificity is accompanied by an increased accuracy of duration estimates at high SNR, theoretically allowing a more precise investigation of rhythmic duration.

3.2. eBOSC detects single-trial alpha rhythms during rest and task states

While the simulations provide a gold standard to assess detection performance, we further probed eBOSC's detection performance in empirical data from resting and task states to investigate the practical feasibility and utility of rhythm detection. As the ground truth in real

data is unknown, we evaluated detection performance by contrasting metrics from detected and undetected timepoints regarding their topography and time course.

Individual power spectra showed clear rhythmic alpha peaks for every participant during eyes closed rest and for most subjects during eyes open rest and the task retention period, indicating the general presence of alpha rhythms during the analysed states (Fig. S4). In line with a putative source in visual cortex, alpha abundance was highest over parieto-occipital channels during the resting state (Fig. 4A) and during the WM retention period (Fig. 8), with high collinearity between abundance and rhythmic amplitudes within resting conditions (Fig. 4B). As expected, rhythmic time-points exhibited increased alpha power compared with arrhythmic time points (Fig. 4A; white cluster). As one of the earliest findings in cognitive electrophysiology (Berger, 1938), alpha amplitudes increase in magnitude upon eye closure. Here, eye closure was reflected by a joint shift towards higher amplitudes and durations for almost all participants (Fig. 4C). To assess unique contributions of the Berger effect on rhythm indices while controlling for the high collinearity between indicators, we performed linear mixed modelling within the common effects cluster (see Supplementary Table 1). We focussed on the continuous condition here, due to the similarity of the effects in the interleaved case. Notably, rhythmic abundance was modulated by eye closure while statistically controlling for either rhythmic or arrhythmic amplitudes. In contrast, rhythmic alpha amplitudes were not modulated by eye closure when controlling for alpha abundance. This suggests that rhythmic duration may be a more sensitive marker of task modulations than amplitude. Finally, arrhythmic amplitudes did not exhibit the Berger effect in either the interleaved or the continuous acquisition when statistically controlling for the collinearity with rhythmic amplitude or rhythmic abundance. Taken together, these results suggest a high, joint sensitivity of rhythm-specific indices to eye closure, which exceeded the residual modulation of arrhythmic backgrounds that may have resulted from specificity impairments during the original detection procedure.

The temporal dynamics of indicated rhythmicity are another characteristic of interest to indicate successful rhythm detection. While such an investigation is difficult for induced rhythmicity during rest, evoked rhythmicity offers an optimal test case due to its systematic temporal deployment. For this reason, we analysed task recordings with stereotypic design-locked alpha power dynamics at encoding, retention and probe presentation (Fig. 5AB). Rhythmic probability closely tracked power dynamics (Fig. 5A) and time points designated as rhythmic exhibited pronounced alpha power compared with those labelled arrhythmic (Fig. 5A left vs. Fig. 5A right). While rhythm-specific dynamics closely captured standard power trajectories, we observed a dissociation concerning arrhythmic power. Here, we observed transient increases during stimulus onsets that were absent from either abundance or rhythmic power (Fig. 5A right). This suggests an increase in high-power transients that were excluded due to the 3 cycle duration threshold. Indeed, a significant increase in transient events was observed without an *a priori* duration threshold (see Fig. 10).

At the single-trial level, rhythmicity was indicated for periods with visibly elevated alpha power with strong task-locking (Fig. 5B left). Conversely, arrhythmicity was indicated for time points with low alpha power and little structured dynamics (Fig. 5B right). However, strong inter-individual differences were apparent, with little detected rhythmicity when global alpha power was low (Fig. 5B bottom; plots are sorted by descending power as indicated by the frame colour of the depicted subjects and scaled using z-scores to account for global power differences). Crucially, those subjects' single-trial power dynamics did not present a clear temporal structure, suggesting a prevalence of noise and therefore a correct rejection of rhythmicity. Notably, those individual rhythmicity estimates were stable across multiple sessions (Fig. 5C), suggesting that they are indicative of trait-like characteristics rather than idiosyncratic measurement noise (Grandy et al., 2013a,b).

In sum, these results suggest that eBOSC successfully separates rhythmic and arrhythmic episodes in empirical data, both at the group and individual level. However, they also indicate prevalent and stable differences in single-trial rhythmicity in the alpha band that may impair an accurate detection of rhythmic episodes.

3.3. Rhythmic SNR constrains empirical duration estimates and rhythm-related metrics

While the empirical results suggest a successful separation of rhythmic and arrhythmic content at the single-trial level, we also observed strong (and stable) inter-individual differences in alpha-abundance. This may imply actual differences in the duration of rhythmic engagement (as indicated in Fig. 5B). However, we also observed a severe underestimation of abundance as a function of the overall signal-to-noise ratio (SNR) in simulations (Fig. 3), thus leading to the question whether empirical data fell into similar ranges where an underestimation was likely. During the resting state, we indeed observed that many overall SNRs were in the range, where simulations with a stationary alpha rhythm suggested an underestimation of abundance (cf. black and blue lines in Fig. 6A. The black line indicates simulation-based estimates for stationary alpha rhythms at different overall SNR levels; see section 2.8). Moreover, the coupling of individual SNR and abundance values took on a deterministic shape in this range, whereas the association was reduced in ranges where simulations suggest sufficient SNR for unbiased abundance estimates (orange line in Fig. 6A). As overall SNR is influenced by the duration of arrhythmic signal, rhythmic SNR may serve as an even better predictor of abundance due to its specific relation to rhythmic episodes (Fig. 2). In line with this consideration, rhythmic SNR exhibited a strong linear relationship to abundance (Fig. 6B). Importantly, the background estimate was not consistently related to abundance (Fig. 6C), emphasizing that it is the 'signal' and not the 'noise' component of SNR that determines detection. Similar observations were made in the task data during the retention phase (Fig. S5), suggesting that this association reflects a general link between the magnitude of the spectral peak and duration estimates. The joint analysis of simulated and empirical data thus questions the accuracy of individual duration estimates, especially at low SNRs, due to the dependence of unbiased estimates on sufficient rhythmic power.

As eBOSC defines single-trial power deviations from a stationary power threshold as a criterion for rhythmicity, it remains unclear whether this association is exclusive to such a 'power thresholding'-approach or whether it constitutes a more general feature of single-trial rhythmicity. To probe this question, we calculated a phase-based measure of rhythmicity, termed 'lagged coherence' (Fransen et al., 2015), which assesses the stability of phase clustering at a single sensor for a chosen cycle lag. Here, 3 cycles were chosen for comparability with eBOSC's duration threshold. Crucially, this definition of rhythmicity led to highly concordant estimates with eBOSC's abundance measure[3] (Fig. 6D), suggesting that power-based rhythm detection above the scale-free background overlaps to a large extent with the rhythmic information captured in the phase-based lagged-coherence measure. Moreover, it suggests that duration estimates are more generally coupled to rhythmic amplitudes, especially when overall SNR is low.

While the previous observations were made at the between-subjects level, we further investigated whether such coupling also persists between trials in the absence of between-person differences. In the present data, we indeed observed a positive coupling of trial-wise fluctuations of rhythmic SNR and abundance (mean Fisher's z: 0.60; $p < 6.5e\text{-}19$)

[3] The eBOSC duration measure was further strongly correlated with the traditional Pepisode measure (estimated at the trial-wise IAF) that results from the standard BOSC algorithm (EC: $r = .96$, $p = 2e\text{-}18$; EC2: $r = .94$, $p = 2e\text{-}15$; EO: $r = .97$, $p = 3e\text{-}20$; EO2: $r = .97$, $p = 2e\text{-}20$), suggesting that both measures are similarly sensitive in our empirical data and reflect to a large extent overlapping information.

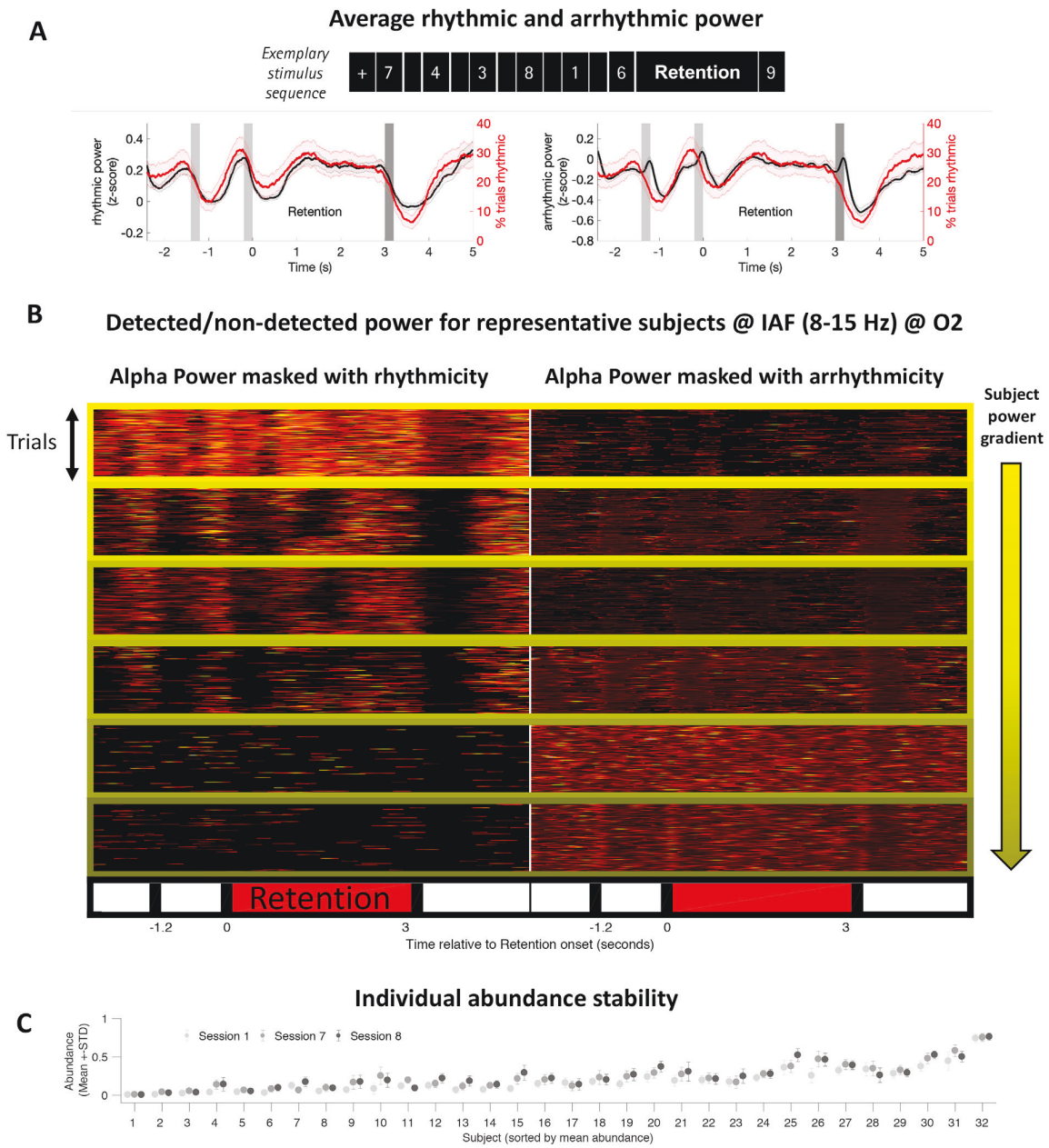

Fig. 5. Detected rhythmicity follows the structure of a working memory task, with stable inter-individual differences in single trial detection. (**A**) Average alpha power (black), split by rhythmic vs. arrhythmic designation, and rhythmic probability (red) at posterior-occipital channels exhibit stereotypic temporal dynamics during encoding (gray bars), retention (0–3 s) and retrieval (black bars). Compared to rhythmic power, arrhythmic power exhibits similar temporal dynamics, but is strongly reduced in power (see y-scales). The arrhythmic power dynamics are characterized by additional transient increases following stimulus presentations. Data are from the first session and the high load condition. Shading indicates standard errors across subjects. (**B**) Task-related alpha dynamics are captured by eBOSC at the single-trial level. Each box displays individual trial-wise z-standardized alpha power at the individual peak frequency, separately for rhythmic (left) and non-rhythmic (right) time points. While rhythmic time points (left) exhibit clear single-trial power increases that are locked to the task design, arrhythmic time points (right) do not show evoked task dynamics that separate them from the background, hence suggesting an accurate rejection of rhythmicity. The subplots' frame colour indicates the subjects' raw power maximum (i.e., the data scaling). Data are from channel O2 during the first session across load conditions. (**C**) Individual abundance estimates are stable across sessions. Data were averaged across posterior-occipital channels and high (i.e., 6) item load trials.

(Fig. 7A), whereas the estimate of the scale-free background was less consistently, though significantly (mean Fisher's z: 0.20; $p = 2.6e\text{-}6$), related to the estimated duration of rhythmicity (Fig. 7B). This suggests that the level of estimated abundance primarily relates to the magnitude of ongoing power fluctuations around the stationary power threshold. Fig. 7C schematically shows how such an amplitude-abundance coupling may be reflected in single trials as a function of rhythmic SNR. These relationships were also observed in our simulations and in other frequency bands, although they were reduced in magnitude at higher levels of simulated empirical SNR (Fig. 3E) and for other frequencies (Fig. S6), suggesting that partial dissociations of the two parameters are feasible.

In sum, these results strongly caution against the interpretation of

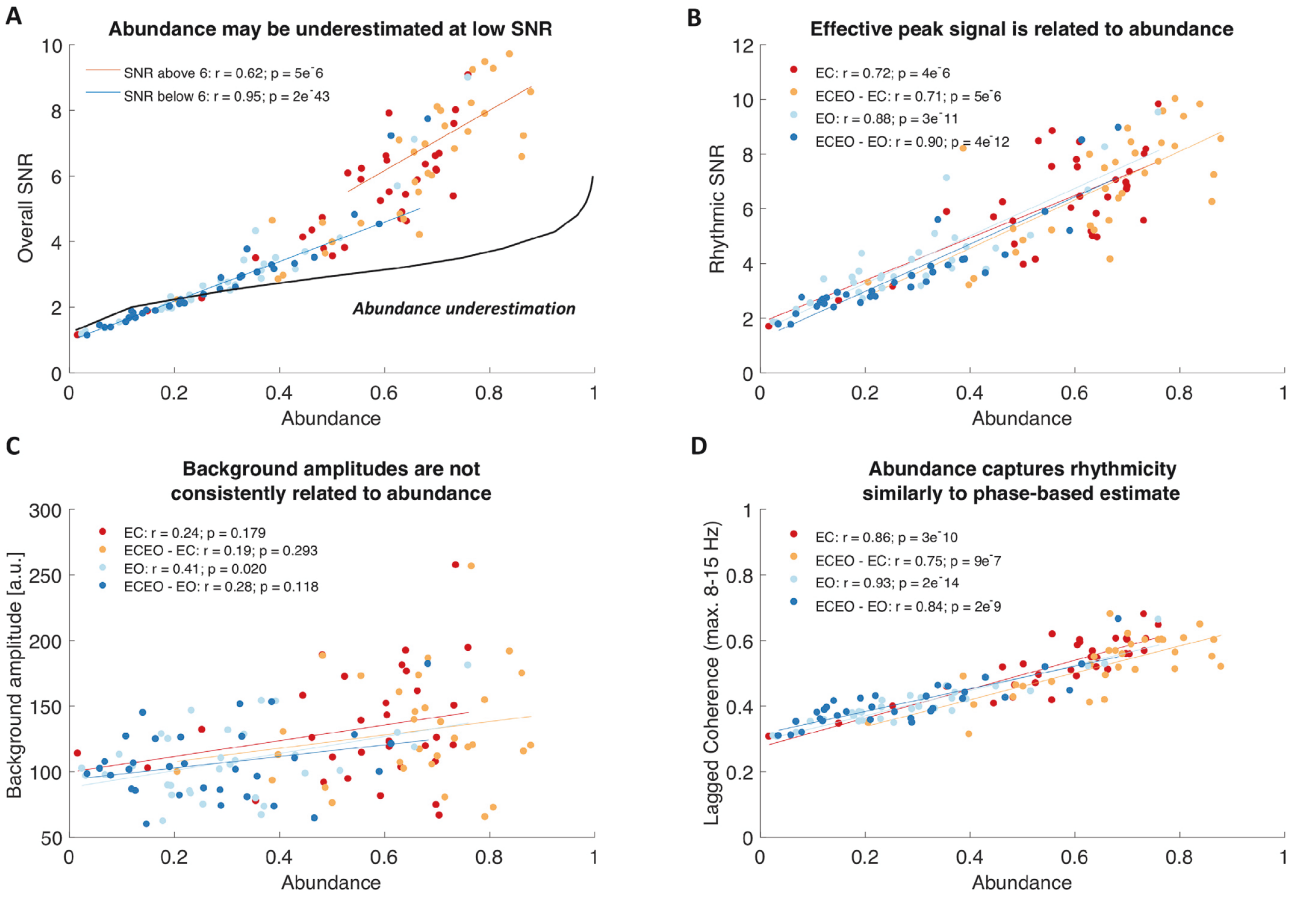

Fig. 6. Inter-individual alpha abundance is strongly associated with rhythmic, but not arrhythmic power and may be underestimated at low rhythmic SNR. (**A**) Individual abundance estimates are strongly related to the overall SNR of the spectral alpha peak. This relationship is also observed when only considering individual data within the SNR range for which simulation analyses indicated an unbiased abundance estimation. The black line indicates interpolated estimates from simulation analyses with a sustained rhythm (i.e., duration = 1; see Fig. 3B left). Hence, it indicates a lower bound for the abundance underestimation that occurs at low SNRs, with notable overlap with the empirical estimates in the same SNR range. (**B**) The effective rhythmic signal can be conceptualized as the background-normalized rhythmic amplitude above the background estimate (rhythmic SNR). This proxy for signal clarity is inter-individually linked to abundance estimates. (**C**) Background estimates are not consistently related to abundance. This implies that the relationship between amplitude and abundance is mainly driven by the signal, but not background amplitude (i.e., the effective signal 'clarity') and that associations do not arise from a misfit of the background. (**D**) Rhythmicity estimates translate between power- and phase-based definition of rhythmicity. This indicates that the BOSC-detected rhythmic spectral peak above the 1/f spectrum contains the rhythmic information that is captured by phase-based duration estimates. All data are from the resting state.

duration measures as a 'pure' duration metric that is independent from rhythmic power, especially at low levels of SNR. The strong within-subject coupling may however also indicate an intrinsic coupling between the strength and duration of neural synchrony as joint representations of a rhythmic mode. Notably, covariations were not constrained to amplitude and abundance, but were widespread, including covariations between 'SNR' and the instability (or variability) of the individual alpha peak frequency (see Supplementary Materials; Fig. S7). Combined, these results suggest that the efficacy of an accurate single-trial characterization of neural rhythms relies on sufficient individual rhythmicity and can not only constrain the validity of duration estimates, but broadly affect a range of rhythm characteristics that can be inferred from single trials.

3.4. Rhythm detection improves amplitude estimates by removing arrhythmic episodes

From the joint assessment of detection performance in simulated and empirical data, it follows that low SNR constitutes a severe challenge for single-trial rhythm characterization. However, while the magnitude of rhythmicity at the single trial level constrains the detectability of rhythms, abundance represents a lower bound on rhythmic duration due to eBOSC's high specificity. This allows the interpretation of rhythm-related metrics for those time points where rhythmicity is indicated, leading to tangible benefits over standard analyses. In this section, we highlight multiple proof-of-concept cases of such benefits.

A considerable problem in standard narrowband power analyses is the superposition of rhythmicity on top of a scale-free 1/f background, effectively mixing the two components in traditional power estimates (e.g. Haller et al., 2018). In contrast, eBOSC uncouples the two signals via explicit modelling of the arrhythmic background. Fig. 8 presents a comparison between the standard narrowband estimate and eBOSC's background and rhythmicity metrics for the alpha band during working memory retention. While high narrowband power is observed in frontal and parietal clusters, eBOSC differentiated a frontally-dominated 1/f component and a posterior-occipital rhythm cluster. Identical comparisons within multiple low-frequency ranges suggest the separation of a stationary 1/f topography and spatially varying superpositions of rhythmicity (Fig. S8). This highlights a successful separation of the scale-free slope magnitude from rhythmicity across multiple frequencies,

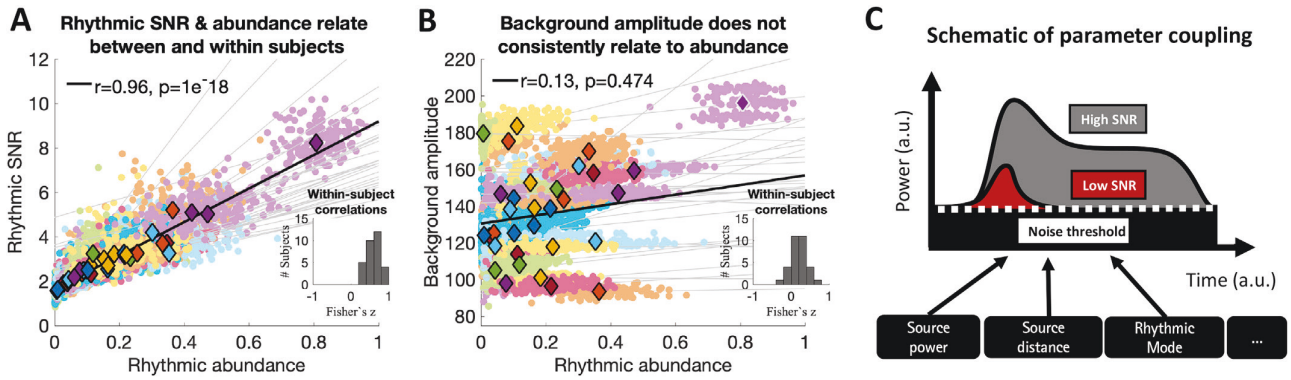

Fig. 7. The magnitude and duration of single-trial rhythmicity are intra-individually associated. Amplitude-abundance association within subjects in the Sternberg task (1st session, all trials). Dots represent single trial estimates, color-coded by subject. Subject means are presented via diamonds. (Inlay) Histogram of within-subject Fisher's z-coefficients of within-subject associations. Relationships are exclusively positive. (B) Background estimates are inter-individually uncorrelated with single-trial abundance fluctuations, excluding the outlier indicated by white edges. (C) Schematic of the potential interdependence of rhythmic SNR and abundance. Low SNR may cause the detection of shorter supra-threshold power periods with constrained amplitude ranges, whereas prolonged periods may exceed the stationary threshold when the rhythmic signal is clearly separated from the background.

even when topographies are partially overlapping as in the case of theta.

Furthermore, the presence of a rhythm is a fundamental assumption for the interpretation of rhythm-related metrics, e.g., phase (Aru et al., 2015). This is often verified by observing a spectral peak at the frequency of interest. However, sparse single-trial rhythmicity may not produce an overt peak in the average spectrum due to the high prevalence of low-power arrhythmic content. Crucially, knowledge about the temporal occurrence of rhythms in the ongoing signal can be used to investigate the spectral content that is specific to those time points, thereby creating 'rhythm-conditional spectra'. Fig. 9A highlights that such rhythm-conditional spectra can recover spectral peaks for multiple canonical frequency bands, even when no clear peak is observed in the grand average spectrum. This showcases that a focus on detected rhythmic time points allows the interpretation of rhythm-related parameters. Abundance topographies for the different peaks observed in the rhythm-conditional spectra, were in line with the canonical separation of these frequencies in the literature (Fig. 9B). Notably, while some rhythmicity was identified in higher frequency ranges, the associated abundance topographies suggests a muscular generator rather than a neural origin for these events.

Related to the recovery of spectral amplitudes from 'overall amplitudes', a central prediction of the present work was that the change from overall to rhythmic amplitudes (i.e., rhythm-specific gain; see Fig. 2 for a schematic) scales with the presence of arrhythmic signal. Stated differently, if most of the overall signal is rhythmic, the difference between overall and rhythm-specific amplitude estimates should be minimal. Conversely, if the overall signal consists largely of arrhythmic periods, rhythm-specific amplitude estimates should strongly increase from their unspecific counterparts. In line with these expectations, we observed a positive, highly linear, relationship between a subject's estimated duration of arrhythmicity and the rhythm-specific amplitude gain (Fig. 9C). Thus, for subjects with sparse rhythmicity, rhythm-specific amplitudes were strongly increased from overall amplitudes, whereas differences were minute for subjects with prolonged rhythmicity. Note however that in the case of inter-individual collinearity of amplitude and abundance (as observed in the present data) the rhythm-specific gains are unlikely to change the rank-order of subjects as the relative gain will not only be proportional to the abundance, but due to the collinearity also to the original amplitude. While such collinearity was high in the alpha band, decreased amplitude-abundance relationships were observed for other canonical frequency bands (Fig. S6), where such 'amplitude recovery' may have the most immediate benefits.

To assess whether these single-trial amplitude estimates validly reflected fluctuations in time series magnitude, we performed a triadic split based on single-trial amplitude estimates across all detected episodes (across channels and sessions) in the alpha band. We aligned time-series representations of rhythmicity to the maximal negative peak and compared power in a window of 200 ms around this peak. Notably, rhythm-specific amplitude estimates reflected time series amplitudes during rhythmic periods (Fig. 9D) with a larger effect size (medium vs. small: p = 4e-7, Cohen's d = 1.13, large vs. medium: p = 4e-9; Cohen's d = 1.42) than overall amplitudes (medium vs. small: p = .002, Cohen's d = .58, large vs. medium: p = 9e-7; Cohen's d = 1.08). Interestingly, despite collinearity between amplitude and abundance at the within-subject level (Fig. 7A), a triadic split based on single-trial abundance estimates did not differentiate rhythmic amplitudes (medium vs. small: p = .34, Cohen's d = .17, large vs. medium: p = .45; Cohen's d = -.14). Hence, rhythm-specific amplitude estimates were better predictors of time series amplitudes than traditional averages that included arrhythmic episodes or estimates of rhythmic duration.

In sum, eBOSC provides sensible single-trial amplitude estimates of narrow-band rhythmicity that are boosted in magnitude due to the removal of arrhythmic episodes.

3.5. *eBOSC separates sustained and transient spectral events*

In addition to specificity gains for rhythmic indices, eBOSC's creation of temporally contiguous rhythmic 'episodes' affords a characterization of rhythmic and transient episodes with significant spectral power in the absence of an *a priori* duration requirement. Using the traditional 3-cycle threshold as a post-hoc criterion for detected episodes, we separated rhythmic and transient spectral events with clear differences in their time-domain representations (Fig. 10A). Notably, while rhythmic SNR related to the number of detected rhythmic events, the same was not observed for the number of transient episodes (Fig. 10B2), thus indicating that rhythms and transients may arise from different mechanisms. In line with the observations made for rhythmic vs. arrhythmic power (cf. Fig. 5A), we observed differences in the temporal prevalence of transient events and sustained rhythms. Specifically, stimulus onsets increased the number of transient events (Fig. 10A1), whereas sustained rhythms were increased during the retention phase. These episodes can be further characterized in terms of their duration in cycles (Fig. 10A2), their mean frequency (Fig. 10A3) and event-specific power (Fig. 10A4). During the retention phase, we observed an increased number of larger and longer rhythms compared with the probe period with no apparent differences in frequency. In contrast, we observed a global increase in the number of transients during probe presentation, with those transients being of higher frequency compared to transients during the retention phase. The

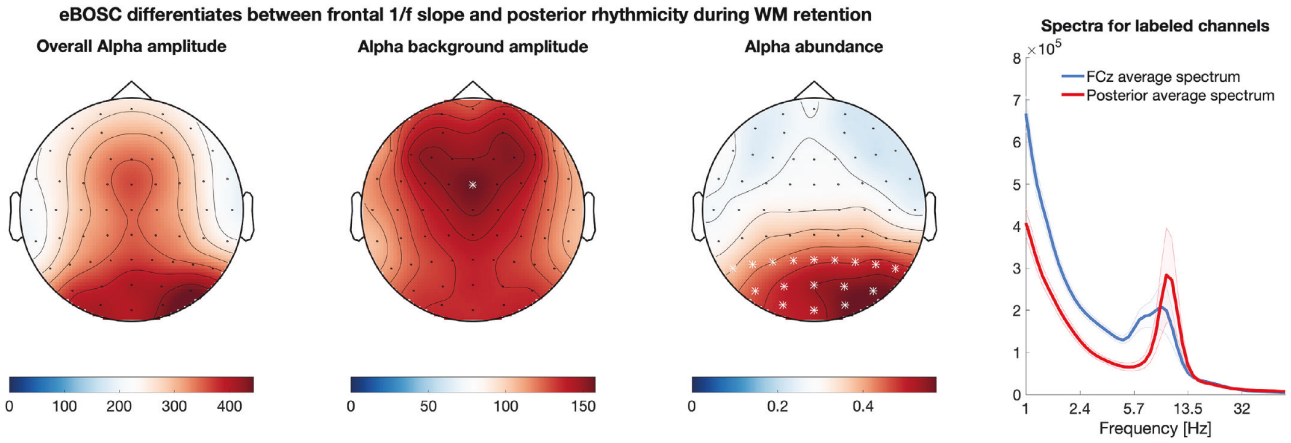

Fig. 8. eBOSC differentiates spatially varying topographies of rhythmic and arrhythmic power during working memory retention. Asterisks mark the channels that were selected for the spectra on the right. The graph shading depicts standard errors. The topographies are grand averages from the retention phase of the Sternberg task across all sessions.

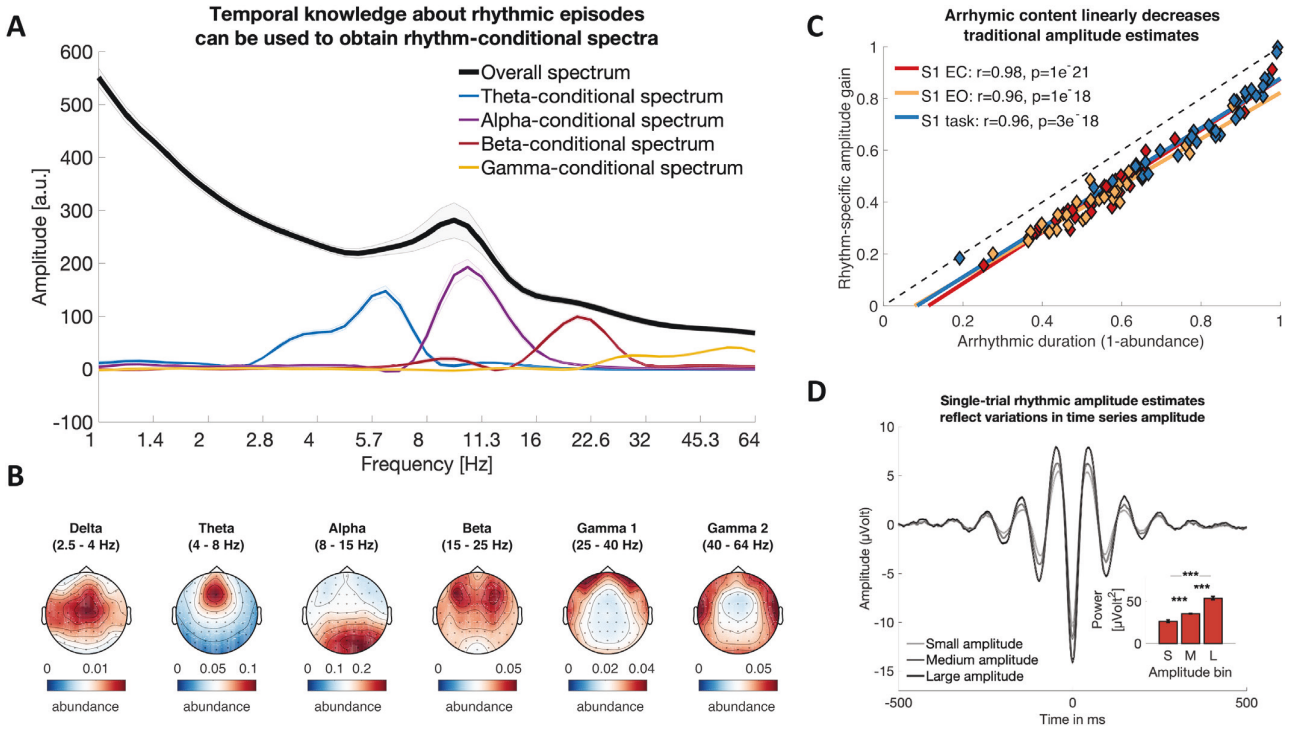

Fig. 9. Time-wise indication of rhythmicity improves rhythmic amplitude estimates and produces rhythm-conditional spectra. (A) Comparison of rhythm-conditional spectra with the standard overall spectrum during the memory retention phase. Rhythm-conditional spectra are created by comparing spectra from time-points where a rhythm in the respective frequency range has been indicated with those where no rhythm was present. Notably, this indicates rhythmic peaks at the frequencies of interest that are not observed in the overall spectrum (e.g. theta, beta) due to the prevalence of non-rhythmic events. Simultaneous peaks beyond the target frequencies indicate cross-spectral coupling. Note that these spectra also suggest sub-clusters of frequencies (e.g. an apparent split of the 'theta-conditional' spectrum into a putative delta and theta component). Data are averaged across sessions, loads, subjects and channels. (**B**) Abundance topographies of the observed rhythm-conditional spectral peaks. (C) Arrhythmic duration linearly biases traditional power estimates during both rest and task states. The relative gain in alpha amplitudes from global intervals to eBOSC's rhythmic periods (see schematic in Fig. 1A and 2A) increases with the arrhythmic duration in the investigated period. That is, if high arrhythmic duration was indicated, a focus on rhythmic periods strongly increased amplitudes by excluding the pervasive low-amplitude arrhythmic periods. In contrast, amplitude estimates were similar when arrhythmicity was low and hence rhythm-unspecific metrics contained little arrhythmic bias. Dots represent individual condition averages during the resting state. Amplitude gain is calculated as the relative change in rhythmic amplitude from the unspecific 'overall' amplitude (i.e., (rhythmic amplitude-overall amplitude)/rhythmic amplitude). (D) Rhythmic amplitudes reflect variations in time series amplitude, here visualized via a triadic split. The inset shows the statistical comparison of squared amplitudes in a 200 ms peri-peak window. Estimates are from Session 1 with data from all channels. *** = $p < .001$.

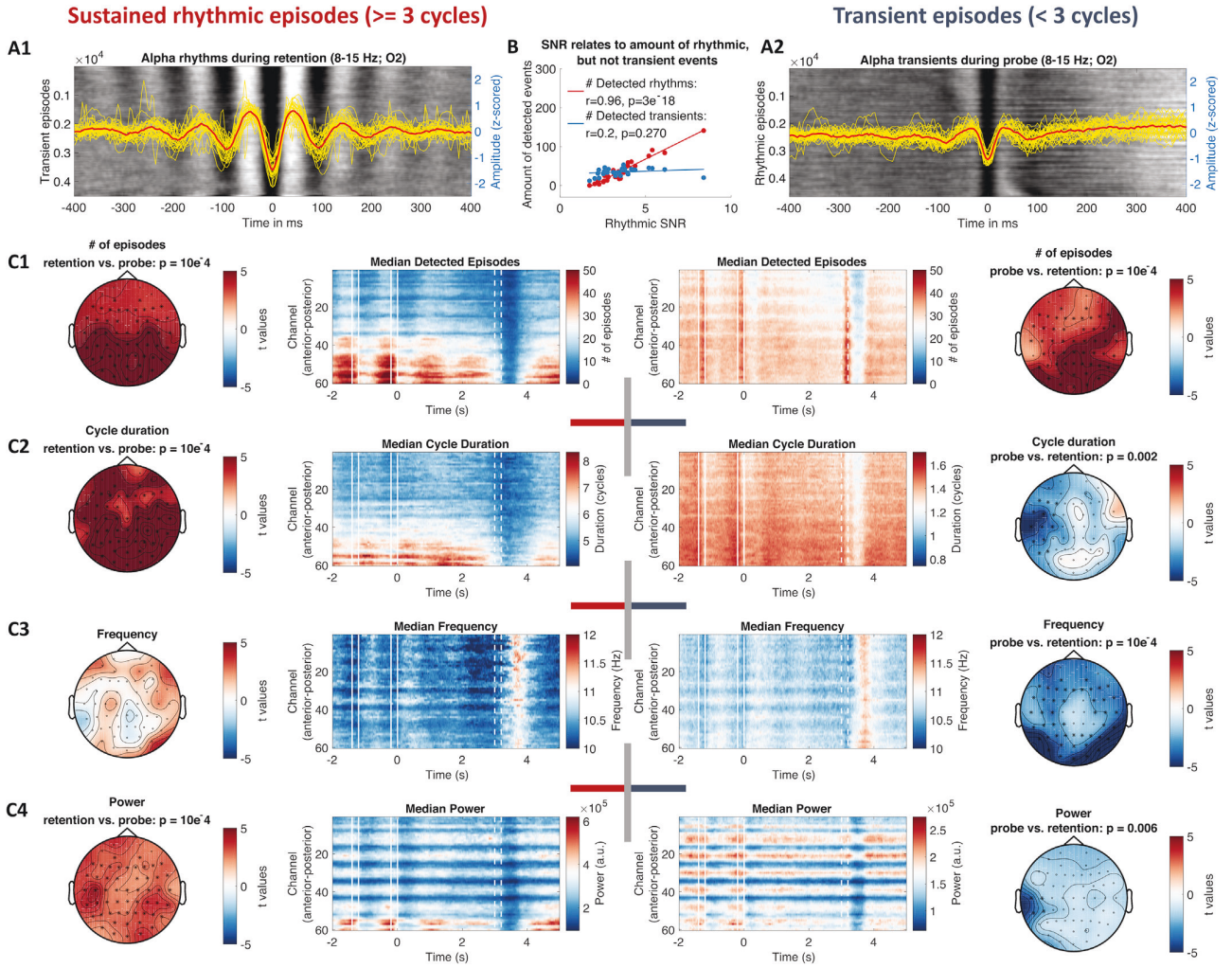

Fig. 10. eBOSC provides a varied characterization of duration-specific frequency content, separating sustained rhythmicity from transients. Episodes with a mean frequency between 8 and 15 Hz were post-hoc sorted by falling below or above a 3-cycle duration threshold. For each index, estimates were averaged across all episodes at any time point, followed by averaging across subjects and sessions. All indices are based on episodes that fulfil the power threshold for rhythmicity. (**A**) Time-domain representation of alpha rhythms (A1) and transients (A2) during retention and probe respectively. Backgrounds display moving averages of 150 raw rhythmic episode time series across all subjects. Events are aligned to the closest trough to the TFR maximum of the identified event. Episodes are sorted by episode onset relative to the identified trough. Individual (yellow) and grand data averages (red) are superimposed. (**B**) Rhythmic SNR linearly relates to the number of rhythmic events during retention, but not transient events during probe presentation. (**C**) Rhythm- and transient-specific estimates of episode prevalence (C1), duration (C2), frequency (C3) and power (C4). Central panels show time-channel representations of group indices for rhythmic (left) and transient episodes (right). Lateral topographies indicate the corresponding statistical comparisons of paired t-tests comparing the retention and the probe period. Asterisks signify significant electrode clusters. Unbroken white lines indicate stimulus presentations, broken white lines indicate probe presentation.

magnitude and duration of transients did not differ globally between these two task periods. Taken together, these analyses suggest a principled separation of sustained and transient spectral events on the bases of temporal post-hoc thresholds.

Finally, the temporal specificity of spectral episodes also enables a characterization of rhythm-'evoked' events (see Supplementary Materials). Whereas an assessment of evoked effects has thus far only been possible with regard to external event markers, the indication of rhythm on- and offsets allows an investigation of concurrent changes that are time-locked to rhythmic events (Fig. S9A). Here, we exemplarily show that the on- and offsets of rhythmic episodes are associated with concurrent power increases and decreases respectively (Fig. S9B), adding further evidence for the high temporal specificity of indicated on- and offsets of rhythmic episodes.

In sum, these proof-of-concept applications suggest that explicit rhythm detection may provide tangible benefits over traditional narrowband analyses due to the specific separation of rhythmic and arrhythmic periods, despite the high collinearity of abundance and power that we observed in the alpha band.

3.6. *Rhythm-specific indices exhibit improved sensitivity to working memory load*

So far, we investigated the potential to derive rhythm-specific estimates and highlighted resulting benefits. It remains unclear however, to what extent these estimates are experimentally modulated in cognitive tasks and whether they add complementary information to extant measures. To attend this question, we probed the effect of working memory load on traditional, rhythm-unspecific power averages and eBOSC's

duration and amplitude in the alpha and theta band.[4] Standard power estimates indicated load-related increases in frontal theta and right posterior alpha power that did not reach statistical significance however (Fig. 11A; see also Fig. S10 for different normalization procedures). In contrast, significant increases were observed for rhythmic abundance (Fig. 11B), but not for rhythm-specific power, despite similar statistical topographies (Fig. 11C). To investigate whether rhythmic abundance captured additional variance of memory load compared to amplitude, we performed linear mixed effects modeling of data averages within the (topographically-similar) abundance clusters. The results are presented in Supplementary Table 2. As expected, we observed high collinearity between different measures, expressed as significant pairwise relations between traditional and rhythm-specific indices. Controlling for this high collinearity however, memory load predicted increases in theta and alpha abundance over and above overall, and rhythmic-specific, amplitudes. In contrast, rhythm-specific amplitudes did not capture unique variance in load level when controlling for overall amplitude, in line with the absence of an indicated effect by the permutation test. Jointly, these analyses suggest that rhythmic abundance, despite high collinearity with overall and rhythmic amplitudes, is more sensitive to working memory load than (traditional) amplitude estimates.

The previous analyses focused on the total rhythmic abundance and power during the retention phase. However, rhythmicity can also be characterized with regard to individual spectral events, such as their rate of occurrence. In line with our observation of high abundance, rhythmic events in the alpha band were characterized by enduring rhythmicity, whereas events in other frequency bands had a more transient signature (Fig. 12A). This poses the question whether the rate of these transient events may be a critical parameter, as has been previously suggested for the beta and gamma band (Lundqvist et al., 2016; Shin et al., 2017). To attend this question, we created rate spectra based on the occurrence of rhythmic episodes in sliding frequency windows. These spectra were then subjected to a cluster-based permutation test to assess their relation with memory load. We observed increased rates of frontal theta and posterior gamma events as well as decreased rates of central beta events with load, whereas no differences were indicated for the alpha band (Fig. 12B). Hence, whereas the sustained appearance of alpha rhythms may render other parameters such as duration and power critical, in other frequency bands, modulation may also affect the number of relatively sparse events.

In turn, focusing on these sparse rhythmic events can drastically increase their amplitude estimates and may thus improve dependent metrics (e.g., see Fig. 9C). During our exploration of rhythmic parameters, we observed a parametric load-related decrease of frontal theta frequency (Fig. 12C) that spatially aligned with the frontal topography of theta rate and abundance increases (see Figs. 12B & 11B). Individual rhythmic frequency decreases between low and high loads were not related to individual abundance ($r = .33$, $p = .06$) or amplitude ($r = .06$, $p = .73$) changes, suggesting that differences in rhythmic SNR cannot solely account for individual frequency shifts. To visualize the shift in theta frequency, we computed FFT spectra with a high spectral resolution (0.33 Hz), separately for rhythmic episodes, and – as traditionally done – for the entire retention period. Critically, frequency-modulated theta peaks at frontal channels were only observed for rhythmic, but not for overall spectra (Fig. 12C) due to a threefold increase in the magnitude of single-trial events across the entire segment. Moreover, in line with the results of eBOSC's wavelet-based frequency estimates, significant negative load-related slopes were indicated for rhythm specific FFT frequency estimates (mean = -.16, SE = .05, $p = .005$) but not rhythm-unspecific global estimates (mean = -.05, SE = .06, $p = .36$). Hence, a focus on rhythmic episodes was necessary to reveal memory-load related frequency decreases of frontal theta rhythms, which would have been missed with traditional analyses.

In sum, these results highlight the potential of single-trial-based rhythm estimates to boost signal of interest to advance analyses regarding the role of rhythmicity in cognition.

4. Discussion

In the present manuscript, we explored the feasibility of characterizing neural rhythms at the level of single trials. To achieve this goal, we extended a previously published rhythm detection method, BOSC (Whitten et al., 2011). Based on simulations we demonstrate that our extended BOSC (eBOSC) algorithm performs well and increases detection specificity. Crucially, the reliance on robust regression in conjunction with removal of the rhythmic power band effectively decoupled estimation of the noise background from the rhythmic signal component (as reflected in the divergent associations with rhythmicity estimates). In real data, we can successfully separate rhythmic and arrhythmic, sometimes transient components, and further characterize e.g., their amplitude, duration and frequency. In total, single-trial characterization of neural rhythms appears promising for improving a mechanistic understanding of rhythmic processing modes during rest and task.

However, the simulations also reveal challenges for accurate rhythm characterization in that the abundance estimates clearly depend on rhythmic power. The comparison to a phase-based rhythm detection further suggests that this a general limitation independent of the chosen detection algorithm. Below, we will discuss the potential and challenges of single-trial rhythm detection in more detail.

4.1. The utility and potential of rhythm detection

Single-trial analyses are rapidly gaining importance (Jones, 2016; Stokes and Spaak, 2016), in part due to a debate regarding the sustained vs. transient nature of neural rhythms that cannot be resolved at the level of data averages (Jones, 2016; van Ede et al., 2018). In short, due to the non-negative nature of power estimates, time-varying transient power increases may be represented as sustained power upon averaging, indicating an ambiguity between the duration and power of rhythmic events (cf., Fig. 2B). Importantly, sustained and transient events may differ in their neurobiological origin (Sherman et al., 2016), indicating high theoretical relevance for their differentiation. Moreover, many analysis procedures, such as phase-based functional connectivity, assume that estimates are directly linked to the presence of rhythmicity, therefore leading to interpretational difficulties when it is unclear whether this condition is met (Aru et al., 2015; Muthukumaraswamy and Singh, 2011). Clear identification of rhythmic time periods in single trials is necessary to resolve these issues. In the current study, we extended a state-of-the-art rhythm detection algorithm, and systematically investigated its ability to characterize the power and duration of neural alpha rhythms at the single-trial level in scalp EEG recordings.

While the standard BOSC method provides a sensible detection of rhythmic activity in empirical data (Caplan et al., 2015; Whitten et al., 2011), its' ability to detect rhythmicity and disambiguate rhythmic power and duration has not yet been investigated systematically. Furthermore, we introduced multiple changes that aimed to create rhythmic episodes with a time-point-wise indication of rhythmicity. For these reasons, we assessed the performance of both algorithms in simulations. We observed that both algorithms were able to approximate the duration of rhythmicity across a large range of simulated amplitudes and durations. However, standard BOSC systematically overestimated rhythmic duration (Fig. 3A). Furthermore, we observed a bias of rhythmicity on the estimated background (Fig. 3C) as also noted by Haller et al. (2018). In contrast, eBOSC accounts for these problems by introducing multiple changes: First, by excluding the rhythmic peak prior to

[4] Regarding traditional metrics, we assessed three normalization procedures: raw signals, single-trial log10-transformation and baseline correction with average power 700 to 500 ms prior to retention onset. In contrast with temporal baselining, eBOSC performs spectral normalization by explicitly modelling the 1/f slope.

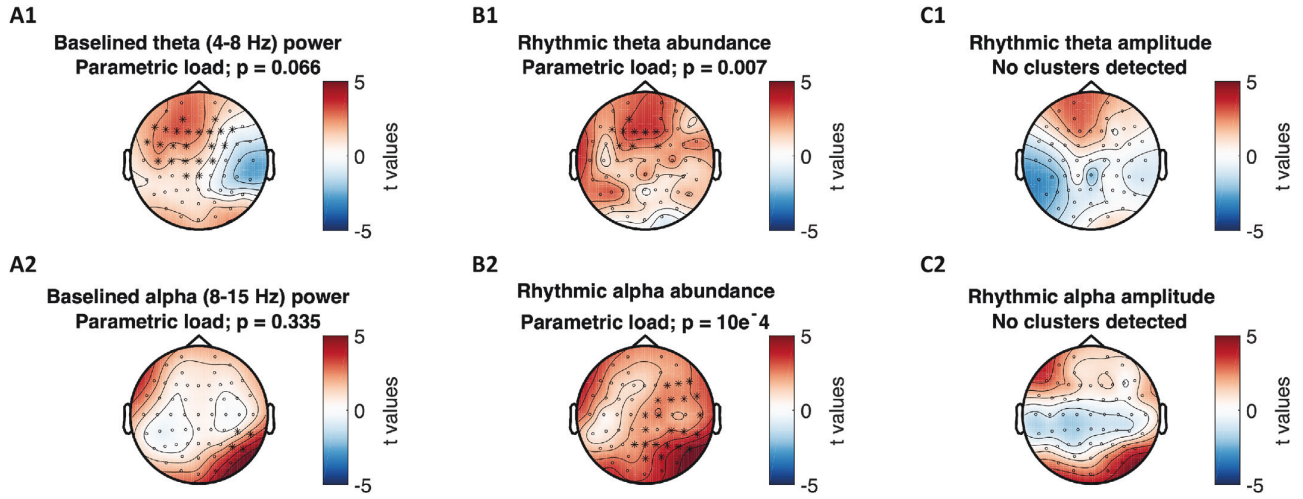

Fig. 11. Memory load-modulation of traditional wavelet power, rhythmic abundance and rhythmic amplitude. Traditional wavelet estimates indicated no significant parametric load of either frontal theta or posterior alpha power (A), whereas a load-related increase was indicated for both theta and alpha abundance (B). In contrast to abundance, no significant relationship with load was indicated for rhythm-specific amplitudes (C).

fitting the arrhythmic background, eBOSC decreased the bias of narrow-band rhythmicity on the background fit (Fig. 3C), thereby effectively uncoupling the estimated background amplitude from the indicated rhythmicity. Second, the post-processing of detected segments provided a more specific characterization of neural rhythms compared to standard BOSC. In particular, accounting for the temporal extension of the wavelet increased the temporal specificity of rhythm detection as indicated by a better adherence to the *a priori* duration threshold along with more precise duration estimates (Fig. 3). In contrast to the high specificity, the algorithm did trade off sensitivity, leading to sensitivity losses that were most pronounced at low signal-to-noise ratios (SNR). In sum, the simulations highlight that eBOSC provides a sensible differentiation of rhythmic and arrhythmic time points as well as accurate duration estimates, but also highlight challenges for empirically disentangling rhythmic power and duration that arise from sensitivity problems when the magnitude of rhythms is low. We discuss this further in section 4.2. In empirical data, eBOSC likewise led to a sensible separation of rhythmic from arrhythmic topographies (Figs. 4A and 8, Fig. S8) and time courses, both at the average (Fig. 5A) and the single-trial level (Fig. 5B). This suggests a sensible separation of rhythmic and arrhythmic time points also in empirical scenarios.

The specific separation of rhythmic and arrhythmic time points has multiple immediate benefits that we validated using empirical data from resting and task states. First, eBOSC separates the scale-free background from superimposed rhythmicity in a principled manner. The theoretical importance of such separation has previously been highlighted (Haller et al., 2018), as narrow-band estimates traditionally confound the two signals. Here, we show that such a separation empirically produces different topographies for the arrhythmic background and the superimposed rhythmicity (Fig. 8 and Fig. S8). In line with these findings, Caplan et al. (2015) described a rhythmic occipital alpha topography, whereas overall power included an additional anterior component across multiple lower frequencies. While that study did not plot topographies for the background estimates, our study suggests that this frontal component is captured by the background magnitude. This provides convergent evidence for a principled separation of rhythmic and arrhythmic spectral content which may be treated as a signal of interest in itself (Buzsáki and Mizuseki, 2014; He et al., 2010).

The separation of these signal sources at single time points can further be used to summarize the rhythmic single-trial content via rhythm-conditional spectra (Fig. 9). Crucially, such a focus on rhythmic periods resolves biases from arrhythmic periods in the segments of interest. In line with our hypotheses, simulations (Fig. 2B) and empirical data (Fig. 9C) indicate that arrhythmic episodes in the analysed segment bias overall power estimates relative to the extent of their duration. Conversely, a focus on rhythmic periods induces the most pronounced amplitude gains when rhythmic periods are sparse. This is in line with previous observations by Cole and Voytek, 2019, showing dissociations between power and frequency estimates when considering 'rhythmic' vs. unspecific periods and extend those observations by showing a strong linear dependence between the rhythm-specific change in estimates and the duration of arrhythmic bias (Fig. 9C).

Moreover, by allowing a post-hoc duration threshold, eBOSC can disentangle transient and sustained events in a principled manner (Fig. 10). This may provide new insights into the contribution of different biophysical signal generators (Sherman et al., 2016) to observed neural dynamics and aid the characterization of these processes. Such characterization includes multiple parameters, such as the frequency of rhythmic episodes, their duration, their amplitude and other indices that we did not consider here (e.g., instantaneous phase, time domain shape). Here, we observed an increased number of alpha transients following stimulus onsets, and more sustained rhythms when no stimulus was presented (Figs. 5A and 10). In line with these observations, Peterson and Voytek (2017) recently proposed alpha 'bursts' to increase visual gain during stimulus onsets and contrasted this role with decreased cortical processing during sustained alpha rhythms. Our data supports such a distinction between sustained and transient events, although it should be noted that the present transients resemble single time-domain deflections that are resolved at alpha frequency (Fig. 10A2) and may therefore not directly relate to the 'rhythmic bursts' proposed by Peterson and Voytek (2017). Note that the reported duration of 'burst' events in the literature is still diverse, often exceeding the 3-cycle threshold used here (Peterson and Voytek, 2017). In contrast to eBOSC however, previous work has not accounted for the impact of wavelet duration. It is thus conceivable that power transients that were previously characterized as 3 cycles or longer are actually shorter after correcting for the impact of wavelet convolution, as is done in the current eBOSC implementation (Fig. S1). This temporal specificity also allows an indication of rhythm-evoked changes, here exemplified with respect to rhythm-evoked power changes (Fig. S9). We observed a precise and systematic time-locking of power changes to the on- and offset of detected rhythmic episodes. This further validates the detection assumptions of the eBOSC method (i.e. significant power increases from the background), and highlights the temporal specificity of eBOSC's rhythmic episodes.

In total, eBOSC's single-trial characterization of neural rhythms provides multiple immediate benefits over traditional average-based analyses temporally precise indication of rhythmic and arrhythmic periods. It thus appears promising for improving a mechanistic understanding of rhythmic processing modes during rest and task.

4.2. Single-trial detection of rhythms: rhythmic SNR as a central challenge

The aforementioned examples highlight the utility of differentiating rhythmic and arrhythmic periods in the ongoing signal. However, the simulations also indicated problems to accurately do so when rhythmic power is low. That is, the recognition of rhythms was more difficult at low levels of SNR, leading to problems with their further characterization. In particular, our simulations suggest that estimates of the duration (Fig. 6A) and frequency stationarity (Fig. S7) increasingly deviate from the simulated parameters as the SNR decreases. Changes in instantaneous alpha frequency as a function of cognitive demands have been theorized and reported in the literature (Haegens et al., 2014; Herrmann et al., 2016; Mierau et al., 2017; Samaha and Postle, 2015; Wutz et al., 2018), with varying degrees of control for power differences between conditions and individuals. Our empirical analyses suggest an increased trial-by-trial variability of individual alpha frequency estimates as SNR decreases (Fig. S7). Meanwhile, simulations suggest that such increased variance - both estimated within indicated rhythmic periods and across whole trials – may result from lower SNR. While our results do not negate the possibility of real frequency variations of the alpha rhythm with changes in task load, they emphasize the importance of controlling for the presence of rhythms, mirroring considerations for the interpretation of phase estimates (Muthukumaraswamy and Singh, 2011) and amplitudes. This exemplifies how stable inter-individual differences in rhythmicity (whether due to a real absence of rhythms or prevalent measurement noise; e.g., distance between source and sensor; head shape; skull thickness) can affect a variety of 'meta'-indices (like phase, frequency, duration) whose estimation accuracy relies on apparent rhythmicity.

The challenges for characterizing rhythms with low rhythmic power also apply to the estimated rhythmic duration, where the issue is particularly challenging in the face of legitimate interest regarding the relationship between the power and duration of rhythmic events. In particular, sensitivity problems at low rhythmic magnitudes challenge the ability to empirically disambiguate rhythmic duration and power, as it makes the former dependent on the latter in the presence of noise (e.g., Fig. 2B). Crucially, a tight link between these parameters was also observed in the empirical data. During both rest and task states, we observed gradual and stable inter-individual differences in the estimated extent of rhythmicity that were most strongly related to the overall SNR in ranges with a pronounced sensitivity loss in simulations (see Fig. 4A black line). Given the observed detection problems in our simulations, this ambiguates whether low empirical duration estimates indicate temporally constrained rhythms or estimation problems. Conceptually, this relates to the difference between lower SNR subjects having (A) low power, transient alpha engagement or (B) low power, sustained alpha engagement that was too faint to be detected (i.e., sensitivity problems). While the second was the case in the simulations, the absence of a ground truth does not allow us to resolve this ambiguity in empirical data.

Empirically, multiple results suggest that the low duration estimates at low SNRs did not exclusively arise from idiosyncrasies of our algorithm. Notably, inter-individual differences in eBOSC's abundance measure were strongly correlated with standard BOSC's Pepisode measure (Whitten et al., 2011) as well as the phase-based lagged coherence index (Fransen et al., 2015), thus showing high convergence with different state-of-the-art techniques (Fig. 6D). Furthermore, detection performance was visually satisfying in single trials given observable task-locked rhythm dynamics for rhythmic, but not arrhythmic periods (Fig. 5B). Moreover, the observed relationship between amplitude gain and abundance suggests a successful exclusion of (low-power) arrhythmic episodes at the individual level (Fig. 9C). These observations indicate that low SNR conditions present a fundamental challenge to single-trial characterization across different methods. The convergence between power- and phase-based definitions of rhythmicity also indicates that rhythmicity can exhaustively be described by the spectral peak above the background, in line with our observations regarding rhythm-conditional spectra (Fig. 9A).

The observation of strong between-person coupling as a function of SNR suggests that such sensitivity limitations may account for the inter-individual amplitude-abundance associations. However, we also observed a positive association between subjects with high alpha SNR. Likewise, we observed positive associations between abundance and rhythmic SNR at the within-subject level (Fig. 5). While trial-wise coupling was also present in our simulations, the magnitude of these relationships was lower at high SNR (Fig. 3E). Conversely, in empirical data, the within-subject association did not vary in magnitude as a function of the individual SNR. Hence, separate sources may contribute to a coupling of rhythmic amplitude and abundance: a methods-induced association in low SNR ranges and an intrinsic coupling between rhythmic strength and duration as a joint representation of rhythmic synchrony. Notably, empirical within-subject coupling between rhythmic amplitude and duration was previously described for LFP beta bursts in the subthalamic nucleus (Tinkhauser et al., 2017), with both parameters being sensitive to a drug manipulation. This association was interpreted as a "progressive synchronization of inputs over time" (Tinkhauser et al., 2017; p. 2978). Due to the absence of a dissociation of these parameters, it remains unclear whether the two measures make independent contributions or whether they can be conceptualized as a single underlying latent 'rhythmicity' index. To resolve this ambiguity, clear dissociations of amplitude and duration estimates in data with high rhythmic SNR are necessary. Notably, potential dissociations between the individual power and duration of beta events has been suggested by Shin et al. (2017), who described differential relationships between event number, power and duration to mean power and behaviour.

The high collinearity between overall amplitude and abundance may be surprising given evidence of their potential dissociation in the case of beta bursts (where overall abundance is low, but burst amplitudes are high) (Lundqvist et al., 2016; Sherman et al., 2016; Shin et al., 2017). In line with this notion, Fransen et al. (2015) reported an increased sensitivity for central beta rhythmicity using the lagged coherence duration index compared with overall power. It may thus be that the alpha range is an outlier in this regard due to the presence of relatively sustained rhythmicity (Fig. 12A). A frequency-wise comparison of the between- and within-subject collinearity between amplitude and abundance collinearity indicated a particularly high overlap for the alpha range (Fig. S6) with relatively lower coupling for delta, theta and beta. In addition, we observed load modulations on rhythm event rate in many bands but alpha (Fig. 12B). Whether these band-specific differences primarily relate to their lower rhythmicity in the current data or reflect systematic differences between frequencies remains an open question and requires data with more prominent rhythmicity in these bands.

The strong collinearity of amplitude and duration estimates also questions the successful disambiguation of the two indices in empirical data and more generally the interpretation of duration as an independent index. In cases where such metrics only serve as a sensitive and/or specific replacement for power (Caplan et al., 2015; Fransen et al., 2015) this may not be problematic, but care has to be taken in interpreting available duration indices as power-independent characteristics of rhythmic episodes. An independent duration index becomes increasingly important however to assess whether rhythms are stationary or transient. For this purpose, both amplitude thresholding and phase-progression criteria have been proposed (Cole and Voytek, 2019; Peterson and Voytek, 2017; Sherman et al., 2016; van Ede et al., 2018; Vidaurre et al., 2016). Here, we show that both methods arrive at similar conclusions regarding individual rhythmic duration and that the mentioned challenges are therefore applicable to both approaches. As an alternative to threshold-based methods, van Ede et al. (2018) propose methods based

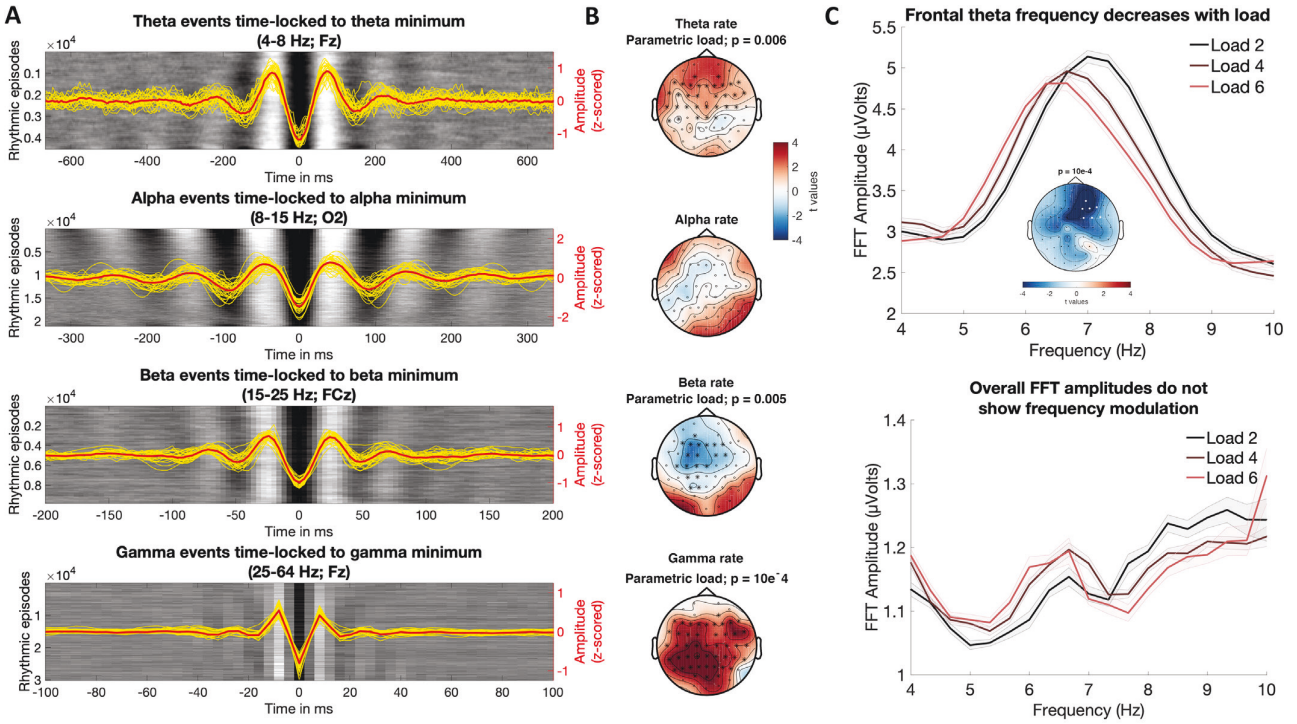

Fig. 12. Descriptors of single-trial rhythmic events relate to working memory load. (A, B) Rhythmic event rates are a relevant parameter for describing band-specific task modulations. (A) Different frequency bands vary in their sustained vs. transient time domain appearance. Conventions are the same as in Fig. 10A. X-axes are scaled to cover approx. 6 cycles at each frequency. (B) Rhythmic event rates are modulated by working memory load except in the alpha band, where events appear the most sustained. Alpha rate was averaged from 8 to 12 Hz here to exclude beta rate decreases. (C) Rhythmic frontal theta frequency decreases with working memory load. (Top) Rhythm-specific spectra indicate a parametric shift in theta frequencies with load. Statistics are based on a cluster-based permutation test. The inset shows the cluster for which a significant relation between load and the average frequency of rhythmic theta episodes is indicated. Spectra are averaged across significant cluster channels. Error bars indicate within-subject standard errors. (Lower) The overall spectrum does not show a clear spectral peak in the theta range or a shift in theta frequency. Note that amplitude values are increased in the rhythm-specific version compared to the rhythm-unspecific estimates.

on e.g., Hidden Markov Models (, 2016) for the estimation of rhythmic duration. These approaches are interesting as the definition of states to be inferred in single trials is based on individual (or group) averages, while the multivariate nature of the signals across channels is also considered. It is a viable question for future investigations whether such approaches can adequately characterize the duration of rhythmic states in scenarios where the present methods fail.

4.3. *Experimental manipulation of rhythm-specific indices*

To establish the practical utility of rhythm detection, we probed the experimental modulation of rhythm-specific indices during working memory retention. We focused on this phase as it has received large interest for distinguishing between transient and sustained retention codes (Lundqvist et al., 2016; Lundqvist et al., 2018), with both theoretical models (Jensen and Lisman, 1998; Lisman and Jensen, 2013; Lundqvist et al., 2011) and empirical evidence (Jensen et al., 2002; Jensen and Tesche, 2002; Jokisch and Jensen, 2007; Meltzer et al., 2008; Michels et al., 2008; Onton et al., 2005; Scheeringa et al., 2009; Tuladhar et al., 2007) suggesting that low-frequency rhythmicity increases with load. In line with this evidence, we observed load-related increases in the total duration of frontal theta and right parietal alpha rhythms during visual working memory retention, despite traditional power estimates not reaching statistical significance. Reinforcing these results, mixed modelling indicated a high sensitivity of rhythmic abundance to both eye closure and working memory load while controlling for its collinearity with traditional estimates. This may be due to multiple advantages: eBOSC's estimates are spectrally normalized and individually specific e.g. to individual peak frequencies, while not assuming stationarity across time. Furthermore, rhythm-specific measures are theoretically agnostic to the magnitude of desynchronization, as they only characterize rhythmicity when it is present. Interestingly, abundance was also more sensitive to the load effect than rhythm-specific amplitudes, suggesting that duration may be a critical parameter to describe cognitive effects despite high collinearity with amplitude.

In addition to our confirmatory analyses in the theta and alpha band, we also explored the load modulation of individual spectral events. Here, we observed that the rate of spectral events during the retention phase was modulated in the theta, beta and gamma, but not the alpha band. This is interesting given that alpha events had a more continuously 'rhythmic' appearance overall, whereas the relative rate of spectral events may be relevant for frequency bands with sparse events, as has been suggested for the beta band (Shin et al., 2017). While we confirm the feasibility of such analyses across multiple frequency bands here, we note that further work on the complementary value of such event rates is required to establish their functional significance.

During our analyses we also observed frequency decreases of rhythmic episodes in the theta band at frontal channels. Decreases in rhythmic theta frequency have previously been hypothesized in the framework of theta-gamma multiplexing serving working memory storage (Bahramisharif et al., 2018; Jensen and Lisman, 1998). In particular, a version of this computational model anticipates that the frequency of theta rhythms determines the amount of gamma cycles that can be multiplexed within a single theta cycle. As the number of targets to be held in memory increases, the theory predicts a slowing of theta with increasing load. Such a load-related decrease in gamma-modulating theta frequencies has been observed in human hippocampus (Axmacher et al., 2010). However, this has been difficult to show outside of invasive recordings. Here

we observed that overall power did not exhibit a clear spectral peak in the theta range, but that such peak became apparent only when estimates were constrained to rhythmic periods. Furthermore, a parametric decrease in the frequency of single-trial rhythmic episodes was indicated. This suggests that the observed frontal theta signature may support the multiplexing of individual items during the retention period and may even have a hippocampal origin. However, as we observed this effect by exploration, further work should confirm these hypotheses.

Taken together, our results highlight that a variety of rhythm-specific characteristics are sensitive to experimental modulations, such as working memory load. Despite the observed high collinearity between estimates, modulations suggest sensitivity differences between different rhythm estimates. Their automatic single-trial estimation using tools such as eBOSC may thus further our understanding of the role of rhythmicity in cognition, without necessitating the (often unchecked) assumptions of data averages.

4.4. Comparison to other single-trial detection algorithms & limitations

The BOSC-family of methods is conceptually similar to other methods that are currently used to identify and describe spectral events in single trials. These methods share the underlying principle of identifying rhythmic events based on momentary power increases relative to an average baseline. Such detection is most common regarding transient beta bursts, for which a beta-specific power threshold is often defined. For example, Sherman et al. (2016) identified transient beta events based on the highest power within the beta range, i.e., without an explicit threshold. Shin et al. (2017) introduced a beta-specific power threshold based on average pre-stimulus power. Similarly, Feingold et al. (2015) defined beta events as exceeding 1.5/3 times the median beta power of that channel, while Tinkhauser et al. (2017) applied a 75th percentile threshold to beta amplitudes. These approaches therefore use a spectrally local power criterion, but no duration threshold. Most closely related to the BOSC-family is the MODAL method by Watrous et al. (2018), which similarly uses a robust fit of the 1/f spectrum to detect rhythmic events in continuous data and then further derives frequency and phase estimates for those rhythmic periods. This is conceptually similar to eBOSC's definition as 'statistically significant' deviations in power from the 1/f background spectrum, except for the absence of a dedicated power or duration threshold. However, all of the above methods share the fundamental assumption of a momentary power deviation from a frequency-specific 'background', with varying implementations of a 1/f model assumption. Such assumption can be useful to avoid a bias of rhythmic content on the power threshold (as a spectrally local power threshold depends on the average magnitude of band-limited rhythmicity, i.e., arrhythmic + rhythmic power). Removing the rhythmic peak prior to background modelling helps to avoid such bias (Fig. 3C). The eBOSC method thereby provides a principled approach for the detection of single-trial events across frequencies (as shown in Fig. 9).

A systematic and general removal of spectral peaks remains a challenge for adequate background estimates. In the current application, we exclusively removed alpha-band power prior to performing the background fit. While the alpha rhythm produced the largest spectral peak in our data (see Fig. S4), this should not be understood as a fixed parameter of the eBOSC approach, as other rhythmic peaks may bias the estimation of the background spectrum depending on the recording's specifics (e.g., type, location etc.). We perceive the need to remove rhythmic peaks prior to background fitting as a general one,[5] as residual spectral peaks bias detection efficacy across the entire spectrum via misfits of the background intercept and/or slope. In particular, rhythmic peaks at higher frequencies disproportionally increase the background estimate at lower frequencies due to the fitting in logarithmic space. Thus, a principled removal of ***any*** spectral peaks in the average spectrum is necessary. Recently, Haller et al. (2018) proposed a principled approach for the removal of rhythmic spectral peaks, which may afford rhythm-unbiased background estimates without requiring priors regarding the location of spectral peaks. It may thus represent a useful pre-processing step for further applications. Regarding the present data, we anticipate no qualitative changes compared to our alpha exclusion approach as (a) we did not consistently observe an association between background and rhythmicity estimates (Fig. 6), and the signal was dominated by an alpha frequency peak, which consistently exceeded eBOSC's power threshold.

Our results further question the adequacy of a stationary power threshold (as traditionally employed and used here) for assessing the amplitude-duration relationship between individual rhythmic episodes. In our empirical analyses, the rhythmic SNR, reflecting the deviation of amplitudes during rhythmic periods from the stationary background, was consistently most strongly associated with the estimated duration (Figs. 6 and 7). While keeping the background (and thus the power threshold) stable conforms with the common assumption of rhythmicity being captured within a spectral peak deviating from a stationary background (Fig. 9), it may also exacerbate an amplitude-abundance coupling on a trial-by-trial basis (see Fig. 7C for a schematic of the assumed association) as ongoing power fluctuations can only be explained by changes in the rhythmic and not the arrhythmic power term. Further research on dynamic thresholds may shed further light on this issue.

Another point worth highlighting is that eBOSC operates on wavelet-derived power estimates. The specific need for wavelet estimates results from model-based assumptions about the time-frequency extension of the wavelet that are used for refining detected rhythmic time points (see Fig. 2 and section 2.6). Naturally, the choice of wavelet parameters, specifically their center frequency and duration, influences the time-frequency representations upon which eBOSC operates. Here, we used 6 cycles as the duration parameter, in line with previous work with standard BOSC (Caplan et al., 2015; Whitten et al., 2011). In a supplementary analysis, we compared detection performance using a 3 cycle wavelet and found increased accuracy only for short rhythmicity, whereas the sensitivity to longer rhythmicity was decreased (Fig. S3). This is consistent with the assumption that wavelet duration regulates the trade-off between temporal and spectral specificity, with longer wavelets allowing for a finer separation of nearby frequencies at the cost of temporal specificity. Another free parameter concerns the choice of center frequencies. In the post-processing procedures, we perform a sort of spectral filtering based on the pass-band of the wavelet (Fig. S1), which is determined by its duration. Resolving rhythms at nearby frequencies thus requires the use of wavelets with sufficient frequency resolution, not only with regard to the sampled frequencies, but also a sufficient duration of the wavelet. This highlights the dependence of eBOSC outputs on the specifics of the wavelet-based transformation from the time into the frequency domain.

An alternative, parallel approach to characterize ongoing rhythmicity is based on characterizing the waveform shape in the time domain, thereby circumventing power analyses entirely (Cole and Voytek, 2019). While such an approach is intriguing, further work is needed to show which analysis sequence is more fruitful: (a) identifying events in the frequency domain and then describing the associated waveform shape in the time domain (e.g., eBOSC) or (b) identifying events and characterizing them based on time domain features (e.g., cycle-by-cycle analysis). As both procedures operate on the basis of single trials, similar challenges (i.e., especially rhythmic SNR) are likely to apply to both approaches.

5. Conclusion

We extended a state-of-the-art rhythm detection method and characterized alpha rhythms in simulated, resting and task data at the single trial level. By using simulations, we show that rhythm detection can be

[5] A potential bias is less likely in the case of sporadic rhythmicity that does not produce a peak in the average spectrum. In this case, the power of the single-trial events would exceed the background estimate that is decreased due to the prevalence of arrhythmic periods.

employed to derive specific estimates of rhythmicity, with fine-grained control over its definition, and to reduce the bias of rhythm duration on amplitude estimates that commonly exists in standard analysis procedures. However, we also observe striking inter-individual differences in the indicated duration of rhythmicity, which for subjects with low alpha power may be due to insufficient single-trial rhythmicity. We further show that low rhythmicity can lead to biased estimates, in particular underestimated duration and increased variability of rhythmic frequency. Given these constraints, we have provided examples of eBOSC's efficacy to characterize rhythms that may prove useful for investigating the origin and functional role of neural rhythms in health and disease, and in turn, the current study works to establish the foundation for ideographic analyses of neural rhythms.

Data availability

The scripts implementing the eBOSC pipelines are available at github.com/jkosciessa/eBOSC alongside the simulation scripts that were used to assess eBOSC's detection properties. Data will be made available upon reasonable request.

Funding

This study was conducted within the project 'Cognitive and Neuronal Dynamics of Memory across the Lifespan (CONMEM)' at the Center for Lifespan Psychology, Max Planck Institute for Human Development (MPIB). MW-B's work was supported by grants from the German Research Foundation (DFG, WE 4269/3–1 and WE 4269/5–1) as well as an Early Career Research Fellowship 2017–2019 awarded by the Jacobs Foundation. JQK is a pre-doctoral fellow of the International Max Planck Research School on Computational Methods in Psychiatry and Ageing Research (IMPRS COMP2PSYCH). The participating institutions are the Max Planck Institute for Human Development, Berlin, Germany, and University College London, London, UK. For more information, see https://www.mps-ucl-centre.mpg.de/en/comp2psych.

Acknowledgements

We thank our research assistants and participants for their contributions to the present work. We thank our anonymous reviewers and Scott R. Cole for their helpful comments on earlier versions of this manuscript.

Appendix A. Supplementary data

Supplementary data to this article can be found online at https://doi.org/10.1016/j.neuroimage.2019.116331.

References

Aru, J., Aru, J., Priesemann, V., Wibral, M., Lana, L., Pipa, G., et al., 2015. Untangling cross-frequency coupling in neuroscience. Curr. Opin. Neurobiol. 31, 51–61. https://doi.org/10.1016/j.conb.2014.08.002.

Atallah, B.V., Scanziani, M., 2009. Instantaneous modulation of gamma oscillation frequency by balancing excitation with inhibition. Neuron 62 (4), 566–577. https://doi.org/10.1016/j.neuron.2009.04.027.

Axmacher, N., Henseler, M.M., Jensen, O., Weinreich, I., Elger, C.E., Fell, J., 2010. Cross-frequency coupling supports multi-item working memory in the human hippocampus. Proc. Natl. Acad. Sci. U. S. A 107 (7), 3228–3233. https://doi.org/10.1073/pnas.0911531107.

Bach, M., 1996. The Freiburg Visual Acuity test–automatic measurement of visual acuity. Optom. Vis. Sci. 73 (1), 49–53.

Bach, M., 2007. The Freiburg visual acuity test-variability unchanged by post-hoc re-analysis, 245, pp. 965–971. https://doi.org/10.1007/s00417-006-0474-4, 7.

Bahramisharif, A., Jensen, O., Jacobs, J., Lisman, J., 2018. Serial representation of items during working memory maintenance at letter-selective cortical sites. PLoS Biol. 16 (8), e2003805–e2003821. https://doi.org/10.1371/journal.pbio.2003805.

Bell, A.J., Sejnowski, T.J., 1995. An information-maximization approach to blind separation and blind deconvolution. Neural Comput. 7 (6), 1129–1159.

Berger, H., 1938. Über das Elektrenkephalogramm des Menschen. Archiv Für Psychiatrie Und Nervenkrankheiten 108 (3), 407–431. https://doi.org/10.1007/BF01824101.

Brookes, M.J., Wood, J.R., Stevenson, C.M., Zumer, J.M., White, T.P., Liddle, P.F., Morris, P.G., 2011. Changes in brain network activity during working memory tasks: a magnetoencephalography study. Neuroimage 55 (4), 1804–1815. https://doi.org/10.1016/j.neuroimage.2010.10.074.

Buzsáki, G., 2006. Rhythms of the Brain. Oxford University Press, New York.

Buzsáki, G., Mizuseki, K., 2014. The log-dynamic brain: how skewed distributions affect network operations. Nat. Rev. Neurosci. 15 (4), 264–278. https://doi.org/10.1038/nrn3687.

Buzsáki, G., Anastassiou, C.A., Koch, C., 2012. The origin of extracellular fields and currents — EEG, ECoG, LFP and spikes. Nat. Rev. Neurosci. 13 (6), 1–14. https://doi.org/10.1038/nrn3241.

Caplan, J.B., Bottomley, M., Kang, P., Dixon, R.A., 2015. Distinguishing rhythmic from non-rhythmic brain activity during rest in healthy neurocognitive aging. Neuroimage 112, 341–352. https://doi.org/10.1016/j.neuroimage.2015.03.001.

Caplan, J.B., Madsen, J.R., Raghavachari, S., Kahana, M.J., 2001. Distinct patterns of brain oscillations underlie two basic parameters of human maze learning. J. Neurophysiol. 86 (1), 368–380.

Cohen, M.X., 2014. Analyzing Neural Time Series Data: Theory and Practice. MIT Press, Cambridge, Massachusetts.

Cohen, M.X., 2017. Where does EEG come from and what does it mean? Trends Neurosci. 40 (4), 208–218. https://doi.org/10.1016/j.tins.2017.02.004.

Cole, S.R., Voytek, B., 2019. Cycle-by-cycle analysis of neural oscillations. J Neurophysiol. 122 (2), 849–861. https://doi.org/10.1152/jn.00273.2019.

Cousineau, D., 2005. Confidence intervals in within-subject designs: a simpler solution to Loftus and Masson's method. Tutorials Quant. Methods Psychol. 1 (1), 42–45.

Feingold, J., Gibson, D.J., DePasquale, B., Graybiel, A.M., 2015. Bursts of beta oscillation differentiate postperformance activity in the striatum and motor cortex of monkeys performing movement tasks. Proc. Natl. Acad. Sci. 112 (44), 13687–13692. https://doi.org/10.1073/pnas.1517629112.

Fransen, A.M.M., van Ede, F., Maris, E., 2015. Identifying neuronal oscillations using rhythmicity. Neuroimage 118 (C), 256–267. https://doi.org/10.1016/j.neuroimage.2015.06.003.

Grandy, T.H., Werkle-Bergner, M., Chicherio, C., Lövdén, M., Schmiedek, F., Lindenberger, U., 2013a. Individual alpha peak frequency is related to latent factors of general cognitive abilities. Neuroimage 79 (C), 10–18. https://doi.org/10.1016/j.neuroimage.2013.04.059.

Grandy, T.H., Werkle-Bergner, M., Chicherio, C., Schmiedek, F., Lövdén, M., Lindenberger, U., 2013b. Peak individual alpha frequency qualifies as a stable neurophysiological trait marker in healthy younger and older adults. Psychophysiology 50 (6), 570–582. https://doi.org/10.1111/psyp.12043.

Grandy, T., Lindenberger, U., Werkle-Bergner, M., 2017. When group means fail: can one size fit all? *bioRxiv*. http://doi.org/10.1101/126490.

Gross, J., 2014. Analytical methods and experimental approaches for electrophysiological studies of brain oscillations. J. Neurosci. Methods 228, 57–66. https://doi.org/10.1016/j.jneumeth.2014.03.007.

Grossmann, A., Morlet, J., 1985. Decomposition of functions into wavelets of constant shape, and related transforms. In: Streit, L. (Ed.), Mathematics 1 Physic. World Scientific, Singapore, pp. 135–165.

Haegens, S., Cousijn, H., Wallis, G., Harrison, P.J., Nobre, A.C., 2014. Inter- and intra-individual variability in alpha peak frequency. Neuroimage 92 (C), 46–55. https://doi.org/10.1016/j.neuroimage.2014.01.049.

Haller, M., Donoghue, T., Peterson, E., Varma, P., Sebastian, P., Gao, R., et al., 2018. Parameterizing neural power spectra. bioRxiv 1–16. https://doi.org/10.1101/299859.

Hansen, E.W., 2014. DFT properties and theorems. Fourier Transforms. Principles and Applications. John Wiley & Sons, Hoboken, New Jersey, p. 128.

He, B.J., Zempel, J.M., Snyder, A.Z., Raichle, M.E., 2010. The temporal structures and functional significance of scale-free brain activity. Neuron 66 (3), 353–369. https://doi.org/10.1016/j.neuron.2010.04.020.

Herrmann, C.S., Murray, M.M., Ionta, S., Hutt, A., Lefebvre, J., 2016. Shaping intrinsic neural oscillations with periodic stimulation. J. Neurosci. 36 (19), 5328–5337. https://doi.org/10.1523/JNEUROSCI.0236-16.2016.

Holland, P.W., Welsch, R.E., 2007. Robust regression using iteratively reweighted least-squares. Commun. Stat. Theor. Methods 6 (9), 813–827. https://doi.org/10.1080/03610927708827533.

Jensen, O., Lisman, J.E., 1998. An oscillatory short-term memory buffer model can account for data on the Sternberg task. J. Neurosci. 18 (24), 10688–10699.

Jensen, O., Tesche, C.D., 2002. Frontal theta activity in humans increases with memory load in a working memory task. Eur. J. Neurosci. 15 (8), 1395–1399.

Jensen, O., Gelfand, J., Kounios, J., Lisman, J.E., 2002. Oscillations in the alpha band (9-12 Hz) increase with memory load during retention in a short-term memory task. Cerebr. Cortex 12 (8), 877–882.

Jokisch, D., Jensen, O., 2007. Modulation of gamma and alpha activity during a working memory task engaging the dorsal or ventral stream. J. Neurosci. 27 (12), 3244–3251. https://doi.org/10.1523/JNEUROSCI.5399-06.2007.

Jones, S.R., 2016. When brain rhythms aren't 'rhythmic': implication for their mechanisms and meaning. Curr. Opin. Neurobiol. 40, 72–80. https://doi.org/10.1016/j.conb.2016.06.010.

Klimesch, W., 2012. alpha-band oscillations, attention, and controlled access to stored information. Trends Cogn. Sci. 16 (12), 606–617. https://doi.org/10.1016/j.tics.2012.10.007.

Linkenkaer-Hansen, K., Nikouline, V.V., Palva, J.M., Ilmoniemi, R.J., 2001. Long-range temporal correlations and scaling behavior in human brain oscillations. J. Neurosci. 21 (4), 1370–1377.

Lisman, J.E., Jensen, O., 2013. The theta-gamma neural code. Neuron 77 (6), 1002–1016. https://doi.org/10.1016/j.neuron.2013.03.007.

Lundqvist, M., Herman, P., Lansner, A., 2011. Theta and gamma power increases and alpha/beta power decreases with memory load in an attractor network model. J. Cogn. Neurosci. 23 (10), 3008–3020. https://doi.org/10.1162/jocn_a_00029.

Lundqvist, M., Herman, P., Warden, M.R., Brincat, S.L., Miller, E.K., 2018. Gamma and beta bursts during working memory readout suggest roles in its volitional control. Nat. Commun. 9 (1), 1–12. https://doi.org/10.1038/s41467-017-02791-8.

Lundqvist, M., Rose, J., Herman, P., Brincat, S.L., Buschman, T.J., Miller, E.K., 2016. Gamma and beta bursts underlie working memory. Neuron 90 (1), 152–164. https://doi.org/10.1016/j.neuron.2016.02.028.

Maris, E., Oostenveld, R., 2007. Nonparametric statistical testing of EEG- and MEG-data. J. Neurosci. Methods 164 (1), 177–190. https://doi.org/10.1016/j.jneumeth.2007.03.024.

Meltzer, J.A., Zaveri, H.P., Goncharova, I.I., Distasio, M.M., Papademetris, X., Spencer, S.S., et al., 2008. Effects of working memory load on oscillatory power in human intracranial EEG. Cerebr. Cortex (New York, N.Y. : 1991) 18 (8), 1843–1855. https://doi.org/10.1093/cercor/bhm213.

Michels, L., Moazami-Goudarzi, M., Jeanmonod, D., Sarnthein, J., 2008. EEG alpha distinguishes between cuneal and precuneal activation in working memory. Neuroimage 40 (3), 1296–1310. https://doi.org/10.1016/j.neuroimage.2007.12.048.

Mierau, A., Klimesch, W., Lefebvre, J., 2017. State-dependent alpha peak frequency shifts: experimental evidence, potential mechanisms and functional implications. Neuroscience 360, 146–154. https://doi.org/10.1016/j.neuroscience.2017.07.037.

Molenaar, P.C.M., Campbell, C.G., 2009. The new person-specific paradigm in psychology. Curr. Dir. Psychol. Sci. 18 (2), 112–117. https://doi.org/10.1111/j.1467-8721.2009.01619.x.

Muthukumaraswamy, S.D., Singh, K.D., 2011. A cautionary note on the interpretation of phase-locking estimates with concurrent changes in power. Clin. Neurophysiol. 122 (11), 2324–2325. https://doi.org/10.1016/j.clinph.2011.04.003.

Nolan, H., Whelan, R., Reilly, R.B., 2010. FASTER: fully automated statistical thresholding for EEG artifact rejection. J. Neurosci. Methods 192 (1), 152–162. https://doi.org/10.1016/j.jneumeth.2010.07.015.

Oldfield, R.C., 1971. The assessment and analysis of handedness: the Edinburgh inventory. Neuropsychologia 9 (1), 97–113. https://doi.org/10.1016/0028-3932(71)90067-4.

Onton, J., Delorme, A., Makeig, S., 2005. Frontal midline EEG dynamics during working memory. Neuroimage 27 (2), 341–356. https://doi.org/10.1016/j.neuroimage.2005.04.014.

Oostenveld, R., Fries, P., Maris, E., Schoffelen, J.M., 2011. FieldTrip: open source software for advanced analysis of MEG, EEG, and invasive electrophysiological data. Comput. Intell. Neurosci. 2011 (1) https://doi.org/10.1155/2011/156869, 156869–9.

Perrin, F., Pernier, J., Bertrand, O., Echallier, J.F., 1989. Spherical splines for scalp potential and current density mapping. Electroencephalogr. Clin. Neurophysiol. 72 (2), 184–187.

Peterson, E.J., Voytek, B., 2017. Alpha oscillations control cortical gain by modulating excitatory-inhibitory background activity. bioRxiv 185074. https://doi.org/10.1101/185074.

Pinheiro, J., Bates, D., DebRoy, S., Sarkar, D., R Core Team, 2019. Nlme: linear and nonlinear mixed effects models. R package version 3.1-141. https://CRAN.R-project.org/package=nlme.

R Core Team, 2019. R: A Language and Environment for Statistical Computing. R Foundation for Statistical Computing, Vienna, Austria. https://www.R-project.org/.

Raghavachari, S., Kahana, M.J., Rizzuto, D.S., Caplan, J.B., Kirschen, M.P., Bourgeois, B., et al., 2001. Gating of human theta oscillations by a working memory task. J. Neurosci. 21 (9), 3175–3183. https://doi.org/10.1523/JNEUROSCI.21-09-03175.2001.

Sadaghiani, S., Kleinschmidt, A., 2016. Brain networks and α-oscillations: structural and functional foundations of cognitive control. Trends Cogn. Sci. 20 (11), 805–817. https://doi.org/10.1016/j.tics.2016.09.004.

Samaha, J., Postle, B.R., 2015. The speed of alpha-band oscillations predicts the temporal resolution of visual perception. Curr. Biol. 25 (22), 2985–2990. https://doi.org/10.1016/j.cub.2015.10.007.

Scheeringa, R., Petersson, K.M., Oostenveld, R., Norris, D.G., Hagoort, P., Bastiaansen, M.C., 2009. Trial-by-trial coupling between EEG and BOLD identifies networks related to alpha and theta EEG power increases during working memory maintenance. Neuroimage 44 (3), 1224–1238. https://doi.org/10.1016/j.neuroimage.2008.08.041.

Schomer, D.L., Lopes da Silva, F.H. (Eds.), 2017. Niedermeyer's Electroencephalography. Oxford Medicine Online, vol. 1. Oxford University Press. https://doi.org/10.1093/med/9780190228484.001.0001.

Sherman, M.A., Lee, S., Law, R., Haegens, S., Thorn, C.A., Hämäläinen, M.S., et al., 2016. Neural mechanisms of transient neocortical beta rhythms: converging evidence from humans, computational modeling, monkeys, and mice. Proc. Natl. Acad. Sci. 113 (33), E4885–E4894. https://doi.org/10.1073/pnas.1604135113.

Shin, H., Law, R., Tsutsui, S., Moore, C.I., Jones, S.R., 2017. The rate of transient beta frequency events predicts behavior across tasks and species. eLife 6. https://doi.org/10.7554/eLife.29086.

Sternberg, S., 1966. High-speed scanning in human memory. Science 153 (3736), 652–654.

Stokes, M., Spaak, E., 2016. The importance of single-trial analyses in cognitive neuroscience. Trends Cogn. Sci. 20 (7), 483–486. https://doi.org/10.1016/j.tics.2016.05.008.

Tinkhauser, G., Pogosyan, A., Tan, H., Herz, D.M., Kühn, A.A., Brown, P., 2017. Beta burst dynamics in Parkinson's disease OFF and ON dopaminergic medication. Brain 140 (11), 2968–2981. https://doi.org/10.1093/brain/awx252.

Tuladhar, A.M., Huurne, ter, N., Schoffelen, J.M., Maris, E., Oostenveld, R., Jensen, O., 2007. Parieto-occipital sources account for the increase in alpha activity with working memory load. Hum. Brain Mapp. 28 (8), 785–792. https://doi.org/10.1002/hbm.20306.

van Ede, F., Quinn, A.J., Woolrich, M.W., Nobre, A.C., 2018. Neural oscillations: sustained rhythms or transient burst- events? Trends Neurosci. 1–3. https://doi.org/10.1016/j.tins.2018.04.004.

Vidaurre, D., Quinn, A.J., Baker, A.P., Dupret, D., Tejero-Cantero, A., Woolrich, M.W., 2016. Spectrally resolved fast transient brain states in electrophysiological data. Neuroimage 126 (C), 81–95. https://doi.org/10.1016/j.neuroimage.2015.11.047.

Wang, X.J., 2010. Neurophysiological and computational principles of cortical rhythms in cognition. Physiol. Rev. 90 (3), 1195–1268. https://doi.org/10.1152/physrev.00035.2008.

Watrous, A.J., Miller, J., Qasim, S.E., Fried, I., Jacobs, J., 2018. Phase-tuned neuronal firing encodes human contextual representations for navigational goals. eLife 7. https://doi.org/10.7554/eLife.32554.

Whitten, T.A., Hughes, A.M., Dickson, C.T., Caplan, J.B., 2011. A better oscillation detection method robustly extracts EEG rhythms across brain state changes: the human alpha rhythm as a test case. Neuroimage 54 (2), 860–874. https://doi.org/10.1016/j.neuroimage.2010.08.064.

Wutz, A., Melcher, D., Samaha, J., 2018. Frequency modulation of neural oscillations according to visual task demands. Proc. Natl. Acad. Sci. 115 (6), 1346–1351. https://doi.org/10.1073/pnas.1713318115.

Supplementary Information for

Single-trial characterization of neural rhythms: potential and challenges

Julian Q. Kosciessa, Thomas H. Grandy, Douglas D. Garrett, Markus Werkle-Bergner

Email: kosciessa@mpib-berlin.mpg.de; werkle@mpib-berlin.mpg.de

This PDF file includes:

Supplementary text
Figures S1 to S10
Tables S1 to S2

SI Methods

Rhythmic frequency variability during rest. As an exemplary characteristic of rhythmicity, we assessed the stability of IAF estimates by considering the variability across trials of the task as a function of indicated rhythmicity. Trial-wise rhythmic IAF variability (Figure S7A) was calculated as the standard deviation of the mean frequency of alpha episodes (8-15 Hz). That is, for each trial, we averaged the estimated mean frequency of rhythmic episodes within that trial and computed the standard deviation across trials. Whole-trial IAF variability (Figure S7B) was similarly calculated as the standard deviation of the IAF, with single-trial IAF defined as the frequency with the largest peak magnitude between 8-15 Hz, averaged across the whole trial, i.e., encompassing segments both designated as rhythmic and arrhythmic. Finally, we compared the empirical variability with that observed in simulations (see section 2.8).

Depiction of rhythm-evoked effects. The temporal specificity of rhythmic episodes further allows the assessment of 'rhythm-evoked' effects in the temporal or spectral domain. Here, we showcase the rhythm-evoked changes in the same frequency band to indicate the temporal specificity of the indicated rhythmic periods (Figure S9). For this purpose, we calculated time-frequency representations (TFRs) using 6-cycle wavelets and extracted power in the theta (3-8 Hz), alpha (8-15 Hz), beta (15-25 Hz) and gamma-band (25-64 Hz) in 2.4 s periods centred on the on- and offset of indicated rhythmic periods in the respective band. Separate TFRs were calculated for the detected episodes in each channel, followed by averaging across episodes and channels. Finally, we z-transformed the individual averages to highlight the consistency across subjects.

SI Results

IAF variability varies as a function of abundance. Given the strong dependence of accurate duration estimates on sufficient rhythmic power, we investigated how the differences in rhythmicity affect the single-trial estimation of another characteristic, namely the individual alpha frequency (IAF) that generally shows high temporal stability (i.e., trait-qualities) within person at the average level (Grandy, Werkle-Bergner, Chicherio, Schmiedek, et al., 2013b) We observed a strong negative association between the estimated rhythmicity and fluctuations in the rhythmic IAF between trials (Figure S7A). That is, for subjects with pervasive alpha rhythms, IAF estimates were reliably stable across trials, whereas frequency estimates varied when rhythmicity was low. Notably a qualitatively and quantitatively similar association was observed in simulations with a stationary alpha frequency (black lines in Figure S7), suggesting that such variation may be artefactual. As lower abundance implies a smaller number of samples from which the IAF is estimated, this effect

could amount to a sampling confound. However, we observed a similar link between overall SNR and IAF variability when the latter was estimated across all timepoints in a trial (Figure S7B). Simulations with stationary 10 Hz rhythms gave rise to similar results, suggesting that estimated frequency fluctuations can arise (at least in part) from the absence of clear rhythmicity. Hence, even when the IAF is intra-individually stable, its moment-to-moment estimation may induce variability when the rhythms are not clearly present.

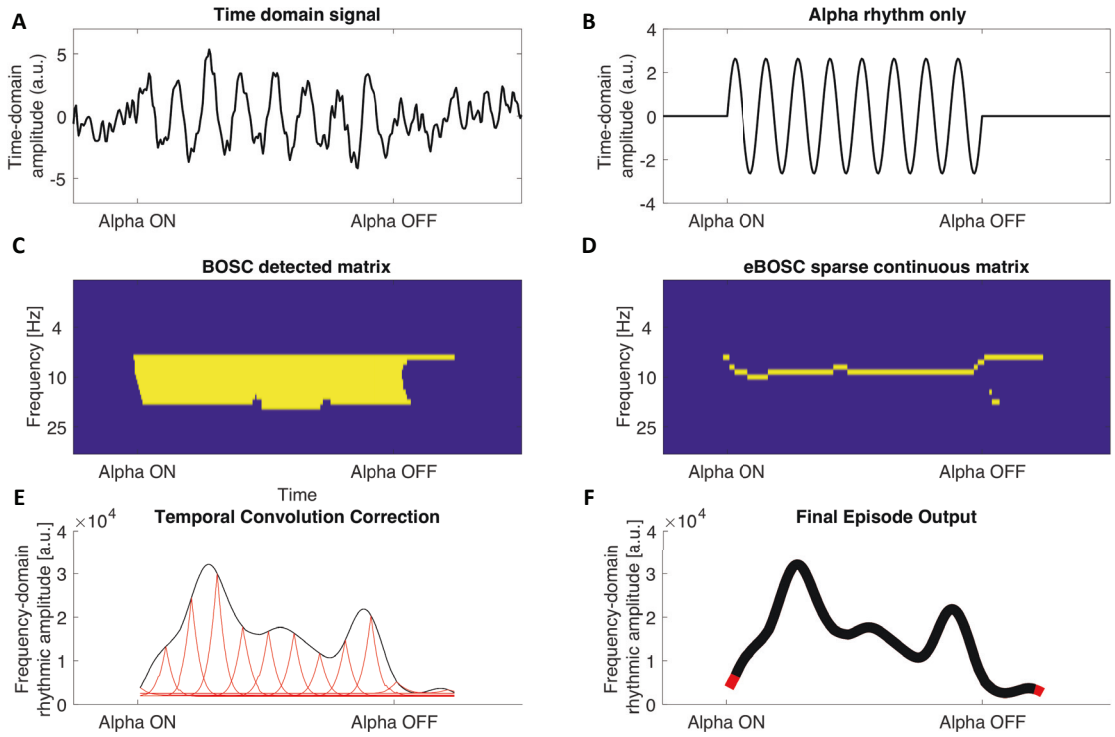

Fig. S1. Example of eBOSC's post-processing routines to derive sparse continuous rhythmic 'episodes'. (A) Simulated signal containing 1/f noise and superimposed 10 Hz rhythmicity. (B) 10 Hz rhythmic signal only. (C) Traditional output of BOSC detection: a binary matrix indicates time-frequency points that adhere to power and duration thresholds (in yellow). These matrices are used to calculate *Pepisode*. (D) First step of eBOSC's post-processing: the detected matrix is 'sparsified' in the spectral dimension to create continuous rhythmic episodes. (E) Second step of eBOSC's post-processing: each episode is temporally corrected for the temporal wavelet convolution by estimating the bias of each time point on adjacent time points (here exemplified for select time points via red traces). Only time points that exceed the bias estimated from surrounding time points are retained. (F) Example of final episode trace. The black line indicates the time points that were retained, whereas the red segments were removed during step E. The final episode output is then characterized according to e.g., mean frequency, duration and amplitude, whereas the time points of rhythmicity can for example be used to define rhythm-conditional spectra. These episodes are used to calculate *abundance*.

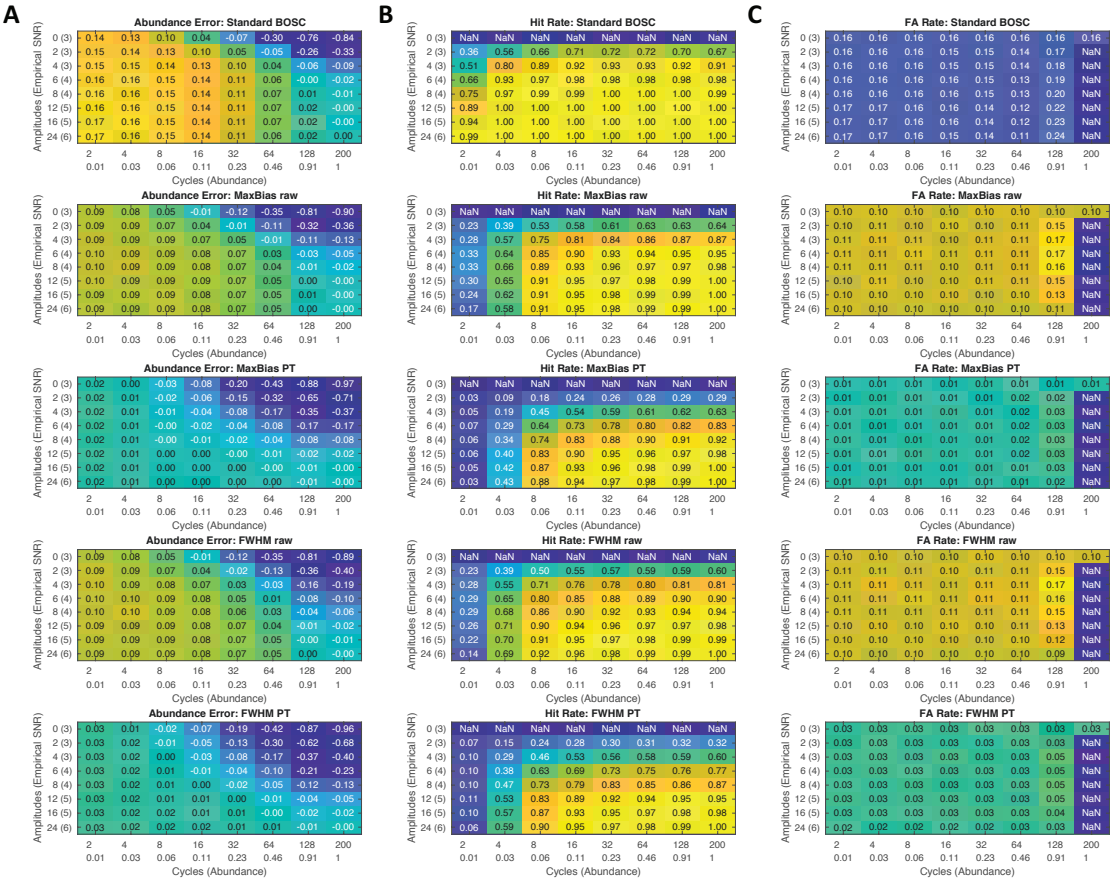

Fig. S2. Rhythm detection performance of different post-processing options. (A) Deviation of abundance estimates from simulated duration. (B) Hit rates. (C) False alarm rates. The subplot structure is the same as in Figure 3A. Rows show detection performance for different routines. The analyses in the main paper use the 'MaxBias PT' method. In the 'PT' method, only power values above the threshold were considered for post-processing, otherwise 'raw' power values were considered. Note that using the PT method, abundance is highly specific and is never over- but only underestimated, thus generally providing a lower bound on the real rhythmic abundance.

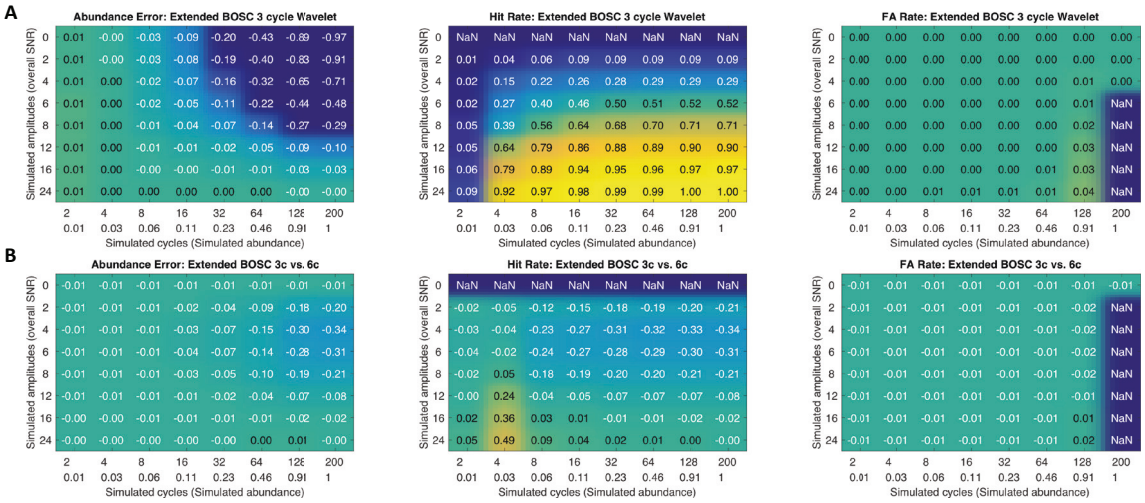

Fig. S3. Signal detection results using a 3 cycle wavelet (compared to the 6 cycle wavelet used for the main analyses). (A) Results for data from a 3 cycle wavelet transform indicate high specificity, with a gradient of sensitivity spanned by overall SNR. (B) Compared to the 6 cycle wavelet, the use of a 3 cycle wavelet increases sensitivity for shorter rhythms (around 4 cycles) at high SNR, whereas it decreases sensitivity for more sustained rhythmicity particularly in lower SNR ranges. Specificity is relatively unaffected.

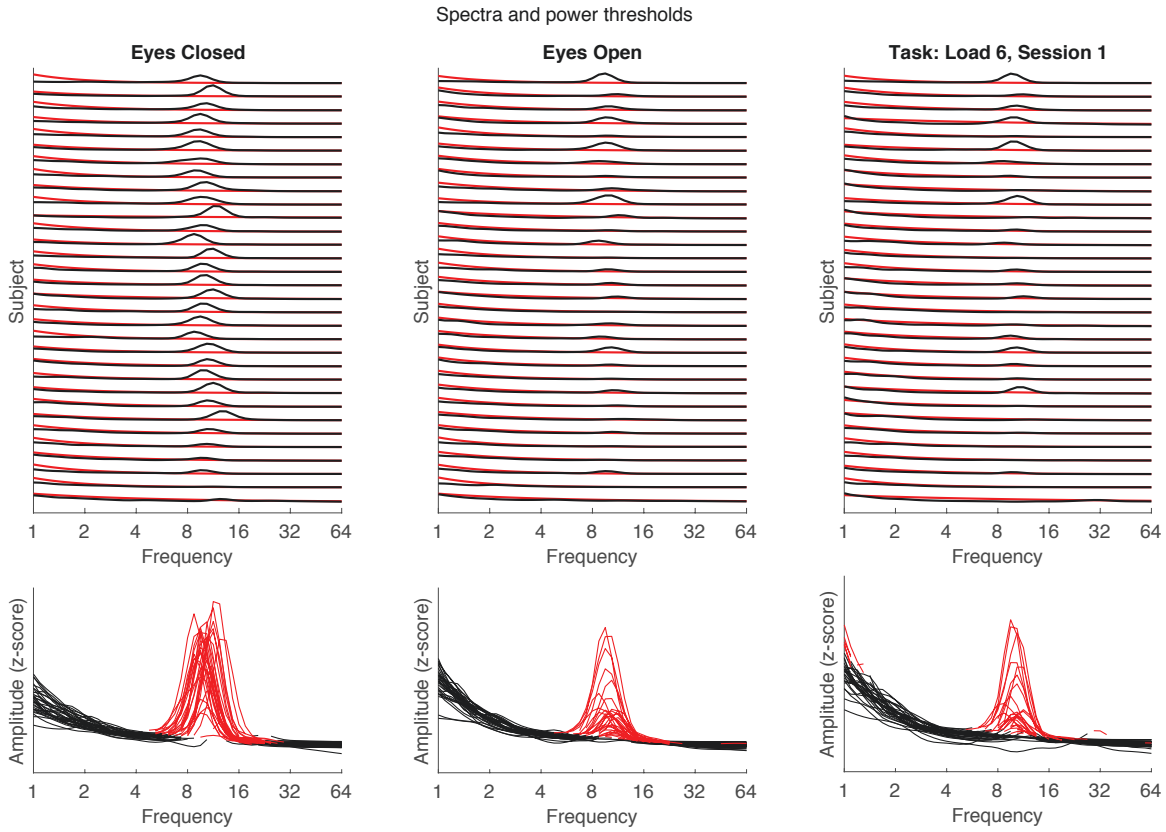

Fig. S4. Individual spectra (black) and power thresholds (red) for the eyes closed and eyes open resting state, as well as task retention period. Power thresholds suggest a successful exclusion of the alpha peak and similar fits across subjects. Large spectral peaks are consistently found in the 8-15 Hz range. Spectra are averaged across posterior-occipital channels. Spectra and power thresholds have been spectrally concatenated and z-scored across frequencies for enhanced visibility. Subjects have been sorted by descending 8-15 Hz power during the eyes closed resting state. (Bottom) The alpha peak is consistently excluded from the background threshold. Red traces indicate the spectral power above the power threshold, black traces indicate the segments below the power threshold. Note that falling below the power threshold does not prevent detection as single-trial power can exceed the average power and thus the power threshold. These fluctuations are crucial for the detection of rhythmicity as the power threshold is fixed (see also Figure 7 in main text).

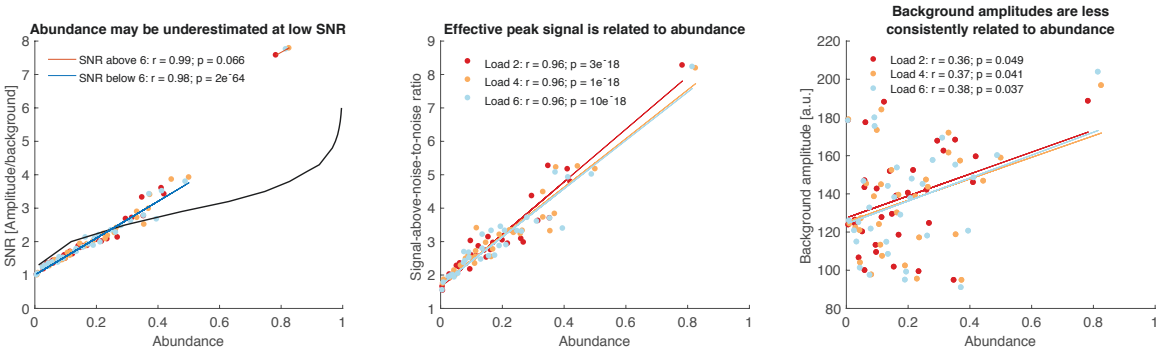

Fig. S5. Amplitude-abundance coupling during the retention phase. Similar to the observations in the resting state data (Figure 6 in the main text), the effective rhythmic peak explains the estimated abundance, whereas the background estimate is less consistently associated with abundance

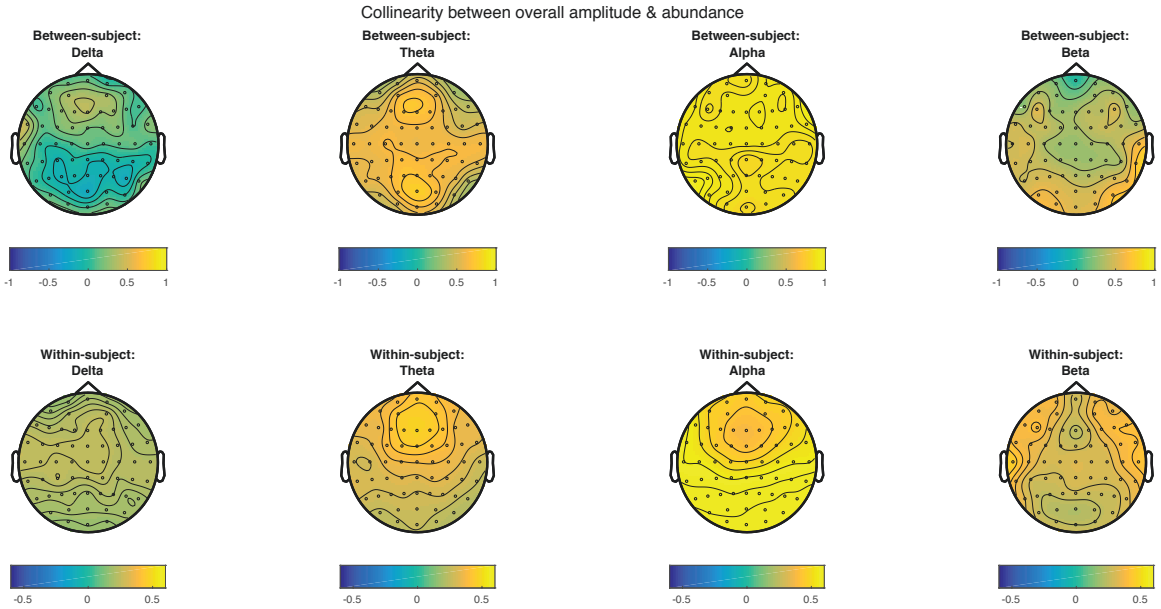

Fig. S6. Topographies of between-subject (1st row) and within-subject (2nd row) collinearity (Pearson correlations) of overall amplitude and abundance for multiple low-frequency ranges. Collinearity is highest for the alpha band. Highest within-subject collinearity is observed for channels with high abundance. Corresponding grand average topographies of overall amplitude and abundance are shown in Figure S8.

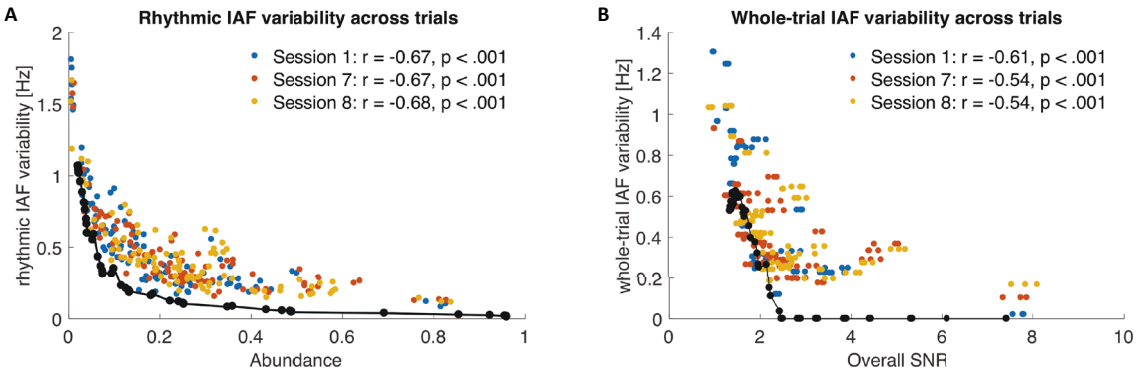

Fig. S7. Trial-by-trial IAF variability is associated with sparse rhythmicity. (A) Individual alpha frequency (IAF) precision across trials is related to abundance. Lower individual abundance estimates are associated with increased across-trial IAF variability. (B) This relationship also exists when considering overall SNR and IAF estimates from across the whole trial. Superimposed black lines show the 6th order polynomial fit for simulation results encompassing varying rhythm durations and amplitudes. Empirically estimated frequency variability is quantitatively similar to the bias observed at low SNRs in the simulated data.

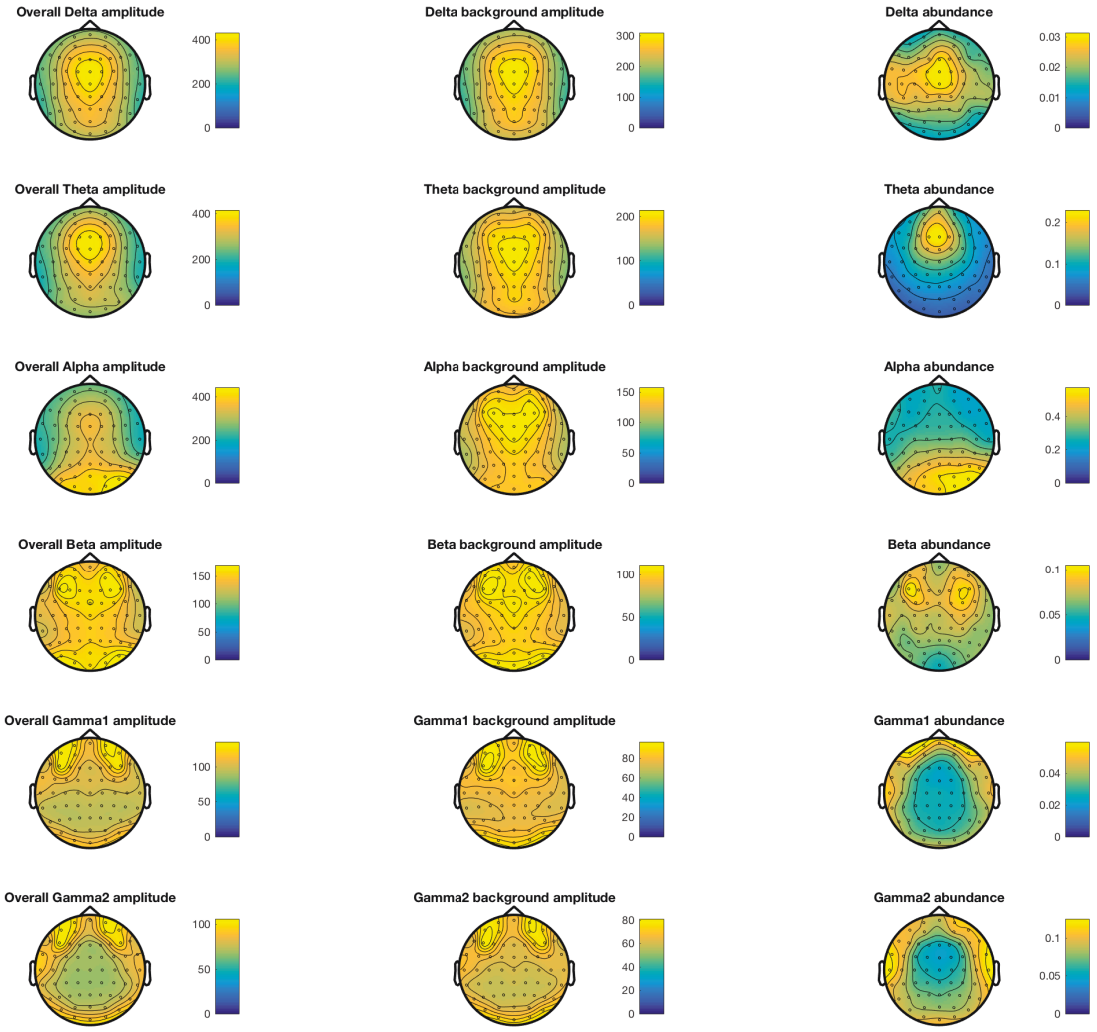

Fig. S8. Topographies of overall (narrowband) amplitudes, estimated background amplitudes and abundance indicate a principled exclusion of stationary scale-free background amplitudes from rhythmicity estimates across multiple frequencies. In addition, the topographies suggest that overall amplitudes represent a mixture of a relatively stationary background and spectrally varying rhythmic components. As in Figure 8, the topographies are grand averages from the retention phase of the Sternberg task across sessions.

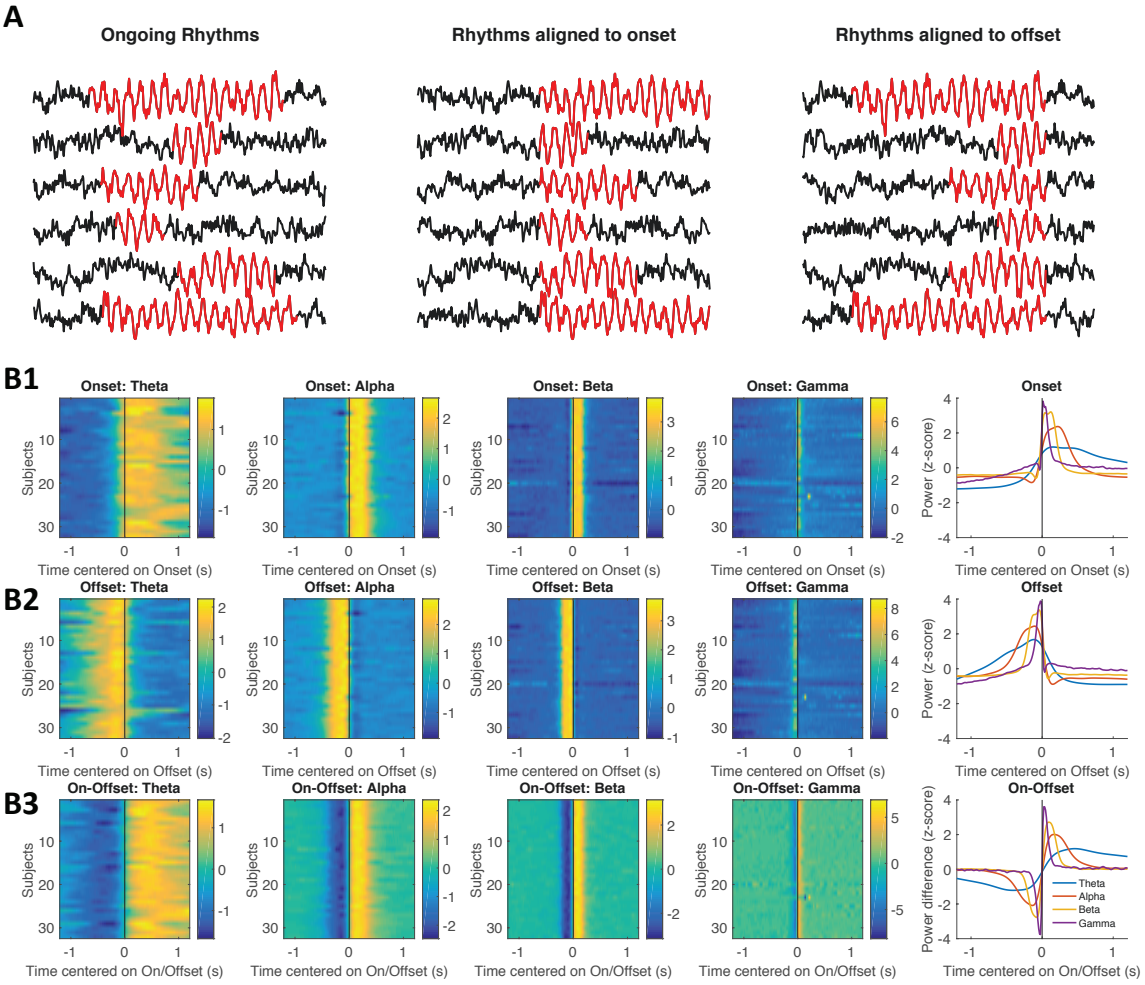

Fig. S9. On- and offsets of rhythmic episodes characterize 'rhythm-evoked' effects. (A) Schematic alignment of data to the on- and offsets of rhythmic periods. (B) Rhythm on- and offsets are marked by sudden power shifts at their respective frequency. Individual normalized wavelet power shows a strong increase at the rhythmic onset (B1) and a decrease once rhythmic episodes end (B2). The difference between on- and offset-related power summarizes the evoked effect of rhythmic episodes on ongoing power (B3). Power was extracted within a fixed peri-onset and peri-offset window for all channels where episodes were detected and subsequently averaged across episodes, loads and channels. Finally, the individual averages were z-normalized. The rightmost plots show the grand average across subjects. Data are from extended periods of the Sternberg task in Session 1.

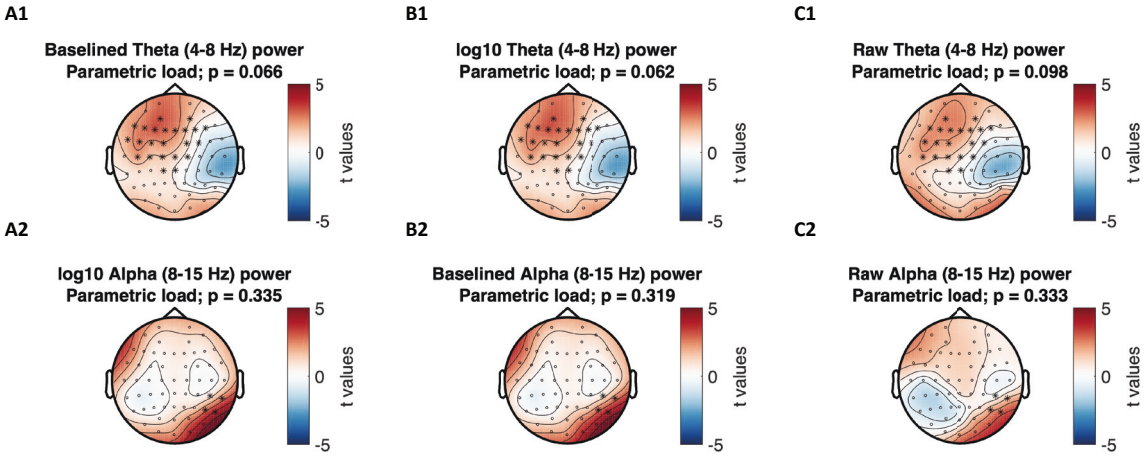

Fig. S10. Results of cluster-based permutation tests for different baseline variants: (A) average baseline, (B) single-trial log10-transform, and (C) raw power. While all normalizations produce similar clusters to the observed abundance effect (Figure 11 in main text), no cluster reached statistical significance.

Table S1. Berger effect of eye closure on rhythmic and arrhythmic alpha indices, controlling for the high collinearity between indicators

			Bootstrap 95% CI				
Dependent variable	Predictor	b	Low	High	SE	F-value	p-value
Rhythmic abundance	Arrhythmic amplitude	0.33	0.15	0.51	0.09	14.0	0.001
	Berger effect	-1.11	-1.44	-0.79	0.16	47.7	0.000
Rhythmic abundance	Rhythmic amplitude	0.46	0.28	0.63	0.09	26.3	0.000
	Berger effect	-0.94	-1.25	-0.63	0.15	36.5	0.000
Rhythmic amplitude	Arrhythmic amplitude	0.85	0.76	0.95	0.05	331.4	0.000
	Berger effect	-0.26	-0.42	-0.10	0.08	10.4	0.003
Rhythmic amplitude	Rhythmic abundance	0.51	0.28	0.75	0.11	19.3	0.000
	Berger effect	-0.37	-0.76	0.02	0.19	3.5	0.070
Arrhythmic amplitude	Rhythmic abundance	0.44	0.14	0.73	0.15	8.6	0.006
	Berger effect	-0.37	-0.89	0.15	0.25	2.0	0.165
Arrhythmic amplitude	Rhythmic amplitude	0.99	0.88	1.09	0.05	370.3	0.000
	Berger effect	0.10	-0.09	0.29	0.09	1.0	0.323

Effects were estimated within linear mixed effects models. Green shading indicates significant ($p < .05$) Berger effects of eye opening that cannot be explained by potential collinearity with the remaining predictor variable; orange shading indicates the absence of an indicated unique Berger effect on the dependent variable.

Table S2. Unique memory load effects on rhythm-specific estimates, controlling for high collinearity with traditional estimates

Dependent variable	Predictor	F-value	p-value
Alpha rhythmic abundance	Alpha overall amplitude	217.8	<0.001
	Load	12.1	<0.001
Theta rhythmic abundance	Theta overall amplitude	75.6	<0.001
	Load	3.3	0.045
Alpha rhythmic abundance	Alpha rhythmic amplitude	112.4	0.000
	Load	13.5	0.000
Theta rhythmic abundance	Theta rhythmic amplitude	59.8	0.000
	Load	5.3	0.008
Alpha rhythmic amplitude	Alpha overall amplitude	81.0	<0.001
	Load	1.3	0.278
Theta rhythmic amplitude	Theta overall amplitude	56.7	<0.001
	Load	0.3	0.744

Effects were estimated within linear mixed effects models. Green shading indicates significant ($p < .05$) memory load effects that cannot be explained by potential collinearity with the remaining predictor variable; orange shading indicates the absence of an indicated unique memory load effect on the dependent variable. Overall amplitudes refer to baselined alpha power as depicted in Figure 11A.

PLOS COMPUTATIONAL BIOLOGY

RESEARCH ARTICLE

Standard multiscale entropy reflects neural dynamics at mismatched temporal scales: What's signal irregularity got to do with it?

Julian Q. Kosciessa[1,2,3]*, **Niels A. Kloosterman**[1,2], **Douglas D. Garrett**[1,2]*

1 Max Planck UCL Centre for Computational Psychiatry and Ageing Research, Berlin, Germany, **2** Center for Lifespan Psychology, Max Planck Institute for Human Development, Berlin, Germany, **3** Department of Psychology, Humboldt-Universität zu Berlin, Berlin, Germany

* kosciessa@mpib-berlin.mpg.de (JQK); garrett@mpib-berlin.mpg.de (DDG)

OPEN ACCESS

Citation: Kosciessa JQ, Kloosterman NA, Garrett DD (2020) Standard multiscale entropy reflects neural dynamics at mismatched temporal scales: What's signal irregularity got to do with it? PLoS Comput Biol 16(5): e1007885. https://doi.org/10.1371/journal.pcbi.1007885

Editor: Daniele Marinazzo, Ghent University, BELGIUM

Received: January 10, 2020

Accepted: April 18, 2020

Published: May 11, 2020

Peer Review History: PLOS recognizes the benefits of transparency in the peer review process; therefore, we enable the publication of all of the content of peer review and author responses alongside final, published articles. The editorial history of this article is available here: https://doi.org/10.1371/journal.pcbi.1007885

Data Availability Statement: Raw empirical data is provided at https://osf.io/q3vxm/ (DOI 10.17605/OSF.IO/Q3VXM). Code used to produce simulations, empirical analyses and figures is

Abstract

Multiscale Entropy (MSE) is used to characterize the temporal irregularity of neural time series patterns. Due to its' presumed sensitivity to non-linear signal characteristics, MSE is typically considered a complementary measure of brain dynamics to signal variance and spectral power. However, the divergence between these measures is often unclear in application. Furthermore, it is commonly assumed (yet sparingly verified) that entropy estimated at specific time scales reflects signal irregularity at those precise time scales of brain function. We argue that such assumptions are not tenable. Using simulated and empirical electroencephalogram (EEG) data from 47 younger and 52 older adults, we indicate strong and previously underappreciated associations between MSE and spectral power, and highlight how these links preclude traditional interpretations of MSE time scales. Specifically, we show that the typical definition of temporal patterns via "similarity bounds" biases coarse MSE scales–that are thought to reflect slow dynamics–by high-frequency dynamics. Moreover, we demonstrate that entropy at fine time scales–presumed to indicate fast dynamics–is highly sensitive to broadband spectral power, a measure dominated by low-frequency contributions. Jointly, these issues produce counterintuitive reflections of frequency-specific content on MSE time scales. We emphasize the resulting inferential problems in a conceptual replication of cross-sectional age differences at rest, in which scale-specific entropy age effects could be explained by spectral power differences at mismatched temporal scales. Furthermore, we demonstrate how such problems may be alleviated, resulting in the indication of scale-specific age differences in rhythmic irregularity. By controlling for narrowband contributions, we indicate that spontaneous alpha rhythms during eyes open rest transiently reduce broadband signal irregularity. Finally, we recommend best practices that may better permit a valid estimation and interpretation of neural signal irregularity at time scales of interest.

provided at https://git.mpib-berlin.mpg.de/LNDG/rhythms_entropy. The code implementing the mMSE algorithm is available from https://github.com/LNDG/mMSE.

Funding: This study was conducted within the 'Lifespan Neural Dynamics Group' within the Max Planck UCL Centre for Computational Psychiatry and Ageing Research in the Max Planck Institute for Human Development (MPIB) in Berlin, Germany. DDG and NAK were supported by an Emmy Noether Programme grant (to DDG) from the German Research Foundation, and by the Max Planck UCL Centre for Computational Psychiatry and Ageing Research. JQK is a pre-doctoral fellow supported by the International Max Planck Research School on Computational Methods in Psychiatry and Ageing Research (IMPRS COMP2PSYCH). The participating institutions are the Max Planck Institute for Human Development, Berlin, Germany, and University College London, London, UK. For more information, see https://www.mps-ucl-centre.mpg.de/en/comp2psych. The funders had no role in study design, data collection and analysis, decision to publish, or preparation of the manuscript.

Competing interests: The authors have declared that no competing interests exist.

Author summary

Brain signals exhibit a wealth of dynamic patterns that are thought to reflect ongoing neural computations. Multiscale sample entropy (MSE) intends to describe the temporal irregularity of such patterns at multiple time scales of brain function. However, the notion of time scales may often be unintuitive. In particular, traditional implementations of MSE are sensitive to slow fluctuations at fine time scales, and fast dynamics at coarse time scales. This conceptual divergence is often overlooked and may lead to difficulties in establishing the unique contribution of MSE to effects of interest over more established spectral power. Using simulations and empirical data, we highlight these issues and provide evidence for their relevance for valid practical inferences. We further highlight that standard MSE and traditional spectral power are highly collinear in our example. Finally, our analyses indicate that spectral filtering can be used to estimate temporal signal irregularity at matching and intuitive time scales. To guide future studies, we make multiple recommendations based on our observations. We believe that following these suggestions may advance our understanding of the unique contributions of neural signal irregularity to neural and cognitive function across the lifespan.

Introduction

Entropy as a measure of signal irregularity

Neural times series exhibit a wealth of dynamic patterns that are thought to reflect ongoing neural computations. While some of these patterns consist of stereotypical deflections [e.g., periodic neural rhythms; 1, 2], the framework of nonlinear dynamics and complex systems also emphasizes the importance of temporal irregularity (or variability) for healthy, efficient, and flexible neural function [3–6]. Specifically, functional network dynamics may reflect the non-linear interaction of local and global population activity, for which intermediate levels of network noise theoretically afford high network capacity and dynamic range [7–10]. In parallel with such conceptual advances, multiscale entropy (MSE) [11, 12], an information-theoretic index that estimates sample entropy [13] at multiple time scales (Fig 1A), has become a promising tool to quantify the irregularity of neural time series across different brain states, the lifespan, and in relation to health and disease [14–22]. However, we argue that outstanding methodological issues regarding the mapping of neural-to-MSE time scales reduce the current interpretability of MSE results, and–if not properly accounted for–limit MSE's utility for investigating substantive neurocomputational questions of interest.

In general, sample entropy quantifies the irregularity of temporal patterns in a given signal (for an example of its calculation, see Fig 1B). Whereas signals with a repetitive structure (like stationary signals or rhythmic fluctuations) are estimated as having low entropy, less predictable (or random) signals are ascribed high entropy. As an extension of this principle, MSE aims to describe temporal irregularity at different time scales–varying from fine (also referred to as 'short') to coarse (or 'long'). In conventional Fourier analysis of time series data, time scales are quantified in terms of lower and higher frequencies present in the signal. This has been shown to be a principled time scale descriptor that relates at least in part to structural properties of the generating neural circuits [2, 23–26]. Given this meaningful definition of fast and slow events, it is a common assumption–including in guides to MSE's interpretation in neural applications [27]–that fine-to-coarse scales characterize the irregularity of high-to-low frequency dynamics, respectively. However, here we highlight one methodological and one

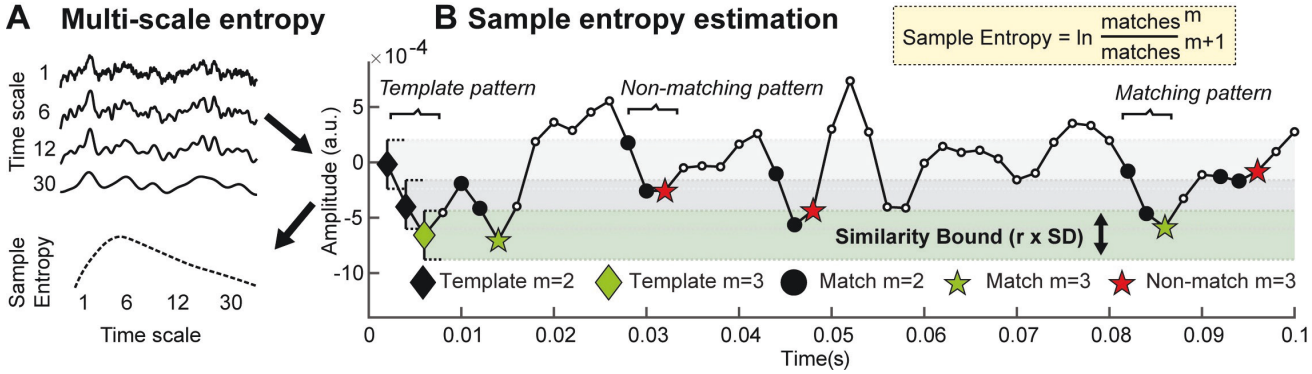

Fig 1. Traditional MSE estimation procedure. (**A**) Multi-scale entropy is an extension of sample entropy, an information-theoretic metric intended to describe the temporal irregularity of time series data. To estimate entropy for different time scales, the original signal is traditionally 'coarse-grained' using low-pass filters, followed by the calculation of the sample entropy. (**B**) Sample entropy estimation procedure. Sample entropy measures the conditional probability that two amplitude patterns of sequence length m (here, 2) remain similar (or matching) when the next sample ***m*** + 1 is included in the sequence. Hence, sample entropy increases with temporal irregularity, i.e., with the number of m-length patterns that do not remain similar at length m+1 (non-matches). To discretize temporal patterns from continuous amplitudes, similarity bounds (defined as a proportion ***r***, *here .5*, of the signal's standard deviation [SD]) define amplitude ranges around each sample in a given template sequence, within which matching samples are identified in the rest of the time series. These are indicated by horizontal grey and green bars around the first three template samples. This procedure is applied to each template sequence in time, and the pattern counts are summed to estimate the signal's entropy. The exemplary time series is a selected empirical EEG signal that was 40-Hz high-pass filtered with a 6th order Butterworth filter.

https://doi.org/10.1371/journal.pcbi.1007885.g001

conceptual issue regarding the computation of MSE that challenge such a direct scale-to-frequency mapping. First, we show that the traditional definition of temporal patterns may lead to an influence of high frequencies on coarse entropy time scales (Issue 1). Second, we highlight that the signal content at fine time scales renders entropy estimates sensitive to a conjunction of scale-free and narrowband signals, including slow fluctuations (Issue 2).

Due to its assessment of temporal patterns rather than sinusoidal oscillatory dynamics, MSE has been motivated as a complementary measure to spectral variance/power that is sensitive to multi-scale, potentially non-linear, signal characteristics, such as phase shifts or cross-frequency coupling. [Note that we use the terms power and variance interchangeably, as a time domain signal's broadband variance is proportional to the integral of its power spectral density, while narrowband variance in the time domain is identical to narrowband power in the spectral domain.] However, the overlap between these measures is often unclear in application because the mapping between spectral power and scale-wise entropy is ambiguous. Such ambiguity affects both the ability to compare individuals at any scale, and the ability to compare entropy levels across scales within person. We argue that a clarification of these issues is thus necessary for valid inferences of time scale-specific 'neural irregularity' in a growing number of neuroscientific MSE applications.

Issue 1: Global similarity bounds introduce a scale-dependent variance bias

A principle assumption of sample entropy is that "the degree of irregularity of a complex signal [. . .] cannot be entirely captured by the SD [i.e., standard deviation]" [28; i.e., square root of variance]. To ensure this, sample entropy is typically assessed relative to the standard deviation of the broadband signal to intuitively normalize the estimation of irregularity for overall distributional width [13, 14, see also 28]. In particular, the ***similarity bound***–defined by a constant r, by which the signal SD is multiplied–reflects the tolerance for labeling time points as being similar or different, and thus, determines how liberal the algorithm is towards detecting 'matching patterns' (Fig 2A and 2B). While wider bounds decrease entropy estimates,

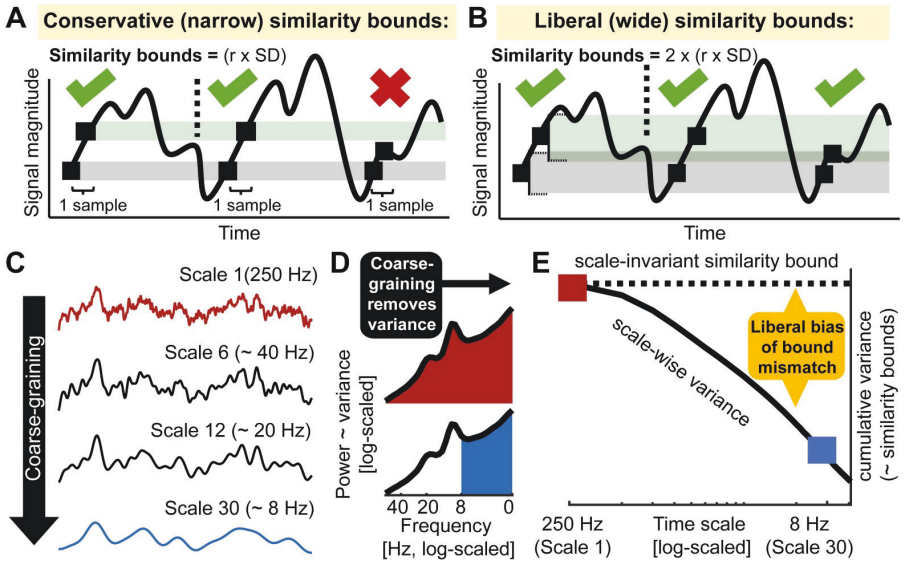

Fig 2. Issue 1: Global similarity bounds systematically confound the entropy of coarse-scale signals with removed spectral power. (**A, B**) Similarity bounds constrain sample entropy as shown schematically for entropy estimation using narrower (**A**) and wider (**B**) similarity bounds. For clarity, only a subset of pattern matches (green ticks) and mismatches (red cross) are indicated for a sequence length m = 1(cf. Fig 1B). Wider, more liberal similarity bounds indicate more pattern matches than narrow, conservative bounds, thereby decreasing entropy. S2 Fig shows the empirical link between liberal similarity bounds and sample entropy estimates. (**C-E**) Divergence between global similarity bounds and scale-wise signal SD biases coarse-scale entropy. (**C**) Coarse-graining (see Fig 1A) progressively reduces variance from the original broadband signal (as shown in panel E). (**D**) At original sampling rates (i.e., time scale 1; marked red in panels DE and F), neural signal variance is usually composed of broadband 1/f content and narrowband rhythmic peaks. Note that the x-axis plots decreasing frequencies to align with the traditional MSE low-pass filter direction. Towards coarser scales (e.g., scale 30; marked blue in CD and E), signal variance progressively decreases, as the signal becomes more specific to low frequencies. (**E**) Due to the systematic and cumulative reduction of variance in scale-wise signals, global similarity bounds become liberally biased ('broad'). Critically, systematic differences in the magnitude of this bias (e.g., due to different spectral slopes) introduce systematic entropy differences at coarser scales.

https://doi.org/10.1371/journal.pcbi.1007885.g002

narrower bounds increase them [13, 29, 30] (S2 Fig). Crucially, the similarity bound is often not equally liberal across time scales, resulting in an entropy estimation bias. Specifically, to characterize temporal irregularity at coarser time scales, signals are typically successively low-pass filtered [or 'coarse-grained'; 31] (Fig 2C), whereas the similarity bound typically (in its 'Original' implementation) is set only once–namely relative to the SD of the original unfiltered signal. Due to the progressive filtering, coarse-graining successively reduces the signal's SD, yet a single global (i.e., scale-invariant) similarity bound remains based on the cumulative variance of all estimable frequencies (Fig 2D and 2E). As a result, the similarity bound becomes increasingly liberal towards pattern similarity at coarser scales, thereby reducing entropy estimates. This is most clearly illustrated by the observation that white noise signals, which should be characterized as equally random at each time scale, exhibit decreasing entropy values towards coarser scales when global *similarity bounds* are used [27, 29, 32]. This issue has been recognized previously [29], and provided a rationale for recomputing the *similarity bound* for each time scale [29, 33–35]. But despite the benefits of this refinement that was already proposed fifteen years ago, our review of the literature revealed that the use of global bounds remains dominant in over 90% of neuroscientific MSE applications (see S1 Text) and in previous validation work [27]. Crucially, the consequences of this bias for practical inference remain

unclear. We therefore argue that a comprehensive assessment of the resulting bias is needed to highlight this issue, both to clarify previous results and to guide future studies.

Issue 2: Traditional scale definitions lead to diffuse time scale reflections of spectral content

While matched similarity bounds account for *total signal variation* at any specific time scale, sample entropy remains related to *the variance structure* (i.e., the power spectrum) of the signal as ***one*** indicator of its temporal irregularity [4]. Most neural signals exhibit a scale-free $\frac{1}{f^x}$ power distribution [36–38], for which the exponent x indicates the prevalence of low-to-high-frequency components in the signal. This ratio is also referred to as the power spectral density (PSD) slope. Smaller exponents (indicating shallower PSD slopes) characterize signals with relatively strong high-frequency contributions (i.e., reduced temporal autocorrelations, and less predictability) compared to larger exponents that indicate steeper slopes. This conceptual link between PSD slopes (or high-to-low frequency power ratios that may have strong broadband slope contributions [39]) and sample entropy has been empirically observed across subjects, wakefulness and task states [14, 17, 40]. However, the sensitivity of fine-scale entropy to PSD slopes–a multi-scale characteristic–highlights that the contribution of slow-to-fast signal content to fine-scale entropy is unclear. This ambiguity arises from the algorithm that derives scale-wise signals. In particular, 'Original' MSE implementations use low-pass filters to derive signals at coarser time scales, which increasingly constrains entropy estimates to slower fluctuations. As such, each scale defines an upper bound for the range of included frequencies (see methods). However, the opposite is not true, resulting in a lack of high-frequency specificity. Hence, finer time scales characterize the *entire* broadband signal (see Fig 3A) which represents a non-specific mixture of low and high-frequency elements across scale-free and rhythmic signal contributions [41, 42]. Crucially, the contribution of these elements to neural broadband signals is not equal. Rather, the variance of $\frac{1}{f^x}$ signals is dominated by the amplitude of low frequencies, which may thus disproportionally impact the assessment of pattern irregularity [35]. As a result, broadband signal characterization challenges the assumption that fine-scale entropy mainly describes 'fast' events. More generally, this highlights large uncertainty regarding the frequencies that are represented at *any* particular time scale.

The projection of narrowband rhythms into simulated noise signals provides a well-controlled situation in which to study the mapping of neural irregularity to MSE, due to their clearly defined time scale (i.e., period = inverse of frequency) and regularity (added rhythmic variance = more regular signal = decreased entropy). Moreover, rhythmic structure remains a dominant target signal in neuroscience [1, 36, 43] for which entropy, as a complementary descriptor, should provide an anti-correlated reflection. However, previous simulations on the mapping of rhythms onto MSE time scales have produced puzzling results that have received little attention in the literature so far; while a linear mapping between rhythmic frequency and entropy time scales has been observed, added rhythmic regularity has been shown to *increase* entropy above baseline in previous work [4, 22, 44]. This notably contrasts with the intuition that added signal regularity should reduce observed entropy. Thus, additional simulations are necessary to assess the intuitive notion that rhythmicity should be anticorrelated with entropy, and to investigate whether this phenomenon indeed occurs at specific time scales, as previously assumed [4, 22, 44]. In particular, we probed the feasibility of using high-pass and band-pass filters (relative to standard low-pass options) to control the MSE time scales at which rhythmicity would be reflected (Fig 3B).

In summary, Issue 1 suggests a coarse-scale bias introduced by global similarity bounds, and Issue 2 highlights a mixture of narrow- and broadband contributions to fine scales. In

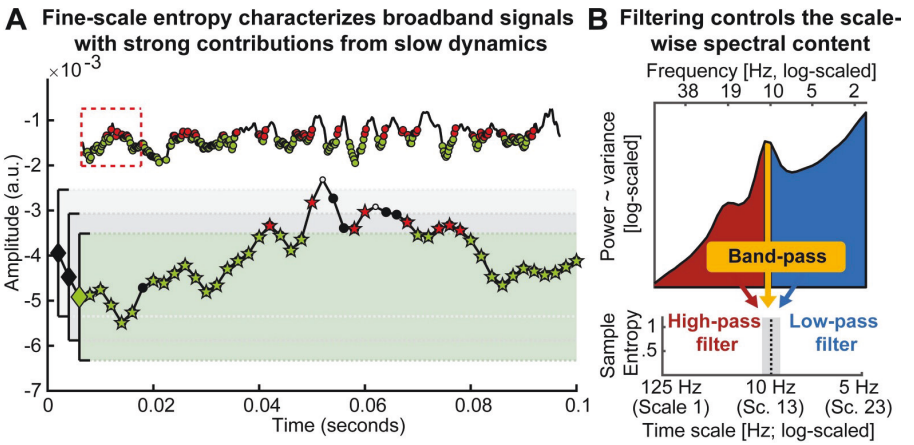

Fig 3. Issue 2: Traditional scale derivation leads to diffuse time-scale reflections of spectral power. (A) Exemplary sample entropy estimation in the same empirical EEG signal shown in Fig 1B, but without application of a high-pass filter, thus including dominant slow dynamics. See Fig 1B for a legend of the Figure elements. In brief, green elements indicate pattern matches at m+1, whereas red elements indicate pattern mismatches at m+1. In the presence of large low-frequency fluctuations, sample entropy at fine scales (here scale 1) may to a large extent characterize the temporal regularity of slow dynamics. Note that this is not a case of biased similarity bounds, but a desired adjustment to the large amplitude of slow fluctuations. The inset shows an extended segment (800 ms) of the same signal, allowing for an assessment of the slower signal dynamics. The red box indicates the 100 ms signal shown in the main plot. (B) A scale-wise filter implementation controls the scale-wise spectral content, as schematically shown here for the filter-dependent representation of spectral content at a time scale of approximately 10 Hz (for a note on the x-axis labeling, see methods: *Calculation of multi-scale sample entropy*). Traditionally, low-pass filters are used to derive coarser scales, which introduces a sensitivity to slower fluctuations. However, other filter implementations can be used to e.g., investigate the pattern irregularity of fast signal variations. No matter whether low or high pass filters are used, the spectral content influencing entropy estimates is by definition not specific to any particular time scale; band-pass filters provide one viable solution permitting such specificity.

https://doi.org/10.1371/journal.pcbi.1007885.g003

worst-case scenarios, a conjunction of these issues may lead to a reflection of fast dynamics in coarse entropy and a reflection of slow dynamics in fine entropy, thus paradoxically *inverting* the intuitive time scale interpretation. These issues have not been jointly assessed, however, and there is little evidence of whether and how these methodological issues may impact practical inferences motivated by neurobiological questions of interest. We focus on two example scenarios in the current study.

Impact of issues on practical inferences: (1) age differences in neural irregularity at fast and slow time scales

One principal application of multiscale entropy is in the domain of lifespan covariations between neural dynamics and structural brain network ontogeny [for a review see 45]. Within this line of inquiry, it has been proposed that structural brain alterations across the lifespan manifest as entropy differences at distinct time scales [16, 18, 40, 46]. Specifically, it has been suggested that coarse-scale entropy decreases and fine-scale entropy rises with increasing adult age as a reflection of senescent shifts from global to increasingly local information processing [16, 18]. Crucially, this mirrors observations based on spectral power, where age-related decreases in the magnitude of low-frequencies [47, 48] are accompanied by increases in high-frequency activity, conceptualized also as a flattening of power spectral density (PSD) slopes [16, 18, 40, 49]. These results seemingly converge towards a joint decrease of low-frequency power and coarse-scale entropy in older adults (and an increase for both regarding fast dynamics). However, this correspondence is surprising upon closer inspection given the

presumed anticorrelation between the magnitude of signal regularity (as indicated by heightened spectral power) and entropy. In light of concerns regarding the interpretation of entropy time scales (see above), we assessed cross-sectional age effects on both MSE and spectral power as a test case for potential mismatches in scale-dependent inferences.

Impact of issues on practical inferences: (2) narrowband modulations of broadband irregularity

Identifying the time scale contributors to MSE is further relevant due to the assumed functional separability of narrow- and broadband brain dynamics. Whereas narrowband rhythms have been closely associated with synchronous population spiking at the service of temporal information coordination [50], scale-free broadband dynamics may provide a complementary index of the level of neocortical activation and aggregate spiking activity in humans [38, 51–53]. In particular, shallower PSD slopes have been proposed as a signature of enhanced cortical excitability (or 'neural noise') [54]. Such excitability in turn may regulate the available range of network dynamics as reflected in information entropy [10]. Notably, interactions between narrow- and broadband activity are neurobiologically expected. In particular, as the magnitude of narrowband alpha synchronization increases, population output is thought to decrease [55]. However, the methodological conflation of narrow- and broadband contributions to entropy (see "Issue 2" above) may complicate principled investigations regarding their neurobiological coupling in practice. As a corollary goal in the present work, we therefore investigate whether a principled separation of narrow- and broadband contributions to entropy is tractable.

Current study

Here, we aimed to address two issues of frequency-to-scale mapping and their relevance for empirical applications. First, we simulated variations in rhythmic power and frequency to probe the relationship between rhythmicity and MSE time scales. Primarily, our goal was to assess how global similarity bounds (Issue 1) and the scale-wise spectral content of the analyzed signal (Issue 2) influence the time scales at which added rhythmicity is observed. Then, we attempted to replicate reported cross-sectional age differences in human electroencephalography (EEG) signals recorded during rest. We assessed whether younger adults would show increased coarse scale and decreased fine-scale entropy compared to older adults, and we probed the extent to which such scale-specific results depend on mismatched spectral power via the issues above. As corollary goals, we assessed the potential of band-pass and band-stop approaches for deriving more intuitive insights regarding the time scales of signal irregularity. First, we probed the potential of 'frequency-specific' estimates of signal irregularity via band-pass filters, and assessed age differences therein. Second, we assessed the relation between alpha rhythms and broadband signal irregularity, after accounting for their methodological coupling. We refer to traditional settings that use global bounds and low-pass filtering as 'Original' throughout the remainder of the manuscript (see methods for details).

Results

Simulations indicate a diffuse mapping between rhythmicity and MSE time scales as a function of global similarity bounds and spectral signal content

Our first aim was to probe how scale-specific events, namely rhythms of a given frequency, modulate MSE time scales. For this purpose, we simulated 10 Hz (alpha) rhythms of varying power on top of pink noise and calculated the MSE of those signals. First, we probed the influence of global similarity bounds (as used in 'Original' implementations) on the time scale

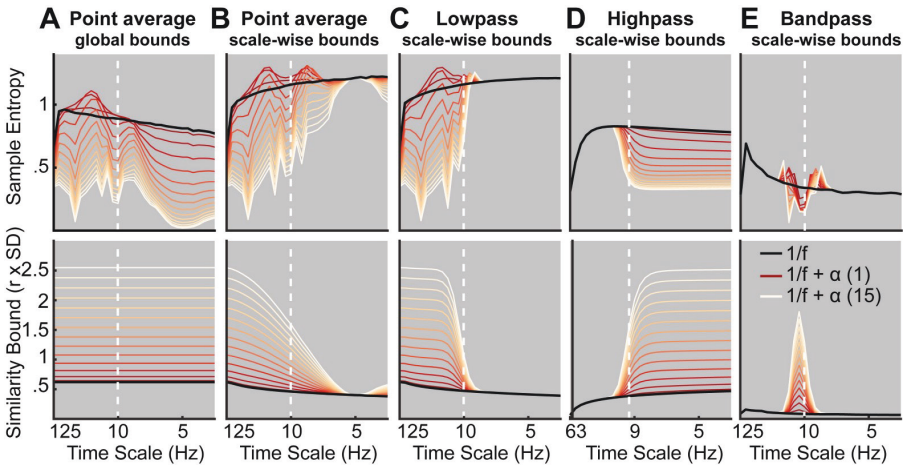

Fig 4. Rhythmic power manifests at different time scales depending on filter choice and similarity bound. Simulations indicate at which time scales the addition of varying magnitudes of stereotypic narrowband 10 Hz rhythms (red-to-white line color gradient) modulate entropy compared to the baseline 1/f signal (black line). Simulations indicate that increases in rhythmicity strongly reduce entropy estimates alongside increases in the similarity bound. The affected scales vary as a function of global vs. scale-dependent similarity bounds and the spectral filtering used to derive coarser time scales. Crucially, in 'Original' implementations, added narrowband rhythmicity decreased entropy with low scale-specificity, in line with global increases in the similarity bound (A). In contrast, the use of scale-varying thresholds (B) and dedicated filtering (C-E) increased specificity regarding the time scales at which rhythmicity was reflected. Note that timescales are presented in Hz to facilitate the visual assessment of rhythmic modulation. For all versions except high pass, the scale represents the upper Nyquist bound of the embedding dimension. For the high pass variant, the scale represents the high pass frequency (see *methods*). Time scales are log-scaled. Spectral attenuation properties of the Butterworth filters are shown in S4 Fig.

https://doi.org/10.1371/journal.pcbi.1007885.g004

mapping (Issue 1). Crucially, as a result of using a global similarity bound for all time scales, strong rhythmic power decreased MSE estimates across a range of time scales, including time scales at which added 10 Hz rhythmicity did not contribute to the scale-wise signal (Fig 4A, upper panel). As highlighted in Issue 1, this can be explained by a general increase in the liberality of bounds (Fig 4A, lower panel) that introduced a bias on coarse-scale entropy below 10 Hz. In contrast, when scale-dependent similarity bounds were used with low-pass filters (Fig 4B and 4C), strong rhythmicity systematically affected entropy only at finer time scales than the simulated frequency (i.e., to the left of the vertical line in Fig 4C, albeit in a diffuse manner, which we will examine next).

Second, we assessed the influence of the scale-wise filters (and hence, the spectral signal content) on frequency-to-scale mapping (see Issue 2, Fig 3B). In particular, we expected that low-pass filters (A-C) would lead to entropy decreases at finer time scales than the simulated frequency, whereas high-pass filters would lead to a rhythm representation at coarser time scales (Fig 3B). In line with these expectations, low-pass filters constrained the influence of narrowband rhythms to finer time scales (Fig 4C). As in previous work [33], Butterworth filters (Fig 4C) improved the removal of 10 Hz rhythms at coarser time scales and produced less aliasing compared with 'Original' point-averaging (see methods, Fig 4A and 4B), with otherwise comparable results. Hence, low-pass filters rendered multiscale entropy sensitive to variance from low frequencies, suggesting that slow events (e.g. event-related potentials) are reflected in a diffuse manner across time scales. In contrast, high-pass filters constrained rhythm-induced entropy decreases to coarser time scales that included 10 Hz signal content, hence leading to estimates of high frequency entropy that were independent of low frequency power (Fig 4D). Finally, when band-pass filters were used (Fig 4E), rhythmicity decreased

sample entropy at the target scales (despite producing edge artifacts surrounding the time scale of rhythmicity). In sum, these analyses highlight that rhythmic power increases will diffusely and non-specifically modulate MSE time scales as a function of the coarse-graining filter choice, unless a narrowband filter is applied.

Such diffuse reflection of rhythms across MSE time scales is at odds with previous simulations suggesting a rather constrained, linear mapping between the frequency of simulated rhythms and entropy time scales [4, 22, 44]. Furthermore, those studies indicated entropy *increases* with added rhythmicity, in contrast with the marked (and expected) decreases in entropy observed here. Crucially, increased entropy relative to baseline runs counter to the idea that the addition of a stereotypic pattern should decrease rather than increase pattern irregularity. To assess whether these seemingly divergent results can be reconciled, we repeated our simulation for different frequencies. We focused on a comparatively low level of rhythmicity (amplitude level = 2; SNR ~ 1.3 (see methods); S3 Fig displays exemplary time series), for which Fig 4A–4C suggested transient entropy increases above baseline. Similar to previous reports, we observed a positive association between simulated frequencies and peak entropy time scales (Fig 5) across implementations, such that rhythms of a given frequency increased entropy at slightly finer time scales (see increases in entropy above baseline to the left of the dotted vertical lines in Fig 5A–5C). However, as shown in Fig 4A–4C, such increases were counteracted when rhythmic strength increased, while global *similarity bounds* (Fig 5A) liberally biased, and thus decreased, entropy at coarser time scales (i.e., to the right of the dotted lines in Fig 5A) independent of rhythmic strength. While the mechanistic origin of entropy increases remains unclear, previous conclusions may thus have overemphasized the scale-specificity of rhythmic influences.

In sum, our simulations highlight that the choice of similarity bound and the signal's spectral content grossly affect one's ability to interpret MSE time scales. Our frequency-resolved simulations suggest that a previously argued direct frequency-to-scale mapping is not tenable when typical estimation procedures are used. Supplementing these narrowband contributions to MSE, we report results from simulations of varying spectral slopes in S2 Text and S7 Fig.

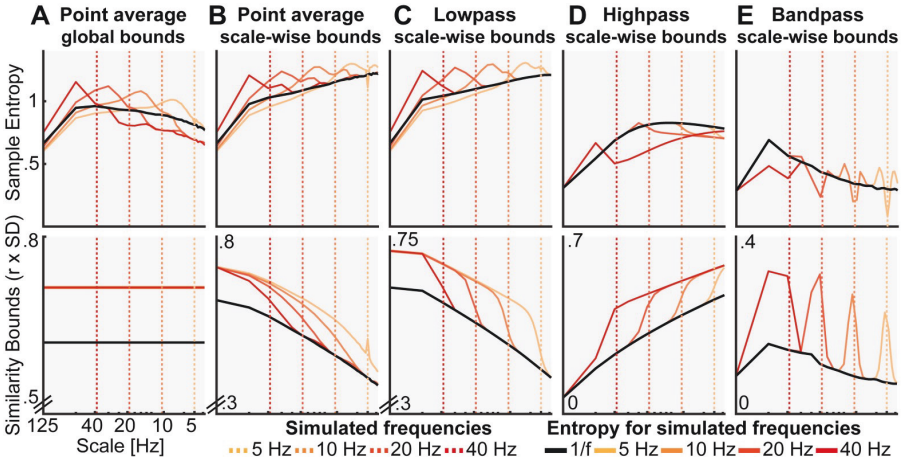

Fig 5. Influence of rhythmic frequency on MSE estimates and similarity bounds across different MSE variants. Simulations of different frequencies indicate a linear frequency-to-scale mapping of simulated sinusoids. Broken vertical lines indicate the simulated frequency. The original MSE variant (A) shows increased entropy at time scales finer than the simulated frequency in combination with a global entropy decrease. Low-, high- and band-pass variants exhibit the properties observed in the alpha case, with a reduction above (B, C), below (D) or at the simulated frequency (E). Time scales are log-scaled.

https://doi.org/10.1371/journal.pcbi.1007885.g005

Probing the impact of spectral power on MSE in a cross-sectional age comparison

Our simulations suggest profound influences of the choice of similarity bound (Issue 1) and spectral content (Issue 2) on scale-dependent MSE estimates. However, whether these issues affect inferences in empirical data remains unclear. Entropy differences across the lifespan are an important application [6], where 'Original' MSE implementations suggest that older adults exhibit higher entropy at finer time scales and lower entropy at coarser time scales compared to younger adults [for a review see 45]. Importantly, a shallowing of PSD slopes with age has also been reported, as represented by higher power at high frequencies and lower power at low frequencies [40, 49]. The raised issues of a potential (1) reflection of high frequency power on coarse scales and (2) diffuse reflection of slow spectral content thus question whether traditional MSE group differences reflect veridical differences in signal irregularity at matching time scales. Given those two issues, we specifically hypothesized that:

a. Adult age differences in coarse-scale MSE can be accounted for by group differences in high frequency power, due to the typical use of global similarity bounds (Issue 1).

b. Adult age differences in fine-scale MSE reflect differences in PSD slopes and thus depend on the contribution of low frequencies to broadband signals (Issue 2).

To assess these hypotheses, we first attempted to replicate previously reported scale-wise age differences in MSE and spectral power during eyes open rest. 'Original' settings replicated scale-dependent entropy age differences (Fig 6A1). Specifically, compared with younger adults, older adults exhibited lower entropy at coarse scales, and higher entropy at fine scales (Fig 6A1). Mirroring these results in spectral power, older adults had lower parieto-occipital alpha power and increased frontal high frequency power (Fig 6A2) compared to younger adults. This was globally associated with a shift from steeper to shallower PSD slopes with increasing age (Fig 6D). At face value, this suggests joint shifts of both power and entropy, in the same direction and at matching time scales. Crucially, however, the spatial topography of entropy differences inverted the time scale of power differences (Fig 6B and C; cf., upper and lower topographies), such that frontal high frequency power topographies resembled coarse entropy topographies (Fig 6B), while parieto-occipital age differences in slow frequency power resembled fine-scale entropy differences (Fig 6C). This rather suggests scale-mismatched associations between entropy and power.

Next, we assessed the impact of scale-wise similarity bounds and different scale-wise filters on the indication of MSE age differences (Fig 7).

Briefly, we observed three main results that deserve highlighting:

a. The implementation of scale-wise similarity bounds affected MSE age differences (Fig 7; Hypothesis A; Issue 1). In particular, with global bounds, MSE indicated increased fine-scale and decreased coarse-scale entropy for older compared to younger adults (Fig 7A1 and 7A2), in the absence of group differences in the global *similarity bound* (Fig 7A3 and 7A4). In contrast, scale-varying bounds captured age differences in variance at finer scales (Fig 7B) and abolished age differences in coarse-scale entropy (effect size was significantly reduced from r = .58 to r = .07; p = 6.8*10^-5; see Statistical analyses).

b. The chosen scale-wise filtering method also affected MSE age differences (Hypothesis B; Issue 2). Specifically, fine-scale entropy age differences were indicated when low-pass filters rendered those scales sensitive to low-frequency content (Fig 7B and 7C). Effect size did not significantly change with the adoption of scale-varying similarity bounds (from r = .44 to r = .45; p = .934). In contrast, when high-pass filters constrained fine scales to high

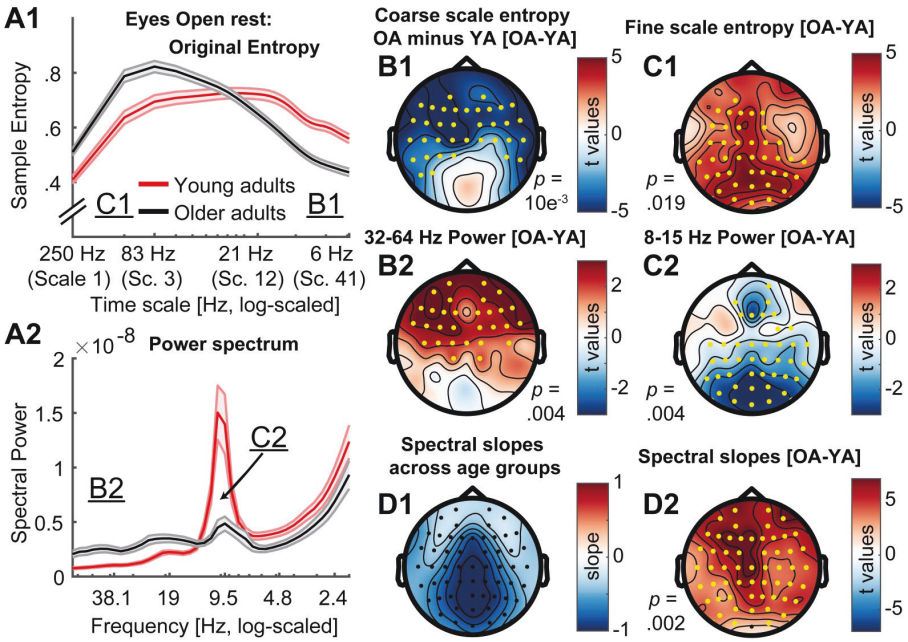

Fig 6. Timescale-dependent age differences in spectral power and entropy during eyes open rest. (A) MSE (A1) and power (A2) spectra for the two age groups. Error bars show standard errors of the mean. Note that in contrast to standard presentations of power, the log-scaled x-axis in A2 is sorted by decreasing frequency to enable a better visual comparison with entropy time scales (see also Fig 2D). Similarly, the x-axis in A1 has been log-scaled to allow easier visual comparison with log-scaled values in A2 and emphasize fine-scale differences (cf. Fig 7A1). Inset labels refer to the approximate time scales across which topographies are plotted in B & C. T-values of power age contrast are shown in S5 Fig. (B, C) Topographies of age differences indicate mirrored age differences in fast entropy and low frequency power, as well as coarse entropy and high frequency power. Significant differences are indicated by yellow dots. P-values correspond to the two/sided significance test of the cluster-level statistic. (D1) Spectral slopes across age groups. (D2) Age differences in spectral slopes.

https://doi.org/10.1371/journal.pcbi.1007885.g006

frequency signals (Fig 7D), no fine-scale age differences were observed and the age effect was significantly reduced to r = .09 (p = .008).

c. Strikingly, the implementation of narrowband filters (Fig 7E) indicated two unique age effects not recoverable using other approaches: larger 'narrowband' alpha-band entropy and lower beta-band entropy for older adults compared with younger adults.

In the following sections, we assess these results more closely.

Global similarity bounds bias coarse-scale entropy to reflect high-frequency power

Scale-dependent entropy effects in the face of global similarity bounds (as observed in the 'Original' implementation; Fig 7A) may intuitively suggest scale-specific variations in signal irregularity in the absence of variance differences. However, global similarity bounds increasingly diverge from the scale-wise signal variance towards coarser scales (Issue 1; Fig 8A). This introduces a liberal bias that systematically varies as a function of the removed variance, thereby rendering coarse MSE scales sensitive to differences in higher frequency power (i.e., Issue 1), as observed in the case of aging (Fig 8A and 8B).

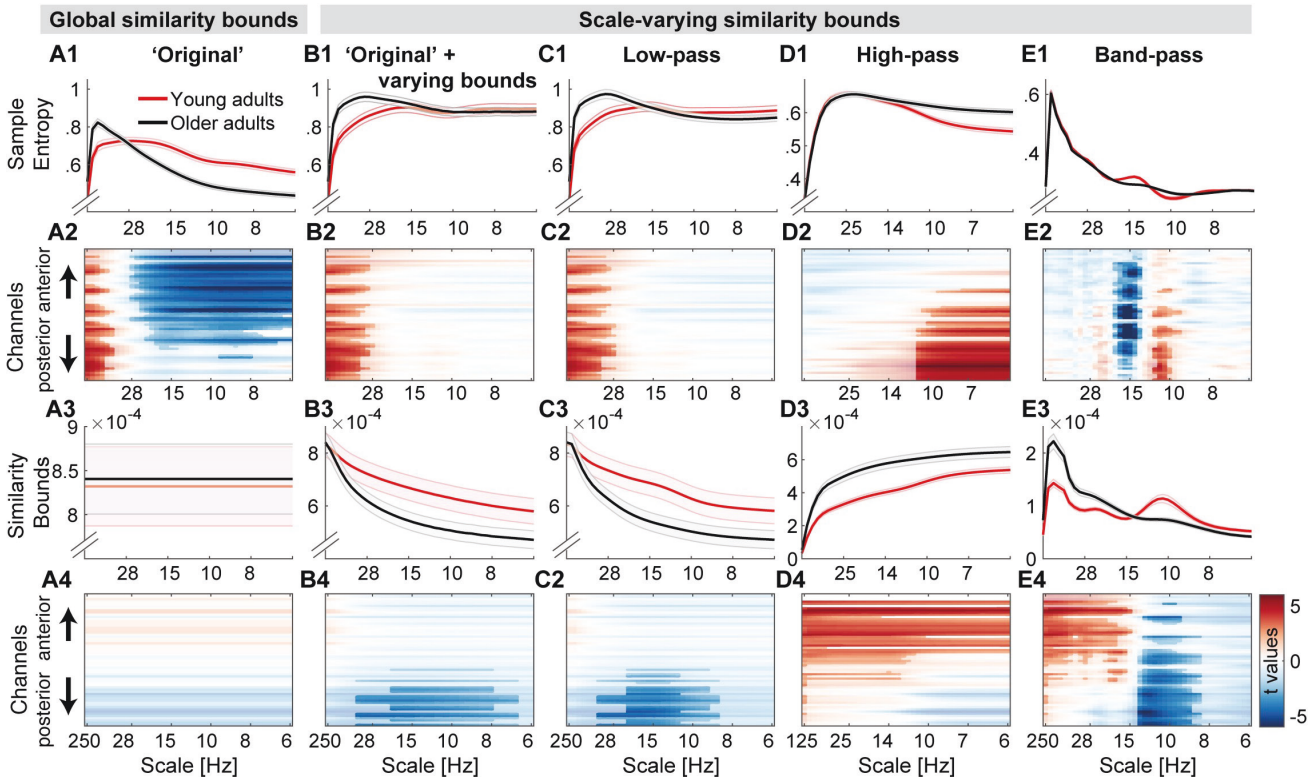

Fig 7. Multiscale entropy age differences depend on the specifics of the estimation method. Grand average traces of entropy (1st row) and similarity bounds (3rd row) alongside t-maps from statistical contrasts of age group differences (2nd + 4th row: younger minus older adults for entropy and bounds, respectively), shown by channel on the y-axis. Age differences were assessed by means of cluster-based permutation tests and are indicated via opacity. Original MSE (A) replicated reported scale-dependent age differences, with older adults exhibiting higher entropy at fine scales and lower entropy at coarse scales, compared with younger adults. The coarse-scale difference was exclusively observed when using global similarity bounds, whereas the fine-scale age difference was indicated with all low-pass versions (A, B, C), but not when signals were constrained to high-frequency or narrow-band ranges (D, E). In contrast, narrowband MSE indicated inverted age differences within the alpha and beta band (E).

https://doi.org/10.1371/journal.pcbi.1007885.g007

To assess whether global bounds introduced an association between high frequency power and coarse scale entropy in the case of aging, we probed changes in *similarity bounds* and MSE between the use of global and scale-varying bounds. As expected, we observed a strong anti-correlation between inter-individual changes in *similarity bounds* and MSE (Fig 8C). That is, the more similarity bounds were re-adjusted to match the scale-wise variance, the more entropy estimates increased. Crucially, this difference was more pronounced for older adults (paired t-test; r: p = 5e-6; MSE: p = 3e-4). Due to their increased high frequency power, coarse-graining decreased older adults' scale-wise variance more so than younger adults' variance. Thus, global similarity bounds presented a more liberal threshold at coarser scales for older adults than for younger adults, in turn producing lower MSE estimates. In line with this assumed link between high frequency power and coarse scale entropy as a function of global bounds, individual high frequency power at frontal channels was anticorrelated with coarse-scale entropy estimates when a global similarity bound was applied (Fig 8D), but was dramatically weaker when the similarity bound was recomputed for each scale (YA: r = -0.15; p = .302; OA: r = .20, p = .146). This is in line with our observation that coarse-scale age differences (Fig 7A) were not found when scale-wise bounds were used (Fig 7B).

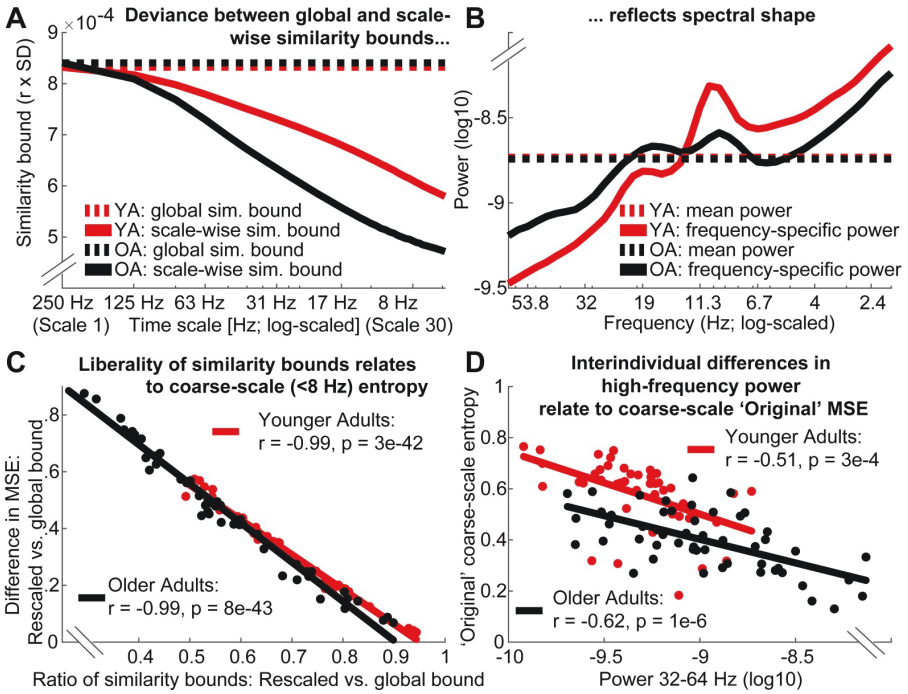

Fig 8. Divergence of scale-specific signal variance from global similarity bounds accounts for age differences in coarse-scale entropy. (A, B) A global similarity bound does not reflect the spectral shape, thus leading to disproportionally liberal criteria at coarse scales following the successive removal of high-frequency variance (see Fig 2C–2E for the schematic example). Scale-dependent variance is more quickly reduced in older compared to younger adults (A) due to the removal of more prevalent high-frequency variance in the older group (B). This leads to a differential bias across age groups, as reflected in the differentially mismatched distance between global and scale-dependent similarity bounds at coarser scales. (C) Removing this bias by adjusting the similarity bounds to the scale-dependent signal is associated with increases in coarse-scale entropy. This shift is more pronounced in older adults following the removal of a more prevalent bias. (D) With global similarity bounds, coarse-scale entropy strongly reflects high frequency power due to the proportionally more liberal similarity threshold associated. Low frequency power < 8 Hz was not consistently related to coarse-scale entropy (log10-power as in D; *YA*: $r = .12$; $p = .419$; *OA*: $r = .36$, $p = .009$). Data in A and B are global averages, data in C and D are averages from frontal 'Original' effect cluster (see Fig 7A) at entropy time scales below 8 Hz.

https://doi.org/10.1371/journal.pcbi.1007885.g008

Taken together, these results indicate that increased high frequency power with age can account for entropy decreases at coarse time scales, whereas the pattern irregularity of slow dynamics *per se* was not modulated by age.

Low-frequency contributions render fine-scale entropy a proxy measure of PSD slope

A common observation in the MSE literature is that MSE is highly sensitive to task and behavioral differences at fine time scales, which are assumed to reflect fast dynamics. This is surprising given that high-frequency activity remains challenging to measure [56]. Moreover, previous studies suggest that fine-scale entropy reflects power spectral density (PSD) slopes [e.g., 14, 40]. Given that 'Original' MSE implementations contain both high- and low-frequency components due to the assessment of broadband signals, we probed whether fine-scale associations with PSD slopes depend on the presence of slow fluctuations and whether age-related slope variations can account for fine-scale entropy age differences (Hypothesis B).

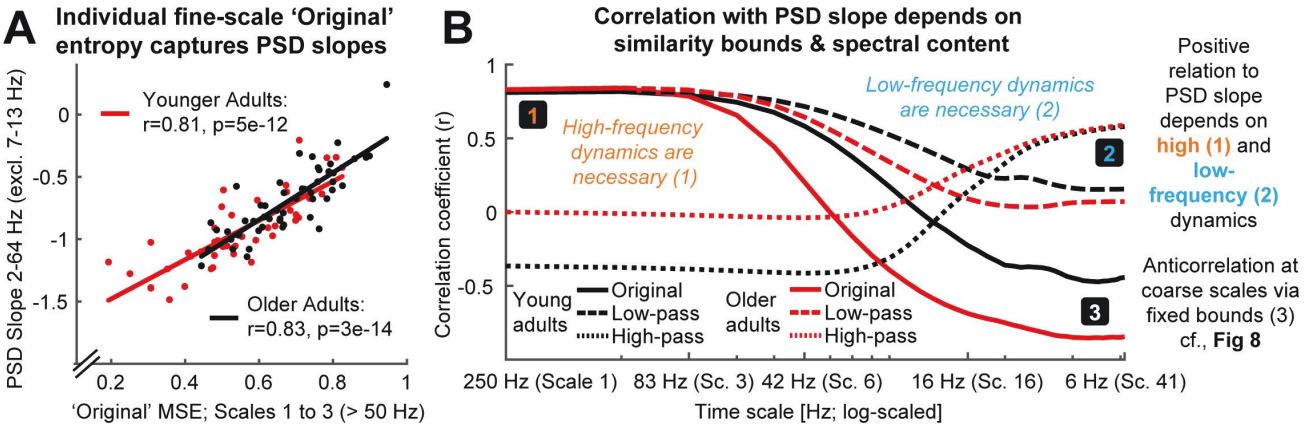

Fig 9. The presence of low- and high-frequency content renders fine entropy slopes sensitive to PSD slopes. A) Sample entropy at fine time scales represents the slope of power spectral density across age groups. The 7–13 Hz range was excluded prior to the PSD slope fit to exclude the rhythmic alpha peak (see Fig 8B). (B) The presence of both slow and fast dynamics is required for positive associations with PSD slopes to emerge. The direction and magnitude of correlations of scale-wise entropy with PSD slopes depends on the choice of global vs. rescaled similarity bounds, as well as the choice of filtering. Original entropy inverts from a positive correlation with PSD slope at fine scales to a negative association at coarse scales. Rescaling of the similarity bound abolishes the negative correlation of coarse-scale entropy with PSD slopes. S6 Fig presents scatter plots of these relationships. The x-axis indicates the upper frequency bounds for the low-pass version.

https://doi.org/10.1371/journal.pcbi.1007885.g009

As expected, individual fine-scale entropy was strongly and positively related to PSD slopes (Fig 9A) in both younger and older adults. Notably, after high-pass filtering the signal, the positive relation of fine-scale entropy to PSD slopes disappeared in both age groups (Fig 9B, dotted lines), and turned negative in older adults (see S6 Fig for scatter plots), while age differences in fine-scale entropy disappeared (Fig 7D). Relations between entropy and PSD slopes–and age differences–re-emerged once low-frequency content was included in the entropy estimation (Fig 9B, dashed and dotted lines), indicating that the presence of slow fluctuations was necessary for PSD slope relations. To assess whether varying PSD slopes accounted for fine-scale age differences in 'Original' MSE, we computed partial correlations between the measures. No significant prediction of age group status by fine-scale entropy was observed when controlling for the high collinearity with PSD slopes ($r = -.04$, $p = .69$), whereas PSD slopes significantly predicted age group status when controlling for fine-scale entropy ($r = .37$, $p = 2e\text{-}4$).

Finally, spectral slopes were anticorrelated with coarse-scale entropy when global similarity bounds were used (Fig 9B, solid lines), but not when criteria were scale-wise re-estimated (Fig 9B, dashed and dotted lines). This again suggests a presence of the scale-wise bias noted in Issue 1 (i.e., scale-wise bound divergence); subjects with shallower slopes (more high frequency power) had increasingly liberally-biased thresholds at coarser scales, resulting in overly low entropy estimates.

In sum, age differences in fine-scale entropy were conditional on the presence of both low- and high-frequency dynamics and reflected differences in PSD slopes; while the pattern irregularity of fast dynamics *per se* was not modulated by age.

Narrowband MSE indicates age differences in signal irregularity in alpha and beta band

The previous analyses highlighted how the spectral content of the signal can give rise to MSE time scale mismatches. However, our simulations also suggest a far more accurate mapping between entropy and power when scale-wise bandpass filters are used (Fig 4E). Concurrently, application of the band-pass implementation indicates a partial decoupling between entropy

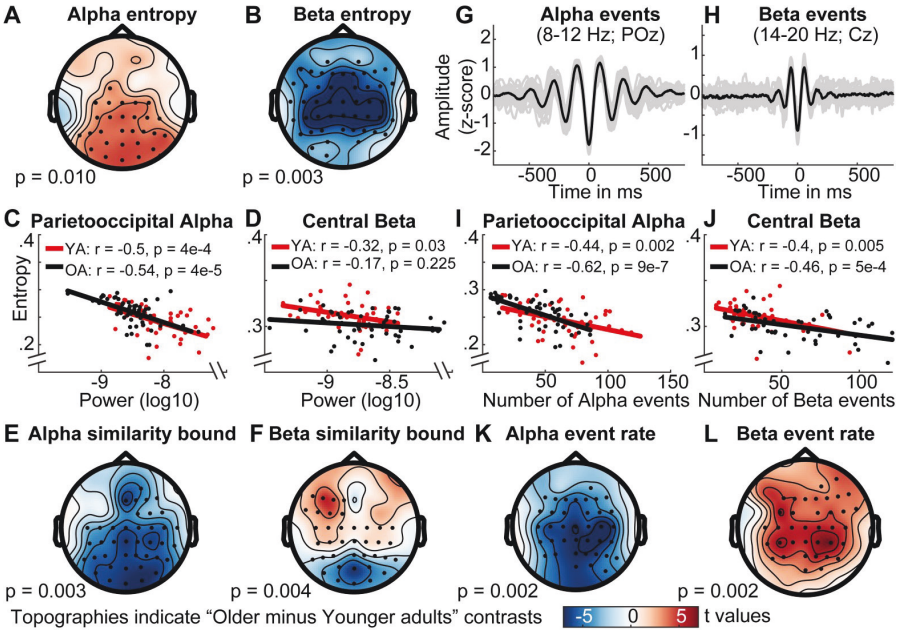

Fig 10. Narrowband MSE reflects age differences in alpha- and beta-specific event (ir)regularity. (A, B) Narrowband MSE indicates age differences in the pattern complexity at alpha (A) and beta (B) frequencies. (C, D) Alpha, but not beta power consistently correlates negatively with individual narrowband entropy within clusters of age differences. (E, F) Similarly, alpha but not beta similarity bounds show an inverted age effect with similar topography. (G, H) Single-trial rhythm detection highlights a more transient appearance of beta compared with alpha events. Data are collapsed across age groups. (I, J) The rate of stereotypical single-trial alpha and beta events is anticorrelated with individual narrowband entropy. (K, L) The rate of spectral events exhibits age differences that mirror those observed for entropy. Note that the same color range, plotted in the lower row, was plotted for all topographies.

https://doi.org/10.1371/journal.pcbi.1007885.g010

and variance (as reflected in the *similarity bound*) age differences (Fig 7E). Specifically, older adults exhibited higher parieto-occipital entropy at alpha time scales (˜8–12 Hz) and lower central entropy at beta time scales (˜12–20 Hz) than younger adults (Fig 7; Fig 10A and 10B). Whereas alpha-band entropy was moderately and inversely correlated with alpha power (Fig 10C) and the age difference was inversely reflected in the similarity bound in a topographically similar fashion (Fig 10E), the same was not observed for entropy in the beta range for both age groups (Fig 10D and 10F). Promisingly, this indicates evidence for what many who employ MSE measures in cognitive neuroscience presume–that power and entropy *can* be decoupled, providing complementary signatures of neural dynamics.

This divergence of entropy and power in the beta band is particularly interesting as beta events have been observed to exhibit a more transient waveform shape [57, 58], while occupying a lower total duration during rest than alpha rhythms [42]. Indeed, it should be the rate of stereotypic spectral events that reduces pattern irregularity rather than the overall power within a frequency band. To better test this assumption in our data, we applied single-trial rhythm detection to extract the individual rate of alpha (8–12 Hz) and beta (14–20 Hz) events. As predicted, alpha events had a more sustained appearance compared with beta events as shown in Fig 10G and 10H (events were time-locked to the trough of individual events; see methods). Importantly, both alpha and beta event rate were inversely and moderately correlated with entropy estimates (Fig 10I and 10J) at matching time scales in the band-pass version. Correlations were also numerically higher than between power and entropy (Fig 10C and

10D), suggesting that entropy captured the non-stationary character of the rhythmic episodes that are not captured by sustained power estimates. The relationships remained stable after controlling for individual event rate and entropy in the age effect cluster of the other frequency band (partial correlations: alpha for younger adults: r = -.52, p = 2e-4; alpha for older adults: r = -.71, p = 8e-9; beta for younger adults r = -.49, p = 6e-4; beta for older adults: r = -.56, p = 2e-5), indicating separable associations between event rate and entropy between the two frequency bands. This is important, as our simulations suggest increased entropy estimates around narrow-band filtered rhythmicity (see Fig 4E). Furthermore, a permutation test indicated age differences in beta rate that were opposite in sign to the entropy age difference (see Fig 10L). In particular, older adults had a higher number of central beta events during the resting state compared with younger adults, thus rendering their beta-band dynamics more stereotypic. In sum, these results suggest that narrowband MSE estimates approximate the irregularity of non-stationary spectral events at matching time scales.

Rhythmic alpha events transiently reduce broadband signal irregularity

Finally, the neurobiological relation between narrowband rhythms and broadband signal characteristics (spectral slopes in particular; Fig 9) is a substantive question of considerable interest [59–61]. Rhythmic alpha events have been theorized to phasically modulate cortical excitability, with higher amplitudes of alpha events thought to reflect an overall reduction in population activity due to reduced excitability [55]. Such activation levels in turn have been related to scale-free broadband characteristics in human electrophysiological data [38, 51–54], which strongly contribute to fine-scale entropy estimates (Fig 9; S7 Fig). It is thus conceivable that alpha rhythms transiently reduce broadband irregularity. In line with this notion, negative associations between alpha power and fine-scale entropy have been observed [40, 62]. However, sample entropy's joint sensitivity to broad- and narrowband dynamics ("Issue 2") (see Fig 4) makes it ambiguous whether such associations truly reflect shifts in broadband features. We confirm this ambiguity in simulations (Fig 11A; sample entropy calculated for 250 ms signals consisting of varying slope coefficients in the presence or absence of alpha rhythms), where we observe that increased rhythmic regularity during alpha events concurrently decreases sample entropy, even when no change has occurred in the aperiodic signal component (Fig 11A: red panels). Controlling the spectral signal content via band-stop filters (here: 8–15 Hz) removes such circular entropy decreases due to increased narrowband regularity in the alpha band, while accurately indicating entropy changes due to changes in spectral slopes (Fig 11: green panels).

We used fine-scale sample entropy's sensitivity to aperiodic slopes determined above (Fig 9; S7 Fig) to probe the relationship between broadband irregularity and rhythmic alpha events with high temporal precision in empirical data. To test transient modulations of irregularity during alpha rhythms, we leveraged the temporal on- and offsets of individual alpha segments (8–15 Hz; $>$ 3 cycles) during eyes-open rest as uniquely identified by rhythm detection (see Fig 11B; see S8 Fig for exemplary traces). We created 250 ms segments surrounding the on- and offsets of alpha activity, followed by the calculation of sample entropy. To investigate potential differences as a function of magnitude, we median-split high- and low-amplitude alpha events. For both splits, we observed that sample entropy decreased upon alpha onset, whereas it recovered to high levels following alpha offset (Fig 11C1 and 11D1; red panels). However, due to the aforementioned circularity, the observation of transient entropy decreases during alpha periods offers little unambiguous insight beyond the successful identification of rhythmic event on- and offsets by the eBOSC algorithm. Importantly, transient entropy decreases during high-amplitude alpha events were also observed after removal of the alpha

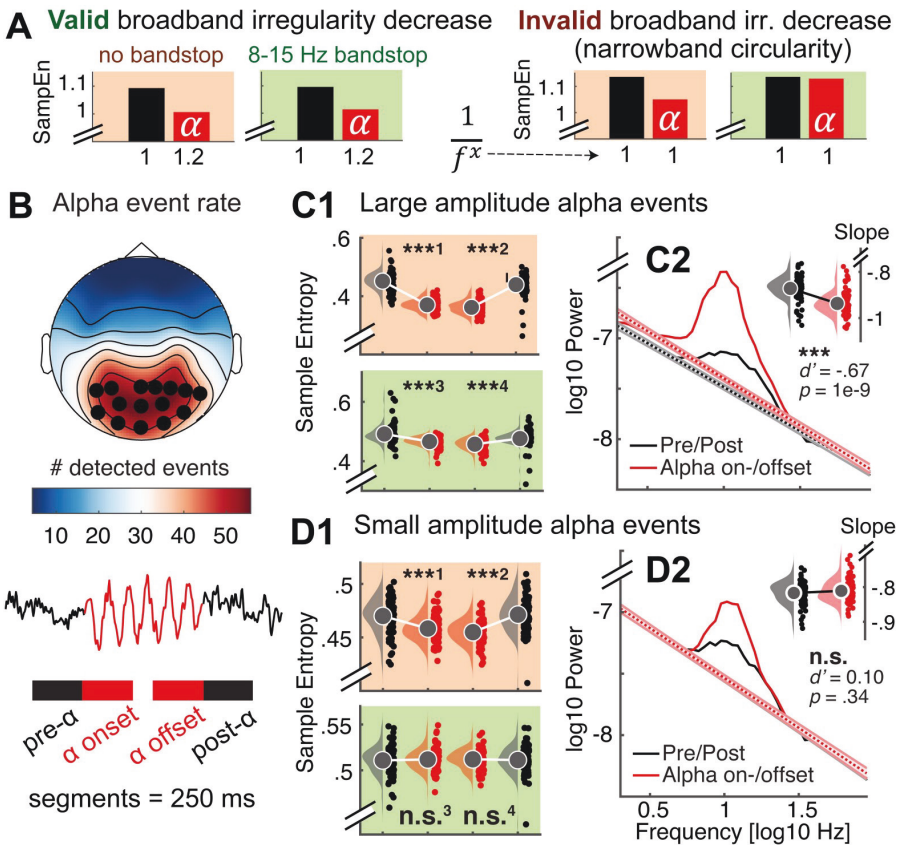

Fig 11. Nonstationary alpha events transiently reduce broadband irregularity. (**A**) Testing for transient broadband changes during alpha events requires control for narrowband circularity. We simulated 250 ms signals consisting of varying slope coefficients (plotted on the x-axis) in the presence or absence of alpha rhythms. Bars indicate first-scale entropy estimates (i.e., sample entropy; SampEn) for these signals, as well as bandstop-filtered versions. Left: Valid slope shallowing in the presence of alpha events was indicated both when alpha was included in estimates (red background), as well as when band-stop filters removed the influence of alpha regularity (green background). Right: Crucially, when no bandstop filters were applied, sample entropy decreased also in the absence of slope variations due to the added alpha regularity (red background). This effectively represents narrowband circularity in the analysis. In contrast, bandstop filters removed the influence of alpha regularity and permitted estimation of valid reductions in broadband irregularity (green background). (**B, C, D**) Empirical analysis of transient entropy decreases during alpha events. (B Alpha events were selected across channels with high amounts of detected events (black dots). Lower: Broadband entropy was calculated for 250 ms segments preceding and following the on- and offset of alpha events. (**C1**) During eyes open rest, nonstationary alpha events of high strength transiently reduce broadband irregularity, also after accounting for alpha circularity. Raincloud plots (RCPs) indicate the intervals schematically plotted in the bottom panel of B. For visualization, RCPs display estimates that are centered within-subject (condition-wise data minus individual across-condition average plus global average); statistics were calculated on uncentered estimates. ^{***1}: d' = -1.91; $p \sim 0$. ^{***2}: d' = -1.61; p ~ 0. ^{***3}: d' = -0.63; p = 1e-8. ^{***4} d' = -0.54; p = 6e-7 [d' = $(\bar{X}_{alpha} - \bar{X}_{pre/post})$/STD($X_{alpha}$-$X_{pre/post}$)]. (**C2**) Slope fits indicate a shallowing of slopes during alpha events. The inset bar plot indicates mean slopes estimates with within-subject standard errors. (**D1**) In contrast, irregularity decreases were indicated for low-amplitude alpha events only when circularity was not accounted for, but not after alpha was removed. This indicates that bandstop filtering successfully avoids circularity in empirical use cases. ^{***1}: d' = -0.52; p = 1e-6. ^{***2}: d' = -0.75; p = 3e-11. n.s.^{3}: d' = -0.05; p = 0.63. n.s.^{4} d' = -0.04; p = 0.67. (**D2**) No significant slope changes were observed during low-amplitude alpha events. Note that black dotted line is covered here. Error bars reflect within-subject standard errors.

https://doi.org/10.1371/journal.pcbi.1007885.g011

band (Fig 11C1; green panel), indicating that narrowband amplitude increases in the alpha-band were not sufficient to explain the observed entropy differences. This provides evidence that spontaneous, large-amplitude alpha rhythms during eyes open rest transiently decrease broadband signal irregularity, supporting their suggested role in the modulation of cortical excitability. We did not observe an interaction between alpha status and age for any of the contrasts (all $p > .05$), suggesting that decreased irregularity during transient alpha events is a preserved characteristic of cortical alpha rhythms across the adult lifespan. To further investigate a broadband effect, we calculated spectral slopes (using an auto-sandwiching approach, see methods). This analysis revealed a transient steepening of slopes during alpha events, in line with a broadband shift towards decreased excitability (Fig 11C2). In contrast to high-amplitude events, entropy decreases were not indicated for low-amplitude events after accounting for circularity bias (Fig 11D1, green panel). Similarly, no shift in aperiodic slopes was observed (Fig 11D2). This suggests that the originally indicated entropy decreases during low-amplitude events do not represent broadband shifts. This analysis highlights sample entropy's potential to indicate fluctuations in signal irregularity with high temporal precision. Notably, the analysis reinforces the need for a targeted modulation of spectral content to avoid circular inferences, and reduce the ambiguity of results. Our findings suggest an alternative use case for dedicated bandpass filters that retains high sensitivity to broadband effects of interest. Specifically, the mechanistically informed use of band-stop filters here affords analyses into the modulators of signal irregularity and thereby can reveal non-trivial neurocomputational/-biological insights.

Discussion

MSE aims to characterize the temporal irregularity of (neural) time series at multiple temporal scales. In the present study, we have highlighted two primary issues that may render the interpretation of time scales unintuitive in traditional applications: (Issue 1) biases from global similarity bounds, and; (Issue 2) the characterization of broadband, low-frequency dominated signals (see Fig 12A for a schematic summary). In the following, we discuss these effects and how they can impact traditional inferences regarding signal irregularity, in particular with regard to empirical age differences. Then, we discuss age effects in narrowband signal irregularity at interpretable temporal scales. Finally, we recommend procedures to improve scale-specific MSE inferences.

Issue 1: Global similarity bounds bias coarse-scale entropy estimates

The ability to estimate entropy at coarser time scales provides the main motivation for a multi-scale implementation. Towards coarser scales, entropy is generally thought to represent the irregularity of increasingly slow dynamics. However, MSE's traditionally global similarity bounds systematically bias coarse scale entropy estimates. Given that scale-wise variance decreases across scales, the liberality of global similarity bounds increases, causing entropy to decrease despite no ostensible shift in pattern irregularity. This bias is independent of the values of the global similarity bound–which did not differ across groups here–but rather depends on the *removed* variance at the time scale of interest. This issue has led to puzzling results in past work. For example, several papers using 'original' MSE have shown that in white noise signals (which by definition should be equally irregular at all time scales due to their randomness), entropy unintuitively decreases towards coarser scales, whereas pink noise signals undergo less entropy reduction across initial scales due to the removal of less high-frequency content [29] (S7 Fig). Strikingly, such puzzling effects have been used to *validate* the most common implementation of MSE [e.g., 27, 32] rather than to indicate the presence of a

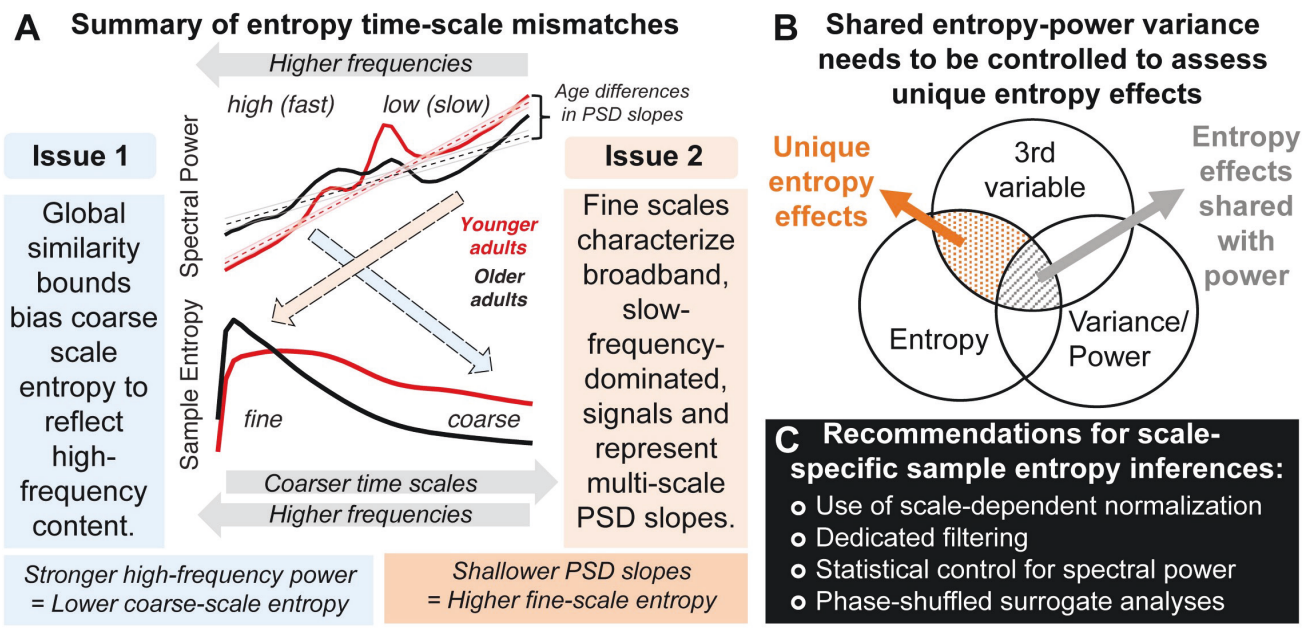

Fig 12. Summary of the identified time-scale mismatches and recommendations for future studies. (**A**) We highlight two scale-dependent mismatches that run counter to the intuition that entropy at fine scales primarily refers to fast dynamics, and vice-versa: (1) Coarse-scale entropy is biased towards reflecting high-frequency content when signals of decreasing variance are compared to a global, and increasingly inadequate, similarity bound. (2) Fine-scale entropy characterizes scale-free 1/f slopes when broadband signals include slow frequency content. Dashed colored arrows indicate the mismatched relations observed in the current study. (**B**) Beyond time-scale mismatches, brain signal entropy and variance/power can often be collinear, in part due to their shared description of linear signal characteristics, such as rhythmicity. To identify complementary and unique relations of pattern complexity compared to more established measures of variance, explicit statistical control is required for the latter. (**C**) We propose multiple strategies to safeguard future applications against the highlighted issues.

https://doi.org/10.1371/journal.pcbi.1007885.g012

systematic bias in estimation. This appears motivated by the assumption that "changes of the variance due to the coarse-graining procedure are related to the temporal structure of the original time series, and should be accounted for by the entropy measure" [12]. We rather consider the similarity bound divergence a clear bias that invalidates the intuitive interpretation of time scales in MSE applications, and highlight that more intuitive broad-scale offsets are indicated when bound biases are removed (see S2 Text for elaboration on this issue).

Importantly, we highlight that this bias affects practical inferences. In the current resting-state EEG data, an age-related increase in high frequency power manifested unintuitively as a decrease in coarse-scale entropy via systematic group differences in the divergence of similarity bounds. Note that we presume that this age difference arises from a relative bias. As such, variations in high-frequency power suffice, even at low levels in 1/f scenarios, to systematically impact coarse-scale estimates and to specifically explain variance in a third variable of interest (e.g., age; see Fig 12B). Given that global similarity bounds remain prevalent in applications (see S1 Text), we hope that our practical example motivates the adoption of scale-varying parameters. Overall, we perceive little justification for the use of scale-invariant parameters in MSE estimation in future work. Indeed, as most previous work included biased, global bounds, reported coarse-scale effects may dominantly reflect false positives, while the sensitivity to true coarse-scale effects may have suffered, hence jointly increasing false negatives. Hence, results obtained with global bounds are ambiguous and hard to interpret. A critical task for future work (potentially including the re-analysis of existing data) will thus be to establish specific coarse-scale effects that provide empirical evidence for the practical utility of a multi-scale

entropy computation. Recent advances for the robust estimation of coarse-scale entropy from sparse neuroimaging data [34, 63, 64] may be required to better estimate coarse-scale effects in *in vivo* data.

Issue 2: Fine-scale entropy relates to PSD slopes in the presence of slow frequency content

In parallel to the assumption of dominantly slow signal contributions to coarser scales, fine-scale entropy is often interpreted as a signature of "fast" temporal irregularity. However, it is typically estimated from broadband signals. As such, slow trends [35], neural rhythms at characteristic time scales [65] (Fig 4) and scale-free 'background' or 'noise' activity with a $\frac{1}{f^x}$ power-law form [38, 50, 53] (Fig 9; S7 Fig) jointly contribute to fine-scale entropy estimates. By linking fine-scale entropy to broadband PSD slopes, we replicated previous observations of increasing sample entropy with shallower slopes [14, 17, 29, 40, 46, 66] and shorter temporal autocorrelations [4, 27, 67]. However, we qualify this association by highlighting that the *joint* presence of slow and fast dynamics in the signal is necessary to produce such effects, hence verifying a broadband origin. At a mechanistic level, differences in spectral slopes and fine-scale entropy may jointly index variations in cortical excitability. Cortical neurons constantly receive a barrage of synaptic inputs. Variations in the excitatory and inhibitory summary statistics of these inputs robustly alter the conductance state of membrane potentials [for a review see 68], thereby producing variations in the irregularity of spike output and the appearance of global EEG signals [for a review see 69]. Whereas excitability is reduced during synchronized states characterized by strong low-frequency fluctuations, "desynchronized" cortical states feature enhanced sensitivity to external stimuli [70–72]. From a functional perspective, cortical information capacity, approximated via the entropy of cortical activity, may non-linearly vary alongside such excitation/inhibition (E/I) ratio, with highest information capacity afforded at intermediate levels of systemic excitability [10]. From a technical perspective, spectral (PSD) slopes have been proposed as a functional index of such an E/I ratio [49, 54, 73–75]. However, frequency-dependent filtering of current flow in the extracellular medium [76] or at the dendrite [77] may also contribute to the observed inter-individual differences in spectral slopes.

More generally, the association between broadband signal entropy and spectral slopes coheres with the notion that shallower slopes have a more 'noisy' or irregular appearance in the time domain. Thus, spectral slopes and temporal predictability are–at least in part–different perspectives on the same signal characteristic. Practically however, the correspondence between fine-scale entropy and 1/f slopes should nonetheless be tested, given that these scales are also sensitive to other signals characteristics, such as narrowband rhythmicity (Fig 4). Such necessity for narrowband control is highlighted by our analysis of transient fine-scale entropy changes during non-stationary alpha events (Fig 11). Only the removal of narrowband rhythmic regularity afforded non-circular insights. Specifically, we observed that broadband entropy transiently reduces following the onset and prior to the offset of parieto-occipital alpha rhythms, alongside a steepening of spectral slopes. This result is in line with alpha rhythms reflecting synchronized states with reduced cortical excitability [55, 59, 60, 78–81], but extends prior applications by characterizing non-stationary events at the single-trial level with high temporal precision, rather than temporal averages. Notably, our results contradict a prior observation that increased spontaneous alpha amplitudes at rest relate to a shallowing of low-frequency slopes, both in time and space [61]. Whether differences in frequency range, temporal specificity, or the stability of slope estimates contribute to this difference is an interesting question for future research that sample entropy may help to resolve. Notably, the fine-scale sensitivity of this effect highlights that single-scale broadband (sample) entropy–in the absence

of multiscale implementations–is *per se* sensitive to broadband effects of interest, benefitting applications with limited available data and time [e.g., closed-loop setups: 62].

Spectral power and entropy: What's irregularity got to do with it?

For entropy to be a practical and non-redundant measure in cognitive neuroscience, both its convergent and discriminant validity to known signal characteristics should be established. Multiple features can influence the temporal irregularity of neural time series. These include traditional 'linear' PSD features, (e.g., temporal autocorrelation, rhythmicity, etc.) as well as 'non-linear' features (e.g., phase resets, cross-frequency coupling, etc.). It is therefore worth noting that associations between spectral power characteristics and entropy estimates are partly anticipated (Fig 12B). For example, as noted before, entropy should reduce with increased rhythmic irregularity, and increase with shallowing of PSD slopes (and hence, shortening of temporal autocorrelations). However, the use of MSE is often motivated by its partial sensitivity to non-linear properties of brain dynamics [27, 46] that cannot be captured by traditional PSD analyses [e.g., 82, 83, 84]. In extreme cases, the absence of linear contributions may be erroneously inferred from the use of variance-based similarity bounds. Contrary to such orthogonality assumptions, our analyses highlight that differences in spectral variance (as captured by the similarity bound, which is typically neglected as a measure of interest when estimating MSE) *can* account for a large proportion of reported MSE effects [see also appendix in 27]. As such, non-linear characteristics *per se* may often do little to drive MSE estimates (see also results from a surrogate analysis in S3 Text, S9 Fig). This is in line with dominant linear power contributions to non-linear measures [85]. Conversely, the specificity to valid and unique non-linear effects increases after methodologically accounting for linear contributions.

Relevance of identified time scale mismatches to previous work

Although the highlighted issues broadly apply to applications in which MSE is a measure of interest (e.g., assessment of clinical outcomes [e.g., 22]; prediction of cognitive performance [e.g., 46]), our results are especially relevant for MSE differences across the lifespan. Previous applications indicated that older adults exhibit lower coarse-scale entropy and higher fine-scale entropy compared with younger adults [16, 18, 27, 86]. While we conceptually replicate these results with the standard MSE implementation, our analyses question the validity of previous interpretations. In particular, our results suggest that age-related increases in coarse-scale entropy do not reflect valid differences in the irregularity of slow dynamics, but rather reflect differential high frequency power biases [see also 19]. Moreover, our analyses ascribe age differences in fine-scale irregularity to a flattening of PSD slopes, as observed from child- to adulthood [46] and towards old age [16, 18, 40, 49]. Such shallowing of scale-free slopes suggests relative shifts from distributed to local processing, and coheres with the notion of increased "neural noise" due to increases in the local excitation/inhibition ratio [54].

Across development, altered time scales of neural computations (as indicated by broadband changes in autocorrelations) [87] may reflect changes in intra- and inter-cortical connectivity [88], arising from reductions in grey matter density [89, 90], the integrity of associative white matter tracts [91], and changes in local receptor distributions and neuromodulation [92–96]. Dynamic interactions between such morphological changes may jointly shape control over local excitability and 'neural noise' across the lifespan [97]. Two alternative functional consequences of developmental noise increases have been proposed. On the one hand, intermediate levels of noise may provide beneficial stochastic resonance effects [9, 98–100], in line with relations between higher entropy and behavioral benefits in child- and adulthood [46], as well as in older adults [86]. In contrast, overwhelming amounts of local noise can produce adverse

consequences [49, 101], supported by the observation that shallower slopes with advanced adult age relate to impaired working memory performance [49]. While further work including longitudinal assessments and behavioral probes will be necessary to disentangle the functional relevance of developmental changes, we argue that a principled separation of narrow- and broadband changes [102] will help to guide the search for neurobiological mechanisms driving entropy effects.

Taken together, our results suggest that entropy age differences dominantly arise from linear power differences, and appear at counterintuitive time scales. We confirmed the dominant contribution of age group differences in power characteristics using a surrogate analysis (see S3 Text, S9 Fig). Our surrogate analysis replicates a previous surrogate analysis that attributed age group differences mainly to linear auto-correlative properties [see appendix in 27, see also 85]. As we exclusively focused on univariate entropy, it remains an interesting question for future work whether our results are applicable to age-related decreases in 'distributed' entropy that capture the mutual information between distinct sensors [16].

Cross-sectional age differences in narrowband MSE

Complementing traditional broadband applications, our use of narrowband MSE suggested age-related entropy increases in the posterior-occipital alpha band and decreases in central beta entropy that inversely tracked the regularity of alpha and beta events, respectively. Posterior-occipital decreases in alpha power and frequency with age are fundamental findings in many age-comparative studies [103]. While age-related increases in beta power are not observed as consistently [see e.g., 103 for a review], age-related increases in their prevalence have been observed during eyes open rest [104]. In addition, beta power increases over contralateral motor cortex during rest may reflect greater GABAergic inhibition in healthy aging [105]. While our results are not hemisphere-specific, they may similarly reflect increased inhibition in older adults, potentially reflected in an increased number of stereotypical beta events [58]. However, further work is required to establish the functional interpretation of narrowband age differences, as well as technical impacts of filter bandwidth, and individual center frequencies on narrowband results, especially given age differences in rhythmic peak frequencies [103]. Nevertheless, these results highlight that scale-specific narrowband filtering can provide novel, frequency-specific, insights into event/signal irregularity.

Notably, a narrowband approach may warrant different use cases than broadband entropy. In particular, the sensitivity to multi-scale information, such as cross-frequency interactions and waveform shape, is a defining characteristic of (and motivation for using) entropy as opposed to spectral analysis. However, this sensitivity trades off with specificity when a narrowband approach is chosen, which by definition enforces a more rhythmic appearance than the raw signal may convey [106]. Nonetheless, frequency-specific phenomena such as variations in the amplitude or the presence of rhythmic events are complementary signatures of irregularity in their own right. For example, long-range temporal correlations (LRTCs) of narrowband amplitudes provide an alternative window on the irregularity of temporal dynamics [107–109]. As such, targeted filter applications–either chosen *a priori* or as a follow-up to broadband entropy effects–may prove useful to delineate spectrally specific effects at directly interpretable neural time scales. Hence, we do not regard narrowband MSE as a replacement for the traditional low-pass implementation of MSE, but rather as a parallel tool for the exploration and probing of broadband effects. Moreover, sensitivity to broad-scale phenomena remains high when band-stop filters are used (e.g., Fig 11), highlighting the general feasibility of applying narrowband filters to derive broadband insights beyond the band-stop range.

Recommendations for future applications

The issues raised here suggest that additional steps need to be taken to achieve valid scale-wise estimates of MSE, and to support the perceived complementary nature of MSE relative to more typical measures (such as spectral power, etc.). We are optimistic that the following recommendations Fig 12C, which have already been partially proposed [33–35, 63, 110], improve the utility of MSE as a principled tool for the estimation of complex brain dynamics.

a. We see little motivation for the use of global similarity bounds as they introduce challenges rather than benefits. We therefore recommend the MSE field to abandon *global* similarity bounds in favor of scale-specific bounds. We hope that our showcase of their detrimental consequences contributes to the wide-scale adoption of 'refined' approaches [e.g., 33, 34, 110], which we consider the minimum requirement for novel neurocomputational insights.

b. We recommend spectral filters to validate the scale-specificity and/or broadband nature of effects. For example, if effects are observed at fine temporal scales with a low-pass filter, additional high-pass filters may inform about the spectral extent of the effect. For entropy estimates of slow dynamics, traditional low-pass filter settings already apply this principle by becoming increasingly specific to slow fluctuations (if scale-dependent normalization is used)–but crucially, specify to high-frequency content is never attained. This proposal represents a general extension of proposed solutions based on high-pass filtering to remove slow trends [35], or based on incorporating slow temporal correlations into parametric models for the MSE estimation [34, 63].

c. We regard statistical control as necessary to establish entropy effects that are not capturable by traditional linear indices (such as PSD characteristics). While some studies have shown joint effects of interest in MSE and (band-limited) spectral power [15, 16, 18, 19, 111–117], others identified unique MSE effects [22, 118–120]. However, the (mis)match between time-scales and frequencies may not always be readily apparent, at least in part due to the various issues raised here. As shown here, controls should include both narrowband ('rhythmic') power and the arrhythmic signal background. As the scale-wise *similarity bound* is used for normalization, it should at the very least be controlled for. The choice of features may further be aided by comparing effect topographies of spectral power and entropy, as done in the present study. An important point to note is the relevance of statistical controls for relations to third variables (see Fig 12B). While some studies highlight scale-dependent associations of entropy with power, a large amount of shared variance (e.g., of coarse-scale entropy with slow frequency power) does not guarantee that a smaller portion of residual variance (e.g., shared with normalization biases) systematically does or does not relate to other effects of interest. This is equally relevant for identifying unique non-linear contributions. For example, while we observed moderate associations between band-specific rhythm events and entropy here, this non-redundant association nevertheless leaves room for the two measures to diverge in relation to third variables. This is in line with prior work [27, 121] showing that despite a dominant influence of linear characteristics on entropy estimates, non-linear contributions can uniquely explain a (smaller) portion of entropy variance.

d. Finally, a principled way to dissociate non-linear signal characteristics from linear signal variance is to use phase-shuffled surrogate data [5, 122–125]. Phase randomization (see S3 Text, S9 Fig) effectively alters original time series patterns while preserving linear PSD characteristics and "is unavoidable if conclusions are to be drawn about the existence of nonlinear dynamics in the underlying system" [5]. While such surrogate approaches have been

utilized in select entropy applications [4, e.g., appendix of 27] to highlight entropy's non-linear sensitivity [e.g., 30, 32, 46], it has not become common practice in application. Given that MSE is sensitive to many linear characteristics, some of which are shown in the present work, we consider surrogate analyses as an optimal approach to verify the contribution of non-linear signal characteristics.

In combination, such controls may go a long way toward establishing unique, complementary, and valid contributions of MSE in future work.

Conclusions

Many inferences regarding multiscale entropy in cognitive/clinical neuroscience rely on the assumption that estimates uniquely relate to pattern irregularity at specific temporal scales. Here we show that both assumptions may be invalid depending on the consideration of signal normalization and spectral content. Using simulations and empirical examples, we showed how spectral power differences can introduce entropy effects that are inversely mapped in time scale (i.e., differences in the high frequency power may be reflected in coarse entropy and vice versa; see Fig 12A). As these results suggest fundamental challenges to traditional MSE analysis procedures and inferences, we highlight the need to test for unique entropy effects (Fig 12B) and recommend best practices and sanity checks (Fig 12C) to increase confidence in the complementary value of pattern irregularity for cognitive/clinical neuroscience. While the warranted claim has been made that "it would be unreasonable simply to reduce sample entropy to autocorrelation, spectral power, non-stationarity or any of their combinations" [4], this should not mean that we cannot test whether one or more of these contributors may sufficiently explain MSE effects of interest. We thus propose that MSE effects may be taken as a starting point to explore the linear and nonlinear features of brain signals [e.g., 126]. We believe that empirical identification of the unique predictive utility of MSE will advance the quest for reliable mechanistic indicators of flexible brain function across the lifespan, and in relation to cognition, health, and disease.

Methods

Simulations of relations between rhythmic frequency, amplitude, and MSE

To assess the influence of rhythmicity on entropy estimates, we simulated varying amplitudes (0 to 7 arbitrary units in steps of 0.5) of 10 Hz (alpha) rhythms on a fixed 1/f background. This range varies from the absence to the clear presence of rhythmicity (see S3 Fig for an example). The background consisted of $\frac{1}{f^x}$-filtered Gaussian white noise (mean = 0; std = 1) with x = 1 that was generated using the function f_alpha_gaussian [127]. The background was additionally band-pass filtered between .5 and 70 Hz using 4th order Butterworth filters. Eight second segments (250 Hz sampling rate) were simulated for 100 artificial, background-varying trials, and phase-locked 10 Hz sinusoids were superimposed. To analyze the reflection of rhythmic frequency on time scales and to replicate a previously observed linear frequency-to-timescale mapping between the spectral and entropy domains [4, 22, 44], we repeated our simulations with sinusoids of different frequencies (5 Hz, 10 Hz, 20 Hz, 40 Hz, 80 Hz), that covered the entire eight second-long segments. For a specified amplitude level, the magnitude of frequency-specific power increases (or narrowband signal-to-noise ratio) increased alongside simulated frequencies due to the decreasing frequency power of pink noise, while the ratio of rhythmic-to-global signal variance (or global signal-to-noise ratio (SNR)) remained constant across simulated frequencies. We used the following definition: $SNR_{global} = \left(\frac{RMS_{signal}}{RMS_{noise}}\right)^2$, where

RMS_{noise} is the root mean square of the pink noise time series and RMS_{signal} characterizes the pink noise signal with added rhythmicity.

Resting state data and preprocessing

To investigate the influence of similarity bounds and filter ranges in empirical data, we used resting-state EEG data collected in the context of a larger assessment prior to task performance and immediately following electrode preparation. Following exclusion of three subjects due to recording errors, the final sample contained 47 younger (mean age = 25.8 years, SD = 4.6, range 18 to 35 years; 25 women) and 52 older adults (mean age = 68.7 years, SD = 4.2, range 59 to 78 years; 28 women) recruited from the participant database of the Max Planck Institute for Human Development, Berlin, Germany (MPIB). Participants were right-handed, as assessed with a modified version of the Edinburgh Handedness Inventory [128], and had normal or corrected-to-normal vision. Participants reported to be in good health with no known history of neurological or psychiatric incidences, and were paid for their participation (10 € per hour). All older adults had Mini Mental State Examination (MMSE) [129, 130] scores above 25. All participants gave written informed consent according to the institutional guidelines of the Deutsche Gesellschaft für Psychologie (DGPS) ethics board, which approved the study.

Participants were seated at a distance of 80 cm in front of a 60 Hz LCD monitor in an acoustically and electrically shielded chamber. Following electrode placement, participants were instructed to rest for 3 minutes with their eyes open and closed, respectively. During the eyes open interval, subjects were instructed to fixate on a centrally presented fixation cross. An auditory beep indicated to the subjects when to close their eyes. Only data from the eyes open resting state were analyzed here. EEG was continuously recorded from 64 active (Ag/AgCl) electrodes using BrainAmp amplifiers (Brain Products GmbH, Gilching, Germany). Sixty scalp electrodes were arranged within an elastic cap (EASYCAP GmbH, Herrsching, Germany) according to the 10% system [131], with the ground placed at AFz. To monitor eye movements, two electrodes were placed on the outer canthi (horizontal EOG) and one electrode below the left eye (vertical EOG). During recording, all electrodes were referenced to the right mastoid electrode, while the left mastoid electrode was recorded as an additional channel. Online, signals were digitized at a sampling rate of 1 kHz.

Preprocessing and analysis of EEG data were conducted with the FieldTrip toolbox [132] and using custom-written MATLAB (The MathWorks Inc., Natick, MA, USA) code. Offline, EEG data were filtered using a 4^{th} order Butterworth filter with a pass-band of 0.2 to 125 Hz. Subsequently, data were downsampled to 500 Hz and all channels were re-referenced to mathematically averaged mastoids. Blink, movement and heart-beat artifacts were identified using Independent Component Analysis [ICA; 133] and removed from the signal. Artifact-contaminated channels (determined across epochs) were automatically detected using (a) the FASTER algorithm [134], and by (b) detecting outliers exceeding three standard deviations of the kurtosis of the distribution of power values in each epoch within low (0.2–2 Hz) or high (30–100 Hz) frequency bands, respectively. Rejected channels were interpolated using spherical splines [135]. Subsequently, noisy epochs were likewise excluded based on FASTER and on recursive outlier detection. Finally, recordings were segmented to participant cues to open their eyes, and were epoched into non-overlapping 3 second pseudo-trials. To enhance spatial specificity, scalp current density estimates were derived via 4^{th} order spherical splines [135] using a standard 10–05 channel layout (conductivity: 0.33 S/m; regularization: 1^-05; 14^{th} degree polynomials).

Calculation of (modified) multi-scale sample entropy (mMSE)

MSE characterizes signal irregularity at multiple time scales by estimating sample entropy (SampEn) at each time scale of interest. A schematic of the estimation pipeline is shown in S1 Fig. The mMSE code is provided at https://github.com/LNDG/mMSE. A tutorial for computing mMSE has been published on the FieldTrip website (http://www.fieldtriptoolbox.org/example/entropy_analysis/).

Sample entropy estimation procedure. The estimation of SampEn involves counting how often patterns of m successive data points reoccur in time ($\boldsymbol{p^m}$) and assessing how many of those patterns remain similar when the next sample m+1 is added to the sequence ($\boldsymbol{p^{m+1}}$). Given that amplitude values are rarely exactly equal in physiological time series, a *similarity bound* defines which individual data points are considered similar. This step discretizes the data and allows to compare data patterns rather than exact data values. The similarity bound is defined as a proportion r of the time series standard deviation (SD; i.e., square root of signal variance) to normalize the estimation of sample entropy for total signal variation. That is, for any data point k, all data points within $k \pm r \times SD$ are by definition equal to k, which forms the basis for assessing sequence patterns. SampEn is finally given as the natural log of $\boldsymbol{p^m}(r)/\boldsymbol{p^{m+1}}(r)$. Consequently, high SampEn values indicate low temporal regularity as many patterns of length m are not repeated at length m+1. In our applications, m was set to 2 and r was set to .5, in line with prior recommendations [13] and EEG applications [27, 46, 136].

Multi-scale signal derivation procedure. To extend sample entropy to multiple time scales, MSE 'coarse-grains' the original time series for multiple scale factors $\boldsymbol{\tau}$ (here 1 to 42, where 1 refers to the original signal). The 'Original' MSE method [11, 12] averages time points within non-overlapping time bins (i.e., 'point averaging'). Such point averaging is equivalent to a low-pass finite-impulse response (FIR) filter, which can introduce aliasing however [33, 137] and constrains the specificity towards increasingly slow signals, while not allowing specificity to fast dynamics or any particular frequency range of interest. To implement control over the scale-wise filter direction and to reduce aliasing, we applied either low- [31, 33, 137], high-, or band-pass filters at each scale factor. The low-pass cut-off was defined as $\mathrm{LP} = \frac{1}{\boldsymbol{scale}} * \boldsymbol{nyquist}$ and was implemented using a 6th order Butterworth filter, with nyquist defined as half the sampling rate of the signal. Similarly, the high-pass cut-off was defined as $\mathrm{HP} = \frac{1}{\boldsymbol{scale}+1} * \boldsymbol{nyquist}$, implemented via 6th order Butterworth filters. Note that these cut-offs describe the upper and lower frequency bounds at each time scale, respectively. Finally, band-pass filters were applied to obtain narrowband estimates by sequentially applying Chebyshev Type I low- and high-pass filters (4th order with passband ripple of 1dB; chosen to achieve a fast filter roll-off), thus ensuring that each scale captured frequency-specific information. The passband was defined as BP = ***LP*** +- 0.05*$\mathbf{LP}$. To avoid pronounced passband ripple for broad passbands, 10th order Butterworth filters replaced the Chebyshev filters at scales where the passband was larger than 0.5*Nyquist. At scale 1, only a high-pass 10th order Butterworth filter was applied as the sampling rate of the signal set the upper (Nyquist) frequency bound. These settings were chosen to optimize the pass-through of signals within the pass-band and the attenuation of signals outside the pass-band. Two-pass filtering using MATLAB's filtfilt function was applied to achieve zero-phase delay. S4 Fig shows the spectral attenuation properties [138] of the filters. To avoid edge artefacts, input signals were symmetrically mean-padded with half the pseudo-trial duration (i.e., 1500 ms). After filtering, we implemented a point-skipping procedure to down-sample scale-wise signals (see S1 Fig). Since point-skipping allows for increasing starting point permutations k for increasing scale factors $\boldsymbol{\tau}$, we counted patterns separately for each starting point k, summed the counts of pattern matches and non-matches across them, and computed sample entropy based on the summed counts as described above:

$\mathbf{MSE}(\mathbf{x}, \boldsymbol{\tau}, \mathbf{m}, \mathbf{r}) = \boldsymbol{ln}\left(\frac{\sum_{k=1}^{\tau} p^m}{\sum_{k=1}^{\tau} p^{m+1}}\right)$. This implementation is equivalent to "refined composite MSE" [110] and can improve the stability of entropy results for short or noisy signals [31, 110]. Note that no point skipping was performed in the 'high-pass' implementation to avoid low-pass filtering. As a result, the signals at increasing scale factors remained at the original sampling rate. To alleviate computational cost, scale factors were sampled in step sizes of 3 for empirical data (only for the 'high-pass' implementation) and later spline-interpolated. An adapted version of MSE calculations was used for all settings [64], in which scale-wise entropy was estimated across discontinuous data segments. The estimation of scale-wise entropy across trials allows for reliable estimation of coarse-scale entropy without requiring long, continuous signals, while quickly converging with estimates from continuous segments [64].

Multi-scale calculation of similarity bounds. Following scale-specific filtering, all implementations re-calculated sample entropy for the scale-specific signal. Crucially, in 'Original' applications [11, 12], the *similarity bound* is calculated only once from the original broadband signal. As a result of filtering, the scale-wise signal SD decreases relative to the global, scale-invariant similarity bound [29]. To overcome this limitation, we recomputed the similarity bound for each scale factor, thereby normalizing MSE with respect to changes in overall time series variation at each scale (.5 x SD of scale-wise signal).

Scale factor notation. As the interpretation of estimates at each scale is bound to the scale-wise spectral content, our Figures indicate spectral bounds of the scale-wise signals alongside the scale factor as follows: for the low- and band-pass implementation, we indicate the low-pass frequency as calculated above as the highest resolvable (i.e., Nyquist) frequency in the scale-specific signal. Likewise, for the high-pass implementation, we indicate the high-pass limit as the lowest resolvable frequency in the scale-specific signal. In the main text, we refer to higher scale factors as 'coarser' scales' and lower scale factors as 'finer' scales, in line with the common use in the literature. Note that the sampling rate of the simulated data was 250 Hz, whereas the empirical data had a sampling rate of 500 Hz.

Calculation of power spectral density (PSD)

Power spectral density estimates were computed by means of a Fast Fourier Transform (FFT) over 3 second pseudo-trials for 41 logarithmically spaced frequencies between 2 and 64 Hz (employing a Hanning-taper; segments zero-padded to 10 seconds) and subsequently averaged. Spectral power was $\log_{10}$-transformed to render power values more normally distributed across subjects. Power spectral density (PSD) slopes were derived by linearly regressing power values on $\log_{10}$-transformed frequencies (i.e., log-log fit). The spectral range from 7–13 Hz was excluded from the background fit to exclude a bias by the narrowband alpha peak [40, 49].

Detection of single-trial spectral events

Spectral power, even in the narrowband case, is unspecific to the occurrence of systematic rhythmic events as it also characterizes periods of absent rhythmicity [e.g., 139]. Specifically detecting rhythmic episodes in the ongoing signal alleviates this problem, as periods of absent rhythmicity are excluded. To investigate the potential relation between the occurrence of stereotypic spectral events and narrowband entropy, we detected single-trial spectral events using the extended BOSC method [42, 140, 141] and probed their relation to individual entropy estimates. In short, this method identifies stereotypic 'rhythmic' events at the single-trial level, with the assumption that such events have significantly higher power than the 1/f background and occur for a minimum number of cycles at a particular frequency. This effectively dissociates narrowband spectral peaks from the arrhythmic background spectrum. Here, we used a

one cycle threshold during detection, while defining the power threshold as the 95th percentile above the individual background power. A 5-cycle wavelet was used to provide the time-frequency transformations for 49 logarithmically-spaced center frequencies between 1 and 64 Hz. Rhythmic episodes were detected as described in [42]. Following the detection of spectral events, the rate of spectral episodes longer than 3 cycles was computed by counting the number of episodes with a mean frequency that fell in a moving window of 3 adjacent center frequencies. This produced a channel-by-frequency representation of spectral event rates, which were the basis for subsequent significance testing. Event rates and statistical results were averaged within frequency bins from 8–12 Hz (alpha) and 14–20 Hz (beta) to assess relations to narrowband entropy and for the visualization of topographies. To visualize the stereotypic depiction of single-trial alpha and beta events, the original time series were time-locked to the trough of individual spectral episodes and averaged across events [c.f., 57]. More specifically, the trough was chosen to be the local minimum during the spectral episode that was closest to the maximum power of the wavelet-transformed signal. To better estimate the local minimum, the signal was low-pass filtered at 25 Hz for alpha and bandpass-filtered between 10 and 25 Hz for beta using a 6th order Butterworth filter. A post-hoc duration threshold of one cycle was used for the visualization of beta events, whereas a three-cycle criterion was used to visualize alpha events. Alpha and beta events were visualized at channels POz and Cz, respectively.

Examination of transient irregularity shifts during alpha events

The relation of narrowband alpha events to broadband irregularity represents an empirical question of interest (see Introduction). We examined the relation between these signatures, while controlling for the circular, intrinsic relation between alpha-based regularity and entropy. To highlight the issue of circularity, we first simulated expected links between the two signals by creating 250 ms of data, consisting of (a) aperiodic slopes of $\frac{1}{f^1}$, (b) aperiodic slopes of $\frac{1}{f^{1.2}}$, as well as equivalent versions with superimposed alpha rhythms of unit amplitude (c, d). We probed the practical potential of a 8–15 Hz band-stop filter (6th order Butterworth) to remove the influence of alpha on broadband entropy. Entropy was calculated for the first MSE scale, reflecting broadband sample entropy. Next, in empirical data, we leveraged the temporal on- and offsets of individual alpha segments (8–15 Hz; $>$ 3 cycles) as identified via rhythm detection and segmented the original data to include 250 ms preceding and following event on- and offsets (see S8 Fig for empirical examples). For each subject, all events across posterior-occipital channels at which event number was highest (see Fig 11B) were included in this analysis. At each channel we performed a median split of events according to their amplitude (high/low). We created versions with and without application of 8–15 Hz bandstop filters (S8 Fig), followed by the calculation of sample entropy. We assessed the impact of transient alpha events on irregularity via paired t-tests between alpha on vs. off contrasts, both at event on- and the offset, and individually for low and high amplitude events. As post-hoc tests, we assessed potential interactions between alpha presence and age via linear mixed effect models (random subject intercept). To probe the presence of a broadband effect, we assessed the spectral slopes for the same segments. To improve spectral resolution, we"auto-sandwiched" each 250 ms segment by appending it in x- & y-inverted forms at the original segment's on- and offset. This effectively increased segment duration to 750 ms, while retaining autocorrelative properties. We then calculated an FFT of each segment (2–90 Hz; 45 2^x steps; Hanning taper; 4 Hz smoothing box; zero-padded to 10 s). Linear slopes were fit in log-log space, after excluding the 5–20 Hz range to remove the influence of the rhythmic alpha peak. Individual entropy estimates were averaged across alpha on- and offsets to remove measurement noise, and were statistically compared between alpha on & off periods via paired t-tests.

Statistical analyses

Spectral power and entropy were compared across age groups within condition by means of independent samples t-tests; cluster-based permutation tests [142] were performed to control for multiple comparisons. Initially, a clustering algorithm formed clusters based on significant t-tests of individual data points ($p < .05$, two-sided; cluster entry threshold) with the spatial constraint of a cluster covering a minimum of three neighboring channels. Then, the significance of the observed cluster-level statistic, based on the summed t-values within the cluster, was assessed by comparison to the distribution of all permutation-based cluster-level statistics. The final cluster p-value that we report in figures was assessed as the proportion of 1000 Monte Carlo iterations in which the cluster-level statistic was exceeded. Cluster significance was indicated by p-values below .025 (two-sided cluster significance threshold). Effect sizes for MSE age differences with different filter settings were computed on the basis of the cluster results in the 'Original' version. This was also the case for analyses of partial correlations. Raw MSE values were extracted from channels with indicated age differences at the initial three scales 1–3 (>65 Hz) for fine MSE and scales 39–41 (<6.5 Hz) for coarse MSE. R^2 was calculated based on the t-values of an unpaired t-test: $R^2 = \frac{t^2}{t^2+df}$ [143]. The measure describes the variance in the age difference explained by the measure of interest, with the square root being identical to Pearson's correlation coefficient between continuous individual values and binary age group. Effect sizes were compared using the r-to-z-transform and a successive comparison of the z-value difference against zero: $Z_{Diff} = \frac{z1-z2}{sqrt\left(\frac{1}{N1-3}+\frac{1}{N2-3}\right)}$ [144]. Unmasked t-values are presented in support of the assessment of raw statistics in our data [145].

Supporting information

S1 Text. Systematic literature search assessing the prevalence of global similarity bounds.
(PDF)

S2 Text. Simulation of MSE's sensitivity to PSD slope variation.
(PDF)

S3 Text. Surrogate analysis of age effects.
(PDF)

S1 Fig. Overview of modified (mMSE) adaptations. First, mMSE uses data aggregation across (here: pseudo-) trials to allow the estimation of coarse scales also from sparse neuroimaging data [64]. These aggregated signals are then filtered at each scale prior to sample entropy calculation. The 'Original' implementation uses 'point averaging' for different scale factors, which is equivalent to a FIR low-pass filter. In adapted applications, we used a two-step implementation, which we refer to as 'filt-skip', which first applies a scale-wise low-, high- or band-pass filter, and then performs point skipping to down-sample the resulting signals. Finally, the sample entropy of these signals is similarly assessed using the sample entropy algorithm, which results in multiscale entropy estimates. Figure adapted with permission from [121].
(TIF)

S2 Fig. Liberal similarity bounds reduce sample entropy in simulations. (**A**) The plot shows the sample entropy of simulated white noise signals with constant signal standard deviation (SD) of 1, but varying similarity bounds. We denote this as a function of a scaling factor (SF) to highlight that such variation may arise from either variation in r, SD or both. Note that the r parameter is usually fixed and the SD matches the signal SD (gray line), thus normalizing total signal variance. However, when the similarity bound systematically increases relative to the

signal SD, entropy estimates progressively decrease (black line). (**B**) A similar scenario applies when fixed and large bounds are applied to signals of decreasing variance, as is the case across MSE time scales due to scale-wise filtering (Fig 2). Whereas no bias is observed when scale-wise signal SD is used for the calculation of similarity bounds (grey line), entropy estimates systematically decrease when the SD of the original signal are used (black line). Hence, the mismatched similarity bounds introduced entropy decreases although no changes to the structure of the (here white noise) signals were introduced.
(TIF)

S3 Fig. Examples of simulated rhythmicity projected into pink noise. (A) Top-down view of time-series from an exemplary simulated trial for a pure 1/f signal pink noise signal and at different magnitudes of added alpha rhythmicity. **(B)** Exemplary time series in 2D view. The red time series indicates an example time series for the level of rhythmicity shown in Fig 5. (**C**) Simulated SNR as a function of amplitude level. The dots indicate SNR for the levels depicted in panel B.
(TIF)

S4 Fig. Filter magnitude responses. (A) Filter magnitude responses at 10 Hz. Note that magnitude responses have been squared due to two-pass filtering to achieve zero-phase offsets. (**B**) Filter magnitudes of Bandpass filters (3^{rd} order type I Chebyshev filter with 1dB passband ripple) at different time scales (red-to-orange indicating fine-to-coarse time scales). Note that only a high-pass filter (6^{th} order Butterworth filter) is applied at the first scale.
(TIF)

S5 Fig. T-values for age group differences in spectral power (OA > YA). Statistical significance ($p < .05$) was assessed by means of cluster-based permutation tests and is indicated via opacity.
(TIF)

S6 Fig. Methods- and scale-dependent associations between sample entropy and PSD slopes. 'Original' settings indicate a strong positive association at fine scales (A1) that turns negative at coarse scales (A2), likely due to coarse-scale biases by the scale-invariant similarity criterion. In line with this notion, scale-wise adaptation of thresholds retains the fine-scale effect (B1), while abolishing the coarse-scale inversion (B2). Crucially, the entropy of exclusively high-frequency signals does not positively relate to PSD slopes (C1), whereas the association reemerges once slow fluctuations are added into the signal (C2).
(TIF)

S7 Fig. Results of different simulated spectral slope coefficients for the different filter implementations. (**A**) Using traditional implementations, 1/f variation introduces scale-dependent crossover effects, including scale-dependent entropy decreases for the signals approaching white noise. (**B, C, D**) In contrast, control for scale-wise variance indicates broad scale entropy offsets without crossovers. (**E**) Bandpass entropy is not modulated by broadband effects, as expected by the absence of multi-scale information at local scales.
(TIF)

S8 Fig. Signal traces around indicated large alpha event on- and offsets. (**A**) Thirty randomly selected traces across subjects for alpha on- (A1) and offsets (A2). The grey background indicates the 250 ms pre- and post-alpha windows used for the calculation of sample entropy (see Fig 11). The red background highlights segments following indicated alpha onsets, and preceding alpha offsets, that were used to assess irregularity during transient alpha events. Note that 250 ms segments may overlap in the case of short rhythmicity of around 3 cycles. (**B**)

All events around on- and offsets. Data were sorted by the instantaneous phase at +100 ms after indicated alpha onset (B1) and -100 ms prior to indicated alpha offset (B2). Instantaneous phase was calculated from a Hilbert transform applied to 8–15 Hz bandpass filtered signals. (**C**) Same as in B, but plotted for signals after 8–15 Hz bandstop filter application. All displayed traces were z-scored for presentation purposes.
(TIF)

S9 Fig. Results of surrogate analysis, testing for non-linear contributions to MSE age effects. (**A**) Examples of original and surrogate data for a random 3 s segment from an occipital channel with strong alpha rhythms. Phase randomization alters higher-order (non-linear) frequency interactions while preserving the linear power characteristics of the original data. If non-linear contributions are necessary for MSE age effects, no age effects should be indicated for entropy estimates of surrogate data (**B**) Results for "Original" MSE analysis on phase-shuffled data indicate similar effects as observed for original data (Fig 7A), suggesting that linear characteristics were sufficient for the observed age effects. (**C**) Results for low-pass MSE analysis on phase-shuffled data indicate similar effects as observed for original data (Fig 7C), suggesting that linear characteristics were sufficient for the observed age effects. (**D, E**) In addition to assessing the necessity of non-linear contributions, we further assessed whether age differences would be indicated for non-linear contributions, after accounting for linear power characteristics. The ratio of MSE estimates for original vs. surrogate data indicates unique non-linear contributions for either age group. The obtained results were remarkably similar for both original (D) and low-pass implementations (E), indicating the successful elimination of power-based biases. However, no statistically significant age differences were indicated, suggesting that non-linear contributions are at most minor, and may require higher statistical power for their assessment.
(TIF)

Acknowledgments

We thank our research assistants and participants for their contributions to the present work.

Author Contributions

Conceptualization: Julian Q. Kosciessa, Niels A. Kloosterman, Douglas D. Garrett.

Data curation: Julian Q. Kosciessa, Niels A. Kloosterman.

Formal analysis: Julian Q. Kosciessa.

Funding acquisition: Douglas D. Garrett.

Investigation: Julian Q. Kosciessa, Douglas D. Garrett.

Methodology: Julian Q. Kosciessa, Niels A. Kloosterman, Douglas D. Garrett.

Project administration: Julian Q. Kosciessa, Douglas D. Garrett.

Resources: Niels A. Kloosterman, Douglas D. Garrett.

Software: Julian Q. Kosciessa, Niels A. Kloosterman.

Supervision: Douglas D. Garrett.

Validation: Julian Q. Kosciessa.

Visualization: Julian Q. Kosciessa.

Writing – original draft: Julian Q. Kosciessa.

Writing – review & editing: Julian Q. Kosciessa, Niels A. Kloosterman, Douglas D. Garrett.

References

1. Buzsaki G, Draguhn A. Neuronal oscillations in cortical networks. Science. 2004; 304(5679):1926–9. https://doi.org/10.1126/science.1099745 WOS:000222241600031. PMID: 15218136
2. Wang XJ. Neurophysiological and computational principles of cortical rhythms in cognition. Physiol Rev. 2010; 90(3):1195–268. Epub 2010/07/29. https://doi.org/10.1152/physrev.00035.2008 PMID: 20664082; PubMed Central PMCID: PMC2923921.
3. Breakspear M. Dynamic models of large-scale brain activity. Nat Neurosci. 2017; 20(3):340–52. https://doi.org/10.1038/nn.4497 WOS:000394920400007. PMID: 28230845
4. Vakorin VA, McIntosh AR. Mapping the Multiscale Information Content of Complex Brain Signals. Comput Neurosci-Mit. 2012:183–208. WOS:000315291000011.
5. Stam CJ. Nonlinear dynamical analysis of EEG and MEG: review of an emerging field. Clin Neurophysiol. 2005; 116(10):2266–301. Epub 2005/08/24. https://doi.org/10.1016/j.clinph.2005.06.011 PMID: 16115797.
6. Garrett DD, Samanez-Larkin GR, MacDonald SW, Lindenberger U, McIntosh AR, Grady CL. Moment-to-moment brain signal variability: a next frontier in human brain mapping? Neurosci Biobehav Rev. 2013; 37(4):610–24. Epub 2013/03/06. https://doi.org/10.1016/j.neubiorev.2013.02.015 PMID: 23458776; PubMed Central PMCID: PMC3732213.
7. Ghosh A, Rho Y, McIntosh AR, Kotter R, Jirsa VK. Noise during rest enables the exploration of the brain's dynamic repertoire. Plos Comput Biol. 2008; 4(10):e1000196. Epub 2008/10/11. https://doi.org/10.1371/journal.pcbi.1000196 PMID: 18846206; PubMed Central PMCID: PMC2551736.
8. Garrett DD, Samanez-Larkin GR, MacDonald SWS, Lindenberger U, McIntosh AR, Grady CL. Moment-to-moment brain signal variability: A next frontier in human brain mapping? Neuroscience and Biobehavioral Reviews. 2013; 37(4):610–24. https://doi.org/10.1016/j.neubiorev.2013.02.015 WOS:000318580100006. PMID: 23458776
9. Garrett DD, McIntosh AR, Grady CL. Moment-to-moment signal variability in the human brain can inform models of stochastic facilitation now. Nat Rev Neurosci. 2011; 12(10):612; author reply Epub 2011/09/08. https://doi.org/10.1038/nrn3061-c1 PMID: 21897432.
10. Shew WL, Yang HD, Yu S, Roy R, Plenz D. Information Capacity and Transmission Are Maximized in Balanced Cortical Networks with Neuronal Avalanches. J Neurosci. 2011; 31(1):55–63. https://doi.org/10.1523/JNEUROSCI.4637-10.2011 WOS:000285915100007. PMID: 21209189
11. Costa M, Goldberger AL, Peng CK. Multiscale entropy analysis of complex physiologic time series. Phys Rev Lett. 2002; 89(6). https://doi.org/10.1103/PhysRevLett.89.068102 WOS:000177009600047. PMID: 12190613
12. Costa M, Goldberger AL, Peng CK. Multiscale entropy analysis of biological signals. Phys Rev E. 2005; 71(2). https://doi.org/10.1103/PhysRevE.71.021906 WOS:000228245700047. PMID: 15783351
13. Richman JS, Moorman JR. Physiological time-series analysis using approximate entropy and sample entropy. Am J Physiol-Heart C. 2000; 278(6):H2039–H49. WOS:000087573500038.
14. Bruce EN, Bruce MC, Vennelaganti S. Sample Entropy Tracks Changes in Electroencephalogram Power Spectrum With Sleep State and Aging. J Clin Neurophysiol. 2009; 26(4):257–66. https://doi.org/10.1097/WNP.0b013e3181b2f1e3 WOS:000268746000007. PMID: 19590434
15. Jaworska N, Wang HY, Smith DM, Blier P, Knott V, Protzner AB. Pre-treatment EEG signal variability is associated with treatment success in depression. Neuroimage-Clin. 2018; 17:368–77. https://doi.org/10.1016/j.nicl.2017.10.035 WOS:000426180300040. PMID: 29159049
16. McIntosh AR, Vakorin V, Kovacevic N, Wang H, Diaconescu A, Protzner AB. Spatiotemporal Dependency of Age-Related Changes in Brain Signal Variability. Cereb Cortex. 2014; 24(7):1806–17. https://doi.org/10.1093/cercor/bht030 WOS:000338110900010. PMID: 23395850
17. Miskovic V, MacDonald KJ, Rhodes LJ, Cote KA. Changes in EEG multiscale entropy and power-law frequency scaling during the human sleep cycle. Hum Brain Mapp. 2019; 40(2):538–51. https://doi.org/10.1002/hbm.24393 WOS:000460481300014. PMID: 30259594
18. Wang H, McIntosh AR, Kovacevic N, Karachalios M, Protzner AB. Age-related Multiscale Changes in Brain Signal Variability in Pre-task versus Post-task Resting-state EEG. J Cogn Neurosci. 2016; 28(7):971–84. Epub 2016/03/05. https://doi.org/10.1162/jocn_a_00947 PMID: 26942319.

19. Sleimen-Malkoun R, Perdikis D, Muller V, Blanc JL, Huys R, Temprado JJ, et al. Brain Dynamics of Aging: Multiscale Variability of EEG Signals at Rest and during an Auditory Oddball Task(1,2,3). Eneuro. 2015; 2(3). https://doi.org/10.1523/ENEURO.0067-14.2015 WOS:000218581400012. PMID: 26464983

20. Werkle-Bergner M, Grandy TH, Chicherio C, Schmiedek F, Lovden M, Lindenberger U. Coordinated within-Trial Dynamics of Low-Frequency Neural Rhythms Controls Evidence Accumulation. J Neurosci. 2014; 34(25):8519–28. https://doi.org/10.1523/JNEUROSCI.3801-13.2014 WOS:000338449200014. PMID: 24948807

21. Yang AC, Wang SJ, Lai KL, Tsai CF, Yang CH, Hwang JP, et al. Cognitive and neuropsychiatric correlates of EEG dynamic complexity in patients with Alzheimer's disease. Prog Neuro-Psychoph. 2013; 47:52–61. https://doi.org/10.1016/j.pnpbp.2013.07.022 WOS:000326682300009. PMID: 23954738

22. Takahashi T, Cho RY, Mizuno T, Kikuchi M, Murata T, Takahashi K, et al. Antipsychotics reverse abnormal EEG complexity in drug-naive schizophrenia: A multiscale entropy analysis. Neuroimage. 2010; 51(1):173–82. https://doi.org/10.1016/j.neuroimage.2010.02.009 WOS:000276480200018. PMID: 20149880

23. Mejias JF, Murray JD, Kennedy H, Wang XJ. Feedforward and feedback frequency-dependent interactions in a large-scale laminar network of the primate cortex. Sci Adv. 2016; 2(11). https://doi.org/10.1126/sciadv.1601335 WOS:000391267800032. PMID: 28138530

24. Buzsaki G, Logothetis N, Singer W. Scaling Brain Size, Keeping Timing: Evolutionary Preservation of Brain Rhythms. Neuron. 2013; 80(3):751–64. https://doi.org/10.1016/j.neuron.2013.10.002 WOS:000326609900019. PMID: 24183025

25. von Stein A, Sarnthein J. Different frequencies for different scales of cortical integration: from local gamma to long range alpha/theta synchronization. Int J Psychophysiol. 2000; 38(3):301–13. https://doi.org/10.1016/s0167-8760(00)00172-0 WOS:000165915000009. PMID: 11102669

26. Fries P. Neuronal Gamma-Band Synchronization as a Fundamental Process in Cortical Computation. Annu Rev Neurosci. 2009; 32:209–24. https://doi.org/10.1146/annurev.neuro.051508.135603 WOS:000268504100009. PMID: 19400723

27. Courtiol J, Perdikis D, Petkoski S, Muller V, Huys R, Sleimen-Malkoun R, et al. The multiscale entropy: Guidelines for use and interpretation in brain signal analysis. J Neurosci Meth. 2016; 273:175–90. https://doi.org/10.1016/j.jneumeth.2016.09.004 WOS:000387195800017. PMID: 27639660

28. Costa M, Goldberger AL, Peng CK. Comment on "Multiscale entropy analysis of complex physiologic time series"—Reply. Phys Rev Lett. 2004; 92(8). https://doi.org/10.1103/PhysRevLett.92.089804 WOS:000189266100069.

29. Nikulin VV, Brismar T. Comment on "Multiscale entropy analysis of complex physiologic time series". Phys Rev Lett. 2004; 92(8). https://doi.org/10.1103/PhysRevLett.92.089803 WOS:000189266100068. PMID: 14995828

30. Shafiei G, Zeighami Y, Clark CA, Coull JT, Nagano-Saito A, Leyton M, et al. Dopamine Signaling Modulates the Stability and Integration of Intrinsic Brain Networks. Cereb Cortex. 2019; 29(1):397–409. https://doi.org/10.1093/cercor/bhy264 WOS:000459518500030. PMID: 30357316

31. Azami H, Escudero J. Coarse-Graining Approaches in Univariate Multiscale Sample and Dispersion Entropy. Entropy. 2018; 20(2). https://doi.org/10.3390/e20020138 WOS:000426793900061.

32. Miskovic V, Owens M, Kuntzelman K, Gibb BE. Charting moment-to-moment brain signal variability from early to late childhood. Cortex. 2016; 83:51–61. Epub 2016/08/02. https://doi.org/10.1016/j.cortex.2016.07.006 PMID: 27479615; PubMed Central PMCID: PMC5042835.

33. Valencia JF, Porta A, Vallverdu M, Claria F, Baranowski R, Orlowska-Baranowska E, et al. Refined Multiscale Entropy: Application to 24-h Holter Recordings of Heart Period Variability in Healthy and Aortic Stenosis Subjects. Ieee T Bio-Med Eng. 2009; 56(9):2202–13. https://doi.org/10.1109/Tbme.2009.2021986 WOS:000269154100008. PMID: 19457745

34. Faes L, Porta A, Javorka M, Nollo G. Efficient Computation of Multiscale Entropy over Short Biomedical Time Series Based on Linear State-Space Models. Complexity. 2017. Artn 1768264 https://doi.org/10.1155/2017/1768264 WOS:000418241600001.

35. Xiong WT, Faes L, Ivanov PC. Entropy measures, entropy estimators, and their performance in quantifying complex dynamics: Effects of artifacts, nonstationarity, and long-range correlations. Phys Rev E. 2017; 95(6). ARTN 062114 https://doi.org/10.1103/PhysRevE.95.062114 WOS:000403077800001. PMID: 28709192

36. Buzsaki G, Mizuseki K. The log-dynamic brain: how skewed distributions affect network operations. Nat Rev Neurosci. 2014; 15(4):264–78. https://doi.org/10.1038/nrn3687 WOS:000333256600012. PMID: 24569488

37. He BYJ. Scale-free brain activity: past, present, and future. Trends Cogn Sci. 2014; 18(9):480–7. https://doi.org/10.1016/j.tics.2014.04.003 WOS:000341613000010. PMID: 24788139

38. Miller KJ, Sorensen LB, Ojemann JG, den Nijs M. Power-Law Scaling in the Brain Surface Electric Potential. Plos Comput Biol. 2009; 5(12). ARTN e1000609 https://doi.org/10.1371/journal.pcbi.1000609 WOS:000274229000027. PMID: 20019800

39. Donoghue T, Dominguez J, Voytek B. Electrophysiological Frequency Band Ratio Measures Conflate Periodic and Aperiodic Neural Activity. bioRxiv. 2020.

40. Waschke L, Wostmann M, Obleser J. States and traits of neural irregularity in the age-varying human brain. Sci Rep-Uk. 2017; 7. https://doi.org/10.1038/s41598-017-17766-4 WOS:000417689400005. PMID: 29234128

41. Haller M, Donoghue T, Peterson E, Varma P, Sebastian P, Gao R, et al. Parameterizing neural power spectra. bioRxiv. 2018.

42. Kosciessa JQ, Grandy TH, Garrett DD, Werkle-Bergner M. Single-trial characterization of neural rhythms: Potential and challenges. Neuroimage. 2019:116331. https://doi.org/10.1016/j.neuroimage.2019.116331.

43. Lopes da Silva F. EEG and MEG: relevance to neuroscience. Neuron. 2013; 80(5):1112–28. Epub 2013/12/10. https://doi.org/10.1016/j.neuron.2013.10.017 PMID: 24314724.

44. Park JH, Kim S, Kim CH, Cichocki A, Kim K. Multiscale entropy analysis of EEG from patients under different pathological conditions. Fractals. 2007; 15(4):399–404. https://doi.org/10.1142/S0218348x07003691 WOS:000252021600010.

45. McIntosh AR. Neurocognitive Aging and Brain Signal Complexity. Oxford University Press; 2019.

46. McIntosh AR, Kovacevic N, Itier RJ. Increased Brain Signal Variability Accompanies Lower Behavioral Variability in Development. Plos Comput Biol. 2008; 4(7). https://doi.org/10.1371/journal.pcbi.1000106 WOS:000260039300027. PMID: 18604265

47. Leirer VM, Wienbruch C, Kolassa S, Schlee W, Elbert T, Kolassa IT. Changes in cortical slow wave activity in healthy aging. Brain Imaging Behav. 2011; 5(3):222–8. https://doi.org/10.1007/s11682-011-9126-3 WOS:000293498500007. PMID: 21698438

48. Vlahou EL, Thurm F, Kolassa IT, Schlee W. Resting-state slow wave power, healthy aging and cognitive performance. Sci Rep-Uk. 2014; 4. https://doi.org/10.1038/srep05101 WOS:000336516800002. PMID: 24869503

49. Voytek B, Kramer MA, Case J, Lepage KQ, Tempesta ZR, Knight RT, et al. Age-Related Changes in 1/f Neural Electrophysiological Noise. J Neurosci. 2015; 35(38):13257–65. https://doi.org/10.1523/JNEUROSCI.2332-14.2015 WOS:000363660200027. PMID: 26400953

50. Buzsáki G. Rhythms of the brain. Oxford; New York: Oxford University Press; 2006. xiv, 448 p. p.

51. Manning JR, Jacobs J, Fried I, Kahana MJ. Broadband Shifts in Local Field Potential Power Spectra Are Correlated with Single-Neuron Spiking in Humans. J Neurosci. 2009; 29(43):13613–20. https://doi.org/10.1523/JNEUROSCI.2041-09.2009 WOS:000271266600020. PMID: 19864573

52. Miller KJ, Honey CJ, Hermes D, Rao RPN, denNijs M, Ojemann JG. Broadband changes in the cortical surface potential track activation of functionally diverse neuronal populations. Neuroimage. 2014; 85:711–20. https://doi.org/10.1016/j.neuroimage.2013.08.070 WOS:000328870400009. PMID: 24018305

53. Miller KJ, Zanos S, Fetz EE, den Nijs M, Ojemann JG. Decoupling the Cortical Power Spectrum Reveals Real-Time Representation of Individual Finger Movements in Humans. J Neurosci. 2009; 29(10):3132–7. https://doi.org/10.1523/JNEUROSCI.5506-08.2009 WOS:000264093200015. PMID: 19279250

54. Gao R, Peterson EJ, Voytek B. Inferring synaptic excitation/inhibition balance from field potentials. Neuroimage. 2017; 158:70–8. https://doi.org/10.1016/j.neuroimage.2017.06.078 WOS:000411450600008. PMID: 28676297

55. Klimesch W, Sauseng P, Hanslmayr S. EEG alpha oscillations: the inhibition-timing hypothesis. Brain Res Rev. 2007; 53(1):63–88. Epub 2006/08/05. https://doi.org/10.1016/j.brainresrev.2006.06.003 PMID: 16887192.

56. Hipp JF, Siegel M. Dissociating neuronal gamma-band activity from cranial and ocular muscle activity in EEG. Front Hum Neurosci. 2013; 7. https://doi.org/10.3389/fnhum.2013.00338 WOS:000321588600001. PMID: 23847508

57. Sherman MA, Lee S, Law R, Haegens S, Thorn CA, Hamalainen MS, et al. Neural mechanisms of transient neocortical beta rhythms: Converging evidence from humans, computational modeling, monkeys, and mice. P Natl Acad Sci USA. 2016; 113(33):E4885–E94. https://doi.org/10.1073/pnas.1604135113 WOS:000381399200018. PMID: 27469163

58. Shin H, Law R, Tsutsui S, Moore CI, Jones SR. The rate of transient beta frequency events predicts behavior across tasks and species. Elife. 2017; 6. https://doi.org/10.7554/eLife.29086 WOS:000414984800001. PMID: 29106374

59. Haegens S, Nacher V, Luna R, Romo R, Jensen O. alpha-Oscillations in the monkey sensorimotor network influence discrimination performance by rhythmical inhibition of neuronal spiking. P Natl Acad Sci USA. 2011; 108(48):19377–82. https://doi.org/10.1073/pnas.1117190108 WOS:000297463100057. PMID: 22084106

60. Peterson EJ, Voytek B. Alpha oscillations control cortical gain by modulating excitatory-inhibitory background activity. bioRxiv. 2017.

61. Becker R, Van de Ville D, Kleinschmidt A. Alpha Oscillations Reduce Temporal Long-Range Dependence in Spontaneous Human Brain Activity. J Neurosci. 2018; 38(3):755–64. Epub 2017/11/24. https://doi.org/10.1523/JNEUROSCI.0831-17.2017 PMID: 29167403; PubMed Central PMCID: PMC6596188.

62. Waschke L, Tune S, Obleser J. Local cortical desynchronization and pupil-linked arousal differentially shape brain states for optimal sensory performance. Elife. 2019; 8. Epub 2019/12/11. https://doi.org/10.7554/eLife.51501 PMID: 31820732.

63. Faes L, Pereira MA, Silva ME, Pernice R, Busacca A, Javorka M, et al. Multiscale information storage of linear long-range correlated stochastic processes. Phys Rev E. 2019; 99(3). ARTN 032115 https://doi.org/10.1103/PhysRevE.99.032115 WOS:000461060500002. PMID: 30999519

64. Grandy TH, Garrett DD, Schmiedek F, Werkle-Bergner M. On the estimation of brain signal entropy from sparse neuroimaging data. Sci Rep-Uk. 2016; 6. https://doi.org/10.1038/srep23073 WOS:000372915300001. PMID: 27020961

65. Berger H. Über das Elektrenkephalogramm des Menschen. Archiv für Psychiatrie und Nervenkrankheiten. 1929; 87(1):527–70. https://doi.org/10.1007/BF01797193

66. Sheehan TC, Sreekumar V, Inati SK, Zaghloul KA. Signal Complexity of Human Intracranial EEG Tracks Successful Associative-Memory Formation across Individuals. J Neurosci. 2018; 38(7):1744–55. https://doi.org/10.1523/JNEUROSCI.2389-17.2017 WOS:000424987700012. PMID: 29330327

67. Kaffashi F, Foglyano R, Wilson CG, Loparo KA. The effect of time delay on Approximate & Sample Entropy calculations. Physica D. 2008; 237(23):3069–74. https://doi.org/10.1016/j.physd.2008.06.005 WOS:000261463000010.

68. Ferguson KA, Cardin JA. Mechanisms underlying gain modulation in the cortex. Nat Rev Neurosci. 2020; 21(2):80–92. https://doi.org/10.1038/s41583-019-0253-y WOS:000508147700001. PMID: 31911627

69. Destexhe A, Rudolph M, Pare D. The high-conductance state of neocortical neurons in vivo. Nat Rev Neurosci. 2003; 4(9):739–51. https://doi.org/10.1038/nrn1198 WOS:000185052600017. PMID: 12951566

70. Contreras D, Steriade M. Synchronization of low-frequency rhythms in corticothalamic networks. Neuroscience. 1997; 76(1):11–24. WOS:A1997VY25600003. https://doi.org/10.1016/s0306-4522(96)00393-4 PMID: 8971755

71. Harris KD, Thiele A. Cortical state and attention. Nat Rev Neurosci. 2011; 12(9):509–23. https://doi.org/10.1038/nrn3084 WOS:000294049200013. PMID: 21829219

72. Marguet SL, Harris KD. State-Dependent Representation of Amplitude-Modulated Noise Stimuli in Rat Auditory Cortex. J Neurosci. 2011; 31(17):6414–20. https://doi.org/10.1523/JNEUROSCI.5773-10.2011 WOS:000289934600018. PMID: 21525282

73. Peterson EJ, Rosen BQ, Campbell AM, Belger A, Voytek B. 1/f neural noise is a better predictor of schizophrenia than neural oscillations. bioRxiv. 2018.

74. Freeman WJ, Zhai J. Simulated power spectral density (PSD) of background electrocorticogram (ECoG). Cognitive Neurodynamics. 2009; 3(1):97–103. https://doi.org/10.1007/s11571-008-9064-y WOS:000266413200009. PMID: 19003455

75. Lombardi F, Herrmann HJ, de Arcangelis L. Balance of excitation and inhibition determines 1/f power spectrum in neuronal networks. Chaos. 2017; 27(4). Artn 047402 https://doi.org/10.1063/1.4979043 WOS:000399154600012. PMID: 28456161

76. Bedard C, Gomes JM, Bal T, Destexhe A. A framework to reconcile frequency scaling measurements, from intracellular recordings, local-field potentials, up to EEG and MEG signals. Journal of Integrative Neuroscience. 2017; 16(1):3–18. https://doi.org/10.3233/JIN-160001 WOS:000395669700002. PMID: 28891497

77. Linden H, Pettersen KH, Einevoll GT. Intrinsic dendritic filtering gives low-pass power spectra of local field potentials. J Comput Neurosci. 2010; 29(3):423–44. https://doi.org/10.1007/s10827-010-0245-4 WOS:000284162900005. PMID: 20502952

78. Dugue L, Marque P, VanRullen R. The Phase of Ongoing Oscillations Mediates the Causal Relation between Brain Excitation and Visual Perception. J Neurosci. 2011; 31(33):11889–93. https://doi.org/10.1523/JNEUROSCI.1161-11.2011 WOS:000293950300016. PMID: 21849549

79. Lange J, Oostenveld R, Fries P. Reduced Occipital Alpha Power Indexes Enhanced Excitability Rather than Improved Visual Perception. J Neurosci. 2013; 33(7):3212–20. https://doi.org/10.1523/JNEUROSCI.3755-12.2013 WOS:000314887200042. PMID: 23407974

80. Romei V, Rihs T, Brodbeck V, Thut G. Resting electroencephalogram alpha-power over posterior sites indexes baseline visual cortex excitability. Neuroreport. 2008; 19(2):203–8. https://doi.org/10.1097/WNR.0b013e3282f454c4 WOS:000252645000014. PMID: 18185109

81. Romei V, Brodbeck V, Michel C, Amedi A, Pascual-Leone A, Thut G. Spontaneous fluctuations in posterior alpha-band EEG activity reflect variability in excitability of human visual areas. Cereb Cortex. 2008; 18(9):2010–8. Epub 2007/12/21. https://doi.org/10.1093/cercor/bhm229 PMID: 18093905; PubMed Central PMCID: PMC2517102.

82. Misic B, Vakorin VA, Paus T, McIntosh AR. Functional embedding predicts the variability of neural activity. Front Syst Neurosci. 2011; 5:90. Epub 2011/12/14. https://doi.org/10.3389/fnsys.2011.00090 PMID: 22164135; PubMed Central PMCID: PMC3225043.

83. Deco G, Jirsa VK, McIntosh AR. Resting brains never rest: computational insights into potential cognitive architectures. Trends Neurosci. 2013; 36(5):268–74. Epub 2013/04/09. https://doi.org/10.1016/j.tins.2013.03.001 PMID: 23561718.

84. Deco G, Jirsa VK, McIntosh AR. Emerging concepts for the dynamical organization of resting-state activity in the brain. Nat Rev Neurosci. 2011; 12(1):43–56. Epub 2010/12/21. https://doi.org/10.1038/nrn2961 PMID: 21170073.

85. Pereda E, Gamundi A, Rial R, Gonzalez J. Non-linear behaviour of human EEG: fractal exponent versus correlation dimension in awake and sleep stages. Neurosci Lett. 1998; 250(2):91–4. Epub 1998/08/11. https://doi.org/10.1016/s0304-3940(98)00435-2 PMID: 9697926.

86. Heisz JJ, Gould M, McIntosh AR. Age-related Shift in Neural Complexity Related to Task Performance and Physical Activity. J Cognitive Neurosci. 2015; 27(3):605–13. https://doi.org/10.1162/jocn_a_00725 WOS:000349078000015. PMID: 25244121

87. Murray JD, Bernacchia A, Freedman DJ, Romo R, Wallis JD, Cai XY, et al. A hierarchy of intrinsic timescales across primate cortex. Nat Neurosci. 2014; 17(12):1661–3. https://doi.org/10.1038/nn.3862 WOS:000345484000012. PMID: 25383900

88. Duarte R, Seeholzer A, Zilles K, Morrison A. Synaptic patterning and the timescales of cortical dynamics. Curr Opin Neurobiol. 2017; 43:156–65. https://doi.org/10.1016/j.conb.2017.02.007 WOS:000403424400021. PMID: 28407562

89. Sowell ER, Peterson BS, Thompson PM, Welcome SE, Henkenius AL, Toga AW. Mapping cortical change across the human life span. Nat Neurosci. 2003; 6(3):309–15. https://doi.org/10.1038/nn1008 WOS:000181178300020. PMID: 12548289

90. Raz N, Lindenberger U, Rodrigue KM, Kennedy KM, Head D, Williamson A, et al. Regional brain changes in aging healthy adults: General trends, individual differences and modifiers. Cereb Cortex. 2005; 15(11):1676–89. https://doi.org/10.1093/cercor/bhi044 WOS:000232595700003. PMID: 15703252

91. Bender AR, Volkle MC, Raz N. Differential aging of cerebral white matter in middle-aged and older adults: A seven-year follow-up. Neuroimage. 2016; 125:74–83. https://doi.org/10.1016/j.neuroimage.2015.10.030 WOS:000366647500008. PMID: 26481675

92. Tatti R, Haley MS, Swanson OK, Tselha T, Maffei A. Neurophysiology and Regulation of the Balance Between Excitation and Inhibition in Neocortical Circuits. Biol Psychiat. 2017; 81(10):821–31. https://doi.org/10.1016/j.biopsych.2016.09.017 WOS:000400335100003. PMID: 27865453

93. Hua TM, Kao CC, Sun QY, Li XR, Zhou YF. Decreased proportion of GABA neurons accompanies age-related degradation of neuronal function in cat striate cortex. Brain Research Bulletin. 2008; 75(1):119–25. https://doi.org/10.1016/j.brainresbull.2007.08.001 WOS:000252489900017. PMID: 18158105

94. Leventhal AG, Wang YC, Pu ML, Zhou YF, Ma YY. GABA and its agonists improved visual cortical function in senescent monkeys. Science. 2003; 300(5620):812–5. https://doi.org/10.1126/science.1082874 WOS:000182579800055. PMID: 12730605

95. Lalwani P, Gagnon H, Cassady K, Simmonite M, Peltier S, Seidler RD, et al. Neural distinctiveness declines with age in auditory cortex and is associated with auditory GABA levels. Neuroimage. 2019; 201. UNSP 116033 https://doi.org/10.1016/j.neuroimage.2019.116033 WOS:000487755700019. PMID: 31326572

96. Schliebs R, Arendt T. The cholinergic system in aging and neuronal degeneration. Behav Brain Res. 2011; 221(2):555–63. https://doi.org/10.1016/j.bbr.2010.11.058 WOS:000291282700021. PMID: 21145918

97. Li SC, Rieckmann A. Neuromodulation and aging: implications of aging neuronal gain control on cognition. Curr Opin Neurobiol. 2014; 29:148–58. https://doi.org/10.1016/j.conb.2014.07.009 WOS:000347128200021. PMID: 25064177

98. Mcnamara B, Wiesenfeld K. Theory of Stochastic Resonance. Phys Rev A. 1989; 39(9):4854–69. https://doi.org/10.1103/PhysRevA.39.4854 WOS:A1989U565300060. PMID: 9901841

99. Wiesenfeld K, Moss F. Stochastic Resonance and the Benefits of Noise—from Ice Ages to Crayfish and Squids. Nature. 1995; 373(6509):33–6. https://doi.org/10.1038/373033a0 WOS: A1995QA23900046. PMID: 7800036

100. McDonnell MD, Ward LM. The benefits of noise in neural systems: bridging theory and experiment. Nat Rev Neurosci. 2011; 12(7):415–26. Epub 2011/06/21. https://doi.org/10.1038/nrn3061 PMID: 21685932.

101. MacDonald SWS, Nyberg L, Backman L. Intra-individual variability in behavior: links to brain structure, neurotransmission and neuronal activity. Trends in Neurosciences. 2006; 29(8):474–80. https://doi.org/10.1016/j.tins.2006.06.011 WOS:000240184400007. PMID: 16820224

102. Voytek B, Knight RT. Dynamic Network Communication as a Unifying Neural Basis for Cognition, Development, Aging, and Disease. Biol Psychiat. 2015; 77(12):1089–97. https://doi.org/10.1016/j.biopsych.2015.04.016 WOS:000355138500011. PMID: 26005114

103. Ishii R, Canuet L, Aoki Y, Hata M, Iwase M, Ikeda S, et al. Healthy and Pathological Brain Aging: From the Perspective of Oscillations, Functional Connectivity, and Signal Complexity. Neuropsychobiology. 2017; 75(4):151–61. Epub 2018/02/22. https://doi.org/10.1159/000486870 PMID: 29466802.

104. Caplan JB, Bottomley M, Kang P, Dixon RA. Distinguishing rhythmic from non-rhythmic brain activity during rest in healthy neurocognitive aging. Neuroimage. 2015; 112:341–52. Epub 2015/03/15. https://doi.org/10.1016/j.neuroimage.2015.03.001 PMID: 25769279; PubMed Central PMCID: PMC4408255.

105. Rossiter HE, Davis EM, Clark EV, Boudrias MH, Ward NS. Beta oscillations reflect changes in motor cortex inhibition in healthy ageing. Neuroimage. 2014; 91:360–5. Epub 2014/01/21. https://doi.org/10.1016/j.neuroimage.2014.01.012 PMID: 24440529; PubMed Central PMCID: PMC3988925.

106. Cole S, Voytek B. Cycle-by-cycle analysis of neural oscillations. J Neurophysiol. 2019; 122(2):849–61. Epub 2019/07/04. https://doi.org/10.1152/jn.00273.2019 PMID: 31268801.

107. Linkenkaer-Hansen K, Nikouline VV, Palva JM, Ilmoniemi RJ. Long-range temporal correlations and scaling behavior in human brain oscillations. J Neurosci. 2001; 21(4):1370–7. WOS:000166819700034. https://doi.org/10.1523/JNEUROSCI.21-04-01370.2001 PMID: 11160408

108. Mahjoory K, Cesnaite E, Hohlefeld FU, Villringer A, Nikulin VV. Power and temporal dynamics of alpha oscillations at rest differentiate cognitive performance involving sustained and phasic cognitive control. Neuroimage. 2019; 188:135–44. https://doi.org/10.1016/j.neuroimage.2018.12.001 WOS:000460064700012. PMID: 30517844

109. Hardstone R, Poil SS, Schiavone G, Jansen R, Nikulin VV, Mansvelder HD, et al. Detrended fluctuation analysis: a scale-free view on neuronal oscillations. Frontiers in Physiology. 2012; 3. ARTN 450 https://doi.org/10.3389/fphys.2012.00450 WOS:000209173000440. PMID: 23226132

110. Wu SD, Wu CW, Lin SG, Lee KY, Peng CK. Analysis of complex time series using refined composite multiscale entropy. Phys Lett A. 2014; 378(20):1369–74. https://doi.org/10.1016/j.physleta.2014.03.034 WOS:000335704900007.

111. Heisz JJ, Shedden JM, McIntosh AR. Relating brain signal variability to knowledge representation. Neuroimage. 2012; 63(3):1384–92. https://doi.org/10.1016/j.neuroimage.2012.08.018 WOS:000310379100040. PMID: 22906786

112. Lippe S, Kovacevic N, McIntosh AR. Differential maturation of brain signal complexity in the human auditory and visual system. Front Hum Neurosci. 2009;3. https://doi.org/10.3389/neuro.09.003.2009 WOS:000274619300008.

113. Mizuno T, Takahashi T, Cho RY, Kikuchi M, Murata T, Takahashi K, et al. Assessment of EEG dynamical complexity in Alzheimer's disease using multiscale entropy. Clin Neurophysiol. 2010; 121(9):1438–46. https://doi.org/10.1016/j.clinph.2010.03.025 WOS:000280555400007. PMID: 20400371

114. Szostakiwskyj JMH, Willatt SE, Cortese F, Protzner AB. The modulation of EEG variability between internally-and externally-driven cognitive states varies with maturation and task performance. Plos One. 2017; 12(7). https://doi.org/10.1371/journal.pone.0181894 WOS:000406575700098. PMID: 28750035

115. Takahashi T, Cho RY, Murata T, Mizuno T, Kikuchi M, Mizukami K, et al. Age-related variation in EEG complexity to photic stimulation: A multiscale entropy analysis. Clin Neurophysiol. 2009; 120(3):476–83. https://doi.org/10.1016/j.clinph.2008.12.043 WOS:000265772400006. PMID: 19231279

116. Carpentier SM, McCulloch AR, Brown TM, Faber SEM, Ritter P, Wang Z, et al. Complexity Matching: Brain Signals Mirror Environment Information Patterns during Music Listening and Reward. J Cognitive Neurosci. 2020; 32(4):734–45. https://doi.org/10.1162/jocn_a_01508 WOS:000520063300012. PMID: 31820677

117. Raja Beharelle A, Kovacevic N, McIntosh AR, Levine B. Brain signal variability relates to stability of behavior after recovery from diffuse brain injury. Neuroimage. 2012; 60(2):1528–37. Epub 2012/01/21. https://doi.org/10.1016/j.neuroimage.2012.01.037 22261371; PubMed Central PMCID: PMC3303989. PMID: 22261371

118. Catarino A, Churches O, Baron-Cohen S, Andrade A, Ring H. Atypical EEG complexity in autism spectrum conditions: A multiscale entropy analysis. Clin Neurophysiol. 2011; 122(12):2375–83. https://doi.org/10.1016/j.clinph.2011.05.004 WOS:000296583000008. PMID: 21641861

119. Misic B, Doesburg SM, Fatima Z, Vidal J, Vakorin VA, Taylor MJ, et al. Coordinated Information Generation and Mental Flexibility: Large-Scale Network Disruption in Children with Autism. Cereb Cortex. 2015; 25(9):2815–27. https://doi.org/10.1093/cercor/bhu082 WOS:000361464000042. PMID: 24770713

120. Ueno K, Takahashi T, Takahashi K, Mizukami K, Tanaka Y, Wada Y. Neurophysiological basis of creativity in healthy elderly people: A multiscale entropy approach. Clin Neurophysiol. 2015; 126(3):524–31. https://doi.org/10.1016/j.clinph.2014.06.032 WOS:000349616700015. PMID: 25066939

121. Kloosterman NA, Kosciessa JQ, Lindenberger U, Fahrenfort JJ, Garrett DD. Boosting Brain Signal Variability Underlies Liberal Shifts in Decision Bias. bioRxiv. 2019.

122. Theiler J, Eubank S, Longtin A, Galdrikian B, Farmer JD. Testing for Nonlinearity in Time-Series—the Method of Surrogate Data. Physica D. 1992; 58(1–4):77–94. https://doi.org/10.1016/0167-2789(92)90102-S WOS:A1992JV85800006.

123. Garrett DD, Grandy TH, Werkle-Bergner M. The neural forest and the trees: On distinguishing the variance of a brain signal from its information content. Annual Alpine Brain Imaging Meeting; Champéry, Switzerland2014.

124. Grandy TH, Garrett DD, Lindenberger U, Werkle-Bergner M. Exploring the limits of complexity measures for the analysis of age differences in neural signals. Dallas Aging and Cognition Conference; Dallas, TX, USA2013.

125. Takens F. Detecting Nonlinearities in Stationary Time Series. Int J Bifurcat Chaos. 1993; 3(2):241–56. https://doi.org/10.1142/S0218127493000192 WOS:000209750900002.

126. Simpraga S, Alvarez-Jimenez R, Mansvelder HD, van Gerven JMA, Groeneveld GJ, Poil SS, et al. EEG machine learning for accurate detection of cholinergic intervention and Alzheimer's disease. Sci Rep-Uk. 2017; 7. https://doi.org/10.1038/s41598-017-06165-4 WOS:000405746500086. PMID: 28720796

127. Stoyanov M, Gunzburger M, Burkardt J. Pink noise, 1/f (alpha) noise, and their effect on solutions of differential equations. Int J Uncertain Quan. 2011; 1(3):257–78. https://doi.org/10.1615/Int.J.UncertaintyQuantification.2011003089 WOS:000209100100005.

128. Oldfield RC. The Assessment and Analysis of Handedness: The Edinburgh Inventory. Neuropsychologia. 1971; 9(1):97–113. https://doi.org/10.1016/0028-3932(71)90067-4 WOS:A1971J199600013. PMID: 5146491

129. Folstein MF, Robins LN, Helzer JE. The Mini-Mental State Examination. Arch Gen Psychiat. 1983; 40(7):812–. WOS:A1983QX57000014. https://doi.org/10.1001/archpsyc.1983.01790060110016 PMID: 6860082

130. Kessler J, Markowitsch H, Denzler P. Mini-mental-status-test (MMST). Göttingen: Beltz Test GMBH; 2000.

131. Oostenveld R, Praamstra P. The five percent electrode system for high-resolution EEG and ERP measurements. Clin Neurophysiol. 2001; 112(4):713–9. https://doi.org/10.1016/s1388-2457(00)00527-7 WOS:000168113100018. PMID: 11275545

132. Oostenveld R, Fries P, Maris E, Schoffelen JM. FieldTrip: Open Source Software for Advanced Analysis of MEG, EEG, and Invasive Electrophysiological Data. Comput Intel Neurosc. 2011. https://doi.org/10.1155/2011/156869 WOS:000208906100004. PMID: 21253357

133. Bell AJ, Sejnowski TJ. An Information Maximization Approach to Blind Separation and Blind Deconvolution. Neural Comput. 1995; 7(6):1129–59. https://doi.org/10.1162/neco.1995.7.6.1129 WOS:A1995RZ70200001. PMID: 7584893

134. Nolan H, Whelan R, Reilly RB. FASTER: Fully Automated Statistical Thresholding for EEG artifact Rejection. J Neurosci Meth. 2010; 192(1):152–62. https://doi.org/10.1016/j.jneumeth.2010.07.015 WOS:000283477500020. PMID: 20654646

135. Perrin F, Pernier J, Bertrand O, Echallier JF. Spherical Splines for Scalp Potential and Current-Density Mapping. Electroen Clin Neuro. 1989; 72(2):184–7. https://doi.org/10.1016/0013-4694(89)90180-6 WOS:A1989T157400011.

136. Heisz JJ, McIntosh AR. Applications of EEG Neuroimaging Data: Event-related Potentials, Spectral Power, and Multiscale Entropy. Jove-Journal of Visualized Experiments. 2013;(76). https://doi.org/10.3791/50131 WOS:000209227800013. PMID: 23851571

137. Semmlow JL. Biosignal and medical image processing: CRC press; 2008.

138. Widmann A, Schroger E, Maess B. Digital filter design for electrophysiological data—a practical approach. J Neurosci Meth. 2015; 250:34–46. https://doi.org/10.1016/j.jneumeth.2014.08.002 WOS:000356978900005.

139. Jones SR. When brain rhythms aren't 'rhythmic': implication for their mechanisms and meaning. Curr Opin Neurobiol. 2016; 40:72–80. https://doi.org/10.1016/j.conb.2016.06.010 WOS:000386405800012. PMID: 27400290

140. Caplan JB, Madsen JR, Raghavachari S, Kahana MJ. Distinct patterns of brain oscillations underlie two basic parameters of human maze learning. J Neurophysiol. 2001; 86(1):368–80. WOS:000169955100033. https://doi.org/10.1152/jn.2001.86.1.368 PMID: 11431517

141. Whitten TA, Hughes AM, Dickson CT, Caplan JB. A better oscillation detection method robustly extracts EEG rhythms across brain state changes: The human alpha rhythm as a test case. Neuroimage. 2011; 54(2):860–74. https://doi.org/10.1016/j.neuroimage.2010.08.064 WOS:000285486000013. PMID: 20807577

142. Maris E, Oostenveld R. Nonparametric statistical testing of EEG- and MEG-data. J Neurosci Meth. 2007; 164(1):177–90. https://doi.org/10.1016/j.jneumeth.2007.03.024 WOS:000248170300019. PMID: 17517438

143. Lakens D. Calculating and reporting effect sizes to facilitate cumulative science: a practical primer for t-tests and ANOVAs. Front Psychol. 2013; 4. https://doi.org/10.3389/fpsyg.2013.00863 WOS:000331576200001. PMID: 24324449

144. Brandner FA. A test of the significance of the difference of the correlation coefficients in normal bivariate samples. Biometrika. 1933; 25:102–9. https://doi.org/10.1093/biomet/25.1–2.102 WOS:000200863000008.

145. Allen EA, Erhardt EB, Calhoun VD. Data Visualization in the Neurosciences: Overcoming the Curse of Dimensionality. Neuron. 2012; 74(4):603–8. https://doi.org/10.1016/j.neuron.2012.05.001 WOS:000304747200004. PMID: 22632718

Supplementary Information for

Standard multiscale entropy reflects neural dynamics at mismatched temporal scales

Julian Q. Kosciessa, Niels A. Kloosterman, and Douglas D. Garrett

Email: kosciessa@mpib-berlin.mpg.de; garrett@mpib-berlin.mpg.de

S1 Text. Systematic literature search assessing the prevalence of global similarity bounds.

We performed a systematic literature search to assess the prevalence of global similarity bounds in current neuroscientific applications (heart rate variability applications are specifically marked). We searched Pubmed (https://www.ncbi.nlm.nih.gov/pubmed) with the following terms: *(MSE AND sample entropy AND EEG) OR (MSE AND brain AND variability) OR (MSE AND EEG AND variability) OR (multiscale entropy AND EEG AND variability).* We excluded any studies that did not assess multiscale entropy, including studies that were restricted to sample entropy at scale 1. In addition, we added references from the main text that were not captured by the systematic search (highlighted in grey). For MSE applications, we checked the text for a notion of how similarity bounds were computed, i.e., whether it was calculated as r*SD of the original time series or the coarse-grained time series. The following sections list the results of this qualitative review and is purely intended to characterize the prevalence of global similarity bounds, not as a qualitative judgement on the claims made in any particular paper. Our literature search revealed the following papers. The relative amount of studies with presumably global similarity bounds was as follows (39+13)/(39+13+4) = 0,928; i.e., > 90%.

Scale-invariant similarity bounds (r x global SD)

We chose this category, when the article contained the specific information that r was calculated from the original signal (i.e., scale-invariant).

Azami, Fernandez, and Escudero (2017)
Azami, Rostaghi, Abasolo, and Escudero (2017)
Carpentier et al. (2019)
Escudero, Abasolo, Hornero, Espino, and Lopez (2006) [but they note the issue]
Grandy, Garrett, Schmiedek, and Werkle-Bergner (2016)
Hadoush, Alafeef, and Abdulhay (2019)
Kaur et al. (2019)
M. Liu, Song, Liang, Knopfel, and Zhou (2019)
H. Liu et al. (2017) [HRV]
Lu et al. (2015)
McIntosh, Kovacevic, and Itier (2008)
Mizuno et al. (2010)
Weng et al. (2015)

#: 13

Unclear, assumed scale-invariant similarity bounds (r x global SD)

We chose this category, when the article did not contain any information about how r was calculated, or no reference was made to scale-specific adaptations. For many papers, Costa, Goldberger, and Peng (2002, 2005) or Richman and Moorman (2000) were cited, which use scale-invariant implementations.

Raja Beharelle, Kovacevic, McIntosh, and Levine (2012)
Bertrand et al. (2016)
Catarino, Churches, Baron-Cohen, Andrade, and Ring (2011)
Chen et al. (2015)(HRV)

Chen et al. (2018) (HRV)
Li, Chen, Li, Wang, and Liu (2016)
Chiu et al. (2015) (HRV)
Courtiol et al. (2016)
Gao, Hu, Liu, and Cao (2015)
Harati, Crowell, Huang, Mayberg, and Nemati (2019)
Harati, Crowell, Mayberg, Jun, and Nemati (2016)
Hasegawa et al. (2018)
Heisz and McIntosh (2013)
Heisz, Shedden, and McIntosh (2012)
Hu and Liang (2012) [RM]
Hussain, Saeed, Awan, and Idris (2018)
Hussain, Aziz, et al. (2018)
Jaworska et al. (2018)
Kuntzelman, Jack Rhodes, Harrington, and Miskovic (2018)
Lin et al. (2019) [BOLD]
H. Liu et al. (2018)
H. Y. Liu et al. (2018)
Q. Liu, Chen, Fan, Abbod, and Shieh (2015)
Q. Liu, Chen, Fan, Abbod, and Shieh (2017)
McIntosh et al. (2014)
Misic et al. (2015)
Misic, Vakorin, Paus, and McIntosh (2011)
Miskovic, Owens, Kuntzelman, and Gibb (2016)
Park, Kim, Kim, Cichocki, and Kim (2007)
Roldan, Molina-Pico, Cuesta-Frau, Martinez, and Crespo (2011)
Szostakiwskyj, Willatt, Cortese, and Protzner (2017)
Takahashi et al. (2009)
Takahashi et al. (2010)
Takahashi et al. (2016)
Ueno et al. (2015)
Yang et al. (2013)
H. Y. Wang, McIntosh, Kovacevic, Karachalios, and Protzner (2016)
H. Wang, Pexman, Turner, Cortese, and Protzner (2018)
Wei et al. (2014)

#: 39

Scale-wise similarity bounds (r x scale-wise SD)
We chose this category, when the article either specified that scale-wise recalculation of r parameters was performed, or when the description could allow that inference.

Fabris et al. (2014) [but with unclear variations in r]
Sleimen-Malkoun et al. (2015)
Valencia et al. (2009) [HRV]
Zavala-Yoe, Ramirez-Mendoza, and Cordero (2015)

#: 4

Not applicable
We chose this category, when multi-scale entropy was not used in the study (i.e., erroneous listing of paper).

El-Gohary, McNames, and Elsas (2008)
Erdogan, Yucel, and Akin (2014)
Fernandez, Gomez, Hornero, and Lopez-Ibor (2013)
Heunis, Aldrich, and de Vries (2016)
Hier, Jao, and Brint (1994)
Kielar et al. (2016) [BOLD MSE, single scale]
Nazari et al. (2019)
Puce, Berkovic, Cadusch, and Bladin (1994)
Sinai, Phillips, Chertkow, and Kabani (2010)
Verhaeghe, Gravel, and Reader (2010)
Xu, Cui, Hong, and Liang (2015)

Supplementary References

Azami, H., Fernandez, A., & Escudero, J. (2017). Refined multiscale fuzzy entropy based on standard deviation for biomedical signal analysis. *Med Biol Eng Comput, 55*(11), 2037-2052. doi:10.1007/s11517-017-1647-5

Azami, H., Rostaghi, M., Abasolo, D., & Escudero, J. (2017). Refined Composite Multiscale Dispersion Entropy and its Application to Biomedical Signals. *Ieee Transactions on Biomedical Engineering, 64*(12), 2872-2879. doi:10.1109/tbme.2017.2679136

Bandt, C., & Pompe, B. (2002). Permutation entropy: A natural complexity measure for time series. *Physical Review Letters, 88*(17). doi:10.1103/PhysRevLett.88.174102

Bertrand, J. A., McIntosh, A. R., Postuma, R. B., Kovacevic, N., Latreille, V., Panisset, M., . . . Gagnon, J. F. (2016). Brain Connectivity Alterations Are Associated with the Development of Dementia in Parkinson's Disease. *Brain Connectivity, 6*(3), 216-224. doi:10.1089/brain.2015.0390

Carpentier, S. M., McCulloch, A. R., Brown, T. M., Ritter, P., Wang, Z., Salimpoor, V., . . . McIntosh, A. R. (2019). Complexity matching: brain signals mirror environment information patterns during music listening and reward. *bioRxiv*.

Catarino, A., Churches, O., Baron-Cohen, S., Andrade, A., & Ring, H. (2011). Atypical EEG complexity in autism spectrum conditions: A multiscale entropy analysis. *Clinical Neurophysiology, 122*(12), 2375-2383. doi:10.1016/j.clinph.2011.05.004

Chen, C. H., Huang, P. W., Tang, S. C., Shieh, J. S., Lai, D. M., Wu, A. Y., & Jeng, J. S. (2015). Complexity of Heart Rate Variability Can Predict Stroke-In-Evolution in Acute Ischemic Stroke Patients. *Sci Rep, 5*, 17552. doi:10.1038/srep17552

Chen, C. H., Tang, S. C., Lee, D. Y., Shieh, J. S., Lai, D. M., Wu, A. Y., & Jeng, J. S. (2018). Impact of Supratentorial Cerebral Hemorrhage on the Complexity of Heart Rate Variability in Acute Stroke. *Sci Rep, 8*(1), 11473. doi:10.1038/s41598-018-29961-y

Chiu, H. C., Lin, Y. H., Lo, M. T., Tang, S. C., Wang, T. D., Lu, H. C., . . . Peng, C. K. (2015). Complexity of cardiac signals for predicting changes in alpha-waves after stress in patients undergoing cardiac catheterization. *Scientific Reports, 5*. doi:10.1038/srep13315

Costa, M., Goldberger, A. L., & Peng, C. K. (2002). Multiscale entropy analysis of complex physiologic time series. *Physical Review Letters, 89*(6). doi:10.1103/PhysRevLett.89.068102

Costa, M., Goldberger, A. L., & Peng, C. K. (2005). Multiscale entropy analysis of biological signals. *Physical Review E, 71*(2). doi:10.1103/PhysRevE.71.021906

Courtiol, J., Perdikis, D., Petkoski, S., Muller, V., Huys, R., Sleimen-Malkoun, R., & Jirsa, V. K. (2016). The multiscale entropy: Guidelines for use and interpretation in brain signal analysis. *Journal of Neuroscience Methods, 273*, 175-190. doi:10.1016/j.jneumeth.2016.09.004

El-Gohary, M., McNames, J., & Elsas, S. (2008). User-guided interictal spike detection. *Conf Proc IEEE Eng Med Biol Soc, 2008*, 821-824. doi:10.1109/iembs.2008.4649280

Erdogan, S. B., Yucel, M. A., & Akin, A. (2014). Analysis of task-evoked systemic interference in fNIRS measurements: insights from fMRI. *Neuroimage, 87*, 490-504. doi:10.1016/j.neuroimage.2013.10.024

Escudero, J., Abasolo, D., Hornero, R., Espino, P., & Lopez, M. (2006). Analysis of electroencephalograms in Alzheimer's disease patients with multiscale entropy. *Physiological Measurement, 27*(11), 1091-1106. doi:10.1088/0967-3334/27/11/004

Fabris, C., Sparacino, G., Sejling, A. S., Goljahani, A., Duun-Henriksen, J., Remvig, L. S., . . . Cobelli, C. (2014). Hypoglycemia-Related Electroencephalogram Changes Assessed by Multiscale Entropy. *Diabetes Technology & Therapeutics, 16*(10), 688-694. doi:10.1089/dia.2013.0331

Fernandez, A., Gomez, C., Hornero, R., & Lopez-Ibor, J. J. (2013). Complexity and schizophrenia. *Prog Neuropsychopharmacol Biol Psychiatry, 45*, 267-276. doi:10.1016/j.pnpbp.2012.03.015

Gao, J., Hu, J., Liu, F., & Cao, Y. (2015). Multiscale entropy analysis of biological signals: a fundamental bi-scaling law. *Front Comput Neurosci, 9*, 64. doi:10.3389/fncom.2015.00064

Grandy, T. H., Garrett, D. D., Schmiedek, F., & Werkle-Bergner, M. (2016). On the estimation of brain signal entropy from sparse neuroimaging data. *Scientific Reports, 6*. doi:10.1038/srep23073

Hadoush, H., Alafeef, M., & Abdulhay, E. (2019). Brain Complexity in Children with Mild and Severe Autism Spectrum Disorders: Analysis of Multiscale Entropy in EEG. *Brain Topogr*. doi:10.1007/s10548-019-00711-1

Harati, S., Crowell, A., Huang, Y., Mayberg, H., & Nemati, S. (2019). Classifying Depression Severity in Recovery from Major Depressive Disorder via Dynamic Facial Features. *IEEE J Biomed Health Inform*. doi:10.1109/jbhi.2019.2930604

Harati, S., Crowell, A., Mayberg, H., Jun, K., & Nemati, S. (2016). Discriminating clinical phases of recovery from major depressive disorder using the dynamics of facial expression. *Conf Proc IEEE Eng Med Biol Soc, 2016*, 2254-2257. doi:10.1109/embc.2016.7591178

Hasegawa, C., Takahashi, T., Yoshimura, Y., Nobukawa, S., Ikeda, T., Saito, D. N., . . . Kikuchi, M. (2018). Developmental Trajectory of Infant Brain Signal Variability: A Longitudinal Pilot Study. *Front Neurosci, 12*, 566. doi:10.3389/fnins.2018.00566

Heisz, J. J., & McIntosh, A. R. (2013). Applications of EEG Neuroimaging Data: Event-related Potentials, Spectral Power, and Multiscale Entropy. *Jove-Journal of Visualized Experiments*(76). doi:10.3791/50131

Heisz, J. J., Shedden, J. M., & McIntosh, A. R. (2012). Relating brain signal variability to knowledge representation. *Neuroimage, 63*(3), 1384-1392. doi:10.1016/j.neuroimage.2012.08.018

Heunis, T. M., Aldrich, C., & de Vries, P. J. (2016). Recent Advances in Resting-State Electroencephalography Biomarkers for Autism Spectrum Disorder-A Review of Methodological and Clinical Challenges. *Pediatr Neurol, 61*, 28-37. doi:10.1016/j.pediatrneurol.2016.03.010

Hier, D. B., Jao, C. S., & Brint, S. U. (1994). The Mental Status Expert (MSE): an expert system for scoring and interpreting the mental status examination. *Proc Annu Symp Comput Appl Med Care*, 1053.

Hu, M., & Liang, H. (2012). Adaptive multiscale entropy analysis of multivariate neural data. *IEEE Trans Biomed Eng, 59*(1), 12-15. doi:10.1109/tbme.2011.2162511

Hussain, L., Aziz, W., Saeed, S., Shah, S. A., Nadeem, M. S. A., Awan, I. A., . . . Kazmi, S. Z. H. (2018). Quantifying the dynamics of electroencephalographic (EEG) signals to distinguish alcoholic and non-alcoholic subjects using an MSE based K-d tree algorithm. *Biomed Tech (Berl), 63*(4), 481-490. doi:10.1515/bmt-2017-0041

Hussain, L., Saeed, S., Awan, I. A., & Idris, A. (2018). Multiscaled Complexity Analysis of EEG Epileptic Seizure Using Entropy-Based Techniques. *Archives of Neuroscience, 5*(1). doi:10.5812/archneurosci.61161

Jaworska, N., Wang, H., Smith, D. M., Blier, P., Knott, V., & Protzner, A. B. (2018). Pre-treatment EEG signal variability is associated with treatment success in depression. *Neuroimage Clin, 17*, 368-377. doi:10.1016/j.nicl.2017.10.035

Kaur, Y., Ouyang, G., Junge, M., Sommer, W., Liu, M., Zhou, C., & Hildebrandt, A. (2019). The reliability and psychometric structure of Multi-Scale Entropy measured from EEG signals at rest and during face and object recognition tasks. *J Neurosci Methods, 326*, 108343. doi:10.1016/j.jneumeth.2019.108343

Kielar, A., Deschamps, T., Chu, R. K., Jokel, R., Khatamian, Y. B., Chen, J. J., & Meltzer, J. A. (2016). Identifying Dysfunctional Cortex: Dissociable Effects of Stroke and Aging on Resting State Dynamics in MEG and fMRI. *Front Aging Neurosci, 8*, 40. doi:10.3389/fnagi.2016.00040

Kuntzelman, K., Jack Rhodes, L., Harrington, L. N., & Miskovic, V. (2018). A practical comparison of algorithms for the measurement of multiscale entropy in neural time series data. *Brain Cogn, 123*, 126-135. doi:10.1016/j.bandc.2018.03.010

Li, C. X., Chen, Y. N., Li, Y. J., Wang, J., & Liu, T. (2016). Complexity analysis of brain activity in attention-deficit/hyperactivity disorder: A multiscale entropy analysis. *Brain Research Bulletin, 124*, 12-20. doi:10.1016/j.brainresbull.2016.03.007

Lin, C., Lee, S. H., Huang, C. M., Chen, G. Y., Ho, P. S., Liu, H. L., . . . Wu, S. C. (2019). Increased brain entropy of resting-state fMRI mediates the relationship between depression severity and mental health-related quality of life in late-life depressed elderly. *J Affect Disord, 250*, 270-277. doi:10.1016/j.jad.2019.03.012

Liu, H., Yang, Z., Meng, F., Guan, Y., Ma, Y., Liang, S., . . . Li, L. (2017). Impairment of heart rhythm complexity in patients with drug-resistant epilepsy: An assessment with multiscale entropy analysis. *Epilepsy Research, 138*, 11-17. doi:10.1016/j.eplepsyres.2017.10.002

Liu, H., Yang, Z., Meng, F., Huang, L., Qu, W., Hao, H., . . . Li, L. (2018). Chronic vagus nerve stimulation reverses heart rhythm complexity in patients with drug-resistant epilepsy: An assessment with multiscale entropy analysis. *Epilepsy Behav, 83*, 168-174. doi:10.1016/j.yebeh.2018.03.035

Liu, H. Y., Yang, Z., Meng, F. G., Guan, Y. G., Ma, Y. S., Liang, S. L., . . . Li, L. M. (2018). Preoperative Heart Rate Variability as Predictors of Vagus Nerve Stimulation Outcome in Patients with Drug-resistant Epilepsy. *Sci Rep, 8*(1), 3856. doi:10.1038/s41598-018-21669-3

Liu, M., Song, C., Liang, Y., Knopfel, T., & Zhou, C. (2019). Assessing spatiotemporal variability of brain spontaneous activity by multiscale entropy and functional connectivity. *Neuroimage, 198*, 198-220. doi:10.1016/j.neuroimage.2019.05.022

Liu, Q., Chen, Y. F., Fan, S. Z., Abbod, M. F., & Shieh, J. S. (2015). EEG Signals Analysis Using Multiscale Entropy for Depth of Anesthesia Monitoring during Surgery through Artificial Neural Networks. *Computational and Mathematical Methods in Medicine*. doi:10.1155/2015/232381

Liu, Q., Chen, Y. F., Fan, S. Z., Abbod, M. F., & Shieh, J. S. (2017). EEG artifacts reduction by multivariate empirical mode decomposition and multiscale entropy for monitoring depth of

anaesthesia during surgery. *Medical & Biological Engineering & Computing, 55*(8), 1435-1450. doi:10.1007/s11517-016-1598-2

Lu, W. Y., Chen, J. Y., Chang, C. F., Weng, W. C., Lee, W. T., & Shieh, J. S. (2015). Multiscale Entropy of Electroencephalogram as a Potential Predictor for the Prognosis of Neonatal Seizures. *Plos One, 10*(12). doi:10.1371/journal.pone.0144732

McIntosh, A. R., Kovacevic, N., & Itier, R. J. (2008). Increased Brain Signal Variability Accompanies Lower Behavioral Variability in Development. *Plos Computational Biology, 4*(7). doi:10.1371/journal.pcbi.1000106

McIntosh, A. R., Vakorin, V., Kovacevic, N., Wang, H., Diaconescu, A., & Protzner, A. B. (2014). Spatiotemporal Dependency of Age-Related Changes in Brain Signal Variability. *Cerebral Cortex, 24*(7), 1806-1817. doi:10.1093/cercor/bht030

Misic, B., Doesburg, S. M., Fatima, Z., Vidal, J., Vakorin, V. A., Taylor, M. J., & McIntosh, A. R. (2015). Coordinated Information Generation and Mental Flexibility: Large-Scale Network Disruption in Children with Autism. *Cerebral Cortex, 25*(9), 2815-2827. doi:10.1093/cercor/bhu082

Misic, B., Vakorin, V. A., Paus, T., & McIntosh, A. R. (2011). Functional embedding predicts the variability of neural activity. *Frontiers in Systems Neuroscience, 5*, 90. doi:10.3389/fnsys.2011.00090

Miskovic, V., Owens, M., Kuntzelman, K., & Gibb, B. E. (2016). Charting moment-to-moment brain signal variability from early to late childhood. *Cortex, 83*, 51-61. doi:10.1016/j.cortex.2016.07.006

Mizuno, T., Takahashi, T., Cho, R. Y., Kikuchi, M., Murata, T., Takahashi, K., & Wada, Y. (2010). Assessment of EEG dynamical complexity in Alzheimer's disease using multiscale entropy. *Clinical Neurophysiology, 121*(9), 1438-1446. doi:10.1016/j.clinph.2010.03.025

Nazari, A., Alavimajd, H., Shakeri, N., Bakhshandeh, M., Faghihzadeh, E., & Marzbani, H. (2019). Prediction of Brain Connectivity Map in Resting-State fMRI Data Using Shrinkage Estimator. *Basic Clin Neurosci, 10*(2), 147-156. doi:10.32598/bcn.9.10.140

Ouyang, G. X., Li, J., Liu, X. Z., & Li, X. L. (2013). Dynamic characteristics of absence EEG recordings with multiscale permutation entropy analysis. *Epilepsy Research, 104*(3), 246-252. doi:10.1016/j.eplepsyres.2012.11.003

Park, J. H., Kim, S., Kim, C. H., Cichocki, A., & Kim, K. (2007). Multiscale entropy analysis of EEG from patients under different pathological conditions. *Fractals-Complex Geometry Patterns and Scaling in Nature and Society, 15*(4), 399-404. doi:10.1142/S0218348x07003691

Puce, A., Berkovic, S. F., Cadusch, P. J., & Bladin, P. F. (1994). P3 latency jitter assessed using 2 techniques. I. Simulated data and surface recordings in normal subjects. *Electroencephalogr Clin Neurophysiol, 92*(4), 352-364. doi:10.1016/0168-5597(94)90103-1

Raja Beharelle, A., Kovacevic, N., McIntosh, A. R., & Levine, B. (2012). Brain signal variability relates to stability of behavior after recovery from diffuse brain injury. *Neuroimage, 60*(2), 1528-1537. doi:10.1016/j.neuroimage.2012.01.037

Richman, J. S., & Moorman, J. R. (2000). Physiological time-series analysis using approximate entropy and sample entropy. *American Journal of Physiology-Heart and Circulatory Physiology, 278*(6), H2039-H2049.

Riedl, M., Muller, A., & Wessel, N. (2013). Practical considerations of permutation entropy. *European Physical Journal-Special Topics, 222*(2), 249-262. doi:10.1140/epjst/e2013-01862-7

Roldan, E. M., Molina-Pico, A., Cuesta-Frau, D., Martinez, P. M., & Crespo, S. O. (2011). Characterization of entropy measures against data loss: application to EEG records. *Conf Proc IEEE Eng Med Biol Soc, 2011*, 6110-6113. doi:10.1109/iembs.2011.6091509

Sinai, M., Phillips, N. A., Chertkow, H., & Kabani, N. J. (2010). Task switching performance reveals heterogeneity amongst patients with mild cognitive impairment. *Neuropsychology, 24*(6), 757-774. doi:10.1037/a0020314

Sleimen-Malkoun, R., Perdikis, D., Muller, V., Blanc, J. L., Huys, R., Temprado, J. J., & Jirsa, V. K. (2015). Brain Dynamics of Aging: Multiscale Variability of EEG Signals at Rest and during an Auditory Oddball Task(1,2,3). *Eneuro, 2*(3). doi:10.1523/ENEURO.0067-14.2015

Szostakiwskyj, J. M. H., Willatt, S. E., Cortese, F., & Protzner, A. B. (2017). The modulation of EEG variability between internally-and externally-driven cognitive states varies with maturation and task performance. *Plos One, 12*(7). doi:10.1371/journal.pone.0181894

Takahashi, T., Cho, R., Mizuno, T., Kikuchi, M., Murata, T., Takahashi, K., & Wada, Y. (2010). Antipsychotics reverse abnormal EEG complexity in drug-naive schizophrenia: A multiscale entropy analysis. *International Journal of Neuropsychopharmacology, 13*, 242-243.

Takahashi, T., Cho, R. Y., Murata, T., Mizuno, T., Kikuchi, M., Mizukami, K., . . . Wada, Y. (2009). Age-related variation in EEG complexity to photic stimulation: A multiscale entropy analysis. *Clinical Neurophysiology, 120*(3), 476-483. doi:10.1016/j.clinph.2008.12.043

Takahashi, T., Yoshimura, Y., Hiraishi, H., Hasegawa, C., Munesue, T., Higashida, H., . . . Kikuchi, M. (2016). Enhanced brain signal variability in children with autism spectrum disorder during early childhood. *Human Brain Mapping, 37*(3), 1038-1050. doi:10.1002/hbm.23089

Ueno, K., Takahashi, T., Takahashi, K., Mizukami, K., Tanaka, Y., & Wada, Y. (2015). Neurophysiological basis of creativity in healthy elderly people: A multiscale entropy approach. *Clinical Neurophysiology, 126*(3), 524-531. doi:10.1016/j.clinph.2014.06.032

Valencia, J. F., Porta, A., Vallverdu, M., Claria, F., Baranowski, R., Orlowska-Baranowska, E., & Caminal, P. (2009). Refined Multiscale Entropy: Application to 24-h Holter Recordings of Heart Period Variability in Healthy and Aortic Stenosis Subjects. *Ieee Transactions on Biomedical Engineering, 56*(9), 2202-2213. doi:10.1109/Tbme.2009.2021986

Verhaeghe, J., Gravel, P., & Reader, A. J. (2010). Task-oriented quantitative image reconstruction in emission tomography for single- and multi-subject studies. *Phys Med Biol, 55*(23), 7263-7285. doi:10.1088/0031-9155/55/23/006

Wang, H., Pexman, P. M., Turner, G., Cortese, F., & Protzner, A. B. (2018). The relation between Scrabble expertise and brain aging as measured with EEG brain signal variability. *Neurobiology of Aging, 69*, 249-260. doi:10.1016/j.neurobiolaging.2018.05.015

Wang, H. Y., McIntosh, A. R., Kovacevic, N., Karachalios, M., & Protzner, A. B. (2016). Age-related Multiscale Changes in Brain Signal Variability in Pre-task versus Post-task Resting-state EEG. *Journal of Cognitive Neuroscience, 28*(7), 971-984. doi:10.1162/jocn_a_00947

Wei, Q., Li, Y., Fan, S. Z., Liu, Q., Abbod, M. F., Lu, C. W., . . . Shieh, J. S. (2014). A critical care monitoring system for depth of anaesthesia analysis based on entropy analysis and physiological information database. *Australasian Physical & Engineering Sciences in Medicine, 37*(3), 591-605. doi:10.1007/s13246-014-0285-6

Weng, W. C., Jiang, G. J., Chang, C. F., Lu, W. Y., Lin, C. Y., Lee, W. T., & Shieh, J. S. (2015). Complexity of Multi-Channel Electroencephalogram Signal Analysis in Childhood Absence Epilepsy. *Plos One, 10*(8), e0134083. doi:10.1371/journal.pone.0134083

Xu, Y., Cui, J., Hong, W., & Liang, H. (2015). [Automatic Classification of Epileptic Electroencephalogram Signal Based on Improved Multivariate Multiscale Entropy]. *Sheng Wu Yi Xue Gong Cheng Xue Za Zhi, 32*(2), 256-262.

Yang, A. C., Wang, S. J., Lai, K. L., Tsai, C. F., Yang, C. H., Hwang, J. P., . . . Fuh, J. L. (2013). Cognitive and neuropsychiatric correlates of EEG dynamic complexity in patients with Alzheimer's disease. *Progress in Neuro-Psychopharmacology & Biological Psychiatry, 47*, 52-61. doi:10.1016/j.pnpbp.2013.07.022

Zanin, M., Zunino, L., Rosso, O. A., & Papo, D. (2012). Permutation Entropy and Its Main Biomedical and Econophysics Applications: A Review. *Entropy, 14*(8), 1553-1577. doi:10.3390/e14081553

Zavala-Yoe, R., Ramirez-Mendoza, R., & Cordero, L. M. (2015). Novel way to investigate evolution of children refractory epilepsy by complexity metrics in massive information. *Springerplus, 4*. doi:10.1186/s40064-015-1173-6

Supplementary Information for

Standard multiscale entropy reflects neural dynamics at mismatched temporal scales

Julian Q. Kosciessa, Niels A. Kloosterman, and Douglas D. Garrett

Email: kosciessa@mpib-berlin.mpg.de; garrett@mpib-berlin.mpg.de

S2 Text. Simulation of MSE's sensitivity to PSD slope variation.

Our simulations have focused on narrowband rhythmicity as one contributor to time series irregularity. However, MSE is theoretically sensitive to many features that add alter the irregularity of time series, with fixed 1/f slopes. Due to the assumed contribution of variations in autocorrelative structure to signal irregularity, we systematically assessed the impact of variations in pink noise on MSE. For this purpose, we simulated 100 trials of 8 s segments with unit variance and varying pink noise ($\frac{1}{f^x}, x = [.5, 1, 1.2, 1.5]$) as generated using the function f_alpha_gaussian (Stoyanov, Gunzburger, & Burkardt, 2011).

Previous simulations of the impact of varying slopes on 'Original' MSE have produced a multi-scale sensitivity that we consider counterintuitive (e.g., Courtiol et al., 2016; Miskovic, Owens, Kuntzelman, & Gibb, 2016). For white noise signals (x = 0), entropy decreases have been observed towards coarser scales, opposing the notion of 'scale-free' randomness. We and others (Nikulin & Brismar, 2004) argue that this results from increasingly mismatched similarity bounds. Our results closely replicate the traditional observations of scale-dependent entropy crossovers in 'Original' implementations (S7 Figure A), while adding that adequate scale-wise implementation of similarity bounds eliminates such cross-over effects (S7 Figure BC), and instead differentiates different autocorrelative structures by constant offsets in sample entropy (S7 Figure BCD). This result more closely reflects the notion of 'scale-free' irregularity. Notably, a bandpass implementation loses sensitivity to such broadband effects, as narrowband-filtered irregularity is equal across varying slopes (S7 Figure E).

Supplementary References

Courtiol, J., Perdikis, D., Petkoski, S., Muller, V., Huys, R., Sleimen-Malkoun, R., & Jirsa, V. K. (2016). The multiscale entropy: Guidelines for use and interpretation in brain signal analysis. *Journal of Neuroscience Methods, 273*, 175-190. doi:10.1016/j.jneumeth.2016.09.004

Miskovic, V., Owens, M., Kuntzelman, K., & Gibb, B. E. (2016). Charting moment-to-moment brain signal variability from early to late childhood. *Cortex, 83*, 51-61. doi:10.1016/j.cortex.2016.07.006

Nikulin, V. V., & Brismar, T. (2004). Comment on "Multiscale entropy analysis of complex physiologic time series". *Physical Review Letters, 92*(8). doi:10.1103/PhysRevLett.92.089803

Stoyanov, M., Gunzburger, M., & Burkardt, J. (2011). Pink noise, 1/f (alpha) noise, and their effect on solutions of differential equations. *International Journal for Uncertainty Quantification, 1*(3), 257-278. doi:10.1615/Int.J.UncertaintyQuantification.2011003089

Supplementary Information for

Standard multiscale entropy reflects neural dynamics at mismatched temporal scales

Julian Q. Kosciessa, Niels A. Kloosterman, and Douglas D. Garrett

Email: kosciessa@mpib-berlin.mpg.de; garrett@mpib-berlin.mpg.de

S3 Text. Surrogate analysis of age effects.

The use of multiscale entropy is at least in part motivated by its partial sensitivity to multi-scale, potentially non-linear, signal characteristics, such as phase shifts or cross-frequency coupling. However, the contribution of non-linear characteristics to MSE estimates and modulations thereof is unclear in practice. A principled way to dissociate non-linear signal characteristics from linear signal variance is to use phase-shuffled surrogate data (Garrett, Grandy, & Werkle-Bergner, 2014; Grandy, Garrett, Lindenberger, & Werkle-Bergner, 2013; McIntosh, Kovacevic, & Itier, 2008; Stam, 2005; Takens, 1993; Theiler, Eubank, Longtin, Galdrikian, & Farmer, 1992; Vakorin & McIntosh, 2012).

To probe whether linear contributions were sufficient to explain the main MSE age effects observed in our study, we created surrogate data and estimated 'Original' MSE – including a presumed similarity bound bias – as well as the low-pass variant that matches similarity bounds to the standard deviation of scale-specific signals. In line with previous surrogate analyses for entropy applications (Miskovic, MacDonald, Rhodes, & Cote, 2019), we used an iterated amplitude-adjusted Fourier transform (IAAFT), which minimizes the spurious detection of nonlinearity (Schreiber & Schmitz, 1996). In short, the IAAFT produces surrogate data with random phases, while the power spectrum and value distribution are iteratively approximated to the original data (for an example see S9 Figure A). We separately generated surrogate time series for each subject, channel and pseudo-trial, using a maximum number of 100 iterations until convergence.

Results in S9 Figure show that the surrogate data can recover the main age effects presented in Fig 7 A and C, indicating that linear properties are sufficient to account for the main age effects observed in the original data. This result coheres with a similar surrogate analysis of age effects in resting state data (Courtiol et al., 2016) and suggests at best limited non-linear contributions that were not necessary for the indicated age differences. However, this does not answer the question whether there are also age effects in non-linear contributions after controlling for linear characteristics. To answer this question, we calculated a surrogate ratio score as $\frac{MSE\ (original)}{MSE\ (surrogate)}$, in line with previous surrogate analyses (Miskovic et al., 2019; Schartner et al., 2017). While a score of 1 would indicate the absence of structured information, lower values suggest the presence of non-linear structure in the original data relative to the random structure of surrogates. In contrast with MSE for surrogates or original data only, this ratio indicated similar scale-dependent patterns across 'Original' and low-pass variants in average traces (S9 Figure D, E). At face value, average traces hinted at age-related increases in posterior fine-scale entropy, and age-related decreases in frontal coarse-scale entropy, in line with prior proposals of a shift from global-to-local processing with increased adult age (McIntosh, 2019). However, no significant clusters were indicated via cluster-based permutation tests at traditional thresholds (two-sided p = .025). Even relaxing two-sided significance thresholds to p = .1 only led to the indication of decreased sample entropy with age exclusively at very fine scales and central channels (not shown). We further assessed the correspondence of linear and non-linear effects to the 'Original' MSE age differences in fine- and coarse-scale clusters in the original data. We assessed t-value ratios to evaluate relative effect sizes. We exclusively probed results from the 'Original' implementation given that non-linear results were comparable across implementations. Linear contributions were approximated by t-values for the surrogate data, whereas non-linear contributions were estimated by t-values of the original/surrogate ratio, averaged within the fine- and coarse scale clusters. Linear contributions, approximated by t-values for the surrogate data, accounted for 98% of the original fine-scale effect size and 99% for the coarse-scale effect size. In stark contrast, non-linear contributions captured only .1 % of the original fine-scale effect size, and 20% of the coarse-scale effect size. These results underline that the evaluation of non-linear contributions requires stringent control for linear PSD properties to

evaluate. Smaller (potentially under-powered) non-linear contributions to age effects are further in line with previous surrogate analyses. Crucially, the absence of significant effects suggests that more statistical power is necessary to indicate smaller non-linear effects of interest in future work. Reassuringly, the similarity between surrogate ratio scores for different implementations underline the notion that surrogate analyses provide a powerful tool to identify non-linearities in the presence of linear power differences.

Supplementary References

Courtiol, J., Perdikis, D., Petkoski, S., Muller, V., Huys, R., Sleimen-Malkoun, R., & Jirsa, V. K. (2016). The multiscale entropy: Guidelines for use and interpretation in brain signal analysis. *Journal of Neuroscience Methods, 273*, 175-190. doi:10.1016/j.jneumeth.2016.09.004

Garrett, D. D., Grandy, T. H., & Werkle-Bergner, M. (2014). *The neural forest and the trees: On distinguishing the variance of a brain signal from its information content*. Paper presented at the Annual Alpine Brain Imaging Meeting, Champéry, Switzerland.

Grandy, T. H., Garrett, D. D., Lindenberger, U., & Werkle-Bergner, M. (2013). *Exploring the limits of complexity measures for the analysis of age differences in neural signals*. Paper presented at the Dallas Aging and Cognition Conference, Dallas, TX, USA.

McIntosh, A. R. (2019). Neurocognitive Aging and Brain Signal Complexity: Oxford University Press.

McIntosh, A. R., Kovacevic, N., & Itier, R. J. (2008). Increased Brain Signal Variability Accompanies Lower Behavioral Variability in Development. *Plos Computational Biology, 4*(7). doi:10.1371/journal.pcbi.1000106

Miskovic, V., MacDonald, K. J., Rhodes, L. J., & Cote, K. A. (2019). Changes in EEG multiscale entropy and power-law frequency scaling during the human sleep cycle. *Human Brain Mapping, 40*(2), 538-551. doi:10.1002/hbm.24393

Schartner, M. M., Pigorini, A., Gibbs, S. A., Arnulfo, G., Sarasso, S., Barnett, L., . . . Barrett, A. B. (2017). Global and local complexity of intracranial EEG decreases during NREM sleep. *Neurosci Conscious, 2017*(1), niw022. doi:10.1093/nc/niw022

Schreiber, T., & Schmitz, A. (1996). Improved surrogate data for nonlinearity tests. *Physical Review Letters, 77*(4), 635-638. doi:DOI 10.1103/PhysRevLett.77.635

Stam, C. J. (2005). Nonlinear dynamical analysis of EEG and MEG: review of an emerging field. *Clinical Neurophysiology, 116*(10), 2266-2301. doi:10.1016/j.clinph.2005.06.011

Takens, F. (1993). Detecting Nonlinearities in Stationary Time Series. *International Journal of Bifurcation and Chaos, 3*(2), 241-256. doi:10.1142/S0218127493000192

Theiler, J., Eubank, S., Longtin, A., Galdrikian, B., & Farmer, J. D. (1992). Testing for Nonlinearity in Time-Series - the Method of Surrogate Data. *Physica D-Nonlinear Phenomena, 58*(1-4), 77-94. doi:10.1016/0167-2789(92)90102-S

Vakorin, V. A., & McIntosh, A. R. (2012). Mapping the Multiscale Information Content of Complex Brain Signals. *Principles of Brain Dynamics: Global State Interactions*, 183-208.

Supplementary Figures for

Standard multiscale entropy reflects neural dynamics at mismatched temporal scales

Julian Q. Kosciessa, Niels A. Kloosterman, and Douglas D. Garrett

Email: kosciessa@mpib-berlin.mpg.de; garrett@mpib-berlin.mpg.de

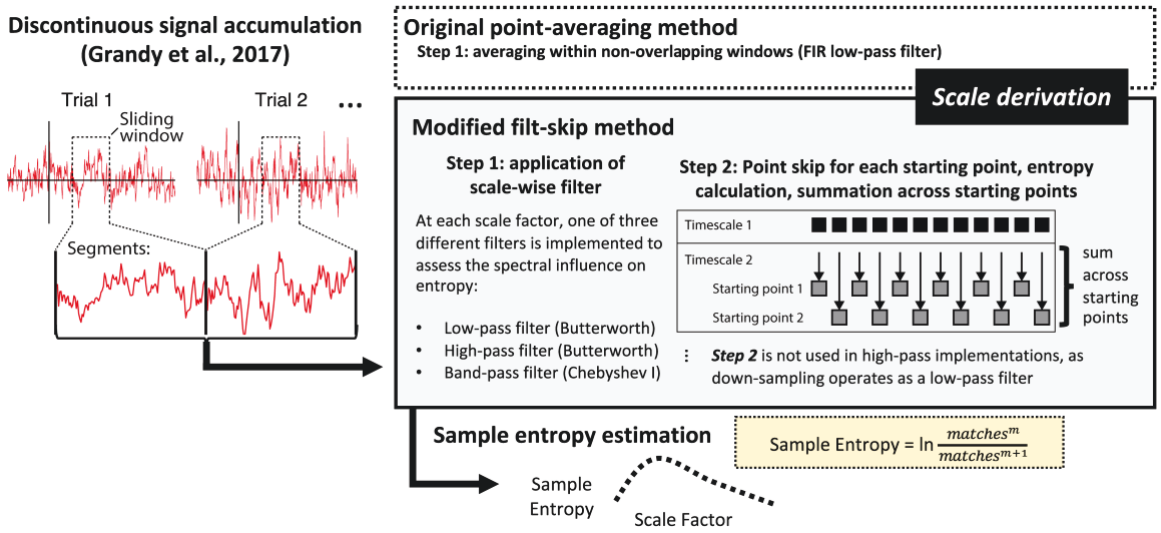

S1 Fig. Overview of modified (mMSE) adaptations. First, mMSE uses data aggregation across (here: pseudo-) trials to allow the estimation of coarse scales also from sparse neuroimaging data [64]. These aggregated signals are then filtered at each scale prior to sample entropy calculation. The 'Original' implementation uses 'point averaging' for different scale factors, which is equivalent to a FIR low-pass filter. In adapted applications, we used a two-step implementation, which we refer to as 'filt-skip', which first applies a scale-wise low-, high- or band- pass filter, and then performs point skipping to down-sample the resulting signals. Finally, the sample entropy of these signals is similarly assessed using the sample entropy algorithm, which results in multiscale entropy estimates. Figure adapted with permission from [121].

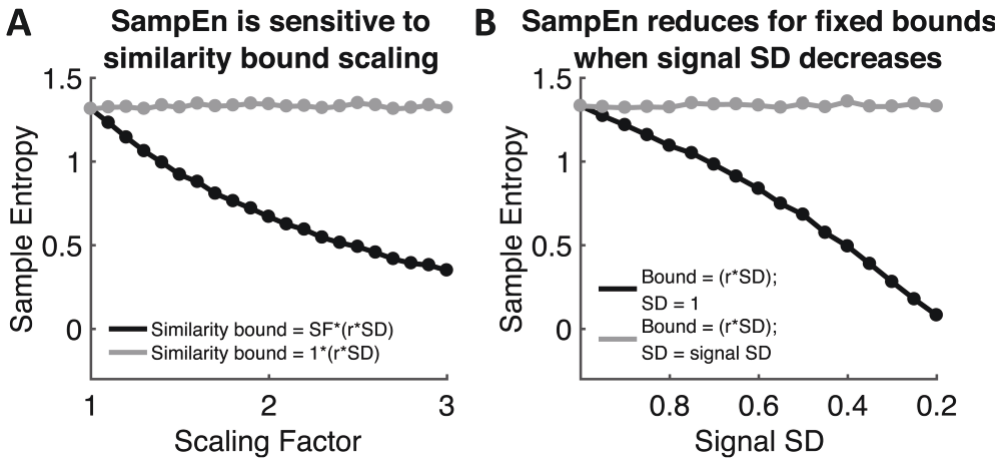

S2 Fig. Liberal similarity bounds reduce sample entropy in simulations. (**A**) The plot shows the sample entropy of simulated white noise signals with constant signal standard deviation (SD) of 1, but varying similarity bounds. We denote this as a function of a scaling factor (SF) to highlight that such variation may arise from either variation in r, SD or both. Note that the r parameter is usually fixed and the SD matches the signal SD (gray line), thus normalizing total signal variance. However, when the similarity bound systematically increases relative to the signal SD, entropy estimates progressively decrease (black line). (**B**)

A similar scenario applies when fixed and large bounds are applied to signals of decreasing variance, as is the case across MSE time scales due to scale-wise filtering (Fig 2). Whereas no bias is observed when scale-wise signal SD is used for the calculation of similarity bounds (grey line), entropy estimates systematically decrease when the SD of the original signal are used (black line). Hence, the mismatched similarity bounds introduced entropy decreases although no changes to the structure of the (here white noise) signals were introduced.

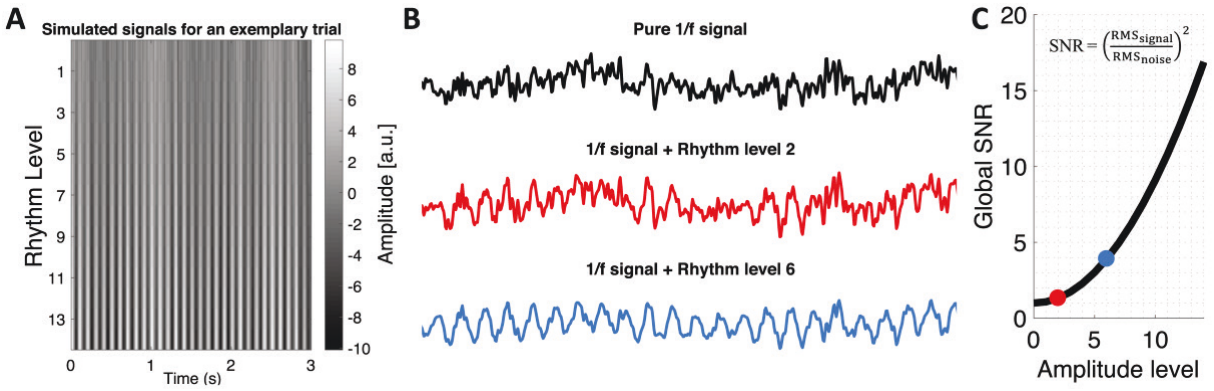

S3 Fig. Examples of simulated rhythmicity projected into pink noise. (A) Top-down view of time-series from an exemplary simulated trial for a pure 1/f signal pink noise signal and at different magnitudes of added alpha rhythmicity. **(B)** Exemplary time series in 2D view. The red time series indicates an example time series for the level of rhythmicity shown in Fig 5. (**C**) Simulated SNR as a function of amplitude level. The dots indicate SNR for the levels depicted in panel B.

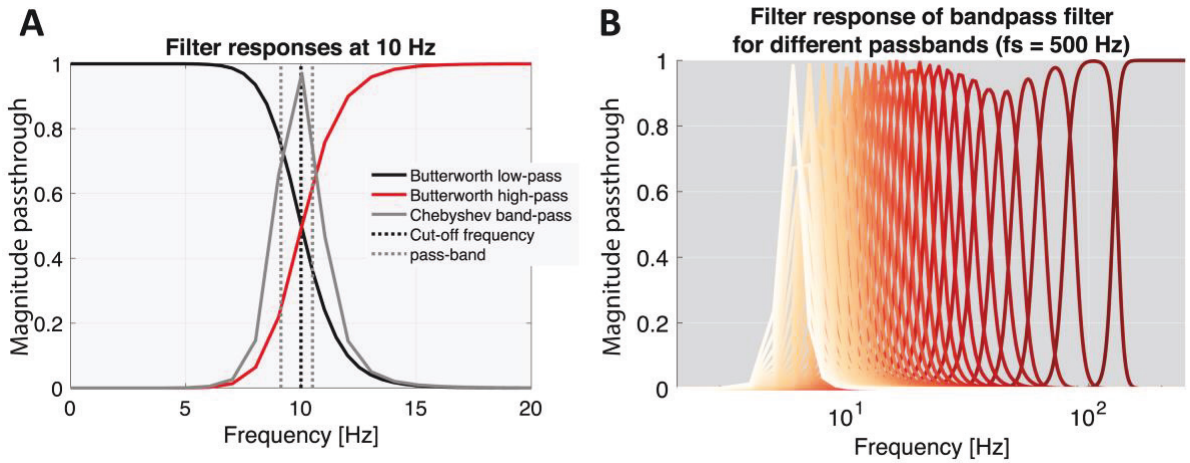

S4 Fig. Filter magnitude responses. (A) Filter magnitude responses at 10 Hz. Note that magnitude responses have been squared due to two-pass filtering to achieve zero-phase offsets. (**B**) Filter magnitudes of Bandpass filters (3rd order type I Chebyshev filter with 1dB passband ripple) at different time scales (red-to-orange indicating fine-to-coarse time scales). Note that only a high-pass filter (6th order Butterworth filter) is applied at the first scale.

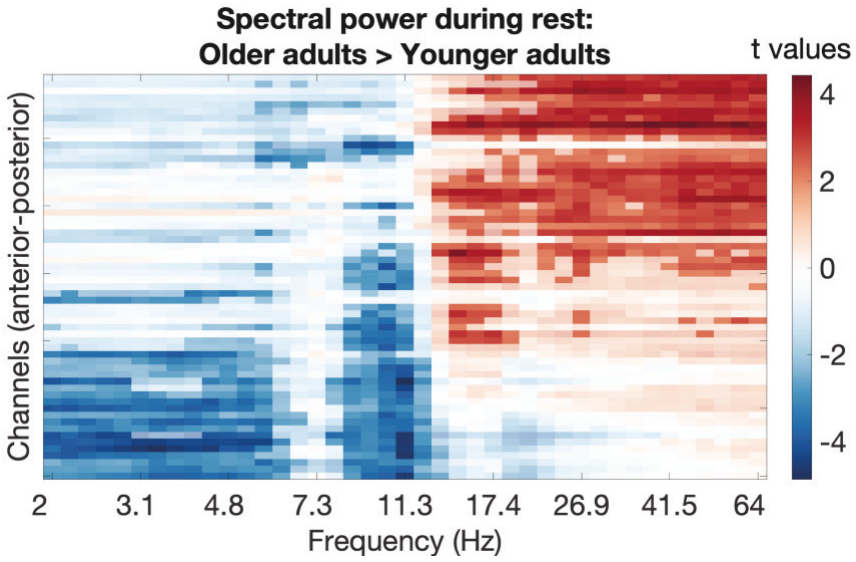

S5 Fig. T-values for age group differences in spectral power (OA > YA). Statistical significance ($p < .05$) was assessed by means of cluster-based permutation tests and is indicated via opacity.

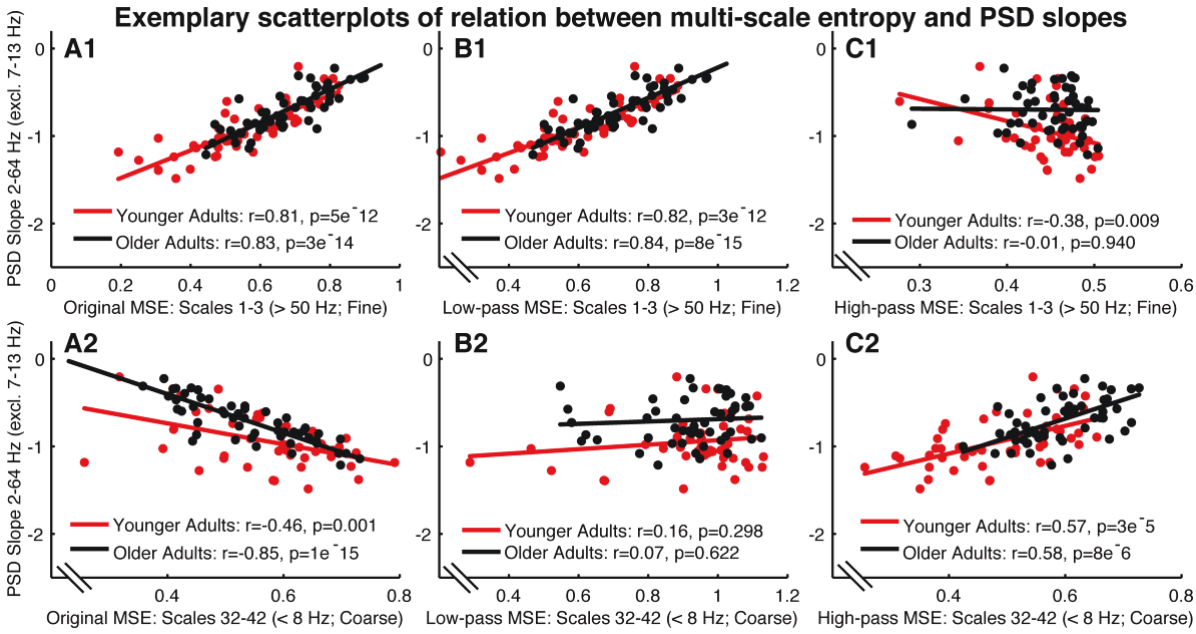

S6 Fig. Methods- and scale-dependent associations between sample entropy and PSD slopes. 'Original' settings indicate a strong positive association at fine scales (A1) that turns negative at coarse scales (A2), likely due to coarse-scale biases by the scale-invariant similarity criterion. In line with this notion, scale-wise adaptation of thresholds retains the fine-scale effect (B1), while abolishing the coarse-scale inversion (B2). Crucially, the entropy of exclusively high-frequency signals does not positively relate to PSD slopes (C1), whereas the association reemerges once slow fluctuations are added into the signal (C2)

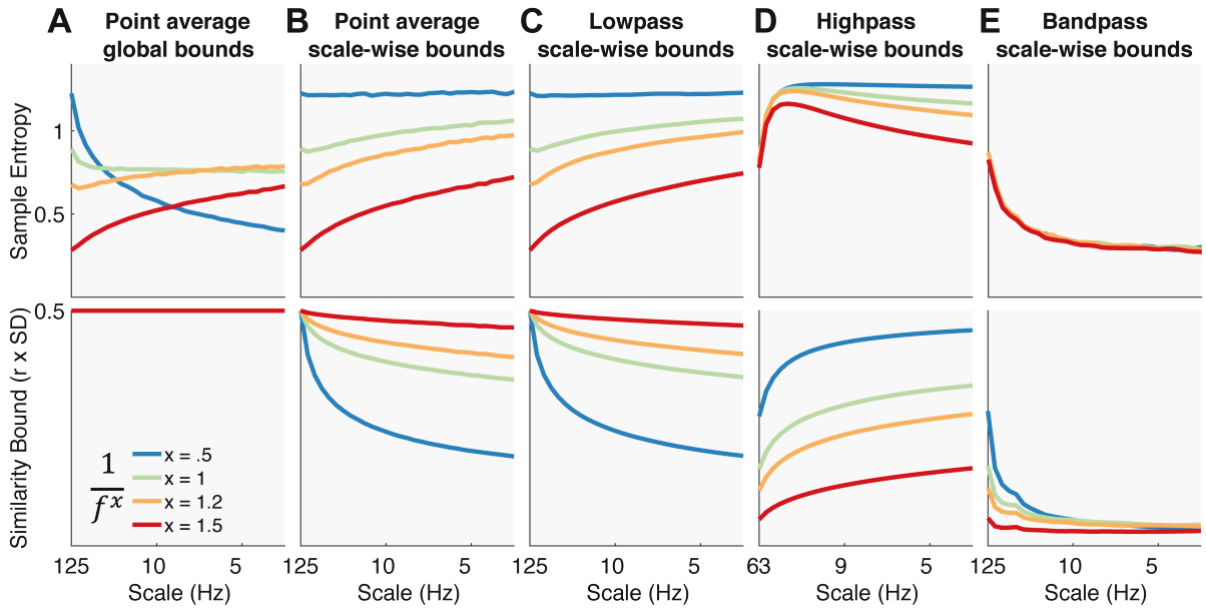

S7 Fig. Results of different simulated spectral slope coefficients for the different filter implementations. (**A**) Using traditional implementations, 1/f variation introduces scale- dependent crossover effects, including scale-dependent entropy decreases for the signals approaching white noise. (**B, C, D**) In contrast, control for scale-wise variance indicates broad scale entropy offsets without crossovers. (**E**) Bandpass entropy is not modulated by broadband effects, as expected by the absence of multi-scale information at local scales.

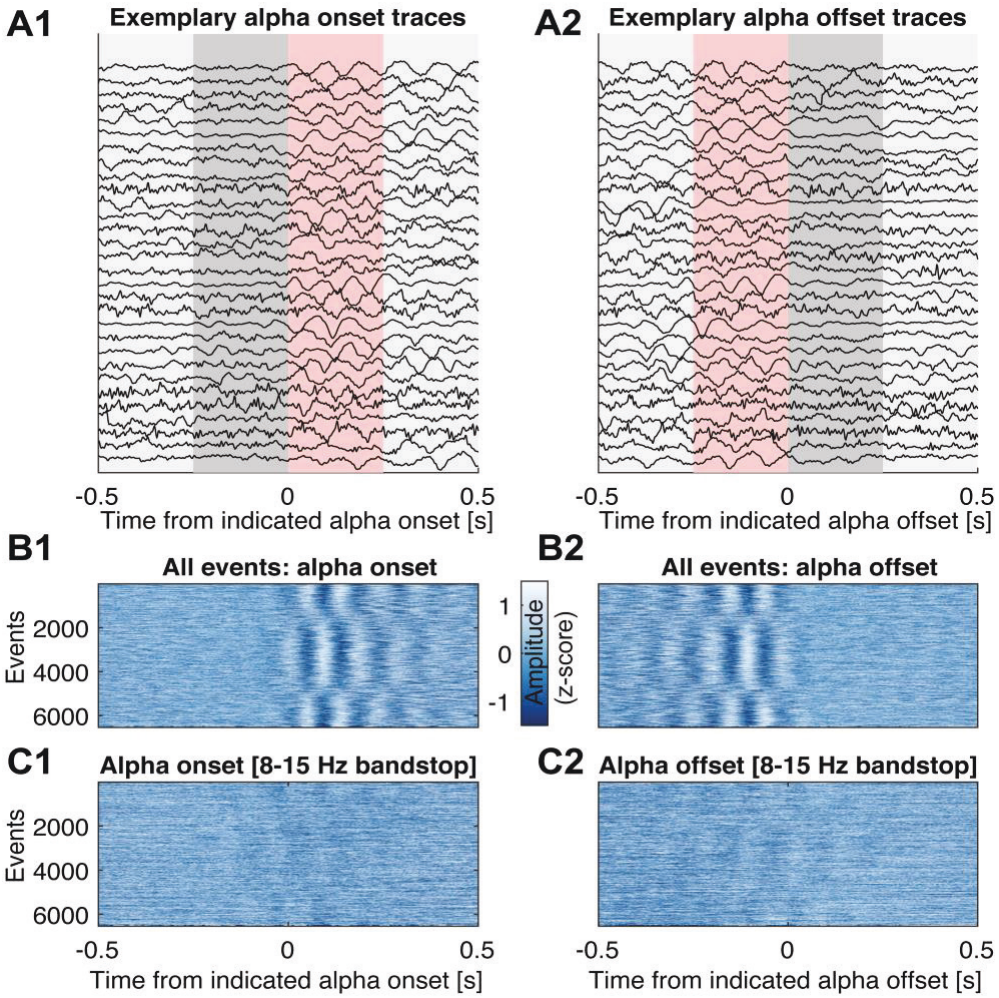

S8 Fig. Signal traces around indicated large alpha event on- and offsets. (**A**) Thirty randomly selected traces across subjects for alpha on- (A1) and offsets (A2). The grey background indicates the 250 ms pre- and post-alpha windows used for the calculation of sample entropy (see Fig 11). The red background highlights segments following indicated alpha onsets, and preceding alpha offsets, that were used to assess irregularity during transient alpha events. Note that 250 ms segments may overlap in the case of short rhythmicity of around 3 cycles. (**B**) All events around on- and offsets. Data were sorted by the instantaneous phase at +100 ms after indicated alpha onset (B1) and -100 ms prior to indicated alpha offset (B2). Instantaneous phase was calculated from a Hilbert transform applied to 8–15 Hz bandpass filtered signals. (**C**) Same as in B, but plotted for signals after 8–15 Hz bandstop filter application. All displayed traces were z-scored for presentation purposes.

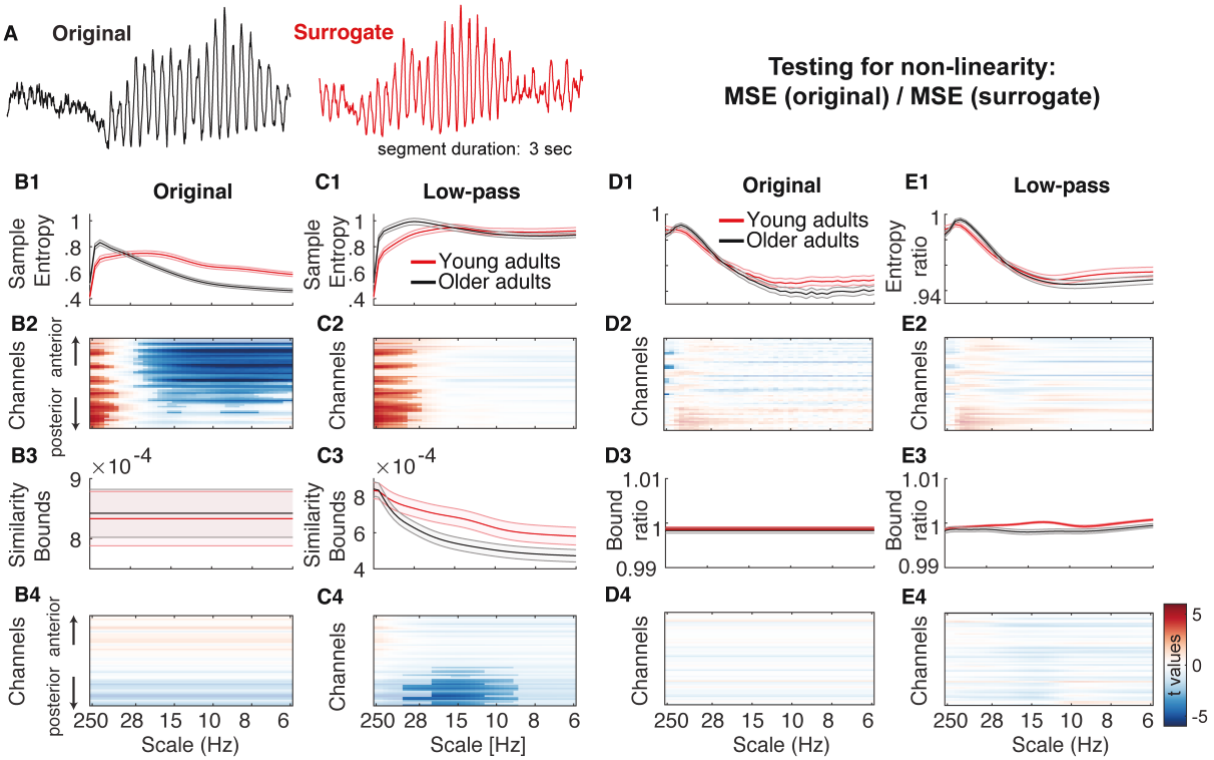

S9 Fig. Results of surrogate analysis, testing for non-linear contributions to MSE age effects. (**A**) Examples of original and surrogate data for a random 3 s segment from an occipital channel with strong alpha rhythms. Phase randomization alters higher-order (non-linear) frequency interactions while preserving the linear power characteristics of the original data. If non-linear contributions are necessary for MSE age effects, no age effects should be indicated for entropy estimates of surrogate data (**B**) Results for "Original" MSE analysis on phase-shuffled data indicate similar effects as observed for original data (Fig 7A), suggesting that linear characteristics were sufficient for the observed age effects. (**C**) Results for low-pass MSE analysis on phase-shuffled data indicate similar effects as observed for original data (Fig 7C), suggesting that linear characteristics were sufficient for the observed age effects. (**D, E**) In addition to assessing the necessity of non-linear contributions, we further assessed whether age differences would be indicated for non-linear contributions, after accounting for linear power characteristics. The ratio of MSE estimates for original vs. surrogate data indicates unique non-linear contributions for either age group. The obtained results were remarkably similar for both original (D) and low-pass implementations (E), indicating the successful elimination of power-based biases. However, no statistically significant age differences were indicated, suggesting that non-linear contributions are at most minor, and may require higher statistical power for their assessment.

Thalamocortical excitability adjustments guide human perception under uncertainty

Julian Q. Kosciessa[1,2,3]*, Ulman Lindenberger[1,2], Douglas D. Garrett[1,2]*

[1]Max Planck UCL Centre for Computational Psychiatry and Ageing Research, Berlin and London; [2]Center for Lifespan Psychology, Max Planck Institute for Human Development, Lentzeallee 94, 14195 Berlin, Germany. [3]Department of Psychology, Humboldt-Universität zu Berlin, Berlin, Germany

Julian Q. Kosciessa: https://orcid.org/0000-0002-4553-2794
Ulman Lindenberger: https://orcid.org/0000-0001-8428-6453
Douglas D. Garrett: https://orcid.org/0000-0002-0629-7672

* Correspondence:

kosciessa@mpib-berlin.mpg.de (Lead Contact); garrett@mpib-berlin.mpg.de

Abstract

Adaptive human behavior builds on prior knowledge about stimulus relevance. Some environments cue such knowledge more than others. To behave adaptively, observers need to flexibly adjust sensory processing to the degree of contextual uncertainty. We hypothesize that the neural basis for these perceptual adjustments consists in the ability of the cortical network to switch back and forth between a rhythmic state that serves selective processing, and a state of elevated asynchronous neural activity that boosts sensitivity. To test this hypothesis, we recorded non-invasive EEG and fMRI BOLD dynamics while 47 healthy young adults performed a parametric visual attention task with varying numbers of relevant stimulus features. Drift-diffusion modeling of response behavior and electrophysiological signatures revealed that greater contextual uncertainty lowered the rate of evidence accumulation while increasing thalamocortical engagement, with concomitant increments in cortical excitability and pupil dilation. As predicted, uncertainty-related processing adjustments were expressed as switches between a state of phase-dependent excitability modulation in the alpha band and a state of increased irregularity of brain dynamics. We conclude that humans dynamically adjust sensory excitability according to the processing fidelity afforded by an upcoming choice, and that neuromodulatory processes involving the thalamus play a key role in adjusting excitability in the human brain.

Highlights

- With increasing contextual uncertainty, human cortical networks shift from a state of phase-dependent excitability modulation in the alpha band into a state of elevated excitatory tone and asynchronous neural activity
- Evidence based on joint modeling of behavior, EEG, and BOLD suggests that neuromodulatory processes involving the thalamus regulate these shifts
- Theoretical and empirical considerations suggest contributions of both frequency-specific and aperiodic neural dynamics to human behavior

Introduction

Adaptive behavior requires dynamic adjustments to the perception of high-dimensional inputs. Prior knowledge about the momentary relevance of specific environmental features selectively enhances their processing while suppressing distractors (for reviews see Buschman & Kastner, 2015; Desimone & Duncan, 1995; Maunsell, 2015), which can be implemented via gain modulation in sensory cortex (Ferguson & Cardin, 2020). Crucially, *a priori* information regarding feature relevance is not always available; and how the brain flexibly adjusts the processing of complex inputs according to contextual uncertainty remains unclear (Bach & Dolan, 2012).

Selective gain control has been associated with ***phasic*** (i.e., phase-dependent) inhibition of task-irrelevant stimulus dimensions during cortical alpha (~8-12 Hz) rhythms (Klimesch, Sauseng, & Hanslmayr, 2007; Sadaghiani & Kleinschmidt, 2016). In particular, rhythmic modulations of feedforward excitability (Haegens, Nacher, Luna, Romo, & Jensen, 2011; Lorincz, Kekesi, Juhasz, Crunelli, & Hughes, 2009) may provide temporal 'windows of opportunity' for high-frequency gamma synchronization in sensory cortex (Spaak, Bonnefond, Maier, Leopold, & Jensen, 2012; van Kerkoerle et al., 2014) and increased sensory gain (Fries, 2015; Ni et al., 2016; Peterson & Voytek, 2017). However, specifically increasing the fidelity of single stimulus dimensions is theoretically insufficient when uncertain environments require joint sensitivity to multiple stimulus features (Pettine, Louie, Murray, & Wang, 2020). During high uncertainty, transient increases to the ***tonic*** excitation/inhibition (E/I) ratio in sensory cortex provide a principled mechanism for elevated sensitivity to – and a more faithful processing of – high-dimensional stimuli (Destexhe, Rudolph, & Pare, 2003; Marguet & Harris, 2011). In electrophysiological recordings, scale-free 1/f slopes are sensitive to differences in E/I ratio (Gao, Peterson, & Voytek, 2017), and vary alongside sensory stimulation (Billig et al., 2019; Podvalny et al., 2015) and arousal states (Colombo et al., 2019; Lendner et al., 2019). Whether contextual demands modulate scale-free activity is unknown however. We hypothesize that high uncertainty shifts cortical regimes from rhythmic excitability modulations towards tonic excitability increases.

Such state switches in network excitability may be shaped by neuromodulation and subcortical activity (Harris & Thiele, 2011). Neuromodulation potently alters cortical states (Froemke, 2015; Thiele & Bellgrove, 2018) and sensory processing (Berridge & Waterhouse, 2003; McCormick, Pape, & Williamson, 1991; McGinley, David, & McCormick, 2015), and noradrenergic arousal in particular may permit high sensitivity to incoming stimuli (Posner & Rothbart, 2007). Yet, non-invasive evidence is lacking for whether/how neuromodulation affects contextual adaptability. Moreover, despite early proposals for thalamic involvement in attentional control (Crick, 2003; Jasper, 1948; Rafal & Posner, 1987), studies have dominantly focused on cortical information flow (e.g., Siegel, Buschman, & Miller, 2015), at least in part due to technical difficulties in characterizing thalamic contributions. Crucially, the thalamus provides a nexus for the contextual modulation of cortical circuits (Halassa & Kastner, 2017; Honjoh et al., 2018), is a key component of neuromodulatory networks (McCormick et al., 1991; Schiff, 2008; Song et al., 2017) and robustly modulates system excitability via rhythmic and aperiodic membrane fluctuations (Jones, 2009). However, human evidence for a central thalamic role in cortical state adjustments at the service of behavioral flexibility is missing.

Here, we aimed at overcoming this lacuna by assessing the effects of contextual uncertainty during stimulus encoding on cortical excitability, neuromodulation, and thalamic activity in humans. We performed a multi-modal (parallel) EEG-fMRI experiment to capture both fast cortical dynamics (EEG) and subcortical activity (fMRI) while recording pupil dilation as a non-invasive proxy for neuromodulatory drive (Joshi & Gold, 2020). Participants performed a parametric adaptation of the classic dot motion task (Gold & Shadlen, 2007) (Figure 1). Specifically, we manipulated the number of stimulus dimensions that are task-relevant in a given trial while holding the sensory features of the task (i.e., its appearance on the screen) constant across trials. By applying drift-diffusion modeling to participants' choice behavior while jointly assessing electrophysiological signatures of decision processes, we found that uncertainty during sensation reduces the rate of subsequent evidence integration. This reduction in available sensory evidence for single targets was associated with increased cortical excitability, as indexed by joint low-frequency (~alpha) desynchronization and high-frequency (~gamma) synchronization, and an increase in E/I ratio, as indicated by increased sample entropy and flatter scale-free 1/f slopes, during stimulus processing, in lines with broad sensitivity increases during periods of higher uncertainty. These excitability adjustments occurred in parallel with increases in pupil-based arousal. Finally, inter-individual differences in the modulation of cortical excitability, drift rates and arousal were jointly associated with the extent of thalamic BOLD signal modulation, pointing to the importance of subcortical mechanisms for cortical state adjustments. Together, these findings suggest that neuromodulatory processes involving the thalamus shape cortical excitability states in humans, and that a shift from alpha-rhythmic to aperiodic neural dynamics adjusts the processing fidelity of external stimuli in service of upcoming decisions.

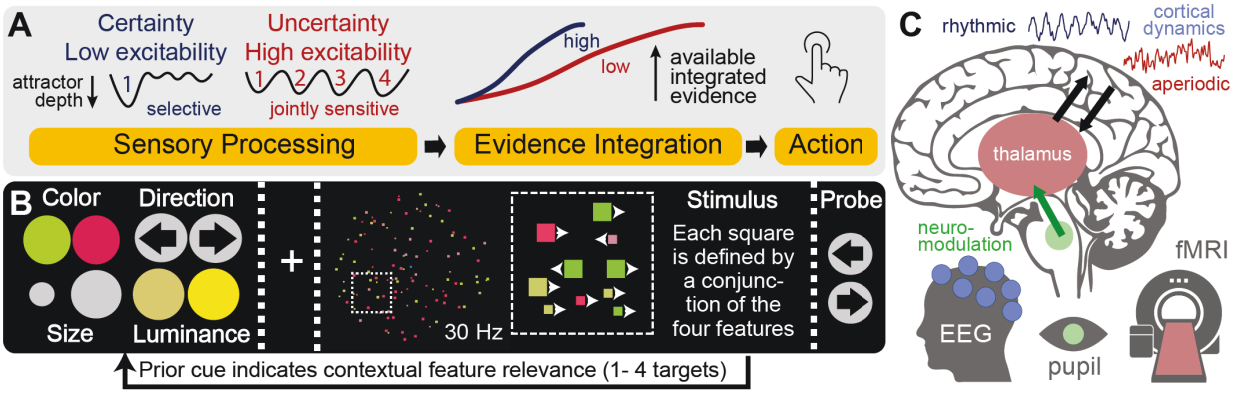

Figure 1. Hypotheses & task design. (**A**) We probed whether participants modulate cortical excitability during stimulus processing to guide subsequent evidence accumulation. We hypothesized that when valid attentional cues about a single target feature are available in advance, a low excitability regime may optimize subsequent choices via the targeted selection of relevant – and inhibition of irrelevant – information. This can be conceptualized as the creation of a "single feature attractor." In contrast, under high probe uncertainty, higher excitability may afford the concurrent sampling of multiple relevant features, but at the cost of a relative reduction of subsequently available evidence for any individual feature. (**B**) Participants performed a **M**ulti-**A**ttribute **A**ttention **T**ask ("MAAT") during which they had to sample up to four visual features in a joint display for immediate subsequent recall. Prior to stimulus presentation, participants were validly cued to a set of potential target probes. The number and identity of cues were varied to experimentally manipulate the level of expected probe uncertainty. (**C**) We hypothesized that increasing probe uncertainty would induce a joint increase in neuromodulation and thalamic activity, associated with shifts from a phasic gain control mode (implemented via neural alpha rhythms) toward transient increases in tonic excitability (as indicated by aperiodic cortical activity). Participants performed the same task in both an EEG and

an fMRI session, allowing us to assess joint inter-individual differences in fast cortical dynamics (EEG) and subcortical sources (fMRI).

Results

We developed a dynamic visual **M**ulti-**A**ttribute **A**ttention **T**ask ("MAAT") to uncover rapid adjustments to stimulus processing and perceptual decisions under expected uncertainty (Figure 1). Participants visually sampled a moving display of small squares, which were characterized by four stimulus features, with two exemplars each: their color (red/green), their movement direction (left/right), their size (large/small), and their color saturation (high/low). Any individual square was characterized by a conjunction of the four features, while one exemplar of each feature (e.g., green color) was most prevalent in the entire display. Following stimulus presentation, participants were probed on a single feature as to which of the two exemplars was most prevalent (via 2-AFC). Probe uncertainty was parametrically manipulated using valid pre-stimulus cues, indicating the feature set from which a probe would be selected. The feature set remained constant for a sequence of eight trials to reduce set switching demands. Optimal performance required flexible sampling of the cued feature set while jointly inhibiting uncued features; participants had to thus rapidly encode a varying number of targets ("target load") to prepare for an upcoming probe. Participants performed the task well above chance level for different features and for different levels of probe uncertainty (Figure S1A). As the number of relevant targets increased, participants systematically became slower (median RT; EEG: β = .138, p ~ 0; MRI: β = .107, p ~ 0) and less accurate (EEG: β = -.032, p ~ 0; MRI: β = -.025, p = 2.4e-07) in their response to single-feature probes (Figure S1B).

Probe uncertainty during sensation decreases the rate of subsequent evidence integration

We leveraged the potential of sequential sampling models to disentangle separable decision processes in order to assess their modulation by probe uncertainty. In particular, drift-diffusion models estimate (a) the non-decision time (NDT), (b) the drift rate at which information becomes available, and (c) the internal evidence threshold or boundary separation (see Figure 2A; for a review see Forstmann, Ratcliff, & Wagenmakers, 2016). We fitted a hierarchical drift-diffusion model (HDDM) separately for each testing session, and assessed individual parameter convergence with established EEG signatures (Donner, Siegel, Fries, & Engel, 2009; O'Connell, Dockree, & Kelly, 2012; Twomey, Kelly, & O'Connell, 2016; van Vugt, Beulen, & Taatgen, 2019). In particular, we investigated the Centroparietal Positive Potential (CPP) and lateralized beta suppression as established neural signatures of evidence integration from eidetic memory traces (Twomey et al., 2016). The best behavioral fit was obtained by a model incorporating probe uncertainty-based variations in drift rate, non-decision time and boundary separation (Figure S1B). Yet, there was no evidence for modulation of the threshold of the CPP or the contralateral beta response (Figure S1C). In line with prior work (McGovern, Hayes, Kelly, & O'Connell, 2018), we therefore selected an EEG-informed model with fixed thresholds across target load levels. With this model, reliability of individual parameters as well as of their load-related changes was high across EEG and MRI sessions (see below and Figure S1E, F). Parameter interrelations are reported in Text S1.

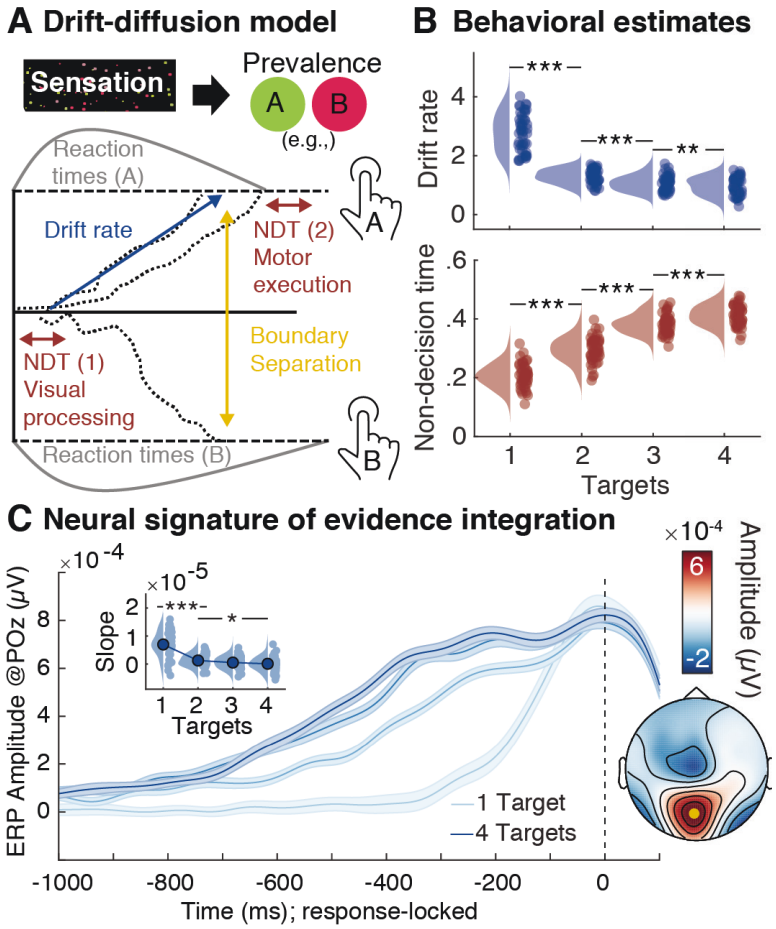

Figure 2: Evidence integration upon probe presentation decreases as a function of prior uncertainty. (**A**) Schematic of drift-diffusion model. Following visual encoding, evidence is successively accumulated towards either of two bounds when probed for the dominant prevalence of one of two options of a single feature. A button press indicates the decision once one of the bounds has been reached and motor preparation has concluded. A non-decision time parameter captures visual encoding and motor preparation, drift rate captures the amount of available information, and boundary separation captures response bias i.e., conservative vs. liberal). (**B**) Behavioral parameter estimates for drift rate and non-decision time (NDT; discussed in Text S3), as indicated by the hierarchical drift-diffusion model (HDDM). (**C**) Modulation of the Centroparietal Positive Potential (CPP) as a neural signature of evidence accumulation (mean +- within-subject SE). The probe-locked CPP indicates decreases in drift rate with prior probe uncertainty. Insets show CPP slope estimates from -250 to -100 ms relative to response execution, as well as the corresponding topography (CPP channel shown in yellow). [*** p < .001, ** p < .01, * p < .05]

Behavioral model estimates (Figure 2B) and EEG signatures (Figure 2C, Figure S2A) jointly indicated that probe uncertainty during stimulus presentation decreased the drift rate during subsequent evidence accumulation. This indicates a reduction of available evidence for single features when more features had to be sampled. Individual drift rate estimates for a single target were positively correlated with the slope of the CPP (r = 0.52, 95%CI [0.26, 0.71], p = 3.59e-4), while individual drift rate reductions reflected the shallowing of CPP slopes (r(137) = 0.34, 95%CI [0.18, 0.48], p = 4.87e-5). Notably, the magnitude of evidence decreases with increasing probe uncertainty was strongly anticorrelated with the available evidence when the target attribute was known in advance (i.e., the single target condition; EEG session: *r* = -.93, *p* = 4e-22, MRI session: *r* = -.88, *p* = 1e-15). That is, participants with more available evidence after selectively attending to a single target showed larger drift rate

decreases under increased probe uncertainty. Importantly however, participants with higher drift rates for single targets also retained higher drift rates at higher probe uncertainty (i.e., high reliability for e.g., four targets: EEG: r = .48; p = 6e-4; MRI: r = .53, p = 2e-4). Moreover, individuals with higher drift rates across target loads exhibited lower average RTs (EEG: r = -.42, p = .003; MRI: r = -.41, p = .007) and higher task accuracy (EEG: r = .86, p = 2e-14; MRI: r = .89, p = 4e-16). Thus, in the present paradigm, more pronounced drift rate decreases with increasing probe uncertainty index a successful modulation of feature-based attention during encoding, and better overall performance.

We performed multiple control analyses to further elucidate decision properties. First, we did not observe a similar ramping of the CPP during stimulus presentation (Figure S2B), suggesting that evidence accumulation was primarily initiated by the probe. Second, drift rate reductions were not primarily driven by differences between feature attributes (Figure S2C). Third, concurrent variations in response agreement across cued attributes could not account for the observed effects (Text S2; Figure S1D). Fourth, individual drift rates for single targets were unrelated to threshold estimates (EEG: r = -.005, p = .74; MRI: r = -.006; p = .72), thus suggesting a lack of differences in response bias (Ratcliff & McKoon, 2008). Finally, participants with larger drift rate decreases exhibited more constrained non-decision time increases (EEG: r(137) = 0.32, 95% CI [0.16, 0.47], p = 1.04e-4; MRI: r(122) = 0.37, 95%CI [0.2, 0.51], p = 2.48e-5), indicating reduced additional motor transformation demands (see Text S3) in high performers.

Cortical excitability increases under uncertainty guide subsequent evidence integration

Decreases in the rate of evidence integration indicate the detrimental consequences of probe uncertainty, but not the mechanisms by which sensory processing is altered. To investigate the latter, we examined rhythmic and aperiodic cortical signatures during stimulus processing. To jointly assess multivariate changes in spectral power as a function of probe uncertainty, we performed a partial-least-squares (PLS) analysis that produces low-dimensional, multivariate relations between brain-based data – in this case time-frequency-space matrices – and other variables of interest (see methods). First, we assessed evoked changes compared to baseline using a task PLS. We observed a single latent variable (LV; permuted p < .001) with jointly increased power in the delta-theta and gamma bands and decreased alpha power upon stimulus onset (Figure S3A, Figure S4A), in line with increased cognitive control (Cavanagh & Frank, 2014) and heightened bottom-up visual processing (van Kerkoerle et al., 2014). We next performed a task PLS to assess spectral power changes as a function of target load. A single LV (permuted p < .001; Figure 3) indicated a stronger expression of this control- and excitability-like pattern with increasing probe uncertainty. Next, we assessed the link between individual changes in multivariate loadings on this “spectral power modulation factor” (SPMF) and behavioral modulations. We performed *partial repeated measures correlations (*see methods), a mixed modelling approach that controls for the main effect of probe uncertainty in both variables of interest and indicates interindividual associations independent of the specific shape of condition modulation in individual participants. Crucially, individual SPMF loadings were positively correlated with interindividual performance differences during selective attention (Figure 3F) and uncertainty-related performance changes (Figure 3G). Participants with stronger spectral power modulation during sensation exhibited faster evidence integration in the selective attention condition, as well as a stronger drift rate decreases under uncertainty [r(137) = -0.4,

95%CI [-0.53, -0.25], p = 1.12e-6], while showing constrained increases in non-decision time [r(137) = -0.26, 95%CI [-0.41, -0.1], p ~ 0]. In sum, this suggests that high performers flexibly increased visual throughput as more features became relevant via top-down control of cortical excitability.

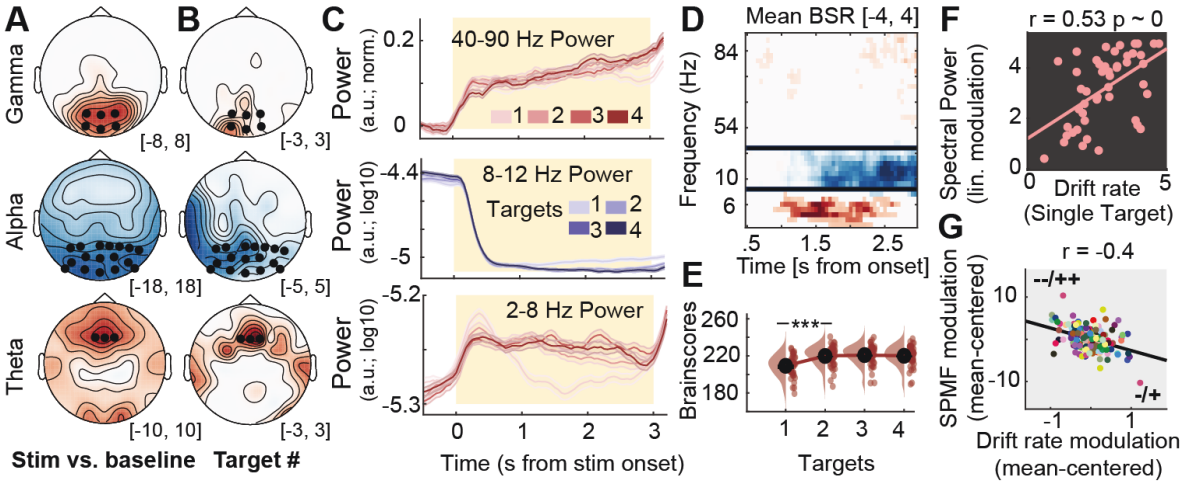

Figure 3: Multivariate power changes with probe uncertainty during stimulus encoding. (**A, B**) Topographies of stimulus-evoked power changes relative to pre-stimulus baseline (A, see Figure S3-1) and load-related power modulation (B). With increasing attentional demands, theta and 'broadband' gamma power increased, whereas alpha rhythms desynchronize. Asterisks indicate the sensors across which data were averaged for presentation in D. Values indicate maximum (theta/gamma) or minimum (alpha range) bootstrap ratios (BSR) across time in the clusters. (**C**) Temporal traces of band-limited power as a function of target load, extracted from the clusters presented in D (mean +- within-subject SE). (**D, E**) Multivariate loading pattern (D) for spectral power changes under uncertainty and associated multivariate brain scores at different levels of target load (E). Black bars in panel D indicate discrete frequency ranges or sensors (shown in A). (**F, G**) Participants with stronger multivariate power modulation exhibit stronger drift rates for single targets (F), as well as stronger drift rate decreases under uncertainty (G). In G, dots represent linear model residuals (see methods), colored by participant. Coupled changes across target conditions are indicated by the black line. We indicate the direction of main effects for each variable via + and - (- = small decreases, -- = large decreases, + = small increases, ++ = large increases), with directions of variables on the x-axis indicated first. [*** p < .001]

Here too, we performed multiple control analyses. First, the same multivariate power-band relations noted in our task PLS model (SPMF above) were also identified in a behavioral PLS model intended to estimate optimal statistical relations between power bands and behavior (Text S4, Figure S4B). Second, while we observed increases in pre-stimulus alpha power with increasing probe uncertainty, these changes did not relate to behavioral changes or power changes during stimulus processing (Text S5, Figure S4C). Third, the entrained steady-state visual evoked potential (SSVEP) magnitude was not modulated by target load (Text S6, Figure S4D). Fourth, multivariate power changes corresponded to narrow-band, rhythm-specific indices in the theta and alpha band (Text S7, Figure S4E), and thus did not exclusively result from changes in the aperiodic background spectrum (see below).

Alpha phase modulates gamma power during sensation

Alpha rhythms have been related to phasic control over bottom-up input, as putatively encoded in gamma power (Spaak et al., 2012). To assess phase-amplitude coupling (PAC)

in the present data, we selected temporal alpha episodes at the single-trial level (see methods, Figure 4A) and assessed the coupling between alpha phase and gamma power. We observed significant alpha-gamma PAC (Figure 4B, D left), consistent with alpha-phase-dependent excitability modulation. This was constrained to the occurrence of alpha episodes, as no significant alpha-gamma PAC was observed prior to indicated alpha episodes (grey shading in Figure 4A; Figure 4D right). Phasic gamma power modulation was observed across target load levels (Figure 4F), but alpha duration decreased as a function of load (Figure 4C). This suggests that alpha rhythms consistently regulated gamma power, but that alpha engagement decreased as more targets became relevant.

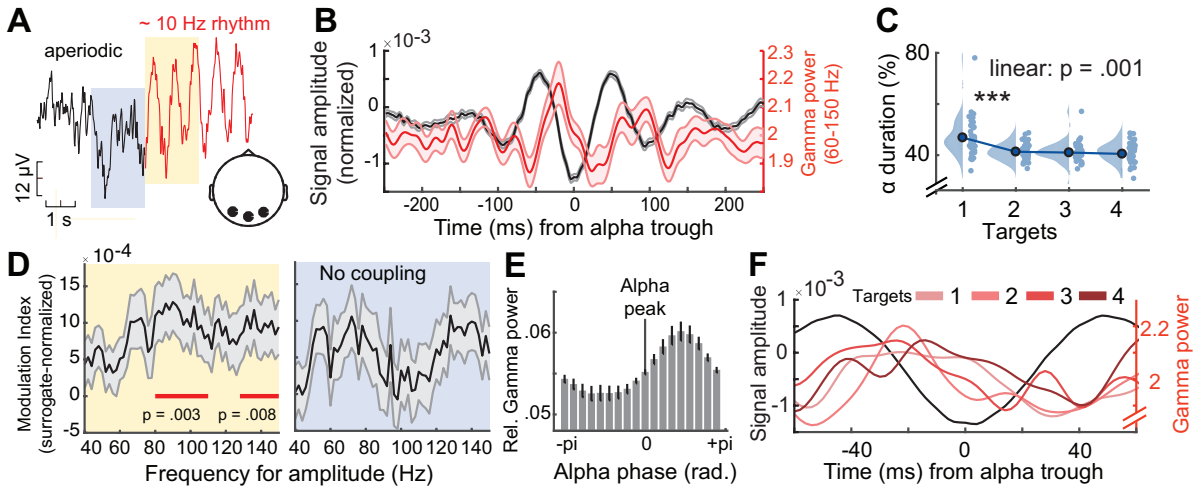

Figure 4. Alpha phase modulates gamma power during sensation. (**A**) Exemplary time series around the onset of a detected alpha event (example from 4-target condition). Segments were pooled across occipital channels (black dots in inset topography) and target load conditions. (**B**) Normalized gamma power (red; mean +- SE) during alpha events (yellow shading in A), is modulated by alpha phase (see methods). The unfiltered ERP aligned to the alpha trough is shown in black. Shaded regions indicate standard errors. (**C**) The relative duration of alpha events decreased with increased feature relevance. Data are individually centered across target loads. (**D**) Modulation index (MI) indicated significant coupling between the phase of alpha and gamma power during rhythmic events (left), but not during periods immediately prior to rhythm onset (right). MI was normalized using surrogate data to reduce erroneous coupling (see methods). Shaded regions indicate standard errors. (**E**) Gamma power (averaged from 60-150 Hz; mean +- SE) was maximal following alpha peaks. Power was normalized across all phase bins (see methods). (**F**) Gamma power systematic peaks between the peak and trough of alpha rhythms across target levels. For this analysis, alpha events were collapsed across all participants. [*** p < .001]

Sample entropy and scale-free dynamics indicate shifts towards increased excitability

Next, we assessed whether reduced alpha engagement was accompanied by increases in temporal irregularity, a candidate signature for system excitability (Kosciessa, Kloosterman, & Garrett, 2020). We probed time-resolved fluctuations in sample entropy (SampEn), an information-theoretic estimate of signal irregularity. As sample entropy is jointly sensitive to broadband dynamics and narrowband rhythms, we removed the alpha frequency range using band-stop-filters (8-15 Hz) to avoid contributions from alpha rhythms (see Kosciessa, Kloosterman, & Garrett, 2020). A cluster-based permutation test indicated SampEn increases under probe uncertainty over posterior-occipital channels (Figure 5A). Notably, the magnitude of individual entropy modulation in this cluster scaled with increases in the SPMF

[r(137) = 0.22, 95%CI [0.05, 0.37], p = 0.01], indicating that alpha desynchronization was accompanied by broadband changes in signal irregularity.

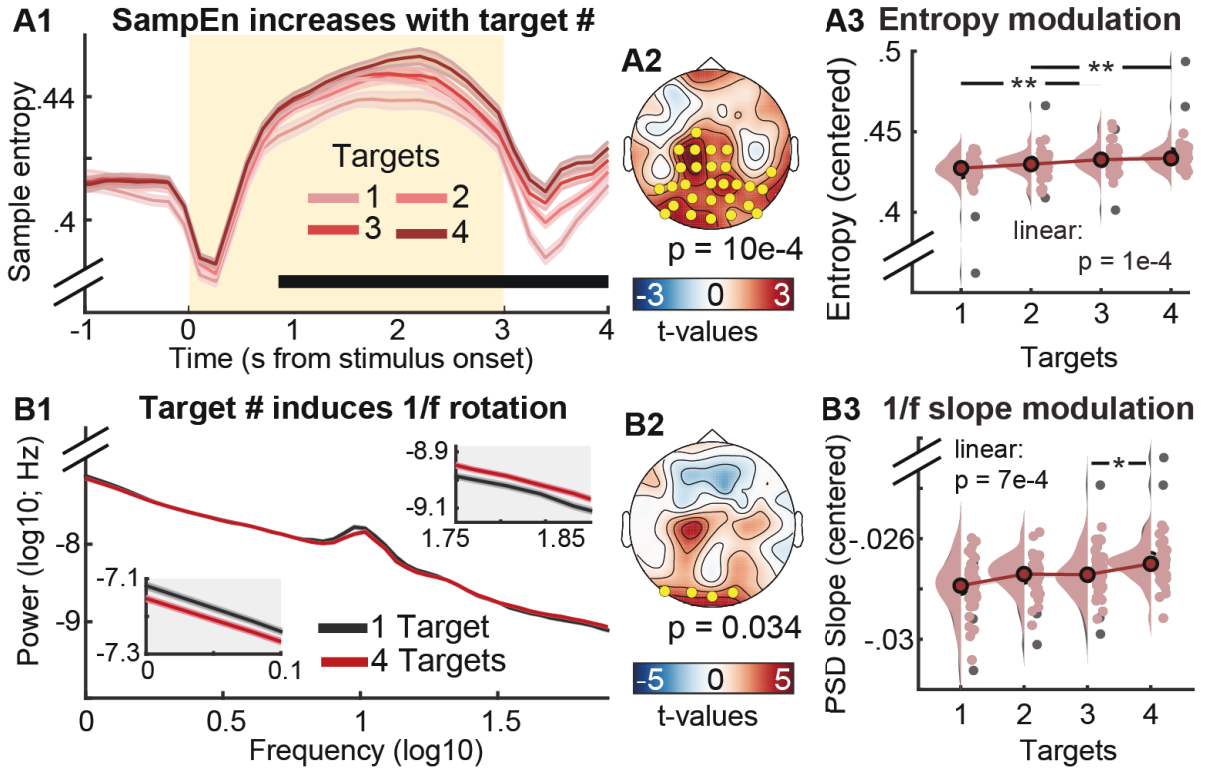

Figure 5: Uncertainty increases aperiodic dynamics during sensation as reflected in neural entropy (A) and 1/f slopes (B). (A1) Temporal traces of sample entropy (mean +- within-subject SE). The yellow background indicates the period of stimulus presentation. The black bar indicates time points at which permutation tests indicated linear load effects. (A2) Topography of linear load effect estimates, with yellow dots representing the significant cluster. (A3) Post-hoc analysis of entropy estimates within significant cluster. Grey dots indicate individual outliers (defined as Cook's distance > 2.5*mean (Cook's distance)) and have been removed from the statistical post-hoc assessment. Estimates have been within-subject centered for display purposes, while statistical analyses were run on uncentered data. (B1) Aperiodic slopes shallow with increased target load (i.e., spectral rotation across low- and high-frequencies; mean +- within-subject SE). Lower and upper insets highlight slope differences at low and high frequencies, respectively. (B2) Topography of linear load effects on 1/f slopes. Yellow dots indicate the significant occipital cluster used for post-hoc assessments. (B3) Same as A3, but for occipital aperiodic slopes. [*** p < .001, ** p < .01, * p < .05]

Aperiodic, scale-free spectral slopes are a major contributor to broadband SampEn, due to their joint sensitivity to autocorrelative structure (Kosciessa, Kloosterman, et al., 2020), and a shallowing of aperiodic (1/f) slopes has theoretically been associated with system excitability (Gao et al., 2017). We therefore assessed aperiodic slope changes during the stimulus period (excluding onset transients). In line with our hypothesis, participants' PSD slopes shallowed under uncertainty (Figure 5B), suggesting that participants increased their excitatory tone in posterior cortex. In line with the expectation that sample entropy should be highly sensitive to scale-free dynamics, sample entropy was strongly related to individual PSD slopes across conditions (r = .77, p <.001) and with respect to linear changes in PSD slope with increasing uncertainty [r(137) = 0.44, 95%CI [0.3, 0.57], p = 4.92e-8]. In sum, heightened probe uncertainty desynchronized low-frequency alpha rhythms, and elevated the irregularity of cortical dynamics, in line with enhanced tonic excitability.

Increases in phasic pupil diameter relate to transient excitability adjustments

Phasic arousal changes modulate perception and local cortical excitability (for reviews see Lee & Dan, 2012; McGinley, Vinck, et al., 2015). To test whether arousal increased alongside uncertainty, we assessed phasic changes in pupillometric responses as a proxy for arousal during stimulus presentation. We quantified phasic pupil responses via the 1st temporal derivative (i.e. rate of change), as this measure has higher temporal precision and has been more strongly associated with noradrenergic responses than the overall pupil response (Reimer et al., 2014). Phasic pupil dilation systematically increased with probe uncertainty (Figure 6). This modulation occurred on top of a general pupil constriction due to stimulus-evoked changes in luminance (Figure 6A, inset), while the linear modulation occurred – by stimulus design – in the absence of systematic luminance changes.

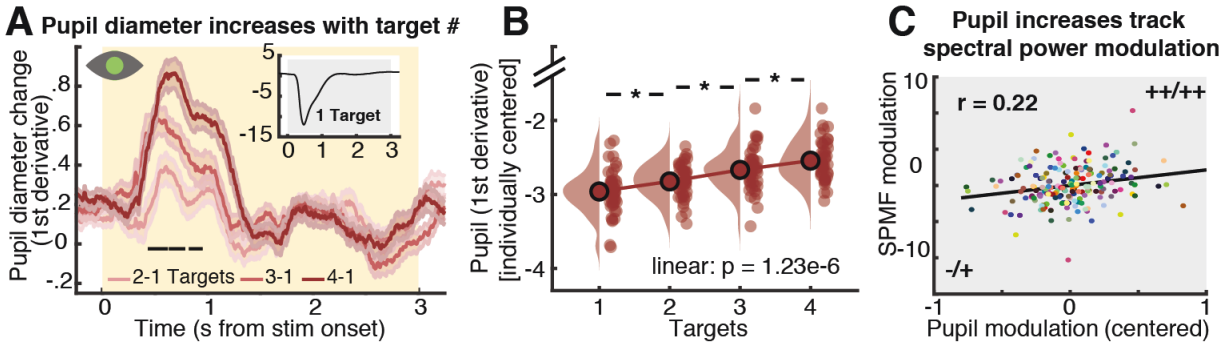

Figure 6: Effect of probe uncertainty on pupil diameter as a proxy for neuromodulation. (A) Phasic changes in pupil diameter increase with number of targets (mean +- within-subject SE). Significant linear load effects as indicated by a cluster-based permutation test are indicated via the black line. For follow-up analyses, we extracted median pupil values from 0 to 1.5 s. For display purposes but not statistics, derivative estimates were smoothed via application of a 200 ms median running average. (**B**) Post-hoc analysis of load effects in extracted median values. (**C**) Coupled changes between our spectral power modulation factor (SPMF) and pupil modulation. Dots represent linear model residuals (see methods), colored by participant. We indicate the direction of main effects for each variable via + and - (- = small decreases, -- = large decreases, + = small increases, ++ = large increases). [* p < .05]

Next, we assessed the relation between individual modulations in pupil diameter, cortical excitability and behavior. The magnitude of pupil increases tracked increases on the spectral power modulation factor (SPMF) [r(137) = 0.22, 95%CI [0.06, 0.38], p = 0.01], but did not directly relate to entropy [r(137) = -0.06, 95%CI [-0.23, 0.1], p = 0.45] or aperiodic slope changes [r(137) = -0.04, 95%CI [-0.2, 0.13], p = 0.67]. Participants with larger increases in pupil dilation also were faster integrators at baseline (r = .31, p = .033), and decreased integration more so with increasing probe uncertainty [r(137) = -0.17, 95%CI [-0.33, 0], p = 0.05], while showing more constrained NDT increases [r(137) = -0.21, 95%CI [-0.36, -0.04], p = 0.01]. This suggests that arousal jointly related to increases in local cortical excitability and subsequent choices.

Thalamic BOLD modulation tracks excitability increases during sensation

Finally, we probed whether the thalamus acts as a subcortical nexus for sensory excitability adjustments under probe uncertainty. To allow spatially resolved insights into thalamic involvement, participants took part in a second, fMRI-based testing session during which

they performed the same task. First, we investigated uncertainty-related changes in BOLD magnitude during stimulus processing via a task PLS. This analysis suggested two reliable (LV1: permuted p = .001; LV2: permuted p = .007) latent variables (Figure 7; see Table S1 for peak coordinates/statistics and Figure S5A, B for complete multivariate spatial patterns for the two LVs), with the first LV explaining the dominant amount of variance (89.6% crossblock covariance) compared to the second LV (8.7% crossblock covariance).

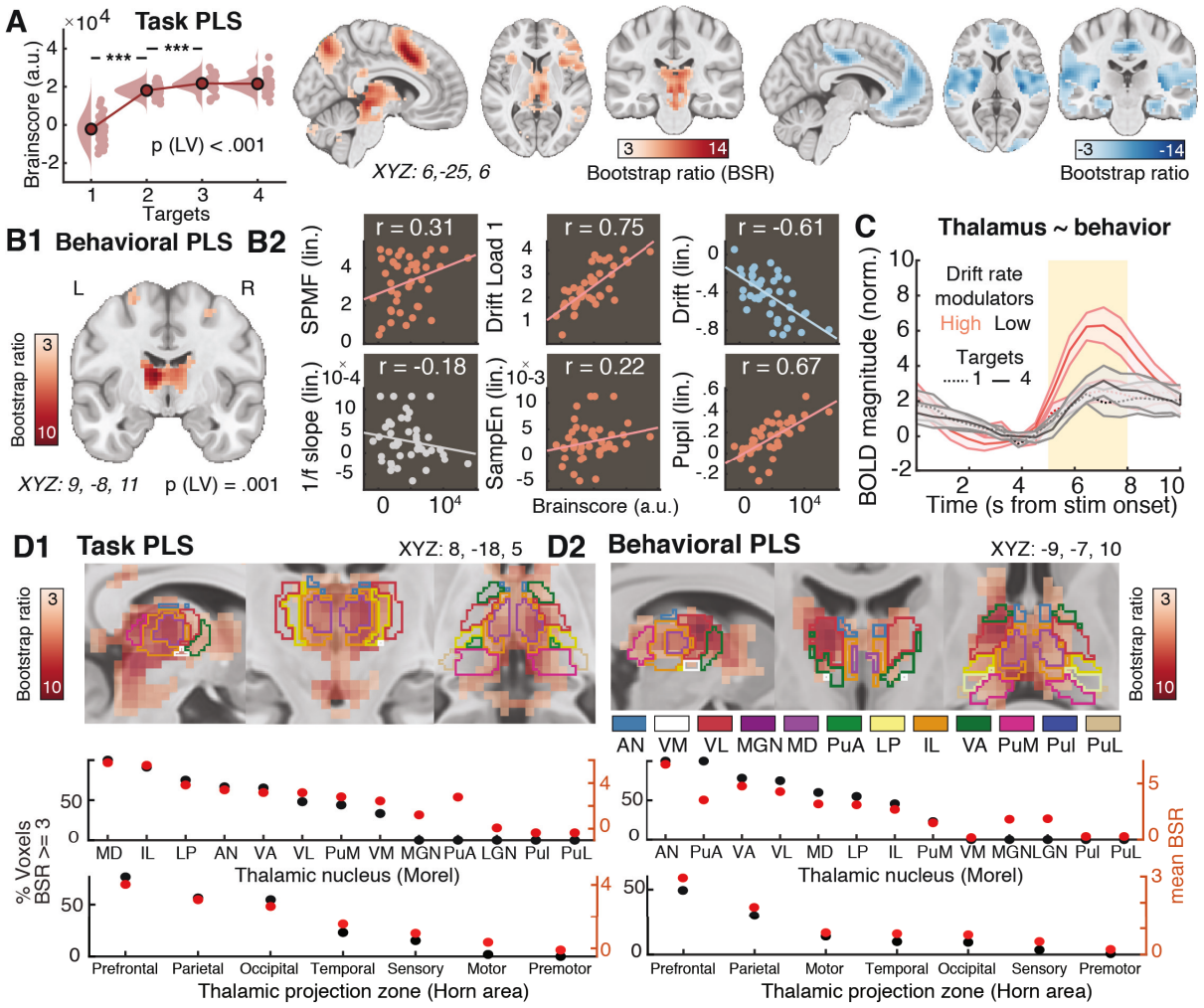

Figure 7: Upregulation of thalamic BOLD responses during stimulus processing is related to stronger excitability increases and better performance in upcoming decision task. (**A**) Results from multivariate task PLS investigating the relation of BOLD magnitude to attentional uncertainty. Data are individually centered across target loads. Activity maps show positive (left) and negative (right) bootstrap ratios of LV1, thresholded at a bootstrap ratio of 3 (p ~.001). Figure S5A presents the full loading matrices for LV1 and LV2. (**B**) Results from behavioral PLS, probing the association between linear changes in BOLD magnitude with behavioral, electrophysiological and pupillary changes under uncertainty. Figure S5B presents the complete factor loadings. (**C**) Visualization of thalamic modulation with uncertainty, split between low- and high- behavioral drift modulators (mean +- SE). The yellow shading indicates the approximate stimulus presentation period after accounting for the delay in the hemodynamic response function. Figure S5C plots all target conditions by group. (**D**) Thalamic expression pattern of the first task LV (D1) and the behavioral LV (D2). Scatters below indicate the major nuclei and projection zones in which behavioral relations are maximally reliable. For abbreviations see methods. Strongest expression is observed in antero-medial nuclei that project to fronto-parietal cortical targets. [*** p < .001]

The first latent variable (LV1) indicated load-related increases dominantly in cortical areas encompassing the fronto-parietal and the salience network, as well as thalamus. Primary positive contributors to LV1 (i.e., representing increases in BOLD with increasing probe uncertainty) were located in mid-cingulate cortex (MCG), inferior parietal lobule (IPL), bilateral anterior insula (aINS), inferior occipital gyrus (IOG), thalamus and bilateral inferior frontal gyrus (IFG). In contrast, relative uncertainty-related decreases in BOLD magnitude were dominantly observed in pallidum (potentially reflecting reduced motor preparation), bilateral posterior insula (pINS), left SFG, and left mid-cingulate cortex. Individual brain score increases were associated with stronger drift rate decreases [r(122) = -0.36, 95%CI [-0.5, -0.19], p = 5.11e-5], but not NDT, SPMF, or entropy (all p >.05). See Text S8 for results from the second latent variable (LV2), which might reflect decreased engagement at higher levels of target uncertainty.

Finally, we performed a behavioral PLS to probe whether regional BOLD modulation tracked a unified set of individual differences in the modulation of cortical excitability, arousal and behavior. In fact, we observed a single significant LV (permuted *p* = .001, 46.2% crossblock covariance) that dominantly loaded on anterior and midline thalamic nuclei with fronto-parietal projection zones (Figure 7D), and extended broadly across almost the entirety of thalamus. BOLD magnitude increases were more pronounced in participants exhibiting higher drift rates (i.e., more available evidence) (r = 0.75, 95% bootstrapped (bs) CI = [0.72,0.86]) and stronger drift reductions under probe uncertainty (r = -0.6, 95% bsCI = [-0.78,-0.54]; Figure 7B), as well as lower baseline non-decision times (r = -.37, 95% bsCI = [-.58, -.08]), confirming that increased thalamic responses reflected behaviorally adaptive contextual adjustments. This association was specific to the behavioral adjustments of interest, as we noted no relations with NDT modulation (r = .05, 95% bsCI = [-.31, .3]) or boundary separation (r = .08, 95% CI = [-.24, .37]). Importantly, higher (dominantly thalamic) BOLD modulation was further associated with greater increases on the SPMF (r = 0.31, 95% CI = [0.16,0.58]), in phasic pupil dilation (r = 0.67, 95% bsCI = [0.51,0.81]) and in entropy assessed during the EEG session (r = 0.22, 95% bsCI = [0.08,0.46]; Figure 7B). 1/f shallowing was not stably related to BOLD modulation (r = -0.18, 95% bsCI = [-0.38,0.17]), potentially due to noisier individual estimates. BOLD modulation was unrelated to chronological age (r = -.19, p = .21), gender (male vs. female; r = -.27, p = .08), subjective task difficulty (rated on 5-point Likert scale; r = -.02, p = .89), or framewise displacement of BOLD signals (an estimate of in-scanner motion; r = -.24, p = .13). Taken together, these results suggest a major role of the thalamus in integrating phasic neuromodulation to regulate rhythmic and aperiodic cortical excitability according to contextual demands.

Discussion

To efficiently process information, cortical networks must be flexibly tuned to environmental demands. Invasive studies indicate a crucial role of the thalamus in such adaptations (for a review see Halassa & Kastner, 2017), but human evidence on thalamic involvement in rapid cortical regime switches at the service of behavioral flexibility has been missing. By combining a multi-modal experimental design with a close look at individual differences, we found that processing under contextual uncertainty is associated with a triad characterized by thalamic BOLD modulation, EEG-based cortical excitability, and pupil-based indicators of arousal. In the light of this triad, we propose that thalamic regulation of sensory excitability is crucial for adaptive sensory filtering in information-rich environments.

By cueing relevant dimensions of otherwise physically identical stimuli, we observed that increases in the number of attentional targets reliably reduced participants' available evidence (as evidenced by drift rate decreases) during subsequent perceptual decisions. We interpret these changes as a negative (Dube, Emrich, & Al-Aidroos, 2017) but necessary and adaptive consequence of the need to encode multiple relevant features for an eventual decision regarding a single target. Concurrently, BOLD activity increased in the frontoparietal network (Dosenbach et al., 2007), composed of the inferior frontal junction (Zanto, Rubens, Thangavel, & Gazzaley, 2011), inferior frontal gyrus (Hampshire, Chamberlain, Monti, Duncan, & Owen, 2010), and posterior parietal cortex (Weerda, Vallines, Thomas, Rutschmann, & Greenlee, 2006; Wojciulik & Kanwisher, 1999), and the salience network (Uddin, 2015) – including anterior insula (Nelson et al., 2010) and dorsal anterior cingulate cortex (Weissman, Gopalakrishnan, Hazlett, & Woldorff, 2005). These cortical networks are thought to establish the contextual relevance of environmental stimuli, and to communicate this information to sensory cortex (Siegel et al., 2015). Accordingly, their BOLD activity often increases alongside multifaceted demands (see above), further in line with increased mediofrontal theta engagement (Cavanagh & Frank, 2014).

Besides such cortical responses at the group level however, we noted that individual increases in cortical excitability, drift rates, and arousal were tracked primarily by the extent of thalamic signal elevation, dominantly in areas with fronto-parietal projections. While past work emphasized the thalamic relay of peripheral information to cortex, recent theories highlight its dynamic involvement in cortical and cognitive function (for reviews see Dehghani & Wimmer, 2019; Halassa & Kastner, 2017; Halassa & Sherman, 2019; Pergola et al., 2018; Saalmann & Kastner, 2011; Ward, 2013; Wolff & Vann, 2019), with empirical support in humans (Garrett, Epp, Perry, & Lindenberger, 2018; Hwang, Bertolero, Liu, & D'Esposito, 2017; Shine et al., 2019), monkeys (Fiebelkorn, Pinsk, & Kastner, 2019; Saalmann, Pinsk, Wang, Li, & Kastner, 2012) and mice (Lewis et al., 2015; Schmitt et al., 2017; Wimmer et al., 2015). Notably, our task responds to demands for "tasks with multifaceted cognitive demands" (Pergola et al., 2018, p. 1017) to enhance sensitivity to higher-order thalamic involvement. In particular, anterior and midline thalamic nuclei, in which neuro-behavioral relations were maximal, may be essential for attentional set shifting (Marton, Seifikar, Luongo, Lee, & Sohal, 2018; Rikhye, Gilra, & Halassa, 2018; Wright, Vann, Aggleton, & Nelson, 2015) and to communicate such top-down information to sensory cortex via frontoparietal network coherence (Schmitt et al., 2017). Sensory processing in turn is shaped by thalamocortical transmission modes (Sherman, 2001). In 'burst mode', thalamic nuclei elicit synchronous activity that can boost stimulus detection (Alitto, Rathbun, Vandeleest, Alexander, & Usrey, 2019; Reinagel, Godwin, Sherman, & Koch, 1999) via non-linear gains of cortical responses (G. D. Smith, Cox, Sherman, & Rinzel, 2000; Swadlow & Gusev, 2001), whereas spike activity during 'tonic mode' more faithfully tracks incoming signals (Hartings, Temereanca, & Simons, 2003; Sherman, 2001). Shifts from sparse bursts towards tonic activity may underlie attention-related increases in thalamic BOLD magnitude observed here and in previous fMRI studies (Jagtap & Diwadkar, 2016; Kim, Cilles, Johnson, & Gold, 2012; Tomasi, Chang, Caparelli, & Ernst, 2007), although further work needs to elucidate the relation between thalamic transmission modes and BOLD responses (but see Liu et al., 2015).

Associated with thalamic bursting (Palva & Palva, 2007), cortical alpha rhythms may control sensory gain via periodic fluctuations in excitability (Dugue, Marque, & VanRullen, 2011; Haegens et al., 2011; Klimesch et al., 2007; Lorincz et al., 2009; Roux, Wibral, Singer, Aru, &

Uhlhaas, 2013) that can signify rapid temporal imbalances between excitation and inhibition (Atallah & Scanziani, 2009; Poo & Isaacson, 2009). Supporting this notion, we observed a coupling between alpha phase and high-frequency power during stimulus processing, with participants engaging alpha rhythms most prevalently when prior cues afforded them a focus on single stimulus features (i.e., high available sensory evidence). Alpha rhythms have been consistently linked to the pulvinar nucleus (Halgren et al., 2019; Lopes da Silva, Vos, Mooibroek, & Van Rotterdam, 1980; Saalmann et al., 2012; Stitt, Zhou, Radtke-Schuller, & Frohlich, 2018), which also contributed to our multi-modal model. The pulvinar diffusely connects to visual and fronto-parietal cortices (Arcaro, Pinsk, & Kastner, 2015), affording it to build up contextual priors (Kanai, Komura, Shipp, & Friston, 2015; O'Reilly, Wyatte, & Rohrlich, 2017; Rikhye, Wimmer, & Halassa, 2018) that can regulate 'bottom-up' stimulus processing (Jaramillo, Mejias, & Wang, 2019), potentially via alpha rhythms (Saalmann et al., 2012; Suffczynski, Kalitzin, Pfurtscheller, & da Silva, 2001). While the localization of effects within the thalamus remains challenging in BOLD signals (Hwang et al., 2017), our results support a perspective in which alpha rhythms – shaped via thalamocortical circuits – dynamically extract relevant sensory information (Sadaghiani & Kleinschmidt, 2016) when contexts afford joint distractor suppression and target enhancement (Wöstmann, Alavash, & Obleser, 2019).

Complementing such selective gain control, overall increases in excitatory tone may serve multi-feature attention when only broad attentional guidance is available. Our results provide initial evidence that probe uncertainty transiently (a) desynchronizes alpha rhythms, (b) increases gamma power, and (c) elevates sample entropy while shallowing spectral slopes, a pattern that suggests increases in excitatory contributions to E/I mixture currents (Destexhe & Rudolph, 2004; Gao et al., 2017) and asynchronous neural firing (Destexhe et al., 2003). Conceptually, elevated excitability during high probe uncertainty facilitates an efficient and rapid switching between parallel feature activations. In agreement with this idea, joint activation of neural populations coding multiple relevant features has been observed during multi-feature attention (Mo et al., 2019). Furthermore, computational modeling indicates that E/I modulations in hierarchical networks optimally adjust multi-attribute choices (Pettine et al., 2020). Similar to our observation of enhanced excitability during probe uncertainty, Pettine et al. (2020) found increases in excitatory tone optimal for a linear weighting of multiple features, whereas inhibitory engagement increased the gain for specific features during more difficult perceptual decisions. As discussed above, such inhibitory tuning may regulate selective target gains via alpha rhythms, in line with the presumed importance of inhibitory interneurons in alpha rhythmogenesis (Lorincz et al., 2009).

Finally, probe uncertainty increased phasic pupil diameter, with strong links to parallel adjustments in behavior, EEG-based excitability, and thalamic BOLD modulation. Fluctuations in pupil diameter provide a non-invasive proxy of particularly noradrenergic drive in mice (Breton-Provencher & Sur, 2019; Reimer et al., 2014; Zerbi et al., 2019), monkeys (Aston-Jones & Cohen, 2005; Joshi, Li, Kalwani, & Gold, 2016) and humans (de Gee et al., 2017). As such, our results support neuromodulation as a potent regulator of excitability both directly at cortical targets (Constantinople & Bruno, 2011; McGinley, Vinck, et al., 2015) and via thalamic circuits (Liu et al., 2015; McCormick, 1989; McCormick, McGinley, & Salkoff, 2015; Schiff, 2008). Functionally, pupil diameter rises during states of heightened uncertainty (Krishnamurthy, Nassar, Sarode, & Gold, 2017; Nassar et al., 2012; Urai, Braun, & Donner, 2017), such as change points in dynamic environments (Murphy, Wilming, Hernandez-Bocanegra, Prat Ortega, & Donner, 2020; Nassar et al., 2012), and multi-feature attention

(Alnaes et al., 2014; Koelewijn, Shinn-Cunningham, Zekveld, & Kramer, 2014), while increasing alongside cortical desynchronization (Dahl, Mather, Sander, & Werkle-Bergne, 2020; Murphy et al., 2020; Stitt et al., 2018; Waschke, Tune, & Obleser, 2019). Our results extend those observations, and suggest that neuromodulatory drive accompanies excitability increases especially when contexts prevent the formation of single attentional targets, potentially to serve a more faithful processing of complex environments (Berridge & Waterhouse, 2003; McGinley, David, et al., 2015).

Multiple neuromodulators, prominently noradrenaline and acetylcholine, regulate thalamocortical excitability (Lee & Dan, 2012; McCormick et al., 2015) and pupil responses (Reimer et al., 2014), but may differentially serve perceptual sensitivity vs. specificity demands (Shine, 2019). Specifically, noradrenergic drive may increase sensitivity to external stimuli (McCormick et al., 1991; Waterhouse & Navarra, 2019) by increasing E/I ratios (Froemke, Merzenich, & Schreiner, 2007; Martins & Froemke, 2015; Pfeffer et al., 2018), whereas cholinergic innervation might facilitate response selectivity (Bauer et al., 2012; Furey, Pietrini, & Haxby, 2000). However, as contrasting effects have also been observed for these modulators (e.g., Hirata, Aguilar, & Castro-Alamancos, 2006; Minces, Pinto, Dan, & Chiba, 2017; Vinck, Batista-Brito, Knoblich, & Cardin, 2015; Yu & Dayan, 2005), their functional separability necessitates further work.

To conclude, we report initial evidence that thalamocortical excitability adjustments guide human perception and decisions under uncertainty. Our results point to neuromodulatory changes regulated by the thalamus that trigger behaviorally relevant switches in cortical dynamics, from alpha-rhythmic gain control to increased tonic excitability, when contexts require a more faithful processing of information-rich environments. Given that difficulties in dealing with uncertainty, neuro-sensory hyperexcitability, and deficient E/I control are hallmarks of several clinical disorders (e.g., McFadyen, Dolan, & Garrido, 2020; Yang et al., 2016; Yizhar et al., 2011), we surmise that further research on individual differences in the modulation of contextual excitability might advance our understanding of cognitive flexibility in both healthy and diseased populations.

Methods

Sample

47 healthy young adults (18-35 years, mean age = 25.8 years, SD = 4.6, 25 women) performed a dynamic visual attention task during 64-channel active scalp EEG acquisition, 42 of whom returned for a subsequent 3T fMRI session. Due to participant and scanner availability, the average span between EEG and MR testing sessions was 9.8 days (SD = 9.5 days). Participants were recruited from the participant database of the Max Planck Institute for Human Development, Berlin, Germany (MPIB). Participants were right-handed, as assessed with a modified version of the Edinburgh Handedness Inventory (Oldfield, 1971), and had normal or corrected-to-normal vision. Participants reported to be in good health with no known history of neurological or psychiatric incidences, and were paid for their participation (10 € per hour). All participants gave written informed consent according to the institutional guidelines of the Deutsche Gesellschaft für Psychologie (DGPS) ethics board, which approved the study.

Procedure: EEG Session

Participants were seated at a distance of 60 cm in front of a monitor in an acoustically and electrically shielded chamber with their heads placed on a chin rest. Following electrode placement, participants were instructed to rest with their eyes open and closed, each for 3 minutes. Afterwards, participants performed a standard Stroop task, followed by the visual attention task instruction & practice (see below), the performance of the task and a second Stroop assessment (Stroop results are not reported here). Stimuli were presented on a 60 Hz 1920x1080p LCD screen (AG Neovo X24) using PsychToolbox 3.0.11 (Brainard, 1997; Kleiner, Brainard, & Pelli, 2007; Pelli, 1997). The session lasted ~3 hours. EEG was continuously recorded from 60 active (Ag/AgCl) electrodes using BrainAmp amplifiers (Brain Products GmbH, Gilching, Germany). Scalp electrodes were arranged within an elastic cap (EASYCAP GmbH, Herrsching, Germany) according to the 10% system (Oostenveld & Praamstra, 2001), with the ground placed at AFz. To monitor eye movements, two additional electrodes were placed on the outer canthi (horizontal EOG) and one electrode below the left eye (vertical EOG). During recording, all electrodes were referenced to the right mastoid electrode, while the left mastoid electrode was recorded as an additional channel. Online, signals were digitized at a sampling rate of 1 kHz. In addition to EEG, we simultaneously tracked eye movements and assessed pupil diameter using EyeLink 1000+ hardware (SR Research, v.4.594) with a sampling rate of 1kHz.

Procedure: MRI session

Forty-two participants returned for a second testing session that included structural and functional MRI assessments. First, participants took part in a short refresh of the visual attention task (“MAAT”, see below) instructions and practiced the task outside the scanner. Then, participants were located in the TimTrio 3T scanner and were instructed in the button mapping. We collected the following sequences: T1w, task (4 runs), T2w, resting state, DTI, with a 15 min out-of-scanner break following the task acquisition. The session lasted ~3 hours. Whole-brain task fMRI data (4 runs á ~11,5 mins, 1066 volumes per run) were collected via a 3T Siemens TrioTim MRI system (Erlangen, Germany) using a multi-band EPI

sequence (factor 4; TR = 645 ms; TE = 30 ms; flip angle 60°; FoV = 222 mm; voxel size 3x3x3 mm; 40 transverse slices. The first 12 volumes (12 × 645 ms = 7.7 sec) were removed to ensure a steady state of tissue magnetization (total remaining volumes = 1054 per run). A T1-weighted structural scan was also acquired (MPRAGE: TR = 2500 ms; TE = 4.77 ms; flip angle 7°; FoV = 256 mm; voxel size 1x1x1 mm; 192 sagittal slices). A T2-weighted structural scan was also acquired (GRAPPA: TR = 3200 ms; TE = 347 ms; FoV = 256 mm; voxel size 1x1x1 mm; 176 sagittal slices).

The multi-attribute attention task ("MAAT")

We designed a task to parametrically control top-down attention to multiple feature dimensions, in the absence of systematic variation in bottom-up visual stimulation (see Figure 1). Participants attended a dynamic square display that jointly consisted of four attributes: color (red/green), movement direction (left, right), size (small, large) and saturation (low, high). The task incorporates features from random dot motion tasks which have been extensively studied in both animal models (Gold & Shadlen, 2007; Hanks & Summerfield, 2017; Siegel et al., 2015) and humans (Banca et al., 2015; Kelly & O'Connell, 2013). Following the presentation of these displays, a probe queried the prevalence of one of the four attributes in the display (e.g. whether the display comprised a greater proportion of either smaller or larger squares). Prior to stimulus onset, valid cue presentation informed participants about the active feature set, out of which one feature would be chosen as the probe. We parametrically manipulated uncertainty regarding the upcoming probe by systematically varying both the number and type of relevant features in the display.

The difficulty of each feature was determined by (a) the fundamental feature difference between the two alternatives and (b) the sensory evidence for each alternative in the display. For (a) the following values were used: high (RGB: 192, 255, 128) and low saturation green (RGB: 255, 128, 149) and high (RGB: 128, 255, 0) and low saturated red (RGB: 255, 0, 43) for color and saturation, 5 and 8 pixels for size differences and a coherence of .2 for directions. For (b) the proportion of winning to losing option (i.e. sensory evidence) was chosen as follows: color: 60/40; direction: 80/20; size: 65/35; luminance: 60/40. Parameter difficulty was established in a pilot population, with the aim to produce above-chance accuracy for individual features.

The experiment consisted of four runs of ~10 min, each consisting of eight blocks of eight trials (i.e., a total of 32 trial blocks; 256 trials). The size and constellation of the cue set was held constant within eight-trial blocks to reduce set switching and working memory demands. Each trial was structured as follows: cue onset during which the relevant targets were centrally presented (1 s), fixation phase (2 s), dynamic stimulus phase (3 s), probe phase (incl. response; 2 s); ITI (un-jittered; 1.5 s). At the onset of each block, the valid cue (attentional target set) was presented for 5 s. At the offset of each block, participants received feedback for 3 s. The four attributes spanned a constellation of 16 feature combinations (4x4), of which presentation frequency was matched within subjects. The size and type of cue set was pseudo-randomized, such that every size and constellation of the cue set was presented across blocks. Within each run of four blocks, every set size was presented once, but never directly following a block of the same set size. In every block, each feature in the active set acted as a probe in at least one trial. Moreover, any attribute equally often served as a probe across all blocks. Winning options for each feature were balanced across trials, such that (correct) button responses were equally distributed across

the experiment. To retain high motivation during the task and encourage fast and accurate responses, we instructed participants that one response would randomly be drawn at the end of each block; if this response was correct and faster than the mean RT during the preceding block, they would earn a reward of 20 cents. However, we pseudo-randomized feedback such that all participants received a fixed payout of 10 € per session. This extra money was paid in addition to the participation fee at the end of the second session, at which point participants were debriefed.

Behavioral estimates of probe-related decision processes

Sequential sampling models, such as the drift-diffusion model (DDM (Ratcliff & McKoon, 2008)), have been used to characterize evolving perceptual decisions in 2-alternative forced choice (2AFC) random dot motion tasks (Kelly & O'Connell, 2013), where the evolving decision relates to overt stimulus dynamics. In contrast with such applications, evidence integration here is tied to eidetic memory traces following the probe onset, similar to applications during memory retrieval (Ratcliff, 1978) or probabilistic decision making (Frank et al., 2015). Here, we estimated individual evidence integration parameters within the HDDM 0.6.0 toolbox (Wiecki, Sofer, & Frank, 2013) to profit from the large number of participants that can establish group priors for the relatively sparse within-subject data. Independent models were fit to data from the EEG and the fMRI session to allow reliability assessments of individual estimates. Premature responses faster than 250 ms were excluded prior to modeling, and the probability of outliers was set to 5%. 7000 Markov-Chain Monte Carlo samples were sampled to estimate parameters, with the first 5000 samples being discarded as burn-in to achieve convergence. We judged convergence for each model by visually assessing both Markov chain convergence and posterior predictive fits. Individual estimates were averaged across the remaining 2000 samples for follow-up analyses.

We fitted data to correct and incorrect RTs (termed ‘accuracy coding‘ in Wiecki et al. (2013)). To explain differences in decision components, we compared four separate models. In the ‘full model’, we allowed the following parameters to vary between conditions: (i) the mean drift rate across trials, (ii) the threshold separation between the two decision bounds, (iii) the non-decision time, which represents the summed duration of sensory encoding and response execution. In the remaining models, we reduced model complexity, by only varying (a) drift, (b) drift + threshold, or (c) drift + NDT, with a null model fixing all three parameters. For model comparison, we first used the Deviance Information Criterion (DIC) to select the model which provided the best fit to our data. The DIC compares models on the basis of the maximal log-likelihood value, while penalizing model complexity. The full model provided the best fit to the empirical data based on the DIC index (Figure S1B) in both the EEG and the fMRI session. However, this model indicated an increase in decision thresholds (i.e., boundary separation) without an equivalent in the electrophysiological data (Figure S1C). We therefore fixed the threshold parameter across conditions, in line with previous work constraining model parameters on the basis of electrophysiological evidence (McGovern et al., 2018).

EEG preprocessing

Preprocessing and analysis of EEG data were conducted with the FieldTrip toolbox (Oostenveld, Fries, Maris, & Schoffelen, 2011) and using custom-written MATLAB (The MathWorks Inc., Natick, MA, USA) code. Offline, EEG data were filtered using a 4th order

Butterworth filter with a pass-band of 0.5 to 100 Hz. Subsequently, data were down-sampled to 500 Hz and all channels were re-referenced to mathematically averaged mastoids. Blink, movement and heart-beat artifacts were identified using Independent Component Analysis (ICA; Bell & Sejnowski, 1995) and removed from the signal. Artifact-contaminated channels (determined across epochs) were automatically detected using (a) the FASTER algorithm (Nolan, Whelan, & Reilly, 2010), and by (b) detecting outliers exceeding three standard deviations of the kurtosis of the distribution of power values in each epoch within low (0.2-2 Hz) or high (30-100 Hz) frequency bands, respectively. Rejected channels were interpolated using spherical splines (Perrin, Pernier, Bertrand, & Echallier, 1989). Subsequently, noisy epochs were likewise excluded based on FASTER and on recursive outlier detection. Finally, recordings were segmented to participant cues to open their eyes, and were epoched into non-overlapping 3 second pseudo-trials. To enhance spatial specificity, scalp current density estimates were derived via 4th order spherical splines (Perrin et al., 1989) using a standard 1005 channel layout (conductivity: 0.33 S/m; regularization: 1^-05; 14th degree polynomials).

Electrophysiological estimates of probe-related decision processes

Centroparietal Positive Potential (CPP). The centroparietal positive potential (CPP) is an electrophysiological signature of internal evidence-to-bound accumulation (Kelly & O'Connell, 2013; McGovern et al., 2018; O'Connell et al., 2012). We probed the task modulation of this established signature and assessed its convergence with behavioral parameter estimates. To derive the CPP, preprocessed EEG data were low-pass filtered at 8 Hz with a 6th order Butterworth filter to exclude low-frequency oscillations, epoched relative to response and averaged across trials within each condition. In accordance with the literature, this revealed a dipolar scalp potential that exhibited a positive peak over parietal channel POz (see Figure 2). We temporally normalized individual CPP estimates to a condition-specific baseline during the final 250 ms preceding probe onset. As a proxy of evidence drift rate, CPP slopes were estimates via linear regression from -250 ms to -100 ms surrounding response execution, while the average CPP amplitude from -50 ms to 50 ms served as an indicator of decision thresholds (i.e., boundary separation) (e.g., McGovern et al., 2018).

To investigate whether a similar 'ramping' potential was observed during stimulus presentation, we aligned data to stimulus onset and temporally normalized signals to the condition-specific signal during the final 250 ms prior to stimulus onset. During stimulus presentation, no 'ramp'-like signal or load modulation was observed at the peak CPP channel. This suggests that immediate choice requirements were necessary for the emergence of the CPP, although prior work has shown the CPP to be independent of explicit motor requirements (O'Connell et al., 2012).

Finally, we assessed whether differences between probed stimulus attributes could account for load-related CPP changes (Figure S2C). For this analysis, we selected trials separately by condition and probed attribute. Note that for different probes, but not cues, trials were uniquely associated with each feature and trial counts were approximately matched across conditions. We explored differences between different conditions via paired t-tests. To assess load effects on CPP slopes and thresholds as a function of probed attribute, we calculated 1st-level load effects by means of a linear model, and assessed their difference from zero via paired t-tests.

Contralateral mu-beta. Decreases in contralateral mu-beta power provide a complementary, effector-specific signature of evidence integration (Donner et al., 2009; McGovern et al., 2018). We estimated mu-beta power using 7-cycle wavelets for the 8-25 Hz range with a step size of 50 ms. Spectral power was time-locked to probe presentation and response execution. We re-mapped channels to describe data recorded contra- and ipsi-lateral to the executed motor response in each trial, and averaged data from those channels to derive grand average mu-beta time courses. Individual average mu-beta time series were baseline-corrected using the -400 to -200 ms prior to probe onset, separately for each condition. For contralateral motor responses, remapped sites C3/5 and CP3/CP5 were selected based on the grand average topography for lateralized response executions (see inset in Figure S2A). As a proxy of evidence drift rate, mu-beta slopes were estimates via linear regression from -250 ms to -50 ms prior to response execution, while the average power -50 ms to 50 ms served as an indicator of decision thresholds (e.g., McGovern et al., 2018).

Electrophysiological indices of top-down modulation during sensation

Low-frequency alpha and theta power. We estimated low-frequency power via a 7-cycle wavelet transform, using, for linearly spaced center frequencies in 1 Hz steps from 2 to 15 Hz. The step size of estimates was 50 ms, ranging from -1.5 s prior to cue onset to 3.5 s following stimulus offset. Estimates were log10-transformed at the single trial level (Smulders, ten Oever, Donkers, Quaedflieg, & van de Ven, 2018), with no explicit baseline.

High-frequency gamma power. Gamma responses were estimated using multi-tapers (five tapers; discrete prolate spheroidal sequences) with a step size of 200 ms, a window length of 400 ms and a frequency resolution of 2.5 Hz. The frequency range covered frequencies between 45-90 Hz, with spectral smoothing of 8 Hz. Estimates were log10-transformed at the single trial level. We normalized individual gamma-band responses via single-trial z-normalization. In particular, for each frequency, we subtracted single-trial power -700 to -100 ms prior to stimulus onset, and divided by the standard deviation of power values during the same period. Finally, to account for baseline shifts during the pre-stimulus period, we subtracted condition-wise averages during the same baseline period.

Multivariate assessment of spectral power changes with stimulus onset and uncertainty. To determine changes in spectral power upon stimulus onset, and during stimulus presentation with load, we entered individual power values into multivariate partial least squares (PLS) analyses (see *Multivariate partial least squares analyses*) using the MEG-PLS toolbox [version 2.02b] (Cheung, Kovacevic, Fatima, Misic, & McIntosh, 2016). We concatenated low- (2-15 Hz) and high-frequency (45-90 Hz) power matrices to assess joint changes in the PLS models. To examine a multivariate contrast of spectral changes upon stimulus onset (averaged across conditions) with spectral power in the pre-stimulus baseline period, we performed a task PLS on data ranging from 500 ms pre-stim to 500 ms post-stim. Temporal averages from -700 to -100 ms pre-stimulus onset were subtracted as a baseline. To assess power changes as a function of probe uncertainty, we segmented the data from 500 ms post stim onset to stimulus offset (to exclude transient evoked onset responses), and calculated a task PLS concerning the relation between experimental uncertainty conditions and time-space-frequency power values. As a control, we performed a behavioral PLS analysis to assess the relevance of individual frequency contributions to the behavioral relation. For this analysis, we computed linear slopes (target amount) for each

time-frequency point at the 1st (within-subject) level, which were subsequently entered into the 2nd level PLS analysis. On the behavioral side, we assessed both linear changes in pupil diameter, as well as drift rates during selective attention and linear decreases in drift rate under uncertainty. Finally, spontaneous fluctuations in pre-stimulus power have been linked to fluctuations in cortical excitability (Iemi, Chaumon, Crouzet, & Busch, 2017; Lange, Oostenveld, & Fries, 2013). We thus probed the role of upcoming processing requirements on pre-stimulus oscillations, as well as the potential relation to behavioral outcomes using task and behavioral PLS analyses. The analysis was performed as described above, but restricted to time points occurring during the final second prior to stimulus onset.

Steady State Visual Evoked Potential (SSVEP). The SSVEP characterizes the phase-locked, entrained visual activity (here 30 Hz) during dynamic stimulus updates (e.g., Ding, Sperling, & Srinivasan, 2006). These features differentiate it from induced broadband activity or muscle artefacts in similar frequency bands. We used these properties to normalize individual single-trial SSVEP responses prior to averaging: (a) we calculated an FFT for overlapping one second epochs with a step size of 100 ms (Hanning-based multitaper), averaged them within each load condition and, (b) spectrally normalized 30 Hz estimates by subtracting the average of estimates at 28 and 32 Hz, effectively removing broadband effects (i.e., aperiodic slopes), (c) and finally, we subtracted a temporal baseline -700 to -100 ms prior to stimulus onset. Linear load effects on SSVEPs were assessed by univariate cluster-based permutation tests on channel x time data (see *Univariate statistical analyses using cluster-based permutation tests*).

Time-resolved sample entropy. Sample entropy (Richman & Moorman, 2000) quantifies the irregularity of a time series of length *N* by assessing the conditional probability that two sequences of *m* consecutive data points will remain similar when another sample (*m+1*) is included in the sequence (for a visual example see Figure 1A). Sample entropy is defined as the inverse natural logarithm of this conditional similarity: $\mathrm{SampEn}(m, r, N) = -\log\left(\frac{p^{m+1}(r)}{p^{m}(r)}\right)$. The similarity criterion (*r*) defines the tolerance within which two points are considered similar and is defined relative to the standard deviation (~variance) of the signal (here set to r = .5). We set the sequence length *m* to 2, in line with previous applications (Kosciessa, Kloosterman, et al., 2020). An adapted version of sample entropy calculations was used (Grandy, Garrett, Schmiedek, & Werkle-Bergner, 2016; Kloosterman, Kosciessa, Lindenberger, Fahrenfort, & Garrett, 2019; Kosciessa, Kloosterman, et al., 2020), wherein entropy is estimated across discontinuous data segments to provide time-resolved estimates. The estimation of scale-wise entropy across trials allows for an estimation of coarse scale entropy also for short time-bins, i.e., without requiring long, continuous signals, while quickly converging with entropy estimates from continuous recordings (Grandy et al., 2016). To remove the influence of posterior-occipital low-frequency rhythms on entropy estimates, we notch-filtered the 8-15 Hz alpha band using 6th order Butterworth filter prior to the entropy calculation (Kosciessa, Kloosterman, et al., 2020). Time-resolved entropy estimates were calculated for 500 ms windows from -1 s pre-stimulus to 1.25 s post-probe with a step size of 150 ms. As entropy values are implicitly normalized by the variance in each time bin via the similarity criterion, no temporal baselining was used. Linear load effects on entropy were assessed by univariate cluster-based permutation tests on channel x time data (see *Univariate statistical analyses using cluster-based permutation tests*).

Aperiodic (1/f) slopes. The aperiodic 1/f slope of neural recordings is closely related to the sample entropy of broadband signals (Kosciessa, Kloosterman, et al., 2020), and has been

suggested as a proxy for 'cortical excitability' and excitation-inhibition balance (Gao et al., 2017). Spectral estimates were computed by means of a Fast Fourier Transform (FFT) over the final 2.5 s of the presentation period (to exclude onset transients) for 41 logarithmically spaced frequencies between 2 and 64 Hz (Hanning-tapered segments zero-padded to 10 s) and subsequently averaged. Spectral power was log10-transformed to render power values more normally distributed across subjects. Power spectral density (PSD) slopes were derived by linearly regressing log-transformed power values on log-transformed frequencies. The spectral range from 7-13 Hz was excluded from the background fit to exclude a bias by the narrowband alpha peak (Kosciessa, Kloosterman, et al., 2020) and thus to increase the specificity to aperiodic variance. Linear load effects on 1/f slopes were assessed by univariate cluster-based permutation tests on channel data (see *Univariate statistical analyses using cluster-based permutation tests*).

Rhythm-specific estimates. Spectral power estimates conflate rhythmicity with aperiodic events in time, space and magnitude (Kosciessa, Grandy, Garrett, & Werkle-Bergner, 2020). Given that we observed changes in aperiodic slopes, we verified that observed narrowband effects in the theta and alpha band describe narrowband changes in rhythmicity. For this purpose, we identified single-trial spectral events using the extended BOSC method (Caplan, Madsen, Raghavachari, & Kahana, 2001; Kosciessa, Grandy, et al., 2020; Whitten, Hughes, Dickson, & Caplan, 2011). In short, this method identifies stereotypic 'rhythmic' events at the single-trial level, with the assumption that such events have significantly higher power than the 1/f background and occur for a minimum number of cycles at a particular frequency. This procedure dissociates narrowband spectral peaks from the aperiodic background spectrum. Here, we used a three-cycle threshold during detection, while defining the power threshold as the 95th percentile above the individual background power. A 5-cycle wavelet was used to provide the time-frequency transformations for 49 logarithmically-spaced center frequencies between 1 and 64 Hz. Rhythmic episodes were detected as described in (Kosciessa, Grandy, et al., 2020). Prior to fitting the 1/f slopes, the most dominant individual rhythmic alpha peak between 8 and 15 Hz was removed, as well as the 28-32 Hz range, to exclude the SSVEP. Detection of episodes was restricted to the time of stimulus presentation, excluding the first 500 ms to reduce residual pre-stimulus activity and onset transients. Within each participant and channel, the duration and SNR of individual episodes with a mean frequency between 4-8 Hz (Theta) and 8-15 Hz (Alpha) were averaged across trials. Effects of target number were assessed within the averaged spatial clusters indicated in Figure 3 by means of paired t-tests.

Alpha-gamma phase-amplitude coupling (PAC)

We assessed alpha-phase-to-gamma-amplitude coupling to assess the extent of phasic modulation of gamma power within the alpha band. As phase information is only interpretable during the presence of a narrowband rhythm (Aru et al., 2015), we focused our main analysis on 250 ms time segments following the estimated onset of a rhythm in the 8-15 Hz alpha range (see *Rhythm-specific estimates* above; Figure 4A). This time window ensured that segments fulfilled the 3-cycle criterion imposed during eBOSC rhythm detection to ensure that a rhythm was present. We selected three occipital channels with maximal gamma power (O1, O2, Oz; shown in Figure 4A) and pooled detected alpha episodes across these channels. We pooled data across load conditions, as we observed no consistent PAC within individual load conditions (data not shown), perhaps due to low episode counts. To derive the alpha carrier phase, we band-pass filtered signals in the 8-15 Hz band, and

estimated the analytic phase time series via Hilbert transform. For the amplitude of modulated frequencies, we equally applied band-pass filters from 40 to 150 Hz (step size: 2 Hz), with adaptive bandwidths (+/- 20% of center frequency). Filtering was implemented using MATLAB's acausal filtfilt() routine using linear finite impulse response (FIR) filters with an adaptive filter order set as 3 times the ratio of the sampling frequency to the low-frequency cutoff (Tort et al., 2008). For each applied bandpass filter, we removed 250 ms at each edge to avoid filter artifacts. For each frequency, narrowband signals were z-scored to normalize amplitudes across frequencies, and absolute values of the Hilbert-derived complex signal were squared to produce instantaneous power time series. We estimated the MI between the 8-15 Hz phase and high-frequency power via normalized entropy (Tort et al., 2008) using 16 phase bins. Power estimates were normalized by dividing the bin-specific power by the sum of power across bins. To make MI estimates robust against random coupling, we estimated MI for 1000 surrogate data, which shuffled the trial association of phase and amplitude information. We subtracted the mean surrogate MI value from the original MI index for a final, surrogate-normalized MI estimate. The resulting MI estimates across frequencies were then subjected to a cluster-based permutation test to assess significant clusters from zero using paired t-tests. For Figure 4B, we followed the procedure by Canolty et al. (2006). Alpha troughs were identified as local minima of phases < [-pi+.01]. For visualization, data were averaged across center frequencies from 80-150 Hz, as significant coupling overlapped with this range. We performed identical analyses for the 250 ms periods prior to rhythm onset (grey shading in Figure 4A) as a control condition. We performed analogous phase-amplitude-coupling analyses for the Mean Vector Length (MVL; Canolty et al., 2006) index, with comparable results (data not shown).

Analyses of pupil diameter

Pupil diameter was recorded during the EEG session using EyeLink 1000 at a sampling rate of 1000 Hz, and was analyzed using FieldTrip and custom-written MATLAB scripts. Blinks were automatically indicated by the EyeLink software (version 4.40). To increase the sensitivity to periods of partially occluded pupils or eye movements, the first derivative of eye-tracker-based vertical eye movements was calculated, z-standardized and outliers >= 3 STD were removed. We additionally removed data within 150 ms preceding or following indicated outliers. Finally, missing data were linearly interpolated and data were epoched to 3.5 s prior to stimulus onset to 1 s following stimulus offset. We quantified phasic arousal responses via the 1st temporal derivative (i.e. rate of change) of pupil diameter traces, as this measure (i) has higher temporal precision and (ii) has been more strongly associated with noradrenergic responses than the overall response (Reimer et al., 2014). We downsampled pupil time series to 200 Hz. For visualization, but not statistics, we smoothed pupil traces using a moving average median of 200 ms. We statistically assessed a linear load effect using a cluster-based permutation test on the 1D pupil traces (see *Univariate statistical analyses using cluster-based permutation tests*). For post-hoc assessments, we extracted the median pupil derivative during the first 1.5 s following stimulus onset.

fMRI-based analyses

Preprocessing of functional MRI data. fMRI data were preprocessed with FSL 5 (RRID:SCR_002823) (Jenkinson, Beckmann, Behrens, Woolrich, & Smith, 2012; S. M. Smith et al., 2004). Pre-processing included motion correction using McFLIRT, smoothing (7mm)

and high-pass filtering (.01 Hz) using an 8th order zero-phase Butterworth filter applied using MATLAB's filtfilt function. We registered individual functional runs to the individual, ANTs brain-extracted T2w images (6 DOF), to T1w images (6 DOF) and finally to 3mm standard space (ICBM 2009c MNI152 nonlinear symmetric) (Fonov et al., 2011) using nonlinear transformations in ANTs (Avants et al., 2011). (For one participant, no T2w image was acquired and 6 DOF transformation of BOLD data was preformed directly to the T1w structural scan.) We then masked the functional data with the ICBM 2009c GM tissue prior (thresholded at a probability of 0.25), and detrended the functional images (up to a cubic trend) using SPM8.

We also used a series of extended preprocessing steps to further reduce potential non-neural artifacts (Garrett, Kovacevic, McIntosh, & Grady, 2010; Garrett et al., 2015). Specifically, we examined data within-subject, within-run via spatial independent component analysis (ICA) as implemented in FSL-MELODIC (Beckmann & Smith, 2004). Due to the high multiband data dimensionality in the absence of low-pass filtering, we constrained the solution to 30 components per participant. Noise components were identified according to several key criteria: a) Spiking (components dominated by abrupt time series spikes); b) Motion (prominent edge or "ringing" effects, sometimes [but not always] accompanied by large time series spikes); c) Susceptibility and flow artifacts (prominent air-tissue boundary or sinus activation; typically represents cardio/respiratory effects); d) White matter (WM) and ventricle activation (Birn, 2012); e) Low-frequency signal drift (A. M. Smith et al., 1999); f) High power in high-frequency ranges unlikely to represent neural activity (≥ 75% of total spectral power present above .10 Hz;); and g) Spatial distribution ("spotty" or "speckled" spatial pattern that appears scattered randomly across ≥ 25% of the brain, with few if any clusters with ≥ 80 contiguous voxels [at 2x2x2 mm voxel size]). Examples of these various components we typically deem to be noise can be found in (Garrett, McIntosh, & Grady, 2014). By default, we utilized a conservative set of rejection criteria; if manual classification decisions were challenging due to mixing of "signal" and "noise" in a single component, we generally elected to keep such components. Three independent raters of noise components were utilized; > 90% inter-rater reliability was required on separate data before denoising decisions were made on the current data. Components identified as artifacts were then regressed from corresponding fMRI runs using the regfilt command in FSL.

To reduce the influence of motion and physiological fluctuations, we regressed FSL's 6 DOF motion parameters from the data, in addition to average signal within white matter and CSF masks. Masks were created using 95% tissue probability thresholds to create conservative masks. Data and regressors were demeaned and linearly detrended prior to multiple linear regression for each run. To further reduce the impact of potential motion outliers, we censored significant DVARS outliers during the regression as described by (Power et al., 2014). In particular, we calculated the 'practical significance' of DVARS estimates and applied a threshold of 5 (Afyouni & Nichols, 2018). The regression-based residuals were subsequently spectrally interpolated during DVARS outliers as described in (Power et al., 2014) and (Parkes, Fulcher, Yucel, & Fornito, 2018). BOLD analyses were restricted to participants with both EEG and MRI data available (N = 42).

1st level analysis: univariate beta weights for load conditions. We conducted a 1st level analysis using SPM12 to identify beta weights for each load condition separately. Design variables included stimulus presentation by load (4 volumes; parametrically modulated by sequence position), onset cue (no mod.), probe (2 volumes, parametric modulation by RT).

Design variables were convolved with a canonical HRF, including its temporal derivative as a nuisance term. Nuisance regressors included 24 motion parameters (Friston, Williams, Howard, Frackowiak, & Turner, 1996), as well as continuous DVARS estimates. Autoregressive modelling was implemented via FAST. Output beta images for each load condition were finally averaged across runs.

2nd level analysis: Multivariate modulation of BOLD responses. We investigated the multivariate modulation of the BOLD response at the 2nd level using PLS analyses (see *Multivariate partial least squares analyses*). Specifically, we probed the relationship between voxel-wise 1st level beta weights and probe uncertainty within a task PLS. Next, we assessed the relationship between task-related BOLD signal changes and interindividual differences in the joint modulation of decision processes, cortical excitability, and pupil modulation by means of a behavioral PLS. For this, we first calculated linear slope coefficients for voxel-wise beta estimates. Then, we included behavioral variables including HDDM parameter estimates during selective attention, as well as linear changes with load, individual linear condition modulation of the following variables: multivariate spectral power, pupil dilation, 1/f modulation and entropy residuals. Prior to these covariates in the model, we visually assessed whether the distribution of linear changes variables was approximately Gaussian. In the case of outliers (as observed for the SPMF, 1/f slopes, and entropy), we winsorized values at the 95th percentile. For visualization, spatial clusters were defined based on a minimum distance of 10 mm, and by exceeding a size of 25 voxels. We identified regions associated with peak activity based on cytoarchitectonic probabilistic maps implemented in the SPM Anatomy Toolbox (Version 2.2c) (Eickhoff et al., 2005). If no assignment was found, the most proximal assignment to the coordinates reported in Table S1 within the cluster was reported.

Temporal dynamics of thalamic engagement. To visualize the modulation of thalamic activity by load, we extracted signals within a binary thalamic mask extracted from the Morel atlas, including all subdivisions. Preprocessed BOLD timeseries were segmented into trials, spanning the period from the stimulus onset to the onset of the feedback phase. Given a time-to-peak of a canonical hemodynamic response function (HRF) between 5-6 seconds, we designated the 3 second interval from 5-8 seconds following the stimulus onset trigger as the stimulus presentation interval, and the 2 second interval from 3-5 s as the fixation interval, respectively. Single-trial time series were then temporally normalized to the temporal average during the approximate fixation interval. To visualize inter-individual differences in thalamic engagement, we performed a median split across participants based on their individual drift modulation.

Thalamic loci of behavioral PLS. To assess the thalamic loci of most reliable behavioral relations (Figure S5C), we assessed bootstrap ratios within two thalamic masks. First, for nucleic subdivisions, we used the Morel parcellation scheme as consolidated and kindly provided by (Hwang et al., 2017) for 3 mm data at 3T field strength. The abbreviations are as follows: AN: anterior nucleus; VM: ventromedial; VL: ventrolateral; MGN: medial geniculate nucleus; LGN: lateral geniculate nucleus; MD: mediodorsal; PuA: anterior pulvinar; LP: lateral-posterior; IL: intra-laminar; VA: ventral-anterior; PuM: medial pulvinar; PuI: pulvinar proper; PuL: lateral pulvinar. Second, to assess cortical white-matter projections we considered the overlap with seven structurally-derived cortical projection zones suggested by (Horn & Blankenburg, 2016), which were derived from a large adult sample ($N = 169$). We

binarized continuous probability maps at a relative 75% threshold of the respective maximum probability, and re-sliced masks to 3 mm size.

Statistical analyses

Assessment of covarying load effect magnitudes between measures. To assess a linear modulation of dependent variables, we calculated 1st level beta estimates for the effect of load (y = intercept+β*LOAD+e) and assessed the slope difference from zero at the group level using paired t-tests. We assessed the relation of individual load effects between measures of interest by means of partial repeated measures correlations. In a simplified form, repeated measured correlation (Bakdash & Marusich, 2017) fits a linear model between two variables x1 and x2 of interest, while controlling for repeated assessments within subjects [x1~1+β1*ID+β2*x2+e] (1). Crucially, to exclude bivariate relations that exclusively arise from joint main effects of number of targets, we added target load as an additional categorical covariate [x1~1+β1*ID+β2*LOAD+β3*x2+e] (2) to remove group condition means. Resulting estimates characterize the group-wise coupling in the (zero-centered) magnitude of changes between the DV and the IV across the four load levels. To identify the directionality of the coupling, we assessed the direction of main effects for x1 and x2. We statistically compared this model to a null model without the term of interest [x1~1+β1*ID+β2*LOAD +e] (3) to assess statistical significance. We report the bivariate residual effect size by assessing the square root of partial eta squared. We extend this model with additional beta*covariate terms when reporting control for additional covariates.

Within-subject centering. To better visualize effects within participants, we use within-subject centering across repeated measures conditions by subtracting individual condition means, and adding global means. For these visualizations, only the mean of the dependent values is directly informative, as the plotted spread reflects within-subject, and not between-subject, variation. This procedure is similar to the creation of within-subject standard errors. Within-subject centering is exclusively used for display, but not statistical calculations.

Univariate cluster-based permutation analyses. For data with a low-dimensional structure (e.g., based on a priori averaging or spatial cluster assumptions), we used univariate cluster-based permutation analyses (CBPAs) to assess significant modulations by target load or with stimulus onset. These univariate tests were performed by means of dependent samples t-tests; cluster-based permutation tests (Maris & Oostenveld, 2007) were performed to control for multiple comparisons. Initially, a clustering algorithm formed clusters based on significant t-tests of individual data points ($p < .05$, two-sided; cluster entry threshold) with the spatial constraint of a cluster covering a minimum of three neighboring channels. Then, the significance of the observed cluster-level statistic, based on the summed t-values within the cluster, was assessed by comparison to the distribution of all permutation-based cluster-level statistics. The final cluster p-value that we report in all figures was assessed as the proportion of 1000 Monte Carlo iterations in which the cluster-level statistic was exceeded. Cluster significance was indicated by p-values below .025 (two-sided cluster significance threshold).

Multivariate partial least squares analyses. For data with a high-dimensional structure, we performed multivariate partial least squares analyses (Krishnan, Williams, McIntosh, & Abdi, 2011; McIntosh, Bookstein, Haxby, & Grady, 1996; McIntosh & Lobaugh, 2004). To assess

main effect of probe uncertainty or stimulus onset, we performed Task PLS analyses. Task PLS begins by calculating a between-subject covariance matrix (COV) between conditions and each neural value (e.g., time-space-frequency power), which is then decomposed using singular value decomposition (SVD). This yields a left singular vector of experimental condition weights (U), a right singular vector of brain weights (V), and a diagonal matrix of singular values (S). Task PLS produces orthogonal latent variables (LVs) that reflect optimal relations between experimental conditions and the neural data. To examine multivariate relations between neural data and other variables of interest, we performed behavioral PLS analyses. This analysis initially calculates a between-subject correlation matrix (CORR) between (1) each brain index of interest (e.g., spectral power, 1st level BOLD beta values) and (2) a second 'behavioral' variable of interest (note that although called behavioral, this variable can reflect any variable of interest, e.g., behavior, pupil dilation, spectral power). CORR is then decomposed using singular value decomposition (SVD): $SVD_{CORR} = USV'$, which produces a matrix of left singular vectors of cognition weights (*U*), a matrix of right singular vectors of brain weights (*V*), and a diagonal matrix of singular values (*S*). For each LV (ordered strongest to weakest in *S*), a data pattern results which depicts the strongest available relation to the variable of interest. Significance of detected relations of both PLS model types was assessed using 1000 permutation tests of the singular value corresponding to the LV. A subsequent bootstrapping procedure indicated the robustness of within-LV neural saliences across 1000 resamples of the data (Efron & Tibshirani, 1986). By dividing each brain weight (from *V*) by its bootstrapped standard error, we obtained "bootstrap ratios" (BSRs) as normalized robustness estimates. We generally thresholded BSRs at values of ±3.00 (~99.9% confidence interval). We also obtained a summary measure of each participant's robust expression of a particular LV's pattern (a within-person "brain score") by either (1) multiplying the vector of brain weights (*V)* from each LV by within-subject vectors of the neural values (separately for each condition within person) for the Task PLS models, or (2) in the behavioral PLS model, by multiplying the model-based vector of weights (*V*) by each participant's vector of neural values (*P*), producing a single within-subject value: Brain score = *VP´*.

Acknowledgements

We thank our research assistants and participants for their contributions to the present work, Alistair Perry for assistance in fMRI preprocessing, and Steffen Wiegert for organizational support.

Funding

This study was conducted within the 'Lifespan Neural Dynamics Group' at the Max Planck UCL Centre for Computational Psychiatry and Ageing Research in the Max Planck Institute for Human Development (MPIB) in Berlin, Germany. DDG was supported by an Emmy Noether Programme grant from the German Research Foundation, and by the Max Planck UCL Centre for Computational Psychiatry and Ageing Research. JQK is a pre-doctoral fellow supported by the International Max Planck Research School on Computational Methods in Psychiatry and Ageing Research (IMPRS COMP2PSYCH). The participating institutions are the Max Planck Institute for Human Development, Berlin, Germany, and University College London, London, UK. For more information, see https://www.mps-ucl-

centre.mpg.de/en/comp2psych. The funders had no role in study design, data collection and analysis, decision to publish, or preparation of the manuscript.

Declaration of Interests

The authors declare no competing interests.

Author contributions

JQK: Conceptualization, Methodology, Investigation, Software, Formal analysis, Visualization, Writing – original draft, Writing – review and editing, Validation, Data Curation; UL: Conceptualization, Resources, Writing – review and editing, Supervision, Funding acquisition; DDG: Conceptualization, Methodology, Software, Resources, Writing—review and editing, Supervision, Project administration, Funding acquisition.

Data and Code Availability

Experiment code is available from https://git.mpib-berlin.mpg.de/LNDG/multi-attribute-task. Primary EEG and fMRI data (excluding structural images exempt from informed consent) will be made available following publication. Code to reproduce the analyses will be made available at https://git.mpib-berlin.mpg.de/LNDG/stateswitch.

References

Afyouni, S., & Nichols, T. E. (2018). Insight and inference for DVARS. *Neuroimage, 172*, 291-312. doi:10.1016/j.neuroimage.2017.12.098

Alitto, H., Rathbun, D. L., Vandeleest, J. J., Alexander, P. C., & Usrey, W. M. (2019). The augmentation of retinogeniculate communication during thalamic burst mode. *Journal of Neuroscience, 39*(29), 5697-5710. doi:10.1523/Jneurosci.2320-18.2019

Alnaes, D., Sneve, M. H., Espeseth, T., Endestad, T., de Pavert, S. H. P. V., & Laeng, B. (2014). Pupil size signals mental effort deployed during multiple object tracking and predicts brain activity in the dorsal attention network and the locus coeruleus. *Journal of Vision, 14*(4). doi:10.1167/14.4.1

Arcaro, M. J., Pinsk, M. A., & Kastner, S. (2015). The anatomical and functional organization of the human visual pulvinar. *Journal of Neuroscience, 35*(27), 9848-9871. doi:10.1523/Jneurosci.1575-14.2015

Aru, J., Aru, J., Priesemann, V., Wibral, M., Lana, L., Pipa, G., . . . Vicente, R. (2015). Untangling cross-frequency coupling in neuroscience. *Current Opinion in Neurobiology, 31*, 51-61. doi:10.1016/j.conb.2014.08.002

Aston-Jones, G., & Cohen, J. D. (2005). An integrative theory of locus coeruleus-norepinephrine function: Adaptive gain and optimal performance. *Annual Review of Neuroscience, 28*, 403-450. doi:10.1146/annurev.neuro.28.061604.135709

Atallah, B. V., & Scanziani, M. (2009). Instantaneous modulation of gamma oscillation frequency by balancing excitation with inhibition. *Neuron, 62*(4), 566-577. doi:10.1016/j.neuron.2009.04.027

Avants, B. B., Tustison, N. J., Song, G., Cook, P. A., Klein, A., & Gee, J. C. (2011). A reproducible evaluation of ANTs similarity metric performance in brain image registration. *Neuroimage, 54*(3), 2033-2044. doi:10.1016/j.neuroimage.2010.09.025

Bach, D. R., & Dolan, R. J. (2012). Knowing how much you don't know: A neural organization of uncertainty estimates. *Nature Reviews Neuroscience, 13*(8), 572-586. doi:10.1038/nrn3289

Bakdash, J. Z., & Marusich, L. R. (2017). Repeated measures correlation. *Frontiers in Psychology, 8*. doi:10.3389/fpsyg.2017.00456

Banca, P., Vestergaard, M. D., Rankov, V., Baek, K., Mitchell, S., Lapa, T., . . . Voon, V. (2015). Evidence accumulation in obsessive-compulsive disorder: The role of uncertainty and monetary reward on perceptual decision-making thresholds. *Neuropsychopharmacology, 40*(5), 1192-1202. doi:10.1038/npp.2014.303

Bauer, M., Kluge, C., Bach, D., Bradbury, D., Heinze, H. J., Dolan, R. J., & Driver, J. (2012). Cholinergic enhancement of visual attention and neural oscillations in the human brain. *Current Biology, 22*(5), 397-402. doi:10.1016/j.cub.2012.01.022

Beckmann, C. F., & Smith, S. A. (2004). Probabilistic independent component analysis for functional magnetic resonance imaging. *Ieee Transactions on Medical Imaging, 23*(2), 137-152. doi:10.1109/Tmi.2003.822821

Bell, A. J., & Sejnowski, T. J. (1995). An information maximization approach to blind separation and blind deconvolution. *Neural Computation, 7*(6), 1129-1159. doi:10.1162/neco.1995.7.6.1129

Berridge, C. W., & Waterhouse, B. D. (2003). The locus coeruleus-noradrenergic system: Modulation of behavioral state and state-dependent cognitive processes. *Brain Research Reviews, 42*(1), 33-84. doi:10.1016/S0165-0173(03)00143-7

Billig, A. J., Herrmann, B., Rhone, A. E., Gander, P. E., Nourski, K. V., Snoad, B. F., . . . Johnsrude, I. S. (2019). A sound-sensitive source of alpha oscillations in human non-primary auditory cortex. *Journal of Neuroscience, 39*(44), 8679-8689. doi:10.1523/Jneurosci.0696-19.2019

Birn, R. M. (2012). The role of physiological noise in resting-state functional connectivity. *Neuroimage, 62*(2), 864-870. doi:10.1016/j.neuroimage.2012.01.016

Brainard, D. H. (1997). The psychophysics toolbox. *Spatial Vision, 10*(4), 433-436. doi:10.1163/156856897x00357

Breton-Provencher, V., & Sur, M. (2019). Active control of arousal by a locus coeruleus GABAergic circuit. *Nature Neuroscience, 22*(2), 218-228. doi:10.1038/s41593-018-0305-z

Buschman, T. J., & Kastner, S. (2015). From behavior to neural dynamics: An integrated theory of attention. *Neuron, 88*(1), 127-144. doi:10.1016/j.neuron.2015.09.017

Canolty, R. T., Edwards, E., Dalal, S. S., Soltani, M., Nagarajan, S. S., Kirsch, H. E., . . . Knight, R. T. (2006). High gamma power is phase-locked to theta oscillations in human neocortex. *Science, 313*(5793), 1626-1628. doi:10.1126/science.1128115

Caplan, J. B., Madsen, J. R., Raghavachari, S., & Kahana, M. J. (2001). Distinct patterns of brain oscillations underlie two basic parameters of human maze learning. *Journal of Neurophysiology, 86*(1), 368-380.

Cavanagh, J. F., & Frank, M. J. (2014). Frontal theta as a mechanism for cognitive control. *Trends in Cognitive Sciences, 18*(8), 414-421. doi:10.1016/j.tics.2014.04.012

Cheung, M. J., Kovacevic, N., Fatima, Z., Misic, B., & McIntosh, A. R. (2016). [MEG]PLS: A pipeline for MEG data analysis and partial least squares statistics. *Neuroimage, 124*, 181-193. doi:10.1016/j.neuroimage.2015.08.045

Colombo, M. A., Napolitani, M., Boly, M., Gosseries, O., Casarotto, S., Rosanova, M., . . . Sarasso, S. (2019). The spectral exponent of the resting EEG indexes the presence of consciousness during unresponsiveness induced by propofol, xenon, and ketamine. *Neuroimage, 189*, 631-644. doi:10.1016/j.neuroimage.2019.01.024

Constantinople, C. M., & Bruno, R. M. (2011). Effects and mechanisms of wakefulness on local cortical networks. *Neuron, 69*(6), 1061-1068. doi:10.1016/j.neuron.2011.02.040

Crick, F. (2003). Function of the thalamic reticular complex: The searchlight hypothesis. *Essential Sources in the Scientific Study of Consciousness*, 263-272.

Dahl, M. J., Mather, M., Sander, M. C., & Werkle-Bergne, M. (2020). Noradrenergic responsiveness supports selective attention across the adult lifespan. *Journal of Neuroscience, 40*(22), 4372-4390. doi:10.1523/Jneurosci.0398-19.2020

de Gee, J. W., Colizoli, O., Kloosterman, N. A., Knapen, T., Nieuwenhuis, S., & Donner, T. H. (2017). Dynamic modulation of decision biases by brainstem arousal systems. *Elife, 6*. doi:10.7554/eLife.23232

Dehghani, N., & Wimmer, R. D. (2019). A computational perspective of the role of the thalamus in cognition. *Neural Computation, 31*(7), 1380-1418. doi:10.1162/neco_a_01197

Desimone, R., & Duncan, J. (1995). Neural mechanisms of selective visual-attention. *Annual Review of Neuroscience, 18*, 193-222. doi:10.1146/annurev.ne.18.030195.001205

Destexhe, A., & Rudolph, M. (2004). Extracting information from the power spectrum of synaptic noise. *Journal of Computational Neuroscience, 17*(3), 327-345. doi:Doi 10.1023/B:Jcns.0000044875.90630.88

Destexhe, A., Rudolph, M., & Pare, D. (2003). The high-conductance state of neocortical neurons in vivo. *Nature Reviews Neuroscience, 4*(9), 739-751. doi:10.1038/nrn1198

Ding, J., Sperling, G., & Srinivasan, R. (2006). Attentional modulation of SSVEP power depends on the network tagged by the flicker frequency. *Cerebral Cortex, 16*(7), 1016-1029. doi:10.1093/cercor/bhj044

Donner, T. H., Siegel, M., Fries, P., & Engel, A. K. (2009). Buildup of choice-predictive activity in human motor cortex during perceptual decision making. *Current Biology, 19*(18), 1581-1585. doi:10.1016/j.cub.2009.07.066

Dosenbach, N. U., Fair, D. A., Miezin, F. M., Cohen, A. L., Wenger, K. K., Dosenbach, R. A., . . . Petersen, S. E. (2007). Distinct brain networks for adaptive and stable task control in humans. *Proc Natl Acad Sci U S A, 104*(26), 11073-11078. doi:10.1073/pnas.0704320104

Dube, B., Emrich, S. M., & Al-Aidroos, N. (2017). More than a filter: Feature-based attention regulates the distribution of visual working memory resources. *Journal of Experimental Psychology-Human Perception and Performance, 43*(10), 1843-1854. doi:10.1037/xhp0000428

Dugue, L., Marque, P., & VanRullen, R. (2011). The phase of ongoing oscillations mediates the causal relation between brain excitation and visual perception. *Journal of Neuroscience, 31*(33), 11889-11893. doi:10.1523/Jneurosci.1161-11.2011

Efron, B., & Tibshirani, R. (1986). Bootstrap methods for standard errors, confidence intervals, and other measures of statistical accuracy. *Statist. Sci., 1*(1), 54-75. doi:10.1214/ss/1177013815

Eickhoff, S. B., Stephan, K. E., Mohlberg, H., Grefkes, C., Fink, G. R., Amunts, K., & Zilles, K. (2005). A new SPM toolbox for combining probabilistic cytoarchitectonic maps and functional imaging data. *Neuroimage, 25*(4), 1325-1335. doi:10.1016/j.neuroimage.2004.12.034

Ferguson, K. A., & Cardin, J. A. (2020). Mechanisms underlying gain modulation in the cortex. *Nature Reviews Neuroscience, 21*(2), 80-92. doi:10.1038/s41583-019-0253-y

Fiebelkorn, I. C., Pinsk, M. A., & Kastner, S. (2019). The mediodorsal pulvinar coordinates the macaque fronto-parietal network during rhythmic spatial attention. *Nature Communications, 10*. doi:10.1038/s41467-018-08151-4

Fonov, V., Evans, A. C., Botteron, K., Almli, C. R., McKinstry, R. C., Collins, D. L., & Grp, B. D. C. (2011). Unbiased average age-appropriate atlases for pediatric studies. *Neuroimage, 54*(1), 313-327. doi:10.1016/j.neuroimage.2010.07.033

Forstmann, B. U., Ratcliff, R., & Wagenmakers, E. J. (2016). Sequential sampling models in cognitive neuroscience: Advantages, applications, and extensions. *Annual Review of Psychology, Vol 67, 67*, 641-666. doi:10.1146/annurev-psych-122414-033645

Frank, M. J., Gagne, C., Nyhus, E., Masters, S., Wiecki, T. V., Cavanagh, J. F., & Badre, D. (2015). fMRI and EEG predictors of dynamic decision parameters during human reinforcement learning. *Journal of Neuroscience, 35*(2), 485-494. doi:10.1523/Jneurosci.2036-14.2015

Fries, P. (2015). Rhythms for cognition: Communication through coherence. *Neuron, 88*(1), 220-235. doi:10.1016/j.neuron.2015.09.034

Friston, K. J., Williams, S., Howard, R., Frackowiak, R. S., & Turner, R. (1996). Movement-related effects in fMRI time-series. *Magn Reson Med, 35*(3), 346-355. doi:10.1002/mrm.1910350312

Froemke, R. C. (2015). Plasticity of cortical excitatory-inhibitory balance. *Annual Review of Neuroscience, 38*, 195-219. doi:10.1146/annurev-neuro-071714-034002

Froemke, R. C., Merzenich, M. M., & Schreiner, C. E. (2007). A synaptic memory trace for cortical receptive field plasticity. *Nature, 450*(7168), 425-429. doi:10.1038/nature06289

Furey, M. L., Pietrini, P., & Haxby, J. V. (2000). Cholinergic enhancement and increased selectivity of perceptual processing during working memory. *Science, 290*(5500), 2315-2319. doi:10.1126/science.290.5500.2315

Gao, R., Peterson, E. J., & Voytek, B. (2017). Inferring synaptic excitation/inhibition balance from field potentials. *Neuroimage, 158*, 70-78. doi:10.1016/j.neuroimage.2017.06.078

Garrett, D. D., Epp, S. M., Perry, A., & Lindenberger, U. (2018). Local temporal variability reflects functional integration in the human brain. *Neuroimage, 183*, 776-787. doi:10.1016/j.neuroimage.2018.08.019

Garrett, D. D., Kovacevic, N., McIntosh, A. R., & Grady, C. L. (2010). Blood oxygen level-dependent signal variability is more than just noise. *Journal of Neuroscience, 30*(14), 4914-4921. doi:10.1523/Jneurosci.5166-09.2010

Garrett, D. D., McIntosh, A. R., & Grady, C. L. (2014). Brain signal variability is parametrically modifiable. *Cerebral Cortex, 24*(11), 2931-2940. doi:10.1093/cercor/bht150

Garrett, D. D., Nagel, I. E., Preuschhof, C., Burzynska, A. Z., Marchner, J., Wiegert, S., . . . Lindenberger, U. (2015). Amphetamine modulates brain signal variability and working memory in younger and older adults. *Proceedings of the National Academy of Sciences of the United States of America, 112*(24), 7593-7598. doi:10.1073/pnas.1504090112

Gold, J. I., & Shadlen, M. N. (2007). The neural basis of decision making. *Annual Review of Neuroscience, 30*, 535-574. doi:10.1146/annurev.neuro.29.051605.113038

Grandy, T. H., Garrett, D. D., Schmiedek, F., & Werkle-Bergner, M. (2016). On the estimation of brain signal entropy from sparse neuroimaging data. *Scientific Reports, 6*. doi:10.1038/srep23073

Haegens, S., Nacher, V., Luna, R., Romo, R., & Jensen, O. (2011). alpha-Oscillations in the monkey sensorimotor network influence discrimination performance by rhythmical inhibition of neuronal spiking. *Proceedings of the National Academy of Sciences of the United States of America, 108*(48), 19377-19382. doi:10.1073/pnas.1117190108

Halassa, M. M., & Kastner, S. (2017). Thalamic functions in distributed cognitive control. *Nature Neuroscience, 20*(12), 1669-1679. doi:10.1038/s41593-017-0020-1

Halassa, M. M., & Sherman, S. M. (2019). Thalamocortical circuit motifs: A general framework. *Neuron, 103*(5), 762-770. doi:10.1016/j.neuron.2019.06.005

Halgren, M., Ulbert, I., Bastuji, H., Fabo, D., Eross, L., Rey, M., . . . Cash, S. S. (2019). The generation and propagation of the human alpha rhythm. *Proceedings of the National Academy of Sciences of the United States of America, 116*(47), 23772-23782. doi:10.1073/pnas.1913092116

Hampshire, A., Chamberlain, S. R., Monti, M. M., Duncan, J., & Owen, A. M. (2010). The role of the right inferior frontal gyrus: Inhibition and attentional control. *Neuroimage, 50*(3), 1313-1319. doi:10.1016/j.neuroimage.2009.12.109

Hanks, T. D., & Summerfield, C. (2017). Perceptual decision making in rodents, monkeys, and humans. *Neuron, 93*(1), 15-31. doi:10.1016/j.neuron.2016.12.003

Harris, K. D., & Thiele, A. (2011). Cortical state and attention. *Nature Reviews Neuroscience, 12*(9), 509-523. doi:10.1038/nrn3084

Hartings, J. A., Temereanca, S., & Simons, D. J. (2003). State-dependent processing of sensory stimuli by thalamic reticular neurons. *Journal of Neuroscience, 23*(12), 5264-5271.

Hirata, A., Aguilar, J., & Castro-Alamancos, M. A. (2006). Noradrenergic activation amplifies bottom-up and top-down signal-to-noise ratios in sensory thalamus. *Journal of Neuroscience, 26*(16), 4426-4436. doi:10.1523/JNEUROSCI.5298-05.2006

Honjoh, S., Sasai, S., Schiereck, S. S., Nagai, H., Tononi, G., & Cirelli, C. (2018). Regulation of cortical activity and arousal by the matrix cells of the ventromedial thalamic nucleus. *Nature Communications, 9*. doi:10.1038/s41467-018-04497-x

Horn, A., & Blankenburg, F. (2016). Toward a standardized structural-functional group connectome in mni space. *Neuroimage, 124*, 310-322. doi:10.1016/j.neuroimage.2015.08.048

Hwang, K., Bertolero, M. A., Liu, W. B., & D'Esposito, M. (2017). The human thalamus is an integrative hub for functional brain networks. *Journal of Neuroscience, 37*(23), 5594-5607. doi:10.1523/Jneurosci.0067-17.2017

Iemi, L., Chaumon, M., Crouzet, S. M., & Busch, N. A. (2017). Spontaneous neural oscillations bias perception by modulating baseline excitability. *Journal of Neuroscience, 37*(4), 807-819. doi:10.1523/JNEUROSCI.1432-16.2016

Jagtap, P., & Diwadkar, V. A. (2016). Effective connectivity of ascending and descending frontalthalamic pathways during sustained attention: Complex brain network interactions in adolescence. *Human Brain Mapping, 37*(7), 2557-2570. doi:10.1002/hbm.23196

Jaramillo, J., Mejias, J. F., & Wang, X. J. (2019). Engagement of pulvino-cortical feedforward and feedback pathways in cognitive computations. *Neuron, 101*(2), 321-336. doi:10.1016/j.neuron.2018.11.023

Jasper, H. H. (1948). Charting the sea of brain waves. *Science, 108*(2805), 343-347. doi:10.1126/science.108.2805.343

Jenkinson, M., Beckmann, C. F., Behrens, T. E., Woolrich, M. W., & Smith, S. M. (2012). Fsl. *Neuroimage, 62*(2), 782-790. doi:10.1016/j.neuroimage.2011.09.015

Jones, E. G. (2009). Synchrony in the interconnected circuitry of the thalamus and cerebral cortex. *Disorders of Consciousness, 1157*, 10-23. doi:10.1111/j.1749-6632.2009.04534.x

Joshi, S., & Gold, J. I. (2020). Pupil size as a window on neural substrates of cognition. *Trends in Cognitive Sciences, 24*(6), 466-480. doi:10.1016/j.tics.2020.03.005

Joshi, S., Li, Y., Kalwani, R. M., & Gold, J. I. (2016). Relationships between pupil diameter and neuronal activity in the locus coeruleus, colliculi, and cingulate cortex. *Neuron, 89*(1), 221-234. doi:10.1016/j.neuron.2015.11.028

Kanai, R., Komura, Y., Shipp, S., & Friston, K. (2015). Cerebral hierarchies: Predictive processing, precision and the pulvinar. *Philosophical Transactions of the Royal Society B-Biological Sciences, 370*(1668), 69-81. doi:10.1098/rstb.2014.0169

Kelly, S. P., & O'Connell, R. G. (2013). Internal and external influences on the rate of sensory evidence accumulation in the human brain. *Journal of Neuroscience, 33*(50), 19434-19441. doi:10.1523/Jneurosci.3355-13.2013

Kim, C., Cilles, S. E., Johnson, N. F., & Gold, B. T. (2012). Domain general and domain preferential brain regions associated with different types of task switching: A meta-analysis. *Human Brain Mapping, 33*(1), 130-142. doi:10.1002/hbm.21199

Kleiner, M., Brainard, D., & Pelli, D. (2007). What's new in psychtoolbox-3? *Perception, 36*, 14-14.

Klimesch, W., Sauseng, P., & Hanslmayr, S. (2007). EEG alpha oscillations: The inhibition-timing hypothesis. *Brain Res Rev, 53*(1), 63-88. doi:10.1016/j.brainresrev.2006.06.003

Kloosterman, N. A., Kosciessa, J. Q., Lindenberger, U., Fahrenfort, J. J., & Garrett, D. D. (2019). Boosting brain signal variability underlies liberal shifts in decision bias. *bioRxiv*.

Koelewijn, T., Shinn-Cunningham, B. G., Zekveld, A. A., & Kramer, S. E. (2014). The pupil response is sensitive to divided attention during speech processing. *Hearing Research, 312*, 114-120. doi:10.1016/j.heares.2014.03.010

Kosciessa, J. Q., Grandy, T. H., Garrett, D. D., & Werkle-Bergner, M. (2020). Single-trial characterization of neural rhythms: Potential and challenges. *Neuroimage, 206*, 116331. doi:10.1016/j.neuroimage.2019.116331

Kosciessa, J. Q., Kloosterman, N. A., & Garrett, D. D. (2020). Standard multiscale entropy reflects neural dynamics at mismatched temporal scales: What's signal irregularity got to do with it? *Plos Computational Biology, 16*(5), e1007885. doi:10.1371/journal.pcbi.1007885

Krishnamurthy, K., Nassar, M. R., Sarode, S., & Gold, J. I. (2017). Arousal-related adjustments of perceptual biases optimize perception in dynamic environments. *Nature Human Behaviour, 1*(6). doi:10.1038/s41562-017-0107

Krishnan, A., Williams, L. J., McIntosh, A. R., & Abdi, H. (2011). Partial least squares (PLS) methods for neuroimaging: A tutorial and review. *Neuroimage, 56*(2), 455-475. doi:10.1016/j.neuroimage.2010.07.034

Lange, J., Oostenveld, R., & Fries, P. (2013). Reduced occipital alpha power indexes enhanced excitability rather than improved visual perception. *Journal of Neuroscience, 33*(7), 3212-3220. doi:10.1523/Jneurosci.3755-12.2013

Lee, S. H., & Dan, Y. (2012). Neuromodulation of brain states. *Neuron, 76*(1), 209-222. doi:10.1016/j.neuron.2012.09.012

Lendner, J. D., Helfrich, R. F., Mander, B. A., Romundstad, L., Lin, J. J., Walker, M. P., . . . Knight, R. T. (2019). An electrophysiological marker of arousal level in humans. *bioRxiv*.

Lewis, L. D., Voigts, J., Flores, F. J., Schmitt, L. I., Wilson, M. A., Halassa, M. M., & Brown, E. N. (2015). Thalamic reticular nucleus induces fast and local modulation of arousal state. *Elife, 4*, e08760. doi:10.7554/eLife.08760

Liu, J., Lee, H. J., Weitz, A. J., Fang, Z. N., Lin, P., Choy, M., . . . Lee, J. H. (2015). Frequency-selective control of cortical and subcortical networks by central thalamus. *Elife, 4*. doi:10.7554/eLife.09215

Lopes da Silva, F. H., Vos, J. E., Mooibroek, J., & Van Rotterdam, A. (1980). Relative contributions of intracortical and thalamo-cortical processes in the generation of alpha rhythms, revealed by partial coherence analysis. *Electroencephalogr Clin Neurophysiol, 50*(5-6), 449-456. doi:10.1016/0013-4694(80)90011-5

Lorincz, M. L., Kekesi, K. A., Juhasz, G., Crunelli, V., & Hughes, S. W. (2009). Temporal framing of thalamic relay-mode firing by phasic inhibition during the alpha rhythm. *Neuron, 63*(5), 683-696. doi:10.1016/j.neuron.2009.08.012

Marguet, S. L., & Harris, K. D. (2011). State-dependent representation of amplitude-modulated noise stimuli in rat auditory cortex. *Journal of Neuroscience, 31*(17), 6414-6420. doi:10.1523/Jneurosci.5773-10.2011

Maris, E., & Oostenveld, R. (2007). Nonparametric statistical testing of EEG- and MEG-data. *Journal of Neuroscience Methods, 164*(1), 177-190. doi:10.1016/j.jneumeth.2007.03.024

Martins, A. R. O., & Froemke, R. C. (2015). Coordinated forms of noradrenergic plasticity in the locus coeruleus and primary auditory cortex. *Nature Neuroscience, 18*(10), 1483-1492. doi:10.1038/nn.4090

Marton, T. F., Seifikar, H., Luongo, F. J., Lee, A. T., & Sohal, V. S. (2018). Roles of prefrontal cortex and mediodorsal thalamus in task engagement and behavioral flexibility. *Journal of Neuroscience, 38*(10), 2569-2578. doi:10.1523/Jneurosci.1728-17.2018

Maunsell, J. H. R. (2015). Neuronal mechanisms of visual attention. *Annual Review of Vision Science, Vol 1, 1*, 373-391. doi:10.1146/annurev-vision-082114-035431

McCormick, D. A. (1989). Cholinergic and noradrenergic modulation of thalamocortical processing. *Trends in Neurosciences, 12*(6), 215-221. doi:10.1016/0166-2236(89)90125-2

McCormick, D. A., McGinley, M. J., & Salkoff, D. B. (2015). Brain state dependent activity in the cortex and thalamus. *Current Opinion in Neurobiology, 31*, 133-140. doi:10.1016/j.conb.2014.10.003

McCormick, D. A., Pape, H. C., & Williamson, A. (1991). Actions of norepinephrine in the cerebral cortex and thalamus: Implications for function of the central noradrenergic system. *Prog Brain Res, 88*, 293-305. doi:10.1016/s0079-6123(08)63817-0

McFadyen, J., Dolan, R. J., & Garrido, M. I. (2020). The influence of subcortical shortcuts on disordered sensory and cognitive processing. *Nature Reviews Neuroscience, 21*(5), 264-276. doi:10.1038/s41583-020-0287-1

McGinley, M. J., David, S. V., & McCormick, D. A. (2015). Cortical membrane potential signature of optimal states for sensory signal detection. *Neuron, 87*(1), 179-192. doi:10.1016/j.neuron.2015.05.038

McGinley, M. J., Vinck, M., Reimer, J., Batista-Brito, R., Zagha, E., Cadwell, C. R., . . . McCormick, D. A. (2015). Waking state: Rapid variations modulate neural and behavioral responses. *Neuron, 87*(6), 1143-1161. doi:10.1016/j.neuron.2015.09.012

McGovern, D. P., Hayes, A., Kelly, S. P., & O'Connell, R. G. (2018). Reconciling age-related changes in behavioural and neural indices of human perceptual decision-making. *Nature Human Behaviour, 2*(12), 955-966. doi:10.1038/s41562-018-0465-6

McIntosh, A. R., Bookstein, F. L., Haxby, J. V., & Grady, C. L. (1996). Spatial pattern analysis of functional brain images using partial least squares. *Neuroimage, 3*(3), 143-157. doi:10.1006/nimg.1996.0016

McIntosh, A. R., & Lobaugh, N. J. (2004). Partial least squares analysis of neuroimaging data: Applications and advances. *Neuroimage, 23*, S250-S263. doi:10.1016/j.neuroimage.2004.07.020

Minces, V., Pinto, L., Dan, Y., & Chiba, A. A. (2017). Cholinergic shaping of neural correlations. *Proceedings of the National Academy of Sciences of the United States of America, 114*(22), 5725-5730. doi:10.1073/pnas.1621493114

Mo, C., Lu, J. S., Wu, B. C., Jia, J. R., Luo, H., & Fang, F. (2019). Competing rhythmic neural representations of orientations during concurrent attention to multiple orientation features. *Nature Communications, 10*. doi:10.1038/s41467-019-13282-3

Murphy, P. R., Wilming, N., Hernandez-Bocanegra, D. C., Prat Ortega, G., & Donner, T. H. (2020). Normative circuit dynamics across human cortex during evidence accumulation in changing environments. *bioRxiv*.

Nassar, M. R., Rumsey, K. M., Wilson, R. C., Parikh, K., Heasly, B., & Gold, J. I. (2012). Rational regulation of learning dynamics by pupil-linked arousal systems. *Nature Neuroscience, 15*(7), 1040-1046. doi:10.1038/nn.3130

Nelson, S. M., Dosenbach, N. U. F., Cohen, A. L., Wheeler, M. E., Schlaggar, B. L., & Petersen, S. E. (2010). Role of the anterior insula in task-level control and focal attention. *Brain Structure & Function, 214*(5-6), 669-680. doi:10.1007/s00429-010-0260-2

Ni, J. G., Wunderle, T., Lewis, C. M., Desimone, R., Diester, I., & Fries, P. (2016). Gamma-rhythmic gain modulation. *Neuron, 92*(1), 240-251. doi:10.1016/j.neuron.2016.09.003

Nolan, H., Whelan, R., & Reilly, R. B. (2010). FASTER: Fully automated statistical thresholding for EEG artifact rejection. *Journal of Neuroscience Methods, 192*(1), 152-162. doi:10.1016/j.jneumeth.2010.07.015

O'Connell, R. G., Dockree, P. M., & Kelly, S. P. (2012). A supramodal accumulation-to-bound signal that determines perceptual decisions in humans. *Nature Neuroscience, 15*(12), 1729-1735. doi:10.1038/nn.3248

O'Reilly, R. C., Wyatte, D. R., & Rohrlich, J. (2017). Deep predictive learning: A comprehensive model of three visual streams. Retrieved from doi:arXiv:1709.04654

Oldfield, R. C. (1971). The assessment and analysis of handedness: The edinburgh inventory. *Neuropsychologia, 9*(1), 97-113. doi:10.1016/0028-3932(71)90067-4

Oostenveld, R., Fries, P., Maris, E., & Schoffelen, J. M. (2011). Fieldtrip: Open source software for advanced analysis of MEG, EEG, and invasive electrophysiological data. *Computational Intelligence and Neuroscience*. doi:10.1155/2011/156869

Oostenveld, R., & Praamstra, P. (2001). The five percent electrode system for high-resolution EEG and ERP measurements. *Clinical Neurophysiology, 112*(4), 713-719. doi:10.1016/S1388-2457(00)00527-7

Palva, S., & Palva, J. M. (2007). New vistas for alpha-frequency band oscillations. *Trends in Neurosciences, 30*(4), 150-158. doi:10.1016/j.tins.2007.02.001

Parkes, L., Fulcher, B., Yucel, M., & Fornito, A. (2018). An evaluation of the efficacy, reliability, and sensitivity of motion correction strategies for resting-state functional MRI. *Neuroimage, 171*, 415-436. doi:10.1016/j.neuroimage.2017.12.073

Pelli, D. G. (1997). The VideoToolbox software for visual psychophysics: Transforming numbers into movies. *Spatial Vision, 10*(4), 437-442. doi:10.1163/156856897x00366

Pergola, G., Danet, L., Pitel, A. L., Carlesimo, G. A., Segobin, S., Pariente, J., . . . Barbeau, E. J. (2018). The regulatory role of the human mediodorsal thalamus. *Trends in Cognitive Sciences, 22*(11), 1011-1025. doi:10.1016/j.tics.2018.08.006

Perrin, F., Pernier, J., Bertrand, O., & Echallier, J. F. (1989). Spherical splines for scalp potential and current-density mapping. *Electroencephalography and Clinical Neurophysiology, 72*(2), 184-187. doi:10.1016/0013-4694(89)90180-6

Peterson, E. J., & Voytek, B. (2017). Alpha oscillations control cortical gain by modulating excitatory-inhibitory background activity. *bioRxiv*.

Pettine, W. W., Louie, K., Murray, J. D., & Wang, X.-J. (2020). Hierarchical network model excitatory-inhibitory tone shapes alternative strategies for different degrees of uncertainty in multi-attribute decisions. *bioRxiv*.

Pfeffer, T., Avramiea, A. E., Nolte, G., Engel, A. K., Linkenkaer-Hansen, K., & Donner, T. H. (2018). Catecholamines alter the intrinsic variability of cortical population activity and perception. *Plos Biology, 16*(2), e2003453. doi:10.1371/journal.pbio.2003453

Podvalny, E., Noy, N., Harel, M., Bickel, S., Chechik, G., Schroeder, C. E., . . . Malach, R. (2015). A unifying principle underlying the extracellular field potential spectral responses in the human cortex. *Journal of Neurophysiology, 114*(1), 505-519. doi:10.1152/jn.00943.2014

Poo, C., & Isaacson, J. S. (2009). Odor representations in olfactory cortex: "Sparse" coding, global inhibition, and oscillations. *Neuron, 62*(6), 850-861. doi:10.1016/j.neuron.2009.05.022

Posner, M. I., & Rothbart, M. K. (2007). Research on attention networks as a model for the integration of psychological science. *Annual Review of Psychology, 58*, 1-23. doi:10.1146/annurev.psych.58.110405.085516

Power, J. D., Mitra, A., Laumann, T. O., Snyder, A. Z., Schlaggar, B. L., & Petersen, S. E. (2014). Methods to detect, characterize, and remove motion artifact in resting state fMRI. *Neuroimage, 84*, 320-341. doi:10.1016/j.neuroimage.2013.08.048

Rafal, R. D., & Posner, M. I. (1987). Deficits in human visual spatial attention following thalamic lesions. *Proc Natl Acad Sci U S A, 84*(20), 7349-7353. doi:10.1073/pnas.84.20.7349

Ratcliff, R. (1978). Theory of memory retrieval. *Psychological Review, 85*(2), 59-108. doi:10.1037//0033-295x.85.2.59

Ratcliff, R., & McKoon, G. (2008). The diffusion decision model: Theory and data for two-choice decision tasks. *Neural Computation, 20*(4), 873-922. doi:10.1162/neco.2008.12-06-420

Reimer, J., Froudarakis, E., Cadwell, C. R., Yatsenko, D., Denfield, G. H., & Tolias, A. S. (2014). Pupil fluctuations track fast switching of cortical states during quiet wakefulness. *Neuron, 84*(2), 355-362. doi:10.1016/j.neuron.2014.09.033

Reinagel, P., Godwin, D., Sherman, S. M., & Koch, C. (1999). Encoding of visual information by lgn bursts. *Journal of Neurophysiology, 81*(5), 2558-2569.

Richman, J. S., & Moorman, J. R. (2000). Physiological time-series analysis using approximate entropy and sample entropy. *American Journal of Physiology-Heart and Circulatory Physiology, 278*(6), H2039-H2049.

Rikhye, R. V., Gilra, A., & Halassa, M. M. (2018). Thalamic regulation of switching between cortical representations enables cognitive flexibility. *Nature Neuroscience, 21*(12), 1753-1763. doi:10.1038/s41593-018-0269-z

Rikhye, R. V., Wimmer, R. D., & Halassa, M. M. (2018). Toward an integrative theory of thalamic function. *Annual Review of Neuroscience, Vol 41, 41*, 163-183. doi:10.1146/annurev-neuro-080317-062144

Roux, F., Wibral, M., Singer, W., Aru, J., & Uhlhaas, P. J. (2013). The phase of thalamic alpha activity modulates cortical gamma-band activity: Evidence from resting-state MEG recordings. *Journal of Neuroscience, 33*(45), 17827-17835. doi:10.1523/Jneurosci.5778-12.2013

Saalmann, Y. B., & Kastner, S. (2011). Cognitive and perceptual functions of the visual thalamus. *Neuron, 71*(2), 209-223. doi:10.1016/j.neuron.2011.06.027

Saalmann, Y. B., Pinsk, M. A., Wang, L., Li, X., & Kastner, S. (2012). The pulvinar regulates information transmission between cortical areas based on attention demands. *Science, 337*(6095), 753-756. doi:10.1126/science.1223082

Sadaghiani, S., & Kleinschmidt, A. (2016). Brain networks and alpha-Oscillations: Structural and functional foundations of cognitive control. *Trends in Cognitive Sciences, 20*(11), 805-817. doi:10.1016/j.tics.2016.09.004

Schiff, N. D. (2008). Central thalamic contributions to arousal regulation and neurological disorders of consciousness. *Ann N Y Acad Sci, 1129*, 105-118. doi:10.1196/annals.1417.029

Schmitt, L. I., Wimmer, R. D., Nakajima, M., Happ, M., Mofakham, S., & Halassa, M. M. (2017). Thalamic amplification of cortical connectivity sustains attentional control. *Nature, 545*(7653), 219-223. doi:10.1038/nature22073

Sherman, S. M. (2001). Tonic and burst firing: Dual modes of thalamocortical relay. *Trends in Neurosciences, 24*(2), 122-126. doi:10.1016/S0166-2236(00)01714-8

Shine, J. M. (2019). Neuromodulatory influences on integration and segregation in the brain. *Trends in Cognitive Sciences, 23*(7), 572-583. doi:10.1016/j.tics.2019.04.002

Shine, J. M., Hearne, L. J., Breakspear, M., Hwang, K., Muller, E. J., Sporns, O., . . . Cocchi, L. (2019). The low-dimensional neural architecture of cognitive complexity is related to activity in medial thalamic nuclei. *Neuron, 104*(5), 849-855. doi:10.1016/j.neuron.2019.09.002

Siegel, M., Buschman, T. J., & Miller, E. K. (2015). Cortical information flow during flexible sensorimotor decisions. *Science, 348*(6241), 1352-1355. doi:10.1126/science.aab0551

Smith, A. M., Lewis, B. K., Ruttimann, U. E., Ye, F. Q., Sinnwell, T. M., Yang, Y. H., . . . Frank, J. A. (1999). Investigation of low frequency drift in fMRI signal. *Neuroimage, 9*(5), 526-533. doi:10.1006/nimg.1999.0435

Smith, G. D., Cox, C. L., Sherman, S. M., & Rinzel, J. (2000). Fourier analysis of sinusoidally driven thalamocortical relay neurons and a minimal integrate-and-fire-or-burst model. *Journal of Neurophysiology, 83*(1), 588-610.

Smith, S. M., Jenkinson, M., Woolrich, M. W., Beckmann, C. F., Behrens, T. E. J., Johansen-Berg, H., . . . Matthews, P. M. (2004). Advances in functional and structural MR image analysis and implementation as fsl. *Neuroimage, 23*, S208-S219. doi:10.1016/j.neuroimage.2004.07.051

Smulders, F. T. Y., ten Oever, S., Donkers, F. C. L., Quaedflieg, C. W. E. M., & van de Ven, V. (2018). Single-trial log transformation is optimal in frequency analysis of resting EEG alpha. *European Journal of Neuroscience, 48*(7), 2585-2598. doi:10.1111/ejn.13854

Song, A. H., Kucyi, A., Napadow, V., Brown, E. N., Loggia, M. L., & Akeju, O. (2017). Pharmacological modulation of noradrenergic arousal circuitry disrupts functional connectivity of the locus ceruleus in humans. *Journal of Neuroscience, 37*(29), 6938-6945. doi:10.1523/Jneurosci.0446-17.2017

Spaak, E., Bonnefond, M., Maier, A., Leopold, D. A., & Jensen, O. (2012). Layer-specific entrainment of gamma-band neural activity by the alpha rhythm in monkey visual cortex. *Current Biology, 22*(24), 2313-2318. doi:10.1016/j.cub.2012.10.020

Stitt, I., Zhou, Z. C., Radtke-Schuller, S., & Frohlich, F. (2018). Arousal dependent modulation of thalamo-cortical functional interaction. *Nature Communications, 9*(1), 2455. doi:10.1038/s41467-018-04785-6

Suffczynski, P., Kalitzin, S., Pfurtscheller, G., & da Silva, F. H. L. (2001). Computational model of thalamo-cortical networks: Dynamical control of alpha rhythms in relation to focal attention. *International Journal of Psychophysiology, 43*(1), 25-40. doi:Doi 10.1016/S0167-8760(01)00177-5

Swadlow, H. A., & Gusev, A. G. (2001). The impact of 'bursting' thalamic impulses at a neocortical synapse. *Nature Neuroscience, 4*(4), 402-408. doi:10.1038/86054

Thiele, A., & Bellgrove, M. A. (2018). Neuromodulation of attention. *Neuron, 97*(4), 769-785. doi:10.1016/j.neuron.2018.01.008

Tomasi, D., Chang, L., Caparelli, E. C., & Ernst, T. (2007). Different activation patterns for working memory load and visual attention load. *Brain Research, 1132*(1), 158-165. doi:10.1016/j.brainres.2006.11.030

Tort, A. B. L., Kramer, M. A., Thorn, C., Gibson, D. J., Kubota, Y., Graybiel, A. M., & Kopell, N. J. (2008). Dynamic cross-frequency couplings of local field potential oscillations in rat striatum and hippocampus during performance of a t-maze task. *Proceedings of the National Academy of Sciences of the United States of America, 105*(51), 20517-20522. doi:10.1073/pnas.0810524105

Twomey, D. M., Kelly, S. P., & O'Connell, R. G. (2016). Abstract and effector-selective decision signals exhibit qualitatively distinct dynamics before delayed perceptual reports. *Journal of Neuroscience, 36*(28), 7346-7352. doi:10.1523/Jneurosci.4162-15.2016

Uddin, L. Q. (2015). Salience processing and insular cortical function and dysfunction. *Nature Reviews Neuroscience, 16*(1), 55-61. doi:10.1038/nrn3857

Urai, A. E., Braun, A., & Donner, T. H. (2017). Pupil-linked arousal is driven by decision uncertainty and alters serial choice bias. *Nature Communications, 8*. doi:10.1038/ncomms14637

van Kerkoerle, T., Self, M. W., Dagnino, B., Gariel-Mathis, M. A., Poort, J., van der Togt, C., & Roelfsema, P. R. (2014). Alpha and gamma oscillations characterize feedback and feedforward processing in monkey visual cortex. *Proceedings of the National Academy of Sciences of the United States of America, 111*(40), 14332-14341. doi:10.1073/pnas.1402773111

van Vugt, M. K., Beulen, M. A., & Taatgen, N. A. (2019). Relation between centro-parietal positivity and diffusion model parameters in both perceptual and memory-based decision making. *Brain Research, 1715*, 1-12. doi:10.1016/j.brainres.2019.03.008

Vinck, M., Batista-Brito, R., Knoblich, U., & Cardin, J. A. (2015). Arousal and locomotion make distinct contributions to cortical activity patterns and visual encoding. *Neuron, 86*(3), 740-754. doi:10.1016/j.neuron.2015.03.028

Ward, L. M. (2013). The thalamus: Gateway to the mind. *Wiley Interdisciplinary Reviews-Cognitive Science, 4*(6), 609-622. doi:10.1002/wcs.1256

Waschke, L., Tune, S., & Obleser, J. (2019). Local cortical desynchronization and pupil-linked arousal differentially shape brain states for optimal sensory performance. *Elife, 8*. doi:10.7554/eLife.51501

Waterhouse, B. D., & Navarra, R. L. (2019). The locus coeruleus-norepinephrine system and sensory signal processing: A historical review and current perspectives. *Brain Res, 1709*, 1-15. doi:10.1016/j.brainres.2018.08.032

Weerda, R., Vallines, I., Thomas, J. P., Rutschmann, R. M., & Greenlee, M. W. (2006). Effects of nonspatial selective and divided visual attention on fMRI BOLD responses. *Experimental Brain Research, 173*(4), 555-563. doi:10.1007/s00221-006-0403-0

Weissman, D. H., Gopalakrishnan, A., Hazlett, C. J., & Woldorff, M. G. (2005). Dorsal anterior cingulate cortex resolves conflict from distracting stimuli by boosting attention toward relevant events. *Cerebral Cortex, 15*(2), 229-237. doi:10.1093/cercor/bhh125

Whitten, T. A., Hughes, A. M., Dickson, C. T., & Caplan, J. B. (2011). A better oscillation detection method robustly extracts EEG rhythms across brain state changes: The human alpha rhythm as a test case. *Neuroimage, 54*(2), 860-874. doi:10.1016/j.neuroimage.2010.08.064

Wiecki, T. V., Sofer, I., & Frank, M. J. (2013). HDDM: Hierarchical bayesian estimation of the drift-diffusion model in python. *Frontiers in Neuroinformatics, 7*. doi:10.3389/fninf.2013.00014

Wimmer, R. D., Schmitt, L. I., Davidson, T. J., Nakajima, M., Deisseroth, K., & Halassa, M. M. (2015). Thalamic control of sensory selection in divided attention. *Nature, 526*(7575), 705-709. doi:10.1038/nature15398

Wojciulik, E., & Kanwisher, N. (1999). The generality of parietal involvement in visual attention. *Neuron, 23*(4), 747-764. doi:10.1016/S0896-6273(01)80033-7

Wolff, M., & Vann, S. D. (2019). The cognitive thalamus as a gateway to mental representations. *Journal of Neuroscience, 39*(1), 3-14. doi:10.1523/Jneurosci.0479-18.2018

Wöstmann, M., Alavash, M., & Obleser, J. (2019). Alpha oscillations in the human brain implement distractor suppression independent of target selection. *Journal of Neuroscience, 39*(49), 9797-9805. doi:10.1523/JNEUROSCI.1954-19.2019

Wright, N. F., Vann, S. D., Aggleton, J. P., & Nelson, A. J. D. (2015). A critical role for the anterior thalamus in directing attention to task-relevant stimuli. *Journal of Neuroscience, 35*(14), 5480-5488. doi:10.1523/Jneurosci.4945-14.2015

Yang, G. J., Murray, J. D., Wang, X. J., Glahn, D. C., Pearlson, G. D., Repovs, G., . . . Anticevic, A. (2016). Functional hierarchy underlies preferential connectivity disturbances in schizophrenia. *Proceedings of the National Academy of Sciences of the United States of America, 113*(2), E219-E228. doi:10.1073/pnas.1508436113

Yizhar, O., Fenno, L. E., Prigge, M., Schneider, F., Davidson, T. J., O'Shea, D. J., . . . Deisseroth, K. (2011). Neocortical excitation/inhibition balance in information processing and social dysfunction. *Nature, 477*(7363), 171-178. doi:10.1038/nature10360

Yu, A. J., & Dayan, P. (2005). Uncertainty, neuromodulation, and attention. *Neuron, 46*(4), 681-692. doi:10.1016/j.neuron.2005.04.026

Zanto, T. P., Rubens, M. T., Thangavel, A., & Gazzaley, A. (2011). Causal role of the prefrontal cortex in top-down modulation of visual processing and working memory. *Nature Neuroscience, 14*(5), 656-U156. doi:10.1038/nn.2773

Zerbi, V., Floriou-Servou, A., Markicevic, M., Vermeiren, Y., Sturman, O., Privitera, M., . . . Bohacek, J. (2019). Rapid reconfiguration of the functional connectome after chemogenetic locus coeruleus activation. *Neuron, 103*(4), 702-718. doi:10.1016/j.neuron.2019.05.034

Supplementary Information for

Thalamocortical excitability adjustments guide human perception under uncertainty

Julian Q. Kosciessa*, Ulman Lindenberger, Douglas D. Garrett*

* Email: kosciessa@mpib-berlin.mpg.de; garrett@mpib-berlin.mpg.de

This PDF file includes:

Text S1. Parameter interrelations. To better understand individual differences in behavioral performance, we explored inter-individual associations between model parameter estimates and 'raw' median RT and mean accuracy. Linear drift rate decreases were inter-individually associated with decreases in accuracy (EEG: r = .35, p = .015, MRI: r = .46, p = .001), but not RT increases (both p > .05), whereas non-decision-time (NDT) increases tracked individual RT increases (EEG: r = .56, p = 3e-5, MRI: r = .64, p = 2e-6), but not accuracy decreases (both p > .05). For single targets, faster RTs were associated with larger drift rates (EEG: r = -.63, p = 3e-6, MRI: r = -.47, p = .002), lower non-decision times (EEG: r = .41, p = .005, MRI: r = .58, p = 3e-5), and lower boundary separation (EEG: r = .58, p = 3e-5, MRI: r = .5, p = 6e-4). More accurate performance for single targets was related to higher drift rates (EEG: r = .74, p = 3e-9; MRI: r = .79, p = 3e-10), but unrelated to boundary separation (EEG: r = .23, p = .121, MRI: r = .18, p = .244) or non-decision times (EEG: r = -.27, p = .069, MRI: r = -.38, p = .011). Amongst model parameters, we observed no parameter relations for single targets (all p > .05). However, we observed intercept-change correlations: subjects with larger drift rates for single targets exhibited strong linear drift rate reductions (EEG: r = -.93, p = 4e-22, MRI: r = -.88, p = 1e-15). Moreover, subjects with larger boundary separation showed stronger linear increases in non-decision time (r = .46, p = 9e-4, MRI: r = .59, p =2e-5). Non-decision time under selective attention, putatively dominantly reflecting visual encoding time, did not relate to changes in drift rate or NDT (both p > .05). Similarly, boundary separation did not relate to drift rate decreases (both p > .05) and drift rates under selective attention were unrelated to NDT increases (both p > .05).

Text S2. Behavioral benefits due to convergent responses. To reduce response mapping demands following probe presentation, we fixed response mapping for the two options of each feature throughout the experiment. Given that multiple attributes converge onto a similar response in a given trial, the potential to prepare motor action prior to probe presentation co-varies as a function of load. To assess the influence of this response agreement on our results, we ran an additional HDDM that simultaneously modelled both a main effect of load, as well as categorical response agreement. Notably, the obtained target load effects on drift rate and NDT were virtually identical to those observed in the selected model in both sessions (reliability of all linear effects: r >= .9 p <.001; data not shown), while linear decreases in drift and increases in NDT were also observed as a function of response divergence (i.e., lower drift and higher NDT if the probed attribute required a differential response than the other cued attributes; shown in Figure S1D for the EEG session; qualitatively similar results were obtained for MRI session; all linear effects p < .001). This suggests that response agreement systematically impacted decision processes, but cannot account for the main effects of target load. However, the large amount of added model parameters introduced partial convergence issues. We therefore chose the simpler model without response agreement for our main analyses.

Text S3. NDT increases indicate extended motor preparation demands. We observed a parametric increase in non-decision time (NDT) with target uncertainty (Figure 2B) that described shifts in RT distribution onset (Figure S3A). NDT is thought to characterize the duration of processes preceding and following evidence accumulation, i.e., probe encoding and planning/execution of the motor response. We therefore examined sensory probe- and response-related ERP components regarding their modulation by prior target uncertainty. We time-locked the CPP to the NDT group estimate for a single target – for which no button remapping was required – and (2) to the condition-wise NDT estimate. However, we observed no shift in CPP onset (Figure S3B), suggesting constant visual encoding time. To probe increases during response preparation, we assessed parametric changes in ERP amplitudes during the interval spanning the final 100 ms prior to response. This interval covered the timeframe of indicated NDT increases, after accounting for the constant probe encoding duration (Figure S3B). Notably, we observed a late frontal potential that increased in amplitude (Figure S3D) and whose onset corresponded to the temporal NDT shift (Figure S3C) after controlling for constant encoding duration (Figure S3B). This suggests that baseline NDT estimates approximate the duration of probe encoding (Nunez, Vandekerckhove, & Srinivasan, 2017), whereas NDT increases characterize increased

demands for transforming the sensory decision into a motor command (Lui et al., 2018). This further suggests that drift diffusion modelling successfully dissociated contributions from evidence integration, sensory encoding, and motor preparation. Interestingly, evidence accumulation consistently peaked at/near response execution, suggesting that additional motor demands may unravel in parallel, rather than succeed finished integration (as is often assumed in sequential sampling models).

Text S4. Behavioral PLS of spectral power during sensation. Task PLS describes the multivariate co-variation of spectral power with load. However, inter-individual behavioral differences may relate to power changes in specific bands. To probe whether inter-individual relations of power modulation to behavior would vary from the mean changes as identified via task PLS, we calculated a behavioral PLS by considering the individual linear change in spectral power with target uncertainty. This revealed a similar multivariate loading pattern as observed for the task PLS (**Figure S4B**), with high agreement between individual brainscores ($r = .7$, $p < .001$), suggesting that the identified frequency ranges jointly contributed to behavioral relations.

Text S5. Pre-stimulus alpha power increases with load, but does not relate to behavioral changes or power changes during sensation. Furthermore, decreases in pre-stimulus alpha power have been linked to increases in cortical excitability at stimulus onset (Iemi, Chaumon, Crouzet, & Busch, 2017; Lange, Oostenveld, & Fries, 2013). To probe whether expected uncertainty modulated pre-stimulus alpha power, we performed another task PLS, covering the final second of the fixation interval prior to stimulus onset. This analysis indicated that pre-stimulus alpha power increased alongside uncertainty (**Figure S4C**). Notably, in contrast to current results, elevated levels of anticipatory alpha power are often associated with decreased gamma power upon stimulus onset. Notably, linear models did not indicate associations between pre-stimulus alpha power increases across load with either drift rate decreases [$r(137) = 0.02$, 95%CI [-0.15, 0.18], $p = 0.86$], non-decision time increases [$r(137) = 0.06$, 95%CI [-0.1, 0.23], $p = 0.45$] or increases on the SPMF [$r(137) = -0.13$, 95%CI [-0.29, 0.04], $p = 0.13$]. These results are in line with increasing evidence suggesting that anticipatory alpha power modulation more closely tracks subjective confidence in upcoming decisions than sensory fidelity (Benwell et al., 2017; Limbach & Corballis, 2016).

Text S6. SSVEP magnitude is not modulated during sensation. Moreover, SSVEP magnitude has been suggested as a signature of encoded sensory information (O'Connell, Dockree, & Kelly, 2012), that is enhanced by attention (Morgan, Hansen, & Hillyard, 1996; Muller et al., 2006) and indicates fluctuations in excitability (Zhigalov, Herring, Herpers, Bergmann, & Jensen, 2019). However, despite a clear SSVEP signature, we did not observe significant effects of encoding demands on the global SSVEP magnitude (**Figure S4D**). As attentional effects on SSVEP magnitude have been shown to vary by SSVEP frequency (Ding, Sperling, & Srinivasan, 2006), the 30 Hz range may have been suboptimal here. Furthermore, the SSVEP frequency was shared across different features, thus not allowing us to assess whether uncertainty modulated the selective processing of single features. Implementing feature-specific flicker frequencies may overcome such limitations in future work, and allow to assess the changes in feature-specific processing under uncertainty.

Text S7. Rhythm-specific indices in theta and alpha band relate to multivariate spectral power modulation. Finally, as spectral power conflates rhythmic and arrhythmic signal contributions in magnitude, space and time (Kosciessa, Grandy, Garrett, & Werkle-Bergner, 2020), we performed single-trial rhythm detection, observing similar decreases in the duration and power of alpha rhythms (see **Figure S4E**) that were jointly related to stronger increases on the latent factor [duration: $r(137) = -0.61$, 95%CI [-0.71, -0.49], $p = 1.31e\text{-}15$; power: $r(137) = -0.63$, 95%CI [-0.72, -0.52], $p = 9.66e\text{-}17$]. Notably, this analysis indicated increases in theta duration, but not power, suggesting that narrowband theta power changes mainly reflected modulations in the duration of non-stationary theta rhythms, rather than changes in their strength. In line with this suggestion, increases on the spectral power factor related

to increases in theta duration [r(137) = 0.19, 95%CI [0.02, 0.35], p = 0.03], but not theta SNR [r(137) = 0.09, 95%CI [-0.08, 0.25], p = 0.31].

Text S8. A second LV may indicate decreased task engagement due to heightened difficulty at higher uncertainty levels. A 2nd significant LV (p =.012) indicated strong positive loadings in angular gyrus, middle frontal gyrus, and inferior frontal gyrus, as well as occipital cortex (see **Figure S5A**). Negative loadings were observed dominantly in medial PFC, precuneus and V5. This component increased from selective attention to target load 2, but then declined towards higher loads. Decreases in angular gyrus have been strongly to increased visual working memory load (Sheremata, Somers, & Shomstein, 2018; Todd & Marois, 2004). Increases in DMN regions, in addition to decreased prefrontal activity suggest that this component reflects relative task disengagement towards high load conditions, while increases in lateral visual cortex may reflect increased entrainment, and lack of top-down inhibition. In line with more negative loadings on this component being detrimental, we observed that inter-individually higher brainscores (i.e., positive loadings) were associated with lower non-decision times during selective attention (r = -0.46, p = .002), while stronger within-subject decreases with load were associated with larger individual NDT increases [r(122) = -0.18, 95%CI [-0.35, -0.01], p = 0.04] but not changes in drift rate [r(122) = 0.01, 95%CI [-0.17, 0.18], p = 0.95]. Larger decreases on this component were moreover related to more constrained increases in spectral modulation [r(122) = 0.39, 95%CI [0.23, 0.53], p = 6.83e-6]. Jointly, this suggests that individual drop-offs in the positive cluster of regions reflects decreased task engagement under increased difficulty, with adverse behavioral consequences.

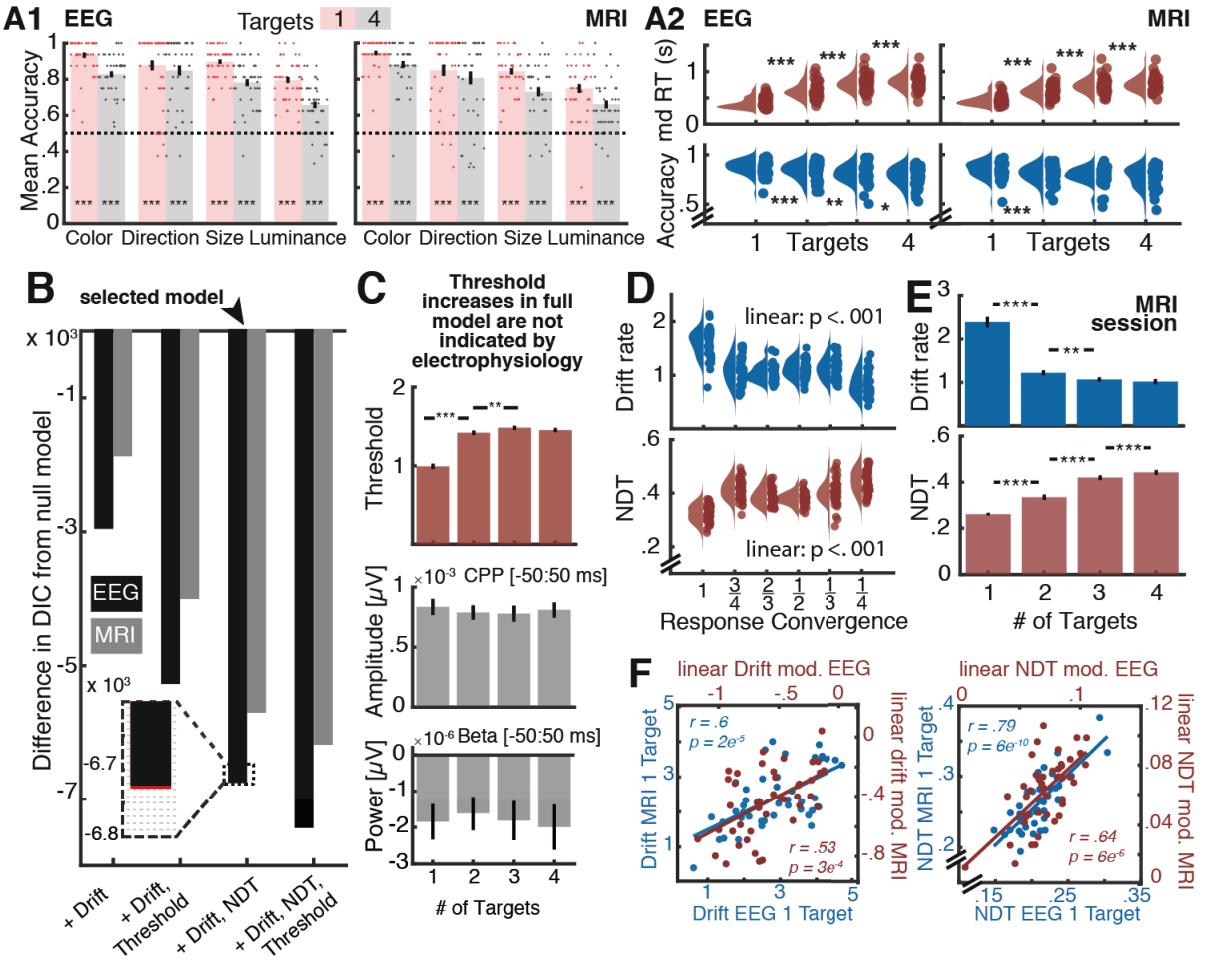

Figure S1. Additional behavioral analyses. **(A1) Accuracies for single target cue and maximum target uncertainty.** For all features, mean accuracy was above chance accuracy (0.5, indicated by broken lines) at the group level. Dots indicate individual accuracies. *** = p < .001 (paired t-test vs. chance accuracy). **(A2) Reaction times and accuracies by load.** All linear effects were significant (p < .001). **(B-C) HDDM model comparison.** (**B**) DIC-based model comparison indicates that full model, including threshold modulation, provides the best group fit to the behavioral data. However, load-related threshold increases (C) were not supported by EEG-based signatures (D). The inset shows an additional comparison of the selected model with an alternative model including starting point variation across load levels (displayed in red). Due to very constrained fit improvements, we selected the simpler model without starting point variation for further analyses. (**C**) **Threshold increases in full model are not indicated by electrophysiology.** The full model indicates additional threshold (also called boundary separation) increases with added target load, with qualitatively identical effects on drift rate and NDT (not shown). Boundary separation captures the conservativeness of the decision criterion and has been related to decision conflict during the choice process (e.g., Cavanagh et al., 2011). EEG-based signatures of evidence integration do not indicate threshold differences. While the full model suggested increased boundary separation, neither of the electrophysiological proxies (i.e., CPP, contralateral beta) of evidence bounds mirrors such increases. While this suggests the absence of threshold increases (McGovern, Hayes, Kelly, & O'Connell, 2018), it alternately questions the sensitivity of electrophysiological threshold estimates, which should be investigated with specific threshold modulations, such as speed-accuracy trade-off instructions, in future work. **(D) Differences in response convergence do not account for main effects of target load.** A separate model including both target load and response convergence indicated practically identical NDT and drift rate effects of target amount, while highlighting additional linear effects of response convergence. Data are individually-centered across conditions. **(E-F) Reliability of individual parameter estimates across sessions.** A separate hierarchical DDM was fit to data from each session. (**E**) Similar group-level effects were indicated for the MRI and EEG (cf. Figure 2B) session: whereas drift rate decreased with load, non-decision time increased. (**F**) Session reliability of inter-individual differences was high both for

single-target performance and for linear changes with target load. Reliability was also high for threshold estimates (r = .79, p = 6e-10). [* p <.05; ** p <.01; *** p < .001]

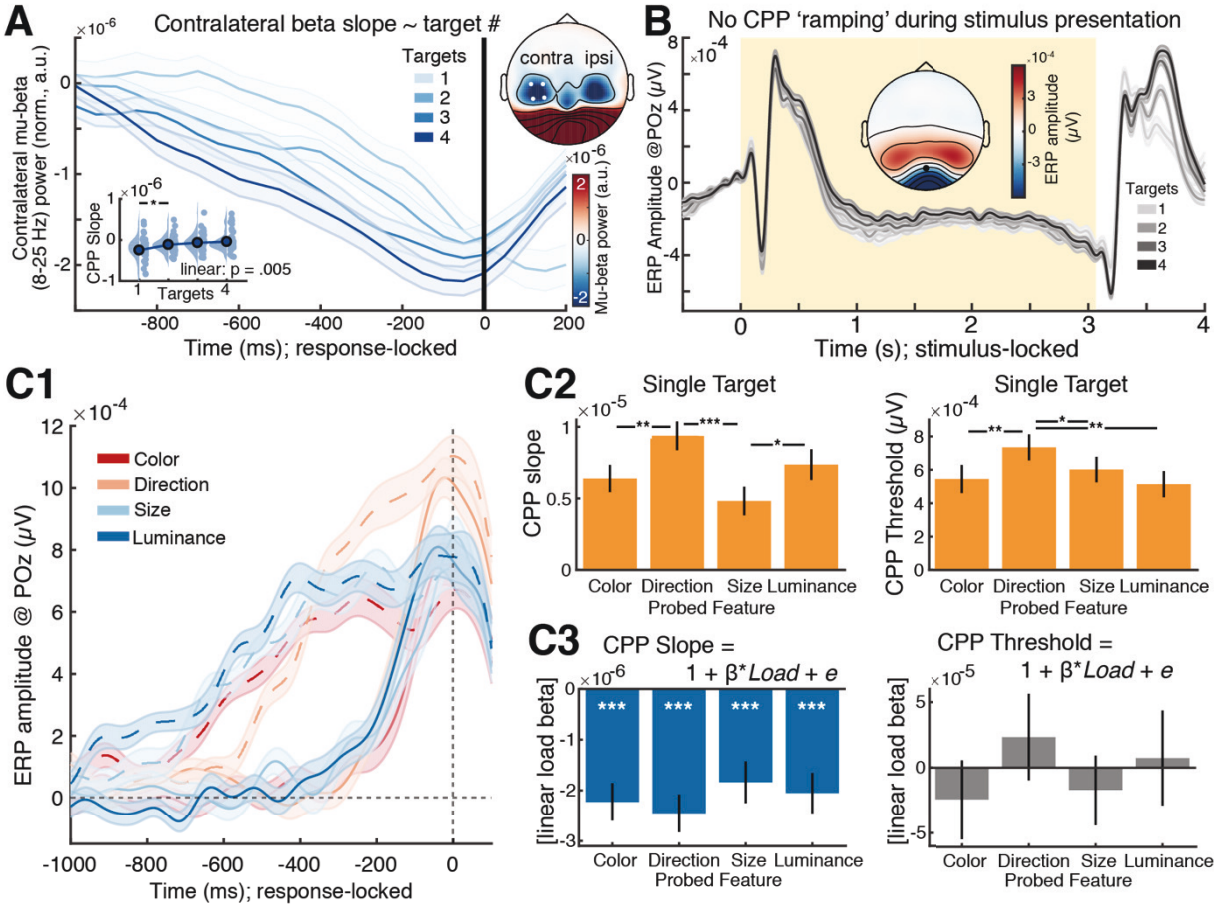

Figure S2. Additional drift rate analyses. **(A) The slope of lateralized motor preparation indicates load-related decreases in drift rate.** (A) Slopes of contralateral mu-beta power shallows with increasing attentional load levels. The inset displays linear slope estimates, estimated via linear regression from -250 ms to -50 ms, relative to response. (B) Topography of response-locked mu-beta power, averaged from -50 ms to +50 ms around response. White dots indicate the contralateral channels from which data was extracted. **(B) The centro-parietal positive potential (CPP) does not show clear ramping increases during stimulus presentation.** The yellow background indicated the stimulus presentation period. Note the modulated ramping following the probe onset at the end of stimulus presentation. The inset shows the topography of the grand average ERPs, temporally averaged during the final 2 seconds of the stimulus presentation period. The black dot indicates channel POz, at which the group-wise CPP was maximal (see Figure 2C1). **(C) Differences between probed stimulus attributes do not account for drift rate decreases under target load.** (A) Response-locked CPP as a function of probed attribute, shown for the single target (complete lines) and four target (broken lines) conditions. Data were selected by condition and probed (cf. cued), attribute, ensuring that unique trials contributed to each load condition. (B) Comparison of CPP slopes and thresholds for different probed features, when the probe target was known in advance. Slopes and thresholds were increased for direction than for other attributes, indicating relatively larger available evidence and more cautious responses (putatively 'easier' feature). (C) Load effect of CPP slopes and thresholds for different probed feature attributes. CPP slopes (i.e., evidence drift) exhibited load-related decreases for each probed attribute, whereas no threshold modulation was indicated for any of the probed attributes. [* p <.05; ** p <.01; *** p < .001]

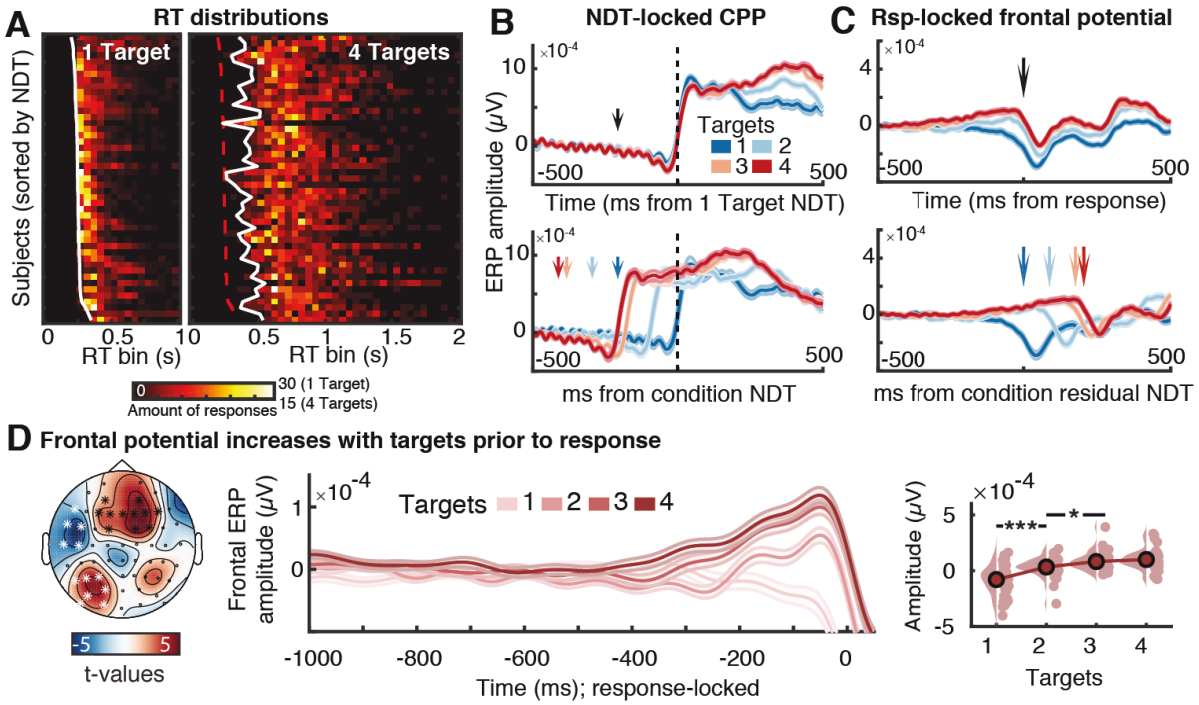

Figure S3. Non-decision time (NDT) increases putatively relate to additional motor demands, not temporal delays in CPP onset. **(A) NDT estimates describe the onset of individual RT distributions (see also Lui et al., 2018).** Response counts (here shown for EEG session) were sorted into 40 bins of 50 ms each. White lines indicate individual NDT estimates; the red dotted line indicates NDT estimates for the single-target condition. **(B, C) Relation of visual encoding and frontal potential to indicated NDT increases.** When response preparation can be made in advance (i.e., when only a single target is indicated) and probe onset only requires response execution, the average NDT estimate aligns with the onset of the CPP (B, top). However, load-related increases in NDT occur in the absence of temporal shifts in CPP onset (B, bottom). In C, arrows indicate the average probe onset time in each condition. In contrast, a frontal potential (see D) increases around the time of residual NDT increases (i.e., NDT estimate for each condition minus constant NDT from single-target condition; C, bottom). In D, arrows indicate the average response time in each condition. **(D) A frontal potential increase prior to response, suggesting that observed NDT increase reflect additional motor preparation demands (e.g., button remapping).** Left: Topography of test for linear ERP changes as a function of load during the final 200 ms prior to response. Clusters in white did not exhibit changes that were exclusive to the period preceding the response (data not shown). Center: Extracted traces averaged within the frontal cluster shown with black asterisks on the left. Right: Post-hoc tests on amplitudes of the frontal potential across the final 100 ms prior to response. Data are individually centered across target loads. [* p <.05; ** p <.01; *** p < .001]

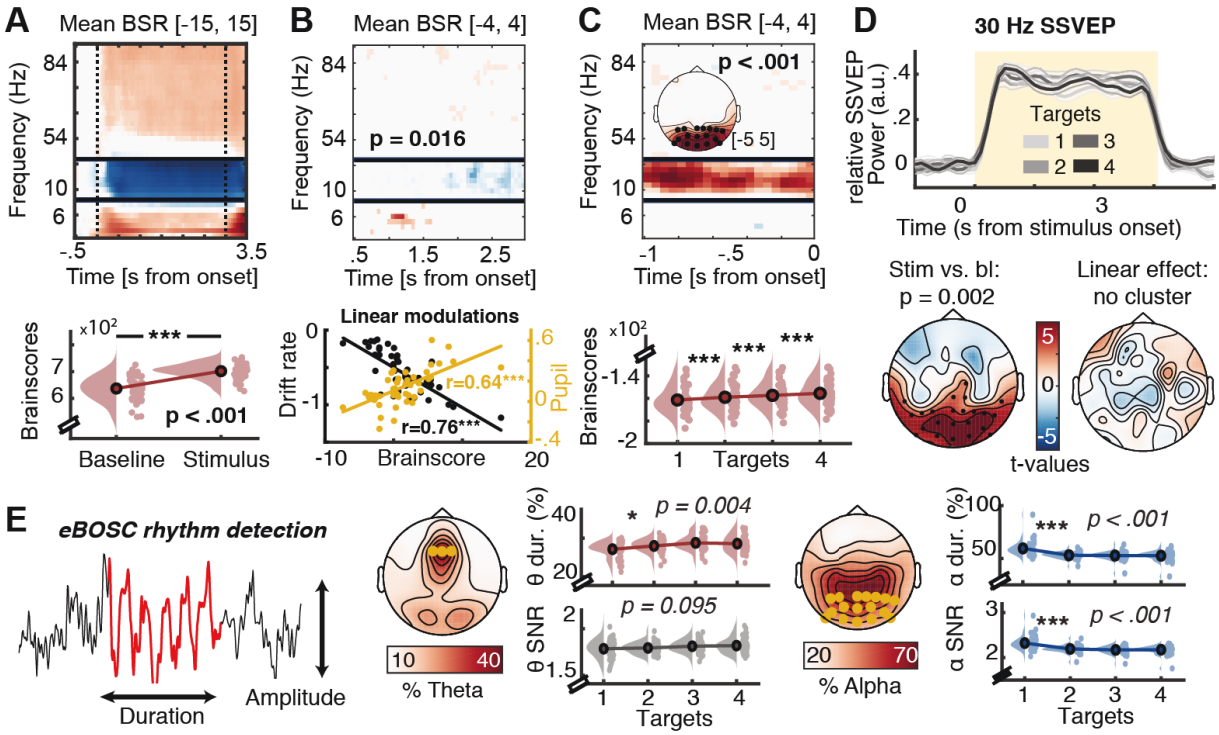

Figure S4. Additional spectral power analyses prior and during sensation. **(A) Multivariate baseline changes and behavioral PLS.** Note that data correspond to the different clusters indicated in Figure 3A. **(B) Behavioral PLS, linking linear multivariate spectral power changes with target # to drift rate decreases and pupil diameter modulation. (C) Parieto-occipital pre-stimulus alpha power increases with target load but is not related to drift changes (see Text S4). (D) SSVEP amplitude is not modulated by attentional load.** Top: Time-resolved, spectrally-normalized, SSVEP power, averaged across occipital channels (O1, Oz, O2), indicates SSVEP presence during stimulus presentation. Bottom left: Topography of stimulus-evoked SSVEP contrast minus baseline. Black dots indicate significant channels as indicated by CBPA. Bottom right: No linear load-related SSVEP modulation was indicated by CBPA. **(E) Modulation of rhythm-specific duration and power by target number.** Left: Schematic of the assessment of amplitude and duration from non-stationary rhythmic events. Right: Topographies of relative theta and alpha occurrence ('abundance'), averaged across target levels. Orange dots indicate the channels used to extract the data in E, which were the same channels also used in Figure 3AB. Target load decreased alpha duration and power and increased theta duration, but not power. Data are individually centered across target loads. [* p <.05; ** p <.01; *** p < .001]

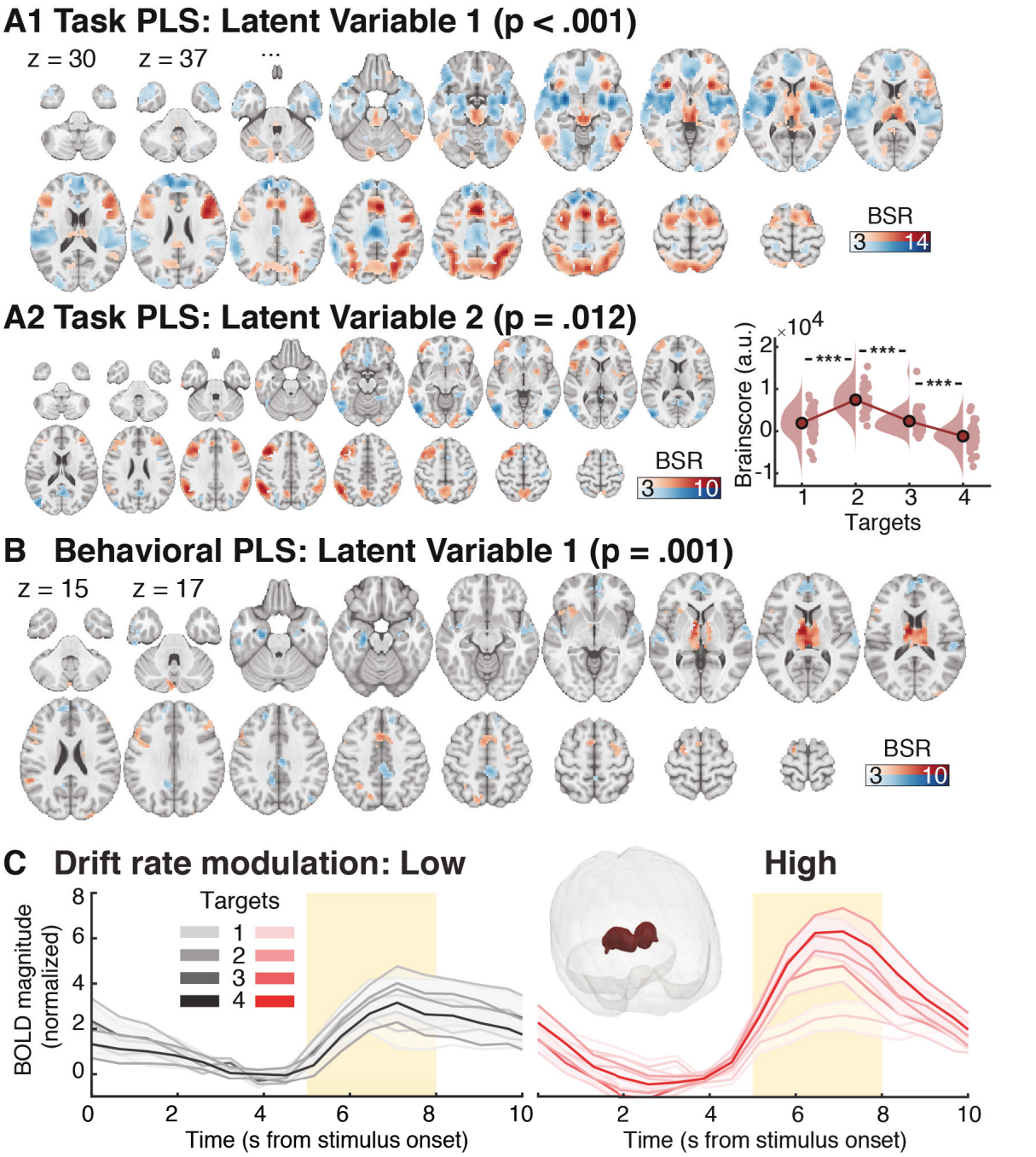

Figure S5. Additional BOLD analyses. **(A, B) Full multivariate brainscore loadings for the two significant latent variables (LVs) produced by the task PLS (A) and behavioral PLS (B).** (A2 left) The brainscore loadings of the second LV designate an initial increase followed by a subsequent decrease towards higher target loads. Data are individually centered across target loads. Thus, the negative components of the pattern expressed on the right become more strongly activated at low and high loads, whereas the positive components are maximally expressed when two targets are relevant. **(C) Thalamic BOLD magnitude for a median split of high- and low drift rate modulators.** The inset shows the thalamic ROI in a glass brain view. [* p <.05; ** p <.01; *** p < .001]

Table S1. PLS model peak activations, bootstrap ratios, and cluster sizes.

			MNI Coordinates				
Model	Region	Hem	X	Y	Z	BSR	#Voxels
taskPLS LV1 BSR [-3 3]	Mid-cingulate cortex (MCC)	L	-6	15	42	13.42	2708
	Inferior Parietal Lobule (IPS)	L	-45	-45	45	11.14	2664
	Insula Lobe (anterior) [33.0 21.0 -3]	R	33	18	-3	10.86	175
	Inferior Occipital Gyrus [-54 -69 -12]	L	-57	-69	-12	10.1	702
	Thalamus [-8 -27 -2]	L	-6	-30	-3	9.93	1121
	Superior Frontal Gyrus	R	27	-3	54	9.47	880
	Inferior Temporal Gyrus	R	51	-60	-12	6.72	265
	Superior Orbital Gyrus	L	-27	54	-3	6.2	232
	Cerebellum (Crus 1)	R	6	-81	-24	6.12	109
	PCC [-6.0 -35.0 28.0]	L	-9	-33	27	5.72	62
	Cerebellum (VI)	R	30	-63	-30	5.64	59
	Cerebellar Vermis (9)		0	-57	-36	4.32	32
	Cerebellum (Crus 2)	L	-6	-84	-33	3.82	26
	Pallidum [24.0 3.0 -6.0]; bilateral	R	24	0	-9	-11.74	3882
	Insula Lobe	L	-33	-18	6	-11.05	3776
	Superior Frontal Gyrus	L	-12	36	54	-10.6	2096
	MCC	L	0	-15	36	-9.72	706
	Lingual Gyrus	R	21	-84	-6	-7.43	440
	Superior Occipital Gyrus	R	27	-96	15	-5.54	318
	Middle Frontal Gyrus	L	-33	24	39	-5.48	44
	Angular Gyrus	L	-48	-63	27	-5.31	106
	Superior Parietal Lobule	L	-21	-45	63	-5.12	94
	Postcentral Gyrus	R	21	-39	63	-4.98	89
BSR [-6 6] (additional clusters that were merged in +/- 3 threshold)	IFG	L	-45	9	30	12.576	790
	Insula Lobe	L	-33	18	-3	10	93
	IFG	R	42	27	18	7	32
	IFG	R	51	33	-9	-8.69	125
	SMG	R	57	-39	39	-7.80	56
	Inferior Temporal Gyrus	L	-57	-6	-33	-7.57	96
taskPLS LV2	Angular Gyrus	R	54	-51	36	8.69	638
	Middle Frontal Gyrus	R	39	18	39	8.24	1238
	IFG (p. Orbitalis)	R	42	45	-12	6.37	141
	SupraMarginal Gyrus	L	-60	-45	33	6.36	317
	Middle Frontal Gyrus	L	-42	24	33	6.21	477
	Inferior Occipital Gyrus	L	-27	-90	-12	5.66	110
	Precuneus	R	3	-60	45	5.54	383
	Middle Temporal Gyrus	R	60	-33	-12	5.26	154
	IFG (p. Triangularis)	R	48	18	3	5.07	115
	Lingual Gyrus	R	21	-84	-6	4.99	77
	Putamen	L	-30	3	-3	4.62	115
	Cerebelum (Crus 2)	L	-9	-81	-27	4.22	34
	Putamen	R	24	0	6	3.93	30
	Inferior Occipital Gyrus	L	-48	-75	-6	-7.92	378
	Inferior Occipital Gyrus	R	51	-72	-15	-7.61	706
	Olfactory cortex	L	-3	18	-12	-5.63	502
	Precuneus	L	-6	-63	21	-5.56	220
	Superior Parietal Lobule	R	27	-54	63	-4.46	39
	Fusiform Gyrus	L	-24	-45	-15	-4.43	83
	Postcentral Gyrus	L	-57	-3	42	-4.38	58
	Postcentral Gyrus	L	-45	-27	57	-4.36	85
	Superior Orbital Gyrus	R	21	27	-15	-4.32	25
	Superior Occipital Gyrus	R	27	-69	36	-4.29	58
	Precentral Gyrus	L	-42	0	30	-4.23	28
	Middle Temporal Gyrus	L	-54	-57	12	-4.18	38
			-69	-42	9	-4.13	51
	Middle Occipital Gyrus	L	-30	-81	36	-4.1	60
	Posterior-Medial Frontal	L	-6	6	60	-3.95	33
	Hippocampus	L	-27	-18	-21	7.04	111

behavioral PLS: LV1	Inferior Temporal Gyrus [-56 -24 -30]	L	-57	-24	-30	5.5	40
	Superior Medial Gyrus	R	3	63	15	5.43	345
	ParaHippocampal Gyrus	R	21	-12	-24	5.35	35
	MCC	R	3	-33	48	5.3	174
	Middle Temporal Gyrus	L	-60	0	-30	4.77	27
	MCC	L	-12	-45	36	4.72	64
	Superior Frontal Gyrus	R	18	51	30	4.68	33
	Fusiform Gyrus	R	24	12	-45	4.67	30
	Middle Temporal Gyrus	R	57	-3	-15	4.64	239
	Superior Frontal Gyrus	L	-21	42	36	4.61	26
	Superior Temporal Gyrus	L	-57	-21	3	4.6	61
	Angular Gyrus	R	39	-72	39	4.59	36
	Middle Temporal Gyrus	L	-51	-3	-21	4.52	72
	Temporal Pole	R	36	6	-21	4.42	25
	Superior Medial Gyrus	L	9	36	45	4.25	29
	Thalamus	L	-9	-9	12	-9.73	591
	Superior Frontal Gyrus	L	-24	-3	69	-5.59	38
	Posterior-Medial Frontal	L	-3	15	45	-5.22	154
	Superior Occipital Gyrus	R	27	-96	21	-5.15	39
	SupraMarginal Gyrus	L	-60	-48	24	-5.13	28
	Cerebelum (Crus 2)	L	-6	-84	-33	-5.09	35
	Superior Parietal Lobule	L	-18	-69	48	-5.07	36
	IFG (p. Opercularis)	L	-57	15	33	-4.87	173
	Insula Lobe	L	-30	21	-3	-4.37	44
	Inferior Parietal Lobule	L	-33	-54	45	-4.03	30
	Superior Frontal Gyrus	R	24	0	54	-3.9	51
	Middle Frontal Gyrus	R	45	36	33	-3.78	35

Note: Locations where peaks had to be shifted for a label are indicated with coordinates in the label.

Supplementary References

Benwell, C. S. Y., Tagliabue, C. F., Veniero, D., Cecere, R., Savazzi, S., & Thut, G. (2017). Prestimulus EEG power predicts conscious awareness but not objective visual performance. *Eneuro, 4*(6). doi:10.1523/ENEURO.0182-17.2017

Cavanagh, J. F., Wiecki, T. V., Cohen, M. X., Figueroa, C. M., Samanta, J., Sherman, S. J., & Frank, M. J. (2011). Subthalamic nucleus stimulation reverses mediofrontal influence over decision threshold. *Nature Neuroscience, 14*(11), 1462-1467. doi:10.1038/nn.2925

Ding, J., Sperling, G., & Srinivasan, R. (2006). Attentional modulation of SSVEP power depends on the network tagged by the flicker frequency. *Cerebral Cortex, 16*(7), 1016-1029. doi:10.1093/cercor/bhj044

Iemi, L., Chaumon, M., Crouzet, S. M., & Busch, N. A. (2017). Spontaneous neural oscillations bias perception by modulating baseline excitability. *Journal of Neuroscience, 37*(4), 807-819. doi:10.1523/JNEUROSCI.1432-16.2016

Kosciessa, J. Q., Grandy, T. H., Garrett, D. D., & Werkle-Bergner, M. (2020). Single-trial characterization of neural rhythms: Potential and challenges. *Neuroimage, 206*, 116331. doi:10.1016/j.neuroimage.2019.116331

Lange, J., Oostenveld, R., & Fries, P. (2013). Reduced occipital alpha power indexes enhanced excitability rather than improved visual perception. *Journal of Neuroscience, 33*(7), 3212-3220. doi:10.1523/Jneurosci.3755-12.2013

Limbach, K., & Corballis, P. M. (2016). Prestimulus alpha power influences response criterion in a detection task. *Psychophysiology, 53*(8), 1154-1164. doi:10.1111/psyp.12666

Lui, K. K., Nunez, M. D., Cassidy, J. M., Vandekerckhove, J., Cramer, S. C., & Srinivasan, R. (2018). Timing of readiness potentials reflect a decision-making process in the human brain. *bioRxiv*.

McGovern, D. P., Hayes, A., Kelly, S. P., & O'Connell, R. G. (2018). Reconciling age-related changes in behavioural and neural indices of human perceptual decision-making. *Nature Human Behaviour, 2*(12), 955-966. doi:10.1038/s41562-018-0465-6

Morgan, S. T., Hansen, J. C., & Hillyard, S. A. (1996). Selective attention to stimulus location modulates the steady-state visual evoked potential. *Proceedings of the National Academy of Sciences of the United States of America, 93*(10), 4770-4774. doi:10.1073/pnas.93.10.4770

Muller, M. M., Andersen, S., Trujillo, N. J., Valdes-Sosa, P., Malinowski, P., & Hillyard, S. A. (2006). Feature-selective attention enhances color signals in early visual areas of the human brain. *Proceedings of the National Academy of Sciences of the United States of America, 103*(38), 14250-14254. doi:10.1073/pnas.0606668103

Nunez, M. D., Vandekerckhove, J., & Srinivasan, R. (2017). How attention influences perceptual decision making: Single-trial EEG correlates of drift-diffusion model parameters. *Journal of Mathematical Psychology, 76*, 117-130. doi:10.1016/j.jmp.2016.03.003

O'Connell, R. G., Dockree, P. M., & Kelly, S. P. (2012). A supramodal accumulation-to-bound signal that determines perceptual decisions in humans. *Nature Neuroscience, 15*(12), 1729-+. doi:10.1038/nn.3248

Sheremata, S. L., Somers, D. C., & Shomstein, S. (2018). Visual short-term memory activity in parietal lobe reflects cognitive processes beyond attentional selection. *Journal of Neuroscience, 38*(6), 1511-1519. doi:10.1523/Jneurosci.1716-17.2017

Todd, J. J., & Marois, R. (2004). Capacity limit of visual short-term memory in human posterior parietal cortex. *Nature, 428*(6984), 751-754. doi:10.1038/nature02466

Zhigalov, A., Herring, J. D., Herpers, J., Bergmann, T. O., & Jensen, O. (2019). Probing cortical excitability using rapid frequency tagging. *Neuroimage, 195*, 59-66. doi:10.1016/j.neuroimage.2019.03.056